OBJECTIVES OF COAL BIOPROCESSING AND APPROACHES

Ramani Narayan and Nancy W. Y. Ho
Laboratory of Renewable Resources Engineering
Purdue University
West Lafayette, IN 47907

INTRODUCTION

There has been a great deal of excitement about various practical applications of biotechnology, including the production of chemicals, fuels, foods, and drugs; waste treatment; clinical and chemical analyses; toxicological assays; and uses in medicine. In fact, in the last four years there have been four issues of *Science* devoted to this "revolution" in biology. The two most recent were entitled "Biological Frontiers" (1) and "Biotechnology" (2).

Microbe-catalyzed processes constitute industrial microbiology, which today is a diversified multi-billion dollar industry (3,4). The applications of living microbial, plant and animal cells for the production of useful compounds has been extensive. The microbial conversions of lignocellulosic material, the biological precursor to coal, have also been studied in detail.

Studies in coal bioprocessing, however, is just getting underway and still in its infancy. Conceptually coal bioprocessing can be categorized into two areas: 1) coal cleaning--removal of undesirable components such as sulfur, nitrogen, trace metals; and 2) coal conversion--microbial liquefaction, microbial gasification, microbial pretreatment, methane production. The ability of any microbe or microbial consortia to break down a complex structure depends on the types of chemical bonds and the three dimensional environment around the bonds. Therefore, intertwined with coal bioprocessing is an understanding of the coal macromolecular structure and biochemical mechanisms by which microbes/enzymes break bonds. These relationships are depicted in Figure 1.

The objectives of microbial coal cleaning are clear. Removal of sulfur, nitrogen and trace metals by mild microbial processes for the production of clean coal is the overall goal. However, in the area of microbial coal conversion it seems that the objectives are not very clear. For example, in the case of microbial lignin degradation the objective is very clear; that is the complete degradation of the lignin. Obviously, one does not want to completely degrade the coal, but convert the coal into a more usable form by the application of microbial transformations.

Thus, the overall objective in any coal conversion scheme, whether microbial or chemical, is to produce a better fuel form, be it liquid fuel (transportation fuels), solid fuel, or even a new fuel form for direct utilization. This essentially entails depolymerizing of the coal macromolecule, removal of oxygen, increase in H/C ratio. This concept is depicted in Figure 2. It must be borne in mind that unlike in the lignin degradation, the coal can not just be subjected to a non-specific degradation, but must undergo microbial transformations resulting in a depolymerized, deoxygenated, denitrated product which would result in a better fuel.

The area of microbial conversion of coal is receiving a lot of attention these days. Cohen and Gabriel (5) reported that fungi could grow directly on and metabolize naturally occurring coal. Scott (6), Wilson (7), Ward (8), and Faison (9) have also reported degradation or solubilization of lignites by various fungal strains including the solubilization of a Wyodak subbituminous coal (6). However, little is known about the products of the degradation or solubilization. As

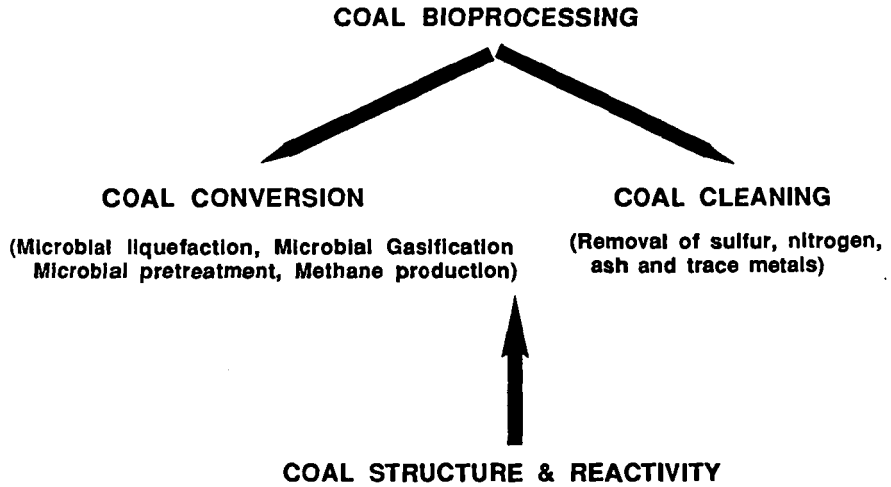

Figure 1. Coal bioprocessing areas

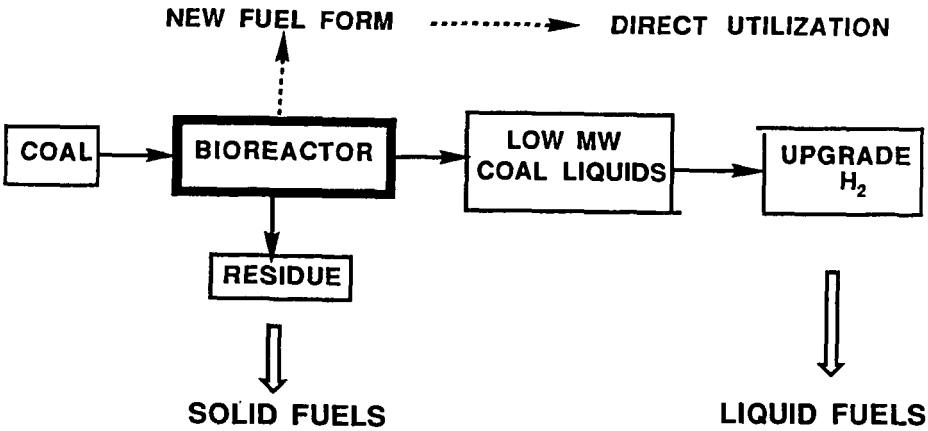

Figure 2. Coal bioprocessing schematics

indicated earlier, the overall objective in any coal conversion scheme whether microbial or chemical is to produce a better fuel form.

Towards achieving this goal, there are two basic approaches to microbial processing of coal. The first approach involves the oxidative solubilization or depolymerization of the coal macromolecule. It involves using enzyme systems or microorganisms to hydroxylate aromatic rings followed by ring fission to a carboxylic acid. Since all of this involves introduction of oxygen into the coal, the question of whether coal is being converted to a less desirable fuel form (converting coal into biomass?) becomes an important issue. On the other hand, if the oxygenated material is more receptive to deoxygenation and/or upgrading than the starting coal, or has other uses, then this type of microbial conversion makes sense.

A second approach to microbial processing of coal, which, according to me promises to be much more rewarding and exciting. The approach envisions using facultative *anaerobic bacteria* to reductively depolymerize/solubilize coal, i.e., reduction of aromatic rings and reductive cleavages to product a hydrogenated product. In other words, hydrogenation of coal via an anaerobic microbial process resulting in a more desirable fuel form rather than oxidation via an aerobic microbial process which results in a less desirable fuel form. Indeed, coal scientists throughout the ages have been trying to do exactly this; i.e., inexpensive approach to product a depolymerized, hydrogen-rich coal fuel.

MICROBIAL COAL TRANSFORMATION IN AEROBIC SYSTEMS
(Oxidative Solubilization/Depolymerization)

All of the microbial conversions (degradation or solubilization) reported so far in literature involves aerobic systems. The mechanism operating under these conditions is oxidative, depolymerization that is hydroxylation of the aromatic ring followed by ring scission. Indeed, it has been shown that biodegradation/oxidation of aromatics are initiated by a series of enzymes known collectively as the oxygenases. The oxygenases can be further sub-divided into dioxygenases and monoxygenases. Molecular oxygen is essential for them to function since it is incorporated into the end product. The reaction pathway is shown in Figure 3 (10) with ring cleavage occurring at the bond between the hydroxyls (orthocleavage) or the bond adjacent to the hydroxyl. Two- (11,12) and three-ring aromatics (13-15) can also be degraded although free ortho ring positions must be available (Figure 4). Low-ranked coals have a number of hydroxy and dihydroxy aromatic structures, as well as carboxy groups. *Pseudomonas* species are capable of carrying out oxidation ring cleavage reactions (16-20) (Figure 5), or aromatic rings containing these functional groups. Therefore, the *Pseudomonas* species should be capable of oxidizing low-rank coals. It would be interesting to compare the products obtained from the microbial oxidative cleavage reactions with that obtained from the ruthenium tetraoxide catalyzed oxidation of the coal. This is because the mechanism of the ruthenium tetraoxide oxidations involves hydroxylation of the aromatic rings followed by ring cleavage which is similar to the mechanism of microbial oxidative ring cleavages.

Again, the question that pops up is whether such microbial processing approaches for depolymerization/solubilization of the coal makes sense. The reason being that we have introduced a number of oxygen functional groups during the process, which could result in less desirable fuel qualities.

Lignin Biodegradation

Lignin is considered as the precursor to coal and some young lignites may contain 35%-70% of lignin-like compounds. It is, therefore, not surprising that lignin degrading microorganisms and enzymes are being employed for microbial coal conversion. For example *Phanerochaete chrysosporium* and *Polyporous versicolor* have been used in microbial coal conversions.

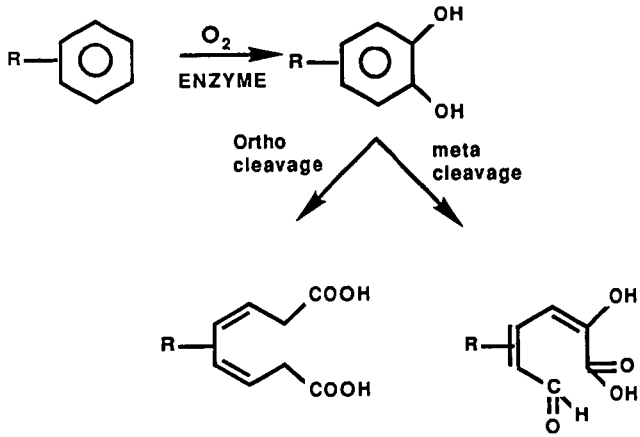

Figure 3. Mechanism of aromatic degradation by oxygenases

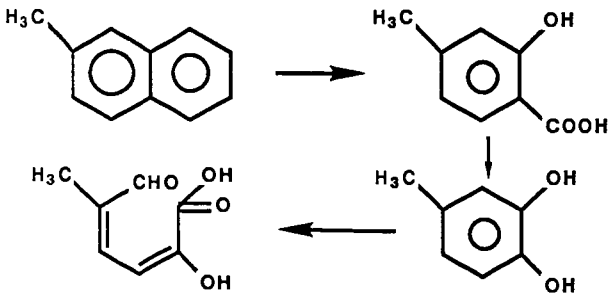

Figure 4. Degradation of two ring compounds

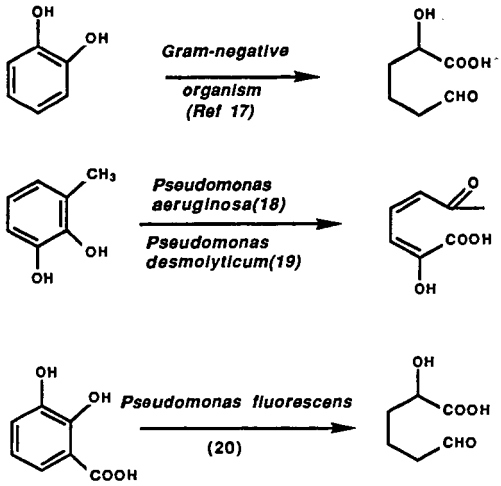

Figure 5. Oxdative ring opening reactions by *Pseudomonas*

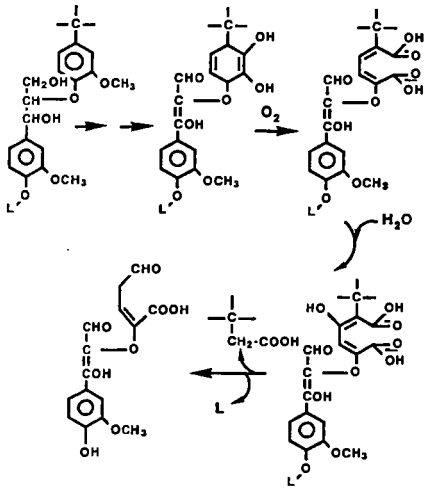

Figure 6. Mechanism of lignin degradation

These are "white rot" fungi and their mechanism of action for lignin degradation involving the enzymes ligninase and laccase have been extensively studied by Kirk and others (21-23). They report that the degradation proceeded by non-specific hydroxylation and ring opening just like the oxygenases functions and, not as previously believed, by beta-arylether cleavage initiated by a specific etherase enzyme (Figure 6).

ENZYMES VS WHOLE CELLS

The question also arises as to whether coal bioprocessing would be better achieved with growing cells or isolated enzymes. Multistep transformations such as the synthesis of interferon or the production of ethanol from cellulose involves a number of different enzymes acting sequentially and regeneration of co-factors is required. Therefore, it is clearly advantageous to use whole cells. For one step or two step transformations however, enzymes are probably superior because their use is free of drawbacks such as competing side reactions, sterility problems, and the cell lysis often associated with fermentations. Enzyme systems like the ligninases, oxygenase could promote selective transformations. There also exists the capability of overproducing the coal processing enzymes using recombinant DNA or genetic engineering techniques. In fact, the ligninase enzyme has been cloned in *Escherichia coli*. It therefore seems to me that the use of isolated enzymes for coal bioprocessing is advantageous and should be pursued.

In our laboratory, we are evaluating enzymes present in various microorganisms to carry out decarboxylation, hydrogenation and non-oxidative depolymerization of the coal. Preliminary results have shown that microorganisms such as *Bacillus megaterium* containing decarboxylase(s) can remove CO_2 from *model compound* vanallic acid and coal. The resulting coal has a higher H/C ratio. Low rank coals have a substantial number of oxygen tied up as carboxyls.

ANAEROBIC BIOCONVERSION OF COAL (Reductive Depolymerization/Solubilization)

A more exciting and potentially rewarding field is the area of coal bioprocessing under anaerobic conditions. To the best of our knowledge, almost no work has been done in this area. This approach envisions the use of facultative anaerobic bacteria to reduce the aromatic ring systems in the coal and produce a depolymerized hydrogenated product. In other words, instead of adding oxygen via an aerobic process and producing a less desirable fuel, we can add hydrogen to the coal using an anaerobic process and produce a richer fuel.

Anaerobic Aromatic Ring Metabolism

Under anaerobic conditions, aromatics are degraded by either hydration or hydrogenation followed by non-oxidative ring fission. In all cases investigated the microorganisms initially reduce the ring structure (24). Tarvin and Buswell (25) reported the complete utilization of benzoate, phenylacetate, phenyl propionate and cinnamate by anaerobes. Healy and Young (26) found that 11 simple lignin derivatives were biodegraded to methane and carbon dioxide under strict anaerobic conditions. Anaerobic degradation of two and three ring lignin fragments has been proposed to occur via an overlap of the ferulate and benzoate degradative pathways (27).

Cleavage of the benzene nucleus anaerobically occurs by at least three different reaction schemes as shown in Figure 7.

A. Photometabolism; ex *Rhodopseudomonas palustris*..

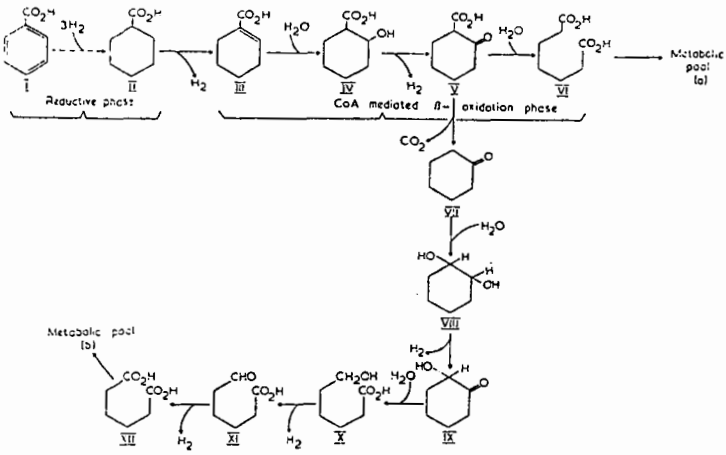

Figure 7. Anaerobic aromatic - ring metabolism

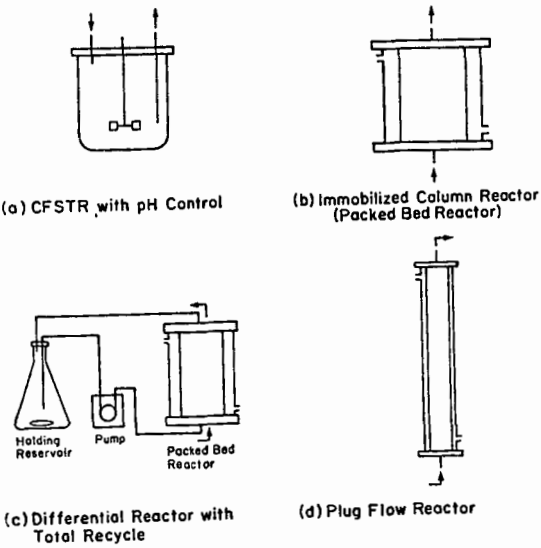

Figure 8. Bioreactor configurations.

B. Nitrate respiration; ex *Moraxella sp.*

C Methanogenic fermentation; ex occurs via a consortium of gram negative organisms and various methane bacteria.

Several species of the purple non-sulfur bacteria, the *Rhodospirillaceae*, are able to use aromatic compounds as sole carbon sources by photometabolism. When cell suspensions of *R. palustris were* incubated with (^{14}C) benzoate the seven carbon atoms of benzoate remained together until after the ring cleavage stage. These results suggested a series of reactions involving the reduction of benzoate (or a derivative) to a cyclohexanecarboxylate moiety followed by a coenzyme-A mediated beta-oxidation sequence. Because the reduced acid is acyclic, breakage of the bond in the 1,2 position occurs to yield pimelate (or its equivalent). This new reductive pathway is illustrated in Figure 7b. Evans (28) has recently demonstrated the occurrence of these reactions using subcellular fractions from *R. palustris* grown photosynthetically on benzoate with the following results: (a) a washed chromatophore or benzyl-Co A under illuminated, anaerobic conditions; (b) a cell-free extract in the presence of CoA, ATP, NAD^+ and Mg^{2+} ions converted cyclohex-1-enecarboxylate to pimelate in anaerobic or aerobic conditions in the light or dark.

These results provide strong evidence for the presence of a light-dependent membrane bound proton-translocating redox system in these chromatophores; the low potential reductant may be a ferrodoxin, which also plays a part in photosynthetic electron transport. In addition, they confirm the presence of the appropriate beta-oxidation suite of enzymes in these cells responsible for the subsequent series of reactions resulting in ring-cleavage.

This is an exciting approach to the bioconversion of coal. One can take advantage of the capability of phototrophic bacteria for reductive bioconversion of aromatics to carry out coal bioconversions.

MICROBIAL COAL CLEANING

Unlike microbial conversions, the microbial cleaning objectives are much better defined. Removal of sulfur primarily trace metals, chlorine and nitrogen by microorganisms is the focus of attention. Microbial desulfurization, especially, pyrite removal has received a lot of attention, and a number of papers by different research groups have been published on the subject (29,30). *Thiobacillus* is used for pyritic sulfur removal and a host of literature is available on the subject. The question arises whether it is cost-effective to use *Thiobacillus* or other microorganisms for pyritic sulfur removal because it takes weeks and even months for the reaction to go to completion. A more viable option in which Atlantic Research Corp. and Illinois Geological Survey, are working in the use of microorganism to surface modify the pyrite is coal and make it more hydrophilic. This type of conditioning takes only three to four hours and a conventional flotation process can now eliminate almost all of the pyritic sulfur from this microbially pretreated coal. Another approach would be to let loose the microorganism in a coal storage pile and then come back later to have a sulfur-free coal available. The idea is not as far fetched as one thinks. Indeed, in Cuba, such an approach is used for the removal of lignin from cane sugar--called the Cubanine process. Lignin-degrading enzymes from the white rot fungus are put together with the biomass cane sugar material in a large chamber and after a month has elapsed the biomass is taken up, ground and made ready for use. The Cubans have found that this method is cost-effective in removing lignin and saves them a lot of energy which they would, otherwise, have to expend to remove the lignin.

BIOPROCESS ENGINEERING COMPONENT

Finally, one has to recognize that in order for these microbial conversions to reach a commercial scale, bioprocess considerations are warranted. Bioreactor design, problems about nutrient recycle or other process considerations entails the fact that bioreactor engineering will have to become an integral component of any coal processing scheme. Figure 18 illustrates some of the possible bioreactor configurations that can be used.

REFERENCES

1. Science, 222:657-860 (1983b).
2. Science, 219:609-747 (1983a).
3. Demain, A. L. Sci. Am. 214:987 (1981).
4. Demain, A. L., Sci. Am. 243(3) (1981)..
5. Cohen, N. S. and P. D. Gabriele, Appl. Environ. Microbiol., 44:23-27 (1982).
6. Scott, C. D., G. W. Strandberg, and S. N. Lewis, Biotechnol. Prog., 2:131-139 (1986).
7. Wilson, B. W., R. M. Bean, J. A. Franz, B. L. Thomas, M. S. Cohen, H. Aronson, and E. T. Gray, Jr., J. Energy and Fuels, 1:80-84 (1987).
8. Ward, B., Syst. Appl. Microbial., 6:236 (1985).
9. Faison, B. D. and T. A. Kuster, in Proceedings, Eighth Symposium on Biotechnology for Fuels and Chemicals, Scott, C. D., ed., Wiley, New York (19887).
10. Mahler, J. R. and E. H. Cordes, Biological Chemistry, Harper and Row, New York, p. 631-711 (1971).
11. Rogoff, M. H. and I. Wender, J. Bacteriol., 77:783 (1959).
12. Hill, I. D., U. S. Patent No. 3,318,781, May 9, 1967.
13. Colla, C., C. Biaggi, and V. Treccani, Atti Accad. Naz. Lincei Cl. Sci. Fis. Mat. Nat. Rend., 23:66 (1957); Chem. Abstr., 53:2350 (1959).
14. Rogoff, M. H. and I. Wender, J. Bacteriol., 74:108 (1957).
15. Evans, W. C., H. N. Fernley, and E. Griffiths, Biochem. J., 95:819 (1965).
16. Chapman, P. J., G. Meerman, I. C. Gunsalus, R. Srinivasan, and K. L. Rinehart, Jr., J. Amer. Chem. Soc., 88:618 (1966).
17. Charney, W. and H. C. Herzog, Microbial Transformations of Steroids, Academic Press, New York (1967).
18. Fonken, G. S., H. C. Murray, and L. M. Reineke, J. Amer. Chem. Soc., 82:5507 (1960).
19. Singh, K. and S. Rakhit, Biochim. Biophys. Acta., 144:139 (1967).
20. Carlstrom, K., Acta. Chem. Scand., 21:1297 (1967).
21. Kirk, T. K., M. Tien, K. E. Hammel, P. Kersten, and B. Kalyanaraman, Proceedings International Symp. Wood and Pulping Chem., August, p. 243 (1985).
22. Higuchi, T., M. Shimada, T. Umezawa, and S. Kawai, Proceedings International Symp. Wood and Pulping Chem., August, p. 117 (1985).
23. Kirk, T. K., Degradation of Lignin in Microbial Degradation of Organic Compounds, Gibson, D. E., ed., Marcel Dekker, Inc., New York, p. 399 (1986).
24. Dutton, P. L. and W. C. Evans, Biochem. J., 109:5-6 (1968).
25 Tarvin, D. and A. M. Buswell, J. Am. Chem. Soc., 56:1751-1755 (1934).
26. Healy, Jr., J. B. and L. Y. Young, Appl. (1979).
27. Colberg, P. J., "Microbial Degradation of Lignin-Derived Compounds Under Anaerobic Conditions," Ph.D. Thesis, Stanford University (1983).
28. Evans, W. C., Nature, 270:17-22 (1977).
29. Biotechnology for the Mining, Metal-Refining, and Fossil Fuel Processing Industries, H-L. Ehrlich and D. S. Holmes, eds., Biotechnol. Bioeng. Symp., 16(4):183-231 (1986).
30. Proceedings Biological Treatment of Coals Workshop, U.S. Department of Energy, Office of Fossil Energy Idaho Operations Office in Cooperation with Idaho National Engineering Laboratory Bioprocessing Center, Herndon, VA, June 23-25 (1986).

MICROBIAL DESULFURIZATION OF SOME EUROPEAN COALS: PROGRESS REPORT ON A JOINT ITALIAN PROJECT

M. Agus[1], C. Conti[2], C. Dalmastri[2], N. Orsi[2], G. Rossi[3], P. Trois[3] and P. Valenti[2]

1 Italian National Research Council (CNR)
2 Microbiology Institute 'La Sapienza' University, Rome, Italy
3 Mining and Mineral Dressing Department Cagliari University, Cagliari, Italy

1. INTRODUCTION

The continuing fluctuation of the oil market together with the likelihood of a rise in the current relatively low prices, highlight the ever-present problem of alternative energy resources availability. This problem, of worldwide impact, is particularly pressing in those industrialized countries which, like Italy, can rely on only very limited domestic energy resources and, on account of political decisions, must refrain from resorting to nuclear power.

In the strive towards the exploitation of all available domestic energy resources, The Italian state-owned energy supply company, ENI-AGIP, has reopened the Seruci mine in the Sulcis subbituminous coal basin (Island of Sardinia). The mine is expected to reach full production of two million tonnes per year of marketable coal by 1992. The entire production is intended for the electrical power stations operating in Sardinia. Sulcis coal has the characteristics shown in Table 1: its major drawback is its high sulfur content. Current legislation on industrial air pollution in Italy restricts peak concentrations of SO_2 in power station emissions to 657 micrograms per cubic meter in 30 minutes and 263 micrograms per cubic meter over 24 hours. Even more stringent are the limits suggested by the European Economic Community (EEC). These standards all impose severe limitations on the sulfur contents of coals since they virtually equate to maximum permissible sulfur contents of about 0.8%.

On the other hand, the sulfur contents of world coal reserves vary from 0.38 to 10%, and that of mineable reserves from 0.38 to 5.32%, which means that a considerable portion of the coal mined throughout the world cannot be directly used for combustion without some preliminary measures being taken to keep, in one way or another, emissions within the prescribed limits. Table 2 shows the pollution potential, in terms of grams of SO_2 per MJ of typical coals extracted from European and American mines.

Although most coal mined in the EEC is presently extracted from those parts of the respective basins containing low-sulfur coals, (i.e. coals containing less than 1% total sulfur), the economic importance of the possibility of mining high-sulfur coals too has been given full recognition by the EEC. Thus, in 1986, the EEC launched an R & D programme with the objective of assessing the possibilities offered by biohydrometallurgy in microbial coal desulfurization. This programme is now well under way and four countries are participating therein: Holland (Biotechnology Delft), Italy (University of Cagliari), the United Kingdom (Warren Springs Laboratories, Stevenage) and West Germany (Bergbau-Forschung GmbH).

In Italy the programme is also partly supported by the Italian company ENICHEM-ANIC, which, in 1986, signed a research contract with the Mining and Mineral Dressing Department (MMDD) of Cagliari University. Part of this research project has been entrusted to researchers of the Microbiology Institute of the 'La Sapienza' University (MILSU) in Rome, which is thus closely cooperating with the MMDD of Cagliari University.

The present paper is intended as a progress report on the problems encountered and the results achieved by the two above-mentioned Italian universities.

2. SULFUR COMPOUNDS AND THEIR IDENTIFICATION

Coal contains sulfur in four forms: metallic sulfides, with a predominance of iron sulfides ('pyritic sulfur'), atoms covalently bound in the organic sulfur compounds contained in the coal matrix ('organic sulfur'), iron, calcium sulfates and elemental sulfur. Pyritic and organic sulfur are the most common: elemental sulfur does not usually assay more than 0.2% and sulfates more than 0.1%. Moreover, being soluble in water, the sulfates can be readily removed during coal washing. Whilst pyritic sulfur can be very accurately identified with several procedures (reflected light microscopy, ordinary chemical analysis), much less is known about the nature of the organosulfur compounds forming the coal matrix and it is still the object of intensive research and debate. As a matter of fact, there are no reliable, direct and single methods for quantitatively determining the organosulfur compounds in coal and even their qualitative determination is considered by some workers to suffer from too many uncertainties (1). It has been suggested that organic sulfur is present in coal in at least five main forms, which correspond to the functional groups containing aliphatic or aromatic thiols, aliphatic, aromatic or mixed sulfides and/or disulfide heterocyclic compounds containing the thiophenic ring and the gamma-thiopyrone system (2),(3).

Although no evidence exists of the direct determination of these compounds, the well known diagram of Figure 1 has been proposed (4): it represents the molecular structure of a typical bituminous coal where the sulfur atoms bound in the organic molecules are indicated with arrows. According to Meyer (2), the average pyritic sulfur content of the world's coal reserves ranges from 0.09 to 3.97% and the organic sulfur content from 0.29 to 2.04%. In some high-sulfur coals, like those investigated herein, these percentages can be higher with predominance of organic sulfur. Hence, coal depyritization, be it carried out microbially or by other means, can only produce coals complying with environmental specifications when organic sulfur is negligible. Otherwise, the organic sulfur must necessarily be removed.

For the time being organic sulfur removal can only be attempted by chemical processing (5): however, the costs involved are prohibitive and discourage commercial application. These considerations warrant the investigation of the possibilities of microbial organo-sulfur removal.

3. MATERIALS AND METHODS

3.1 The Investigated Coals

The programme entails the investigation of the amenability to microbial desulfurization of four coals: Sulcis coal, from the Sulcis coal basin in southwestern Sardinia, Monopol coal, from the Monopol coal mine in West Germany, Gardanne coal, from Provence in southern France and a Spanish coal from the Teruel mine. At the time of writing the Teruel coal had not yet been delivered to Cagliari's laboratory. Tables 1, 3 and 4 summarize the most salient characteristics of the above-mentioned coals.

3.1.1. Sulcis coal

On the grounds of 'rank' determinations based on the average reflecting power of vitrinite, Sulcis coal can be considered a sub-bituminous coal according to the ASTM (USA) classification or a 'Glanzbraunkohle' according to the DIN (West Germany) classification. If the additional parameter represented by the upper thermal power - determined on pure coal and with its intrinsic moisture, in compliance with the latest EEC guidelines - is considered, then Sulcis coal can be placed among the 'average rank' coals, near to the limit of 'lower rank' coals. Its maceral composition is characterized by an abundance of the 'vitrinite' group, which in the I Seam ranges from 70 to 75%. After the vitrinite group, the maceral group exinite-liptinite is the most represented, with cutinite predominating: in the I Seam, the exinite-liptinite associa-

tion amounts to 12 to 24%. The maceral group inertinite ranges from 2 to 7%. The main associated mineral phases are dolomite, calcite, pyrite, marcassite, quartz, aragonite and clay.

Pyrite, which is present throughout the Sulcis coal, is syngenetic and finely dispersed within the coal matrix (Fig. 2), where it occurs as individual crystals from submicron to micron size, along with less frequent framboids no larger than 40-50 micrometers. This very fine intergrowth makes pyrite removal with classical physical mineral dressing methods impossible. Pyritic sulfur is always accompanied by higher proportions of organic sulfur.

3.1.2 Gardanne coal

The 'rank' and technological determinations indicate that this coal belongs to the class of 'subbituminous' coals (ASTM). The Gardanne coal is predominantly composed of vitrinite (up to 65%) and, to a lesser extent, of inertinite (inertodetrinite, semifusinite, fusinite) and exinite-liptinite (cutinite, resinite, sporinite). It is characterized by abundant occurrence of pyrite and carbonate phases (dolomite and calcite) accompanied by quartz and clay.

Pyrite, basically syngenetic in nature, is finely dispersed within the coal matrix in the form of individual crystals (sometimes submicronic in size) and of framboidal clusters ranging in size from 5 to 40 micrometers (Figure 3).

Organic sulfur is always present in high percentages: investigations with the electron microprobe revealed that vitrinite contains more organic sulfur than other macerals.

3.1.3 Monopol coal

This is a bituminous coal containing, in decreasing order, vitrinite, exinite and inertinite. Vitrinite occurs as bands of variable thickness, alternated with exinitic and inertinitic bands. The exinite group is predominantly composed of sporinite, cutinite and resinite, whereas the major components of inertinite are fusinite and semifusinite.

Pyrite occurs in Monopol coal in both the syngenetic and epigenetic form. The syngenetic pyrite appears as individual framboids ranging in size from a few micrometers up to 40 micrometers, with a predominance of the 20 micrometer size, and less frequently as groups of framboids. Epigenetic pyrite is present in the form of fissure fillings (Fig. 4) and is frequently accompanied by marcassite. The veins of epigenetic pyrite range in thickness from 20 to 300 micrometers, with 100 micrometers prevailing.

Pyrite is also present in cellular cavities of semifusinite and fusinite structures. Of the carbonates, calcite, and to a lesser extent siderite, can be mentioned. Quartz and clay were also detected.

3.2 The Microbial Strains

3.2.1 Pyritic sulfur removal

For pyrite removal a Thiobacillus ferrooxidans active mixed culture was used, isolated from acid drippings of the Fenice Capanne Mine (Tuscany, central Italy) (6) routinely maintained in Cagliari's laboratory in Silvermann and Lundgren 9K medium.

3.2.2 Organosulfur removal

To the best of the authors' knowledge, only one strain of Pseudomonas sp., denoted CB1 strain and listed as ATCC No. 39381 , obtained by chemical mutagenesis of a wild strain, is claimed to be so effective in removing some organosulfur compounds from coal (7), as to encourage its testing with a view to commercial application. Sulfolobus acidocaldarius is also claimed to be capable of removing some organic sulfur from coal, although it does not perform as well (8). The CB1 strain and Pseudomonas putida PAW 340 were therefore also investigated, at least for comparative purposes.

A campaign of microbial strains collection was undertaken with the aim of isolating microorganisms present in a model mining environment. The following procedure was adopted for isolating microorganisms from the Seruci mine: a 20 dm^3 Mariotte carboy, containing the suitable culture medium, was placed on a platform supported by a steel arch of a gallery located at 250 meters below sea level, where the temperature was 35°C. The medium was allowed to spread and percolate over the coal exposed on the gallery wall and was finally collected in another carboy placed on the gallery floor (Fig. 5). Repeated samplings, carried out with complete and minimal media as well as minimal media supplemented with selective agents, led to the isolation of the following strains:

- from complete medium Bacillus sp., Enterobacter, sp. and Micrococcus sp.;
- from minimal medium, and minimal medium supplemented with dibenzothiophene (DBT) as sole carbon source, several Gram-positive and Gram-negative bacteria, with a prevalence of strains belonging to Bacillus and Pseudomonas genera.

The isolated microorganisms were serially subcultured at 30°C and 26.17 $rad.s^{-1}$ in 300 cm^3 flasks containing 50 cm^3 of basal salt

solution M9 (9), supplemented with 5% powdered coal or a minimal medium supplemented with DBT).

3.2.3 Leaching techniques

All the sulfur removal tests were carried out in 300 cm^3 Erlenmeyer flasks containing either organosulfur compounds presumably present in the investigated coals (e.g. DBT) or coal along with the suitable culture medium. They were incubated on giratory shakers operated at the speeds and temperatures specified in the descriptions of the individual runs.

3.2.4 Reagents

All reagents used in the tests were analytical grade. The culture media were always made up with distilled water and, for laboratory testing, were always sterilized.

3.2.5 Analytical methods

Total sulfur was determined by means of the SC132 Instrument manufactured by LECO (St. Joseph, MI, USA). Pyritic sulfur was determined by gravimetric analysis, whereas iron and other elements were analysed by complexometric titration. Organic sulfur was determined as the difference between total and pyritic plus sulfate sulfur. The analyses of the residual DBT after microbial attack were carried out with an original method developed by the Industrial Chemistry Department of Bologna University (10).

Hydrogen ion concentrations were determined by means of potentiometric pH-meters of various makes (Beckmann, Orion and Hanna) and redox potential measured with a Mod. HI 8418 Hanna electronic potentiometer with Pt combined electrode.

3.2.6 Microbial growth measurements

Cell concentrations were obtained by the dilution plating method and by counting colony-forming units (CFU) per cm^3.

4. RESULTS

4.1 Pyritic sulfur removal

Tests were carried out on Sulcis, Monopol and Gardanne coals, the coal from Teruel (Spain) being unavailable.

4.1.1 Sulcis coal

All tests were performed in 300 cm^3 Erlenmeyer flasks with baffled bottom, containing suspensions of coal powder in 9K medium. The shaker speed was adjusted to 26.3 $rad.s^{-1}$ and temperature maintained at 28±1°C. CO_2 was added to the shaker atmosphere. Owing to the very fine intergrowth of pyrite within the coal matrix and in spite of the relatively high porosity of the coal, a satisfactory access of the solutions and/or microbes to the pyrite crystals can only be achieved provided that most of them are at least partially exposed. Hence grinding to -40 micrometers is required to achieve 90% pyritic sulfur removal in a leaching time ranging from 9 to 12 days. These pyrite removals were achieved for solids-to-liquid ratios (weight of coal divided by weight of liquid medium) ranging from 1:100 to 16:100. Poorer results were obtained for solids-to-liquid ratios higher than 20:100. The initial pH of the medium was adjusted to between 2.20 and 2.25, and pulp acidity had to be stabilized prior to inoculation with about 45 Kg of concentrated sulfuric acid per Mg of coal. The final pH of the leach liquor was usually 1.8. The redox potential of the medium steadily increased from about 370 mV to more than 650 mV.

4.1.2 Monopol coal

Several runs were carried out in the same conditions as those adopted for Sulcis coal, but the results were quite deceptive. Some runs lasted up to 25 days, but no appreciable pyrite removal was observed. The pH of the leach liquor only dropped very slightly (from 2.20 to 2.00) and the redox potential of the solution never rose above 540 mV. Viability tests showed however that microorganisms remained viable well after conclusion of the tests.

Factorial variance analyses are presently under way, with potassium, phosphorus and ammonium sulfate concentrations of the medium as variables.

4.1.3 Gardanne coal

A first series of tests was carried out in the same experimental conditions as those adopted for Sulcis coal. Pyrite removal appears to be of the same order of magnitude, but always lower, as that achieved with Sulcis coal: the solubilization rate is constantly about 20% slower; Preliminary tests carried out on this coal varying phosphorus, potassium and ammonium sulfate concentrations in the medium, seem to indicate that a suitable composition of the medium might considerably improve the effectiveness of microbial attack.

4.2 Organic Sulfur Removal

All the isolated strains were analysed in order to assess their ability to grow in basal salt solution supplemented with powdered coal (5% w/v) or a selective agent (1 per thousand DBT w/v). The data obtained show that all strains can grow on basal salt solution supplemented with coal. On the other hand, only the strains preselected in the mine using basal salt solution plus DBT exhibited significant growth when cultivated in the presence of this selective agent.

As for coal-degrading activity, removal of between 10 and 18% organic sulfur was observed. Under these experimental conditions, no degrading activity was detected for the CB1 strain.

It should be noted that for sulfur contents of the order of magnitude of those of the examined coals (from 1.5 to 6.0%), a certain unpredictable variability was observed in the data provided by the described analytical techniques. This fact stresses the need for analytical methods of adequate sensitivity to detect fraction percent variations in sulfur contents, presently lacking.

The nutritional characteristics of the above-mentioned microorganisms are shown in Table 5.

5. REMARKS AND CONCLUSIONS

The occurrence in several EEC countries of sizeable reserves of high-sulfur coals containing large proportions of organic sulfur as well as the economic potential of the high-sulfur coal zones exhibiting similar characteristics in several coal basins, provide an impetus for needed research aimed at removing both types of sulfur.

Microbial removal of pyritic sulfur is, in principle, a well-defined process, and the effectiveness of Thiobacillus ferrooxidans in dissolving the accessible pyrite from the coal matrix is well documented (11),(12),(13). However, the present research has emphasized the major role played by the chemical composition of the run-of-mine coal. The presence of phosphorus, potassium and nitrogen compounds may, in effect, alter the composition of the nutrient medium to such an extent as to diminish the effectiveness of microbial action, probably due to substrate inhibition. It is therefore advisable to always design the composition of the basal salts medium according to the type of processed coal.

Exposure - not necessarily liberation - of the pyrite component is an essential condition for its microbial removal. Hence, petro-

graphic and porosity analyses of the coal should always provide the information required to avoid excess of expensive grinding. As shown by the diagrammatic sketch of Fig. 6, porosity effectively contributes to the accessibility of solutions and/or microorganisms to pyrite crystals not exposed on the coal grain surface.

Information on microbial organosulfur removal is very scanty. Among the strains claimed in the literature (7),(8) to be effective to a certain extent are Sulfolobus acidocaldarius and Pseudomonas strain CB1 obtained by chemically induced mutation, although little has been published on the organosulfur removal ability from coal . The tests carried out to date in the present investigation do not seem to support the effectiveness claimed for strain CB1 in removing organic sulfur. On the other hand, the organic-sulfur degradation ability exhibited by the strains isolated from the mine environment, appears encouraging.

One hundred percent sulfur removal cannot be achieved inasmuch as the sulfur atoms are dispersed throughout the coal matrix and therefore only those exposed on the coal surface (grain boundaries or pore surfaces) can be removed. The larger the surface-to-volume ratio, the more the sulfur is amenable to microbial attack. However, the surface-to-volume ratio cannot be increased beyond a certain value, owing to the high grinding costs and to the depreciation of coal when its grain size is smaller than market specifications. For the time being, the finest coal particles find commercial application in the coal-water mixtures technique, with an average grain size of 40 micrometers.

It is therefore imperative to exploit other means for increasing the exposed surface. One possibility is preliminary depyritization and dissolution of the carbonate phases present in coal (Fig. 7): the surfaces of all the cavities left by pyrite and carbonates removal contribute to coal matrix, and hence organic sulfur, exposure. On these grounds, a tentative flowsheet for microbial coal desulfurization is proposed in Fig. 8. This flowsheet should be considered, at the present state of progress of the research, as a guideline for the planning of laboratory and pilot plant testing.

It should finally be pointed out that the present inability of analytical chemistry to provide reliable analytical methods for quantitatively determining the organosulfur compounds forming the coal matrix contributed to the difficulties encountered in evaluating the organic sulfur removal by the above-mentioned microorganisms.

ACKNOWLEDGEMENTS

This work was financed partly by the European Economic Comunity (Contract No. EN3F-0061-I) and by ENICHEM (Milan, Italy) and partly by contributions from the Italian Ministry of Public Education and the Italian National Research Council (CNR), Centro Studi Geominerari e Mineralurgici at Cagliari University. The authors wish to express their appreciation for the very useful cooperation of the management and technical staff of Carbosulcis S.p.A., Houillères de Bassin du Centre et du Midi, Houillères de Provence, France, and of Bergbau-Forschung GmbH in providing the coal samples used in the present research. The assistance of Mr. Franco Chessa is also gratefully acknowledged.

REFERENCES

1) BOUDOU, J.P., In verbis, 1988.
2) MEYERS, R.A., Coal Desulfurization, Marcel Dekker, Inc., New York, 1977.
3) CHENG TSAI, S., Sulfur in coal and reactions of sulfur compounds related to coal desulfurization, in Fundamentals of Coal Beneficiation and Utilization, Elsevier, Amsterdam, 1982, 222 (Chap. 5).
4) WHEELOCK, T.D., An overview of coal cleaning technology, in Proceedings of the Coal Water Fuel Technology Workshop, U.S. Dept. Energy Tech. Ctr., Rept. No. BNL 51427, 1981, 82-101.
5) MORRISON, G.F., Chemical desulphurization of coal, Report No. ICTIS/TR15, June 1981, IEA Coal Research, London.
6) ROSSI, G., La lisciviazione microbica dei minerali. I. L'azione dei microorganisms reperiti in acque acide di miniere italiane sulla pirite, Res. Ass. Min. Sarda, Iglesias (Italy), 76, 5-23, 1971.
7) ISBISTER, J.D. and KOBYLINSKY, E.A., Microbial desulfurization of coal, in Processing and Utilization of High Sulfur Coals, ATTIA, Y.A., Ed., Elsevier, Amsterdam, 1985, 627-641.
8) KARGI, F. and ROBINSON, J.M., Removal of organic sulphur from bituminous coal. Use of the thermophilic organism Sulfolobus acidocaldarius, Fuel, 65, 397-399, 1986.
9) MANIATIS, T., FRITSCH, E.S. and SAMBROOK, J., Molecular cloning, Cold Spring Harbor Laboratory, Cold Spring Harbor, New York, 1983.
10) PIFFERI, P.G., In verbis, 1988.
11) DETZ, C.M. and BARVINCHAK, G., Microbial desulfurization of coal, Min. Cong. J., 65, 75-82 and 86, 1979.
12) HOFFMANN, M.R., FAUST, B.C., PANDA, F.A., KOO, H.H. and TSUCHIYA, H.M., Kinetics of the removal of iron pyrite from coal by microbial catalysis, Appl. Environ.Microbiol., 42, 259-271, 1981.

13) HUBER, T.F., KOSSEN, N.W.F., BOS, P. and KUENEN, J.G., Modelling, design and scale-up of a reactor for microbial desulphurization of coal, in Progress in Biohydrometallurgy, ROSSI, G. and TORMA, A.E., Eds., Ass. Min. Sarda, Iglesias (Italy), 1983, 279-289.

Table 1 - Data of a typical Sulcis coal

Analysis of macerals %		Chemico-technological analysis		Reflective power of vitrinite %
Vitrinite	76.4	Ash	7.7 %	0.49
Exinite	15.8	Sulfur, total	5.9 %	
Inertinite	3.8	Pyritic sulfur	1.06%	
		Sulfate sulfur	0.8 %	
		Iron, total	1.4	
		CaO	20.5 % of ash	
		K_2O	n.d.	
		MgO	11.2 % of ash	
		P_2O_5	0.8 % of ash	
		Heating power (dry basis)	20.485 $kJ.kg^{-1}$	
		Porosity	31.46	

n.d. = not detected

Table 2 - Examples of average sulfur, ash and energy content of several coal samples

Country/State	County	Coal Seam	kJ/kg	% Ash	Total S %	g SO_2 per MJ
France		Gardanne	28,360	10.84	5.67	4.0
Italy	Sulcis	I Seam	27,900	10.81	6.46	4.6
Spain		Berga	15,900	41.0	4.75	6.0
		Utrillas	21,850	18.6	7.92	7.2
USA						
-Ohio	Belmont	Pittsburgh	28,600	15.1	6.19	4.3
	Coshocton	Middle Kittanning	28,360	14.1	6.39	4.5
	Muskingum	Lower Kittanning	28,800	11.5	4.85	3.4
-Pennsylvania	Indiana	Lower Kittanning	31,380	12.9	4.68	3.0
-Utah	Emery	Blind Canyon	31,850	5.6	0.58	0.3
-Virginia	Wise	Taggart	33,940	2.9	0.79	0.5
-W.Virginia	Preston	Upper Freeport	28,800	18.5	2.44	1.7
	Nicholas	Middle Kittanning	27,900	20.2	1.06	0.8
-Wyoming	Sweetwater	Rock Spring No.11	29,060	6.5	0.97	0.7

Table 3 - Chemico-technological characteristics of Monopol coal

Component	Weight %		Porosity %
Ash	28.5		4.5
Sulfur, total	1.97		
Pyritic sulfur	1.33		
Sulfate sulfur	0.21		
Iron, total	2.6		
Carbonates	0.4	% of ash	
$-K_2O$	4.4	% of ash	
$-Na_2O$	1.1	% of ash	
-MgO	1.9	% of ash	

Table 4 - Chemico-technological characteristics of Gardanne coal

Component	Weight %		Porosity %
Ash	7.5		29.09
Sulfur, total	5.1		
Pyritic sulfur	1.06		
Sulfate sulfur	0.21		
Iron, total	0.7		
Cao	20.0	% of ash	
K_2O	0.3	% of ash	
MgO	3.4	% of ash	
P_2O_5	2.3	% of ash	

Table 5 - Nutritional characteristics of microorganisms isolated in Seruci coal mine

Colony	Isolation Medium	Glucose 2%	M9 supplemented with NaBenzoate 1.5%	NaBenzoate 1.5%+DBT 1%	DBT 1%
1N	M9+glucose 2%	+	+	+	+
2P	M9+NaBenz. 1.5%	+	+	+	+
1Q	M9+NaBenz.+DBT	+	+	+	+
1R	M9+DBT 1%	+	+	+	+
1H	McConkey	+	+	+	+
1A	LB	-	-	+	-
1B	LB	+	+	+	-
1S	MMA+coal 5%	+	+	+	-
1L	M9+glucose 2%	+	-	+	-
1M	M9+glucose 2%	+/-	-	-	+
2A	LB	+	-	-	-

1 = strains isolated in mine by means of M9+DBT
2 = strains isolated in mine by means of M9

N.B. The strains capable of growing only in the presence of glucose as carbon source are not reported, except 2A, which has been used as control.

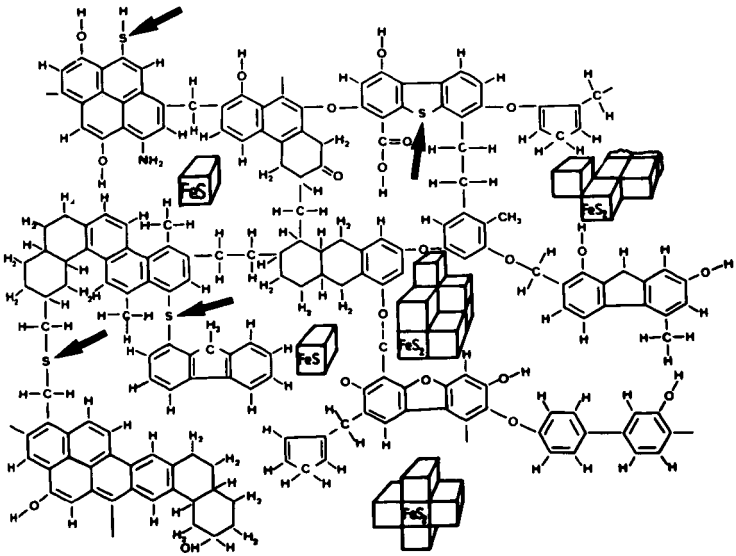

Figure 1 - Molecular structure of a typical bituminous coal after Wendell Wiser. The sulfur atoms bound in organic molecules are indicated by arrows.(Modified from Wheelock ( )).

Figure 2 - Pyrite in Sulcis coal: fine dispersions; refl.light, oil immersion.

Figure 3 - Pyrite in Gardanne coal: framboids; refl. light, oil immersion.

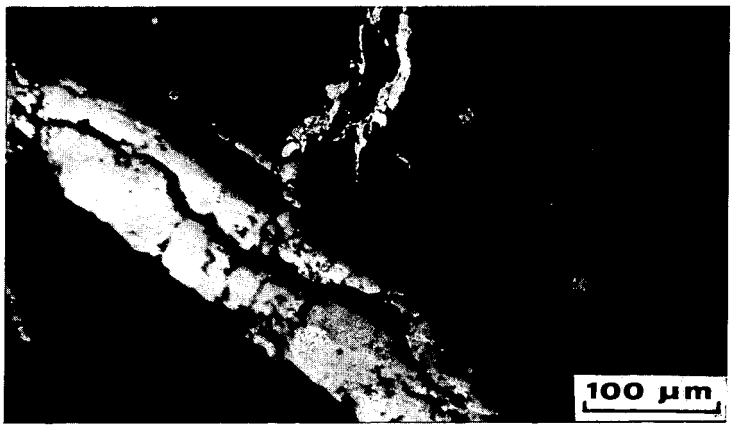

Figure 4 - Pyrite in Monopol coal: epigenetic veins in cleats; refl.light, oil immersion.

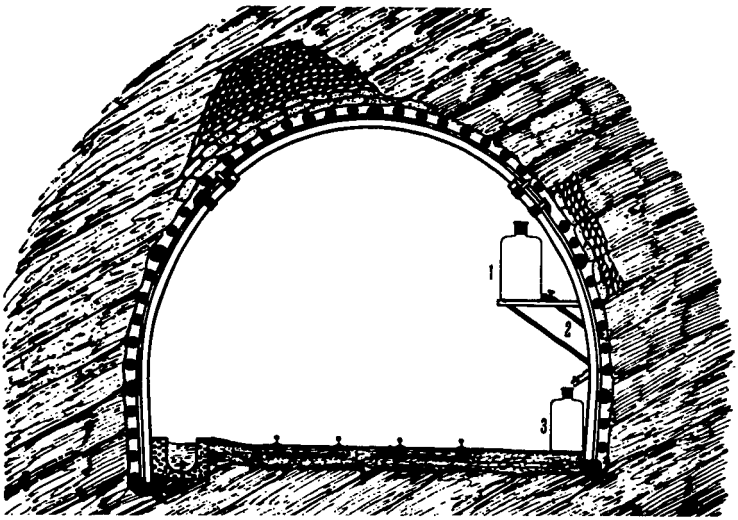

Figure 5 - Set-up for collecting microbes in the Seruci mine.
1 = head tank; 2 = pipe; 3 = medium collecting carboy.

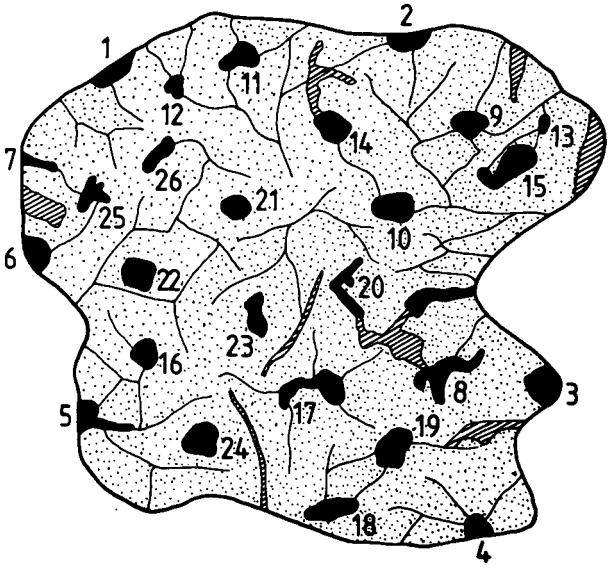

Figure 6 - Two-dimensional model of coal particle. Black grains are pyrite; dashed grains are carbonates; white matrix is coal; lines are pores or cracks.

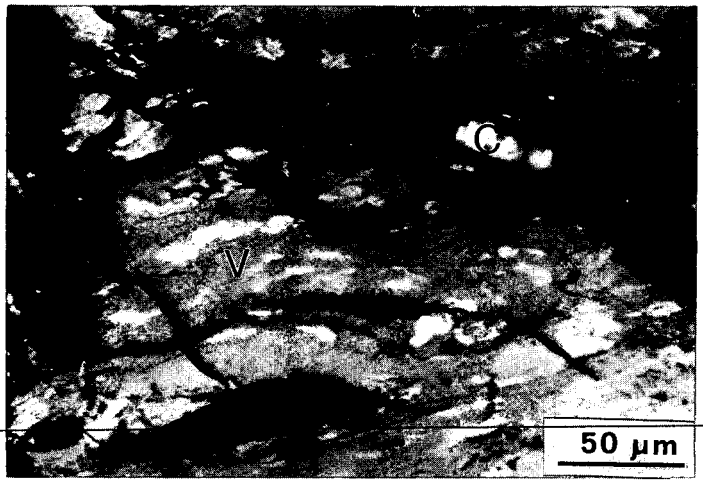

Figure 7 - Sulcis coal: carbonates (C) in fissures in vitrinite (V); refl.light, oil immersion.

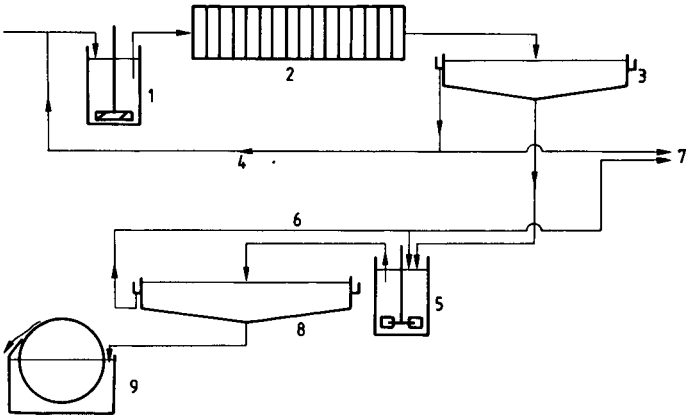

Figure 8 - Microbial coal desulfurization flowsheet. 1: backmix reactor; 2: plug flow reactor for pyrite removal; 3: thickener; 4: medium recycle; 5: backmix reactor for organic sulfur removal; 6: supernatant to waste; 7: tailings disposal; 8: thickener; 9: filter.

BIODEGRADATION OF COAL-RELATED MODEL COMPOUNDS

J. A. Campbell, D. L. Stewart, M. McCulloch, R. B. Lucke and R. M. Bean

Pacific Northwest Laboratory
P. O. Box 999
Richland, WA. 99352

INTRODUCTION

Since 1982 when Cohen and Gabriele (1) first reported that fungi could grow directly on and metabolize naturally occuring coal, biological conversion of low-rank coals by bacteria, fungi, or preparations of the enzymes they produce has been the subject of intensive research. Because these processes occur at ambient temperatures and pressures, they represent a potential savings in the processing of certain coals and lignites. Current technology for coal conversion requires both high temperatures and pressures which may result in the production of components that are more toxic than the original starting material.

Cohen and Gabriele (1) reported that fungi could metabolize leonardite, a naturally oxidized form of lignite coal. Wilson et al. (2) have shown that the leonardite-biodegraded product from *C. versicolor*, a white-rot fungus, was water soluble and contained no detectable polycyclic aromatic hydrocarbons (PAH) having three to six rings. In addition, the bioconverted material was inactive in the microbial histidine reversion assay for mutagenic activity. Linehan et al. (3) determined by gel permeation chromatography that the average molecular weight of the biodegraded product was 1800 daltons.

The details of the specific reactions of lignin biodegradation, and the biochemistry involved, have been primarily based on the use of low molecular weight compounds representing specific substructures rather than the complex, polymeric lignin material. As an example, Gold et al. (4) utilized ß-aryl ether model compounds to examine oxidation by lignin peroxidase from *P. chrysosporium*. We have studied the reactions of model compounds having coal-related functionalities (ester linkages, ether linkages, PAH) with the intact organism, cell-free filtrate, and cell-free enzyme of *C. versicolor* to

better understand the process of biosolubilization. Many of the degradation products have been identified by gas chromatography/mass spectrometry (GC/MS).

EXPERIMENTAL

Preparation of the Enzyme (5). The fungus was grown in a Chemap CF-20 fermentor at 25° C, and was supplied with 4 L of filtered air per minute at atmospheric pressure to 15 L of growth medium. The growth medium used was that published by Fahraeus and Reinhammar (6). A two-stage Rushton turbine (6 blade) agitator system was used at a speed of 400 rpm. The inoculum used for the fermentation was three 50 mL cultures of *C. versicolor* grown on Sabouraud-maltose broth (1) for 7 to 10 days at 25° C with no agitation. The fungi grown under these conditions form a mycelial mat. The mats were then transferred to a stoppered vessel containing 250 mL of distilled water and 50 mL of 3-mm glass beads. This vessel was shaken vigorously and the mycelial fragments were transferred to the fermentor. After three days growth in the fermentor, 0.3 mL of 2,5-xylidine (Aldrich Chemical Co., Milwaukee, Wi) was added to increase levels of extracellular laccase (5).

The extracellular fluid formed during the growth of *C. versicolor* was separated from the cell mass by filtration through several layers of cheesecloth. This fluid was termed the cell-free filtrate. The resulting fluid was then filtered through an ultrafiltration membrane with a molecular weight cutoff of 100,000 (Amicon H5P100-43). The higher molecular weight material in aqueous fluid was concentrated using an ultrafiltration membrane with a molecular weight cutoff of 10,000 (Amicon H5P10-43). The remaining fluid was further washed (diafiltered) with three 300-mL portions of water while being continually passed through the H5P10-43 membrane to maintain a constant volume of 1 L. The concentration and diafiltration steps caused precipitate formation which was removed by either filtration or centrifugation. The concentrated, extracellular fluid was then chromatographed on a 2 cm X 30 cm DEAE-cellulose (Amicon cellufine DEAE-AM) column which had been previously equilibrated to 0.01 M sodium phosphate, pH 7.0 buffer. This final fluid was termed the cell-free enzyme.

Model Compound Preparation. All of the model compounds were prepared in the same manner. Approximately 10 mg of each was dissolved in 10 mL of methanol. Suitable volumes of this stock

solution were added to the incubation system to make the desired concentration in water.

C. versicolor was cultured on Kirk's minimal medium (10 mL) for ten days in 125-mL Erlenmeyer flasks. One hundred microliters of benzylbenzoate and methoxybenzophenone were added to the culture. Controls consisted of (a) cultures with the same volume of methanol added as with the model compounds and (b) benzyl benzoate and methoxybenzophenone were added to the sterile minimal medium. Hyphal growth of fungal cultures was evident following addition of methanol indicating that the volumes of methanol added were not inhibitory. The model compounds and intact organism were incubated for 1 week. The cultures were then filtered through 0.2 μm filters and extracted with three equal volumes of chloroform. The extracts were combined, concentrated to 1 mL, and analyzed by gas chromatography/flame ionization detection (GC/FID) and GC/MS.

Dibenzothiophene, indole, and bibenzyl were incubated with *C. versicolor* for three weeks. The samples were extracted and concentrated in the same manner as discussed above. Controls, as discussed previously, were also obtained and analyzed.

Benzylbenzoate, bibenzyl, phenylbenzoate, methoxybenzopheneone, and benzyl ether were added (100 μL) to a mixture of 1 mL of cell-free filtrate and 1 mL of buffer solution (pH 5.2). After one day, the solutions were extracted with three equal volumes of chloroform. The extracts were combined and concentrated to 1 mL for subsequent GC/FID and GC/MS analysis. Controls were made with the model compounds and the buffer solution. The controls were extracted, concentrated, and analyzed in the same manner. Anthracene was incubated with the cell-free filtrate for three days. The solution was then extracted, concentrated, and analyzed by GC/FID and GC/MS.

Benzylbenzoate and methoxybenzophenone were introduced (100 μL) to the cell-free enzyme and a buffer solution at pH 5.2. After equilibration of the enzyme and buffer for one day, the solution was extracted, concentrated, and analyzed in the same manner as discussed previously.

Extraction efficiencies were determined by GC analysis of a solution of the model compound in the medium that did not contain

enzyme. The peak areas were then compared with the standard to determine the efficiency of extraction and possible reaction of the model compound with the medium.

Molecular Weight Separation of Cell-Free Filtrate. A culture filtrate was passed through ultrafiltration membranes with molecular weight cutoffs of 10,000, 5000, 1000 , and 500 using an Amicon ultrafiltration apparatus.

Analytical Instrumentation. A HP 5880 gas chromatograph with a flame ionization detector was used to determine the amount of degradation for each model compound . The GC was equipped with a DB-5 30m column and appropriate flow rates were utilized as recommended by the manufacturer. The temperature program used was as follows: 50° C for 1 minute, 50-250° C at 8°/min, and 250° C for 10 minutes. The temperature of the injection port was 250° C and the temperature of the detector was 275° C. A HP 5985 GC/MS/DS was used in the electron impact mode at 70 eV to identify specific degradation products. The same type of column and temperature program were used. The temperature of the source was 200° C, the interface temperature was 275° C, and the electron multiplier voltage was 2500 eV.

RESULTS

Intact Organism. The gas chromatograms obtained from the degradation of benzylbenzoate and methoxybenzophenone by *C. versicolor* are illustrated in Figure 1. Figure 1a is a chromatogram of a 100 ppm standard of benzylbenzoate and 1b is a chromatogram after degradation by the intact organism. Figure 1c is a chromatogram of a 100 ppm standard of methoxybenzophenone and 1d is after degradation. These results clearly indicate that both compounds were degraded by the total organism. The data obtained from the degradation of model compounds by the intact organism is summarized in Table 1.

The extracts were analyzed by GC/MS. For benzylbenzoate, the primary degradation products included benzyl alcohol and benzoic acid.

Cell-Free Filtrate. The results for the degradation of benzylbenzoate, methoxybenzophenone, phenylbenzoate, and benzyl ether by the cell-free filtrate of *C. versicolor* are summarized in Table 1. Phenyl

benzoate was degraded the most; methoxybenzophenone was degraded only slightly. This may reflect the difference in reactivity of the two compounds was well as the selectivity of the enzymes.

Analysis of the degradation of anthracene by the cell-free filtrate indicated the presence of 9.10-anthracenedione (anthraquinone) as a degradation product in about 10% yield. Since anthracene can be oxidized to anthraquinone by a number of non-microbial mechanisms, it is important to note that the controls showed no indication of any quinones or any other degradation products.

Cell-Free Enzyme. For benzylbenzoate, the amount of degradation after one day was approximately 50% but methoxybenzophenone was degraded very little. It should be noted that 85-90% of the model compounds were recovered by extraction from the buffer solution, thereby eliminating reaction with the buffer as a possibility for model compound degradation. The results are summarized in Table 1 and are corrected for extraction efficiencies.

Molecular Weight Separation of Cell-Free Filtrate. The molecular weight separations indicated no reaction with the model compounds with the <10,000 MW fraction while the >10,000 MW fraction completely degraded the model compounds. It is interesting to note that the <10,000 MW fraction is primarily responsible for the biosolubilization of coal.

DISCUSSION

The results obtained from degradation studies of oxygen-containing compounds by *C. versicolor* and its extracts, shown in Table 1, indicate that the two compounds tested with the intact fungal organism were completely degraded. Complete degradation refers to no recovery of model compound. We can probably assume that the other two would also be totally degraded, since we have not yet found a simple compound that will survive long-term exposure to the intact fungus. The ease of degradation with the cell-free filtrate appears to be in the order: phenylbenzoate > benzylbenzoate > benzyl ether > methoxybenzophenone. Esters and ethers that are activated by aromatic rings appear to be susceptible to the fungal extract; however, aromatic ketones are not affected by the extract. From the limited results we have obtained from the isolated enzyme, it appears that the activity may parallel the cell-free filtrate. When

the cell-free extract was tested with the model compounds indole, dibenzothiophene, and bibenzyl, no degradation with the enzyme was noted; however, exposure of these compounds to the intact organism resulted in complete degradation.

Our results with anthracene indicate that its degradation by *C. versicolor* may occur through a radical cation mechanism similar to that proposed for trichlorophenol by *P. chrysosporium* (7). Related research has shown that there is a relationship between the ionization potential of the polycyclic aromatic hydrocarbon and the amount of degradation observed (8). Horseradish peroxidase has been shown to degrade polycyclic aromatic hydrocarbons to quinones, but only in the presence of hydrogen peroxide (9). It is of interest to note that our cell-free filtrate tests positive for peroxidase, although no peroxide is added to any of our biodegradation experiments.

The results of the molecular weight separations of the cell-free filtrate by ultrafiltration indicate the possibility of at least two mechanisms taking place during the biosolubilization process, one of which may be hydrolysis. The >10,000 MW fraction has been very reactive with the model compounds we have tried. The <10,000 MW fraction, where most of the biosolubilization occurs, has been found to be fairly unreactive toward most of the model compounds. Some preliminary results indicate the p-methoxyphenol may be a good substrate for this fraction.

Other preliminary results of further molecular weight separations indicate that the fraction of cell-free filtrate responsible for the majority of the biosolubilization activity is between 500 and 1000 MW. We are presently trying to characterize this fraction to determine the source of biosolubilizing activity.

REFERENCES

(1) Cohen, M. J.; Gabriele, P. D. Appl. Environ. Microbiol. (1982), 44, 23-27.

(2) Wilson, B. W.; Bean, R. M.; Franz, J. A.; Thomas, B. L.; Cohen, M. S.; Aronson, H.; Gray, E. T. Jr. Energy and Fuels, (1987), 1, 80-84.

(3) Linehan, J. C.; Campbell, J. A.; Franz, J. A.; Bean, R. M. Submitted to Energy and Fuels.

(4) Miki, K.; Renganathan, V.; Gold, M. H. Biochemistry, (1986), 25, 4790-4796.

(5) Pyne, J. W.; Stewart, D. L.; Fredrickson, J. K.; Wilson, B. W. Appl. Environ. Microbiol., (1987), 53, 2844-2848.

(6) Fahraeus, G.; Reinhammar, B.; Acta. Chem. Scand., (1967), 21, 2367-2378.

(7) Zurer, P. S. Chem. and Engineering News, (1987), 65, 17-23.

(8) Hammel, K. E.; Kalyanaraman, B.; Kirk, T. K. In: American Chemical Society, Division of Environmental Chemistry Preprints, (1987), 23, 624-626.

(9) Cavalieri, E.; Rogan, E. Environ. Health Perspect., (1985), 64, 69-75.

ACKNOWLEDGMENT

This work was supported by the Electric Power Research Institute, Palo Alto, Ca., and by the U. S. Department of Energy, Office of Fossil Energy, under Contract DE-AC06-76RLO 1830.

Table 1. Percent Model Compound Degradation by *Coriolus Versicolor* and its Cell-Free Isolates

Compound	Total Organism	Cell-Free Filtrate	Cell-Free Enzyme
benzylbenzoate	100 (a)(b)	56	55
methoxybenzophenone	100 (b)	1	2
dibenzothiophene	100 (c)		
phenylbenzoate		100	
indole	100 (c)		
bibenzyl	100 (c)		
benzyl ether		45	

(a) 100% = no model compound detected after incubation
(b) incubated one week with total organism
(c) incubated three weeks with total organism

Figure 1. Gas chromatograms of (a) benzylbenzoate, (b) after degradation, (c) methoxybenzophenone, and (d) after degradation by *C. versicolor*.

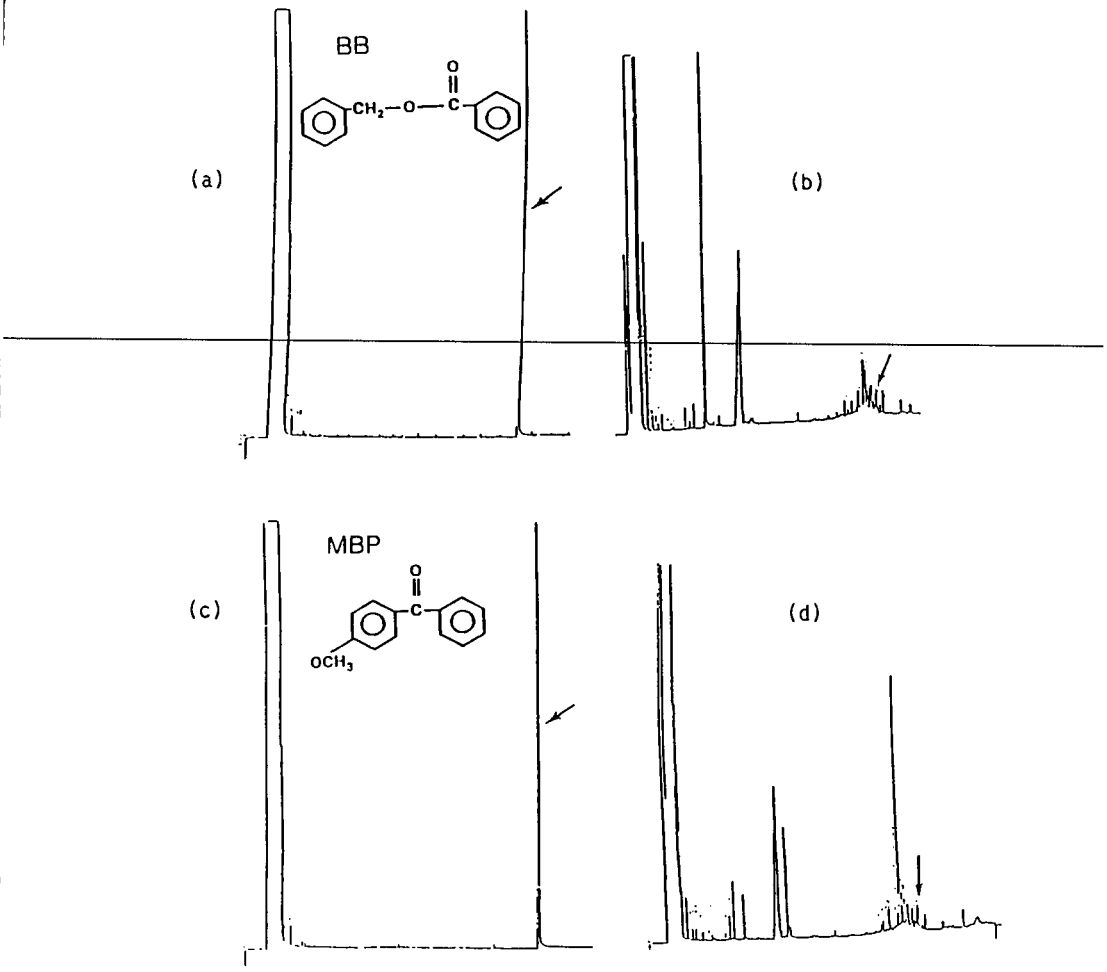

SERIAL BIOLOGICAL CONVERSION OF COAL INTO LIQUID FUELS

by

R. Q. Liu
N. L. Johnson
G. C. Magruder
M. D. Ackerson
J. L. Vega
E. C. Clausen
J. L. Gaddy

ABSTRACT

Recently, several microorganisms have been shown to be capable of directly solubilizing low rank coals. This bioextract has a high molelcular weight and is water soluble, but is not useful as a liquid fuel. This paper presents the results of studies to biologically convert the solubilized coal into more useful compounds. Preliminary experiments have been conducted to isolate cultures for the serial biological conversion of coal into alcohols. Coal particles have been solubilized employing an isolate from the surface of Arkansas lignite. Natural inocula, such as sheep rumen and sewage sludge, are then employed in devloping cultures for converting the bioextract into alcohols. This paper presents preliminary results of experiments in coal solubilization and bioextract conversion.

INTRODUCTION

Microbial solubilization of coals and lignites is being developed as an alternative method of liquid fuels production. The biological approach under study offers the potential of significant cost-savings by converting solid coal to a liquid product, with minimal loss in total energy content, at near ambient conditions of temperature and pressure. The phenomenon of coal utilization and liquefaction by fungal and bacterial species was first reported in the early 1980's (1,2). A number of strains of fungi and filamentous bacteria are now known to interact with low-rank coals, via extracellular processes, to yield a darkened medium when grown in submerged culture (3,4), or dark droplets of liquid on the coal's surface when grown on agar surface culture (1,3,5).

The coal liquid produced by bioliquefaction is a mixture of water soluble, polar organic compounds with relatively high molecular weights. Ultrafiltration and gel permeation chromatography have shown that the molecular weight is in the range of 30,000 to 300,000 (3). The chemical

structure is extremely aromatic, with a large number of hydroxyl groups. Because of the low relative volatility, analysis to quantify the product by mass spectrophometry or gas chromatography has been difficult.

While this technology has great potential, there are a number of serious problems to be solved. In the absence of water, or suitable solvent, the product is a solid. Although the solubilized product has a reasonably high energy content and may be useful as a combustion fuel, it is not suitable as a transportation fuel. Also, most of the organisms require expensive sugars and media for growth over a period of about two weeks. Cheap media and fast growing organisms will be required for commercial application. Another serious economic problem relates to the requirement for pretreatment to achieve high yields. Highly oxidized lignites, such as leonardite, can be converted almost entirely. Higher rank coals must be chemically oxidized before significant liquefaction occurs in a reasonable time (6,7). Chemical treatment is likely to be cost prohibitive.

Research at the University of Arkansas has led to the isolation of a bacterium, as yet unidentified, that is fast growing in cheap mineral salts media and that converts coal into liquid and floculate in a few hours in submerged culture. High rank coals are converted without pretreatment. This rod-shaped bacterium is not a Streptomyces and is likely a previously unknown strain with coal or lignin activity. Further study is required to develop and quantify coal conversion with this organism.

It is highly unlikely that any single organism will be able to completely liquefy coal to low molecular weight fuels. However, it is likely that organisms can be utilized to upgrade the initial microbial products to useful fuels. Such a second-stage conversion should probably be anaerobic to avoid further oxidation of the product. The evaluation of serial biological conversion of coal to liquid fuels is currently underway. This paper presents a brief summary of progress to biologically produce low molecular weight liquid fuels from coal.

MATERIALS AND METHODS

Substrate

The solubilized lignite used as the substrate for the anaerobic bacteria was obtained from submerged culture experiments. An organism isolated from an Arkansas lignite sample was used to solubilize the coal.

The solubilization was carried out in a 1.5 liter Biostat M stirred-tank fermentation system from B Braun Instruments. The fermenter was equipped with pH and temperature control as well as a dissolved oxygen probe. The temperature was maintained at 28°C and the agitation rate was 150 rpm.

The lignite surface culture was allowed to grow for 3 days on a media consisting of 0.5 percent glucose and 0.5 percent peptone. After 3 days, 9g of 8-20 mesh Arkansas lignite were added. Within 24 hours, 35 percent of the lignite was solubilized. The solubilized lignite was collected by filtration and precipitated by adjusting the pH of the solution to 1.0 with acid. The

precipitate was washed and dried and then redissolved in distilled water by adjusting the pH to approximately 6.5. Portions of this solution were then used as substrate in the attempts to produce alcohol fuels.

Media

The original culture media contained yeast extract (Difco), 0.1g; B-vitamins (Wolfe's), 1 ml; KH_2PO_4, 0.6 mg; $(NH_4)_2SO_4$, 0.6 mg; NaCl, 1.2 mg; $MgCl_2 \cdot 6H_2O$, 0.4 mg; $MgSO_4 \cdot 7H_2O$, 0.3 mg; lignite, 0.03 g, added to 100 ml of deionized water, and adjusted to pH 7 with NaOH.

Media for transfers from the original cultures contained yeast extract (Difco), 2.0 g; α-D glucose (Aldrich), 5.0 g; B-vitamins (Wolfe's), 10.0 ml; $ZnSO_4 \cdot 7H_2O$, 0.5 mg; $MnCl_2 \cdot 4H_2O$, 0.15 mg; H_3PO_3, 1.5 mg; $CoCl_2 \cdot 6H_2O$, 1.0 mg; $NiCl_2 \cdot 6H_2O$, 0.1 mg; Na_2MoO_4, 0.5 g; $FeCl_2 \cdot 4H_2O$, 7.5 mg; Na_2SeO_3, 0.05 mg; KH_2PO_4, 0.5 g; $MgCl_2 \cdot 6H_2O$, 0.33 g; NaCl, 0.4 g; NH_4Cl, 0.4 g; $CaCl_2 \cdot 2H_2O$, 50 mg; rumen fluid (filtered and sterilized in autoclave), 100 ml; lignite, 0.3 g, per liter of water, and adjusted to pH 7 with NaOH. The control medium was of the same composition without lignite.

Media solutions were made anaerobic by briefly boiling, then cooling under 80% N_2/20% CO_2; the gases passed over heated copper to remove any oxygen. Anaerobic media was transferred to 100 ml stoppered serum bottles and autoclaved at 15 psig for 20 minutes. Just prior to inoculation of media, $Na_2S \cdot 9H_2O$, 0.05%, was added to each media bottle to lower the oxidation-reduction potential. Resazurin was not added as an indicator of anaerobiosis as it would interfere with spectrophotometric readings; however, experience with the anaerobic techniques used here have shown them to be reliable.

Cultures

Rumen has been used a number of times as source of bacteria capable of breaking down complex structures (8,9,10). Cultures were started with fresh rumen contents from cow and sheep. Only sheep rumen cultures showed lignite-degrading potential and were studied further. Following growth of serial dilutions of a sheep rumen culture, the dilution tube showing the greatest color change from baseline as measured on the spectrophotometer by its absorbance at 580 nm was transferred to fresh media; subsequent sheep rumen cultures were all derived from this dilution tube. Cultures were started generally with a 10% inoculum to fresh media. Incubation was at 37°C, shaking at 100 rpm.

A mixed culture derived from sheep rumen which appeared to degrade lignite at 0.03 g% was streaked onto plates; solid media had the same composition as the liquid media with glucose, with the addition of 2.0 % agar (Difco). Plates were poured, and all inoculating was done inside an anaerobic chamber. Inoculated plates were incubated at 37°C in an anaerobic jar (Oxoid). Three different colonies were transferred to solid media in slant tubes and later to liquid anaerobic media in flasks.

Microscopically, the isolated cultures did not look pure. One showed growth of large rods with endospores, but it appeared there were also smaller

rods present. The other two cultures showed growth of at least two types of rods - a long, slender rod, and a shorter, more refractile one.

Liquid samples were also analyzed on a spectrophotometer. A standard plot of optical density or absorbance at 580 nm versus lignite concentration using dilutions of lignite in water was made and a linear plot was obtained (Figure 1); the darker the solution, the higher the liqnite concentration. Thus, it was concluded that spectrophotometry could be used to follow the lignite utilization of the culture. Liquid samples were centrifuged at 10,000 x g for two minutes. One ml of supernatant was diluted with 1 ml of distilled water. Readings of absorbance at 580 nm were taken on a Bausch and Lomb Spectronic 21. Control media served as reference for corresponding lignite media samples.

Results

Of the initial mixed cultures of sheep rumen and cow rumen, the sheep rumen culture was the only one to show a substantial visual decrease in color during fermentation with a decrease in the absorbance at 580 nm from 0.305 to 0.047 as seen in Tables 1 and 2, indicating a decrease in the lignite concentration of approximately 90 percent.

The three cultures derived from the original sheep rumen culture were also tested for their ability to degrade solubilized lignite based on the decrease in absorbance at a wavelength of 580 nm of a culture containing 0.03 percent solublized lignite. The results of this test are presented in Table 3. As seen in Table 3, culture 2 appears able to degrade solubilized lignite better than cultures 1 and 3.

Due to the apparent ability of culture 2 to degrade solubilized lignite, it was chosen for further work. This culture was inoculated into five culture tubes with the media for transfers described above except the solubilized lignite concentration varied from 0.03 percent to 0.25 percent. The absorbance at 580 nm was monitored on each tube with time to determine the affect of solubilized lignite concentration on the degrading ability of the culture. The results of these experiments are shown in Table 4. Based on these results it appears that solubilized lignite concentrations of 0.1 percent or higher inhibit the cultures ability to degrade the lignite.

Further work is being done with these cultures to determine the ability to produce lower alcohols and organic acids. At this time, none of the cultures have shown the ability to produce substantially higher quantities of ethanol, propanol, butanol, acetic, propionic or butyric acids from solubilized lignite when compared to a control culture without solubilized lignite. Work is continuing, however, on the analysis of these experiments to better determine what compounds are being produced.

CONCLUSIONS

Preliminary results have been obtained in the second step of the serial biological conversion of coal to liquid fuels. Solubilized lignite, derived from the action of a lignite surface culture on Arkansas lignite, was used as the substrate in anaerobic culture with organisms derived from sheep rumen.

In mixed culture, the potential for degrading lignite was shown by the decrease in color and absorbance at 580 nm during fermentation. Analysis of the fermentation products of these cultures, however, has not shown substantial production of lower alcohols. The search for an anaerobic organism capable of producing higher quantities of alcohols is continuing. Work is also being conducted in an attempt to find aerobic organisms capable of degrading solubilized lignite to compounds which can then be converted to alcohols by anaerobic organisms.

REFERENCES

(1) Fakavsa, R. M., "Coal as a Substrate for Microorganism: Investigation with Microbial Conversion of National Coals," Ph.D Thesis, Friedrich Wilhelms University, Bonn, Federal Republic of Germany (1981).

(2) Cohen, M. S. and Gabriele, P. D., "Degradation of Coal by the Fungi Polyporous versicolor and Poria placenta," Appl. Environ. Microbiol. 44(1), 23-27 (1982).

(3) Scott, C.D., Standborg, G. W. and Lewis, S. N.,"Microbial Solubilization of Coal," Biotech. Progress 2(3), 131-139 (1986)

(4) Standborg, G. W. and Lewin, S. N., "Solubilization of Coal by an Extracellular Product from Streptomyces setonii 75 Vi2," J. Industrial Microbiol. 1 370-375 (1987).

(5) Ward, B., "Biodegradation and Bioconversion of Coals by Fungi," US DOE/PC80913 (1987).

(6) Cohen, M. Biological Treatment of Coals Workshop, Proceedings U. S. DOE/ENTEL, Herndon, VA (June 1986).

(7) Dahlberg, M., Biological Treatment of Coals Workshop, Proceedings U. S. DOE/ENTEL, Herndon, VA (June 1986).

(8) Cheng, K. J., Jones, G. A., Simpson, F. J., and Bryant, M. P., "Isolation and Identification of Rumen Bacteria Capable of Anaerobic Rutin Degradation. Can. J. Microbiol. 15 1365-1371 (1969).

(9) Simpson, F. J., Jones, G. A., and Wolin, E. A., "Anaerobic Degradation of Some Bioflavinoids by Microflora of the Rumen. Can. J. Microbiol. 15 972-974 (1969).

(10) Tsai, C. G., and Jones, G. A.. "Isolation and Identification of Rumen Bacteria Capable of Anaerobic Phloroglucinol Degradation. Can. J. Microbiol. 21 794-801 (1975).

Table 1

Optical Density or Absorbance at 580 nm of
Original Cow Rumen Culture

days	A_{580} (Sample)-(Control)	Control
0	0.202	0.360
2	0.310	0.198
4	0.293	0.205
6	0.280	0.280
10	0.285	0.208

Table 2

Optical Density or Absorbance at 580 nm of
Original Sheep Rumen Culture

days	A_{580} (Sample)-(Control)	Control
0	0.305	0.213
1	0.278	0.210
2	0.235	0.238
3	0.158	0.263
6	0.047	0.335

Table 3

Absorbance at 580 nm of Cultures
Derived from Sheep Rumen

Culture	day	A_{580}
1	0	0.328
	10	0.240
2	0	0.328
	10	0.170
3	0	0.328
	17	0.225

Table 4

Optical Density or Absorbance at 580 nm of Culture
With Varying Lignite Concentrations

Lignite Concentration	days	A_{580} (Sample)-(Control)*	Control**
0.03%	0	0.263	0.310
	3	0.085	0.277
	7	0.057	0.267
0.05%	0	0.344	0.310
	3	0.203	0.277
	7	0.033	0.267
0.10%	0	0.740	0.310
	3	0.788	0.277
	7	0.768	0.267
0.15%	0	1.050	0.310
	3	1.013	0.277
	7	1.033	0.267
0.25%	0	--***	0.310
	3	--	0.277
	7	--	0.267

* average of two samples
** average of three samples
*** sample reading was off instrument's scale

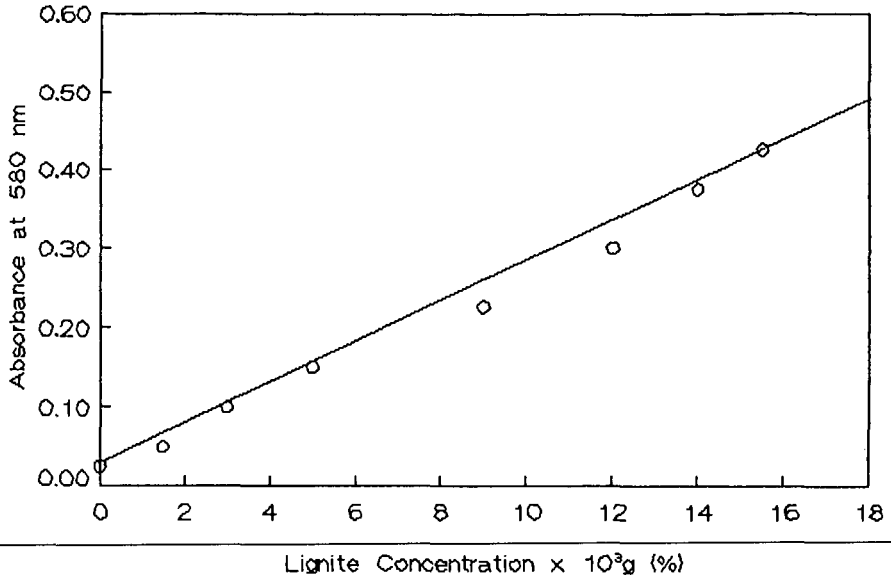

Figure 1. Calibration curve for solubilized lignite concentration using absorbance.

RECENT PROGRESS IN CELL-FREE SOLUBILIZATION OF COAL

Martin S. Cohen[1], Harold Aronson[1], Kathleen Feldman[1],
Cynthia Brown[1] and Edward T. Gray, Jr.[2],
Department of Biology[1] and Department of Chemistry[2],
University of Hartford, West Hartford, CT 06117.

ABSTRACT

Low rank coal has been solubilized using cell-free filtrates separated from cultures of Polyporus versicolor. Solubilization has been obtained with neat filtrates and with fractions collected from the neat filtrates after gel permeation chromatography. The coal solubilizing enzymes have been collected in enriched fractions with gpc. This increased relative purity has allowed the determination of the average molecular weight of this enzyme by gel permeation chromatography and by polyacrylamide gel electrophoresis. Rates of coal solubilization are dependent on the size of coal particles, mass of coal, temperature, pH, concentration of the cell-free filtrate, and the concentration of several inorganic ions.

INTRODUCTION

The focus of experimentation at the beginning of this project was to produce a solubilized product from coal which had been exposed to the fungus Polyporus versicolor. Initially, Polyporus was routinely grown in dishes containing Sabouraud maltose agar and incubated at 30°C. Leonardite was routinely solubilized by adding small pieces directly to the surface of the growing mycelium. In a second stage, Polyporus was grown in a liquid medium consisting of Sabouraud broth. After a suitable period of fungal growth, the hyphae were separated from the culture medium by filtration and aliquots of the cell-free broth were added to samples of leonardite. The general characteristics of the observed (cell-free) solubilization were reported in the open literature (1). The research presented here has the ultimate aim of isolation and purification of the active agent(s) in the solubilization process, which are present in the neat cell-free broth. Ultimate success does, of course, require a knowledge of the presence of those agents and their relative concentrations. Thus, this paper reports the optimization of the characteristics of the solubilization process, and a standard set of conditions for the testing of the solubilization phenomena. From this base, a discussion of the progress towards isolation and purification of the species involved in the solubilization process is presented.

OPTIMIZATION AND STANDARDIZATION OF THE SOLUBILIZATION PROCESS.

Having identified the scope of the solubilization process, it became necessary to determine an optimal set of conditions for the study of the process itself. A standard set of conditions is necessary in order to develop an assay for the solubilization ability of the broth, with some form of assay being required in order to compare the activity of various samples of broth with each other. This set of conditions is also necessary to be able to systematically avoid any inhibitors of the process.

An initial series of tests showed that some ionic strength in the solubilization medium was helpful in improving the solubilization action of the Polyporus broth. While nitrate, perchlorate, and acetate showed little effect at pH = 5.5 (even

though acetate has buffering capacity at this pH), the presence of phosphate (Figure 1) and, to some degree, chloride, did influence the solubilization of coal. The explanation at the time centered around the ability of these latter two bases to coordinate ferric ion, especially phosphate. From this work, a standardized buffering system of 0.050M phosphate and 0.050M acetate (all sodium salts) was established.

Using this medium, it was determined that the broth did not simply act as a catalyst for coal dissolution, but that the broth had a capacity, and that this capacity could be measured (Figure 2). This was the first standardization procedure for the solubilization ability of the broth. Knowing that the action of the broth was not being limited by its inherent capacity, and the fact that the constant medium being used and the constancy of the procedures was dramatically reducing the scatter in the data which was being obtained, it was possible to obtain a solubilization yield of the broth for the first time. This was accomplished by comparing the lyophilized bioextract from the agar plates against the liquid culture solubilizations. A 70% yield of coal solubilization was obtained, and that particular batch of broth had a capacity of 0.32mg/mL at pH = 5.5. At pH = 5.25, the yield was only 32% but the capacity was above 1.5mg/mL.

In a parallel investigation, an increasing amount of the broth was added to a fixed amount of coal. Figure 3 shows that the absorbance of solubilized coal is a function of the concentration of broth at low broth concentrations, and becomes independent of the amount of broth at higher concentrations. It should be noted that undissolved particles were present in all the test mixtures. This supports the concept of enzyme capacity discussed above.

The pH effect mentioned above prompted the generation of a pH profile (Figure 4). The maximum effect appears between pH = 5.3 and pH = 5.5. It is interesting to note that the activity does not rapidly fall to zero as pH decreases, but appears to fall to zero as pH increases by one unit. This rapid drop at higher pH is at least partially due to the much higher background of solubilization by the buffer at higher pH values.

In an attempt to understand the nature of the active agent in the broth, and, thus, to better be able to handle the system, ascorbic acid (a reducing agent) was added to inactivate any oxidative enzymes which might be present in the broth. The addition of ascorbic acid decreased the effectiveness of the broth by 90%, while the addition of oxygen after the ascorbic acid (to oxidize the ascorbic acid and show that the oxidized ascorbate was not responsible for the inactivity of the broth) restored the activity. The addition of oxygen to the broth alone showed a slight increase in the activity of the broth.

A temperature profile of the rate of solubilization activity was developed. Figure 5 shows a steady increase of the rate of cell-free solubilization with increasing temperature until 60°C after which the rate of solubilization turns up very quickly. The active agent for solubilization must be very rugged, and any 3-dimensional property of the agent must not be important in solubilization. Another critical point in the analysis is the presence of cations which are poor Lewis acids (i.e. cations which tend to be "soft" and basic in solution). It was noticed early in 1987 that virtually all the iron which the coal contained was brought into the solution phase during the solubilization process. When various eluents were being used in the HPLC separation of the broth, it was noticed that the presence of added Fe(III) as well as cations such as ammonium ion and

tetraethylammonium ion inhibited the solubilization process. This initial nuisance has become a potential analytical probe for the activity of the broth. In Figure 6, the intersection of the negative slope and the horizontal baseline is a direct function of the concentration of active agent, since the iron content eventually stops the solubilization process. Thus, for the same coal sample and time of contact, the slope of the absorbance vs. Fe(III) line should remain constant as the x-axis intercept changes to reflect the activity of the particular enzyme sample.

Furthermore, the active agent has a very strong binding constant toward iron, which presents itself as an irreversible process in the simple sense. This is seen when EDTA is added to a sample of coal, broth, and excess iron. If the iron is added to the broth before the EDTA, the broth is inhibited under conditions where the EDTA is able to coordinate all the iron. If the EDTA is added before the broth, it coordinates to the iron and the solubilization continues normally. Not all cations act in the same manner as Fe(III). Figure 7 shows the effect of the addition of ammonium ions on the solubilization process. As seen in the Figure, the concentration of NH_4^+ needed for a loss of enzyme activity equivalent to that seen in the Fe(III) system is much greater. The far greater effectiveness of Fe(III) in inhibiting the solubilization process implies that the binding constant of ammonium ion with the active enzyme is clearly much lower than that with Fe(III). Even at 0.5M, the ammonium ion presence has not totally inhibited the solubilization process, although it is significantly decreased.

ISOLATION OF THE ACTIVE AGENT(S) IN THE SOLUBILIZATION PROCESS.

With a set of standard analytical procedures in place, the process of separating the active agent(s) from the broth was begun.

Using a C_{18} column with the standard phosphate/acetate buffer as eluent, two of the nine discernable peaks in the chromatogram showed activity toward coal (Figure 8). In order to further resolve these peaks, the eluent polarity was varied from that of methanol to 5% (w/w) NaCl. Resolution increased with polarity, but the peaks of interest always partially overlapped the void volume. Thus, another separation technique was necessary. Even so, gel electrophoresis separations on the broth produced patterns of protein which mirrored those of the C_{18} chromatography, indicating that the number of large molecules from which a separation had to be effected was not enormous.

Anion exchange initially showed some potential. The compound(s) of interest apparently have weak bases which have pK_a's in the pH = 5.5 region, since the placement of peaks coming off the anion column was quite sensitive to pH and $[Cl^-]$ in this pH region. The work carefully led to ever further refinements of procedure from step gradients to gradient elution through various concentrations of Cl^- and H^+.

The difficulty with all these methods is the high $[Cl^-]$ which was part of the anion-exchange process. Since coordinating agents which might ordinarily be of use in removing the Cl^- are not available to the work because of the inhibition of the system, the method of separation turned to exclusion chromatography. With an analytical gel permeation column (Waters Protein-Pak 125), the active solubilizing agent can be isolated to a single fraction of the chromatogram (Figure 9). A similar pattern of separation can be accomplished on a preparative gpc column (Sephadex, G-25-150) as shown in Figure 10.

In order to determine the molecular weight of the active fraction, the analyticalgpc column was used with six compounds of known molecular weight. The active fraction eluted from the column in an elution volume of 11.9 mL (Figure 11). This corresponds to an average molecular weight of 25,000 Daltons.

FUTURE EXPERIMENTATION

Experiments aimed at purification of the proteins responsible for solubilization of coal will be continued, with the goal of the formulation of a large-scale process of enzyme separation.

REFERENCES

1. Cohen, M.S., W.C. Bowers, N. Aronson, and E.T. Gray, Jr. 1987. "Cell-Free Solubilization of Coal by Polyporus versicolor". Appl. Environ. Microbiol. 53:2840-2843.

ACKNOWLEDGEMENT

This research was supported by contract RP8003-06 from the Electric Power Research Institute.

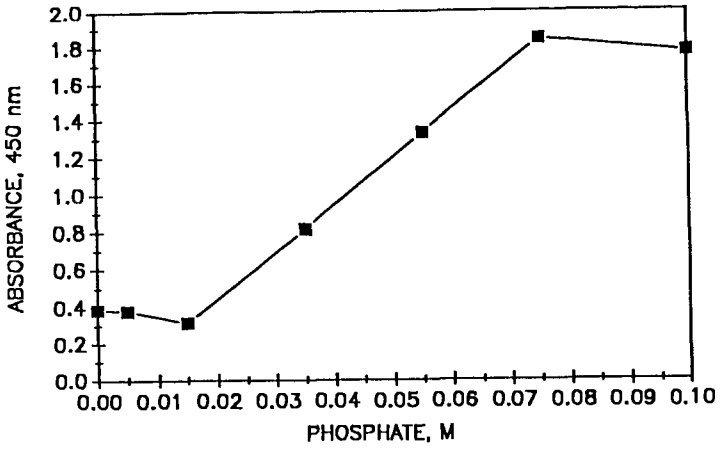

Figure 1. Effect of phosphate concentration on cell-free solubilization of leonardite coal.

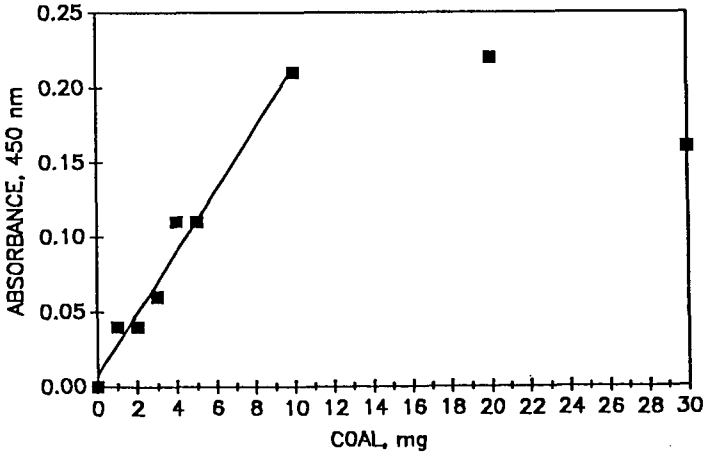

Figure 2. Effect of mass of coal added to a constant amount of cell-free filtrate on extent of solubilization of leonardite.

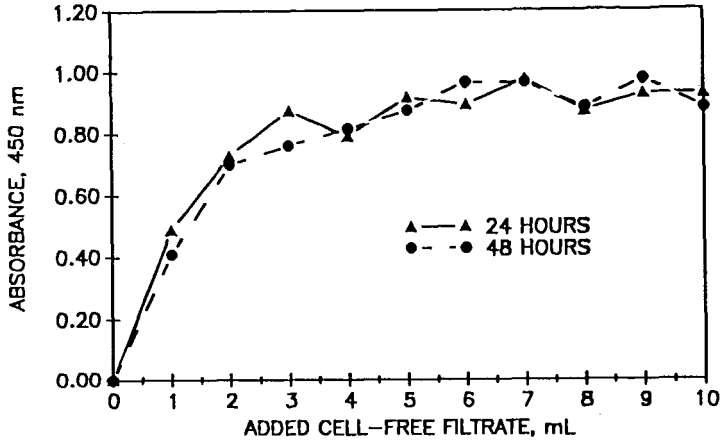

Figure 3. Effect of various amounts of cell-free filtrate added to a constant amount of leonardite on extent of solubilization of leonardite.

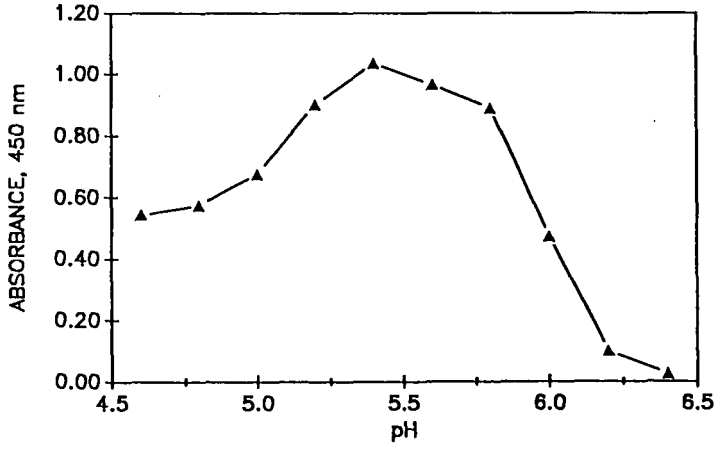

Figure 4. Effect of pH on activity of the cell-free filtrate separated from the SMB in which Polyporus had grown.

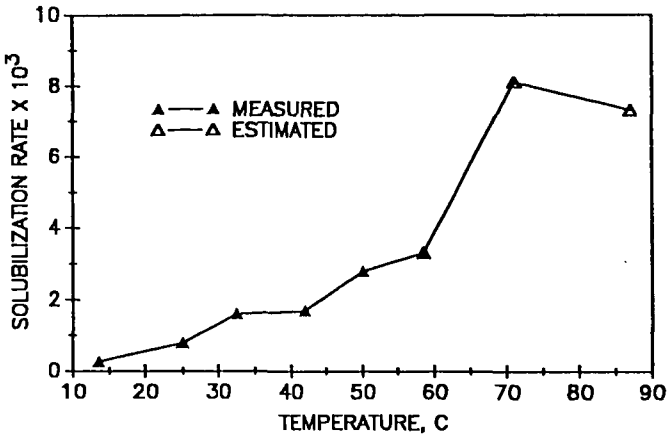

Figure 5. Effect of temperature on the rate of cell-free solubilization of leonardite coal.

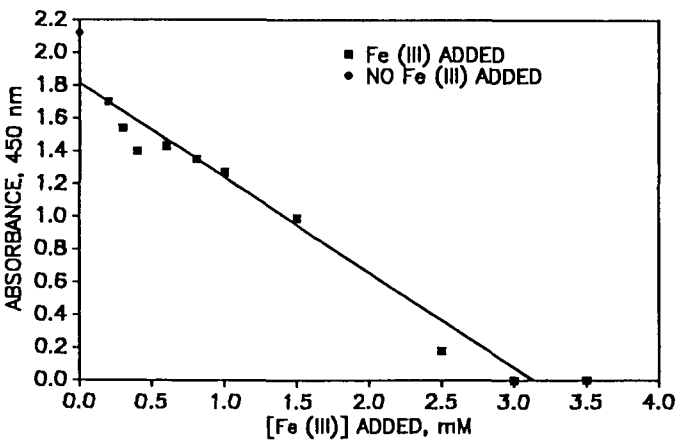

Figure 6. Inhibition of cell-free solubilization of leonardite coal by addition of Fe(III) to the filtrates. The inhibition can be reversed by mixing EDTA with the Fe(III) before addition of the iron solution to the filtrates.

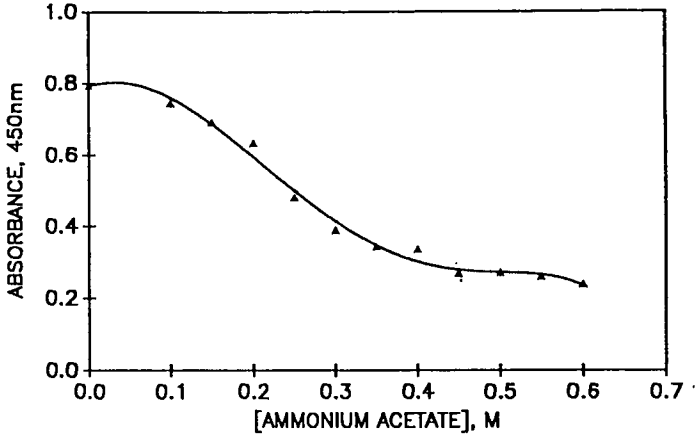

Figure 7. Inhibition of cell-free solubilization of leonardite coal by addition of ammonium ion to the filtrates.

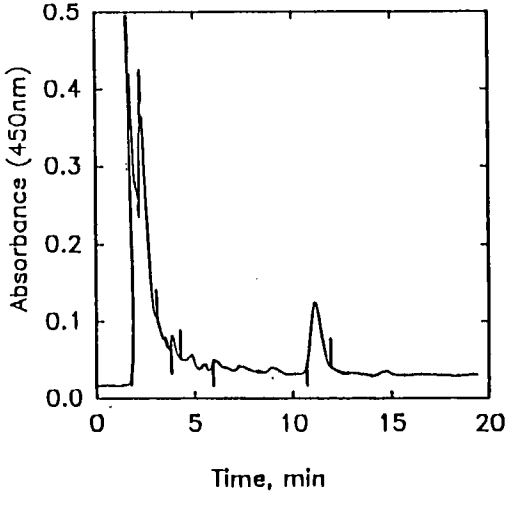

Figure 8. Separation of cell-free filtrate from Polyporus on a C_{18} column.

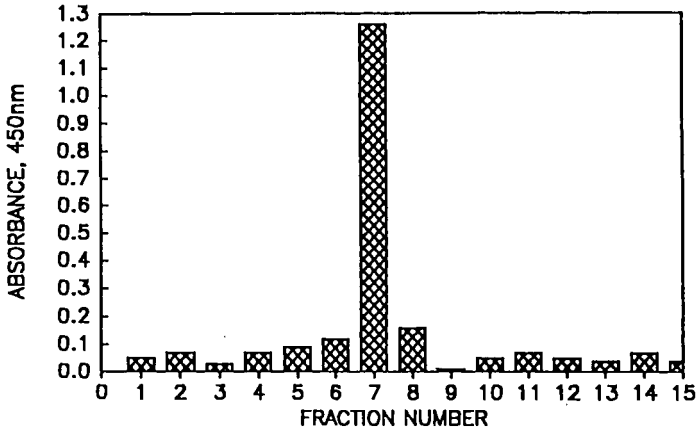

Figure 9. Fractionation of the neat cell-free filtrate on a gel permeation column. The leonardite-degrading activity has been separated into a single fraction.

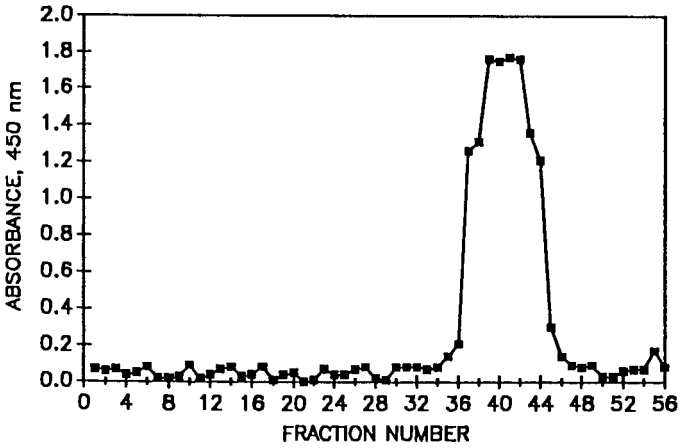

Figure 10. Separation of the coal solubilizing enzyme on a preparative column (1.5 cm X 25 cm) packed with Sephadex G-25-150 resin.

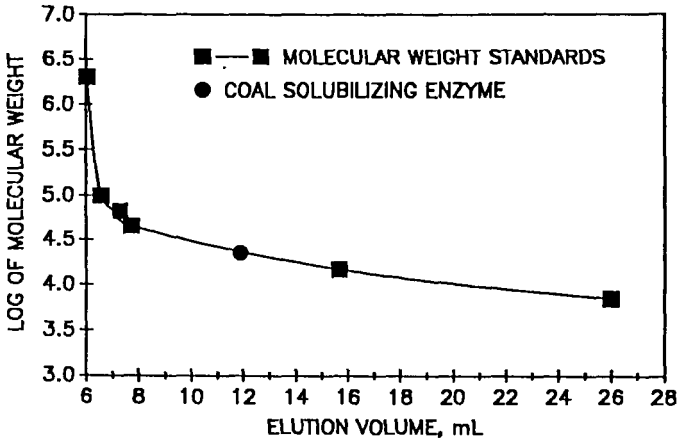

Figure 11. Molecular weight determination of the coal-solubilizing enzyme.

BIOSOLUBILIZATION OF COAL IN AQUEOUS AND NON-AQUEOUS MEDIA

B. D. Faison, C. D. Scott, and B. H. Davison
Chemical Technology Division
Oak Ridge National Laboratory
Oak Ridge, Tennessee 37831-6194

ABSTRACT

Biocatalytic solubilization of coal can be achieved by microorganisms in aqueous medium or by enzymes in aqueous or organic media. In these systems, coal is converted to a liquid product through a variety of oxidative and/or hydrogenative reactions.

The mechanism and control of coal solubilization activity have been studied in organisms associated with coal in nature. The solubilization apparently involves catalysis by alkaline cell metabolites. The aqueous product of this microbial action may be a suitable substrate for other biological interactions such as biogas production by methanogenic organisms.

Enzymatic coal solubilization has been demonstrated in both shake flasks and fluidized-bed reactors. The process has been carried out under both anaerobic and aerobic conditions, with aqueous and hydrous organic solvents. The solubilization product of the anaerobic process is much less polar than that from microbial solubilization.

INTRODUCTION

The application of biotechnology to the utilization of low-ranked coals has become the focus of intense research activity in recent years. Biological systems -- whole organisms or fractions thereof -- have been shown to catalyze a variety of industrially significant reactions. These systems have potential utility in the upgrading and/or transformation of coal.

Biocatalysis generally occurs under mild, "physiological" conditions, e.g. at relatively low temperatures and pressures, and at pH near neutrality. Biological treatments of coal could therefore be conducted under mild reaction conditions relative to those under which conventional thermo/chemical processes are carried out. Biocatalysts characteristically demonstrate high specificity with respect to the products generated. Biological treatment of coal would thus promote the formation of specific products, including perhaps products with higher fuel value than that of the original substrate.

Biotechnology can be applied to various aspects of coal processing. The application which has received the greatest attention is the removal of contaminating heteroatoms, such as sulfur, from low-ranked coals by microorganisms. The use of biocatalysts to modify coal's carbon skeleton is, however, a rapidly developing area of great potential importance. Research at Oak Ridge National Laboratory has focused on the biotransformation of lignite and subbituminous coals by microorganisms or by isolated biochemical catalysts (enzymes). The

synthesis of liquid products from coal by biological systems, i.e. coal biosolubilization, is the subject of this exploratory research. This work will form a basis for the development of technologies for the production of clean-burning liquid or gaseous fuel products from coal substrates. The results of current initiatives in this area are summarized below.

Biosolubilization of coal in aqueous media

The solubilization of coal by microorganisms was first reported in 1982 by Cohen and Gabrielle (1). These and other workers noted the production of liquid droplets from coal, associated with the growth of mycellial organisms on the coal surface. Organisms competent to solubilize coal were isolated from coal in the environment (2) or in the laboratory (3). It was subsequently shown that these organisms solubilized coal when cultured on the surface of common, organic microbiological media. Suitable coal substrates for this activity were leonardite, lignites, and subbituminous coals. In the latter cases, the coals required oxidative pretreatment either through natural weathering or by chemical agents [hydrogen peroxide, ozone, nitric acid, etc.; (4)]. The product of this microbial activity was a water-soluble mixture of oxidized compounds of moderate molecular weight [30,000-300,000 daltons; (3)]. The material was enriched in carbonyl and hydroxyl functions relative to the coal substrate, and was precipitable at pH 1. Its characteristics resembled those of humic acids, except for its water-solubility.

Recent work (5,6) in this laboratory has sought to determine the mechanism by which microorganisms solubilize coal in vivo. Superior isolates (fungi) have been cultivated in a defined growth medium in both surface culture on agar and submerged culture in liquid medium. These culture methods simulate fixed-bed and fluidized-bed bioreactor configurations respectively, which have been proposed for use with this technology (Figure 1). The defined media developed for use in this work consisted of inorganic salts, supplying the organism's mineral requirements, plus a sole carbohydrate carbon source (5). These media support coal solubilization in vivo (Table 1). The use of defined media has minimized contamination of the liquid coal product with organic medium components, and will contribute to further product analysis. product recovery has been expedited by growth and solubilization under submerged culture conditions, i.e. in shake flasks. use of this system has also permitted the development of a spectrophotometric assay for coal solubilization, based on the appearance of chromophoric material (absorbing in the 420-450 nm spectral range) in cultures incubated with coal. Its spectral characteristics were identical to those of the material formed by the nonbiological action of alkali on coal.

The solubilization of coal by dilute alkali had been demonstrated previously, and had been implicated in the activity in vivo (6). Specifically, it was thought that microbial coal solubilization occured as a fortuitous consequence of pH increases associated with growth. Evidence in support of this conclusion had been obtained in alkaligenic systems substantially contaminated with protein and other basic components. In the present work, activity was detected in an acidogenic system of known biochemical composition (Figure 2). These data support an involvement of alkaline catalysis in the microbial activity. The data suggest further that the proposed alkaline catalyst is produced by cultures in specific response to the presence of coal.

The liquid product generated by fungal action on coal may have some utility as

a feed stream for the biological production of other combustible fuels. Possible products are biogas (methane) and fuel alcohols.

Methane production from partially-oxidized compounds analogous to coal substructures has been demonstrated elsewhere. Based on this knowledge, a two-step process for conversion of coal to methane has been proposed. Coal solubilization would be carried out by aerobic microorganisms as described above. Subsequent biogas production would be accomplished through the action of anaerobic organisms. Preliminary tests have been conducted in order to determine the feasibility of the proposed process.

Microbial consortia isolated from a municipal sewage treatment plant or from a coal fly ash settling pond were incubated with biosolubilized coal under anaerobic conditions. The liquid coal product was nontoxic at low concentration toward microbial growth or metabolism. After acclimation, methanogensis from methanol occurred with the same yield with or without the coal liquids present. Model compound studies were carried out with vanillin, which was shown to disappear from metabolically active cultures. A defined growth medium was designed for use with these methanogenic consortia. In that system, either vanillin or the coal liquid could serve as sole carbon source for growth and metabolism. Preliminary data from total organic carbon analysis with the coal liquid as the sole carbon source indicated at least partial degradation. These findings suggest that biosolubilized coal can be utilized by methanogenic consortia for biogas production, accomplishing a two-step conversion of coal to clean-burning gaseous product. These data also support the feasibility of using anaerobic microorganisms for other treatments of liquid coal product, possibly including the conversion of coal to fuel alcohol.

The feasibility of treating coal with enzymes in aqueous buffer has been explored. Preliminary trials were conducted with horseradish peroxidase and laccase from Pyricularia oryzae. These enzymes are a nonspecific oxidoreductase, transferring electrons from H_2O_2, and an oxygenase respectively. The reactions were carried out in shake flasks under aerobic conditions. A measurable increase in coal solubilization occurred when laccase was used, although the extent of solubilization was somewhat low (Table 2). Horseradish peroxidase also increased solubilization, but to a smaller extent. The material yielded by enzymatic solubilization was water-soluble, and of a polarity similar to that of the product of microbial action.

Biosolubilization of coal in non-aqueous media

Bioprocesses involving intact microorganisms generally are carried out in aqueous environments, i.e. growth media or buffers. Considerable excitement has been generated by the finding that isolated enzymes can be used in organic solvents to catalyze certain reactions (8). The bioprocessing of coal in nonaqueous media would favor the formation of nonpolar products, possibly including reduced compounds with high fuel value.

Oxidizing enzymes would be required to catalyze the various reactions involved in coal depolymerization. Additional treatment with reducing enzymes may result in the production of low-molecular-weight nonpolar compounds similar to those generated by nonbiological coal liquefaction. These enzymes would cause a net increase in hydrogen content and a reduction in oxygen content. Recovery of

these products would be facilitated if these reactions were carried out in a non-polar organic solvent. The use of enzymes in organic solvents is complicated by the need to maintain the enzyme within an aqueous microenvironment in order to support activity (8). Hydrous organic media are therefore used in these systems.

The potential for enzymatic coal solubilization in nonaqueous media was evaluated via tests with horseradish peroxidase, alcohol dehydrogenase from yeast, and/or bacterial hydrogenase. Preliminary experiments were performed under aerobic conditions (air) using peroxidase dissolved in hydrous dioxane. The extent of coal solubilization was somewhat increased by this treatment, and was much greater than that previously measured in buffer alone (data not shown). Subsequent tests were carried out with enzyme mixtures in dioxane or pyridine, under a reducing atmosphere of 100% hydrogen. Solubilization of a leonardite was substantially enhanced by enzyme treatment (Table 3). A much smaller positive effect was seen in tests with bituminous coal.

The liquid product from anaerobic coal solubilization in organic solvent was found to be soluble in benzene (data not shown). This product thus differed from that obtained by aerobic treatment with enzymes or intact microorganisms in aqueous systems with respect to polarity and solubility behavior.

Additional studies were carried out in a fluidized-bed bioreactor under aerobic conditions, in which coal was treated with peroxidase in hydrous dioxane. Solubilization was very rapid and was enzyme-dependent (Figure 3).

SUMMARY

Biological treatments with whole cells or isolated enzymes has the potential to yield useful products from low-ranked coals. These products may include clean-burning gaseous or liquid fuels. Coal solubilization is a common element in these conversions. Exploratory research indicates that the characteristics of the product(s) obtained are dependent on the choice of operating conditions, i.e. whether in aqueous or organic solvent, and in the presence or absence of air. The development of future bioprocesses for coal utilization must build upon these findings, to achieve the directed synthesis of desired products.

REFERENCES

1. Cohen, M., and P. Gabrielle. 1982. Appl. Environ. Microbiol. 44:23-27.

2. Ward, B. 1985. System. Appl. Microbiol. 6:236-238.

3. Scott, C., et al. 1986. Biotechnol. Prog. 2:131-139.

4. Strandberg, G., and S. Lewis. 1986. Biotechnol. Bioeng. Symp. Ser. 17: 153-158.

5. Faison, B., and S. Lewis. 1988. Manuscript submitted to Appl. Biochim. Biotechnol.

6. Strandberg, G., and S. Lewis. 1987. J. Indus. Microbiol. 1:371-375.

7. Healy, J. B. Jr., and L. Y. Young. 1979. Appl. Environ. Microbiol. 38:84-89.

8. Dordick, J., et al. 1986. Proc. Nat. Acad. Sci. USA 83:6255-6257.

Table 1. Coal solubilization by *Paecilomyces* TLi (3; surface cultures)[a]

Medium[b]	Coal solubilization[c] (% weight loss)
Complex:	
Sabouraud maltose	12.4
Defined:	
Czapek's	25.9
Minimal I	[5.3]

[a]Cultures were grown at 30°C, 80% RH for 7 d. Coal was added (0.5 g) and cultures reincubated for 7 d under the same conditions.

[b]Media contained 0.1% malose.

[c]Controls (uninoculated medium) exhibit ≤5% weight loss. Weight loss measurements incorporate ≤20% error.

Table 2. Enzymatic solubilization of acid-treated subbituminous coal in the presence of 0.05 M phosphate aqueous buffer at pH 6.0

Aqueous constituents	Average weight loss (%)
Buffer only	2.5
Buffer + 1625 units of peroxidase/mL	4.4
Buffer + 700 units of laccase/mL	6.8

Table 3. Anaerobic solubilization of coal in a hydrogen environment at ambient temperature and pressure by enzymes in organic solvents[a]

Liquid phase	Type of coal	Enzymes	Weight loss of coal (%)
Dioxane + buffer	Lenordite	None	19.6
Dioxane + buffer	Lenordite	Mixed[b]	86.4
Dioxane + buffer	Bituminous	None	1.2
Dioxane + buffer	Bituminous	Mixed[b]	3.7
Pyridine + buffer	Bituminous	None	3.0
Pyridine + buffer	Bituminous	Mixed[b]	6.7
Pyridine + tetralin + buffer	Bituminous	None	4.6
Pyridine + tetralin + buffer	Bituminous	Dehydrogenase	6.0

[a]The tests were carried out for 48 h with 20 mL of liquid and 0.3 g of coal size-reduced to a range of -10 to +30 mesh in 50-mL shake flasks with a controlled gas environment in the flask headspace. When enzymes were used, they were introduced with an activity of 400 units/mL for peroxidase, 0.325 units/mL for hydrogenase, and 3640 units/mL for dehydrogenase. A 0.1 M aqueous phosphate buffer, pH 5.6, that constituted 5% (v/v) of the liquid solution was used.

[b]The enzyme mixture included peroxidase, hydrogenase, and dehydrogenase in equal weight proportions.

Figure 1

ORNL DWG 85-1243

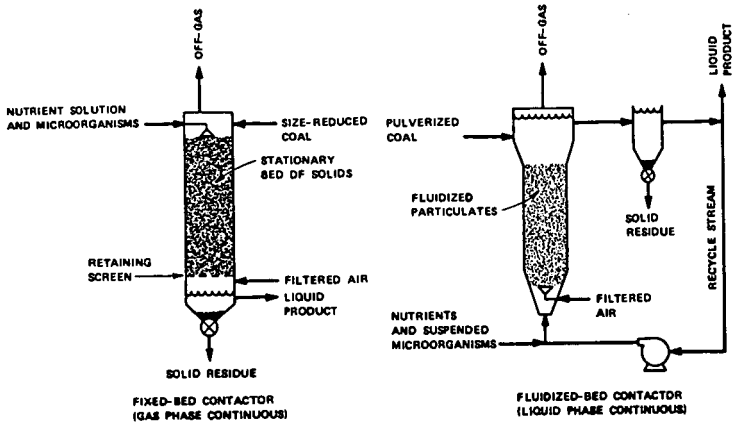

Fig. 1 Two possible bioreactor configurations for the microbial liquefaction of coal.

Figure 2

ORNL DWG 86-9890

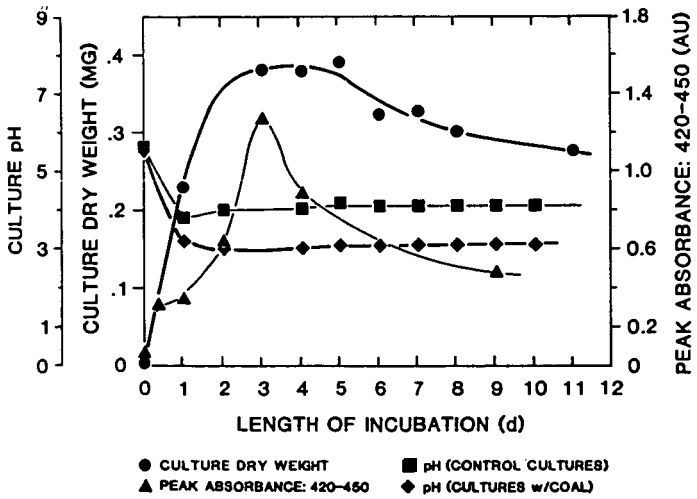

Fig. 2 Coal solubilization in an acidogenic system.

FIGURE 3

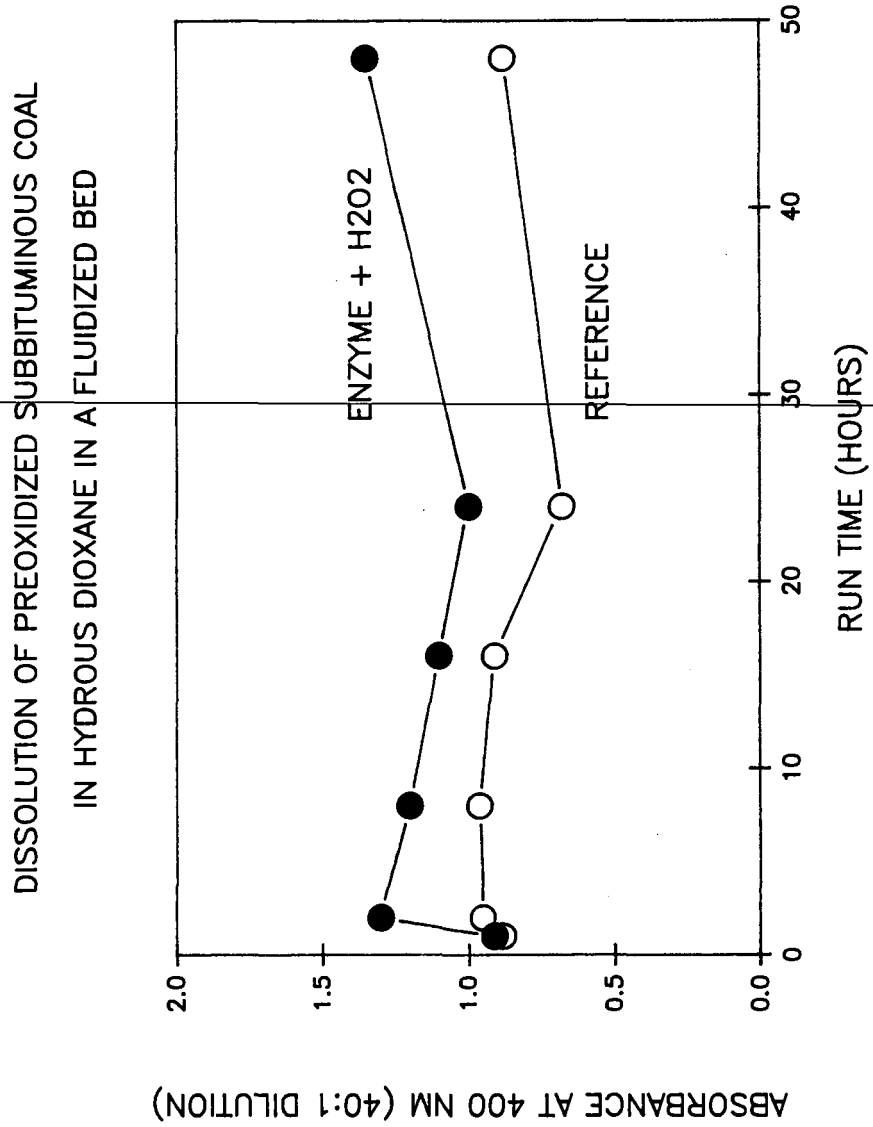
DISSOLUTION OF PREOXIDIZED SUBBITUMINOUS COAL
IN HYDROUS DIOXANE IN A FLUIDIZED BED
ENZYME + H2O2
REFERENCE
ABSORBANCE AT 400 NM (40:1 DILUTION)
2.0
1.5
1.0
0.5
0.0
0
10
20
30
40
50
RUN TIME (HOURS)

MICROBIAL CONVERSION OF COALS TO CLEAN FUEL FORMS

S. Barik, J. Isbister, B. Hawley, T. Forgacs, L. Reed,
G. Anspach, T. Middaugh

ARCTECH, Inc., 5390 Cherokee Avenue, Alexandria, VA, 22312

ABSTRACT

Anaerobic cultures have been used for the production of methane and alcohols from coal. Cultures were adapted from natural inocula collected from sources such as sewage sludge and horse manure. A 1% (w/v) slurry of leonardite, lignite, or subbituminous coal was used in the incubations. Methane was produced from all cultures, including some untreated coals, to a greater extent than in control cultures. Over several months of adaptation, methane production capacity increased considerably. Volatile fatty acids (VFAs) were identified as intermediates in the conversion of coal to methane. A proposed scheme for the conversion is breakdown of the coal polymer by a series of organisms and metabolism of the fragments to methane precursors such as VFAs. A mixture of short chain alcohols was produced by cultures grown in the presence of methane inhibitors. These cultures after prolonged adaptation show potential for use in larger scale bioreactors for the production of gaseous and liquid fuels.

INTRODUCTION

Recent interest in the use of microorganisms to process coal has led to the investigation of sulfur removal from coal as well as the conversion of coal to water soluble forms. Prior work in this laboratory has focused on investigating the mechanisms of formation of these water soluble compounds from coal by microbial as well as chemical means and characterization of the resulting products (ARCTECH, Inc. 1988a). The nonvolatile nature of these coal products inhibits their use as a clean fuel even though a majority of the ash and a proportion of the sulfur has been removed. In the current work, we have investigated the use of these coal products as well as untreated coals for the production of gaseous and liquid fuels (ARCHTECH, Inc. 1988b).

EXPERIMENTAL PROCEDURE

Coals--Both untreated coals and coal depolymerization products were used as substrates (1% w/v and 1% v/v, respectively) for methane, alcohol, and acid production. Two lignites were used as raw coal substrates. For the depolymerization products, three coals, North Dakota lignite, Beulah lignite, and Wyodak subbituminous, were treated with chemical or biological agents to yield water soluble products of a range of molecular weights.

Anaerobic Cultures--Anaerobic samples were collected from environmental sources and inoculated into an anaerobic medium containing coal or coal products. The procedures of Hungate, as modified by Bryant (1972) and by Balch and Wolfe (1976) were followed throughout. Serum stoppered tubes or serum bottles capped with black butyl rubber stoppers and crimp sealed were used for incubations.

Enrichment cultures were developed through successive transfers from each inoculum to fresh medium containing coal or coal depolymerization products every 28-45 days over a period of several months. Slow cultures were adapted to the coal or coal products over longer periods of time. Enrichment cultures were also developed in the presence of the methane inhibitors, 2-bromoethanesulfonic acid (BESA) and monensin, to allow the accumulation of acids and/or alcohols.

Chemical Analysis--All anaerobic fermentation products were quantified using gas chromatography. For gas analysis, a 10' x 1/8" O.D. stainless steel column packed with 100/120 mesh Carbosieve S-II was used. Methane, carbon dioxide, nitrogen, and hydrogen were determined using a thermal conductivity detector. The oven was programmed to hold at 100°C for 1 minute then to increase temperature at a rate of 20°C per minute to 200°C. Total gas production was determined by syringe displacement and was used to calculate mole % of methane in the gas phase.

Alcohol analyses were performed with either a 6' x 2 mm I.D. (1/4" O.D.) glass column packed with 1% SP-1000 on 60/80 mesh Carbopack B (first 3-4 inches 10% SP-1000 on 100/120 mesh Supelcoport) or a 2.4 M x 2 mm I.D. (1/4" O.D.) glass column packed with 0.3% Carbowax 20M on 80/100 mesh Carbopack C using a flame ionization detector. The oven was programmed from 60°C to 150°C at 20°C per minute then to 190°C at 5°C per minute and held. Analysis was performed by direct aqueous injection after centrifugation of samples to remove particulate matter.

Volatile fatty acids were primarily analyzed with an 8' x 2 mm I.D. glass column packed with 4% Carbowax 20M on 80/120 mesh Carbopack B-DA using a flame ionization detector. The oven was programmed to hold at 100°C for 1 minute then increase temperature to 180°C at 15°C per minute then to 205°C at 10°C per minute. Samples were diluted 1:1 with 0.06 M oxalic acid and centrifuged to remove particulates before injection.

RESULTS

Production of Methane From Coal and Coal Products

Figure 1 presents the time course of methane production from an untreated North Dakota coal and from Beulah lignite coal products. Methane production from samples containing coal or coal depolymerization products was higher than that of control cultures, demonstrating the conversion of coal carbon to methane. Similar results were obtained with other natural inocula, although not all cultures produced methane from every coal. A shift in the color of the reaction medium was observed during the course of incubation that was associated

with depolymerizing activity. The flattening out of the production curve indicates depletion of nutrients in the culture.

The effect of biological or chemical depolymerization of the coal on methane production was investigated with several different cultures. Data in Table 1 demonstrate increased production of methane in samples containing biologically produced coal depolymerization products. Methane is also produced from chemically depolymerized substrates although at a lower level. These experiments indicate that the products formed during biological and chemical depolymerization differ.

Identification of Alcohols and Acids in the Culture Medium

Our experiments indicated that methanogens were present and active in the adapted cultures. Methanogens are known to convert only simple organic molecules such as acetate and carbon dioxide to methane. Further experiments were initiated to determine the existence of methane precursors in the medium. To accumulate these precursors, methane inhibitors were added to enrichment cultures. Monensin serves as an inhibitor of specific enzymatic steps of methane production, whereas 2-bromoethane sulfonic acid (BESA) is an analogue of coenzyme-M which is required for methane production.

In almost all of the samples, BESA completely inhibited the production of methane. Monensin, however, inhibited methane production only from a single culture adapted to Beulah coal products. Results of analyses of culture media during methane inhibition studies are reported in Tables 2 and 3. Several short chain alcohols, including methanol, ethanol, propanol, and butanol, were produced by these cultures from either coal or coal depolymerization products. Acetone was also produced in small quantities by some cultures. No alcohols were produced in the absence of coal or coal products.

Product ratios varied depending on the inhibitor added to the medium. Ethanol was clearly the major alcohol produced by all cultures, with concentrations ranging between 757 and 2288 ppm. Methanol accumulated up to 316 ppm only in the presence of monensin. Propanol and butanol formation was favored in the presence of BESA. Total alcohol production decreased as the pH of the medium increased with no production of alcohols at pH 7.

In addition to alcohols, several short chain organic acids were detected in the culture medium (Table 3). Acetic acid was the principal organic acid detected, accumulating to a level of 1312 ppm. Small quantities of propionic, butyric, and valeric acid were also identified. Control samples without coal or coal depolymerization products produced minute quantities of acetic acid. No other organic acids were detected in these control samples.

DISCUSSION

The results reported in this paper demonstrate the feasibility of converting untreated lignite coals or depolymerized products of lignite and

subbituminous coals to methane by anaerobic cultures. Methane is produced from enrichment cultures in excess of that produced in the absence of coal or coal products. The ability of the cultures to produce methane increased as the enrichment period increased, demonstrating bacterial adaptation to use of coal or coal depolymerization products. The next step in culture development will be transfer of the most promising culture to a small bench-scale bioreactor to monitor continuous production of methane from coal or coal products.

Enrichment cultures are also capable of converting coal and coal-derived material to short chain alcohols and acids when methane production is inhibited. Although total alcohol concentration in the medium is less than one percent, the amount of alcohol produced by the cultures has steadily increased as the cultures adapted to the new substrates. Time course experiments are in progress to determine the production of alcohols and acids over an extended period.

Anaerobic enrichment cultures are capable of converting both untreated lignite coal and depolymerized coal products to methane, alcohols, and volatile fatty acids. A distinct preference for biologically derived coal products rather than chemically derived products was observed. Alterations in the coal molecule effected by microorganisms might be more conducive to further microbial attack than chemical modifications.

ACKNOWLEDGEMENTS

The authors gratefully acknowledge the Morgantown Energy Technology Center (contract no. DE-AC21-87MC23285) and the Houston Lighting and Power Company for support of this work.

REFERENCES

ARCTECH, Inc. 1988a. Biochemical Bond Breaking. DOE/PETC Draft Final Report Contract No.

ARCTECH, Inc. 1988b. Biological Gasification of Coals. DOE/METC Topical Report Contract No. DE-AC21-87MC23285.

Balch, W.E., and R.S. Wolfe. 1976. New approach to the cultivation of methanogenic bacteria: 2-mercapto-ethane sulfonic acid (HS-COM) dependent growth of Methanobacterium ruminantium in a pressurized atmosphere. Appl. Environ. Microbiol. 32:781-791.

Bryant, M.P. 1972. Commentary on the Hungate technique for culture of anaerobic bacteria. Am. J. Clin. Nutr. 25:1324-1328.

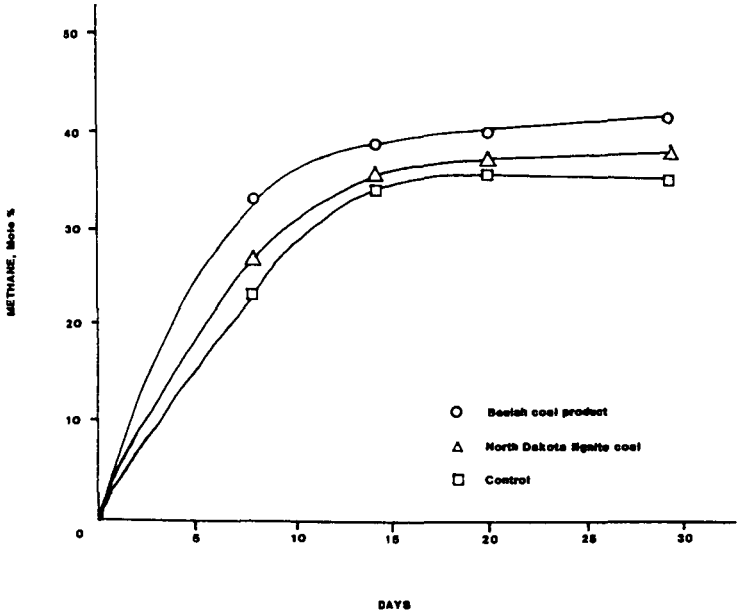

Figure 1. Production of methane from a ND Coal and Beulah Coal Product by Natural Inocula

Table 1. Direct Production of Methane from Coals by Anaerobic Bacteria

Coals	Methane Produced,** Mole % 2 Mos. Adaptation	6 Mos. Adaptation
Leonardite	7.8	25.6
	11.4	19.3
Texas lignite	9.1	----
	6.4	----

* 1% (w/v) coals were used.
** Methane from control samples (no coal) was substracted.

Table 2. Production of Alcohols from Untreated Leonardite Coal and Depolymerized Products of a Beulah Coal Using Anaerobic Microorganisms

			Alcohols Produced, ppm			
pH	Coal	Inhibitors	Methanol	Ethanol	Propanol	Butanol
5.0	L	BESA	7.2	2288.2	22.3	18.6
5.0	L	Monensin	275.3	2053.3	3.9	1.9
5.0	L	Control	0	10.9	25.6	0
6.0	L	BESA	7.06	1335.9	173.5	38.3
6.0	L	Monensin	315.9	1975.5	1.7	0
6.0	L	Control	0	16.2	19.9	1.7
6.0	B	BESA	13.5	756.5	202.9	88.9
6.0	B	Monensin	129.2	911.4	10.1	8.5
6.0	B	Control	29.1	4.9	4.5	6.2

Table 3. Production of Short Chain Acids from Coals and Depolymerized Coal Products Using Anaerobic Microorganisms

		Acids Produced, ppm			
Coal	Inhibitors	Acetic	Propionic	Butyric	Valeric
L	BESA	925.8	70.9	28.8	280.7
L	Monensin	626.5	77.7	34.1	266.1
L	Control	34.7	0	0	0
L	BESA	1311.5	306.5	80.7	501.0
L	Monensin	618.9	92.6	83.8	436.5
L	Control	4.5	0	0	0
B	BESA	932.4	233.9	62.5	0
B	Monensin	805.0	261.8	57.9	0
B	Control	99.6	118.7	0	0
TXL	BESA	885.7	158.4	34.7	0

L - Leonardite
B - Beulah lignite
TXL - Texas lignite
BESA - 2-bromoethanesulfonic acid

MICROBIAL OXIDATION AND REDUCTION OF SULFUR IN COALS FOR SPECIATION AND DESULFURIZATION

R.N. Schicho, S.H. Brown, and R.M. Kelly

Department of Chemical Engineering
The Johns Hopkins University
Baltimore, MD 21218

G.J. Olson

Chemical Performance & Standards Group
National Bureau of Standards
Gaithersburg, MD

1. INTRODUCTION

The microbial removal of sulfur from coal by oxidative means is well documented, especially with regard to pyritic sulfur removal by organisms such as *Thiobacillus ferooxidans* and *Sulfolobus acidocaldarius*. There also have been reports of the removal of organic sulfur from coals, (1,2) although generally less success has been achieved along these lines. Two aspects of microbial coal interaction which have received less attention are the use of microbes to elucidate coal sulfur chemistry and the removal of coal sulfur by bio-reduction. It is unlikely that there are significant amounts of elemental sulfur in pristine coal samples (3) but the recent work of Narayan suggests the presence of elemental and/or polysulfide sulfur in some weathered coals (4). By ASTM techniques these sulfur forms would be counted as "organic" sulfur. The lack of a direct assay for organic sulfur makes it difficult to establish a clear connection between microbial metabolism and the cleaving of covalently bound sulfur from the coal matrix. It also ignores any chemical interconversion of sulfur species which may occur during weathering, desulfurization, or analytical processing.

In this study we have made use of organisms which selectively metabolize elemental sulfur, either oxidizing it to sulfate at 28°C (*Thiobacillus thiooxidans*) or reducing it to hydrogen sulfide at 98°C (*Pyrodictium brockii* and *Pyrococcus furiosus*). We have pursued both the development of a bioassay for the speciation of sulfur in coals and novel desulfurization methods. The quantification of elemental sulfur by bioassay was confirmed with CS_2 extraction of the coals. Narayan has suggested that a significant fraction of so called organic sulfur in coals may be amenable to transformation to free elemental sulfur under mildly oxidative conditions. We will attempt to oxidize several coals using such techniques to investigate the possibilities for novel routes to microbial "organic" sulfur removal. The activity of the organisms toward polysulfide sulfurs (amorphous), partially oxidized species, and other model compounds (i.e. dibenzothiophene) will also be investigated.

The reduction of sulfur to hydrogen sulfide may avoid one of the problems involved with oxidative coal desulfurization, namely, the re-deposition of insoluble sulfate bearing minerals such as jarosite from the leachate when sulfate concentrations become too high. We are also investigating the activity of cell free extracts and lysed membrane preparations towards coal desulfurization.

1.1. The Microorganisms

Thiobacillus thiooxidans is an acidophilic, aerobic, sulfur-oxidizing chemolithotrophic bacterium. Strain 8085 was obtained from the American Type Culture Collection, Rockville, MD. *Pyrodictium brockii*, an autotroph, and *Pyrococcus furiosus*, a heterotroph, are both hyperthermophilic, anaerobic, sulfur-reducing archaebacteria, capable of growth above 100°C (5,6,7). *P. brockii* strain DSM 2708 and *P. furiosus* strain DSM 3638 were both obtained from the Deutsche Sammlung von Mikroorganismen, Gottingen, Federal Republic of Germany.

2. EXPERIMENTAL METHODS

2.1. Coals

Samples of four different coals were used in this study. Indiana no. 5 (IBCSP sample no. 6) and Illinois no. 6 (IBCSP sample no. 1) coals were obtained from C.W. Cruse, Director of the Illinois Basin Coal Sample Program. Victorian brown coal (Australia) was obtained from D.J. Allardice, Coal Corp. of Victoria, through L. Atherton of the Electric Power Research Institute. A waste coal from Indiana (bog coal) was obtained from R. Narayan, Purdue University.

2.2. Coal Biodesulfurization Experiments

2.2.1. Thiobacillus thiooxidans. Coals to be used in these experiments (200-400 mesh) were sterilized by heating in a vacuum oven at 85°C for one hour on each of three successive days. Coal (0.5 to 1.5 g) was aseptically added to 50 ml of the sterile low sulfate medium (minus elemental sulfur) in 250 ml conical flasks. The flasks were inoculated with an active culture of *T. thiooxidans* previously grown in the low sulfate medium containing elemental sulfur. Coals were tested in duplicate or triplicate flasks. Sterile controls and flasks containing cells and no coal were run with each experiment. Flasks were incubated at 28°C with shaking at 200 r.p.m. After sulfate concentrations leveled off (generally after one to two weeks), the difference in solution sulfate concentrations between inoculated and uninoculated flasks was determined. From this value the amount of elemental sulfur converted to sulfate was calculated.

2.3.2. Pyrodictium brockii and Pyrococcus furiosus. Coals to be tested (200-400 mesh) were washed with reverse osmosis water and then dried in an air oven at 70°C for about four hours. Coals were tested in the range of 0.2 to 2.0 % pulp density (w/v). Bottles were incubated quiescently at 98°C. Gas phase H_2S was assayed by syringe injections to a Varian 3700 gas chromatograph using a thermal conductivity detector, a 6-foot, packed Hayesep-N column, and a carrier gas flow rate of 30 cc/min (helium). The total amount of sulfide generated was estimated using Henry's Law. Cell densities were determined by direct count of periodically taken subsamples. The cells were stained with acridine orange and visualized on 0.2 μm filters using epifluorescence microscopy.

2.3. Chemical Determinations

Sulfate ion in solution was determined turbidimetrically using barium chloride precipitation (8). Total sulfur content in coals was determined using a modified high temperature method (9) employing a Leco (St. Joseph MI) furnace and automatic titrator. The method is based on an ASTM method for sulfur in petroleum products (10). NBS coal standard reference materials were used for system calibration. Forms of sulfur in coals (sulfatic, pyritic, organic) were determined using ASTM procedures (11). Elemental sulfur was determined chemically by extracting 0.5 g of coal with 25 ml of CS_2 at room temperature for at least 12 hr. The coal was removed by filtration and the CS_2 was evaporated to dryness. The residue was taken up in hexane and assayed for sulfur colorimetrically (12).

3. RESULTS

3.1. Sulfur Oxidation by *Thiobacillus thiooxidans*

The amount of sulfur in various forms in the test coals is shown in Table 1. Especially noteworthy is the very low level of pyritic sulfur in the Australian coal and the very high level of total and sulfatic sulfur in the bog coal. This latter coal is evidently very weathered.

Small amounts of sulfate above control values were produced when *T. thiooxidans* was incubated with Indiana and Illinois coal samples indicating low levels of elemental sulfur in these coals. No significant differences in sulfate concentrations were found between inoculated and uninoculated flasks containing the Australian brown coal. However, significant sulfate levels above control values were seen with the Indiana bog coal. Calculations of the elemental sulfur content in these coals based on sulfate production are shown in Table 2. Very little elemental sulfur was detected by bioassay in the first three coals, corresponding with the results of CS_2 extraction. About 1.2% (weight) sulfur as elemental sulfur was detected by bioassay in the bog coal. The total sulfur content in the bioprocessed bog coal was about 1% lower than sterile controls. This corresponded closely to the loss in "organic sulfur" from the coal (Table 2). By ASTM definitions, the organisms removed about 25% of the "organic sulfur" from the coal.

3.2. Sulfur Reduction by *Pyrodictium brockii*

Table 3 shows estimates of elemental sulfur content of the bog coal by bioassay. Liquid phase sulfide concentrations were estimated assuming the system was at equilibrium at the end of the experiment and using Henry's law to calculate dissolved sulfide concentrations. Since the pH of the sample was typically about 5.5, it was assumed that all dissolved sulfide was molecular hydrogen sulfide. The inoculated samples containing the bog coal typically yielded gas phase sulfide concentrations 4 to 5 times those obtained from uninoculated controls and inoculated samples containing no coal. Samples of other coals used in this study showed no biotic sulfide generation although bacteria could be grown in these samples if spiked with elemental sulfur (data not shown). It is interesting to note that the drop in ASTM organic sulfur levels of about 30-40% correspond well with the elemental sulfur estimate by bioassay.

3.3. Sulfur Reduction by *Pyrococcus furiosus*

Table 4 shows the activity of *P. furiosus* on the coal samples used in this study. Note that for pulp densities of 0.5% (weight), growth was strongest for the bog coal. In fact, significant amounts of sulfide production were noted only in that sample.

As can be seen, the level of sulfide production and cell yields are proportional to the amount of coal added to the medium. The three replicates at the 2% (weight) pulp density show that reproducibility in these experiments is good. The uninoculated with coal and inoculated without coal control bottles had only trace amounts of H_2S. These results strongly suggest that coal sulfur was used as a substrate by the cells.

Not reported are bioassay estimates of elemental sulfur in the bog coal. Unlike *P. brockii* which grows at a pH of 5.5, *P. furiosus* grows at a pH of about 7.0. Because sulfide levels in the liquid phase were not measured directly, estimates of dissolved sulfide levels at pH 7 or higher are more difficult to make. The liquid phase dissociation of molecular hydrogen sulfide must be accounted for. Nonetheless, initial estimates indicated that elemental sulfur in the bog coal based on sulfur reduction by *P. furiosus* was between 1% and 2% by weight. Direct solution sulfide analysis will improve these estimates.

4. DISCUSSION

Several reports of microbial removal of organic sulfur from coal have appeared in the literature. However, the definition of organic sulfur is not precise or universal. By ASTM methods, organic sulfur represents all sulfur that is not pyritic or sulfatic. If significant elemental sulfur occurs in coal or is produced during studies on coal biodesulfurization, the apparent success of organic sulfur removal will depend on the analytical scheme. By ASTM designations all three organisms used in this study removed significant (25-40%) amounts of the "organic" sulfur present in the bog coal. At the same time, in the other three coals, very little elemental sulfur was detected by bioassay or CS_2 extraction. In these coals, a loss of ASTM organic sulfur following bioprocessing (which we did not detect) would be interpreted as a loss of true organic (C-S) sulfur. It is important, therefore, that investigators determine if elemental sulfur is present in their test coals, or perhaps more important, if it forms during experimentation as a result of biotic and/or abiotic reactions.

A more complicated situation arises in consideration of data presented by Narayan et al. (4) suggesting the presence of polysulfides in coal which oxidize on weathering to produce free elemental sulfur. We have not yet determined with model compounds whether or not it is likely that *T. thiooxidans*, *P. brockii* or *P. furiosus* (or other microorganisms) can attack such polysulfide linkages directly. Experiments are needed to determine if oxidative treatment of coals leads to the production of elemental sulfur and if polysulfides are attacked by these or other microorganisms. If such forms of sulfur are important in coals, there are very good prospects for their removal. However, the organisms which would remove this type of organic sulfur will be different from the organisms which would remove, for example, thiophenic sulfur.

Ultimately, definitions do not matter if the sulfur can be removed from coal. However, the choice of organisms and engineering designs will be quite different depending on the forms of sulfur that the organisms and their enzymes encounter.

5. ACKNOWLEDGMENTS

The authors would like to thank Linda Atherton (EPRI) for her interest and support of this research. The authors also thank R. Narayan (Purdue University) for supplying the bog coal samples used in this study.

6. REFERENCES

1. F. Kargi and J.M. Robinson. "Removal of organic sulfur from bituminous coal. Use of the thermophilic organism *Sulfolobus acidocaldarius*," *Fuel*, **65**, 391, 1986.
2. J.D. Isbister and E.A. Kobylinski. "Microbial Desulfurization of Coal." *Processing and Utilization of High Sulfur Coals*, Y.A. Attia, ed., Elsevier Science Publishers, Amsterdam, 1985, p. 627.
3. J.E. Duran, S.R. Mahasay, and L.M. Stock. "The Occurrence of Elemental Sulphur in Coals," *Fuel*, **65**, 1167, 1986.
4. R. Narayan, G. Kullerud, and Karl V. Wood. "A New Perspective on the Nature of *Organic* Sulfur in Coal." Division of Fuel Chemistry Preprints, 195th Meeting of the American Chemical Society, Toronto, Canada, June, 1988.
5. K.O. Stetter, H. Konig, and E. Stackebrandt. "*Pyrodictium gen. nov.*, a new genus of submarine disc-shaped sulfur-reducing archaebacteria growing optimally at 105°C." *Syst. Appl. Microbiol.*, 4, 535, 1983.
6. R.M. Kelly and J.W. Deming. "Extremely Thermophilic Archaebacteria: Biological and Engineering Considerations." *Biotechnol. Prog.*, in press.

7. G. Fiala and K.O. Stetter. "*Pyrococcus furiosus* sp. nov. represents a novel genus of marine heterotrophic archaebacteria growing optimally at 100°C." *Arch. Microbiol.*, **145**, 56, 1986.

8. ASTM Standard Test Method for Sulfate Ion in Water, *1986 Annual Book of ASTM Standards*, Vol. **11.01**, p. 700.

9. P.T.S. Pei and S.J. Weeks. "Methods and Procedures used at NBS to Certify Sulfur in Coal SRM's for Sulfur Content, Calorific Value, and Ash Content." T.E. Gills, ed., National Bureau of Standards, Gaithersburg, MD, 1984.

10. ASTM Standard Test Method for Sulfur in Petroleum Products, *1982 Annual Book of ASTM Standards*, Vol. **23**, p. 836.

11. ASTM Standard Test Method for Forms of Sulfur in Coal, *1987 Annual Book of ASTM Standards*, Vol. **5.05**, pp. 336-340.

12. J.K. Bartlett and D.A. Skoog, "Colorimetric Determination of Elemental Sulfur in Hydrocarbons." *Anal. Chem.*, **26**, 1008, 1954.

Table 1. Sulfur in Test Coals by ASTM Procedures (%)

	Total S	Sulfate S	Pyritic S	Organic S
Illinois No. 6	4.25	0.08	0.73	3.44
Indiana No. 5	3.91	0.12	1.57	2.22
Australian	4.35	0.63	0.03	3.69
Bog Coal	11.6	5.20	2.32	4.06

Organic S = Total S - Sulfate S - Pyritic S
(ASTM Method 5.05)

Table 2. Elemental Sulfur in Coals - Thiobacillus thiooxidans

			Total Sulfur Determinations (%)		
Coal Type	Total S (%)	S° (%) (bioassay)	After CS_2 extraction	After Thiobacillus thiooxidans	sterile
Ill. #6	4.25	0.02	4.29	3.97	3.84
Ind. #5	3.91	0.03	3.76	3.39	3.49
Aust.	4.35	trace	4.50	nt	nt
Ind. Bog	11.6	1.19	8.37	5.26	6.22

nt - not tested

Table 3. Pyrodictium brockii on Bog Coal

	Total S (wt %)	Sulfatic S (wt %)	Pyritic S (wt %)	Organic S (wt %)	S° (wt %) (bioassay)
sterile + cells (Low Inoc.)	5.97 4.22	0.09 0.14	1.82 1.81	4.06* 2.27 Δ = 1.79	1.62
sterile + cells (High Inoc.)	5.97 4.98	0.09 0.15	1.82 1.96	4.06** 2.87 Δ = 1.19	1.40

apparent organic sulfur removal: * 44.1% and ** 29.3% respectively

Table 4. Activity of Pyrococcus furiosus on Coal Samples

Coal Type	Pulp Density	Cell Growth	Gas phase H_2S Production (μmoles)
Illinois No. 6	5.0	+	trace
Indiana No. 5	5.0	+	trace
Australian	5.0	+	trace
	0.0	+	trace
Bog Coal	5.0	+	43.2
Bog Coal	10.0	++	72.4
Bog Coal	20.0	uninoc.	trace
Bog Coal	20.0	+++	104.4
Bog Coal	20.0	+++	100.8
Bog Coal	20.0	+++	108.9

Microbial Desulfurization of Dibenzothiophene

M. van Afferden, S. Schacht, M. Beyer, J. Klein
Bergbau-Forschung GmbH, Franz-Fischer-Weg 61,
D-4300 Essen 13, FRG

Abstract

Concerning the sulfur removal from coal before combustion there is considerable interest in microbial methods as pyrite oxidation and elimination of organically bound sulfur from coal. Using organic sulfur compounds relevant for coal the mechanism of desulfurization was investigated. We isolated a defined mixed culture (FODO) capable to utilize dibenzothiophene as sole sulfur source for growth, while benzoate was used as carbon source. The mixed culture FODO consists of an *Alcaligenes denitrificans* subspecies and a *Brevibacterium* species. Two metabolites of the degradation and dibenzothiophene-5-dioxide. The subsequent degradation of dibenzothiophene-5-dioxide used as sole sulfur source results in a release of sulfate ions into the medium. The results suggest a sulfur specific oxidative mechanism for removal of sulfur from dibenzothiophene.

Introduction

Coal combustion causes emissions such as dust, NO_x and SO_2, which, if not diminished, are of environmental concern. To prevent SO_2 emissions sulfur removal from coal before combustion can partly be achieved by mechanical and chemical processes (1). However, for future application microbial methods are judged to represent a possible tool for sulfur removal from coal (2;3). Coal contains, apart from pyritic sulfur, traces of sulfates nd elementary sulfur, a considerable amount of organically bound sulfur. This so-called organic sulfur is an element of the chemical coal structure integrated as thiol, disulfide, sulfide or thiophene in the macromolecular coal matrix (4;5). Also the occurrence of sulfur organo metallic species is established for high sulfur coals (6). For the removal of organic sulfur by means of biotechnological methods covalent C-S bonds have to be cleaved. In consideration of the inhomogenous structure of the coal, the enzymes involved should therefore be specific for the sulfur of different sulfur bonding types (regiospecificity). Experience is still limited, concerning the metabolic pathway involved in the removal of reduced sulfur from coal relevant model compounds as dibenzothiophene (DBT). Early reports suggested, that in bacterial DBT degradation the thiophene nucleus remained untouched (9). However sulfate release by an oxidative bacterial attack on DBT is reported by Isbister and Doyle (7) and Kargi and Robinson (8).

This work contributes to the oxidative bacterial desulfurization of DBT, using DBT as sole sulfur source for bacterial growth.

Material and Methods

Chemicals

Dibenzothiophene (DBT) was purchased from Merck, Hohenbrunn, FRG; dibenzothiophene sulfone (DBT-5-dioxide), benzyl methyl sulfide, dibenzyldisulfide, dibenzylsulfinde, diphenylsulfide and poly (phenylene sulfide) from Aldrich-Chemie, Steinheim, FRG. Dibenzothiophene-5-oxide (DBT-5-oxide) was prepared as described by Gilman and Esmay (10). The product of the synthesis was contaminated with DBT and DBT-5-dioxide. Both of which were removed by high pressure liquid chromatography (HPLC). The identity of DBT-5-oxide was confirmed by GC-MS, the purity (98.3% DBT-5-oxide contaminated with 1.7% DBT-5-dioxide) by HPLC and GC. All other chemicals were obtained at the highest purity from commercial sources.

Apparatus and Analytical Methods

DBT was quantitatively removed from bacterial culture fluid by extracting with CH_2Cl_2 using equal volumes. DBT quantification was carried out by gaschromatography (Varian, mod. 3400, Darmstadt, FRG) using a Chrompack Sil 5 capillary column (25mX0.22mm) and a flame ionization detector with the following oven temperature program: 80°C for 5 min, 10°C/min to 300°C which was held for 5 min.

For metabolite characterization, samples of culture fluid were prepared by centrifugation at 10,000 g for 15 minutes to remove particles and cells. Metabolites of DBT degradation in the supernatant were detected at 220 nm or 290 nm after high pressure liquid chromatography (HPLC) using following equipment: Liquid chromatograph 655A-11 with autosampler (Merck, Darmstadt, FRG) and variable wavelength monitor (Knauer, Bad Homburg, FRG); columns (Knauer): length 250 mm, internal diameter 4 mm or 16 mm filled with LiChrosorb RP8 particles (Merck) of 5 um in diameter; solvent system: 50% acetonitril (v/v), 50% water (v/v) containing 0.12% H_2PO_4 (v/v).

Cochromatography was carried out with synthesized DBT-5-oxide and authentic DBT-5-dioxide at approx. the same concentrations as the metabolites.

For identification of metabolites the UV-spectra (spectrophotometer: Shimadzu UV-210 A, Langenfeld, FRG) were compared with authentic DBT-5-dioxide.

GC-MS analyses were performed with a double focussing mass spectrometer (Finnigan MAT-8200, EI 70 eV) and an INCOS datasystem. The determination of sulfate ion concentration in the culture fluid was routinely carried out by the method of Cypionka and Pfennig (11). Additionally sulfate and sulfite ion concentration are detected by ion chromatography (Dionex 2000-I). Growth of the cultures was monitored either spectrophotometrically by measuring the optical density at 578 nm with an Eppendorf photometer 1101 M (Eppendorf, Hamburg, FRG) or as protein using the Lowry method (12).

Media

Sulfur limitation required scrupulously cleaned glassware to prevent bacterial growth on contaminant sulfur. The medium consisted of a salt solution containing, per liter, 2.19 g NH_4Cl, 0.27 g KH_2PO_4, 0.2 g $MgCl_2$ x 6 H_2O, 0.1 g $Ca(NO_3)_2$ x 4 H_2O, 10 mg $FeCl_3$ x 6 H_2O and 1 ml of trace element solution. The medium was adjusted with 20 mM tris/HCl to pH 7.4 and was supplemented with 10 mM benzoate. The required amount of organic sulfur sources were put into culture tubes or flasks from stock solutions (DBT dissolved in diethyl ether, DBT-5-oxide/DBT-5-dioxide dissolved in CH_2Cl_2). AFter the organic solvents had been evaporated medium was added. The tightly closed culture tubes and flasks were sterilized at 121oC for 20 minutes. All organic sulfur sources used are stable as proved by GC and HPLC.

Enrichment and Isolation of Organisms

Enrichment of suitable microrganisms was achieved in a pneumatically operated percolator with external loop as described by Codner (13) containing 33% (w/w) sterilized postbog, 33% (w/w) raschig-rings and 33% (w/w) municipal sewage sludge as inoculum. To adapt the microbial population selectively to organic sulfur compounds, the percolator was supplemented with dibenzothiophene, benzyl methyl sulfide, dibenzyldisulfide, dibenzylsulfide, diphenylsulfide and poly(phenylene sulfide) at concentrations of the percolator fluid were incubated at 30°C on a rotary-shaker at 170 rpm in 10 ml screw-cap culture tubes (3 ml medium) with DBT (200 uM) as sole sulfur source and glucose (10 mM), glycerol (10 mM) or benzoate (10 mM) as carbon source. The isolation of organisms was carried out as described by Cook and Hutter (14), the vitamine soluation being omitted. Bacterial isolates were characterized according to their gram reaction, fatty acid composition and physiological parameters in part by DSM (Braunschweig, FRG).

2.5 Isolation of Metabolites

Cells were removed from the culture fluid by centrifugation (10,000 g, 15 min) and the supernatant was acidified to a final concentration of 0.1 M HCl and extracted with CH_2Cl_2 (1:1 v/v). After concentrating the organic phase to approximately 1% of the original volume the preparation was used for GC-MS analyses. Samples for isolation of metabolites by HPLC were transferred to the aqueous phase again.

Results and Discussion

Isolation and Characterization of Organisms

After simultaneous adaption of an enrichment culture to several organic sulfur compounds using a percolation equipment one stable bacterial mixed culture was obtained from percolator liquid. This culture was able to grow with DBT as sole sulfur source and benzoate as sole carbon source. Without sulfur source bacterial growth was strongly limited. Analogous enrichment procedures with glucose or glycerol as carbon source were not successful. After numerous isolation steps, a two species community (FODO) was obtained. The two organisms could be distinguished by the morphology of their colonies. On nutrient broth (NB) agar plates growth of organism FO (feeding organism) was always superior compared to organism (DO) degrading organism). Pure cultures of strain DO on NB agar plates formed very small and transparent colonies (diameter 0.5 - 1 mm, 30°C, 3 d), whereas colonies growing together with strain FO on the same plate are lightly yellow with a diameter of 4-5 mm (30°C, 3 d). This effect could be due to the need of diffusable nutrients or vitamines by strain DO.

Pure cultures of each strain were not able to grow with DBT as sole sulfur source.

Strain FO was identified as a non-motile subspecies of *Alcaligenes denitrificans* and strain DO as a non-motile *Brevibacterium* species.

Physiology of growth

The mixed culture FODO cultured with DBT (200 uM) as sole sulfur source and benzoate as carbon source grew with a doubling time of 8.5 h at the pH optimum of 7.4.

A molar growth yield of 9.8 kg protein per mol of sulfur was obtained with low concentrations (1-30 uM) of DBT or sulfate as sulfur source (Fig. 1). This indicates that the DBT-sulfur was as accessible to the culture as sulfate.

Comparable ranges of molar growth yields are described by Cook and Hutter (14) for bacteria, isolated from sewage and soil.

Table 1 showed that bacterial growth and DBT-degradation remained almost constant, in spite of sulfate in varying concentrations (0-100 uM) was present as a second sulfur source. This indicates that at least the first step in DBT degradation is not repressed by sulfate.

Catabolism of DBT

The bacterial mixed culture FODO was grown on DBT (200 uM) with benzoate as carbon source. In the course of bacterial growth DBT was degraded to a final concentration of 71 uM concomitant to growth. In parallel sterile controls the DBT concentration remained unchanged.

Furthermore the formation of two metabolites of DBT degradation was observed (Fig. 2). The metabolite occurring first was identified by GC-MS and cochromatography (HPLC) as DBT-5-oxide. The second metabolite was identified by cochromatography (HPLC) and UV-spectrometry as DBT-5-dioxide (Fig. 3 and Tab. 2). DBT-5-oxide was produced concomitant to bacterial growth up to a final concentration of 42 uM after 80 h incubation. At the end of thelogarithmic growth phase production of DBT-5-dioxide was quantified as a final concentration of 18 uM (Fig. 2).

The yield of the products obtained, was about 46% of the amount which would be achieved by totally conversion of DBT to the concentration of about 15 uM sulfur is necessary for an optimal growth of the cells. Several organisms are able to accumulate sulfur intracellularly (15) but this seems not to be true with the mixed culture FODO because DBT grown cells, washed and incubated in sulfate free medium are strongly limited in growth due to sulfur depletion.

The discrepancy in sulfur balance implies that at least one other sulfur compound has to be accumulated during growth. However no sulfate, sulfite or other additional metabolite could be identified up to now.

In order to prove whether DBT-5-oxide and DBT-5-dioxide are utilized by the bacterial culture as sulfur sources too, growth experiments using this compound (25 uM) as sole sulfur source with benzoate as carbon source were carried out. As shown in Fig. 4 both the sulfoxide and the sulfone were degraded in the course of cell growth, whereas the growth of control cultures without any sulfur source was negligible.

Using high concentrations of DBT-5-dioxide (2 mM) as sole source of sulfur with benzoate as carbon source, in the

stationary phase of growth 21.2% (424 uM) of DBT-5-dioxide was degraded and a concentration of 200 uM sulfate, but no sulfite was detected in the supernatant culture fluid. In sterile controls neither sulfate nor sulfite could be measured. Considering the amount of 15 uM sulfur the bacterial cultures needed for optimal growth, these results confirm the aforementioned hypothesis, that at least one additional unknown sulfur compound accumulates.

Further investigations are directed to isolate this "missing sulfur compound" and the first sulfur free metabolite to examine the C-S bond cleavage occurring in the desulfurization of DBT.

The presented data indicate a sulfur specific attack on DBT by a bacterial two species community which utilizes DBT as sole source of sulfur. We propose that sulfur elimination proceeds via the corresponding sulfoxide and sulfone (Fig. 5).

This is the first report of the bacterial degradation of DBT serving as sulfur source, though similar reactions have been reported: The microbial oxidation of thiophenes to the corresponding sulfoxides and sulfones is reported by Holland et al (16) and Fedorak et al (17), but no further degradation could be achieved. Kaufmann and Kearney (18) reported on the degradation of a methylthio-S-triazine by soil bacteria. The desulfurization of this organic sulfide proceeds through the sulfoxide and the sulfone whereby methyl sulfonic acid is suspected to be an intermediate (14). A *Pseudomonas* species is described to desulfurize DBT by cooxidation with benzoate by Isbister and Doyle (7). Using DBT as carbon and energy source for growth of *Sulfolobus acidocaldarius* sulfate release was measured by kargi and Robinson (8). However biochemical reactions of the aforementioned DBT degradation are not reported in detail, the initial attack may be of similar type as presented in this work. This initial reaction occurring in DBT degradation (Fig. 5) support the approach to develop specific mechanisms for microbial removal of organically bound sulfur from coal.

Acknowledgements: We thank the Department of Coal and Environmental Analytics (Bergbau-Forschung GmbH) for performing mass spectra and ion chromatography. Park of this work was supported financially by the Bundesminister fur Forschung and Technologie (BMFT, 03E-6215-A).

References:

1. Stanbaugh, E., In: Kirk Othmer, "Enzymcolopedia of Chemical Technology," (R.E. Kirk, O.F. Othmer, M. Grayson and D. Eckroth, eds), 3rd ed, Vol. 6, Wiley, New York, pp 306-324 (1979).

2. Olson, G.J. and Brinkman, F.E. "Bioprocessing of Coal," Fuel, 65, 1638-1646 (1986).

3. Couch, G.R. "Biotechnology and Coal," IEA Coal Research, London (1987).

4. Markuszewski, R., Fan, C.W., Greer, R.T. and Wheelock, T.D. "Evaluation of the Removal of Organic Sulfur from Coal," In: Symposium on New Approaches in Coal Chemistry, Americal Chemical Society, Pittsburgh, PA, USA (1980).

5. Boudou, J.P., Bouleque, J., Malechaux, L., Nip, M., de Leeuw, J.W. and Boon, J.J. "Identification of Some Sulphur Species in a High Organic Sulphur Coal," Fuel, 66, 1558-1569 (1987).

6. Baruah, M.K. and Upreti, M.C. "Accumulation of Organic Sulfur in Coal," J. Scient. Ind. Res., 45, 17-20 (1986).

7. Isbister, J.D. and Doyle, R.C. "Mutant Microorganism and Its Use in Removing Organic Sulphur Compounds," United States Patent (No. 4., 562, 156) (1985).

8. Kargi, F. and Robinson, J.M. "Microbial Oxidation of Dibenzothiophene by the Thermophilic Organism Sufolobus acidocaldarius," Biotechnol. Bioeng. 25, 687-690 (1984).

9. Kodama, K., Umehara, K., Shimizu, K., Nakatani, S., Midoda, Y., and Yamada, K. "Identification of Microbial Products for Dibenzothiophene and Its Proposed Oxidation Pathway," Agr. Biol. Chem., 37(1), 45-50 (1973).

10. Gilman, H. and Esmay, D.L. "The Oxidation of Dibenzothiophene and Phenoxathin with Hydrogen Peroxide," J. Am. Chem. Soc., 74, pp 2021-2024 (1952).

11. Gypionka, H. and Pfenning, N. "Growth Yields of Desulfotomaculum orientis with Hydrogen in Chemostat Culture," Arch. Microbiol., 143, 396-399 (1986).

12. Lowry, O.H., Rosebrough, N.J., Farr, A.L. and Randall, R.J. "Protein Measurement with the Folin Phenol Reagent," J. Biol. Chem., 193, 265-275 (1951).

13. Codner, R.C. "Solid and Solidified Growth Media in Microbiology," In: Methods in Microbiology (J.R. Norris, D.W. Ribons, eds), Vol. 1, Academic Press, New York, London, pp 427-454 (1969).

14. Cook, A.M. and Hutter, R. "Ametryne and Prometryne as Sulphur Sources for Bacteria," Appl. Environ. Microbiol., 43, 782-786 (1982).

15. Schlegel, H.G. "Allgemeine Mikrobiologie," Thieme, Stuttgart, New York, 5th ed. (1981).

16. Holland, H.L., Khan, S.H., Richards, D. and Riemland, E., "Biotransformation of Polycyclic Aromatic Compounds by Fungi," Xenobiotica, 16 (8), 733-741 (1986).

17. Fedorak, P.M. Payzant, J.D., Montgomery, D.S. and Westlake, D.W. "Microbial Degradation of n-Alkyl Tetrahydrothiophenes Found in Petroleum," Appl. Environ. Microbiol., 54, 1243-1248 (1988).

18. Kaufmann, D.D. and Kearney, P.C., In: Herbicides, Physiology, Biochemistry, Ecology, 2nd ed., 2, (L.J. Andus, ed.), Academic Press, Inc., New York, 29-64 (1976).

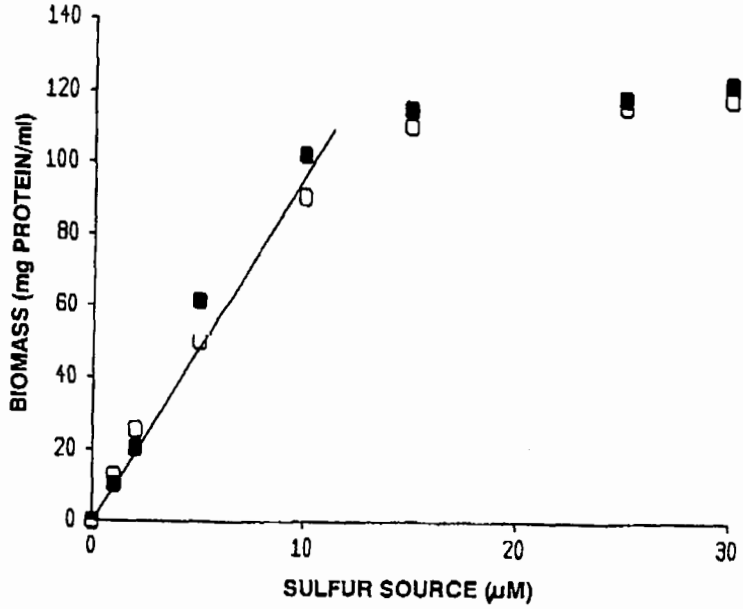

Figure 1: Biomass production at the stationary growth phase of the mixed culture of *Alcaligenes denitrificans* and *Brevibacterium* sp. at different concentrations of sulfur sources. ▢ dibenzothiophene, ■ sulfate

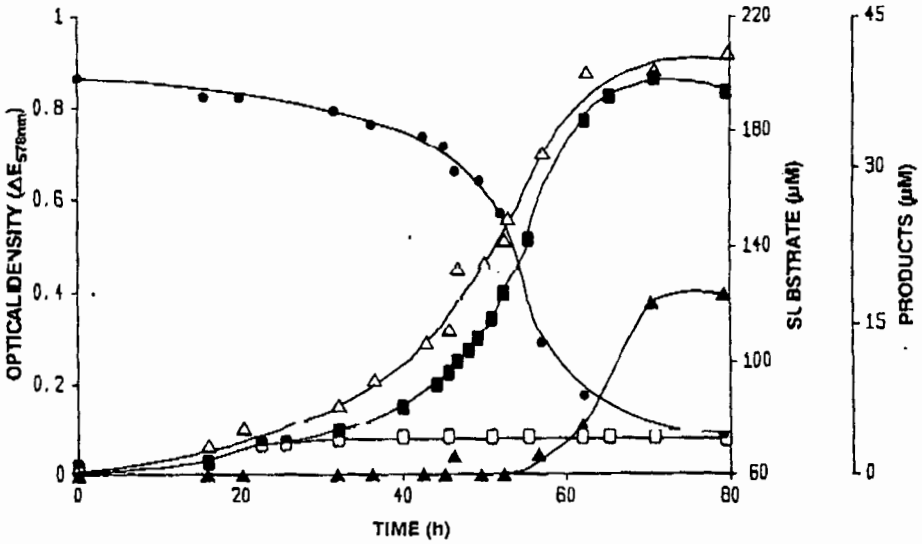

Figure 2: Growth of the mixed culture of *Alcaligenes denitrificans* and *Brevibacterium* sp. with dibenzothiophene as sole sulfur source and benzoate as carbon source. ■ optical density, ▢ optical density without sulfur source added, ● dibenzothiophene, △ dibenzothiophene-5-oxide, ▲ dibenzothiophene-5-dioxide.

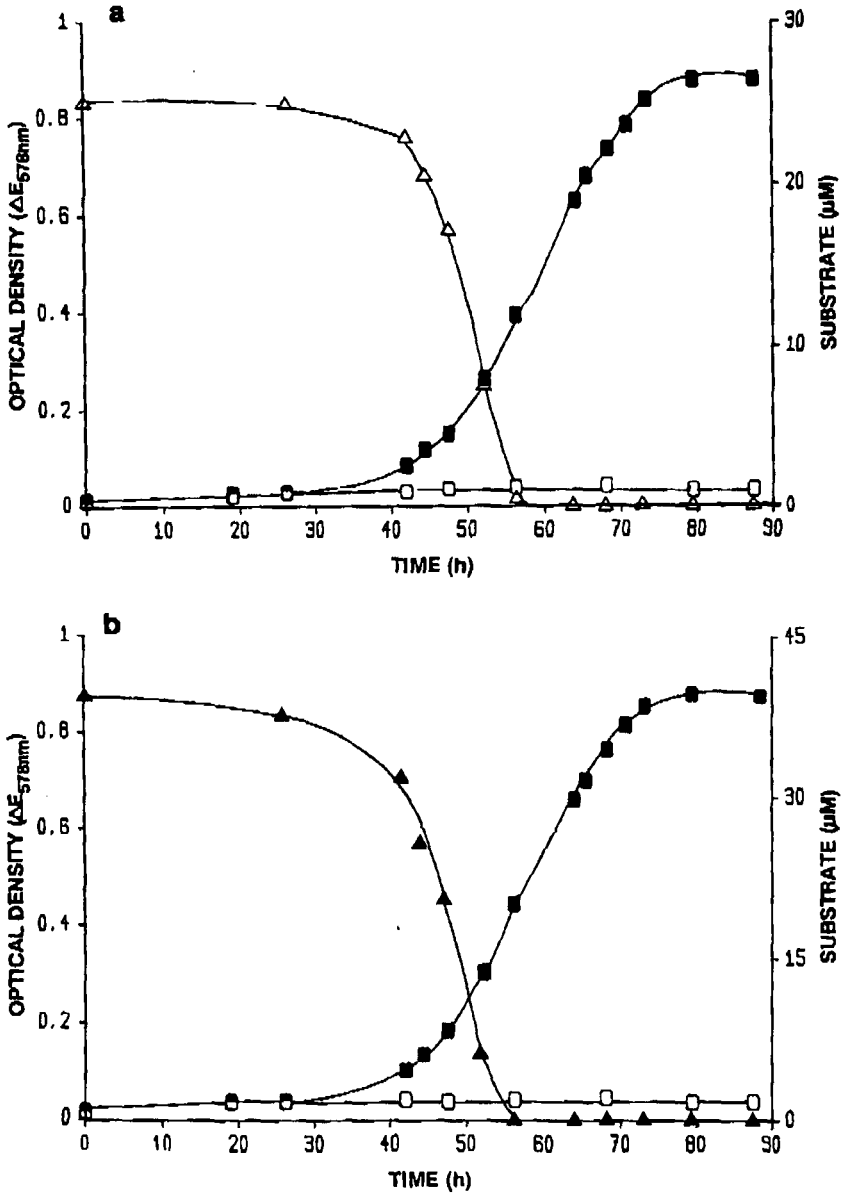

Figure 4: Growth of the mixed culture of *Alcaligenes denitrificans* and *Brevibacterium* sp. with dibenzothiophene-5-oxide (a) and dibenzothiophene-5-dioxide (b) as sole sulfur source and benzoate as carbon source. ■ optical density, □ optical density without sulfur source added, △ dibenzothiophene-5-oxide, ▲ dibenzothiophene-5-dioxide.

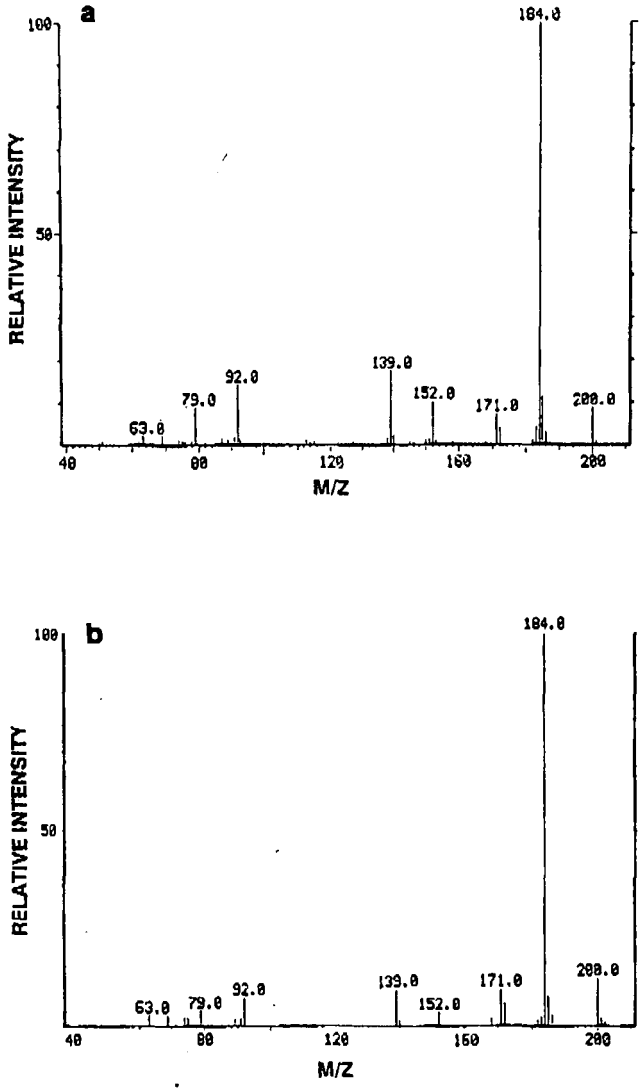

Figure 3: Mass spectra of (a) dibenzothiohpene-5-oxide produced from dibenzothiophene by the mixed culture of *Alcaligenes denitrificans* and *Brevibacterium* sp. and (b) authentic dibenzothiophene-5-oxide (library search).

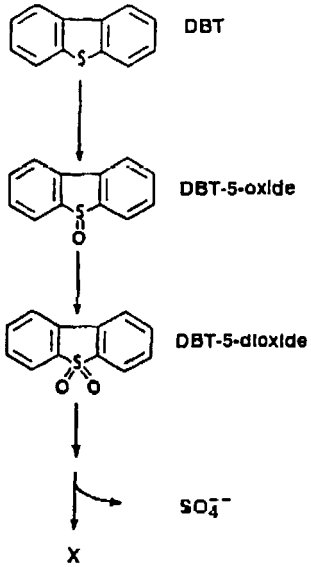

Figure 5:
Proposed initial reactions of the desulfurization of dibenzothiophene (DBT) by the mixed culture of *Alcaligenes denitrificans* and *Brevibacterium* sp..

Table 1: Utilization of dibenzothiophene (100 µM) by the mixed culture of *Alcaligenes denitrificans* and *Brevibacterium* sp. with benzoate as carbon source in presence of various amounts of sulfate.

Sulfate (µM)	optical density (E_{578nm})	dibenzothiophene degradation (%)
0	0.96	85.5
2	1.01	84.5
5	1.02	80.9
10	0.92	90.0
15	1.01	79.5
30	0.96	84.5
50	0.99	91.8
100	1.00	89.6

Table 2: Identification of metabolites fron dibenzothiophene (DBT) released during growth of mixed culture of *Alcaligcnes denitrificans* and *Brevibacterium* sp.

Product	Cochromatography* retention time (min)	UV-spectrometry** maxima (nm)
DBT-5-oxide	5.1	not assayed
DBT-5-dioxide	7.1	236/244/280/292/322

* HPLC, retention times are identic with authentic chemicals
** Maxima are identic with authentic DBT-5-dioxide

COAL DESULFURIZATION THROUGH REVERSE MICELLE BIOCATALYSIS PROCESS

by Kwang-Il Lee and Teh Fu Yen

University of Southern California

Department of Civil and Environmental Engineering

Los Angeles, California 90089-0231

ABSTRACT

A novel bioprocess using micelle biocatalysis has been attempted to minimize several disadvantages of conventional microbial coal desulfurization scale-up processes. The reverse micelle biocatalysis process consists of a water-immiscible organic medium, a surfactant, an aqueous phase and sulfur-oxidizing bacteria or enzymes. This process has been successful for removing sulfur from bituminous coal (Illinois coal #5). The preliminary results showed that coal desulfurization through the use of cell-free enzyme extracts of Thiobacillus ferrooxidans ATCC 19859 was better than that of bacteria itself. The use of enzymes has shown potential for commercial coal desulfurization processes as well. This same process is being applied to the thermophillic bacteria Sulfolobus acidocaldarius ATCC 33909. The implications of these experimental results will be discussed, including a hypothetical mechanism using reverse micelle biocatalytical process for coal desulfurization

INTRODUCTION

Since coal utilization as an alternative energy resource is associated with SO_2 emission, causing acid rain and acid fog during stages in the combustion process, there has been a great interest in the desulfurization of coals.

Microbial desulfurization methods are given great amounts of attention because biological removal of sulfur compounds prior to combustion of coals requires low capital and operating costs. Several researchers have demonstrated the feasibility of sulfur removal from pulverized coals by sulfur-oxidizing bacteria. However, this bacterial desulfurization process has not yet been applied on

a commercial scale. This is partically due to the fact that the reaction rate in the bacterial process in comparatively slow, and the microbial cells must be in physcial contact with pyrite to decompose it[1,2]. In order to overcome these barriers, a new desulfurization process is needed.

During the last decade, there has been a rapid growth of the application of biocatalysts (whole cell, purified enzymes and cell organelles) in non-aqueous media. Recent research has revealed that the reverse micellar system -- solvent/surfactant/water -- affords protein solubilization and enzymatic chemical reactions[3,4,5]. Of special interest is the reversed micelle solution (oil/nonionic surfactant/water) which may generate large swollen micelles (globules). The "water pools" of the reversed micelle created by large head groups of the non-ionic surfactants might be used as a "microreactor."

The objective of this work is directed not only to investigate catalytic oxidation of ferrous ion by biocatalysts (bacteria and cell-free enzyme extracts) entrapped in the water pools of the reversed micellar system, but also to provide feasibility of sulfur removal from coal. We will describe here our preliminary results on the iron oxidation via reverse micelle biocatalysis, and on bituminous coal desulfurization.

EXPERIMENTAL

Pure cultures, Thiobacillus ferrooxidans ATCC 19859 and Sulfolobus acidocaldarius ATCC 33909, were obtained from the American Type Culture Collections and routinely maintained[6,7]. Cells were harvested after they were four days old, suspended in distilled water (pH 2.6 with H_2SO_4), and allowed to stand in the refrigerator. The resulting supernatant fluid was carefully collected, brought to a volume of 30 ml with distilled water (pH 2.8), centrifuged and stored in the refrigerator. 10 ml of stored cell suspensions (0.02 g/ml, dry weight) were sonicated in glycine-SO_4 buffer solution (pH 2.8) for one hour so that cell-free enzyme extracts were prepared.

The reversed micellar system included 0.01% nonionic surfactants (Tween 80) in mineral oil (light) (wt/vol) and 1% water phase (vol/vol). The appropriate rates of blowing air in the reversed micellar system were 40 ml m^{-1} at room temperature.

To measure a change of concentration of ferrous ion in the reversed micelle, the ferrous oxidation measurement described by Tamura et al.[8] was adopted. A stable complex of Fe^{2+} having color density by 1,10-phenanthroline assay was determined at 510 nm with the spectrophotometer (Figure 1).

Table 1. Sulfur content of Illinois coal #5

	PYRITIC %	SULFATIC %	ORGANIC %	TOTAL %
SULFUR	1.82	0.03	2.50	4.35

For this study, an Illinois #5 coal sample was collected from the Burning Stat #4 mine in Illinois. This sample was reported to hold 4.35% total sulfur (Table 1). An Illinois coal #5 was crushed and ground to 100 mesh. The obtained coal powder was slowly poured into the mineral oil containing 0.01% non-ionic surfactant (wt/vol). Then, bacteria and respective media (pH 2.4) were added into the organic phase. The mixed multiphase solution was sonicated and vigorously agitated. After incubation, coal particles were collected by centrifuge and washed with hexane and hot water to remove possible oil associated with the coal particles. The washed coal samples were dried and the content of total sulfur was assessed.

RESULTS & DISCUSSION

The iron assay at 510 nm shows a significant decrease of Fe^{2+} ion complex in the reverse micellar system containing the cell-free enzyme extracts of T. ferrooxidans (Figure 2). The Fe^{2+} level was rapidly dropped during the initial one hour; this could be due to enzymatic compounds responsible for iron oxidation entrapped in the water core of the reversed micelle. Such compounds could be a copper protein, rusticyanin and a Fe (II)-oxidizing enzyme from T. ferrooxidans. The result that iron could be oxidized by reversed micelle biocatalyst would support a feasibility of this system for the coal desulfurization process.

Figure 3 shows the data of total sulfur removal by the reverse micelle system. It was observed that there was about 13% total sulfur loss in coals (control) washed with solvent hexane and hot water, when comparing them with raw Illinois coal. The reason for that could be dissolution of elemental sulfur present in coal by solvent and hot water. It was positively observed that sulfur was removed from coal by the sulfur-oxidizing bacteria in the reverse micelle system. Remarkably, more than 37% of the total sulfur removal was found in the coals treated during a 24 hour period with the cell-free enzyme extracts reverse micelle system. It should be pointed out that the desulfurization reaction time by the cell-free enzyme extracts was comparatively very short. Also, the rate of sulfur removal by the cell-free enzyme extracts of Thiobacillus ferrooxidans was much higher than that of the bacteria. We therefore intrepret the preliminary results as showing that mineral oil/non-ionic surfactant/water allow protein solubilization and catalytic reaction. Hence, a reverse micelle biocatalysis seems to be a promising coal desulferization process. Further studies are being conducted with the thermophilic bacteria S. acidocaldarius. The implications of these results will be addressed.

ACKNOWLEDGEMENTS

We acknowledge Energy and Environmental Labs, Inc. for partial support.

REFERENCES

1. Andrews, G.W. and J. Maczuga, "Bacterial Coal Desulfurization," the 4th Symposium on Biotechnology in Energy Production and Conversion, Gatlinburg, Tenessee, May 11-14, (1982).

2. Hoffmann, M.R., B.C. Faust, F.A. Panda, H.H. Koo and H.M. Tsuchiya, "Kinetics of the Removal of Iron Pyrite from Coal by Microbial Catalysis," Appl. Environ. Microbiol., 42, 259-271 (1981).

3. Luisi, P.L. and C. Laane, "Solubilization of Enzymes in Apolar Solvents via Reverse Micelles," TIBTECH, 153-161, June (1986).

4. Kadam, K.L., "Reverse Micelles as a Bioseparation Tool," Enzyme Microb. Technol., 8, 266-273, (1986).

5. Goklen, K.E. and T.A. Hattan, "Protein Extraction Using Reverse Micelles," Biotechnology Progress, 1(1), 69-74, 1985.

6. Silverman, M.P. and D.G. Lundgren, "Studies on the Chemoautotropic Iron Bacterium Ferrobacillus Ferrooxidans," J. Bacteriol., 77, 641-647 (1959).

7. Kargi, F. and J.M. Robinson, "Removal of Sulfur Compounds from Coal by the Thermophilic Organism Sulfolobus acidocaldarius," Appl. Environ. Microbiol., 44, 878-883, (1982).

8. Tamura, H., K. Goto and M. Nagayama, "Spectrophotometric Determination of Iron (II) with 1,10-phenanthraline in the Presence of Large Amounts of Iron (III)," Talanta, 21, 314-318 (1974).

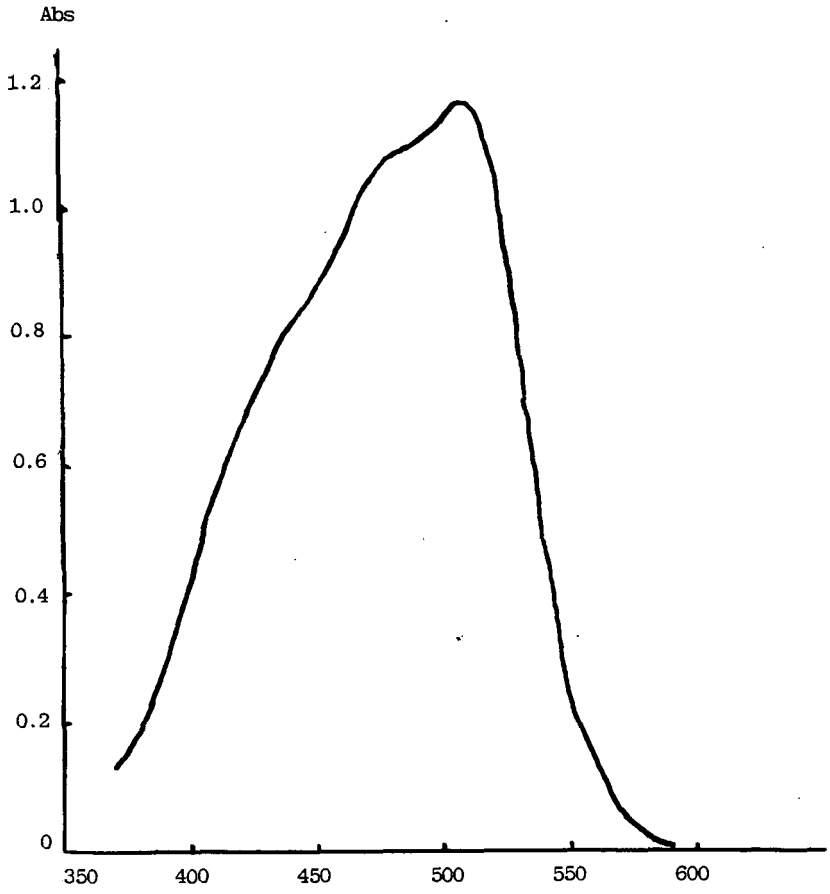

Figure 1. Absorption spectrum of 1,10-phenanthroline-iron complex extracted from reverse micelle system.

Figure 2. Iron oxidation via reverse micelle biocatalysts.

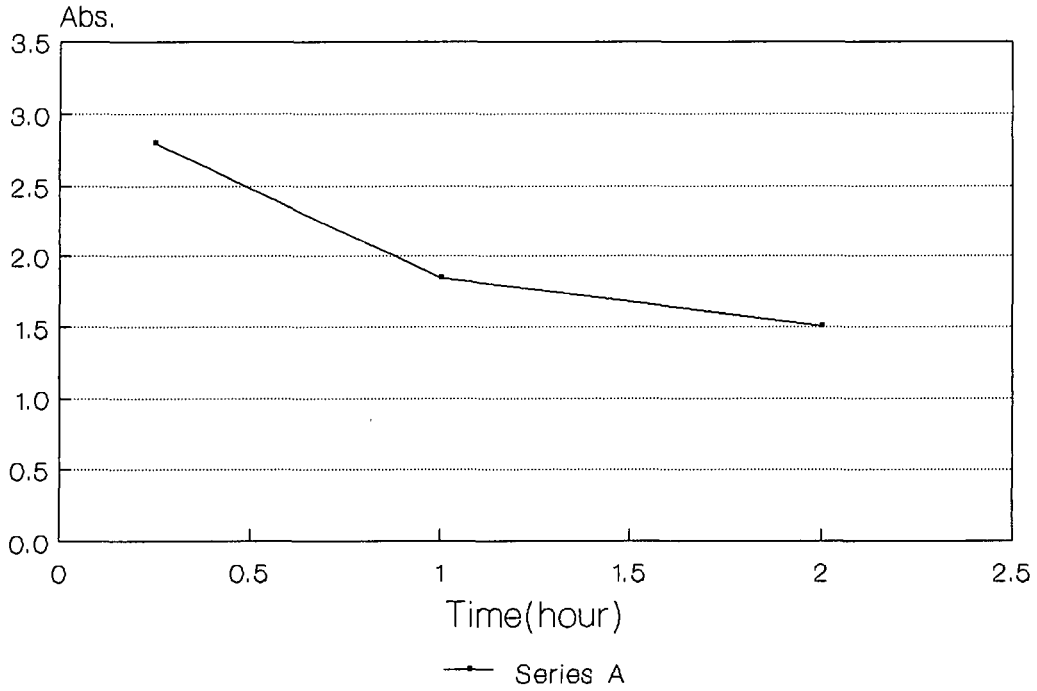

Cell-free enzyme extract of Thiobacillus

Figure 3. Coal desulfurization via reverse micelle biocatalysts.

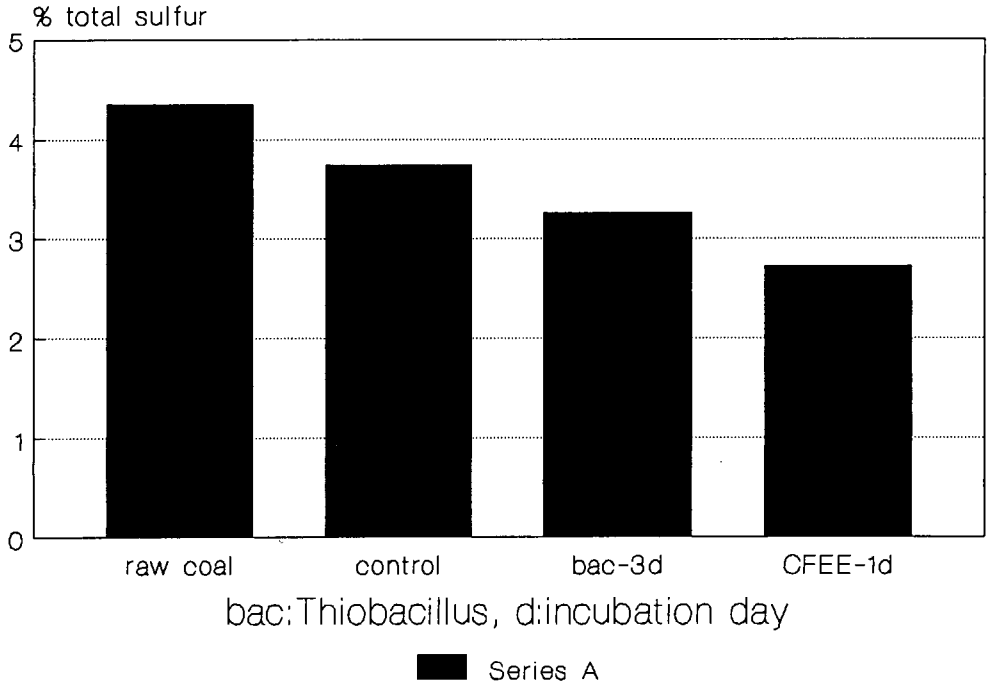

CFEE:cell-free enzyme extract

EFFECTS OF MULTIVALENT CATIONS FOUND IN COAL ON ALKALI- AND BIOSOLUBILITIES

David R. Quigley, Cynthia R. Breckenridge and
Patrick R. Dugan
Idaho National Engineering Laboratory
Biotechnology Group
Idaho Falls, ID 83415

and

Bailey Ward
Department of Biology
University of Mississippi
University, MS 38677

ABSTRACT

Extraction of low-rank coals with dilute hydrochloric acid resulted in the removal of a small percentage of total ash present. Calcium, and to a lesser extent,aluminum, magnesium and iron were present in acid extracts. Resulting coals were significantly more soluble in dilute alkali and more readily biosolubilized than water treated controls. These data suggest that some of the multivalent cations are present in coals as alkali insoluble complexes and contribute to the structural integrity of the coal.

INTRODUCTION

Since the observations of microbial coal solubilization in the early 1980's (1,2), there has been considerable interest in those mechanisms involved. Two mechanisms have been reported to be involved in coal biosolubilization: direct enzyme attack and production of alkaline materials. Enzymes implicated in the biosolubilization process include lacasses (3), ligninases (4), and peroxidases (4). Unfortunately, the degree of involvement of any of these enzymes in coal biosolubilization has yet to be rigorously demonstrated. Microbial production of alkaline materials which are able to solubilize coals has been clearly demonstrated (5-8). These alkaline materials appear to be nitrogenous in nature and increase medium pH sufficiently to cause coal solubilization. This mechanism does not appear to alter coal molecular structure.

There is now suggestive evidence that a third mechanism is involved in coal biosolubilization. This mechanism involves the removal of multivalent metal ions resulting in coal becomming more soluble in dilute alkali. In this paper, we report how the removal of small amounts of ash present in coals dramatically increases coal alkali- and biosolubilization.

EXPERIMENTAL

Texas lignite was obtained from Northwestern Resources, Jewett, TX. Wyodak and Beulah Zap coals were from the Argonne Premium coal sample program, Argonne IL. Mississippi Wilcox lignite was obtained from a

weathered outcrop as previously described (9). Texas and Wilcox lignites were ground to -100 mesh and stored under a nitrogen atmosphere. Wyodak and Beulah Zap coals were recieved preground to -100 mesh and packaged under an inert atmosphere. While under a nitrogen atmosphere, coals were dried (50°C for 48 hours) and aliquots (1g) were extracted with either water or 6N HCl (50ml). Extractions were performed by shaking (140RPM) at ambient temperature (22±2°C). Coals were recovered by centrifugation (10,000xg for 10 min)and washed using deionized water until the pH of the wash water exceeded 3.0. Solubilities of coals in dilute alkali were determined by placing coal aliquots (1g) in 50mM Tris buffer (pH 8.0, 100ml), shaking (140RPM) for 72 hours and measuring the absorbance of the filtered fluid (Gelman GA-8 SUPOR, 0.2μM pore dia.) at indicated wavelengths.

Fungal strains RWL-40 (unidentified Basidiomycete) and YML-1 (Cunninghamella sp.) (9) were grown and maintained on yeast-malt agar slants at room temperature. Biosolubilization was tested by placing coal aliquots (0.5g) in late log cultures of each organism growing in yeast malt broth and monitoring the amounts of coal going into solution as a function of time. The amount of coal solubilized was estimated by measuring the absorbance of filtered culture fluids at indicated wavelengths.

Ultimate and proximate analyses were performed at the Fuel Characterization Laboratory, University of Utah, Salt Lake City, UT. Element analyses were performed on an ARL Model 3520 Atomic Absorption Spectrophotometer using the ICP mode.

RESULTS AND DISCUSSION

Preliminary drying at 50°C under nitrogen did not appear to oxidize coal samples, but did reduce coal moisture content to a consistent 3-6% (data not shown). Extractions of coals with 6N hydrochloric acid likewise did not result in significant increases in coal oxygen content as compared to water extracted controls (Table 1). These data indicate that no significant amounts of either acid catylized hydrolysis (e.g., ethers, esters, etc.) or oxidation occured. Acid extraction of coals reduced total ash content by a consistant 2-5% and appeared to be independent of original ash content. It is unlikely that any of the ash reduction is due to decreasing pyrite content because sulfur contents remain essentially unchanged.

Acid extracts of coals were a deep yellow or yellow-green color and contained a relatively large amount of calcium and lesser amounts of magnesium, aluminum, iron (Table 2). Sodium and potassium were also present. Very low concentrations of metals were observed in controls (water extracts). The total amount of metals observed in each acid extract was between 60% and 180% of the decrease in ash content caused by acid extraction.

Extraction of coals with hydrochloric acid significantly enhanced the amount of coals soluble in pH 8 buffer (Table 3). Initial amounts of coal solubilized were 145% to 675% greater for acid extracted coals than for water washed controls. In all cases, except for Wilcox, increased solubilities of acid extracted coals continued to be observed in all

subsequent extractions. That is, it did not appear to be the case that each acid and water extracted coal had the same total alkali solubility and that the former was initially more readily solubilized.

Treatment of coals with microbial cultures yielded mixed results. Both organisms used produced a yellow pigment with an absorbance maximum at 400nm and little absorbance at 500nm in controls that did not contain coal (data not shown). Because of this, biosolubility experiments were monitored by following absorbances at at 500nm. As control cultures aged, however, the pigment present began to change and absorb more at 500nm.

Mississippi Wilcox lignite was more readily biosolubilized than those other coals tested and did not behave as did other coals. As observed with alkali solubilization, acid treated Wilcox was more readily biosolubilized than water treated controls (Figure 1). It is not likely that the increased biosolubility of acid treated Wilcox was due to an increase in the amount of alkali produced because pH values of cultures containing water extracted Wilcox were consistantly one half pH unit greater than those observed for the acid extracted coal (data not shown).

Cultures containing Texas lignite, Wyodak or Beulah Zap became lightly colored after several days of incubation and then lost color as the experiment proceeded (data not shown). The initial colored material in solution appeared to be solubilized coal. It is unknown if the decolorization of these culture media in the latter stages of incubation represents soluble coal being metabolized and supression of pigment formation or if solubilized coal and extracellular pigments were being removed from solution (e.g., coprecipitated, absorbed...). Since the pH of all cultures were increased and maintained at values greater than 7.5 (data not shown), it is unlikley that coals became insoluble due to pH effects. The net result was that absorptions at 500nm increased initially and then decreased sharply (data not shown). Initial increases in absorbances were small (less than 0.1 absorption unit) but were consistantly greater in cultures containing acid treated Texas lignite, Wyodak or Beulah Zap than those observed in controls.

From these data, it appears that the removal of multivalent metal ions significantly enhances both the alkali- and biosolubility of coals without causing measurable oxidation. It appears that low-rank coals have two types of ash present: peripheral and intergral. Peripheral ash would be that ash present as inclusions (e.g., pyrite, clays, etc.) while integral ash would be that which is incorporated into the molecular structure of the coal as metal complexed with organic components of the coal (e.g., carboxylic acids, phenols, alcohols or their sulfur analogs). The presence of multivalent cations present in coal structure as metal complexes is consistent with the suggested structure for other low-rank coals (10). These metal complexes would be less soluble in dilute alkali and, because multivalent cations are involved, they may act as crosslinks between organic molecules in coal. If this working hypothesis is correct, then removal of integral ash by any method will result in lower molecular weights of coal organics and larger populations of free carboxylic acids, phenols and alcohols which will result in increased coal solubilities and greater opportunity for enzyme attack (bioconversion).

While alkali solubility has been shown to be a mechanism in coal biosolubilization, pyrolysis-mass spectral data has suggests that there may be another mechanism involved (11). This other mechanism may involve direct enzyme attack or it may involve the removal of metal ions by microbes. The illucidation of this other mechanism will be the subject of a subsequent manuscript.

ACKNOWLEDGEMENTS

We thank Mr. J. E. Wey and D. A Johnson for their expert technical assisstance. This work was supported by Department of Energy Contract No. DE-AC07-76ID01570.

REFERENCES

1) Fakoussa, R. M. 1981. Ph.D. Thesis, Freidrich-Wilhelms University, Bonn, Federal Republic of Germany.

2) Cohen, M. S. and Gabriele, P. D. 1982. Appl. Environ. Microbiol. 44:23-27.

3) Pyne, J. W., Stewart, D. L., Fredrickson, J. and Wilson, B. W. 1987. Appl. Environ. Microbiol. 53:2844-2848.

4) Scott, C. D. and Lewis, S. N. 1988. Appl/ Biochem. Biotech. 18:403-412.

5) Quigley, D. R., Wey, J. W., Breckenridge, C. R., Stoner, D. L. and Dugan, P. R. 1987. In Precessing and Utilization of High Sulfur Coals II. Y. P. Chugh and R. D. Caudle, eds. Elsevier, Amsterdam. pp. 315-322.

6) Quigley, D. R., Wey, J. E., Breckenridge, C. R and Hatcher, H. J. 1987. In Proceedings of the Biological Treatment of Coals Workshop, Viennia, Virginia. pp. 151-164.

7) Quigley, D. R., Wey, J. E., Breckenridge, C. R. and Stoner, D. L. 1988. Resourc. Conserv. Recov. In Press.

8) Strandberg, G. W. and Lewis, S. N. 1988. Appl. Biochem. Biotech. 18:355 361.

9) Ward, B. In Biotechnology Applied to Fossil Fuels. D. L. Wise, ed. CRC Press, Inc. Cleveland. In Press.

10) Huttinger, K. J. and Michenfelder, A. W. 1987. Fuel. 66:1164 1165.

11) Meuzelaar, H. L. C. 1988. Personal Communication.

Table 1. Analyses of Treated Coals.

Coal[a]	C[b]	H	N	S	O	Moisture	Ash
Wyodak-W	73.39	5.21	0.98	0.44	19.97	4.00	5.91
Wyodak-A	73.31	5.13	0.91	0.43	20.16	2.00	2.93
Δ				-0.01	+0.19		-2.98
TXL-W	71.61	4.89	0.92	0.68	21.90	5.31	7.95
TXL-A	70.76	4.76	0.97	0.73	22.78	4.41	2.69
Δ				+0.05	+0.88		-5.26
B.Z.-W	72.76	5.6	1.35	1.21	19.08	2.78	13.81
B.Z.-A	71.41	5.49	1.27	1.25	20.58	2.83	9.36
Δ				+0.04	+1.50		-4.45
Wilcoz-W	66.58	4.91	1.11	1.29	26.11	4.56	14.21
Wilcox-A	67.52	5.11	1.16	1.25	24.96	4.12	11.48
Δ				-0.04	-1.15		-2.73

a) Abbreviations are as follows: TXL - Texas lignite, B.Z. - Beulah Zap, W - Water extracted, A - Acid extracted.
b) Values are the average of two determinations.
Δ are the difference between the control and experimental values.

Table 2. Metal Concentrations Present in Coal Extracts.

Coal[a]	Al[b]	Ca	Fe	Mg	Na	K
Wyodak-W	0	0.5	0	0.1	3.6	0.3
Wyodak-A	31	243	36	35	17	1.5
TXL-W	0.1	15	0	5	1.6	0.5
TXL-A	36	453	139	66	9	4
B.Z.-W	0.1	0.3	0.1	0.1	12	0.2
B.Z.-A	29	255	34	69	89	3
Wilcox-W	3.6	41	9	5	0.5	0.5
Wilcox-A	95	427	725	23	5	4

a) Abbreviations are as in Table 1.
b) Concentrations are given as mg per liter.

Table 3. Solubilities of Coals in Tris Buffer, pH 8.0

Coal[a]	Treatment	First[b] Extraction	Second Extraction	Third Extraction
Wyodak	Water	0.126	0.164	0.101
Wyodak	Acid	0.532	0.388	0.243
TXL	Water	0.343	0.278	0.198
TXL	Acid	1.45	1.22	0.780
B.Z.	Water	3.78	0.326	0.152
B.Z.	Acid	25.5	1.58	0.800
Wilcox	Water	85.8	26.9	7.3
Wilcox	Acid	124	13.7	4.40

a) Abbreviations are as in Table 1.
b) Values are given as absorbance at 400nm (corrected for any dilution factors).

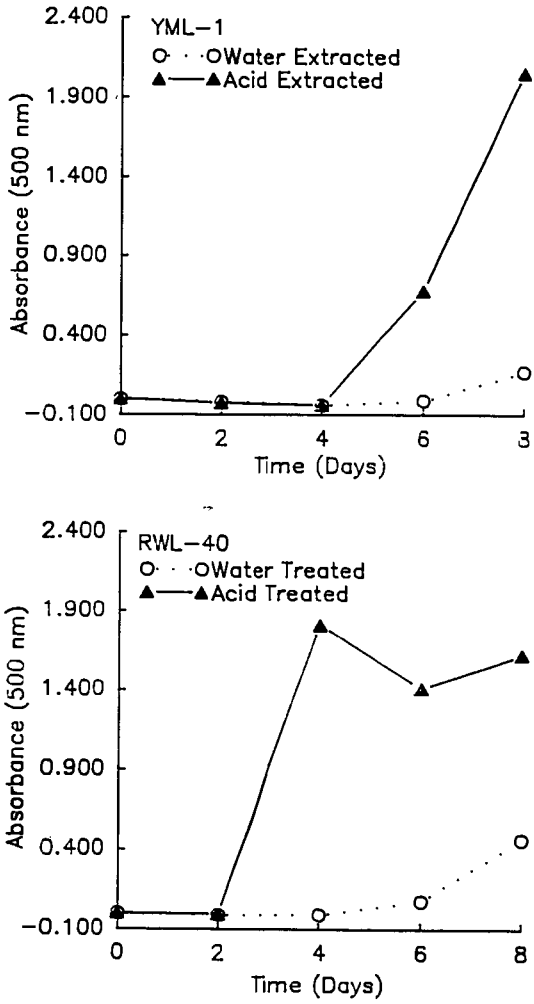

Figure 1. Biosolubilization of acid and water treated Mississippi Wilcox lignite.

MICROBIAL TREATMENT OF COALS AND ITS EFFECT ON ASH FUSION PROPERTIES

C. R. Krishna
and
A. J. Francis
Brookhaven National Laboratory
Upton, NY 11973

INTRODUCTION

Coal is a major source of energy in the United States, generating roughly 50% of the total electricity power produced, and 90% of the electricity used eastof the Mississippi River. Coal usage for electrical power generation currently averages 550-600 million ton/yr, and is expected to increase despite diminishing quantities of high-quality (i.e., low sulfur content, low fouling) coals. Increasingly stringent regulatory standards for reduced levels of atmospheric sulfur emissions have increased demand for low-sulfur coal. The primary objection to high-sulfur coal is the consequent generation of sulfur oxides during combustion, which may play a major role in the formation of acid rain.

In addition to sulfur, the quantity of metals in the coal also affects coal quality. Metals which may be present, mostly in the form of minerals and sulfides, include Si, Fe, Ca, Mg, Al, Na, K, and Ti, as well as traces of As, Cd, Cr, Cu, Pb, Mn, Hg, Ni, and Zn. Coal combustion oxidizes these metals to produce significant quantities of coal ash, the disposal of which can be costly. Additionally, ash entrained with the hot combustion gas tends to foul heat exchange surfaces, which reduces furnace efficiency and causes operational difficulties. The presence of metals like Arsenic, Lead, and Mercury create problems in disposal of ash.

The most common techniques of coal benefication are physical separation methods which exploit density differences between the light organic coal and heavier inorganic impurities. Numerous chemical processes involving reaction and extraction have been proposed. However, these methods generally prove uneconomic due to the high temperature and pressure required to achieve desired removal of impurities. The use of microbial processes in various aspects of energy production has become increasingly important over the past several years. In particular, the isolation and characterization of bacteria which catalyze the solubilization of sulfur compounds in coal and petroleum has suggested the possibility of a biological approach to fossil fuel desulfurization.

Microbial desulfurization of coal presents some important advantages over physical/chemical processes. Ambient temperature and pressure are generally sufficient to promote good microbial growth. The microbes are self-regenerating, so the costs are minimal. Microbial processes offer the possibility of removing not only inorganic sulfur, but also organic sulfur in the coal.

Processes involving the microorganism Thiobacillus ferrooxidans have been considered as an alternative to desulfurization by physical and chemical methods. In addition to desulfurization, it may also be effective in removing pyritic iron, Ca, Mg, Al, Na, K, Pb, Mo, Zn, Cu, and Cr. This concurrent demetalization of the coal may enhance the relative economic attractiveness of microbial desulfurization by reducing the quantity of ash produced and improving the quality of the ash.

OBJECTIVES AND APPROACH

One objective of this study was to characterize the microbial demetalization and desulfurization of coal by the bacterium Thiobacillus ferrooxidans under aerobic conditions. The effects of type of coal, coal particle size, and nutrient concentration on the bacterial leaching of coal were investigated. Ash fusion temperatures of treated and untreated coal samples were measured and an attempt was made to relate variations to the coal and ash properties.

Another objective was to determine the extent of dissolution of different metals from coal residues by the action of native autotrophic bacteria under aerobic conditions. The effects of inorganic nutrient supplements were also studied.

RESULTS AND DISCUSSION

The major results from the aerobic demetalization and desulfurization tests on three bituminous coal are summarized in Table 1. It is obvious that the effectiveness of microbial treatment is dependent on the type of coal and coal ash. More significantly, it can lead to substantial improvements in ash quality (as defined by the ash fusion temperature) as seen with the Pittsburgh Coal.

Some resutls from aerobic dissolution of toxic metals from the fines fractions of coal residues are summarized in Table 2. It is clear that under aerobic conditions substantial fractions of other metals in addition to pyritic iron can be solubilized from coal or coal residues.

CONCLUSIONS

Microbial action on bituminous coals under aerobic conditions can lead to significant reductions in inorganic sulfur, metals and total ash content, as well as considerable increase of ash fusion temperatures of the remaining ash.

Table 1

Coal	Ash Content (%)	Ash Reduction (%)	Inorganic Sulfur Reduction (%)	Increase in Ash Fusion Temperature (°F)
Ohio	25.2	15	80	180
Pittsburgh	10.3	17.5	40	460
Illinois	8.1	27	40	50

Table 2

Metal	Control	With No Nutrients Added	With Nutrients Added
	% Metal in Solution		
As	0.69	6.1	47
Cr	7.7	11	65
Cu	2.4	10	33
Fe (III)	0.1	2.7	26
Mn	16	16	43
Ni	15	20	44
Pb	0.6	0.6	4.6
Zn	8.2	17	48

SULFUR-SPECIFIC METABOLISM OF ORGANIC COMPOUNDS

John J. Kilbane II
Institute of Gas Technology
Biotechnology and Environmental Research
Chicago, Illinois 60616

All fossil fuels (except most natural gas) contain sulfur. When these fuels are combusted, the sulfur present is released into the atmosphere contributing to air pollution in the form of "acid rain." Current air quality standards have already placed strict limitations on the amounts of sulfurous air emissions allowed, and these regulations may well become even more stringent in the future. There is then a need and an incentive to limit sulfurous emissions resulting from the combustion of fossil fuels. The current technology focuses on sulfur removal achieved during or after combustion. At this time there is no cost effective technology that can desulfurize fuel prior to combustion.

The cost of desulfurization equipment currently used to remove sulfur during and/or after combustion, the problems associated with maintaining that equipment, and disposing of the copious quantities of sulfurous wastes generated by these processes are expenses and problems that industry and the utilities would prefer to avoid. If clean low-sulfur fuel (other than natural gas) could be made available, then fuel users could avoid these concerns. Although there are naturally occurring sources of low-sulfur oil and coal, these high-quality fuels are not abundant enough to serve all of the world's energy needs. Biological processes occur under very mild reaction conditions compared to chemical reactions, so it is hoped that if a suitable means of desulfurizing fuels using biological systems can be found, then economically favorable pre-combustion fuel desulfurization processes will result.

It has been known for many years that acidic drainage associated with coal mines or coal storage piles is the result of microbial oxidation of sulfur in coal, which produces sulfuric acid. This microbial desulfurization of coal is almost completely limited to the inorganic forms of sulfur (pyrite) found in coal and is accomplished by the action of well, characterized bacteria: *Thiobacillus ferrooxidans*, *Thiobacillus thiooxidans*, and *Sulfolobus acidocaldarius*. The microbiological removal of sulfur from coal has been shown to be capable of removing 90% or more of the inorganic sulfur, while the microbiological removal of organic sulfur from coal is certainly less complete and is less well-documented. More than 90% of the total sulfur must be removed for any pre-combustion coal desulfurization process to obviate the need for subsequent desulfurization. Therefore, the focus of current research concerning the microbiological removal of sulfur from coal centers on the removal of organic sulfur.

Inorganic sulfur generally exists in coal in the form of discrete particles or crystals of pyrite; whereas organic sulfur occurs as an integral part of the molecular coal matrix and is not readily accessible for microbial attack. The goal, then, of developing a microbiological process for the removal of organic sulfur from coal — while retaining the fuel value of that coal — is a most difficult goal indeed. What is needed are microorganisms that have an affinity for cleaving carbon-sulfur bonds, that is, microorganisms capable of sulfur-specific metabolism of organic compounds.

Enrichment culture techniques are typically used to isolate microorganisms with desired traits, and the search for microorganisms capable of organic sulfur removal from coal is no exception. The chemical dibenzothiophene (DBT) is generally regarded as a good model compound representative of organic sulfur found in coal; it is used as the substrate of choice in most enrichment culture experiments. There are two fundamentally different pathways for the microbial degradation of DBT that have been proposed. Both pathways are outlined in Figure 1. Pathway A (the sulfoxide/sulfone/sulfonate/sulfate "45" pathway) is the sulfur-specific metabolic pathway that results in the removal of sulfur from DBT, while leaving the carbon intact. Pathway B is a carbon-destructive metabolic pathway which results in the overall degradation of DBT. Numerous investigators[1-6] have attempted to isolate or develop microbial cultures that can metabolize or co-metabolize DBT. A summary of the published results of these attempts to isolate DBT-utilizing cultures is presented in Table 1. The nearly universal experience has been the isolation of microorganisms that metabolize DBT by the carbon-destructive pathway. The implication is that the methods of screening bacterial cultures and of performing enrichment culture experiments may be inappropriate and in need of revision. The published reports concerning CB1,[6] the only bacterial strain claimed to metabolize DBT via Pathway A exclusively, do not give any indication of a novel culture enrichment procedure or offer an example of how to purposefully isolate microorganisms with sulfur-specific metabolic capabilities.

There are several major research needs that can clearly be identified at this time. Since the rate and extent of organic sulfur removal from coal by characterized microorganisms is insufficient to warrant process development at this time, there is a need to identify new microorganisms that have sulfur-specific degradation abilities toward the full array of sulfur-containing organic molecules. Toward the isolation of new bacterial strains with appropriate desulfurization activities, there is a need for a convenient and powerful strain selection technique rather than relying on laborious culture screening techniques. There also exists a need to compare the cultures and the results obtained from different laboratories concerning microbial desulfurization. We need a way to normalize the results obtained by different researchers, using different microorganisms, different substrates, and different growth/reaction conditions. Existing strains of bacteria with documented desulfurization abilities are in need of strain improvement and techniques to conveniently monitor the progress of strain improvement efforts. Lastly, there is a need for better analytical techniques to assess the removal of organic sulfur from coal, as the existing methods of physical/chemical analysis of sulfur by type in coal are costly, time consuming, and not particularly accurate — especially regarding the organic sulfur in coal. All of these research needs can be served by taking advantage of the fact that all living organisms require sulfur for growth.

Enrichment cultures can be established to isolate microorganisms that possess an array of characteristics reflective of the incredible diversity present in the microbial kingdom. The challenge is to manipulate the culture conditions such that a very powerful selective pressure exists favoring only those microorganisms that possess the desired trait; then all that remains is to provide a suitable inoculum and allow the selective pressure and the "survival of the fittest" to interact and allow only those microbes that possess the desired characteristic to predominate in the enrichment culture. Enrichment cultures are startlingly simple in theory. The compound to be degraded is supplied as the growth-limiting source of an essential nutrient,

while all other growth requirements are supplied in abundance. Growth under such conditions favors those microorganisms that possess degradative activities toward the target compound — whereby the "appropriate" microorganisms should outgrow all "inappropriate" competitors and rapidly come to dominate the culture. A growth limitation can be achieved by removing, reducing, substituting, or altering any essential nutrient; however, in practice it is usually only the carbon source that is manipulated in enrichment culture experiments. That also seems to be the case for enrichment culture experiments reported for the isolation of microorganisms with the ability to desulfurize DBT or the organic sulfur in coal. It would be much more to the point to establish enrichment cultures utilizing DBT as the growth-limiting source of sulfur.

Enrichment culture experiments were carried out at the Institute of Gas Technology (IGT) in two ways: traditional shake flask enrichment cultures and sulfur-limited chemostats. A sulfur-limited chemostat is a continuous culture bacterial growth experiment in which all of the nutrients, except sulfur, that are needed for growth are supplied in abundance, and sulfur is supplied in the form of coal or organic chemicals. The use of traditional shake flask enrichment culture techniques resulted in the isolation of a Pseudomonas species, designated TG-232, which is capable of co-metabolizing DBT while growing at the expense of naphthalene. The sulfur-limited coal chemostat resulted in the isolation of a mixed bacterial culture, designated IGT-S7, capable of co-metabolizing DBT while growing at the expense of glucose, succinate, or benzoic acid. The bacterial metabolites of DBT produced by TG-232 and IGT-S7 were identified by gas chromatography and mass spectrometry (GC/MS). The results from these analyses are presented in Table 2. It can readily be seen that TG-232 metabolizes DBT by the carbon-destructive Pathway B, while IGT-S7 is capable of sulfur-specific metabolism, which removes sulfur from DBT and leaves the carbon intact. Sulfur-limited chemostats appear to be a useful tool for the purposeful isolation of microorganisms with sulfur-specific metabolic capabilities.

Growth of cultures in a sulfur-limited medium is not only useful for the selection of microorganisms but also the sulfur requirement of all microorganisms for growth can be used as the basis of a quantitative sulfur-specific bioassay by correlating bacterial growth to substrate metabolism. A bioassay can detect sulfur utilization from organic substrates more easily and with greater sensitivity than physical/chemical analyses. Moreover, a bioassay can be used to compare the results of different bacterial strains acting on different substrates. A bioassay relating sulfur metabolism of organic substrates to the rate and extent of growth observed can be a universally applicable method useful in normalizing the data obtained from every researcher in the field of microbial desulfurization of coal.

Because all life requires some amount of sulfur for growth, a situation can be created such that by quantifying bacterial growth one can quantify the utilization of any organic or inorganic compound as a source of sulfur. In work funded by the U.S. Department of Energy, IGT developed a sulfur bioassay to do just that. An inorganic sulfate is usually the form in which sulfur is supplied in a bacterial growth medium. Similarly, various organic sulfur compounds can be tested for their ability to serve as sources of sulfur for bacterial growth. Growth curves of IGT-S7 with glucose serving as a carbon source and various sulfur sources (nothing, sulfate, DBT, and trithiane) are presented in Figure 2. These curves, which constitute sulfur bioavailability assays, illustrate several points. The no-sulfate control shows some growth

because trace amounts of sulfur are present in this medium, but this growth is comparatively slow and essentially complete after 24 hours. The experiment that contains sulfate shows extremely rapid growth that is largely complete within 8 hours. When the same bacterial culture is grown with either DBT or trithiane as sulfur sources, about 78 hours are required to attain maximal growth. Inspection of these growth curves reveals that the bacterial cultures that contain DBT or trithiane grow at approximately the same rate as the no-sulfate control for the first 24 hours. This suggests that DBT and trithiane are not utilized appreciably as sulfur sources until the trace amounts of sulfur compounds present in the medium have been exhausted. Thereafter, a slow rate of growth continues at the expense of the organic sulfur compounds. Moreover, there is no pronounced lag in the growth curves of the DBT or the trithiane cultures after 24 hours coinciding with the exhaustion of the trace sulfur in the medium. This implies that no lengthy induction/adaptation period is required for IGT-S7 to utilize organic sulfur sources.

IGT-S7 is capable of utilizing a variety of organic compounds as sulfur sources including, but not limited to, dibenzothiophene, dibenzothiophene sulfoxide, dibenzothiophene sulfone, thianthrene, thioxanthene, and trithiane. While all of these compounds can be used as sulfur sources by IGT-S7, the time required to achieve maximal cell growth is longer than when sulfate is present. However, when bacterial cultures capable of metabolizing DBT by Pathway B are tested in the sulfur bioavailability assay, the vast majority of these cultures show no growth whatsoever in excess of that observed in the "no-sulfur controls." TG-232 is capable of utilizing DBT as a sulfur source, but it never grows to more than 40% of the maximum growth observed in the sulfate-containing controls, even upon lengthy incubation and multiple sequential subculturing. The sulfur bioavailability assay, therefore, is a convenient inexpensive method to compare quantitatively the abilities of bacterial cultures to utilize organic substrates as sulfur sources.

When IGT-S7 is used to treat coal, as much as 25% removal of organic sulfur has been observed. These results are encouraging, but organic sulfur removal efficiencies of about 90% are required if a microbial coal desulfurization process is to be developed that is competitive with current post-combustion desulfurization technologies. Significant strain improvement research is needed to enhance the desulfurization activity in bacterial cultures, and physical problems associated with the pre-combustion desulfurization of coal must be addressed if a viable technology for the microbial removal of organic sulfur from coal is to be realized.

Sulfur-limited continuous culture chemostats can be used to isolate/develop bacterial cultures capable of sulfur-specific metabolism of organic compounds. Similarly, the sulfur bioavailability assay can be used to evaluate quantitatively the desulfurization abilities of bacterial cultures and can aid in culture evaluation and strain improvement experiments. If the goal of developing a microbiological process for the removal of sulfur from coal is to be achieved, bacterial cultures with expanded and improved abilities to desulfurize organic substrates are needed. The techniques described in this paper are useful tools that can help to achieve that goal.

REFERENCES CITED

1. Malik, K. A. and Claus, D., Fifth Int. Ferment. Symp. 23, 03, 421, Berlin, 1976.

2. Hou, C. T. and Laskin, A. I., "Microbial Conversion of Dibenzothiophene," Dev. Ind. Microbiol. 17, 351, 1976.

3. Laborde, A. L. and Gibson, D. T., "Metabolism of Dibenzothiophene by a Beijerinkia Species," Appl. Environ. Microbiol. 34, 783, 1977.

4. Monticello, D. J., Bakker, D. and Finnerty, W. R., "Plasmid Mediated Degradation of Dibenzothiophene by Pseudomonas Species," Appl. Environ. Microbiol. 49, 756-60, 1985.

5. Kodama, K., Nakatani, S., Umehara, K., Shimizu, K., Minoda, Y. and Yamada, K., "Microbial Conversion of Petrosulfur Compounds: Isolation and Identification of Products From Dibenzothiophene," Agr. Biol. Chem. 34, 1320-24, 1970.

6. Isbister, J. D. and Kobylinski, E. A., "Microbial Desulfurization of Coal in Processing and Utilization of High Sulfur Coals," Coal Science and Technology Series, No. 9, 627, Attia, Y. A., Ed., Elsevier, Amsterdam, 1985.

PAP/JJK-ACSpap-PF

Table 1. SUMMARY OF THE IDENTIFICATION OF DBT METABOLITES PRODUCED BY MICROBIAL DEGRADATION

Research Group	Pathway A Degradation %	Pathway B Degradation %	Most Complete Degradation Products Observed*
Kodama et al.[5]	8	92	A1, B3
Laborde & Gibson[3]	Minor	Major	A1, B3
Monticello et al.[4]	0	100	B3
Kilbane: TG-232	32	68	A1, B6, B10
IGT-S7	100	0	A4
Hou & Laskin[2]	0	100	B2
Malik & Claus[1]	0	100	B2
Isbister & Kobylinski[6]	100	0	A4

* The designations of A1, B1, etc. refer to structures included in the pathways presented in Figure 1.

Table 2. GC/MS ANALYSIS OF BACTERIAL-DERIVED METABOLITES OF DBT

The most abundant metabolites of DBT degradation were analyzed by GC/MS. The concentration of DBT was arbitrarily set at 1.0, and the concentrations of metabolites were reported relative to the concentration of DBT. The numbers in parenthesis (A1, B1, etc.) refer to structures included in the pathways presented in Figure 1.

Compound	Mol. wt	TG-232	IGT-S7
Dibenzothiophene	184	1	1
(A1) Dibenzothiophene-5-oxide	200	0.30	1.8
plus Phenoxathiin	200	--	--
(A4)* Dihydroxybiphenyl	186	BDL**	0.033
(A4)* Hydroxybiphenyl	170	BDL	59
(B3) 3-hydroxy-2-formyl-benzothiophene	178	0.21	BDL
Biphenyl	154	BDL	0.001
(B6) Benzothiophene	134	0.016	BDL
Naphthalene	128	0.001	BDL
(B4) Three isomers of C(8)H(6)OS: (hydroxybenzothiophene)			
No. 1	150	0.01	BDL
No. 2	150	0.02	BDL
No. 3	150	0.048	BDL
(B9) C(9)H(8)OS	164	0.12	BDL
(B7) C(9)H(8)O(2)S	180	0.067	BDL
(B5) C(9)H(6)OS	162	0.022	BDL
C(10)H(10)OS or C(9)H(6)O(2)S	178	0.035	BDL
(B10) C(8)H(8)O(2)S isomers a)	168	0.033	BDL
b)	168	0.025	BDL
Formula (?)	220	0.036	BDL
Total Excluding DBT		0.94	60.8

* Hydroxybiphenyl is the terminal metabolite in a modified A/"4S" pathway.
** BDL = below detection limit.

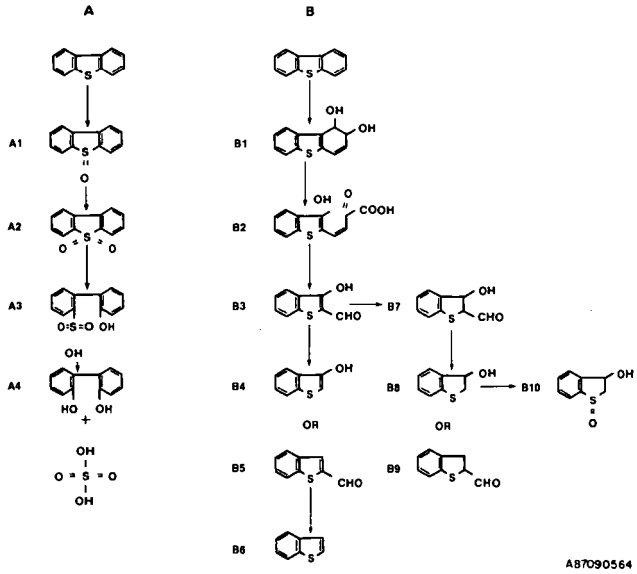

Figure 1. PROPOSED PATHWAY OF DBT DEGRADATION

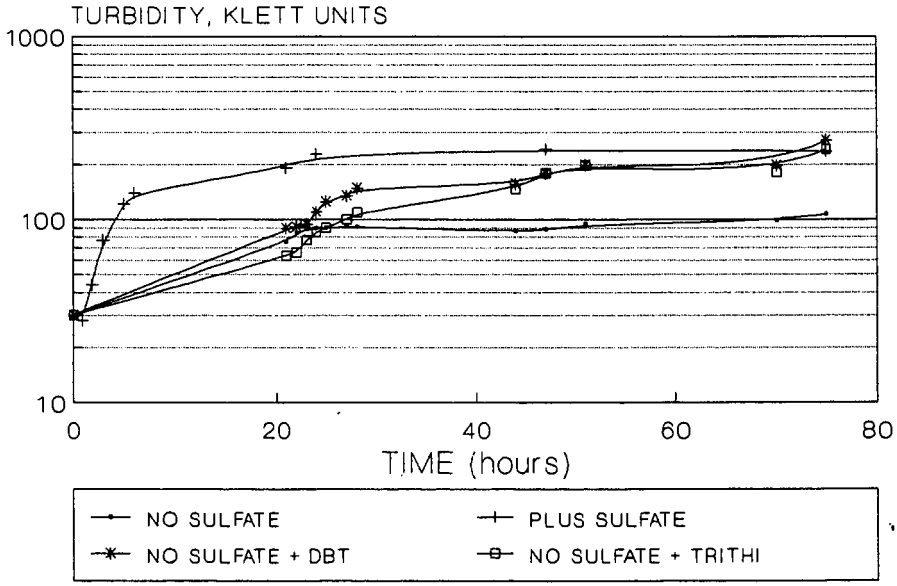

Figure 2. GROWTH CURVES OF IGT-S7 USING ORGANIC AND INORGANIC SULFUR SOURCES

SOLUBILIZATION OF AUSTRALIAN LIGNITES BY MICROORGANISMS

D.E.A. Catcheside[1], K.J. Mallett[1], and R.E. Cox[2]

1 School of Biological Sciences, Flinders University, Bedford Park, South Australia 5042
2 AMDEL, 31 Flemington Street, Frewville, South Australia 5063

INTRODUCTION

Cohen and Gabriel (1982) found that the wood rot fungi *Polyporus versicolor (Trametes versicolor)* and *Poria monticola (Poria placenta)* were able to solubilize Leonardite, a naturally oxidized lignite from a deposit in North Dakota. Lignite pieces placed on the surface of mycelial mats of each species, growing on Sabourauq maltose agar, were reduced to black water soluble products, shown by Wilson *et al* (1987) to contain aromatic, carboxylic and aliphatic carbon and have molecular weights of 10,000 to 50,000 Daltons or more.

Other North American lignites were found to be much less susceptible to solubilization by both these and other fungi (Ward 1985_1 and Scott *et al* 1986). However, Strandberg and Lewis (1986) showed that a range of lignites and a subbituminous coal could be solubilized by Candida (ML13) following oxidation with acid, peroxide or ozone. Several lignin degrading organisms have also been shown to solubilize oxidized lignite, including: *Phanerochaete chrysosporium* (Scott and Lewis 1987), *Streptomyces setonii* and *S. viridosporus* (Strandberg and Lewis 1987). Ward (1985_2) was able to isolate a range of lignite degrading fungi from a naturally exposed lignite seam. These included species of Aspergillus, Candida, Mucor, Paecillomyces and Penicillium. The mechanisms involved are not clear and may not all reflect enzymatic breakdown of lignin like structures remaining in lignite. Fakoussa and Truper (1983) have reported that surfactants produced by the bacterium *Pseudomonao fluorescens* have a solubilizing action on coal.

Australia has substantial lignite deposits, particularly in the Latrobe Valley in Victoria where 4.10^{10} tonnes are accessible with available technologies (Perry *et al* 1984). We have investigated the susceptibility of these coals to solubilization by microorganisms, including species additional to those already identified as active on North American lignites.

MATERIALS AND METHODS

Cultures were obtained from: The American Type Culture Collection, 12301 Parklawn Drive, Rockville, MD, USA (ATCC 11538, 12679 and 24725); CSIRO Division of Chemical and Wood

Technology, P.O. Box 56, Highott, Victoria 3190, Australia (DFP 7522); Dr. G.W. Strandberg, Chemical Technology Division, Oak Ridge National Laboratory, Oak Ridge, TN 37831, USA. *(Streptomyces viridosporus)*; and Dr. B. Ward, Department of Biology, University of Mississippi, University, MS 38667, USA (ML-13, ML-20 and YML-1).

Solubilization tests were conducted at 28°, at a relative humidity exceeding 80%, in 250ml screw capped jars containing 50ml of Sabouraud maltose agar. Tho jar closures had a 10mm perforation plugged with non-absorbent cotton. For *Trametes versicolor*, lignite pieces were placed on the surface of the mycelial mat, 8 days after central inoculation of the medium. For other tests, coal pieces were added at the same time as a spread inoculum of a suspension of conidia or mycelial fragments. Lignite solubilization was detected by the appearance of pigmented droplets on the surface of the coal pieces and by diffusion of dark solubilization products into the medium. The degree of solubilization was quantitated by recovery of remaining lignite pieces which were washed in deionized water, dried at 95° and weighed.

Lignite samples were obtained from the Coal Corporation of Victoria. Run of mine coal came from a 20,0001 sample taken at Morwell in October 1982 and a 40,0001 sample taken at Loy Yang in October 1984. Both had been stored in sealed drums. Weathered lignite came from a deposit at Loy Yang. The samples were pushed through a 4mm screen and fines passing a 2.4mm mesh removed. Lignite was sterilized by autoclaving at 121° and dried to constant weight at 95° prior to use. Lignite was oxidized by reacting with 8M nitric acid for 18 hours, washed with water and dried. Approximately 300mg dry weight of lignite was used for each test.

RESULTS

Mycelial mats of *Trametes versicolor* were able to solubilize both Latrobe Valley lignites following acid oxidation (Table-1). Run of mine lignite was resistant, with the exception that Loy Yang coal showed trace coloration of droplets forming on the coal pieces and diffusion of dark material into the agar surrounding coal fragments. Pigmented droplets formed within 14 days both on acid oxidized Morwell and acid oxidized Loy Yang lignites. There was extensive collapse of the granules by day 38. The incubation was continued to day 118 prior to quantitation. Although pigmented droplets appeared on the Loy Yang run of mine coal at 42 days, there was no extensive solubilization. Mass gain by unoxidized lignite pieces reflects the difficulty of separating them from the pigmented droplets formed and no pigments diffused into the agar in cultures without lignite or when lignite was in contact with medium under aseptic conditions.

Seven strains of six additional species were tested for their effect on acid oxidized and run of mine Morwell lignite, and on a naturally oxidized, weathered, lignite deposit at Loy Yang, Table-2. Each of these species, previously shown to be active on oxidized North American lignites, were able to solubilize acid oxidized Morwell lignite. *Poria placenta* was least effective and the ATCC 11538 strain reported active on Leonardite (Cohen and Gabriel 1982) did not solubilize any of the Latrobe Valley lignites in repeated tests. A strain of *P. placenta* from the CSIRO collection showed some activity on acid oxidized Morwell coal by the diffusion test. Each of the other five species caused extensive or total solubilization of acid oxidized lignite and were also active on the naturally oxidized weathered coal on which *Phanerochaete chrysosporium* was the most effective. None of the isolates tested showed evidence of activity on run of mine coal, with the exception of Candida ML-13 that was positive by the diffusion test but so heavily interpenetrated the coal grains that quantitation of the extent of solubilization was not possible.

DISCUSSION

The data presented here show that acid oxidized lignites from the Latrobe Valley are solubilized by each of seven species of microorganisms previously found to be active on Leonardite and oxidized North American lignites. These are the wood rot fungi: *Trametes versicolor, Poria placenta and Phanerochaete chrysosporium,* the lignin degrading prokaryote *Streptomyces viridosporus* and three fungi isolated from lignite in Mississippi: Candida ML-13, Cunninghamelia YML-1 and *Penicillium waksmanii*.

The completeness of solubilization by these organisms was not correlated with the time of onset of solubilization as indicated by the diffusion of pigment from lignite grains, data not shown, and varied from as soon as 5 days after inoculation in Cunninghamella, that gave 74% solubilization by day 67, to as late as 46 days after inoculation by *Penicillium waksmanii* which gave 100% solubilization by day 67. This suggests that there is substantial potential for the manipulation of conditions and of the organisms themselves to speed solubilization. It should be noted that the extended incubation periods used in these tests do not reflect the speed of the process by the most active species and were chosen such that weak or delayed activity could be detected. It is desirable that even slow acting isolates are identified since they may include species degrading lignite by different mechanisms. Identification of all biological mechanisms of lignite degradation may provide pathways to desirable products that can be manipulated to give good yields at practicable rates.

Further to the work reported here, we have surveyed other lignin and wood degrading species for their activity on Latrobe Valley lignites. Of the lignin degraders, four were inactive but the remaining six solubilized acid oxidized Morwell lignite and also weathered lignite to a substantial extent. Three of these species also showed some activity on run of mine Morwell lignite. In addition, we have established enrichment cultures for lignite degrading species from natural lignite exposures and from mining sites in Victoria. These enrichments have yielded a wide range fungi, Streptomycetes and bacteria able to grow on lignite as their sole carbon source. The isolates include some able to quantitatively solubilize acid oxidized Morwell lignite and some that partially solubilize unoxidized, run of mine Morwell coal. This work has identified a second deposit of lignite at Loy Yang, that like Leonardite is readily solubilized by microorganisms without further treatment.

ACKNOWLEDGEMENTS

This work was supported by grants from the Coal Corporation of Victoria and from The Flinders University of South Australia. We thank Diana Thompson and Karen Ribbons for their skill and patience in separating lignite pieces from microbial growth.

REFERENCES

Cohen, M.S. and P.D. Gabriele. 1982. Degradation of Coal by the fungi *Polyporus versicolor* and *Poria monticola*. Applied and Environmental Microbiology 44: 23-27.

Fakoussa, R.M. and H.G. Truper. 1983. Kohle als microbielles substrat unter aeroben bedingungen. *in* Kolloquium in der Bergbau-Forschung Gmblt, Essen. p 41-49.

Perry, G.J., D.J. Allardice and L.T. Kiss. The Chemical Characteristics of Victorian Brown Coal. 1984. *in* The Chemistry of low-rank coals. H.H. Schobert, Ed. ACS Symposium series, No. 264: 3-14, American Chemical Society.

Scott, C.D. and S.N. Lewis. 1987. Biological Solubilization of Coal Using Both *in vivo* and *in vitro* processes. 9th Symposium on Biotechnology for Fuels and Chemicals, Boulder, May 1987.

Scott, C.D., G.W. Strandberg and S.N. Lewis. 1986. Microbial Solubilization of Coal. Biotechnology Progress 2: 131-139.

Strandberg, G.W. and S.N. Lewis. 1986. A Method to Enhance the Microbial Liquefaction of Lignite Coals. (8th Symposium on Biotechnology for Fuels and Chemicals. Gatlinburg, May 1986) Biotechnology and Bioengineering Symp. 17: 153.

Strandberg, G.W., and S.N. Lewis. 1987. The Solubilization of Coal by an Extracellular Product from Streptomyces Setonii 75Vi2. J. Industrial Microbiology 1: 371-375.

Ward, H.B. 1985_1. Apparent Bioliquefaction of Lignite by Fungi and The Growth on Lignite Components. *in* Bioenergy 84 Proceedings, vol 3, Egneus, E and A. Ellegard, Eds. Elsever, London.

Ward, H.B. 1985_2. Lignite-degrading Fungi Isolated from a Weathered Outcrop. Systematic and Applied Microbiology. 6: 236-238.

Wilson, B.W., R.M. Bean, J.A. Franz, B.L. Thomas, M.S. Cohen, H. Aronson and E.T. Gray. 1987. Microbial Conversion of Low-rank Coal: Characterization of Biodegraded Product. Energy and Fuels 1: 80-84.

TABLE-1 ACTION OF *TRAMETES VERSICOLOR* ON RUN OF MINE AND ACID OXIDIZED AUSTRALIAN LIGNITES.

LIGNITE		COLOURATION OF DROPLETS ON COAL	COLOURATION OF AGAR	MASS CHANGE OF COAL %
MORWELL	ROM	NONE	NONE	+5
	OXIDIZED	BLACK	BLACK	-90
LOY YANG	ROM	TRACE	TRACE	+4
	OXIDIZED	BLACK	BLACK	-83

TABLE-2 SOLUBILIZATION OF MORWELL AND LOY YANG LIGNITE BY MICROORGANISMS.

		LIGNITE					
		MORWELL ROM		MORWELL OXIDIZED		LOY YANG WEATHERED	
		a	*b*	*a*	*b*	*a*	*b*
Candida sp.	ML-13	B	+14	B	-74	B	-13
Cunninghamella sp.	YML-1	0	+1	B	-74	B	-1
Phanerochaete chrysosporium	ATCC24725	0	+1	B	-35	B	-47
Poria placenta	ATCC11538	0		0		0	
	DFP7522	0		B		0	
Penicillium waksmanii	ML-20	0	+2	B	-100	B	-3
Streptomyces viridosporus	T7A	0	+9	B	-75	B	-10

a Formation of pigmented droplets on coal pieces and/or diffusion of black pigment from the coal into the agar: 0 not observed, B black pigment.

b Percentage mass change of lignite pieces following 58 to 70 days incubation. Apparent mass gain is due to mycelium penetrating the lignite pieces.

CONSIDERATIONS FOR THE COMMERCIALIZATION OF COAL BIODESULFURIZATION TECHNOLOGY

Barbara J. Zakheim
NUS Corporation
Gaithersburg, Maryland

S. Rick Gilbert
Pittsburgh Mineral and Environmental Technology, Inc.
Pittsburgh, Pennsylvania

INTRODUCTION

The adverse effects to human health and to the ecological environment caused by the release of sulfur dioxide (SO2) to the atmosphere during coal combustion have gained increasing attention due to the acid rain debate. Control of SO2 emissions, however, have been regulated under various federal, state, and local standards for well over ten years. The 1977 amendments to the Clean Air Act (CAA) introduced Environmental Protection Agency (EPA) regulation of new utility coal-fired boiler emissions under the New Source Performance Standards (NSPS) of 0.6 lbs/mm BTU. Compliance with these standards and National Ambient Air Quality Standards (NAAQS) have required that many utilities purchase coal based on sulfur content, often more expensive feedstocks, and also invest in costly flue gas desulfurization processes, especially scrubbers.

Currently the EPA is in the midst of promulgating SO2 control regulations for the industrial boiler market, which mandate a 90 percent reduction of emissions from all new coal industrial and commercial boilers regardless of the sulfur content of the coal. Compliance with these regulations may prove very difficult for industrial boiler owners. For example, boiler emissions would have to be lowered to 0.6 lbs/mm BTU when using 3 percent sulfur eastern coal. This would cause fuel switching to natural gas, rather than expensive coal cleaning or flue gas treatments.

The pre- or post-combustion removal of sulfur from coal, therefore, is a regulatory driven necessity but is constrained by technological and economic difficulties. Technologies that are commercially available include a variety of physical and chemical coal cleaning techniques and several flue gas treatment processes. Table 1 lists the most common, commercially available technologies with an approximation of their efficiencies and costs. As shown, both capital and operating costs for these processes are quite significant, and in most cases remove less sulfur than required to meet regulations. The successful commercial introduction of any new technology into this marketplace, therefore, requires both efficient sulfur removal and cost competitiveness.

BIODESULFURIZATION OF COAL

One technology for coal desulfurization that is under development, but still far from a commercial reality, is biological treatment. In the past few years, several studies have identified the technical status of coal biodesulfurization research, listing published results of laboratory scale experiments both in the United States and overseas (National Bureau of Standards, 1986; Battelle Pacific Northwest Laboratories, 1986; Couch, 1987). These studies refer to experimental results published since 1914, although the majority have appeared in the past twelve years. Most of these experiments have been concerned with the microbiology and coal chemistry aspects of coal biodesulfurization and very few have looked at the engineering, process, and economics aspects. Notable examples of this latter category include studies by Bos (1985), Dugan (1985), and Sproull (1986).

Results from these studies indicate that pyritic sulfur removal using the acidophilic organism Thiobacillus Ferroxidans has been achieved widely, with over 90 percent removal reported by many researchers. In addition, these sulfur oxidizing microbes remove ash and some metals during the biodesulfurization process. Removal of organic sulfur is more difficult; the use of thermophilic organisms have apparently reduced the organic sulfur component of some high sulfur coals by up to 30 percent (Chandra, 1987; Isbister 1986). What is clear from these studies is that biological treatment provides no utopian solution to the coal desulfurization problem and may only be part of a more complex, multifaceted process. Furthermore, biological treatments may be more suitable for some coals than others and may not deal with both the organic and inorganic sulfur present in coal. On the other hand, there is some indication that biological removal of pyrite may be economically competitive with physical coal cleaning methods, especially as operations and maintenance costs will be limited and a greater percentage of sulfur will be removed.

Given this current status, therefore, what can be done to bring coal biodesulfurization technology to the marketplace within a timeframe that is compatible with the regulatory drivers? In answering this question, it is important to understand the prominent issues impeding the progress of coal bioprocessing research:

- Transfer of fundamental studies to pilot or demonstration activity -- emphasis remains on benchtop studies and, as shown in Figure 1, only about 15 percent of these have given any attention to either process design, engineering, or economics.
- Low level of research funding and emphasis --although clean coal technologies are receiving large-scale

funding from the government, the Electric Power Research Institute (EPRI), and the private sector, fundamental research in biotechnology lags far behind the funding levels available for demonstration activities in other coal cleaning areas, flue gas treatment processes, fluidized bed combustion, or fuel cells.

- Lack of commercial biotechnology company interest -- unlike the pharmaceutical, agricultural, or metals extraction industries, coal bioprocessing leads to a low value-added product.

Overcoming the first of these impediments by transferring fundamental studies to demonstration activity will probably remove the remaining two. Quite often, not all of the components of a given process are fully developed by the inventors, but the overall concept has merit and should be tested at a larger scale. Some see this approach as risky, which it is, while others see it as an opportunity to begin tackling the next phase of problems. Hopefully, by the time the process is brought to commercialization, an acceptable solution to all of the "underdeveloped" portions of the technology have caught up. In making a case for early scale up, this paper presents examples of several industries and their own progress in commercializing biological processing. By offering these examples and comparing them to coal, it is the objective of this paper to stress performance of both applied and fundamental research early on in order to accelerate the implementation of a commercially viable process.

BENCH TO COMMERCIALIZATION -- INDUSTRY EXAMPLES

The importance of achieving a synergism between applied technology and fundamental microbiology was poignantly exemplified in the petroleum industry. When the development of the petroleum industry was in its infancy, neither the petroleum, technologists nor the microbiologists were aware of the others activities (Davis, 1967). It was in fact a Russian geologist who is credited for using bacterial hydrocarbon oxidation as a prospecting tool. He had enlisted the assistance of microbiologists who were working separately on the same problem, and their joint efforts resulted in a practical solution for petroleum exploration. In a similar fashion during the 1940's, petroleum geologists in the United States established the need to involve microbiologists to resolve issues relating to source sediments. In this case as well, those involved with the practical application solicited the assistance of those with a technical understanding of microbial interactions and, together, they engineered a timely and workable solution.

Another example involves waste water management. Even though the biological management of wastes, particularly waste waters, has been employed for centuries, a firm understanding of the

principles has only been achieved in recent decades. Engineers, aided by available biological data, have successfully designed and implemented scores of aerobic waste water treatment systems, and new systems are still in the making. The proper engineering and optimization of biological water treatment systems are continuing to improve the industry as evidenced by the anaerobic bio-reactors now being developed for municipal waste water treatment (Cheremisinoff, 1987).

In the agricultural area, processes for improving crop yields and reducing infestation have also been approached with the fundamental microbiology and genetic engineering research occurring at the same time as the applied system development and the overcoming of policy and regulatory constraints.

The metals mining industry provides one of the most striking examples in recent years of a large, industrial-scale microbiological process that has been snatched from the laboratory beaker and engineered into production before "the ideal" set of microbiological data has been documented.

Much of the practical beginnings of bioextractive metallurgy in the copper industry is attributed to J. Prater, E. Malouf and other engineers at Kennecott Copper Corporation (now BP Minerals America) who, in the 1960's, initiated a dump leaching operation at Bingham Canyon to recover metal values contained in sulfide copper ores. Gleaning what biological information they needed, they successfully engineered and implemented one of the world's first and largest dump leaching operations. Initially, these engineers knew relatively little about how optimal strains of bacteria performed on model compounds, and what conditions might produce the optimal response during leaching. Nevertheless, from their efforts to get the wheel rolling, as well as those of others like them, bioleaching operations in copper and uranium have spread throughout the world. It was the iterative process of engineering design, fed by increased microbiological understanding, that led to the successful implementation of the technology.

In a similar vein, precious metals recovery from sulfide minerals made great strides once the process moved from laboratory investigation to pilot-plant development studies. A number of investigators had been involved in fundamental studies of the biooxidation of pyrite so that encapsulated gold particles could be liberated for subsequent cyanidation (Bruynesteyn, 1984; Lawrence, et. al., 1985; and Murr, et. al., 1980). A few engineering, research, and equipment companies over the past 10 years have undertaken pilot-plant scale-ups of biooxidation systems for precious metal recovery by drawing on the available biological data. Coming to grips with engineering issues such as reactor design, slurry dewatering, effluent water treatment, reagent and nutrient consumption, aeration requirements, materials of construction and interfacing the biooxidation process with pre- and post-

treatment processes have led to the installation and operation of at least three commercial plants in the free world.

Feasibility studies also played an important role in establishing the economic viability and eventual plant implementation of bacterially-enhanced precious metals recovery (Marchant, 1986). It was the present author's experience that the potential for a significant return on investment by biologically treating gold-bearing concentrates prompted a large scale pilot-plant study (Gilbert, et. al., 1988). Certainly, microbiological studies are evolving along with the economics and the practical plant applications, but with a better focus toward the real needs of the process.

LESSONS FOR COAL BIODESULFURIZATION

From the above examples it can be seen that the speed of progress in bringing biotechnology to a commercial reality resulted from early scale up or applied research supporting fundamental studies. Among the reasons for this appear to be motivation and approach, especially evident in the metals extraction area. In that case, the value added by the process was relatively high, especially in bioleaching of gold and other precious metals. Further, due to this motivation of producing a valuable product, the approach to developing an efficient technology focused foremost on the process engineering and economics, utilizing available microorganisms in increasingly larger-scale demonstration programs. As a feasible process became evident, refinements to the process based on an improved understanding of the microbiology and chemistry were made.

Biodesulfurization of coal is now at the stage where pilot plant efforts should begin. By placing the carrot, cart and horse in proper order, productive progress can be made. At present, there is a shortage of engineering data to keep pace with the fundamental microbiological studies now in progress. The bulk of governmental and industrial research support has been focused on microbiological developments dealing with isolated bacteria, model compounds, and sterile coal samples. Progress and funding are now slowing so that in a few years the process development of biodesulfurization might be strictly an academic issue. A solid pilot-scale study accompanied by a thorough economical feasibility study is needed to revitalize the program.

Scale up of coal biodesulfurization experiments will provide essential data about the feasibility of such a process and its application to the numerous coal feedstocks in the market. By applying what is already known, researchers can answer some of the fundamental engineering and economics concerns that will either make or break further efforts in this field. For example:

- Can bioextraction handle large tonnages of coal? Even for industrial boiler application, the volumes of feedstocks involved are far greater than in other biotechnology applications.
- If a superbug is developed that can reduce greater levels of organic sulfur and/or pyritic sulfur will it thrive in the engineered environment?
- What are the pre- and post-treatment requirements?
- What are the environmental benefits and concerns relating to solids, liquids, and gasses involved with the process? What are the volumes of each?
- Is it economical to treat run-of-mine coal or possibly a reject stream?
- Can organic and inorganic be coupled together in the same stage, or handled separately?
- What are the supply and cost constraints of nutrients?
- What impact will coal biodesulfurization have on the overall power plant design and performance?

In terms of pyrite removal, a technical feasibility study of coal biodesulfurization carried out in the Netherlands (Bos, 1985) suggests that the process is a realistic, economic option, although probably in conjunction with other processes. Bos concluded the following:

- Coal must be milled extensively to achieve an acceptable pyrite removal without considerable carbon loss.
- Pyrite removal was achieved on all of the 17 different, worldwide coal samples tested. In addition heavy metals and varying amounts of ash were removed.
- A temperature of 30 degree C. is optiomal for T. Ferrooxidans cultures, but residence times for 90 percent pyrite removal are between 7 to 9 days.
- Long residence times and large tonnages of coal will require large reactors. He recommends a trough-shaped system similar in cross section to the Pachuca-tank reactor.
- For the treatment of 1 ton of coal in a 1 million tons of coal per year installation costs range between $9 - 16.

These results and others presented by Dugan and Sproull certainly suggest further feasibility analyses and scale up studies. In particular, economics data that include the costs and benefits of combined sulfur, ash, and metals removal must be carefully evaluated.

In conclusion, microbial studies have brought us a long way, but they will not satisfy the need to demonstrate the technology at a larger scale. Answering the engineering questions could well be the bucket of cold water that douses

degree has been earned but experience is needed. It is up to the research community to gain the experience from scale up and demonstration programs before earning a higher degree in the fields of microbiology and chemistry.

REFERENCES

Battelle Pacific Northwest Laboratories, "Biologic Coal Beneficiation-Literature Review", EPRI Report AP-4834, 1986.

P. Bos, et. al., "A Dutch Feasibility Study on Microbial Coal Desulfurization", presented at the International Symposium on Biohydrometallurgy, Vancouver, BC, August, 1985.

A. Bruynesteyn, "Bio-leaching of Refractory Gold-Silver Ores", Presented at the 14th Annual Hydro-metallurgical Meeting, CIM, Ontario, Oct. 1984.

D. Chandra and A. Misra, "Desulfurization of Coal by Bacterial Means", Proceedings of the Biological Treatment of Coals Workshop, Vienna, VA, July, 1987.

P.N. Cheremisinoff, Wastewater Treatment, pp 279-324, Pudvan Publishing Co., 1987.

G. Couch, "Biotechnology and Coal", IEA Coal Research Report OCTIS/TR 38, 1987.

J.B. Davis, Petroleum Microbiology, pp 1-15, Elsevier Publishing Co., 1967.

P. Dugan, "Economics of Coal Desulfurization", Proceedings of the Biological Treatment of Coals Workshop, Herndon, VA, June, 1986.

S.R. Gilbert, et. al., "Comparative Economics of Bacterial Oxidation and Roasting as a Pre-treatment Step for Gold Recovery from an Auriferous Pyrite Concentrate", CIM Bulletin, February, 1988.

J. Isbister, "Biological Removal of Organic Sulfur from Coal", Proceedings of the Biological Treatment of Coals Workshop, Herndon, VA, June, 1986.

R.W. Lawrence, et. al. "Biological Pre-oxidation of a Pyrite Gold Concentrate" Frontier Technology In Mineral Processing, AIME, 1985.

P.B. Marchant, "Commercial Piloting and the Economic Feasibility of Plant Scale Continuous Biological Tank Leaching at Equity Silver Mines Limited", Fundamental and Applied Biohydrometallurgy, Elsevier, 1986.

L.E. Murr, et. al., Metallurgical Applications of Bacterial Leaching and Related Microbiological Phenomena, Academic Press, New York, 1978.

National Bureau of Standards, "Processing of Coal with Microorganisms", EPRI Report AP-4472. 1986

NUS Corporation, "An Assessment of Microbial Coal Desulfurization and Microbial Solubilization Experimental and Economics Data", Prepared for EG&G, Idaho, Inc., March, 1988.

R. Sproull, et. al., "Enhancement of Coal Quality by Microbial Demineralization and Desulfurization", Proceedings of the Biological Treatment of Coals Workshop, Herndon, VA, June, 1986.

Table 1: Commercially Available Coal Desulfurization Technologies

TECHNOLOGY	PERCENTAGE SULFUR REMOVAL	OP. COST ($/T)	CAP. COST ($/KWE)
TRW Gravimelt	80-90	30	82
Flue Gas Desulfurization	Up to 90	7-12	150-200
Physical Coal Cleaning	30-40	4-6	50
Advanced Flotation	53	25	110
Oil Agglomeration	49	23	85
Fine Coal, Heavy Medium	59	21	98

Source: Pittsburgh Mineral and Environmental Technology Internal Documentation

Figure 1: Disciplinary Focus of Coal Biodesulfurization Literature

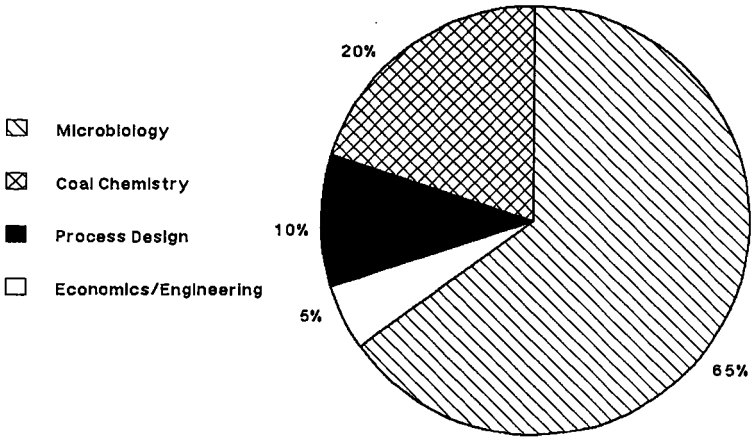

NUMERICAL COMPARISONS BETWEEN THE PYROLYSIS MASS SPECTRA OF TWELVE U.S. COALS AND THEIR RELATIVE SOLUBILITY IN MICROBIAL CULTURES OR ALKALINE BUFFER

Gene J.C. Yeh, Bailey Ward*, David R. Quigley, Don L. Crawford**
and Henk L.C. Meuzelaar***

Idaho National Engineering Laboratory
*University of Mississippi, **University of Idaho
***Center for Micro Analysis & Reaction Chemistry, University of Utah
Salt Lake City, Utah 84112

ABSTRACT

Curie-point pyrolysis mass spectra of twelve low-rank U.S. coals with various degrees of natural weathering were correlated with the results of biosolubility screening tests involving six selected microorganisms as well as with a specially designed alkaline solubility test. The main objective of this study was to determine which mass spectral characteristics, if any, correlate with the degree of biosolubility. The results indicate the possible presence of two biosolubilization trends, a main trend which correlates positively with the presence of severely oxidized aromatic moieties in the coal and apparently enables biosolubilization by all six microorganisms, and a second trend which correlates with relatively high concentrations of acid components and enables biosolubilization by only two or three of the organisms. The chemical and biological significance of these trends is not yet completely understood. Finally, in agreement with previous reports a strong positive correlation was observed between biosolubility and alkaline solubility.

INTRODUCTION

Few areas of coal science are more challenging and intimidating to analytical chemists than the study of coal bioliquefaction phenomena. In recent years, powerful chromatographic and spectroscopic techniques have begun to shed more light on the structural chemistry of coal. However, the added complexity of bioconversion phenomena puts coal bioliquefaction processes well out of the reach of most analytical methods.

A further complicating factor is the lack of standardization with regard to suitable coal samples, microorganisms and experimental conditions. Although several coal sample and data banks are in operation within the USA, none of these banks currently provides the type of relatively strongly weathered, low rank coals which have been used in nearly all coal bioliquefaction experiments reported to date. Moreover, many of the various strains of microorganisms used are not available for general distribution and/or incompletely characterized. Finally, there is no general agreement as to what constitutes "bioliquefaction" or how to measure it objectively.

In order to help solve some of these problems Idaho National Engineering Laboratory has assembled a multidisciplinary task group including researchers at several different universities. The present communication represents one of several reports detailing the results of studies carried out during the past year and primarily aimed at obtaining an improved definition and understanding of coal bioliquefaction phenomena.

A strong correlation between the bioliquefaction yields and alkaline solubilities of a series of low rank U.S. coals was reported by Quigley et al. [1,2]. Together with the observation that the more "successful" microorganisms tend to produce substantial alkalinity of the culture medium, this suggested that simple acid-base solution processes might play a significant role, especially in strongly acidic, e.g., highly weathered coals. Consequently, one of the key questions in any future coal bioliquefaction studies should be whether proof of covalent bond scission can be obtained or not.

In a separate paper, Ward et al. [3], describe a novel bioliquefaction screening and quantitation method which uses objectively measurable product diffusion zones around standard-sized coal sample "disks" imbedded in solid media. After inoculation with selected microorganisms, characteristic "bioliquefaction profiles" can then be obtained.

Here we report the results of a study of 12 low rank coal samples (representing several different U.S. provinces as well as degrees of natural weathering), each of which was submitted to the new "bioliquefaction profiling" procedure using six different strains of microorganisms. Suitable aliquots of each coal sample were further analyzed by means of Curie-point pyrolysis mass spectrometry, using techniques described by Meuzelaar et al. [4]. Also, alkaline solubilities were determined according to Quigley et al. [2].

Finally, biosolubility profiles, pyrolysis MS profiles and alkaline solubility data were compared by means of canonical correlation analysis, a powerful multivariate statistical analysis approach capable of determining common sources of variance between related data sets.

The primary objective of this study was to search for key structural features of coals (as reflected in the pyrolysis MS profiles), directly associated with bioliquefaction response (as reflected in the "bioliquefaction profiles"). A secondary objective was to obtain information on reaction mechanisms, e.g., with regard to the role of acid-base solubilization vs. covalent bond scission processes.

EXPERIMENTAL

Sample Preparation - Suspensions of each of the 12 coals (5 mg of ~200 mesh coal per ml of spectrograde methanol) were prepared. A 5 ul drop of each suspension (25 ug of coal) was applied to a 610°C Curie-point wire. The methanol was evaporated under continuous rotation of the wire.

Pyrolysis Mass Spectrometry - Py-MS was performed with the MS inlet at 25°C and using low voltage (12 eV) electron ionization. For each Py-MS analysis, the total number of scans was 100 and the total scan time was 23 seconds. Each sample was analyzed in triplicate.

Data Analysis - The Py-MS data were first normalized to 100% total ion intensity. For the normalization of the total ion intensities, mass peak signals with high variance were temporarily excluded. 159 mass peaks with high "characteristicity" (outer variance/inner variance ratio) values were used for factor analysis. Furthermore, these Py-MS data were correlated with biosolubility data and alkaline solubility data by canonical correlation techniques.

Biosolubility - A set of six selected fungal strains, e.g., ACL-12, DML-12, P. Chrysosporium, RWL-40, YML-1 and YML-21, representing a diversity of taxonomic types was used for all biosolubility assays. The general methods used for standardized assays (i.e., the "diffusion zone assay") of coal biosolubility were described elsewhere [3]. In brief, 2-3 mm diameter mounds of sized coals (0.25-0.50 mm) were placed with uniform spacing on the surface of Sabouraud Dextrose 1.5% agar ("SDA" Difco Laboratories, U.S.A.). Medium depth was 5.5 mm in 100 mm diameter pyrex-glass; deep-well culture dishes. Two replicate preparations of five coal units were used for each coal type. Spores or hyphal fragments of each organism were inoculated onto the surface of the nutrient medium after which the cultures were incubated in the dark at 30°C, 70 ± 2% RH for 17 days. Circular zone diameters were measured and averaged to give values for comparisons of degree of biosolubility for each coal.

Alkaline solubility - One half gram of sized coal (0.25 - 0.50 mm) was placed in a 250 ml Erlenmeyer flask containing 50 cc of a pH 8, tris buffer. Flasks were shaken (140 rpm) for 24 hours at 25°C. Supernatants were obtained by filtering through 0.2 micron filters. Where necessary, dilutions were made using fresh TRIS buffer and absorbances at 400 nm measured.

RESULTS AND DISCUSSIONS

The wide range of different coal types included in this study is illustrated in Figure 1. At first sight the low voltage pyrolysis mass spectrum of North Dakota Hagel lignite appears to be fairly characteristic of Northern Great Plains lignites, i.e., dominated by homologous series of dihydroxybenzenes and phenols representative of fossil lignins [5]. However the relatively high peak intensities at m/z 45, 46, 60, 87 point to the presence of carboxylic moieties characteristic of oxidative changes [6]. Since the Hagel lignite was originally obtained from the Penn State Coal bank (see Table 1), these oxidative changes are probably due to long term exposure to ambient air in the laboratory. By comparison, the Mississippi Claiborne lignite (see Figure 1b) shows a much more pronounced homologous series of aliphatic hydrocarbon components. This is again in agreement with earlier Py-MS studies of lignites representing the Gulf Province [5] in which higher relative abundances of aliphatic hydrocarbons were found to correlate with aquatic depositional environments. In that study, longer chain aliphatic hydrocarbon moieties in Gulf Province coals were thought to represent liptinitic macerals primarily derived from algal materials. Finally, the spectrum in Figure 1c, obtained from an Arkansas Lower Hartshorne "bituminous" coal, appears to be totally different. Little or no aromatic compound series are seen whereas aliphatic series are not very distinct either. In fact, this spectrum is almost totally dominated by the (off scale) intensities of small mass peaks in the m/z 28-45 range. In our opinion this coal sample, collected from an old roadcut in highway 7 (see Table 1), has undergone severe chemical deterioration and should perhaps be considered as a humic acid type material rather than a coal. The wide range of structural chemical differences between just three of the twelve coals in our study illustrates the magnitude of the analytical problem.

In order to obtain a more systematic overview of the various chemical components and trends in our data set we performed a factor analysis of all 36 coal spectra (each sample was analyzed in triplicate). A description of the variance described by the first 11 factors with eigenvalue >1.0 is given in Table II whereas a score plot of factors II and III (Figure 2a) was found to display some of the most interesting chemical information. A more complete description of

the information in Factors I and IV will be provided in the final publication of the results. Chemical interpretation of the clustering trends in Figure 2a is facilitated by inspection of the so-called variance diagram plot [7] in Figure 2b which reveals the presence of at least 4 major chemical components. These components can be shown in mass spectral form using a "factor spectrum" technique described by Windig et al. [8]. Inspection of the factor spectra in Figure 3a-d shows two vitrinite-like patterns (component axes B and C in Figure 2b), an aliphatic hydrocarbon pattern (component axis E) and a sulfur compound pattern (component axis F). Comparison with component spectra found in earlier Py-MS studies [5,9] of U.S. lignites and coal maceral fractions, respectively, indicates that, whereas components B and C may be regarded as primarily of terrestrial origin, components E and F can be thought to represent a stronger aquatic influence on the ancient depositional environments involved.

In other words, Factors II and III appear to be primarily correlated with differences in depositional environment. Not unexpectedly, Factor I was found to be dominated by differences in the overall degree of oxidation and/or weathering (factor spectrum of component A not shown here because of space limitation). In contrast to the apparent differences in "reported rank" shown in Table I, no obvious rank dependent influence was observed other than the presence of two distinct, possibly rank dependent, vitrinite-like patterns in components B and C. However, it should be pointed out that the highest rank coal (Lower Hartshorne "bituminous") was severely degraded and that the difference in Py-MS patterns between "lignites" and "subbituminous" coals tend to be relatively minor [10].

After examining the major chemical components and trends in the Py-MS patterns of all twelve coals we undertook a thorough analysis of the "biosolubility" data obtained by systematic studies with a panel of six microorganisms (listed in Table III) using a novel technique developed by one of us (B. Ward) and reported in more detail elsewhere [3]. The biosolubility data shown in Figure 4, can be regarded as a multidimensional biological response surface obtained by measuring the diameter of dark diffusion zones of soluble coal components surrounding small disk-shaped coal pellets imbedded in solid culture media inoculated with selected microoganisms under carefully standardized conditions.

Factor analysis of the biosolubility data shown in Figure 4 reveals that the true dimensionality of the biological response surface is close to 2 with the first two factors explaining more than 97% of the cumulative variance (see Table IV). In other words, no more than two independent sources of variance can be present in the biosolubility data. Both trends are clearly identified in Figures 5a and b. All microorganisms appear to be more or less successful in solubilizing coals 3 and 9 (or, less completely, 8 and 10), whereas only organisms c and e (and to some extent b) succeed in solubilizing coals 2 and 11 (or, less completely, 4 and 12).

This can also be seen in Figure 4 where the two response patterns have been arranged to show the differences in the upper and lower rows, respectively. No significant biosolubilization response was observed for coals 1, 5, 6 and 7. It should be noted here that the two distinct biosolubilization patterns were only observed upon factor analysis of the microbiological data but were not immediately apparent in the foregoing examination of the Py-MS data.

This prompted us to resort to the powerful canonical correlation approach in order to determine which, if any, Py-MS signals correlated with the

biosolubilization trends. Moreover, in view of earlier observations by one of us of a strong correlation between biosolubilization and alkaline solubility under abiotic conditions, we decided to include the alkaline solubility values for all twelve coals in the biosolubilization data set.

Two significant canonical correlation functions were found with correlation coefficients 0.99 and 0.92, respectively. Together these two functions explained 25% of the total variance in the Py-MS data set and 92.4% of the total variance in the combined biosolubilization/alkaline solubility data. Moreover, in agreement with the earlier reports by Quigley et al. [1,2], alkaline solubility was found to correlate strongly (correl. coeff. = 0.93) with biosolubilization. Inspection of the scores and loadings of the two canonical correlation functions, as plotted in Figures 6a and b, reveals the same two trends already noticed in Figures 5a and 5b. This brings up the key question: what is the chemical and biological meaning, if any, of these two trends? In order to help answer this question we calculated the two factor spectra correlating with these trends (a further impression of the most important mass peak contributions can be obtained from the combined loadings plots in Figure 6b). Figures 7a and b show the two mass spectral patterns associated with good biosolubilization (and alkaline solubility) by all microorganisms (Figure 7a, 310° component axis) and with good biosolubilization by microorganisms c and e (Figure 7b, 40° component axis), respectively.

At present, we are unable to provide an unambiguous chemical interpretation of these two trends. However, spectrum 7b is dominated primarily by fatty acid and carboxylic moieties, such as commonly observed in coals weathered in a laboratory environment [6]. Spectrum 7a, on the contrary, exhibits a variety of additional aromatic or polyunsaturated aliphatic signals suggestive of oxidative products of aromatic compounds. One hypothetical explanation could be that Figure 7a represents severe oxidative destruction by natural weathering phenomena enabling a broad range of microorganisms to start solubilizing the coal matrix, e.g., by producing alkaline compounds, as suggested by Quigley et al. [1,2], whereas Figure 7b points to a more extreme accumulation of carboxylic acids, and thus a strongly acidic pH, possibly allowing only some of the microorganisms to produce sufficient alkaline compounds to solubilize the coal.

In line with this interpretation, the alkaline solubility vector in Figure 6b can be seen to be intermediate between the two trends. In other words, both conditions produce an equal degree of solubilization in the presence of an unlimited amount of alkaline buffer. If this explanation is correct, the lower acid concentration in Figure 7a could have been caused by secondary natural phenomena, such as the loss of water soluble acidic constituents through leaching, rather than by a different oxidative mechanisms.

Presently, we are investigating possible other explanations, e.g., involving metal chelating agents or the possible involvement of enzyme-mediated bond breaking mechanisms.

CONCLUSIONS

Multivariate analysis of pyrolysis mass spectra of twelve samples of low rank coals exhibiting different degrees of biosolubility revealed a high level of heterogeneity, apparently associated with differences in rank, depositional environment (e.g., as reflected in maceral composition) and degree of weathering.

Multivariate analysis of "biosolubility profiles", obtained by measuring the relative biosolubility response of twelve coal samples to a panel of six different microorganisms, strongly suggests the presence of at least two biosolubility mechanisms. One of these mechanisms is exhibited by all 6 microorganisms whereas a second mechanism appears to be associated with only 3 of the microorganisms.

Canonical correlation analysis of the pyrolysis mass spectrometery and biosolubility profile data sets produced two canonical variate functions with correl. coeff. 0.99 and 0.92, respectively. Together these functions explain approx. 25% of the total variance in the Py-MS data and 92.4% of the biosolubility data.

Coal samples exhibiting good biosolubility appear to have in common a pronounced oxidative degradation of aromatic structural components, thought to represent vitrinitic and related maceral constituents. Besides increased biosolubility, the most obvious effects of these oxidative changes are: (1) an apparent increase in low MW, oxygen containing pyrolysis products; (2) a notable increase in alkaline solubility; and (3) a markedly reduced abundance of characteristic vitrinitic signals in the pyrolysis mass spectrum.

The observed correlations between the biosolubility and pyrolysis MS profiles further suggest that oxidation of a coal sample (evidenced by strongly increased pyrolysis yields of CO_2 and CO) does not produce biosolubility for all six microoganisms. An additional structural change, characterized by the increased evolution of pyrolytic benzene (presumably derived from benzenecarboxylic acids) may be needed to induce biosolubility for all six microorganisms and thus achieve maximum alkaline solubility levels.

A strong linear correlation (corr. coeff. 0.91) was observed between alkaline solubility (as determined by absorbance of the solution at 400 nm) and the two-dimensional canonical variate space obtained by canonical correlation analysis of the pyrolysis MS and biosolubility profiles. This is in agreement with previous reports by Quigley et al. [1,2].

ACKNOWLEDGEMENTS

The work reported here was supported by Idaho National Engineering Laboratory (INEL) under DOE Contract #DE-AC07-76ID01570.

REFERENCES

1. Quigley, D.R., Wey, J.E., Breckenridge, C.R., Stoner, D.L. and Dugan, P.R., in "Processing and Utilization of High Sulfur Coal II," Y.P. Chung and R.D. Caudle (eds.), Elsevier, N.Y., pp. 315-322, 1987.
2. Quigley, D.R., Wey, J.E., Breckenridge, C.R., and Stoner, D.L. Resources, Conservation and Recycling, 1988 (in press).
3. Ward, Bailey, in "Biotechnology Applied to Fossil Fuels," D.L. Wise, (eds.), Chap. 25, CRC Press, Boca Raton, FL, (in press).
4. Meuzelaar, H.L.C., Haverkamp, J., Hileman, F.D., "Pyrolysis Mass Spectrometry of Recent and Fossil Biomaterials," Elsevier, Amsterdam, 1982.
5. Metcalf, G.S., Windig, W., Hill, G.R. and Meuzelaar, H.L.C., Int. J. Coal Geol., 7, (1987) 245-268.
6. Jakab, E., Yun, Y. and Meuzelaar, H.L.C., in "Chemistry of Coal Weathering", C.R. Nelson, (ed.) chapter 6, in press.

7. Windig, W. and Meuzelaar, H.L.C., Anal. Chem., 56, (1984) 2297-2303.
8. Windig, W., Jakab, E., Richards, J.M., and Meuzelaar, H.L.C., Anal. Chem., 59, (1987) 317-323.
9. Meuzelaar, H.L.C., Harper, A.M., Pugmire, R.D. and Karas, J., Int. J. Coal Geol., 4, (1984) 143-171.
10. Meuzelaar, H.L.C., Harper, A.M., Hill, G.R. and Given, P.H., Fuel, 63, (1984) 640-652.

Table I
Origin, Rank and Alkaline Solubility of 12 Coals

Sample #	seam or field (state)	reported rank	description of sampling site	alkaline[a] solubility
1	Coalmont (CO)	subbit	fresh stripmine sample (Kerr Mining CO)	-2.70
2	Coalmont (CO)	subbit	weathered chunks from abandoned mine (near site 1)	-1.09
3	Coalmont (CO)	subbit	erosion gully outcrop in pasture (near site 1)	1.45
4	Kiowa (CO)	lignite	dry gulch outcrop	-1.19
5	Green River (CO)	subbit	weathered chunks from abandoned strip mine (Black Dan, near Hayden)	-2.70
6	Hagel (ND)	lignite	fresh sample (PSOC 1482)	-1.22
7	Clairborne (MS)	lignite	creek bed outcrop near Antioch	-0.78
8	Clairborne (MS)	lignite	ibid, more weathered	-0.36
9	Wilcox (MS)	lignite	I-20 roadcut near Russell	0.91
10	Midway (AL)	lignite	I-20 roadcut between York and Cuba	0.32
11	Lower Hartshorne (AK)	bituminous	Hwy 7 roadcut of excavation near Dardanelle	-0.70
12	Brandon (VT)	lignite	fresh sample stored in H_2O since October, 1984	-0.35

a. Alkaline solubilities (log (absorbance)) were measured at 400 nm

Table II
Factor Analysis Results of Py-MS Data

FACTOR #	EIGENVALUE	%TOTAL VARIANCE	CUMULATIVE VARIANCE
1	88.85	57.86	57.86
2	22.60	14.71	72.57
3	14.99	9.76	82.58
4	8.06	5.25	87.58
5	6.42	4.18	91.77
6	2.85	1.86	93.62
7	2.39	1.56	95.18
8	1.84	1.19	96.38
9	1.64	1.07	97.44
10	1.28	.83	98.28
11	1.06	.69	98.96

Table III
List of Microorganisms and Description of Six Fungal Strains

Bacteria #	Code	Full Name
a	ACL-13	*Candida* sp.
b	DML-12	*Acremonium* sp.
c	*p. chrysosporium*	*phanerochaeta chrysosporium*
d	RML-40	an unidentified Basidiomycete
e	YML-1	*Cunninghamella* sp.
f	YML-21	a *Cunninghamella* - like Hyphomycete

Table IV
Factor Analysis Results of Biosolubility Data

FACTOR	EIGENVALUE	% TOTAL VARIANCE	CUMMULATIVE VARIANCE
1	5.19	86.43	86.43
2	.64	10.59	97.03
3	.14	2.34	99.37
4	.03	.49	99.86
5	.01	.12	99.99
6	.00	.01	100.00

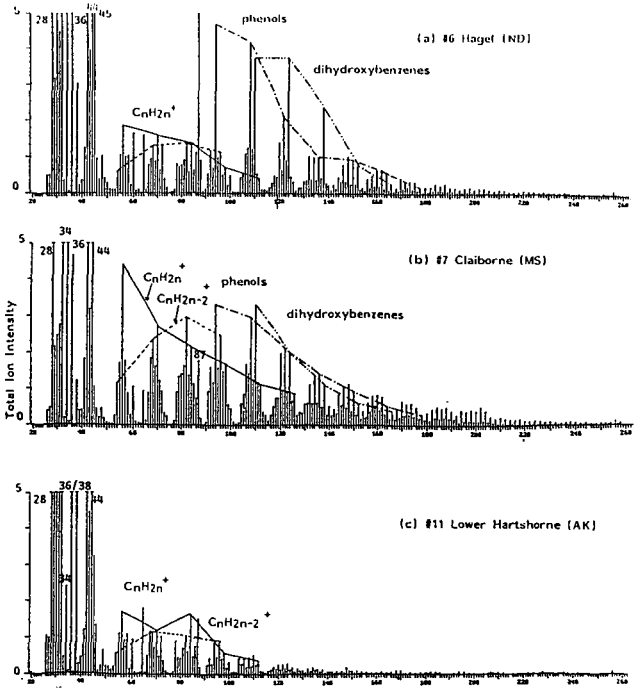

Figure 1. Pyrolysis mass spectra of (a) North Dakota lignite (b) Mississippi Claiborne lignite (c) Arkansas "bituminous" coal.

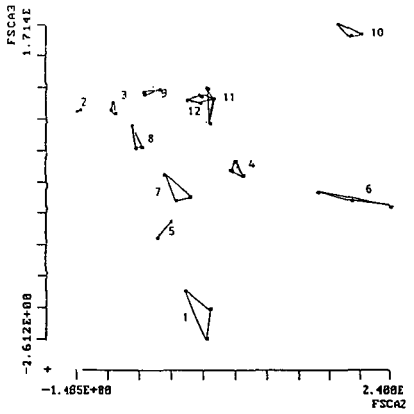

Figure 2a. Score plot of factor 2 vs. factor 3 of MS data.

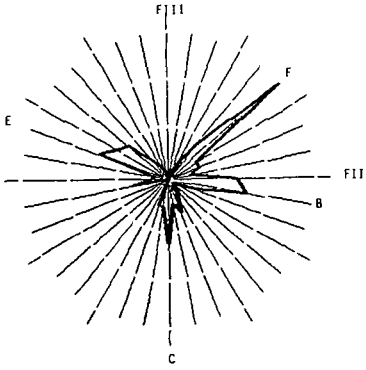

Figure 2b. Variance diagram showing the presence of four major component axes B,C,E,F, in the space spanned by factors II and III.

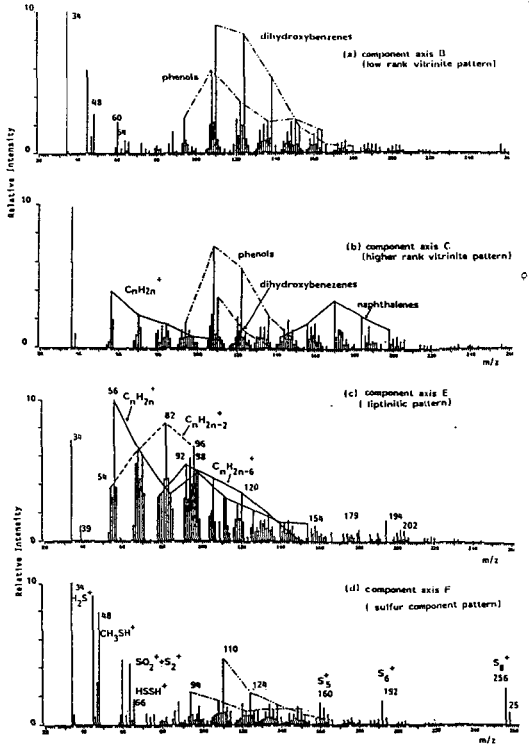

Figure 3. Comparison of numerically extracted factor spectra of (a) component B (low rank vitrinite pattern), (b) component C (higher rank vitrinite pattern) (c) component E (liptinitic pattern) and (d) component F (sulfur component pattern).

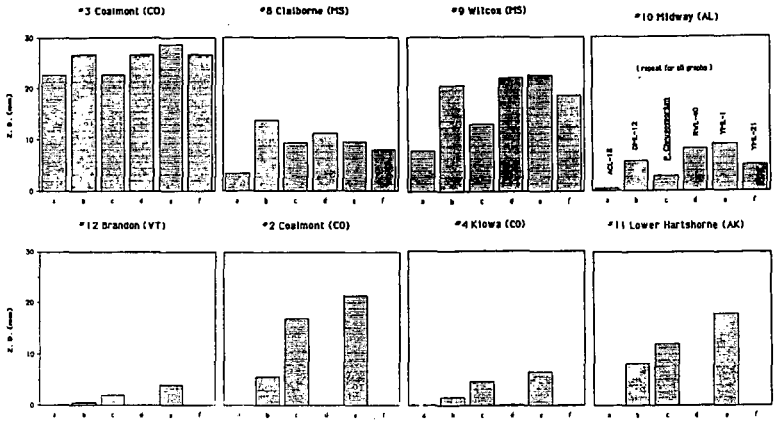

Figure 4. Biosolubility of 8 coals as a function of six microorganisms, expressed by zone diameter (mm). None of the microorganisms shows biosolubility on coals nos. 1, 5, 6 or 7.

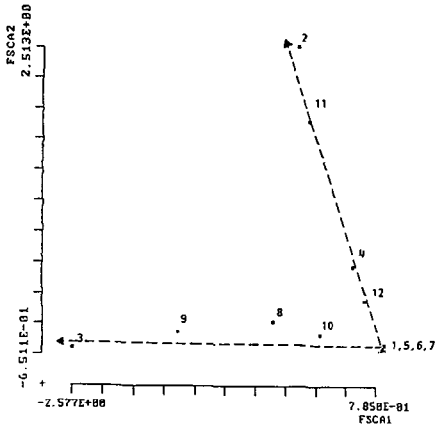

Figure 5a. Score plot of factor I vs. factor II of biosolubility data.

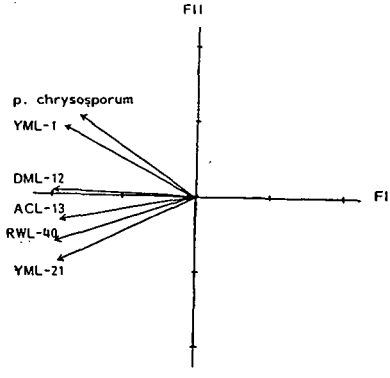

Figure 5b. Variance diagram of factor I vs. factor II of biosolubility data.

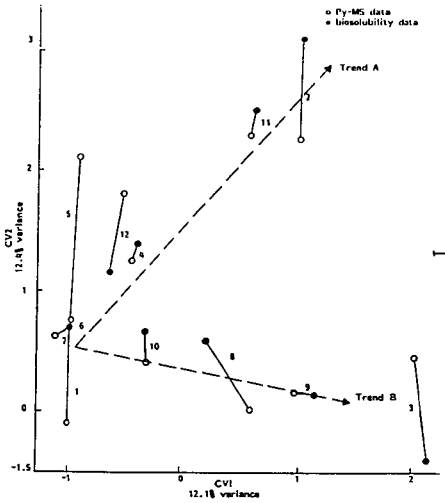

Figure 6a. Combined score plot of the first two canonical variate function of the Py-MS data and the biosolubility data, respectively.

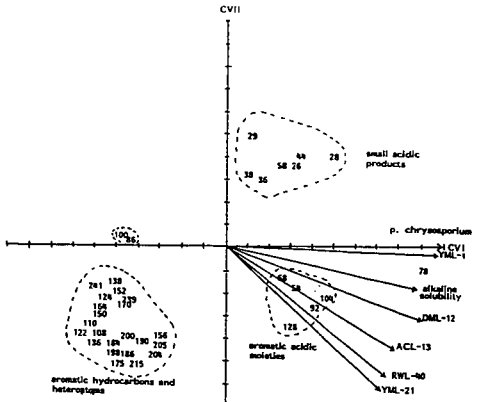

Figure 6b. Loading plot of the mass values and biosolubility parameters contributing most strongly to the first two canonical variate functions.

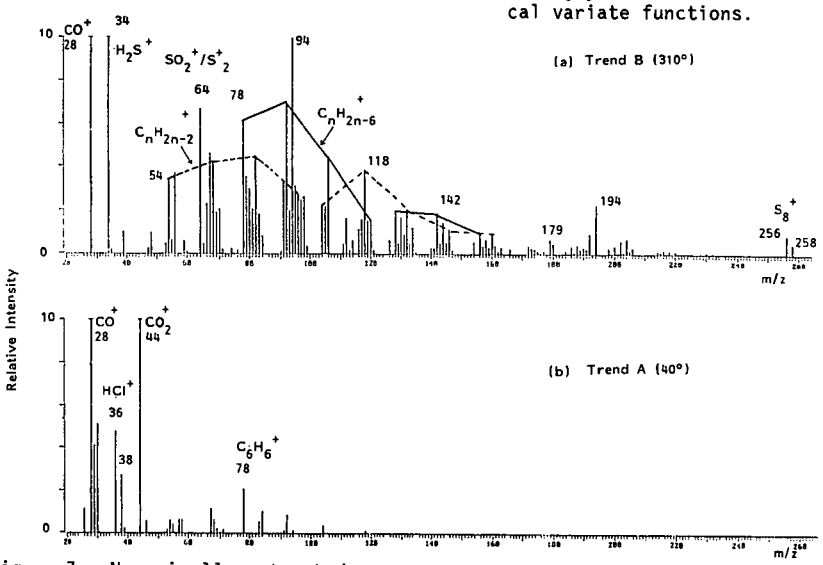

Figure 7. Numerically extracted mass spectra of trends B and A at 310° and 40° in CVI/CVII space, respectively.

ENZYMATIC REMOVAL OF ORGANIC SULFUR FROM COAL

O.G. Ngaiza, D.L. Wise, T.R. Gilbert *
Dept. of Chemical Engineering and
Dept. of Chemistry *
Northeastern University
Boston, MA 02115 U.S.A.

ABSTRACT

A process in described for the enzymatic (not microbiological) removal of organic sulfur from coal. The process evaluated utilizes ultra ground coal (<50 microns) and froth flotation to first removal pyritic sulfur. In this design conceptual mild alkali oxidation followed by enzymatic treatment is then used to reduce the organic sulfur. A preliminary economic analysis for processing 20,000 metric tons of coal/day is being carried out for reducing 4.5% sulfur content bituminous coal (containing an assumed 50:50 W/W pyritic/organic) to under 1% sulfur in order to meet clean air standards. The background work leading to this conceptual process is encouraging. Experimental work is now proceeding and preliminary results are encouraging.

INTRODUCTION

Background to the Problem of Sulfur in Coal

The use of fossil fuels for power generation is expected to increase, despite diminishing world reserves of high quality crude oil and coal. The demand for low-sulfur and low-nitrogen fossil fuels has been intensified by increasingly stringent regulatory standards for reduced levels of sulfur- and nitrogen-oxides in released atmospheric emissions. Amendments to the 1964 Clean Air Act require not only compliance with emission standards but also a percentage reduction in emissions that otherwise would occur from the burning of untreated fuel, requiring that low-quality fuels be subjected to either pre- or post-combustion desulfurization.

Post-combustion processes, e.g., flue-gas desulfurization, are generally inconvenient, expensive, and definitely limited with respect to the scope of their remedial action. These processes usually ignore other aspects of (sulfur) contamination which are certainly as economically important as emissions control, e.g., corrosion of mills and conveyors due to pyritic sulfur. Pre-combustion cleaning processes, on the other hand, can offer significant advantages over post-combustion processes, such as flue gas desulfurization, because these pre-combustion schemes can eliminate problems associated with both environmental pollution and equipment corrosion.

Traditional pre-combustion processes exploit either physical or chemical methods. Physical methods include flotation or magnetic separation of the pyrite from coal. As compared to chemical methods, these are generally more economical. The drawbacks to these physical methods, however, lie in the limited removal of the overall sulfur and the notable energy losses. Chemical pre-combustion cleaning methods usually employ some sort of oxidizing agent, e.g., ferric salts, chlorine, or ozone, or reducing agent, e.g., solvent-hydrogen mixtures. In contrast to physical methods, chemical methods can be reasonably effective in removal of some of the organic sulfur along with the pyrite. Some of the disadvantages which have an impact on the efficiencies associated with chemical

cleaning operations include corrosion problems resulting from the use of high concentrations of the chemical agents, the energy intensiveness of the high temperature/high pressure operations, and the costliness of reagent recovery.

Thus, there is a need for methods of coal desulfurization which improve upon these traditional process. Of particular need is a method for removal of organic sulfur, a contaminant which often is only secondarily removed. This paper focuses on a processing concept for the resolution of that need. Drawing upon the experiences derived from the aforementioned types of cleaning operations, the technical feasibility of a novel concept is considered within the context of process efficiency. Reagent costs, recovery operations, waste products, and operating conditions are also under consideration in this new plan for coal beneficiation while the technical concepts are researched. Development goals and research goals are of coincident interest, as is necessary for programs addressing new cleaning processes.

Background to Biodesulfurization

An obvious means to the circumvention of some of the cost problems found in traditional coal cleaning processes lies in the use of biological methods because of the inherently lower capital and operating costs. Indeed, microbial coal desulfurization already has a history. Early interests in this field focused upon microorganisms for pyritic sulfur removal; these microorganisms were "naturally" suited to this task having themselves adapted to sulfur utilization in mine waters (e.g., as with *Thiobacillus*) or sulfur springs (e.g., as with *Sulfolobus*). However, while interesting from the standpoint of process-type manipulations, these microorganisms do nothing for organic sulfur removal. Thus, if substantial sulfur removal is of interest, biological methods must do more than remove only the inorganic sulfur.

Several more recent efforts have focused upon the adaptation and use of various strains of microorganisms to act upon and remove the organic sulfur (e.g., those projects at the Atlantic Research Corporation(1,2), The Institute of Gas Technology(3), and the University of Georgia(4). These "coal bugs" are becoming well-known and have been shown to have "appetites" for organic sulfur. Oxidation of sulfur for removal as organic sulfate has been the most commonly demonstrated mechanism for microbial removal of organic sulfur; as a result, some of the organic, i.e., the energy, content is often lost as part of the sulfate. While encouraging demonstrations of the feasibility of organic sulfur removal via biological means have been shown, these projects by no means represent optimized solutions. Microbial efficiencies and process operations await improvements. These works continue, for the most part, in that vein while additional lessons in coal cleaning are made available for further conceptual developments of the sort being exploited, as described herein.

A consideration in these microbially-based cleaning operations lies in the potential for some degree of process sensitivity. That is, because these operations exploit live organisms, there is concern as to their maintenance as both viable and selective populations. While ample precedent exists for microbially-based treatment systems, e.g., wastewater treatment, there are recognized sensitivities implicit in the use of live systems, such as mutational problems, reactor upsets, substrate variations, etc. A possible solution may lie in the use of an enzyme-based cleaning process, that is, a process which solely uses the "active extract" of the microbial process to effect desulfurization(5). The concept of enzymatic removal of sulfur from coal is discussed in the following.

Enzymes for Removal of Organic Sulfur From Coal

An enzymatic (not microbiological) process for organic sulfur removal from coal would first require the identification, characterization and production of an enzyme known to cleave sulfur from a representative polymer. These enzymes would then be immobilized or "tethered" on a standard packing material such as is used to support conventional catalytic materials in the bioprocess industries (the enzymes may be in solution, as discussed later, but immobilized enzymes are used in this explanation.) Upon passing the coal/water slurry through the packing material, the immobilized enzymes tethered on the packing would cleave the organic sulfur, acting as a type of biocatalyst. Coal particles, free of organic sulfur, would then be recovered; sulfur could also be readily recovered.

With this introduction, some of the pertinent technical background is given in the following section.

TECHNICAL BACKGROUND

Overview

The subject of sulfur removal from fossil fuels by biologically based means has been receiving increasing attention in recent years(6). This is due, in part, to the enhanced ability of controlling the genetic make-up of various organisms, but also to the possibility of selectively removing the objectionable sulfur compounds at the front-end of a power generation process and without affecting the hydrocarbon structure (hence, the thermal value) of fuel. Other advantages include mild operating conditions, possible use of natural earth formations as reactor systems, and possible longer biocatalyst life under concentrated sulfur and heavy metal conditions observed in refining and cracking operations.

Pyrite Removal

Sulfur content of coal has been reported to be at least 4.5%, approximately equally distributed between organic and inorganic compounds. The latter, predominantly in the form of pyrite, have been investigated recently, with regards to their dissolution potential through the mediation of soil acidophilic bacterial. A large number of such organisms have been isolated to date, the most important among them being members of the genera of Thiobacillus and Sulfolobus. Extensive studies with such organisms, in pure as well as in mixed cultures, demonstrated the feasibility of oxidative dissolution of the pyrite sulfur from coal(7,8,9). Dissolution kinetics were found to be first order with respect to the specific surface area of the coal, and, based on these preliminary kinetic data, a feasibility assessment of a coal water slurry pipeline was carried out for the simultaneous transport and pyritic sulfur removal from the coal.

Organic Sulfur Removal

The removal of organic sulfur from coal is a significantly more demanding task than pyritic sulfur removal mainly because of two reasons. Foremost, organic sulfur is deeply embedded in the coal matrix requiring a very fine pulverization of coal in order to expose the sulfur compounds to the action of chemicals or catalysts. Second, the primary sulfur compounds are far more resistant to degradation or assimilation by organic or biological catalysts and often poisonous or toxic to their activity.

The possibility of using microorganisms for organic sulfur removal from coal

has been examined in the past forty years. The patent literature is rather imaginary and inconclusive. The majority of these studies were carried out with model compounds representative of the three types of organic compounds that the approximately 195 sulfur substances in coal can be classified into, namely, A) sulfides, B) thioles, and C) thiophenes(10). In particular, due to the relative ease of removing aliphatic sulfides and other sulfur compounds of low boiling point by simple chemical means, most of the attention has been focused on aromatic sulfur compounds such as thiophenes, especially benzothiophene (BT) and dibenzothiophene (DBT)(10). Attempts to isolate microorganisms capable of degrading simple thiophene aerobically have been unsuccessful(11). However, microbial degradation of the nucleus of substituted thiophenes has been demonstrated(12). Other studies have addressed the possibility of degrading BT and DBT. For example, a mixed culture of Arthrobacter sp. and Pseudomonas sp. was shown to be able to grow on DBT and residue oil with products being cellular mass and inorganic sulfate(13). DBT could also be converted to water soluble oxygenated derivatives which accumulated during metabolism, but the sulfur in the thiophene nucleus remained untouched by this action(14). Several other studies have confirmed these findings showing that BT, DBT, and related organic sulfur compounds can be converted into soluble sulfur compounds through the use of pure cultures or microbial consortia(15-17).

There are, however, some serious problems associated with the use of living organisms in considering large scale organic sulfur removal from coal. First, the conditions which are optimal for the growth and activity of such organisms are usually incompatible with the concept of the envisioned large-scale process or require expensive additives so that they can be maintained for extended periods of time. Second, objectionable amounts of growth factors and carbon sources are needed which could cause insurmountable economic difficulties. Third, toxic by- products or other compounds in a realistic process environment could be the source of severe poisoning problems that render the microorganisms incapable of performing the tasks for which they were isolated. Finally, culture stability is always a serious concern especially in open, continuous flow ecosystems. For this reason, the concept considered here is a combination of chemical pretreatment with an enzymatic process which could be a viable alternative to the above mentioned possibilities.

Enzymatic Desulfurization Process

It is assumed that it is feasible and economical to pulverize coal down to 10 to 50 micron fine particles so that most of the organic sulfur compounds become either exposed to or reachable by the chemical reagents involved in the pretreatment and the subsequent enzymatic process. If this is not so, significant carbon oxidation may take place before the sulfur compounds can be acted upon by the oxidizing agents.

The coal particles are mixed with water for the preparation of a coal/water slurry (available technology) which is subsequently subjected to a chemical oxidation pretreatment with a hot alkaline reagent. The objective is to partially oxidize the maximum possible amount of the organic sulfur compounds to sulfate. Full oxidation to SO_4 is obviously undesirable and so are many destructive effects of the oxidizing agent on the carbon of the coal matrix. There is clearly an optimum for the degree of oxidation, and this can be achieved by varying the temperature, strength of alkali, and duration of pretreatment, followed by titration for the fraction of overall sulfur converted to sulfate for each combination of operating conditions.

The next step is to remove the sulfates from the coal particles. One way to selectively accomplish this is by contacting the coal/water slurry with a sulfatase enzyme solution. Enzymes are commercially available that have the property of catalyzing the dissolution of sulfur compounds by cleaving the sulfate anions from the aliphatic aromatic backbone. The resulting sulfate solution can be further treated with lime to finally contain sulfur in the form of calcium sulfate solids.

Concept Presented

The present work addresses the feasibility of organic sulfur removal from coal via select enzymatic methods. These methods focus upon the stepwise biochemical transformation of the coal matrix for extraction of the organic sulfur as sulfur oxides such as sulfate. These transformations proceed via enzymatic pretreatment of the coal to both (bio)chemically oxidize the available organic sulfur and (bio)physically "loosen" the matrix followed by enzymatic cleavage about the pretreated sulfur moieties.

Thus, this concept followed from the basic demonstrations of microbial desulfurization in that technical sense which supports oxidative methods for removal of organic sulfur. However, this concept focused on a unique approach to circumvention of the process inefficiencies associated with microbial desulfurization methods by testing the use of only the "active' fractions of microbial populations, i.e., the enzymes, to effect the necessary coal chemistry for sulfur transformations and removal. This evaluation was conducted within the context of considering a feasible process template for an enzymatic coal cleaning operation. A brief discussion of the enzymatic removal of organic sulfur from coal, the concept on which our concept is based, is as follows.

ENZYMATIC COAL BIODESULFURIZATION

Rationale For Processing Concept

The intricacies of coal structures and their chemistries are the subject of continuing study. However, some of the basic elements of coalification and depolymerization chemistries can be considered. Coal is formed via dehydration processes and coal is broken down via combinations of hydrolytic, oxidation, and other displacement chemistries. The understanding of these types of chemical transformations in coals forms the basis for various processes addressing coal upgrading or beneficiation via traditional methods, e.g., liquefaction or chemical desulfurization.

Microorganisms which have been shown capable of interacting with coal also take advantage of these coal chemistries. Basically, microbes establish an interaction with the coal because the coal has something which the microbe can use or, at least, tolerate. The microorganism requires its "balanced diet" for growth and survival. If given coal as the mainstay of that "diet", then it has to acclimate its biological machinery in such a way so as to be able to utilize the coal. This means that the microorganism's consortia of available reagents (e.g., water) and catalysts (i.e., enzymes) must go to work to selectively extract and/or cleave the nutrients it needs, and, in doing so, this microorganism uses established chemistries. There is no reason to suggest that, in these instances, coal is extracted or cleaved in a manner any different than those demonstrated via conventional chemical processing. Indeed, some of the early work which has been done on the mechanisms of microbially-mediated coal

processing shows (through product analysis) that this is certainly so. Studies of microbial liquefaction, for example, demonstrate oxidation and hydrolysis of the coal matrix.

Current knowledge of microbial desulfurization processes lends further support to the cited mechanism for coal breakdown. Those microbial processes specifically intended for organic sulfur removal from coal implicate oxidation of the carbon-sulfur linkages to yield sulfur oxides (in most cases, sulfates) which then are susceptible to a hydrolysis to liberate the sulfur oxides from the remainder of the coal matrix. There have been, however, some serious problems associated with the use of these living organisms in large-scale organic sulfur removal from coal. First, the conditions which are optimal for the growth and activity of such organisms are usually incompatible with the concept of the envisioned large-scale process or required expensive additives so that they can be maintained for extended periods of time. Second, objectionable amounts of the growth factors and carbon sources are needed which could eventually cause insurmountable economic difficulty. Third, toxic by-products or other compounds found in a realistic process environment could be the source of sever poisoning problems that render the microorganisms incapable of performing the desulfurization task for which they were isolated. Finally, culture stability is always a serious concern particularly in an open, continuous-flow ecosystem.

Given microbial ability to effect the coal chemistries necessary for desulfurization, but also given the concerns of a "living" processing system, our team early considered an alternative biologically-based desulfurization scheme. In this alternative concept was seen the advantages of bioprocessing in perhaps an eventually more efficient manner. Specifically, the concept investigated has focused on the sole use of the "active extracts" of the microbes with the consideration that the problems associated with reactor upset can be minimized. The concept subject to the investigation is an enzymatic desulfurization process.

While enzymatic processes have been proven in large-scale industrial applications, it is important to note that their use in coal cleaning is not merely a transfer of technology to a new process substrate. Specific enzymatic action about the organic linkages of interest, as well as the efficiencies of any demonstrated action, must be investigated. The issues of enzymatic accessibility must also be addressed. In addition, the constraints imposed by a solid substrate must be incorporated into design consideration, particularly if the use of raw coal is the major interest. Thus, both scientific and engineering feasibilities are important components to process development.

Processing Concept

Overall, the present concept is a desulfurization system that derives its processing reagents from biological sources. In contrast to chemical operations, processing catalysts (i.e., enzymes) are of natural origin thus, potentially, processing may be more benign. In contrast to microbial operations, the active agents are molecularly discrete; thus, potentially, processing may be less sensitive to the reactor upsets associated with "living" microbial systems.

In this concept enzymes are being used as processing tools in an effort to affect the removal of the organic sulfur from coal. The coal chemistries are those of oxidation and hydrolysis. "Oxidases" are being used to catalyze the oxidation about the sulfur bond; "hydrolases" are being used to catalyze the hydrolysis about the prepared sulfur. In other words, biochemicals are being

investigated for their potential to direct the chemistry of desulfurization thus leading to a potentially more efficient cleaning process. The overall objective is to investigate the feasibility of a practical, bioreactor-based enzymatic desulfurization process specifically intended for organic sulfur removal from coal.

Technical Considerations

The basic premise of our concept for enzymatic desulfurization of coal is that the use of specific hydrolases will reduce the organic sulfur content. For example, the reaction to remove organic sulfur may use one type of hydrolase, namely an "arylsulfatase". That is, in the presence of the arylsulfatase enzyme, the hydrolysis of organic sulfate compounds to organic phenols is catalyzed. The sulfur is effectively isolated from the organic starting components and is retrievable as water-soluble sulfate. Aside from the issues of biocatalyst selectivity and operating efficiency, the use of an arylsulfatase for organic sulfate removal is fairly straightforward.

The complexity which arises from the actual exploitation of arylsulfatases or sulfur removal lies in the consideration of the forms of sulfur in coal. The three major forms of organic sulfur in coal are: (1) thiophenes (approximately 65% of the total organic sulfur), (2) sulfides (approximately 25%), and (3) thiols (approximately 10%). Very little of the accountable sulfur is presumed to be in the form of organic sulfur oxides, such as sulfate. However, it is possible to survey these available sulfur forms and propose their conversion to oxides for removal via hydrolase, e.g., sulfatase, enzymes. Specifically, it is our concept to oxidatively pretreat coal for conversion of as much of the organic sulfur to oxides, such as sulfate, then effect the actual desulfurization via enzymatic hydrolysis of the sulfur oxide.

Thus, our concept for enzymatic desulfurization of coal presently organizes the processing effort into two areas: (1) oxidative pretreatment, and (2) actual desulfurization. The former has as its goal the oxidation about the sulfur moiety and includes investigation of both chemical and enzymatic methods. The latter has as its goal the actual removal of the prepared sulfur from the organic matrix and focuses on enzymatic methods only. The results in each area are intended for use in a reasonable process model, the template of which has been prepared.

Acknowledgement

This work has been sponsored in part by Stone and Webster Engineering Corporation and Houston Lighting & Power Company.

REFERENCES

1. Isbister, J.D. et. al, "Biological Removal of Organic Sulfur From Coal", Paper No. 133, Presented at the Pittsburgh Coal Technology Conf., Sept. 1985.
2. Isbister, J.D. et. al, "Biological Removal of Organic Sulfur From Coal", Proceedings of Workshop on Biological Treatment of Coals, June 23-25, 1986, Herndon, VA.
3. Kilbane, J.J. "Microbial Removal of Organic Sulfur From Coal: Current Status and Research Need" in Biotechnology Applied to Fossil Fuels, D.L. Wise, Editor, CRC Press, Inc., in press, to be published 1988.

4. Finnerty, Univ. of Geo., Athens, Georgia, Personnel Communication.
5. Ngaiza, O.G., Wise, D.L., Sinskey, A.J., "Enzymatic Removal of Organic Sulfur from Coal" to be presented July 12-13, 1988 at Coal: Target of Opportunity, Workshop, Washington, D.C.
6. Wise, D.L., Editor, Biotechnology Applied to Fossil Fuels, CRC Press, Inc., to be Published 1988.
7. Hoffman, M.R., Faust, B.C., Panda, F.A., Koo, H.H. and Tsuchita, H.M., "Kinetics of the Autoxidation of Iron Pyrite in Coal by Microbial Catalysts," Applied Environ. Microbiol., 42, 259, 1981.
8. Hoffman, M.R., "A Reaction Network Model of the Ocidative Dissolution of Iron Pyrite as Catalyzed by Mixed-Culture Microbial Systems," Environ. Sci and Tech, 1982.
9. Lapako, K.L., Eisenrieich, S.J. and Hoffman, M.R., "Kinetics and Mechanisms of the Oxidative Dissolution of Sulfide Minerals from Duluth-Gabbro Ore," Geochim. Cosmochim. Acta, 1983.
10. Takaoka, S., Process Economics Program, Report No. 47, Stanford Research Institute, Menlo Park, CA, 1969.
11. Malik, K.A. and Claus, D., Fifth Intern. Fermen. Symposium, Berlin, 23, 03, 429, 1976.
12. Amphlett, M.J., and Callely, A.G., Biochem J., 112, 12, 1969.
13. Knecht, Jr., A.T., Ph.D. Dissertation, Louisiana State University, 1961.
14. Hou, C.T., and Laskin, A.I., Dev. Ind. Microbiol., 17, 351, 1976.
15. Laborde, A.L. and Gibson, D.T., Appl. Env. Microbiol., 34:783, 1977.
16. Kodama, K., Agro, Bio. Chem., 37:45, 1973.
17. Yamada, K., Agro, Bio. Chem., 32:480, 1968.

SOLUBILIZATION OF LEONARDITE BY WHITE-ROT FUNGI GROWN IN STATIONARY AND SHAKE FLASKS

M.D. Dahlberg, B.C. Bockrath, and V.A. Speers*
U.S. Department of Energy
Pittsburgh Energy Technology Center
Pittsburgh, PA 15236

INTRODUCTION

Oxidized coals, including a naturally oxidized lignite identified as leonardite, are solubilized and sometimes degraded further by a variety of fungi and bacteria. Evidence for biosolubilization of coal was first presented by Fakoussa (1), and Cohen and Gabriele (2). Subsequent studies concentrated on screening organisms (3), characterization of the product (4), and determination of the biochemical mechanisms. Mechanisms of biosolubilization are poorly known and may vary with the species used and the media. There is evidence for both enzymatic degradation (5,6) and alkaline solubilization (7,8).

The objective of this study was to discover critical factors in solubilization and biosolubilization mechanisms by testing a variety of growth media, growth conditions, and fungi. Lignin-degrading species were emphasized because of similarities between the structures in lignin and in low-rank coals. The results indicate that during idiophase (secondary metabolism), the fungi produce alkaline materials that solubilize leonardite.

METHODS

Phanerochaete chrysosporium BKM-F 1767 was obtained from Dr. T.K. Kirk of the U.S.D.A. Forest Products Laboratory; Trametes versicolor (ATCC 12679), from the American Type Culture collection; and Candida ML-13, from Dr. Bailey Ward of the University of Mississippi. Others were isolated at PETC. All were maintained on Sabouraud maltose agar (SMA) or broth at 35°C and 90%-98% humidity. Malt agar was frequently used to promote spore production in P. chrysosporium. P. chrysosporium was inoculated using filtered conidial suspensions (A_{650} = 0.5/cm); other species were inoculated using fungal mats ground in a blender.

To solubilize leonardite on fungal mats, small (1-2 mm) pieces of sterile leonardite were placed on 1- to 3-week-old agar cultures. The pH of the agar was monitored by the use of puncture and surface pH probes, and the black drops of solubilized coal were sampled for pH and other analyses. Elemental analyses were performed on 6-day-old mats and associated agar to study nutrient depletion.

---

*This research was supported in part by an appointment to the Postgraduate Research Training program under contract number DE-AC0570R00033 between the U.S. Department of Energy and Oak Ridge Associated Universities.

Reference in this report to any specific commercial product, process, or service is to facilitate understanding and does not necessarily imply its endorsement or favoring by the United States Department of Energy.

Four broths were tested for their characteristics in supporting fungal growth and promoting solubilization: Sabouraud maltose broth (SMB), nutrient broth (NB), tryptic soy broth (TSB), and a defined broth (DB) (9). Leonardite, a naturally oxidized lignite, was provided by American Colloid Co., Reeder, North Dakota.

Fungi were grown in 125-mL flasks (20 mL of broth) and 250-mL flasks (40 mL of broth). Roughly 40 flasks were set out at one time under the same growth conditions. From this set, duplicate samples were selected once or twice per week. They were filtered (1.0 μ-pore glass fiber) and analyzed for fungal dry weight (using tared filter paper), pH, and absorbance (A_{450}). A routine test was developed to assay the activity of cell-free broth for solubilization using both gravimetric and spectroscopic measures. Unless otherwise stated, leonardite [0.3% (wt/vol), <100-mesh] was added to the cell-free broth, and the mixture was shaken on a wrist shaker for 1 hr. The treated coal was filtered with a tared glass fiber filter (1-μ-pore), washed, dried, and weighed to gravimetrically determine the percentage of coal solubilized. The filtrate was analyzed for pH. The optical density at 450 nm (A_{450}) was measured, using diluted samples when appropriate, to obtain the spectrophotometric determination of the relative amount of coal solubilized. When plotted against each other, the two measures were correlated but showed considerable scatter (R^2=0.820-0.854).

To determine the effect of shake time on solubilization, replicates of cell-free filtrates were shaken and then filtered, and A_{450} of the filtrates were measured at 15-min intervals over the course of 1 hr. The SMB treated with P. chrysosporium was boiled for 1 min or heated at 90°C for 1 hr to determine if denaturation of basic proteins reduced solubilization. Protein concentrations of cell-free extracts were determined with the Bradford test (10).

RESULTS

Solubilization on Agar

Phanerochaete chrysosporium, Trametes versicolor, Candida SL13, Rhizopus arrhizus, and Geosmithia argulus all solubilized 1-2 mm leonardite chunks when grown on SMA at pH over 7 (Fig. 1). Solubilization was evidenced by the appearance of black liquid surrounding the coal within 48 hours after the coals were added to 1- to 3-week cultures. Two possible conversion mechanisms were investigated in the case of P. chrysosporium: degradation by the ligninase enzymes and solubilization by alkaline products. Ligninase is produced by the organism when nitrogen available for growth is nearly exhausted (9). Neither nitrogen nor two other growth essentials, phosphorus and carbon, were depleted in 6-day cultures (Table 1). Thus, conditions for ligninase production are not evident, even though conversion of coal was observed. Furthermore, ligninase is most active at low pH (9). Solubilization appeared to result from production of alkaline materials. This phenomenon was investigated in more detail using suspension cultures.

Solubilization by Fresh Broth

Results of shaking fresh broth with leonardite for 1 hr are shown in Fig. 2. The SMB and NB were preferred for use as growth media in fungal experiments. The TSB was eliminated because of high levels of solubilization in absence of fungi. Later experiments showed that only low levels of biosolubilization were

observed with extracellular fluid harvested from fungi grown in DB. All biosolubilization data presented below have been corrected for the absorbance due to the medium alone.

Solubilization by Harvested Cell-Free Broth

Particle size was expected to affect solubilization because of the larger surface area presented by the smaller particles. The A_{450} did increase as expected (Table 2) but not greatly within the 60- to 300-mesh range. Results for the standard size used in these studies (<100 mesh) were most similar to those for the 200-300 mesh.

The time needed to solubilize leonardite in cell-free broth harvested from an active fungal growth was studied. The absorbance was determined after shaking and reading A_{450} at 15-min periods for 1 hr (Table 3). The solubilization rate is most rapid during the first 15 min, and there is little increase in A_{450} during the next 45 min or for several hours (data not shown). Thus, the solubilizing agent works quickly, and the 1-hr shake time used under standard conditions is more than adequate.

Leonardite is an acidic material. Addition of leonardite to the harvested growth media reduces its pH and adversely affects its solubilization capacity. As may be seen in Table 4, the percentage of leonardite solubilized as measured by the gravimetric method steadily declines as the leonardite loading is increased. The A_{450} passes through a maximum and begins to decline as the pH is progressively reduced. Thus, the pH ultimately reached by a medium must be taken into account when comparisons of activity are made. The lowest coal loading (0.3 wt%) was chosen to minimize the influence of coal acidity.

A large set of flasks (~40) were set out under the same conditions as described under Methods. Duplicate flasks were selected and their cultures were tested regularly for solubilization of leonardite. The relationship of biomass, pH, percent solubilization, and A_{450} with P. chrysosporium in SMB is shown in Fig. 3. In this example, solubilization and A_{450} parallel the change in pH. Solubilization peaked during secondary metabolism and declined during the autolysis stage. Maximum absorbance occurred at 20-25 days in other runs with SMB cultures of P. chrysosporium.

The time to reach maximum absorbance could be reduced by continuous gentle agitation of the cultures at 50 rpm (Fig. 4). The highest absorbance occurred before the pH reached a peak. Agitation at 200 rpm considerably reduced solubilizing ability, although the pH of broth was similar to that obtained with more gentle agitation. Absorbance levels similar to those shown in Fig. 3 were found with filtrates of NB cultures of P. chrysosporium and SMB cultures of Trametes versicolor (data not shown). Absorbance peaked at 20-45 days.

Extracellular proteins are likely agents of biosolubilization. The Bradford test (10) was used to determine protein concentration in harvested broth as a function of growth time over a 35-day period; protein content increased gradually to between 100 and 200 μg/mL. To determine whether denaturing of the proteins could reduce solubilization activity, samples of active broth from P. chrysosporium grown in SMB were boiled for 1 min or heated at 90°C for 1 hr. Boiling for 1 min resulted in decreases in A_{450} of 60% in one case and 33% in another. Heating a third broth at 90°C for 1 hr reduced A_{450} from 2.5 to 0.2

(92%). These reductions are evidence that biochemical activity, possibly due to proteins, is lost on heating.

DISCUSSION

Solubilization of untreated leonardite was shown to occur with fungi grown on agar and neat filtrates of suspension cultures. Biosolubilization of leonardite or oxidized coals has been attributed to enzymes (2,5), alkaline materials (7), and basic polypeptides or polyamines (8). Alkaline materials can neutralize acidic functional groups and render the coal soluble. In the present study, biochemical activity was only observed after the agar or broth pH increased above pH ~7. However, elevated pH was not sufficient for observation of peak biochemical activity because the most active broths appeared for various periods after pH had increased to a plateau. The protein content of the broths increases with growth time but with a pattern different from that for the increase in pH. Heating of the active broths decreased activity, as would be expected if an agent of biosolubilization was protein subject to loss of activity through denaturation. However, the operation of the agent at elevated pH, and the appearance of bioactivity before nutrient nitrogen starvation, are facts inconsistent with ligninases, such as described by Tien and Kirk (9), being responsible agents. Apparently the elevated pH is a condition that enables peak biosolubilization to be observed; this activity is apparently due to heat-sensitive proteins that may act on leonardite within 15 minutes to bring about solubilization in a standard activity test.

ACKNOWLEDGEMENTS

The excellent laboratory assistance of M.J. Schoffstaff is appreciated. Elemental analyses were performed by Huffman Laboratories.

LITERATURE CITED

1. Fakoussa, R.M., Ph.D. Thesis, University of Bonn, 1981.
2. Cohen, M.S.; Gabriele, P.D., Appl. Environ. Microbiol., 1982, 44:23-27.
3. Ward, H.B., Appl. Microbial., 1985, 6:236-238.
4. Wilson, B.W.; Bean, R.M.; Franz, J.A.; Thomas, B.L.; Cohen, M.S.; Aronson, H.; and Gray, E.T., Jr., J. Energy Fuels, 1987, 1:80-84.
5. Pyne, J.W.; Stewart, D.L.; Fredrickson, J.; Wilson, B.W., Appl. Environ. Microbial., 1987, 53(12):2844-2848.
6. Cohen, M.S.; Bowers, W.C.; Aronson, H.; Gray, E.T., Jr., Appl. Environ. Microbial., 1987, 53(12):2840-2843.
7. Quigley, D.R.; Wey, J.E.; Breckenridge, C.R.; Stoner, D.L.; Dugan, P.R., Processing and Utilization of High Sulfur Coals II. Elsevier Sci., 1987, 315-322.
8. Strandberg, G.W.; Lewis, S.N., J. Indust. Microb., 1987; 1:371-375.
9. Tien, M.; Kirk, T.K., Proc. Nat. Acad. Sci., 1984, 81:2280-2284.
10. Bradford, M.M., Analytical Biochem., 1976, 72:248-254.

Table 1. Elemental Composition (mg) of Phanerochaete chrysosporium at 6-Days Old, and Decrease of elements in Sabouraud Maltose Agar Growth Medium

	Fungus	Elements in agar, day 0	Elements in agar, day 6	Decrease of elements in agar
C	248 mg	1150 mg	854 mg	296 mg
H	36	102	102	0
O	162	749	695	54
N	28	63	46	17
S	3	12	11	1
P	5	<=1	1	0
Dry Weight	482 mg	2077 mg	1709 mg	

Table 2. Effect of Particle Size on Solubilization of Leonardite by Filtrates from SMB Cultures of Phanerochaete chrysosporium.

Mesh Size	A_{450}
60 - 100	0.834
100 - 200	1.110
200 - 300	1.122
<100	1.154

Table 3. Effects of Shake Time on Rate of Solubilization (A_{450}) of Leonardite per 15 min and 1 hr by Fungus-Treated Broths.

pH	Absorbance (A_{450}) 15 min	Absorbance (A_{450}) 60 min	Species
7.9	1.80	2.40	TV
7.4	4.00	4.60	PC
7.4	5.10	5.10	TV
5.9	0.25	0.37	TV

Note: TV = Trametes versicolor
PC = Phanerochaete chrysosporium

Table 4. Effect of Leonardite Concentration on Solubilization with P. chrysosporium Culture at Initial pH 7.9 and Initial A_{450} = 1.3.

Concentration % (wt/vol)	A_{450}	% Solubilization	Final pH
0.3	4.0	43	7.9
1.0	5.1	11	7.5
3.0	3.9	2	6.2
10.0	1.3	1	4.6

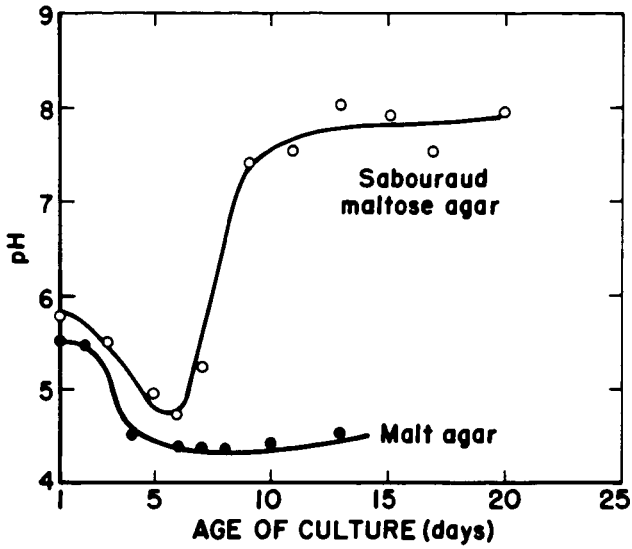

Figure 1. Change in pH of agar associated with growth *P. chrysosporium*.

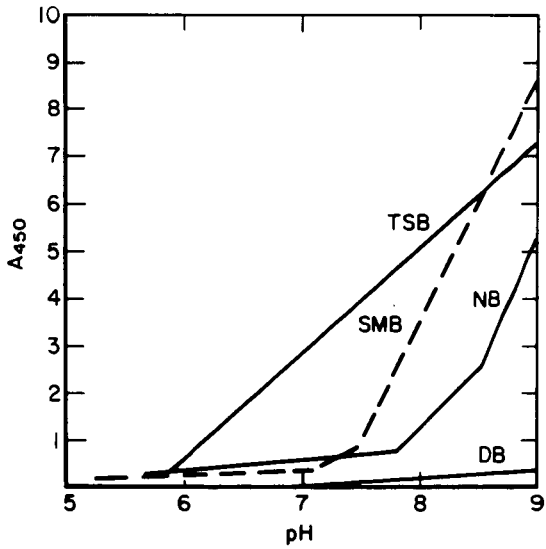

Figure 2. Solubilization of 0.3% leonardite after shaking for one hour with fresh broths.

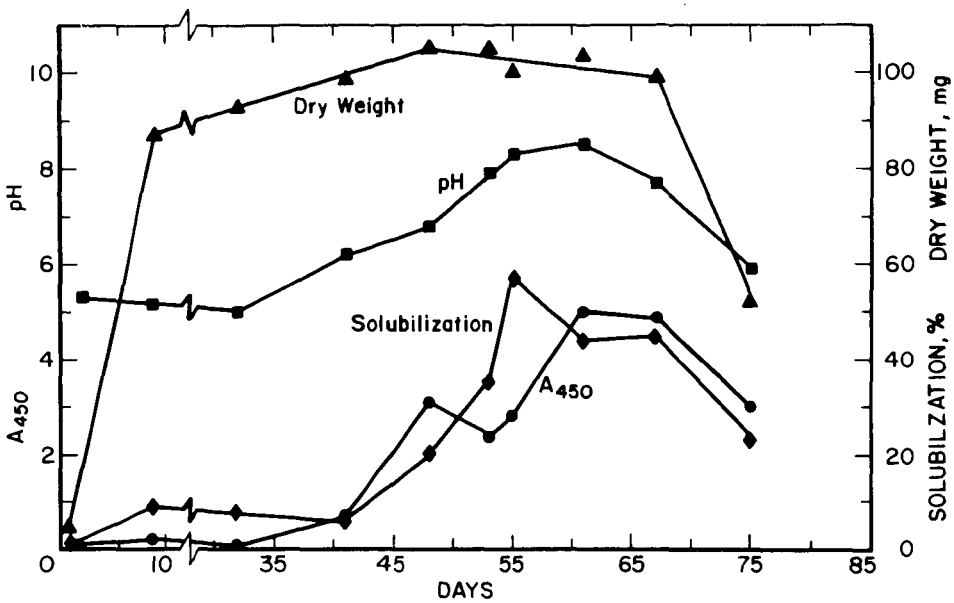

Figure 3. Relationship of dry weight, pH, percent solubilization and A450 from solubilization of leonardite by filtrates from SMB cultures of *P. chrysosporium*.

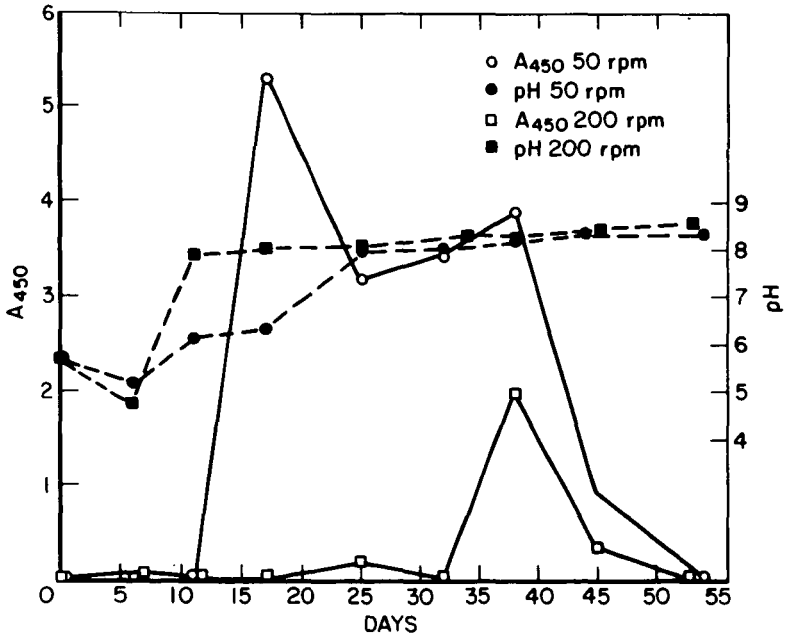

Figure 4. Solubilization of leonardite by filtrates from SMB cultures of *P. chrysosporium* at 50 rpm and 200 rpm.

KINETIC ELEMENTS IN THERMOPHILIC-MICROBIAL LEACHING OF SULFUR FROM COAL

Charles C. Y. Chen and Duane R. Skidmore

Department of Chemical Engineering
Columbus, Ohio 43210

ABSTRACT

A mechanism found suitable for pyritic sulfur removal from coal by mesophilic organisms has been modified and evaluated for the same reaction by the thermophile: Sulfolobus acidocaldarius. The mechanism as modified includes direct and indirect mechanistic elements whose magnitudes were determined experimentally at leaching conditions with and without microbes. Chemical leaching of pyrite by Fe(III) ions and the chemical oxidation of Fe(II) to Fe(III) were found to contribute significantly to overall conversions at thermophilic temperature (72 °C) but not at mesophilic temperature (25-37 °C). The model thus constructed fit overall sulfur leaching data well after suitable assumptions had been made for extent of cell attachment; gas (oxygen) transfer rates, sulfur accessibility, and sulfate reprecipitation rates. The resulting equation is useful for process sumulation, control and design. Further work is needed to define additional sulfur leaching effects.

INTRODUCTION

The Sulfolobus acidocaldarius microbe is thermophilic and acidophilic with optimum growth at temperatures between 70-75 °C and a pH 2-3[1]. The microorganism can grow autotrophically on elemental sulfur, mineral sulfides, and ferrous ions, while it can also grow on glucose and yeast extract[1,2]. Recent reports claimed the oxidation of dibenzothiophene (DBT) and organic sulfur in coal by this organism[3,4].

The thermophilic organism S. acidocaldarius has some advantages over the widely used mesophile Thiobacillus ferrooxidans for microbial coal desulfurization[5-7]. Its extremely thermophilic, acidophilic, aerobic and autotrophic character make it resistant to contamination. The rates of chemical reaction between ferric iron ions and pyrite are higher at high temperature, which benefits the process of sulfur removal. The solubility of some mineral sulfates is higher at low pH and high temperature, which reduces reprecipitation in a process for sulfur reduction. Finally, microbial ability to remove organic sulfur is very important.

Mathematical models have been proposed to describe the kinetics of microbial coal desulfurization[8,9]. The model designed for mesophiles neglected chemical reactions which occurred in parallel with biological reactions in coal-water slurry system. The model proposed in this report considers both chemical and biological reactions, as more realistic for sulfur bioleaching at elevated temperatures. Microbial oxidation of ferrous ions and of sulfur in coal were studied to provide particular values for the model parameters.

MATERIALS AND METHODS

Culture methods

The medium for microbial growth was a basal salts solution and an energy source with or without supplements. The basal salts solution had the

following composition (g/l): $(NH_4)_2SO_4$, 1.3; KH_2PO_4, 0.28; $MgSO_4 \cdot 7H_2O$, 0.25; $CaCl_2 \cdot 2H_2O$, 0.07; in 1 liter of tap water. The energy source can be elemental sulfur, ferrous ions or sulfur in coal. Sometimes yeast extract was a supplement. The pH of the medium was adjusted to 2.0 with 3.0 N H_2SO_4.

The original culture of S. acidocaldarius (ATCC 53230) from Dr. Brierley at the New Mexico Institute of Mining and Technology and transfers from Dr. Kargi at Lehigh University were used throughout the investigation.

Eight hundred ml. of the medium were placed in a three necked, round bottomed flask equipped with a condenser. The system was autoclaved at 121 °C for 15 min and then inoculated with a culture of S. acidocaldarius. Microbial cells were grown and harvested from a medium where elemental sulfur was the energy source 3-5 days after inoculation. The culture was first centrifuged at 1000x g for 5 min to remove the sulfur particles. Then, the cell solution was centrifuged at 4000x g for 20 min to separate the cells. The cells were resuspended in basal salts solution without an energy source. These cells were used as inoculum for ferrous ion oxidation and sulfur leaching from coal.

Accurate cell counts were achieved for experimental runs from protein analyses calibrated with visual cell counts under a phase contrast microscope equipped with a Petroff-Hausser counting chamber. The total protein was assayed by the modified Bradford Method suggested by Peterson[10].

Medium with ferrous sulfate as the energy source was prepared by adding 9 g/l or 3.18 g/l of $FeSO_4 \cdot 7H_2O$ to the basal salts medium to yield an initial iron concentration of 2000 or 700 ppm. Experiments were conducted with and without yeast extract supplement. An uninoculated control flask was run in parallel to show the rate of chemical oxidation of ferrous iron by oxygen from the air. Samples were taken every 12-24 hours for the assay of ferrous and ferric iron concentrations. The analysis followed a procedure using 1,10 phenanthroline hydrochloride as the indicator for iron concentration. Details of the analytical procedures are available in the literature[11].

Other experiments were conducted with 5% coal slurry comprised of Kentucky #9 coal and basal salts solution. The slurry was either inoculated or uninoculated with the cells. Every 12-24 hours, 3 ml of slurry were taken from each flask and filtered through Whatman #1 filter paper. Concentrations of sulfate, ferrous, and ferric iron in the solution and total sulfur content in the coal were measured. Concentration of sulfate was determined by the turbidimetric method specified in ASTM[12]. The sulfur content in coal was measured by combustion and titration using a LECO sulfur analyzer.

KINETIC ELEMENTS

The mechanism for pyritic sulfur oxidation was first proposed by Silverman[13] for Thiobacillus species as comprised of direct and indirect oxidative components. The direct mechanism requires direct contact between bacteria and pyrite since no extracellular enzymes are involved. In the indirect mechanism, the ferric iron chemically reacts with pyrite to give ferrous iron and elemental sulfur. The bacteria then oxidize ferrous iron to ferric iron and oxidize elemental sulfur to sulfate. In the absence of bacteria, the regeneration of ferric iron is the rate limiting step for pyrite oxidation. Bacteria increase the pyrite oxidation rate by oxidizing ferrous iron to ferric iron. Precipitation of iron-sulphate was observed when ferric iron was present at high concentration.

To model the system, kinetics of the following reactions were considered:

1. Chemical oxidation of ferrous ions to ferric ions by dissolved oxygen without bacteria
2. Biological oxidation of ferrous ions by suspended microorganisms with bacteria
3. Chemical oxidation of pyrite to iron and sulfate
4. Biological oxidation of pyrite by attached microbes
5. Precipitation of sulfate and ferric ions

Microbial oxidation of pyrite by Thiobacillus ferrooxidans has been studied and Monod type models were proposed[8]. The basic concept is that the adsorbed cells grow on pyrite surfaces and the suspended cells grow on ferrous ions. An equilibrium exists between the free cells and the adsorbed cells according to the Langmuir isotherm. However, Kargi and Robinson pointed out that in their study of pyrite leaching with S. acidocaldarius, that the number of free cells remained unchanged while the attached cells grew in number[9]. Recent reports showed that in the short term, the cells attached to coal particles following the Langmuir isotherm and that selective adsorption on pyrite surfaces was evident, but irreversiblity was developed through long term cell-coal contact[14,15].

The attached cells are assumed to have a maximum specific growth rate of $\mu_{M,S6}$ which is independent of the amount of pyrite. As suggested by Huber et al.[6], the Monod type of model was not appropriate here since pyrite is not a soluble substrate. The value, X_A is the density of attached cells, defined as cells/mM pyrite, and Y_S is the yield factor for microbial oxidation of pyrite defined as cells/mM FeS_2 oxidized. The microbial growth is considered as occurring in two ways. One is the growth on pyrite surface, the other term is the growth on ferrous iron in solution. For the growth on pyrite surface, the number of attached cells is limited by a saturation cell density designated as X_A^*. For the growth on ferrous iron, the Monod expression can be applied. The density of the cells which did not attach to the pyrite surface (could be free suspended or attached to surfaces other than pyrite) is designated as X_F. Based on the assumptions, the rate equation for each kinetic element is proposed as follow:

$$\text{Rate of chemical oxidation of } Fe^{2+} = k_1 [Fe^{2+}] - k_{-1}[Fe^{3+}] \quad \text{.....(1)}$$

$$\text{Rate of microbial oxidation of } Fe^{2+} = \frac{\mu_{M,Fe}^* [Fe^{2+}]}{K_{Fe} + [Fe^{2+}]} * \frac{X_F}{Y_{Fe}} \quad \text{....(2)}$$

$$\text{Rate of chemical oxidation of } FeS_2 = k_s[Fe^{3+}]\left(\frac{[Fe^{2+}]_{eq}}{[FeS_2]_{eq}} - \frac{[Fe^{2+}]}{[FeS_2]}\right) \quad \text{..(3)}$$

$$\text{Rate of biological oxidation of } FeS_2 = \frac{\mu_{M,S}^* X_A^* [FeS_2]}{Y_S} \quad \text{.....(4)}$$

$$\text{Rate of } Fe^{3+} \text{ precipitation} = k_p [Fe^{3+}] \quad \text{.....(5)}$$

Based on the rate equations proposed above, balance equations for Fe(II), Fe(III), attached cells, free-floating cells and pyritic sulfur can be writen as:

$$\frac{d[Fe^{2+}]}{dt} = -k_1([Fe^{2+}] - K_e\,[Fe^{3+}]) + \frac{\mu_{M,Fe} * [Fe^{2+}]}{K_{Fe} + [Fe^{2+}]}$$

$$+ 3\,k_s[Fe^{3+}]\left(\frac{[Fe^{2+}]_{eq}}{[FeS_2]_{eq}} - \frac{[Fe^{2+}]}{[FeS_2]}\right) + 3\,\frac{\mu_{M,S}\,X_A[FeS_2]}{Y_S} \quad \ldots\ldots\ldots(6)$$

$$\frac{d[Fe^{3+}]}{dt} = k_1([Fe^{2+}] - K_e\,[Fe^{3+}]) + \frac{\mu_{M,Fe}*[Fe^{2+}]}{K_{Fe} + [Fe^{2+}]}\,\frac{X_F}{Y_{Fe}} - k_p[Fe^{3+}] \quad \ldots\ldots(7)$$

$$\frac{d\,X_A}{dt} = L_{M,S}\,X_A \qquad \text{when } X_A < X_A^* \quad \ldots\ldots\ldots\ldots\ldots\ldots\ldots\ldots\ldots\ldots(8)$$

$$= 0 \qquad \text{when } X_A = X_A^*$$

$$\frac{d\,X_F}{dt} = \frac{\mu_{M,Fe}[Fe^{2+}]}{K_{Fe} + [Fe^{2+}]} + X_A * \left(\frac{d[FeS_2]}{dt}\right) \quad \ldots\ldots\ldots\ldots\ldots\ldots\ldots\ldots(9)$$

$$-\frac{d[FeS_2]}{dt} = k_s[Fe^{3+}]\left(\frac{[Fe^{2+}]_{eq}}{[FeS_2]_{eq}} - \frac{[Fe^{2+}]}{[FeS_2]}\right) + \frac{\mu_{M,S} * X_A*[FeS_2]}{Y_S} \quad ..(10)$$

$$= 2\,\frac{d[SO_4^{=}]}{dt}$$

The factor 3 came from the assumption that 3 moles of ferrous iron were released when one mole of FeS_2 was oxidized with 2 moles of ferr iron.

RESULTS AND DISCUSSIONS

Oxidation of ferrous ions in aqueous solution:

In the absence of microorganism and pyrite, the equations to describe the pure chemical oxidation of ferrous ions can be derived simply by dropping the biological terms and sulfur turms in the balance equations for a general bioleahing system. Equilibrium was reached in a few days and no more oxudation occurred. A drop of total iron concentration signified precipitation of ferric ions.

Microbial oxidation of ferrous ions

Figure 1 demonstrates the data from a run with inoculated ferrous sulfate medium. In the presence of microbes, the balance equation can be derived by dropping the sulfur terms in the general equations. The results of simulation are given in Figure 1. The experimental data indicate that ferrous ions were completed oxidized to ferric ions with the help of microorganisms. Ferric ion concentrations in the medium increased rapidly at first and then dropped due to precipitation of ferric-sulfate complex. The drop of ferrous ions was associated with growth of the microorganism.

Oxidation of pyrite in aqueous solution

Experimental results with uninoculated 5% coal slurry are shown in Figure 2. An equilibrium was detected beyond which no more oxidation occurred. Model prediction and data are shown in Figure 2. The model fits the data to a satisfactory degree.

Microbial oxidation of pyrite

The data from batch leaching of -270+325 mesh Kentucky #9 coal was fitted with this model. As Case I, it is assumed that cells preferentially adsorbed on the pyrite surface. In other words, all the attached cells were on pyrite sites in the coal. Case II has only part of the attached cells on the pyrite surface while others were on coal surfaces.

Figure 3 shows the simulation for case I. The predicted ferrous iron concentration was higher than the experimental data. Figure 4 shows the simulation results with the assumption of case II. The predicted ferrous iron concentration in the first two days of leaching was lower than the experimental data, which means that fewer cells were utilizing ferrous iron as energy. In Figure 4 the number of cells which were attached to pyrite surface was assumed to be 10% of the the cells attached to coal particles. The model predicted the general trend, or the dynamics of the leaching system, but more information is required to develop further the model for a better fit to the experimental data.

CONCLUSION

Kinetic elements were proposed to describe the bacterial leaching system. The cells attached to pyrite sites grew on pyrite and yielded ferrous iron and sulfate as the products. The cells which were not on the pyrite sites, either attached to the coal surface or freely suspended utilized ferrous iron as an energy source. Chemical oxidation of pyrite by ferric iron and chemical oxidation of ferrous iron were also considered. The model gave a good description of the dynamics of the leaching system.

There are limitations in applying this model since assumptions were made to simplify the rate equations. Also, cells counts in the coal slurry were not accurately followed due to interference from the materials leached from coal. However, the model predicts the trends of concentration profiles of Fe(II), Fe(III) and sulfate ions in solution. More experiments with accurate cell counts is necessary to make the model more generally applicable.

Nomenclature

k_s: Rate constant for chemical oxidation of pyrite, (mM/day ppm^2)
k_1 : Rate constant for chemical oxidation of ferrous iron, (1/day)
k_{-1} : Rate constant for reduction of ferric ions, (1/day)
$\mu_{M,F}$: Maximum specific growth rate of cells on ferrous iron, 1/day)
K_{Fe}: Saturation constant in the Monod model, (mg Fe/l)
Y_{Fe}: Yield factor for cell growth on ferrous iron, (cells/nM Fe)
$\mu_{M,S}$: Specific growth rate on pyrite (1/day)
Y_S: Yield factor for growth on pyrite, (cells/mM FeS_2)
X_F : Free-floating cell density, (cells/ml solution)
X_A : Attached cell density, (cells/gm coal)

REFERENCES

1. Brock, T. D., K. M. Brock, R. T. Belly and R. L. Weiss., "Sulfolobus: A New Genus of Sulfur-Oxidizing Bacteria Living at Low pH and High Temperature.", Arch. Mikrobiol., 84, (1972), 54-68.
2. Brierley, C. L. and J. A. Brierley., "A Chemoautotroph and Thermophilic Microorganism Isolated from an Acid Hot Spring.", Can. J. Microbiol., 19, (1973), 184-188.

3. Kargi, F. and J. M. Robinson., "Microbial Oxidation of Dibenzothiophene by the thermophilic Organism Sulfolobus acidocaldarius.", Biotech. Bioeng. 26(7), (1984), 687-690.
4. Kargi, F. and J. M. Robinson. "Removal of Organic Sulphur from Bituminous Coal Using the Thermophilic Organism: Sulfolobus acidocaldarius.", Fuel, 65, (1986), 397-399
5. Kargi, F. and J. M. Robinson., "Biological Removal of Pyritic Sulfur from Coal by the Thermophilic Organism Sulfolobus acidocaldarius." Biotech. Bioeng., 27(1), (1985), 41-49.
6. Murphy, J., E. Riestenberg, R. Mohler, D. Marek, B. Beck. and D. Skidmore., "Coal Desulfurization by Microbial Processing.", in Y. A. Attia, (ed.), Processing and Utilization of High Sulfur Coals., Amsterdam: Elsevier, (1985), 643-652.
7. Kargi, F. and J. M. Robinson., "Microbial Desulfurization of Coal by Thermophilic Microorganism Sulfolobus acidocaldarius.", Biotech. Bioeng., 24, (1982), 2115-2121.
8. Chang, Y. C. and A. S. Myerson., "Growth Models of the Continuous Bacterial Leaching of Iron Pyrite by Thiobacillus ferrooxidans.", Biotech. Bioeng., 24, (1982), 889-902.
9. Kargi, F. and J. G. Weissman., "A Dynamic Mathematical Model for Microbial Removal of Pyritic Sulfur from Coal.", Biotech. Bioeng., 26, (1984), 604-612.
10. Peterson, G. L., "Determination of Total Protein.", in C. H. W. Hirs and S. N. Timasheff, (eds.), Methods in Enzymology-Enzyme Structure, Part I., New York: Academic Press., 91, (1983), 95-119.
11. ASTM Standards., "Standard Test Methods for Iron in Water.", 1985 Annual Book of ASTM, Philadelphia: ASTM, 11.01, (1985) 507-511.
12. ASTM Standard., "Standard Test Method for Sulfate Ion in Water., 1986 Annual Book of ASTM. Philadelphia: ASTM., D 516, 11.01, (1986), 700-706.
13. Silverman, M. P., "Mechanism of bacterial Pyrite Oxidation.", J. of Bacteriology, 94, (1967), 1046-1051.
14. Chen, C. Y. and D. R. Skidmore. "Langmuir Adsorption Isotherm for Sulfolobus acidocaldarius on Coal Particles.", Biotech. Letters, 9(3), (1987), 191-194.
15. Chen, C. Y. and D. R. Skidmore. "Attachment of Sulfolobus acidocaldarius Cells on Coals and Other Particles.", Biotech. Progresses, 4(1), 1988, 25-30.
16. Huber, T. F. and N. W. F. Kossen., "Design and Scale-up of a Reactor for the Microbial Desulfurization of Coal: A Kinetic Model for Bacterial Growth and Pyrite Oxidation.", Proc. 3rd Europe Congress on Biotech., Frankfort, Sep. 10-14, (1984), III 151-159.

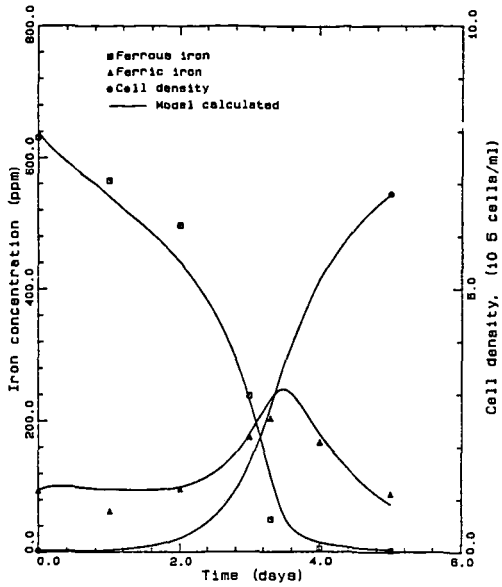

Figure 1 Curve-fitting of experimental data on microbial oxidation of ferrous iron, run #4

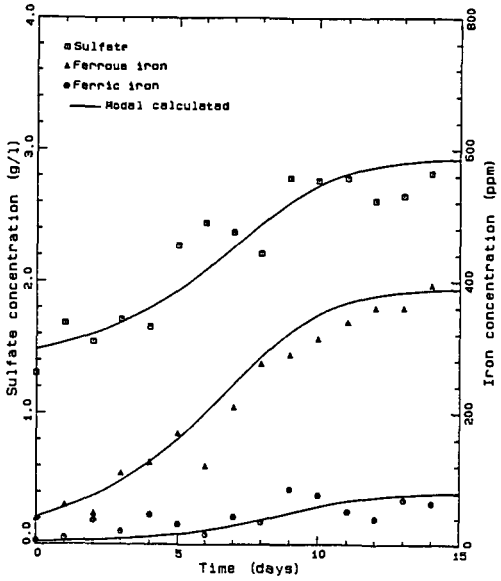

Figure 2 Curve-fitting of experimental data on an uninoculated control of 10% slurry of Kentucky #9 coal with a single dose of basal salts.

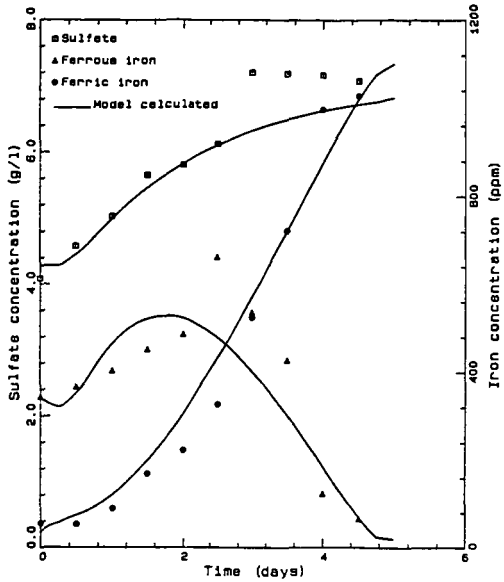

Figure 3. Curve-fitting of experimental data on batch leaching of -270 +325 mesh Kentucky #9 coal, case I.

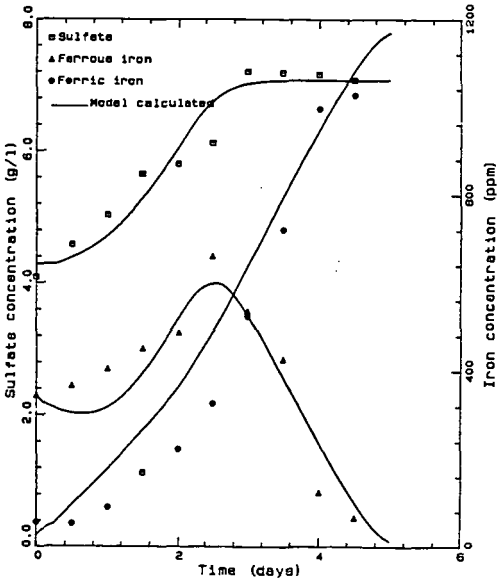

Figure 4. Curve-fitting of experimental data on batch leaching of -270 +325 mesh Kentucky #9 coal, case II.

Theoretical Problems in Modelling of Enzyme Sequences

Marek A. Borowiak
Catalysis Department, Industrial Chemical Res. Inst.,
01-793 Warsaw, Rydygiera 8, POLAND

In vivo enzymes operate in enzyme systems[1] realizing reactions of metabolic networks. Using mechanisms of vectorial flow of matter and energy[2,3] as well as compartment and microcompartment of cells interior[4] the systems achieved high perfection[5] of catalytic action. Non-linear non-equilibrium thermodynamics describe the formation of coherent structures[6] of which enzyme systems are important example. Many of dynamic properties of the systems may be explained by control theory[7] or by more and more complicated kinetic models[8]. Measurable properties of the system reflect both properties of individual enzymes and the system as a whole and its environment. The system simultaneously realizes transport, binding and catalysis functions which are impossible to single out in the models. But rather than to bind or transport a substrate, the most important property of an enzyme is to catalyze the conversion of a substrate into a product[9]. On the other hand, the models in principle base on the approximation of an absolute continuous medium commonly used in most chemical models. This is reasonable for a large chemical system i.e. containing very large numbers of molecules but becomes doubtful for enzymes in conditions extant in vivo. What is even more important is that catalysis itself, viz. quantum mechanical interactions between a catalytic center c, a substrate s and a product p molecules is associated with the particular attributes of the objects c, s, p rather than with properties of an enzyme macrosystem and its environment.

New general models of enzyme systems, composed of elementary catalytic systems were suggested[10] for these reasons. A model of the elementary catalytic system (ECS), derived from the notions of the general theory od systems, which is capable of performing a single elementary catalytic act (ECA) is as simple as possible functional model of a system with the catalysis function only. The term „catalytic system" was first used by Rudenko[11] in his analysis of coupled catalysis and transport functions. To modelling of the optimum cooperation between many ECS´s and its environment the general models of multicatalytic system (MCS) were used[10,12]. The MCS´s were shown to contain finite numbers n of ECS. An effectiveness of an ECS action inside the MCS, described by a maximum classical probability (MPr(ECA)) of succesive ECA occurrence, increases non--linearly with increasing of n incomparison with a system of n ECS non-organized into MCS.For analysis of the catalysis function of enzyme systems the MCS models look to be very useful. It is just the purpose of the present paper to show that optimum value of n for simple MCS is about 15. In term of ECS and MCS a discussion of some modern biophysics and biotechnology problems will be made.

Elementary Catalytic System

The ECS is defined as a discrete, determinated system with purposeful behaviour which is a function of attributes of the system objects and bi-object relations. The purpose of the ECS action is to realize a sequence of bi-object events in a well-defined crder (ECA). A set of the events does not contain those connected with flow of matter into and away of the ECS, which are function of environment attributes.

The ECS is composed (Figure 1) of a set of five objects which are represented by vertices of a structural graph and of the set of bi-object relations represented by the graph branches. The formal objects g and k where g is the source and k is the receiver of energy quanta simplify the modelling of energy flow inside ECS during ECA. Any object of ECS may exist in one of the states belonging to the object set of states, which is the subset of finite

minimal set of states required for ECA to occur. There are two attributes of a state $\underline{x_i}$ of object $\underline{x}$: I_{x_i} and E_{x_i}, where I_{x_i} is a constant time interval between the moments of appearance of two succesive active states (impulses) required for the reaction to occur, so called oscillation time in impulse-oscillation parametric model (IOM) of molecule[12], and E_{x_i} is the internal energy of object $\underline{x}$ in $\underline{x_i}$ state.

In ECS discrete time scale is used. All time parameters are assumed to be natural number counts of arbitrary time units. A bi--object relation (x_i, y_i) arises then and only then if a moment $SYN_{x_i y_j}$ of synchronization can be attained:

$$SYN_{x_i y_j} = a_{x_i} + n_{x_i} \cdot I_{x_i} = a_{y_j} + n_{y_j} \cdot I_{y_j} \qquad 1)$$

where: n_{x_i}, n_{y_j} are natural numbers; a_{x_i}, a_{y_j} are the moments of appearance of first active states in the system. The change of states $\underline{x_i}$, $\underline{y_i}$ of objects $\underline{x}$, $\underline{y}$ is the result of the relation.

To describe a flow of internal energy from $\underline{x}$ object (energy donor) to $\underline{y}$ object (energy acceptor) the following model was adopted:

$$E_{x_i} + E_{y_j} = E_{x_{(i+1)}} + E_{y_{(j+1)}} \qquad 2)$$

$$E_{x_i} > E_{y_j} \qquad 3)$$

$$E_{x_{(i+1)}} \geqslant E_{y_{(j+1)}} \qquad 4)$$

where: 2) follows from the energy concervation law; 3) and 4) define energy gradients before and after the flow, respectively.

The analysis of the general ECS model showed that an ECA process is the sequence of bi-object events (Figure 2) which occur if the conditions 1)-4) are fulfilled. Results obtained with computing of detailed particular ECS model (in preparation) showed, among others, that the catalysis effect (ECA duration time smaller that the time necessary for the relation ($\underline{s}$ $\underline{p}$) to occur) is possible to achieve for particular I_{c_o} values only and that the effect increases when the difference between I_{s_o} and I_{p_o} decreases.

Models of cooperation between ECS and its environment

To make many succesive ECA's occur, it is necessary to carry $\underline{s_o}$ and $\underline{g_o}$ into, and $\underline{p_o}$ and $\underline{k_2}$ away from the ECS. Thus, the ECS model may be simplified and considered (Figure 3) a transformer of the chemical $\underline{s}$ and the energy $\underline{g}$ input signals into the respective signals $\underline{p}$ and $\underline{k}$.

The probability of the succesive ECA occurrence is a function of those events that depend on the interaction of the appropriate inputs/outputs to the ECS with its environment because the probabilities of all bi-object events inside the ECS are equal to unity (the determined system). For the estimation of MPr(ECA) the following simplifying assumptions are made:

- the number of objects in the ECS environment and the number of inputs/outputs with which ECS and its environment cooperate are determined
- the probability P(w) of any object appearance at any ECS input/output is the same
- the objects appear at appropriate moments $\underline{a}$ (eq. 1))
- individual events are independent
- any object $\underline{s}$, $\underline{p}$, $\underline{g}$, $\underline{k}$, $\underline{c}$ may exist in one of its equally probable states (Fig. 2).

1. An ECS inside stochastic environment

   The objects number = 4; the inputs/outputs number = 4

   $MPr(ECA)_1 \approx 2 \cdot 10^{-9}$

2. $\underline{n}$ ECS inside stochastic environment

   The objects number = 4n; the inputs/outputs number = 4n

   $MPr(ECA)_2 \approx 2 \cdot 10^{-9} \cdot n^{-8}$

3. Two ECS energy-coupled inside stochastic environment
First ECS serves as a source of energy quanta for the second. It is possible if:

$$ {}^{1}I_{k_2} = {}^{2}I_{g_o}; \qquad {}^{1}_{m}a_{k_2} = {}^{2}_{m}a_{g_o} \qquad 5) $$

$$ {}^{2}I_{k_o} = {}^{1}I_{g_2}; \qquad {}^{1}_{m+1}a_{k_o} = {}^{2}_{m}a_{g_2} \qquad 6) $$

$$ {}^{2}E_{g_o} = {}^{1}E_{k_2}; \qquad {}^{2}E_{g_2} = {}^{1}E_{k_o} $$

where the left superscripts and subscripts are ECS numerals in the system and ECA numerals in the ECS, respectively.
From the energy flow model 2)-4) and 6) it follows[12] that ${}^{1}E_{c_o} > {}^{2}E_{c_o}$. If the number of objects and inputs/outputs are 6 then $MPr(ECA)_3 \approx 2\cdot10^{-8}$, in comparison with $MPr(ECA)_2 \approx 10^{-11}$ for $\underline{n} = 2$.

4. Two ECS chemically coupled inside stochastic environment
The $\underline{p}$ object in $\underline{p_o}$ state from first ECS serves as the $\underline{s}$ object in $\underline{s_o}$ state inside the second ECS. It is possible if:

$$ {}^{1}I_{p_o} = {}^{2}I_{s_o}; \qquad {}^{1}_{m}a_{p_o} = {}^{2}_{m}a_{s_o} \qquad 7) $$

$$ {}^{1}I_{p_-} = {}^{2}I_{s_-}; \qquad {}^{1}_{m+1}a_{p_-} = {}^{2}_{m}a_{s_-} $$

$$ {}^{1}E_{p_o} = {}^{2}E_{s_o} \qquad 8) $$

$$ {}^{1}E_{p_-} = {}^{2}E_{s_-} \qquad 9) $$

States $\underline{p_-}$ and $\underline{s_-}$ serve to convey information of the lack of object $\underline{p}$ and $\underline{s}$ in the system. For the number of objects and inputs/outputs equal 6 $MPr(ECA)_4 \approx 2.5\cdot10^{-8}$, thus the same order as for model 3.

5. Chain MCS: $\underline{n}$ ECS energy-coupled inside stochastic environment.
   5a. The objects number $\underline{4n}$; the inputs/outputs number (2n+2)
   $MPr(ECA)_{5a} \approx 3\cdot10^{-4}\ [n(2n+2)]^{-2}$
   5b. The objects number (2n+2); the inputs/outputs number (2n+2)
   $MPr(ECA)_{5b} \approx 5\cdot10^{-3}\ (2n+2)^{-4}$
   The above formulas are true for $n \geqslant 3$, with terminal ECS disregarded. The absolute values of $MPr(ECA)_5$ decrease with increasing $\underline{n}$; $MPr(ECA)_{5a} \approx MPr(ECA)_1$ for n=12; $MPr(ECA)_{5b} \approx MPr(ECA)_1$ for n=18. The relative effectiveness $(MPr(ECA)_5/MPr(ECA)_2)$ increases with increasing $\underline{n}$, approximately with $\underline{n}^4$.

6. Chain MCS: $\underline{n}$ ECS chemically coupled inside stochastic environment.
   6a. The objects number 4n; the inputs/outputs number (2n+2)
   $MPr(ECA)_{6a} \approx 4\cdot10^{-4}\ [n(2n+2)]^{-2}$
   6b. The objects number (2n+2); the inputs/outputs number (2n+2)
   $MPr(ECA)_{6b} \approx 7\cdot10^{-3}\ (2n+2)^{-4}$
   The above formulas are true for $n \geqslant 3$, with terminal ECS disregarded. $MPr(ECA)_{6a} \approx MPr(ECA)_1$ for n=14; $MPr(ECA)_{6b} \approx MPr(ECA)_1$ for n=20.

7. Ring MCS: $\underline{n}$ ECS chemically coupled inside stochastic environment.
   7a. The objects number $\underline{4n}$; the inputs/outputs number $\underline{2n}$
   $MPr(ECA)_{7a} \approx 1\cdot10^{-4}\ n^{-4}$
   7b. The objects number $\underline{2n}$; the inputs/outputs number $\underline{2n}$
   $MPr(ECA)_{7b} \approx 4\cdot10^{-4}\cdot n^{-4}$
   $MPr(ECA)_{7a} \approx MPr(ECA)_1$ for $\underline{n} = 15$;
   $MPr(ECA)_{7b} \approx MPr(ECA)_1$ for $\underline{n} = 21$.

Discussion

The general character of the present considerations has prompted us to make the assumptions some of which need not to be obligatorily satisfied in individual cases. The MPr(ECA) estimates should be viewed as the orders of magnitude rather than exact values. On the other hand, the formal general analysis of ECS and MCS models leads to a number of conclusions which are well consistent with the modern biophysics and catalysis. At the same time it seems that the models have a good predictive capability helpful in studies of many biotechnology problems. From this point of view, for example, one should postulate a new look to be given to carriers employed in immobilization of enzymes in order to pick up carriers capable of an additional function of directional energy flow which could significantly enhance enzyme effectiveness; the relations 5)-6) or 7)-9) may be used in experiments with immobilization of bienzyme systems (the estimated effect due to chemical coupling is by at least one order of magnitude higher than established in experimental studies reported in literature); it seems that energetical relations[12)] may help in studies of the formation of new series of chemical transformations in artificial non-biological MCS systems. However to achieve this, more detailed studies in the field are required.

Literature

1. G.R.Welch (editor) Organized Multienzyme Systems: Catalytic Properties (Academic Press Inc. Orlando 1985)
2. G.R.Welch, M.N.Berry in: Organized Multienzyme Systems (Academic Press Inc. Orlando 1985) p.419
3. P.A.Srere in: Organized Multienzyme Systems (Academic Press Inc. Orlando 1985) p.1
4. P.Friedrich in: Organized Multienzyme Systems (Academic Press Inc. Orlando 1985) p.141
5. W.J.Albery, J.R.Knodes, Biochem. 15 (25) 5631 (1976)
6. G.Nicolis, J.Prigogine, Self-organization in Non-equilibrium Systems; From Dissipative Structures to Order Through Fluctuactions (J.Wiley and Sons, New York 1977)
7. B.A.Palsson, E.N.Lightfoot, J.theor.Biol. 113 231 (1985); 113 261 (1985); 113 279 (1985)
8. P.W.Kuchel in: Organized Multienzyme Systems (Academic Press Inc. Orlando 1985) p.303
9. J.Ricard in: Organized Multienzyme Systems (Academic Press Inc. Orlando 1985) p.177
10. M.A.Borowiak The Elementary Catalytic System as a Building Unit of Large Enzymatic Systems (ISSOL 86, Poster No 179, Berkeley (USA) July 1986)
11. A.P.Rudenko The Theory of Self-Development of Open Catalytic Systems (in Russian) (Moscow Uniw.Press 1969)
12. M.A.Borowiak Biophys.Chemistry (in press) (1988).

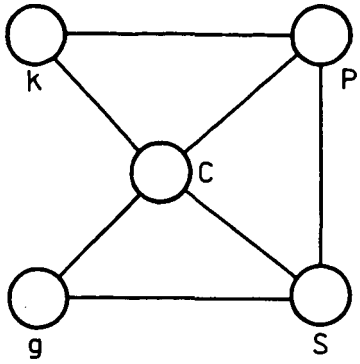

Figure 1. A graph of the ECS structure.

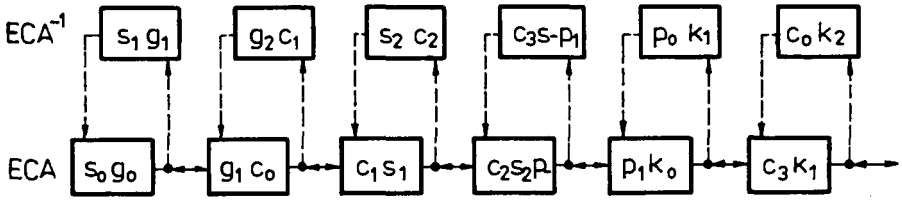

Figure 2. A diagrammatic presentation of an ECA.

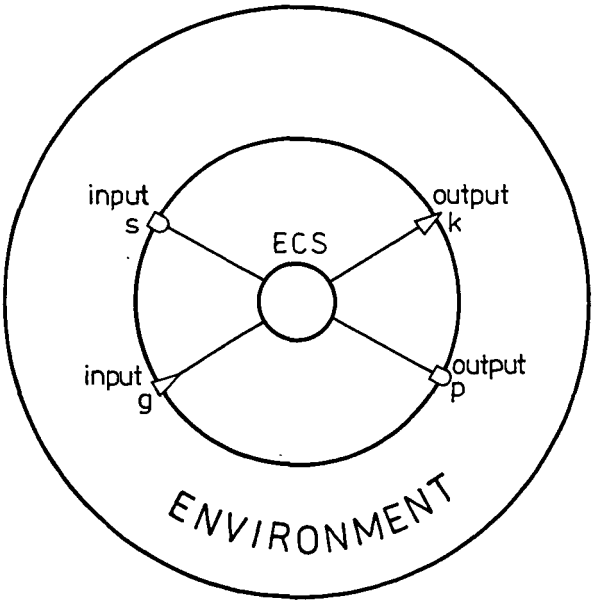

Figure 3. A simplified model of interaction between ECS and surroundings.

Lignin Peroxidase-Catalyzed Depolymerization of Water Soluble Polymer Derived from Subbituminous Coal and Lignite

Lillian Wondrack, Maria Szanto and Willis A. Wood
Salk Institute Biotechnology/Industrial Associates, Inc.
P. O. Box 85200
San Diego, CA 92138

In view of reports that enzymes can depolymerize or otherwise alter lignin, it is to be anticipated that enzymes will also attack some of the linkages in coal. However, the solid and vitreous nature of coal precludes a direct test of this possibility. For this reason, it has been necessary to prepare a coal substrate with minimal chemical alteration which is water soluble in the pH range where enzymes are active.

This report describes the preparation and characterization of a coal liquid substrate suitable for enzymes and the ability of lignin peroxidase to alter this material.

Preparation of Coal Polymer

Use was made of the well-known ability of nitric acid to oxidize low ranked coals and lignite to yield an alkali soluble material. Ground North Dakota lignite or German subbituminous coal was treated with 20% to 40% nitric acid at less than 70°C for 2 to 6 hours. The washed and dried material was suspended in 1N NaOH at room temperature for 30 minutes and then centrifuged. HCl was added to the brown-black supernatant solution to pH 3.5, and the copious brown-black precipitate, which salted out with the 1N NaCl produced on acidification, recovered by centrifugation. In an alternative procedure, the nitric acid-treated subbituminous coal was suspended in water and the pH raised to 10 to 11 with NaOH. After acidification to pH 3.5 with HCl and centrifugation, NaCl was added to the brown-black supernatant to 1M concentration and the precipitate recovered by centrifugation.

The salted out precipitate obtained in either procedure was extracted with water at room temperature for 20 minutes to 12 hours to obtain a dark-brown soluble material which was dialyzed and retained in 12,000-14,000 dalton cut off membranes.

The yield of soluble organic carbon by an acid dichromate colorimetric method was 35 to 61% based on the organic carbon content of the nitric acid-treated material.

The water soluble material was also soluble in dimethyl formamide, dimethyl sulfoxide, tetrahydrofuran, sparingly soluble in methanol, and insoluble in acetonitrile, ethyl acetate, hexane and benzene.

Gel filtration chromatography of the soluble material from North Dakota lignite on Sephadex G-75 and G-200 with effluent monitoring at 254 nm revealed a single relatively narrow peak migrating with Blue Dextran on G-75 and slightly slower than Blue Dextran on G-200. Similar results were obtained with the soluble material from German subbituminous coal by high performance gel filtration chromatography with the exception that in addition to the major peak of about 125,000 daltons, there were minor components of about 50,000 and 32,000 daltons. No low molecular weight components were present in either preparation. In dialysis experiments at 0, 1, and 3M KCl and at acidic and basic pH values, virtually all of the material was retained. From these results it is concluded that the bulk of the pH 3.5 water soluble material had a molecular weight of greater than 100,000 daltons, and as such is a satisfactory substrate for enzyme studies.

Lignin Peroxidase

Lignin peroxidase of *Phanerochaete chrysosporium* is unique among enzymes: (a) in its ability to catalyze reactions without regard for stereoconfiguration of the substrate; and (b) in the seemingly large number of different reactions it catalyzes. In this regard both lignin and coal are appropriate substrates being stereoirregular polymers with a multiplicity of intercomponent linkages.

The partially purified lignin peroxidase used in these experiments was recovered from Phanerochaete chrysosporium cultures by adsorption to and specific elution from DEAE-Sephadex coated porous silica (Macrosorb Kax.DEAE, Sterling Organics US, New York, NY) and concentration on an American YM-10 membrane (American Corporation, Danvers, MA). Manganese peroxidase activity was virtually absent from these preparations. Except for this recovery procedure, growth of the organisms, enzyme assay, etc., followed published procedures.

Incubation of Coal and Lignite Preparations with Lignin Peroxidase

Soluble coal and lignite preparations were incubated at 37°C with lignin peroxidase in tartrate buffer, pH 3.0, and H_2O_2 for 4 to 24 hours. The incubations were oxygenated periodically. Aliquots of reaction mixtures were either directly applied to conventional gel permeation columns of Sephadex G-200 or to high performance gel permeation chromatographic columns. In some analyses samples were first treated with acetone-dimethyl formamide (1:1). Following removal of denatured protein by centrifugation, the supernatant solution was recovered, dried, and dissolved in buffer for gel permeation chromatography (0.02 M KPO_4, pH 7 - 0.5% Tween 80).

The elution diagrams for soluble material from North Dakota lignite obtained by monitoring the effluent at 254 nm showed a substantial loss of the major peak for the polymer and formation of a mixture lower molecular weight components in low yield;no production of "monomeric components" was not observed. With more peroxidase and incubation at pH 4.5, the accumulation of lower molecular fragments was enhanced.

Similar results were obtained with soluble polymer from German subbituminous coal. There was a substantial disappearance of the major peak and an appearance of material of both

higher and lower molecular weight. The addition of veratryl alcohol caused the nearly complete disappearance of the major peak without the appearance of fragments absorbing at 254 nm. This indicates extensive alteration of aromatic rings in the starting material had occurred.

Discussion

The results clearly show that lignin peroxidase can modify soluble coal polymers derived form North Dakota lignite and German subbituminous coal, probably by several reactions involving depolymerization and polymerization. This process probably should be considered as distinct from the liquification of powdered low ranked coals and lignite on mats of growing fungi as has been reported in numerous publications. The nature of the chemical modifications are unknown. Based on the current concepts of the mechanism of lignin peroxidase, it is to be expected that a donation of electrons from oxidizable groups to the Fe(IV)-oxo form of the peroxidase will form a cation radical. This election transfer may occur either directly or via the veratryl alcohol cation radical. Non-enzymatic rearrangement of the cation radical could follow many paths depending on the substructure involved and these could occur with or without the introduction of oxygen. It is, therefore, to be expected that a large number of products of both higher and lower molecular weight will be formed. Hence, it will be necessary in future research to separate the products and to determine their structure so as to establish the nature of the lignin peroxidase attack on soluble coal polymer.

CHARACTERIZATION OF BIODEGRADED COALS

R. M. Bean, J. A. Franz, J. A. Campbell,
J. C. Linehan, D. L. Stewart, and B. L. Thomas

Pacific Northwest Laboratory
P. O. Box 999
Richland, WA 99352

INTRODUCTION

Microbial degradation of coals to materials that are soluble in water has been a topic of intensive research for the last few years. The potential for economical recovery of low-grade coals, coupled with possibilities for further upgrading by microbial desulfurization or methanation has spurred intensive research at a number of laboratories. Until very recently, coal biodegradation has been accomplished using low-grade, naturally oxidized coals such as leonardite (1,2,3), or coals subjected to pretreatment with oxidizing chemicals (4). We have been able to accomplish the biodegradation of bituminous Illinois #6 coal after a pretreatment consisting of air oxidation, using a culture of the fungus *Penicillium* sp. We report in this paper results of chemical and spectrometric analyses of the starting materials and products from Illinois #6 coal biodegradation, and compare the results with those previously reported (2) from the biodegradation of leonardite.

EXPERIMENTAL

Coal and Coal Pretreatment - Illinois #6 coal (mine-washed) was obtained from the Illinois Department of Natural Resources. Prior to microbial treatment, the coal was sized to 0.5 to 5 mm diameter, spread to a layer approximately 1 cm thick on Al foil, and heated in a forced draft oven at 150°C for 7 days. Thermocouple measurements made on the coal during pretreatment showed that the coal temperature did not deviate significantly from the oven temperature.

Coal Biodegradation -Agar plates containing Sabourauds maltose medium (Difco Laboratories, Detroit, MI) were inoculated with a strain of *Penicillium* obtained from Professor Bailey Ward of Louisiana State University. After 7 days incubation at room temperature, 0.3 to 0.4 g of pretreated Illinois #6 coal was placed on each plate, and incubation continued. Water-solubilized coal was harvested by pipette after 5 weeks, passed through 0.45 μ filters, and freeze-dried. The residual material was extracted with 50 mL portions of 0.5 N NaOH until extracts were colorless (approximately 700 mL was used per plate). The base solubilized coal was filtered (0.45 μ), acid precipitated (HCl, pH 2), and dried.

Solubilization of leonardite coal by *Coriolus versicolor* has been described elsewhere (2).

Analysis for conversion to Soluble Products - Conversion of coal to water or base solubles was determined by measurement of optical density at 680 nm after appropriate sample dilution. Standards were prepared from dry acid-precipitated subsamples of solubilized coal product.

Elemental Analysis - Samples were dried for 48 hr under vacuum at 125°C prior to analysis. Elemental analyses were carried out by Schwarzkopf Microanalytical Laboratory, Woodside, NY.

Gel Permeation Chromatography(GPC) - GPC was conducted in tetrahydrofuran solvent containing 0.1% acetic acid flowing at 1 mL/min through two µStyragel columns (100 and 500 Å, Waters Associates (Milford, MA) in series. Detection was by ultraviolet absorbance (Waters Model 490) and by mass detector (Applied Chromatography Systems Ltd, (Bedfordshire, England). Calibration was with polystyrene standards, and with pyrene.

^{13}C NMR Spectroscopy - A Varian VXR-300 equipped with an ultra high speed probe (Doty Scientific, Inc.,Columbia, SC), spinning at 14 kHz, was used to obtain NMR spectra of coal and coal bioproducts. At the high spin rate, no sidebands interfere within the entire spectral window of interest. The instrument was run in the cross-polarization mode, with a 56 kHz decoupling field.

RESULTS

Recoveries of water and base soluble material from the plates after degradation for 5 weeks are shown in Table 1. In contrast to the biosolubilization of leonardite, which is rendered water soluble by *C. versicolor*, yields of water solubles from *Penicillium*-biodegraded pretreated Illinois #6 coal were very low. The total yield of solid material that could be directly pipetted from the plates was on the order of 3%. When this material was recovered from solution by acid precipitation rather than freeze-drying, less than half could be recovered, an indication that the water-solubles were contaminated by the media in which the organism was grown. Recovery of coal material by base extraction was much more satisfactory. Although recovery with 0.5 N NaOH is indicated to be 80 to 90% in Table 1, recent data has shown that after 6 weeks of incubation, over 95% can be extracted from the plates with base. The high degree of solubility in even 0.01 N base is an indication that the solubilization by base results from a metathetical exchange of sodium ions for active hydrogens, rather than solvolysis reactions.

The data in Table 2 indicates that the biodegraded material is different from materials derived from base solubilization of the

air-oxidized coal. Base solubilization of air-oxidized Illinois #6 coal is only accomplished to a significant extent from 24-hr treatment with 2.4 N base. Conditions producing high yields of solubilized material from the biotreated coal give only 6% solubles from the undegraded pretreated coal. In addition, the biodegraded material has significantly different molecular weight properties than the undegraded, base solubilized oxidized coal (Table 2). Although the molecular weight (MW) ranges are similar, the base soluble biodegraded coal exhibits a weight-average MW only one-sixth that of the base solubilized oxidized coal. After recovery by acid precipitation, the water-soluble biodegraded Illinois #6 coal is essentially indistinguishable in MW properties from the corresponding base-soluble material. For comparison, the molecular weight characteristics of biodegraded leonardite are included; there is a significant difference in both weight average MW and MW range between the Illinois #6 product and the leonardite product.

Ash and elemental analyses of the Illinois #6 coal, before and after pretreatment, and the coal-biodegraded products are presented in Table 3. It is clear from the data that the pretreatment caused profound changes in the coal composition. Weight loss upon heating in air was 10%; essentially the same as when the coal is vacuum dried at 125°C. However, Table 3 shows that there was a substantial loss in both carbon and hydrogen after heating, offset by a large increase in oxygen content. The elemental compositions of the biodegraded materials were lower in sulfur, presumably because of pyrite losses during the solubilization and filtration processes. Nitrogen was somewhat elevated, probably due to some contamination with protein material. Oxygen was appreciably elevated in the water soluble product, and oxygen/carbon ratios were elevated in the products over the starting pretreated coal. Low material balances in the acid-precipitated products resulted from relatively high quantities of chlorine were present (2.6% in the water soluble product, and 7.4% in the base soluble product). Chlorine (as chloride ion) would displace metallic oxide oxygen or hydroxyl during the acid precipitation process.

^{13}C NMR spectra of untreated Illinois #6 coal, 150°C air-treated Illinois #6 coal, and the base soluble biodegradation product are shown in Figure 1. Chemical shifts obtained from carbon in different chemical environments have been well-documented in coal samples (5). The chemical shift region from 0 to 75 ppm includes resonance from carbon in aliphatic linkages; the region from 90 to 155 ppm contains resonance from carbon present in aromatic rings; from 155 to 215 ppm is found signal from carbon present in carbonyl structures. Specifically, chemical shifts in the region 165-185 ppm are assigned to carbon in carboxyl groups (6). From Figure 1, it can be seen that upon air treatment at 150°C, the aliphatic region is reduced in intensity relative to the aromatic region, and the aromatic region somewhat broadened. Upon biodegradation, the aliphatic peak is even

further reduced, while a distinct peak in the carboxyl region is produced. For the three Illinois #6 samples, quantitative determinations of the relative abundances of different carbon obtained by integration of the three chemical shift areas are given in Table 4, together with data obtained from leonardite and biodegraded leonardite.

DISCUSSION

Recent studies of the air oxidation of coal between ambient and 150°C (7, 8, 9) indicate that the incorporated oxygen is largely present in ether-type linkages rather than in carboxyl groups as might be expected. Infrared studies of coal during oxidation at temperatures between 25 and 100°C (7,8) have indicated initial formation of carboxyl groups, followed by their disappearance (presumably through thermal decarboxylation), and the evolution of ether bonds. A study of the oxidative weathering of freshly mined Illinois #6 coal (9) in which an additional 26% oxygen was incorporated over 2 months under ambient conditions, found that no carbonyl groups were present. The NMR spectrum obtained from our pretreated coal sample indicates that carboxyl groups are not in high concentration. The broadening of the peak containing chemical shifts from aromatic carbon toward higher chemical shifts in the pretreated sample (Figure 1), may be an indication of carbon involved in ether bonds, since the C-O chemical shift is in the region 148-158 ppm (5). We thus have evidence through the literature and through the NMR spectra that oxygen incorporation into Illinois coal during pretreatment is largely through ether formation, and that losses of carbon and hydrogen are through CO and CO_2 evolution, as well as losses of other volatiles.

Shown in Table 5 are the empirical formulas, based on 100 carbon atoms, obtained from elemental analyses of Illinois #6 and leonardite coals and coal products. In terms of elemental composition, the effect of the microbial action on the oxidized coal does not appear to be great. For the Illinois #6 coal 4 oxygens, 11 hydrogens, and 1 nitrogen were added per 100 carbon atoms; for the leonardite case, 2 oxygens, 7 hydrogens, and 2 nitrogens were added per 100 carbons. Although stoichiometry is not precise, the addition of the elements of water during the microbial degradation indicates that hydrolysis is involved in the biodegradation of oxidized coal. Further, an oxidative hydrolysis mechanism is suggested by the reduction in molecular weight of the microbial product, the appearance of carbonyl in the ^{13}C NMR spectra after biodegradation, the facile solubility of the product in weak base, and the finding in our laboratories that soluble enzymes produced by the coal-degrading organisms readily hydrolyze benzyl ethers and oxidize aromatic hydrocarbons (J. A. Campbell et al., presented at this symposium).

The oxidation of lignin materials has been reported to occur through mechanisms involving cleavage of beta-aryl ethers (10,11), and

aromatic ring cleavage (12). In addition, parallel pathways of side chain degradation, decarboxylation, and aromatic ring opening have been described for the degradation of lignin model compounds (13). From our ^{13}C NMR data (Table 4), leonardite loses 10% aromatic carbon while gaining 10% C=O carbon, which is consistent with a mechanism of aromatic oxidative hydrolysis; however, there does not appear to be a loss of aryl carbon in the case of the Illinois #6 coal (Table 4). For Illinois #6 coal, ether cleavage and side chain degradation seems to be favored, since loss of aliphatic carbon is observed.

REFERENCES

(1) Cohen, M. J.; Gabriel, P. D. Appl. Environ. Microbiol. (1982), 44, 23-27.

(2) Wilson, B. W.; Bean, R. M.; Franz, J. A.; Thomas, B. L.; Cohen, M. S.; Aronson, H.; Gray,E. T., Jr. Energy and Fuels (1987) 1, 80-84.

(3) Pyne, J. W., Jr.; Stewart, D. L.; Fredrickson, J.; Wilson, B. W. Appl. Environ. Microbiol. (1987), 53, 2844-2848.

(4) Quigley,D. R.; Wey,J. E.; Breckinridge, C. R.; Stoner, D. L. In: Processing and Utilization of High Sulfur Coals II, Y. P. Chugh and R. C. Caudle, Eds. Elsevier Science, pp 316-322.

(5) Snape, C. E.; Ladner, W. R.; Bartle, K. D. Anal. Chem., 1979, 51, 2189.

(6) Levy, G. C.; Nelson, G. L. Carbon-13 Nuclear Magnetic Resonance for Organic Chemists, Wiley-Interscience, NY, NY, p 117.

(7) Bouwman, R.; Freriks, I. L. C. Fuel (1980), 59, 315-322.

(8) Gethner, J. S. Appl.Spect. (1987), 41, 50-63.

(9) Liotta, R.; Brons,G.; Isaacs,J. Fuel (1983), 62, 781-791.

(10) Miki, K.; Renganathan, V.; Gold, M. H. Biochem. (1986), 25,4790-4796.

(11) Enoki, A.; Goldsby,G. P.; Gold, M. H. Arch Microbiol. (1981), 129, 141-145.

(12) Umezawa, T.; Higuchi,T. FEBS (1985) 182, 257-259.

(13) Haider, K; Trojanowski, J. Arch. Microbiol. (1975), 105, 33-41.

ACKNOWLEDGMENT

This work was supported by the Electric Power Research Institute, Palo Alto, CA., and by the U. S. Department of Energy, Office of Fossil Energy, under Contract DE-AC06-76RLO 1830

Table 1. Yields of *Penicillium*-Degraded Illinois #6 Coal

Extracting Solvent	% of Biodegraded Illinois #6 Coal Extracted
Water	3.0 ±0.8 (s.d.,n=6)
0.50 N NaOH	79.0 ±10.9 (range,n=2)
0.05 N NaOH	89.4 ±2.2 (range,n=2)
0.01 N NaOH	51.0 ±6.5 (range,n=2)

Table 2. Yields and GPC-Determined Molecular Weights of Soluble Coal Fractions

Sample	Solvent Treatment	% Soluble	Wt. Av. Mole Weight	MW Range (THF Sol*)
Biodeg. Ill #6 (Insol. H_2O, sol. base)	0.05-0.5 N	100	900	200 - 100,000
H_2O-Sol Ill#6 (Acid pptd)	H_2O	100	1000	200 - 100,000
Air Ox. Ill #6 (150°C, 7 days)	2.4 N NaOH	25	6,000	200 - 100,000
Air Ox. Ill #6	0.5 N NaOH	6	-	-
Biodegraded Leonardite	H_2O	100	2,000	200 - 20,000

* Base soluble fractions were 70 to 90% soluble in the GPC solvent

Table 3 Elemental Analysis of Illinois #6 Coal Biodegradation Products: Comparison with Starting Materials and Leonardite Products

Sample	% C	% H	% O	% N	% S	% Ash	Total
ILL #6 Coal	67.43	4.08	11.8	1.5	4.35	14.16	103.32
Air Ox Coal	58.53	2.13	23.42	1.16	4.36	14.42	104.02
Base Sol Prod	52.85	2.41	23.74	1.77	2.57	10.15	93.49
H_2O Sol Prod (acid precip)	56.12	2.14	29.75	3.04	2.59	2.03	95.67
Leonardite	54.95	3.6	30.24	0.8	1.06	8.32	98.97
Leon Prod (acid precip)	53.53	3.83	30.7	2.07	1.06	3.48	94.67

Table 4. Carbon-Type Analysis of Coal and Biodegraded Coal Samples by ^{13}C NMR

	% C=O	% Aromatic C	% Aliphatic C
Illinois #6	5	55	40
Oxidized Illinois #6	17	58	25
Biodegraded Ill #6	28	60	12
Leonardite	10	45	45
Biodegraded Leonardite	20	35	45

Table 5. Empirical Formulas Calculated for Illinois #6 Coal, Leonardite, and Their Biodegradation Products

Illinois #6 Coal	$C_{100}H_{73}O_{13}N_{1.9}S_{2.4}$
Heat-Treated Illinois #6 Coal	$C_{100}H_{44}O_{30}N_{1.7}S_{2.8}$
Base Soluble, Acid Precipitate	$C_{100}H_{55}O_{34}N_{2.9}S_{1.8}$
Leonardite	$C_{100}H_{79}O_{41}N_{1.2}S_{0.7}$
Water Soluble, Acid Precip.	$C_{100}H_{86}O_{43}N_{3.3}S_{0.7}$

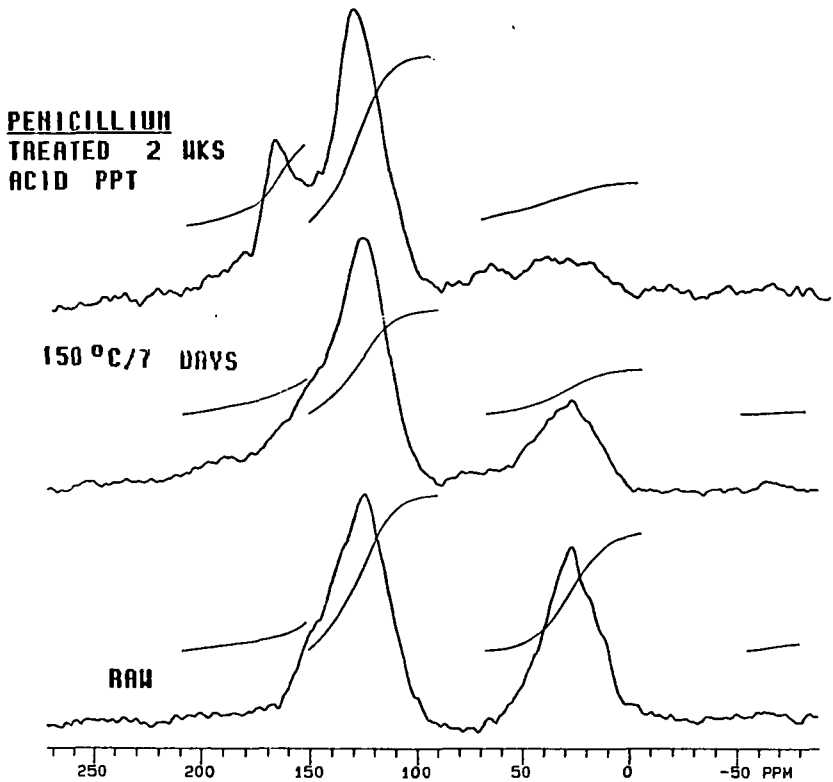

Figure 1. ^{13}C NMR spectrum of Illinois #6 coal and coal products. Bottom, untreated Illinois #6 coal; Middle, coal pretreated by heating at 150° C in air; Top, pretreated coal after degradation by the fungus *Penicillium* sp.

BIOLOGICAL REMOVAL OF HYDROGEN SULFIDE FROM COAL SYNTHESIS GAS

Kerry L. Sublette
Center for Environmental Research and Technology
University of Tulsa
600 South College Ave.
Tulsa, OK 74104

INTRODUCTION

Coal synthesis gas may typically contain up to 1% hydrogen sulfide (H_2S) which, in conventional processing, must be removed prior to methanation to prevent catalyst fouling (1,2). Alternatively, Barik et al (3) have shown that coal synthesis gas may be upgraded microbially in a process which is not particularly sensitive to H_2S. However, H_2S would have to be removed from the resulting upgraded gas prior to distribution and sale.

The work described here was initiated to investigate the feasibility of a microbial process for the removal and oxidation of H_2S from a gas stream such as the product of the shift conversion of coal gas or the product of the microbial methanation process. The high reaction rates and mild reaction conditions characteristic of a microbial process can potentially yield technical and economic advantages over conventional processes. Conceptually, a microbial process can replace an entire conventional gas processing train of H_2S removal (amine system), H_2S disposal (Claus or Stretford system) and tail gas clean-up or any individual processing step.

There are many bacteria capable of H_2S oxidation and therefore serve as potential candidates to form the basis of a microbial gas desulfurization technology. However, the ideal microorganism for this application must possess several other characteristics in addition to the ability to oxidize hydrogen sulfide if the technology is to be economically viable. The bacteria chosen for this study was Thiobacillus denitrificans.

T. denitrificans is a strict autotroph and facultative anaerobe first described by Baalsrud and Baalsrud (4). Thiosulfate, elemental sulfur and soluble sulfide may be utilized as energy sources with oxidation to sulfate which accumulates external to the cells. Under anaerobic conditions nitrate may be used as a terminal electron acceptor with reduction to elemental nitrogen. Reported here is a study of the stoichiometry and kinetics of aerobic and anaerobic oxidation of $H_2S(g)$ by T. denitrificans in batch and continuous flow reactors under sulfide-limiting conditions. The maximum loading of the biomass for aerobic and anaerobic oxidation of H_2S was determined and a study of reactor upset conducted. The effect of heterotrophic contamination was also examined. Lastly, T. denitrificans has also been immobilized by co-culture with floc-forming heterotrophs to produce macroscopic floc with excellent settling properties. A study of the oxidation of H_2S by immobilized T. denitrificans is also reported.

MATERIALS AND METHODS

Organism and Stock Cultures

Stock cultures of wild-type (ATCC 23642) and sulfide-tolerant strains of Thiobacillus denitrificans were grown anaerobically in thiosulfate maintenance medium in 10 ml culture tubes at 30°C. Thiosulfate medium is described in Table 1. The trace metal solution has been described elsewhere (5). Stocks were transferred every 30 days and stored at 4°C until used.

Oxidation of H_2S by Planktonic or Free-Cell T. denitrificans

All investigations of anaerobic growth of planktonic T. denitrificans on $H_2S(g)$ as the energy source were conducted with a B. Braun Biostat M bench scale fermenter (culture volume, 1.4 l). Aerobic experiments also made use of an L. E. Marubishi MD 300 fermenter (culture volume, 2.0 l). In a typical anaerobic batch experiment, T. denitrificans was grown in thiosulfate maintenance medium at 30°C and pH 7.0 to an OD_{460} of 0.5-0.8 prior to the introduction of H_2S. This optical density (OD) corresponds to greater than 10^8-10^9 cells/ml. The purpose of this prior cultivation on thiosulfate was to develop a sufficient concentration of biomass in the reactor so that an appreciable rate of $H_2S(g)$ could be fed to the reactor without exceeding the biooxidation capabilities of the biomass. Otherwise toxic levels of sulfide would accumulate in the culture. The OD level of 0.5-0.8 was initially chosen arbitrarily. While growing on thiosulfate a gas feed of 5 mol% CO_2 in nitrogen was normally fed to the reactor at 30 ml/min to ensure continuous availability of a carbon source. A hydrogen sulfide feed gas typically contained 0.5-1.0 mol% H_2S, 5 mol% CO_2, and balance N_2.

The pathways for sulfide and thiosulfate oxidation to sulfate in T. denitrificans are not independent but have two common intermediates, a membrane bound polysulfide and sulfite (6). In the presence of thiosulfate, the rate of sulfide oxidation would be reduced because of competition between intermediates of thiosulfate and sulfide oxidation for the same enzymes of the sulfur pathway. Therefore, prior to the introduction of H_2S to T. denitrificans cultures, residual thiosulfate was removed. This was accomplished by sedimenting the cells by centrifugation, washing with 20 mM phosphate buffer (pH 7.0) and resuspending the cells in the fermenter in thiosulfate maintenance medium without thiosulfate. The cell suspension was then purged for 1 h with 5 mol% CO_2 in nitrogen to allow residual thiosulfate to be metabolized before the feed gas was changed to include hydrogen sulfide. H_2S oxidizing cultures were also maintained at 30°C and pH 7.0.

The start-up of a continuous-flow, anaerobic reactor began with the establishment of a batch culture as described above. When stable operation on $H_2S(g)$ feed was indicated, the reactor was switched to a continuous flow mode by introducing a continuous stream of nutrient solution (thiosulfate maintenance medium without thiosulfate) and withdrawing a continuous stream of reactor mixed liquor (cells plus medium) at the same rate. A schematic diagram

of the continuous flow reactor system used in these experiments is given in Figure 1.

In batch, aerobic experiments, T. denitrificans was grown in thiosulfate maintenance medium without nitrate at 30°C and pH 7.0 until the thiosulfate was depleted. Aeration was provided at a rate sufficient to maintain 60-100 μM O_2 in the culture medium. Air was supplemented with 5 mol% CO_2 to ensure a continuous availability of a carbon source. When the thiosulfate was depleted the optical density (at 460 nM) of the culture was approximately 1.0 and the T. denitrificans viable count was approximately 10^9 cells/ml. Following thiosulfate depletion the culture received two gas feeds, 0.9-1.1 mol% H_2S, 5 mol% CO_2 and balance nitrogen and air supplemented with 5 mol% CO_2. The aeration rate and agitation rate (300-400 rpm) were adjusted to produce steady-state oxygen concentration of 60-150 μM in the culture medium. The aeration rate was typically in the range of 200-400 ml/min. Foaming was controlled with the addition of 0.5 ml of a 1/10 dilution of General Electric AF93 silicone antifoam emulsion (previously autoclaved at 121°C, 205 kPa) approximately every 18-24 h. All other details of the operation of aerobic batch reactors were identical to those characteristics of the operation of anaerobic, batch reactors described earlier.

With the exception of providing aeration, the start-up and operation of continuous-flow aerobic reactors was virtually identical to the anaerobic systems. The nutrient feed solution was identical to the thiosulfate maintenance medium described in Table 1 with the exceptions that there was no thiosulfate or nitrate in the feed.

Oxidation of H_2S by Immobilized T. denitrificans

T. denitrificans was immobilized by co-culture with floc-forming heterotrophs obtained from activated sludge from the aerobic reactor of a refinery wastewater treatment system. T. denitrificans cells grown aerobically on thiosulfate and washed sludge were resuspended together in fresh thiosulfate maintenance medium without nitrate. The culture was maintained in a fed batch mode at pH 7.0 and 30°C with a gas feed of 5% CO_2 in air. With respect to the growth of T. denitrificans this medium was thiosulfate-limiting. When thiosulfate was depleted, the agitation and aeration were terminated and the flocculated biomass allowed to settle under gravity. The supernatant liquid was then removed and discarded. In this way the culture was enriched for T. denitrificans cells which had become physically associated with the floc. The volume was then made up with fresh medium and aeration and agitation restarted. This fed-batch cycle was repeated 5-6 times.

At the end of the fed batch cycles the biomass was allowed to gravity settle and was washed four times with 20 mM phosphate buffer (pH 7.0) to remove free-cell biomass. Floc were then resuspended in fresh medium (without thiosulfate) in the fermenter and sparged with 500 ml/min of 5% CO_2 in air and 50 ml/min of 1.0% H_2S in nitrogen.

Analytical

All gas analyses were conducted with a Perkin Elmer Sigma I Gas Chromatograph or Hewlett-Packard 5995 GC/MS. The Perkin Elmer featured a thermal conductivity detector with a detection limit for H_2S of 2-4 µM with a 0.25 ml sample at 101.3 kPa and 25°C. The column used was a 10-ft by 1/8-in. ID Teflon column containing 80/100 mesh Porapak QS (Waters Associates). The detection limit of the HP GC/MS for H_2S was found to be approximately 0.05 µM with a 0.25 ml sample at 101.3 kPa and 25°C. The column used was a 6-ft by 1/8-in. ID glass column containing 60/80 mesh Tenax GC (Alltech Associates).

Whole cell protein was determined by sonication followed by protein determination by the micro-modification of the Folin-Ciocalteau method (7,8). The protein content of T. denitrificans cells was determined to be 60% ± 3% by dry weight. Using this figure, protein analyses were converted to dry weight T. denitrificans biomass.

Nitrate was determined by the cadmium reduction method and nitrite by the diazotization method (9). Ammonium ion was determined by the Nessler method without distillation (9). Thiosulfate was determined by titration with standard I_2 solution with a starch indicator (10). Sulfate was determined turbidiometrically (9).

Total sulfide (H_2S, HS^- and S^{-2}) was determined by ion specific electrode using an Orion Research Model 94-16 sulfide/silver electrode and an Orion Research Model 701A pH/mV meter. Elemental sulfur collected by filtration on 0.45-µ Millipore Type HA filters was determined by reaction with cyanide to produce thiocyanate which was quantitated as $Fe(SCN)_6^{-3}$ (11).

Viable counts of T. denitrificans were determined by plating serial dilutions of culture medium on thiosulfate agar plates and incubating anaerobically at 30°C. Heterotrophs were quantitated by plating samples of culture medium on nutrient agar (Difco Labs) plates incubated aerobically at 30°C.

Free-cell or planktonic biomass in reactors containing immobilized T. denitrificans was estimated in terms of the optical density (460 nm) of the supernatant after medium samples were allowed to settle under gravity for 10 min. Settling properties of flocculated biomass were determined during the course of H_2S fermentation by periodically turning off all gas feeds and the agitation and measuring the height of the biomass in the fermenter at intervals for 20 min.

RESULTS AND DISCUSSION

Batch Growth of Planktonic T. denitrificans on H_2S

When H_2S was introduced to anaerobic or aerobic cultures of planktonic or free-cell T. denitrificans previously grown on thiosulfate, the H_2S was immediately metabolized with no apparent

lag. At initial loadings of 4-5 mmoles/h-g biomass the reactor outlet gas generally contained less than 2.0 μM H_2S. When H_2S was detected in the outlet gas, an increase in the agitation rate reduced the H_2S concentration to levels undetectable by GC/MS. The residence time of a bubble of feed gas (average diameter approximately 0.25 cm) under these conditions was 1-2 s. Less than 1 μM of total sulfide (H_2S, HS^-, S^{-2}) was observed in the reactor medium during periods of up to 36 h of operation. No elemental sulfur was detected; however, sulfate accumulated in the reactor medium as H_2S was removed from the feed gas (Figure 2). Oxidation of H_2S to sulfate was accompanied by growth, as indicated by an increase in optical density and protein concentration and a decrease in the NH_4^+ concentration as shown in Figures 2 and 3. Consumption of OH^- equivalents indicated that the reaction was acid producing. Nitrate was consumed under anaerobic conditions as expected (Figure 3), but no nitrite was observed to accumulate.

Sample material balances for batch aerobic and anaerobic H_2S oxidation are given in Table 2. Table 3 presents this type of data as stoichiometric ratios all relative to H_2S oxidized. The stoichiometries of aerobic and anaerobic oxidation of $H_2S(g)$ by T. denitrificans in batch reactors were similar with respect to sulfate production and ammonium and hydroxide utilization. However, the biomass yield under aerobic conditions was only about 37% of that observed under anaerobic conditions. These results suggest that oxygen may be a growth inhibiting substrate for T. denitrificans growing on $H_2S(g)$. Similar results have been reported by Justin and Kelley (12) for aerobic growth of T. denitrificans on thiosulfate.

Growth of Planktonic T. denitrificans on H_2S in a CSTR

T. denitrificans was readily cultured both anaerobically and aerobically on a continuous basis with a H_2S feed. Less than 2 mg/l of elemental sulfur was deterected in the reactors at any time. Nitrite was detected in some anaerobic reactors during start-up (up to 0.25 mM in one instance); however, no nitrite could be detected in any anaerobic reactor at steady state. The steady state concentration of total sulfide in each reactor was less than or equal to 1 μM. This was true throughout each experiment even during start-up. Typical behavior in approach to steady state in an anaerobic CSTR is illustrated by Figures 4 and 5. Small amounts of N_2O (< 40 μM) resulting from the incomplete reduction of nitrate were detected in the outlet gases from anaerobic reactors. With sufficient agitation H_2S was undetectable by GC/MS in the outlet gases of both aerobic and anaerobic reactors.

The stoichiometry of anaerobic and aerobic H_2S oxidation in continuous cultures is also given in Table 3. Under anaerobic conditions the yield of biomass was seen to be greater at the higher dilution rate as expected since a greater fraction of energy yielding substrate will be consumed to support growth as opposed to cell maintenance at higher growth rates. The true growth yield and maintenance coefficient for anaerobic H_2S oxidation by T. denitrificans were calculated by the method given by Pirt (13) to be 21.1 g dry wt biomass/mole H_2S and 1.74 mmoles H_2S/h-g dry wt,

respectively. At D=0.029 h^{-1} the average yield was 9.3 g biomass/mole H_2S oxidized. This compares favorably with that reported by Timmer-ten-Hoor (14,15) (9.41 g biomass/mole S^{-2}) for anaerobic growth of T. denitrificans on Na_2S as limiting substrate at D=0.030 h^{-1}. Under aerobic conditions biomass yield was relatively unaffected by the specific growth rate in the range of 0.030 h^{-1} to 0.053 h^{-1}. As indicated in Table 3 biomass yield under aerobic conditions in continuous cultures was lower than that observed under anaerobic conditions at comparable dilution rates.

Reactor Upset and Recovery

In those experiments described above, the H_2S feed rate was always less than the maximum rate at which the biomass was capable of oxidizing the substrate. If the maximum capacity of the biomass for H_2S oxidation is exceeded, inhibitory levels of sulfide will accumulate in the medium. In order to examine the behavior of a T. denitrificans reactor in an upset condition, the H_2S feed rate to aerobic and anaerobic batch and continuous flow reactors like those described in the previous sections was increased in a stepwise manner until H_2S breakthrough was obtained. At the point at which breakthrough occurred, N_2O was also detected in the outlet gas from anaerobic reactors in concentrations approximately equal to that of the H_2S in the feed gas. Analysis of the reactor medium from both aerobic and anaerobic reactors also indicated an accumulation of sulfide and elemental sulfur in the reactor. Sulfur balances for reactors operated under upset conditions showed that all of the H_2S removed from the feed gas could be accounted for in terms of sulfate, elemental sulfur, and sulfide in the medium. It was observed that the upset condition was reversible if the cultures were not exposed to the accumulated sulfide for more than 2-3 h. Reduction in H_2S feed rate following an upset condition reduced H_2S and N_2O concentrations in the outlet gas to preupset levels. In addition, elemental sulfur, which accumulated during upset, was rapidly oxidized to sulfate.

It is of importance to know at which H_2S loadings the specific activity of the T. denitrificans biomass will be exceeded resulting in upset. The maximum loading of the biomass under anaerobic conditions was observed to be in the range of 5.4-7.6 mmoles/h-g biomass. Under aerobic conditions, the maximum loading was observed to be much higher, 15.1-20.9 mmoles H_2S/h-g biomass.

Effect of Heterotrophic Contamination

The autotrophic medium used in these experiments will not support the growth of heterotrophs since there is no organic carbon source. However, early on in this study it was observed that if aseptic conditions were not maintained, a heterotrophic contamination developed in a T. denitrificans culture. Evidently T. denitrificans releases organic material into the medium in the normal course of growth or through lysis of nonviable cells which supports the growth of heterotrophs. In order to investigate the effect of heterotrophic contamination on the performance of a T. denitrificans CSTR, one anaerobic reactor which became contaminated was allowed to operate for an extended period of time. The reactor

was originally contaminated by two unidentified gram-negative heterotrophs which had distinctly different colony morphology on nutrient agar. After 145 h of operation, the reactor was injected with suspensions of four facultatively anaerobic heterotrophs in phosphate buffer. These were Pseudomonas chlororaphus ATCC 9446, Pseudomonas stutzeri ATCC 11607, Pseudomonas fluorescens ATCC 33512, and an unidentified gram-negative lab isolate. After 315 h of operation, a sample of Desulfovibrio desulfuricans ATCC 13541 in phosphate buffer was also injected. The Desulfovibrio quickly washed out. However, the total heterotroph concentration increased to about 10^8 cells/ml and leveled off. Apparently growth of the contaminants became limited by the availability of suitable carbon sources. The viable count of T. denitrificans at steady state was 5.0×10^9 cells/ml. The steady state composition of the culture medium and outlet gas condition were indistinguishable from that of a pure culture of T. denitrificans operated under the same culture conditions. These observations led to the efforts to immobilize T. denitrificans by co-culture with floc-forming heterotrophs described below.

Oxidation of H_2S by Immobilized T. denitrificans

The activated sludge used as a source of floc-forming heterotrophs in the immobilization of T. denitrificans contained many morphological forms of bacteria as well as fungi and protozoa. However, at the end of the fed-batch cycles (18 days on the average) in co-culture with T. denitrificans in thiosulfate maintenance medium, microscopic examination revealed only short (0.5 μ by 1.0-1.5 μ), gram-negative rods. T. denitrificans and Zoogoea ramigera are both short gram-negative rods. Zoogloea ramigera is the most common floc-forming bacterium found in activated sludge systems.

When $H_2S(g)$ was introduced into batch aerobic reactors containing immobilized T. denitrificans, the H_2S was immediately metabolized. With gas-liquid contact time of approximately 1-2 sec the outlet gas of the reactor typically contained less than 0.1 μM H_2S. Sulfate was observed to accumulate in the medium as H_2S was removed from the feed gas. The oxidation of H_2S was accompanied by growth as indicated by an increase in the total protein concentration and a decrease in the NH_4^+ concentration. In a typical experiment the oxidation of 205.5 mmoles H_2S was accompanied by the production of 204.9 mmoles sulfate and 614.7 mg biomass protein and the utilization of 16.2 mmoles NH_4^+. This stoichiometry is comparable to that given in Table 3 for the aerobic oxidation of H_2S by planktonic or free-cell T. denitrificans biomass.

As noted above, each time fermenters were sampled the sample was allowed to settle under gravity for 10 min and the optical density of the supernatant measured. At the time H_2S feed was initiated the OD_{460} was typically 0.25-0.32. As H_2S was removed from the feed gas the OD after settling was observed to actually decline indicating that no free-cell biomass accumulated in the culture medium. It appears that the growth of the autotroph T. denitrificans was balanced with the growth of the floc-forming heterotrophs through a commensal relationship in which the growth

of the heterotrophs was limited by organic carbon derived from T. denitrificans. The result was an immobilization matrix which grew with the T. denitrificans.

Figure 6 gives typical settling curves for the immobilized T. denitrificans biomass during the course of growth on H_2S. As shown here the settling properties of the biomass were relatively constant during these experiments. When the fed-batch cycles are coupled with the H_2S experiments, the settling properties of the biomass are seen to have been maintained for in excess of 25 days without external addition of organic carbon.

CONCLUSION

It has been demonstrated that the H_2S content of a gas can be reduced to very low levels by contact with an aerobic or anaerobic culture of planktonic or free-cell Thiobacillus denitrificans if the reactor is operated under sulfide-limiting conditions. Hydrogen sulfide was observed to be an inhibitory substrate; however, upset conditions produced by excess H_2S feed were readily detected and reversed. Hydrogen sulfide was oxidized completely to sulfate. Under aerobic conditions the maximum loading of the biomass was 2-3 times higher than that observed for anaerobic conditions.

T. denitrificans has also been immobilized in macroscopic floc by co-culture with floc-forming heterotrophs from an activated sludge treatment facility. Floc with excellent settling characteristics were produced which were subsequently used to remove H_2S from a gas stream bubbled through a batch aerobic culture. No organic carbon addition was required during enrichment for immobilized cells of T. denitrificans or during H_2S oxidation. No free-cell biomass was released into the medium during growth on H_2S. The stoichiometry and kinetics of H_2S oxidation by immobilized T. denitrificans were comparable to that observed in free-cell cultures. Immobilization of T. denitrificans will facilitate concentration of cell suspensions by gravity settling and cell recycle in a continuous system. A corresponding increaase in volumetric productivity is anticipated.

ACKNOWLEDGEMENT

This work was funded by Combustion Engineering, Inc. (Stamford, CT). The author wishes to express his appreciation for the technical assistance of Dr. Marion Woolsey.

REFERENCES

1. Richardson, J. T., Hydro. Process, Dec., 91 (1973).

2. Jockel, H. and B. E. Triebskorn, Hydro. Process, Jan., 93 (1973).

3. Barik, S., R. E. Corder, E. C. Clausen and J. L. Gaddy, Energy Progress, 7, 157 (1987).

4. Baalsrud, K. and K. S. Baalsrud, Arch. Mikrobiol., 20, 34 (1954).

5. American Type Culture Catalog, Catalogue of Strains, ATCC, Rockville, MD (1982).

6. Suzuki, I., Ann. Rev. Microbiol., 28, 85 (1974).

7. Folin, O. and V. Ciocalteau, J. Biol. Chem., 73, 627 (1927).

8. Lowry, O. H., N. J. Rosenberg, A. L. Farr and R. J. Randall, J. Biol. Chem., 193, 265 (1951).

9. American Public Health Association, Standard Methods for the Examination of Water and Wastewater, 14th Ed., APHA, New York (1976).

10. Meites, L., Handbook of Analytical Chemistry, McGraw-Hill, New York (1963).

11. Schedel, M. and H. G. Truper, Arch. Microbiol., 124, 205 (1980).

12. Justin, P. and D. P. Kelley, J. Gen. Micro., 107, 131 (1978).

13. Pirt, S. J., Proc. Royal Soc., B163, 224 (1965).

14. Timmer-ten-Hoor, A., Ant. van Leeuwenh., 42, 438 (1976).

15. Timmer-ten-Hoor, A., Ant. van Leeuwenh., 47, 231 (1981).

TABLE 1. Growth Medium for *Thiobacillus denitrificans*

Component	per liter
Na_2HPO_4	1.2 g
KH_2PO_4	1.8 g
$MgSO_4 \cdot 7H_2O$	0.4 g
NH_4Cl	0.5 g
$CaCl_2$	0.03 g
$MnSO_4$	0.02 g
$FeCl_3$	0.02 g
$NaHCO_3$	1.0 g
KNO_3 (Anaerobic)	5.0 g
$Na_2S_2O_3$ (Grow up only)	10.0 g
Trace metal solution	15.0 ml
Mineral water	50.0 ml

TABLE 2. Material Balances: Aerobic and Anaerobic Oxidation of $H_2S(g)$ in Batch Reactors by *T. denitrificans*

	Anaerobic	Aerobic
H_2S oxidized	18.3 mmoles	86.0 mmoles
SO_4^{-2} produced	18.8 mmoles	81.8 mmoles
Biomass produced	246 mg	453 mg
NO_3^- consumed	27.0 mmoles	-
NH_4^+ consumed	2.2 mmoles	8.4 mmoles
OH^- consumed	31.8 meq	151.3 meq

TABLE 3. Stoichiometry of H_2S Oxidation by *Thiobacillus denitrificans*[a]

Reactor Type	Electron Acceptor	NO_3^-/H_2S (mole/mole)	O_2/H_2S (mole/mole)	SO_4^{-2}/H_2S (mole/mole)
Batch	NO_3^-	1.36		1.04
CSTR $D = 0.029\ h^{-1}$	NO_3^-	1.30		1.03
CSTR $D = 0.058\ h^{-1}$	NO_3^-	1.19		1.00
Batch	O_2		1.81	0.99
CSTR $D = 0.030\ h^{-1}$	O_2			1.06
CSTR $D = 0.053\ h^{-1}$	O_2			1.04

TABLE (continued)

Reactor Type	Electron Acceptor	NH_4^+/H_2S (mole/mole)	OH^-/H_2S (eq/mole)	Biomass/H_2S (g/mole)
Batch	NO_3^-	0.12	1.60	12.1
CSTR $D = 0.029\ h^{-1}$	NO_3^-	0.09	1.37	9.3
CSTR $D = 0.058\ h^{-1}$	NO_3^-	0.10	1.24	12.9
Batch	O_2	0.10	1.75	4.5
CSTR $D = 0.030\ h^{-1}$	O_2	0.11[b]	2.38[b]	8.1
CSTR $D = 0.053\ h^{-1}$	O_2	0.12	1.77	7.9

[a] Average of three or more determinations unless otherwise noted.
[b] Average of two determinations.

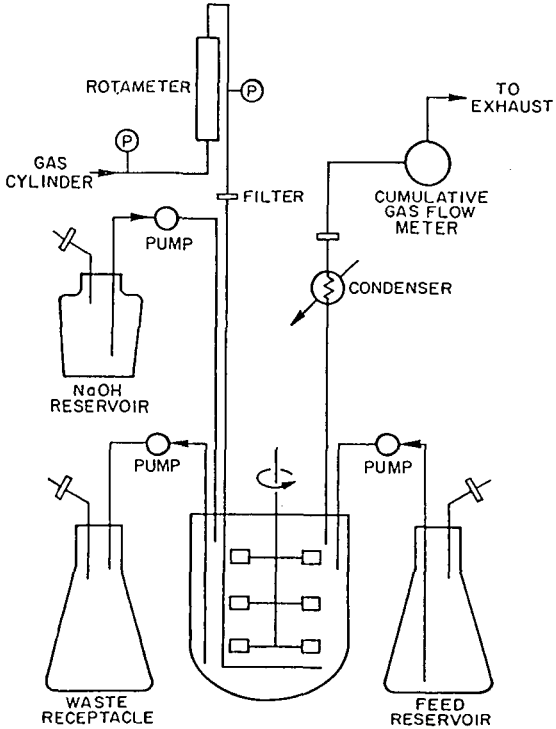

FIGURE 1. Schematic Diagram of Continuous Flow Fermentation System.

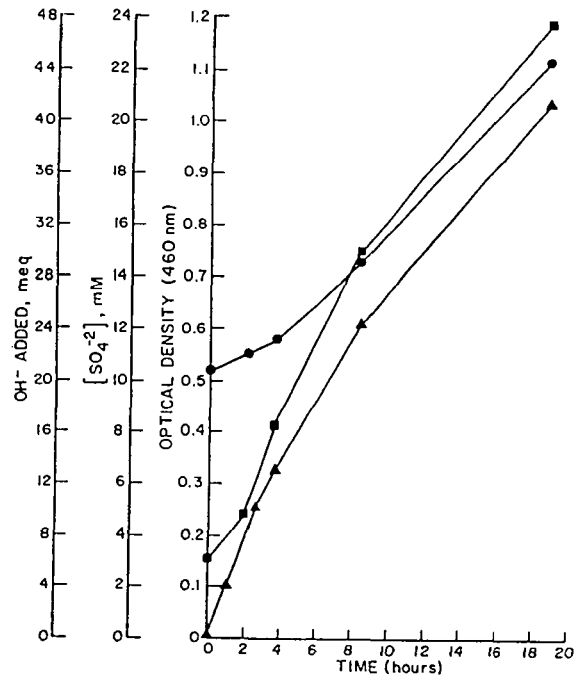

FIGURE 2. Optical Density, Concentration of Sulfate (SO_4^{-2}) and Hydroxide Ion (OH^-) Utilized in an Anaerobic T. denitrificans Batch Reactor Receiving 1.25 mmole/hr Hydrogen Sulfide (H_2S) Feed. OD (●); SO_4^{-2} (■); OH^- (▲).

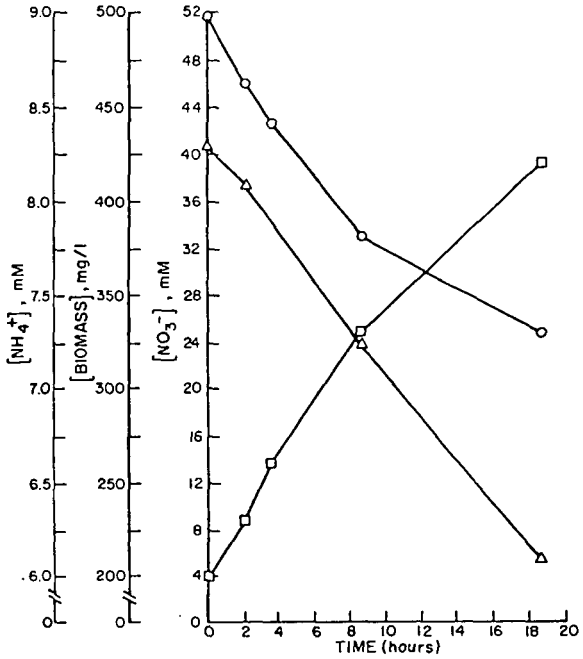

FIGURE 3. Concentrations of Nitrate (NO_3^-), Biomass and Ammonium (NH_4^+) in an Anaerobic T. denitrificans Batch Reactor Receiving 1.25 mmoles/hr Hydrogen Sulfide (H_2S) Feed. NO_3^- (O); NH_4^+ (Δ); Biomass (□).

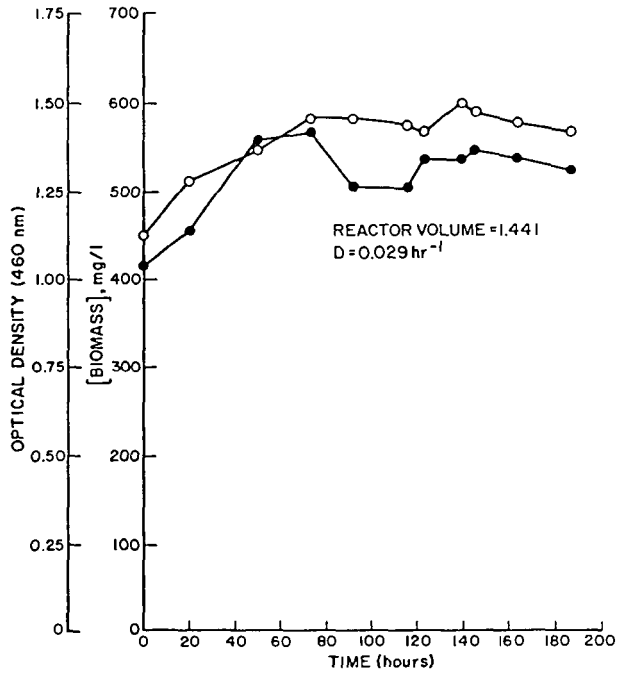

FIGURE 4. Concentration of Biomass and Optical Density in an Anaerobic T. denitrificans CSTR Receiving 2.6 mmoles/hr Hydrogen Sulfide (H_2S) Feed. OD (O); Biomass (●).

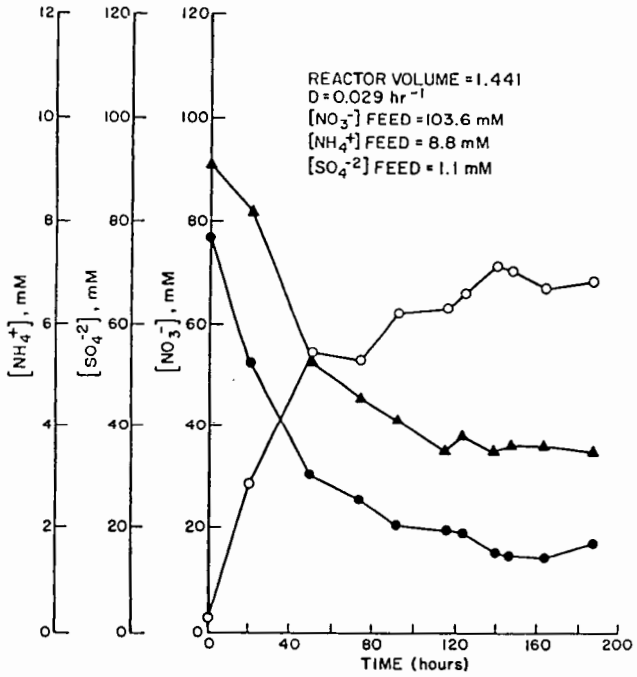

FIGURE 5. Concentrations of Nitrate (NO_3^-), Sulfate (SO_4^{-2}) and Ammonium (NH_4^+) in an Anaerobic T. denitrificans CSTR Receiving 2.6 mmoles/hr Hydrogen Sulfide (H_2S) Feed. NO_3^- (●); SO_4^{-2} (o); NH_4^+ (▲).

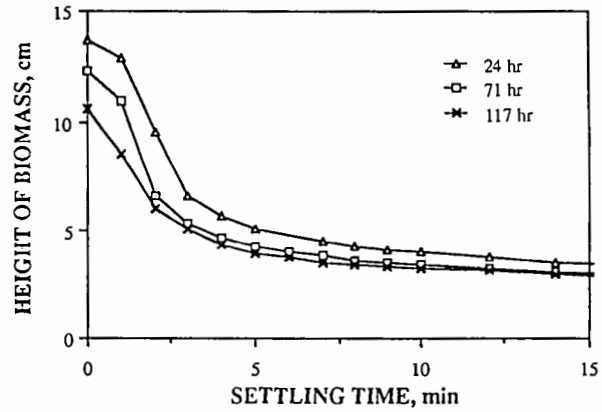

FIGURE 6. Height of Biomass in Settling Test in Marubishi MD 300 Fermenter.

Biological Production of Liquid and Gaseous Fuels from Coal Synthesis Gas

by

G. M. Antorrena
J. L. Vega
E. C. Clausen
J. L. Gaddy

Abstract

Cultures of microorganisms have been isolated that convert CO, H_2 and CO_2 in coal synthesis gas into methane or ethanol. The reactions are severely mass transfer limited and bioreactor design will be a critical factor in the application of this technology. This paper presents results of culture isolation studies and development of continuous reactors for these cultures. The results of bubble columns and stirred tank reactors are presented and discussed. Methods for defining mass transfer coefficients and intrinsic kinetics are presented. Operation of these gaseous fermentations at high pressure has enabled complete conversion in reaction times of a few minutes.

INTRODUCTION

Coal synthesis gas represents an excellent raw material for the production of chemicals and fuels. A typical composition of coal-derived synthesis gas includes 25-35 percent hydrogen, 40-65 percent carbon monoxide, 1-20 percent carbon dioxide, 0-7 percent methane and other compounds in small quantities such as sulfur (as H_2S or COS), chlorine, etc. Many coal gasification processes exist or are currently under development that can produce synthesis gas economically.

Chemical catalytic processes are known to utilize syngas to produce a large variety of compounds such as methanol, formaldehyde, and acetic acid (Courty and Chaumette, 1978). Microorganisms may also be used to convert synthesis gas components into more desired products such as acetate, methane, and alcohols. Biological processes, although generally slower than purely chemical reactions, have several advantages over catalytic processes, such as higher specificity, higher yields, lower energy costs and possibly higher resistance to poisoning. Furthermore, the irreversible character of biological reactions allows complete conversion and avoids thermodynamic equilibrium relationships.

The biological conversion of synthesis gas components to methane and liquid fuels involves contacting the gas and microorganisms in liquid culture. The gas must then absorb into the gas-liquid interface and diffuse through the culture medium to the cell surface to be consumed by the microbes. For sparingly soluble gases such as carbon monoxide, oxygen, etc. in contact with suspended cells it

has been well established that the main resistance to transport lies in the liquid film (Tsao and Lee, 1977; Blanch, 1979; Yoshida, 1982). The rate of transport from the gas phase into the culture medium is, therefore, faster for higher partial pressures in the gas phase. In the case where the overall reaction rate is transport controlled, that is, the dissolved gas concentration in the liquid phase is zero, the rate of transport, and thus the rate of reaction, is proportional to the partial pressure in the gas phase. Contacting schemes to maximize gas-liquid contact are thus very important.

The purpose of this paper is to present the results of laboratory experiments carried out in various contacting schemes for converting synthesis gas components to methane, acetate and ethanol. The batch reactor and two continuous reactors, the continuous stirred tank reactor (CSTR) and the bubble column, are employed. Also, the effects of increased pressure on improving mass transfer and microorganism performance are presented and discussed.

BIOLOGICAL SYNTHESIS GAS CONVERSION

Methane Production

The primary reactions in the biological conversion of synthesis gas to methane are the formation of methane precursors and biomethanation of the precursors. Table 1 shows the known biological routes to methane from synthesis gas components. All of these reactions are carried out anaerobically and usually require very low redox potentials in the liquid medium in which the microorganisms are suspended (Ljungdahl and Wiegel, 1986). As is seen in the table, the formation of methane can be accomplished by direct conversion of CO, CO_2 and H_2 or by the indirect formation of methane intermediates (acetate or H_2 and CO_2). Of the one-step reactions, only reaction I.3, the direct formation of methane from H_2 and CO_2, has been well-studied and verified (Escalante-Semerena *et al*. 1984). This reaction is known to be carried out by most of the methanogens (Jones *et al*., 1987), although some methanogens such as *Methanothrix* sp. are not capable of this conversion (Huser *et al*. 1982).

The one-step reactions that convert carbon monoxide directly to methane have been suggested in the literature. *Methanobacterium thermoautotrophicum* has been reported to produce methane from carbon monoxide according to Equation I.1 (Daniels *et al*. 1977). The growth of *M. thermoautotrophicum* on CO was reported to be very slow and was inhibited by high substrate concentrations. It has also been reported that other methanogenic bacteria may convert carbon monoxide and hydrogen directly to methane according to Equation I.2 (Fisher *et al*. 1932; and Stephenson and Strickland, 1933). It is more likely, however, that the carbon monoxide reduction to methane in these experiments proceeded via the multiple-step reactions II.3 and I.3 (Daniels *et al*. 1977; and Kluyver and Schnellen, 1947).

With the exception of Equation I.3, an indirect formation of methane seems more viable than the direct routes previously discussed. These multi-step reactions may involve the formation of a liquid intermediate, acetate, or the utilization of carbon monoxide to produce carbon dioxide and hydrogen by the water gas shift reaction (Equation II.3). In the latter case, the products hydrogen and carbon dioxide can be directly converted to methane (Equation I.3) or may enter the multiple step process that produces acetate as an intermediate

(Equation II.2). The organisms Rhodopseudomonas gelatinosa (Uffen, 1976; and Dushekvicz and Uffen, 1979), and Rhodospirillum rubrum (Breed et al. 1977) are known to perform the water gas shift reaction.

Another approach to indirect methane production is the formation of acetate as a methane precursor. In anaerobic digestion processes, 80 percent of the methane is produced from acetate by Equation II.4. The organisms Peptostreptococcus productus and Eubacterium woodii (Genther and Bryant, 1983) have been found to produce acetate by Equation II.1. Among these bacteria, P. productus has shown the fastest growth rate and the highest tolerance to carbon monoxide. These microorganisms have also been found to carry out the conversion of hydrogen and carbon dioxide to acetate (Equation II.2), although in P. productus, carbon monoxide appears to be a preferred substrate.

Acetate can be transformed by methanogens of the Methanosarcinaceae family such as Methanosarcina barkeri as well as Methanothrix soehngenii (Jones et al. 1987). While Methanosarcina barkeri, for example, will utilize acetate only in the absence of other preferred substrates (such as H_2 and CO_2), Methanothrix sp. does not utilize normal methanogenic substrates and growth and methane formation is exclusively observed in the presence of acetate (Huser et al. 1982). Both microorganisms show comparable specific growth rates at low acetate concentrations (< 3mM). On the other hand, in view of the Monod saturation constants available for the two microorganisms, (K_s = 0.7 mmol/l for Methanothrix), it is expected that at low acetate concentrations Methanothrix is the more predominant of the two.

Ethanol Production

While many anaerobic, facultatively anaerobic and even some strictly aerobic microorganisms form various amounts of ethanol from glucose (Weigel, 1980), no organism was known to form ethanol autotrophically from synthesis gas components. In 1987, a strict anaerobic mesophilic bacterium was isolated from animal waste that was capable of converting CO, H_2, and CO_2 to a mixture of acetate and ethanol (Barik et al. 1987). Preliminary identification studies have indicated that the bacterium has a strong possibility of being a new clostridium species (Tanner, 1988). It is likely that in the same manner as with other clostridia growing on sugars, ethanol and acetate are formed from acetyl-CoA by this organism, with product distribution highly dependent on the regulation of electron flow (Rao, et al. 1987).

The overall stoichiometry for the formation of ethanol from carbon monoxide and hydrogen/carbon dioxide has been established by Vega et al. (1988):

$$6\ CO + 3\ H_2O \rightarrow CH_3CHOH + 4\ CO_2 \quad \Delta G^\circ = -\ 59.9\ \text{Kcal/g mole}\ CH_3CHOH \qquad (1)$$

$$2\ CO_2 + 6\ H_2 \rightarrow CH_3CHOH + 3\ H_2O \quad \Delta G^\circ = -\ 23.2\ \text{Kcal/g mole}\ CH_3CHOH \qquad (2)$$

Acetate formation from CO, CO_2 and H_2 by the organism is carried out using the same stoichiometric equations presented in Table 1.

BIOREACTOR DESIGN

Gas-Liquid Mass Transfer Concepts in Bioreactors

The transfer of gases in fermentation systems involves three phases: gas, culture medium and microbial cells suspended in the medium. In general, a combination of the following resistances can be expected (Bailey and Ollis, 1977):

1.- Diffusion from the bulk gas to the gas-liquid interface;
2.- Movement through the gas-liquid interface;
3.- Diffusion of the solute through the relatively unmixed liquid region (film) adjacent to the bubble into the well mixed bulk liquid;
4.- Transport of the solute through the bulk liquid to a second stagnant film surrounding the microbial species;
5.- Transport through the second unmixed liquid region associated with the microbes;
6.- Diffusive transport into the microbial floc, mycelia, or particle, if appropriate. (When the microbes take the form of individual cells, this resistance disappears); and,
7.- Consumption of the solute by biochemical reaction within the microorganism.

As is the case with the conventional chemical engineering analysis of absorption processes, interfacical resistance to mass transfer can be neglected. In systems where agitation is provided, transport through the bulk liquid is assumed to be instantaneous. Finally, when individual cells are suspended in a medium, the liquid film resistance around the cells is usually neglected with respect to other resistances because of the minute size and the enormous total surface of the cells (Finn, 1954). Thus for the transfer of sparingly soluble gases such as CO and H_2, the main resistance to transport lies in the liquid film. Reaction schemes should thus concentrate on minimizing the liquid film resistance of the gas transfer into the liquid phase. Other techniques for promoting gas-liquid mass transfer should also be considered, including the use of alternative liquid phases and the use of high pressure to promote higher solubility.

The conversion of carbon monoxide to acetate by reaction II.1 (see Table 1) using P. productus was chosen as a model system for bioreactor comparisons. The mass transfer limited concepts shown for this organism are applicable to other gas phase fermentation systems.

The Batch Reactor

Batch fermentation systems are typically used in determining fermentation kinetics by following the concentration of substrate in the liquid phase with time. For gas phase systems, however, the liquid phase concentration cannot be measured since sensors are not generally available for most systems. A method has been developed for determining mass transfer and intrinsic kinetic parameters in gas phase fermentation systems for sparingly soluble gases such as CO and H_2. In a typical experiment, batch reactors are started with different initial gas, partial pressures, and monitored with time for gas consumption, cell density and product formation.

Figure 1 presents the volumetric rate of disappearance of CO from the gas phase using P. productus as a function of its partial pressure. The data for each partial pressure shows a period of increase in the rate of uptake of carbon monoxide from the gas phase while the partial pressure of the gas decreased slowly. During this period and because the cell concentration is low, the reaction rate is mainly under kinetic control, since the concentration of substrate in the liquid culture is above zero. The actual shape of these curves in the figure bear no physical meaning and the continuous lines drawn correspond to a best visual fitting of the data. As the cell concentration reached a value at which mass transfer controlled, the concentration of carbon monoxide in the liquid became zero and the reaction rate was that of the rate of transport of the substrate into the liquid phase. This rate of transport is then proportional to the partial pressure of carbon monoxide in the liquid phase and the proportionality constant is K_La/H. Because the fermentation conditions for all experiments (medium composition, agitation, temperature, etc.) were very similar if not the same, all the data in Figure 1 followed a single straight line. The value of the slope on the straight line as obtained from least squares of all data in the mass transfer limited region was 5.91 mmol CO/L•hr•atm. Taking for H the value for water at 37°C (H = 1.21 atm•L /mmol CO), the calculated value for K_La was 7.15 hr-1. Once the volumetric mass transfer coefficient is known, intrinsic kinetic parameters may be estimated using the data in the region where mass transfer does not control. Typically, Monod-type kinetics are used, utilizing calculated values of dissolved CO in the liquid phase.

The Stirred Tank Reactor

The traditional reactor used in fermentation processes is the continuous stirred tank reactor or CSTR. As it relates to gas phase substrates, the CSTR has continuous gas flow into a constant volume liquid phase reactor. A smaller liquid feed stream is utilized to supply nutrients to the microorganism in the reactor system. The agitation rate in the system is relatively high in order to promote transfer of the sparingly soluble gas into the liquid culture medium.

Experiments have been conducted with P. productus in a CSTR at different gas flow rates in order to develop suitable equations for modeling and process scale-up. The model which includes material balances for carbon monoxide, methane, and carbon dioxide in the gas phase and for the carbon dioxide/bicarbonate equilibrium system in the liquid medium. The model assumes that the carbon dioxide in equilibrium with the gas phase carbon dioxide partial pressure and the bicarbonate and pH level in the liquid.

Figures 2 and 3 show the solution of the model for various volumetric mass transfer coefficients (Figure 2) and various total operating pressures (Figure 3). Experimental data at 1 atm and a mass transfer coefficient of 30 are also included in the figures. As observed in the model results, increases in the mass transfer coefficient or in total operating pressures lead to higher reactor productivities. However, due to the perfect mixing in a CSTR, complete conversion is only attained when the gas flow rate is zero. The use of the model allows the extrapolation of performance of the CSTR system and permits preliminary economic evaluation of coupled with suitable equations for scale-up of properties such as the mass transfer coefficient.

Bubble Columns

Bubble columns are commonly used in industrial processes both as reactors or absorbers whenever a large liquid retention time and/or a large liquid hold-up is needed. Some advantages of bubble columns are the lack of moving parts, minimum maintenance, relatively low costs, high interfacial area and a high mass transfer coefficient (Charpentier, 1981). The principal disadvantages are a large extent of backmixing and coalescence. These two drawbacks can be minimized by employing packing inside the column.

The performance of a bubble column for CO conversion to acetate by *P. productus* is shown in Figure 4. The bubble column is capable of achieving similar rates of CO conversion as the stirred tank reactor without agitation. In addition, the bubble column is capable of yielding complete conversion due to plug flow operation.

By combining a CO material balance along the column with the rate expression for CO transport into the liquid phase, the following expression for the partial pressure of CO leaving the reactor is obtained:

$$\ln P^{o}_{CO} = \ln P_{CO}{}^{i} - \frac{K_L a}{H} \frac{\epsilon_L \, h \, RTS}{G} \qquad (1)$$

where ϵ_L = fraction of liquid in the column;
h = height of the column;
S = cross-sectional area of the column;
R = ideal gas constant;
T = absolute temperature; and
G = gas flow rate

Verification of Equation (1) is shown in Figure 5 for the data of Figure 4. As is shown, a single straight line is obtained, indicating that the model satisfactorily predicts column performance. In addition, $K_L a/H$ can be obtained from the slope of the line in Figure 5, once the numerical values of the constants in Equation (1) are supplied. This mathematical model can also be used for process design and scale-up in a similar manner as the CSTR model.

Pressure Effects

As was shown in Figure 3, an increase in the operating pressure brought about a significant increase in the rate of CO uptake in a CSTR. Thus, operation at increased pressures can be highly beneficial in minimizing reactor volume requirements. However, CO has been shown to inhibit growth and CO uptake at dissolved CO tensions of 0.8-1.0 atm. Methods to avoid CO inhibition by maintaining low dissolved CO tensions at increased pressures must be developed. The key to maintaining low dissolved CO tensions at increased pressures is to develop high cell concentrations that are capable of uptaking the increased quantities of CO. Higher cell concentrations can be achieved by feeding alternate substrates such as glucose, or by gradually increasing the cell concentration in a stepwise fashion.

When P. productus inside a high pressure Parr reactor with an initial cell concentration of about 18 mg/L was directly pressurized to a total pressure of 5.7 atm (carbon monoxide partial pressure of 3.6 atm), no sign of carbon monoxide consumption was observed after 93 hours. On the other hand, when the pressure was raised stepwise with small increases in the carbon monoxide partial pressure at 10 hr time intervals, carbon monoxide consumption occurred at total pressures as high as 14.6 atm (carbon monoxide partial pressure of 9.3 atm). Figure 6 shows a carbon monoxide disappearance profile for P. productus grown on CO where a 14.6 atm total pressure (9.3 atm carbon monoxide partial pressure) was achieved in five smaller pressure increments. As is seen, carbon monoxide was consumed at fast rates even at these high pressures. Thus, low dissolved CO tensions were achieved by gradually increasing cell growth. A proportional decrease in reactor volume is then possible through increased pressure operation.

CONCLUSIONS

Anaerobic bacteria have been utilized in the biological conversion of sparingly soluble gas phase substrates such as CO and H_2 to the products methane, ethanol and acetate. Several reactor designs may be utilized in these conversions including batch reactors and continuous stirred tank and bubble column reactors. The batch reactor has been utilized to obtain mass transfer correlations for the mass transfer controlled regime, and intrinsic kinetic parameters have been obtained in the non-mass transfer limited regime.

The continuous stirred tank reactor has been utilized to develop suitable equations for modeling and process scale-up. The model includes material balance equations and carbon dioxide/bicarbonate chemical equilibrium. The effects of the mass transfer coefficient and total pressure on CO uptake and conversion were modeled.

The bubble column has also been utilized for CO utilization. Higher conversions and similar rates of CO conversion were obtained without the required agitation in the CSTR. The results were successfully modeled and the resultant mass transfer coefficient obtained.

The benefits of increased pressure on CO utilization were demonstrated in batch and continuous culture. A gradual stepwise procedure was utilized in increasing the cell concentration to achieve low dissolved CO tensions.

LITERATURE CITED

Bailey, J. E. and Ollis, D. F. (1977). Biochemical Engineering Fundamentals. McGraw-Hill, New York.

Barik, S., J. L. Vega, E. R. Johnson, E. C. Clausen and J. L. Gaddy (1987). "Methanation of Synthesis Gas Using Biological Processes," CRC Series, (to be published).

Blanch, H. W. (1979). "Aeration", Annual Reports on Fermentation Processes, 3: 47-74, Academic Press, Inc.

Breed, R. S., E. G. D. Murray, and N.R. Smith (1977). Bergey's Manual of Determinative Bacteriology, The Williams and Wilkins Company, Baltimore, MD (8th Ed.).

Charpentier, J. C. (1981). "Mass Transfer Rates in Gas-Liquid Absorbers and Reactors. Advances in Chemical Engineering, Vol. II, 1-133.

Courty, Ph. and P. Chaummette (1987). "Syngas: A Promising Feedstock in the Near Future," Energy Progress 7: 23-30.

Daniels, L., G. Fuchs, R. K. Thauer and J. G. Zeikus (1977). "Carbon Monoxide Oxidation by Methanogenic Bacteria," J. Bacteriol., 132: 118-126.

Dushekvicz, M. P. and R. L. Uffen (1979). "Identification of a Carbon Monoxide - Metabolizing Bacterium as a Strain of Rhodopseudomonas gelatinosa," International Journal of Systematic Bacteriology, 29 : 145-148.

Escalamte-Semerena, J. C., K. L. Rinehart, Jr., and R. S. Wolfe (1984). "New Insights Into The Biochemistry of Methanogenesis From H_2 and CO_2," p. 191-198, in R. L. Crawford and R. S. Hanson (ed.), Microbial Growth on C_1 Compounds. Proceedings of the 4th International Symposium, American Society for Microbiology, Washington, D. C.

Finn, R. K. (1954). Agitation-aeration in the laboratory and in industry. Bacteriol. Rev. 18: 254-274.

Fisher, F., R. Leiske, and K. Winzer (1932). "Uber die bildung von Essigsaure bei der biologischen Umsetzung von Kohlenoxyd Und Kohlensaure mit Wasserstoff zu Methan," Biochem. Z., 245: 2-12.

Genthner, B. R. S., and M. P. Bryant (1983). "Growth of Eubacterium limosum with Carbon Monoxide as the Energy Source," Appl. and Environ. Microbiol. 43: 70-74.

Huser, B. A., K. Wuhrmann, and A. J. B. Zehnder (1982). "Methanothrix soehgenii gen. nov. sp. nov., a New Acetotrophic Non-hydrogen-oxidizing Methane Bacterium," Arch. Microbiol., 132: 1-9.

Jones, W. J., D. P. Nagle, Jr., and W. B. Whitman (1978). "Methanogens and the Diversity of Archaebacteria," Microbiol. Rev., 51: 135-177.

Kluyver, A. J., and C. G. Schnellen (1947). "On the Fermentation of Carbon Monoxide by Pure Cultures of Methane Bacteria," Arch. Biochem., 14: 57-70.

Ljungdahl, L. G., and J. Wiegel (1986). "Working with Anaerobic Bacteria," A. L. Demain, N. A. Solomon (Ed.) in Manual of Industrial Microbiology and Biotechnology, Chapter 8, pp 84-96, ASM, Washington, D. C.

Rao, G., P. J. Ward, and R. Mutharasan (1987). Annals of the New York Academy of Sciences 506, 76.

Stephenson, M., and L. H. Strickland (1933). "The Bacterial Formation of Methane by the Reduction of One-Carbon Compounds by Molecular Hydrogen," Biochem . J., 27: 1417-1527.

Tanner, R. S. (1988). (The University of Oklahoma, Department of Botany and Microbiology), private communication.

Tsao, G. T., and Y. H. Lee. (1977). "Aeration", Annual Reports on Fermentation Processes, 1: 115-149.

Uffen, R. L. (1976). "Anaerobic Growth of a Rhodopseudomonas Species in the Dark with Carbon Monoxide as Sole Carbon and Energy Substrate," Proc. Natl. Acad. Sci. U.S.A., 73 : 3298-3302.

Vega, J. L., S. Prieto, B. B. Elmore, E. C. Clausen and J. L. Gaddy, "The Biological Production of Ethanol from Synthesis Gas," presented at the 10th Symposium on Biotechnology for Fuels and Chemicals, May 1987, Gatlinburg, TN.

Wiegel, J. (1980). Experientia 36, 1434.

Yoshida, F. (1982). "Aeration and Mixing in Fermentation," Annual Reports on Fermentation Processes, 5: 1-34.

Table 1

Biological Routes to Methane From Synthesis Gas Components

I) ONE-STEP REACTIONS

$$4\ CO + 2\ H_2O \xrightarrow{\text{I.1}} CH_4 + 3\ CO_2 \qquad \Delta G^\circ = -54.4\ \text{kcal/reac.}$$

$$CO + 3\ H_2O \xrightarrow{\text{I.2}} CH_4 + H_2O \qquad \Delta G^\circ = -36.0\ \text{kcal/reac.}$$

$$4\ H_2 + CO_2 \xrightarrow{\text{I.3}} CH_4 + 2\ H_2O \qquad \Delta G^\circ = 31.3\ \text{kcal/reac.}$$

II) MULTIPLE-STEP REACTIONS

$$4\ CO + 2\ H_2O \xrightarrow{\text{II.1}} CH_3COOH + 2\ CO_2 \xrightarrow{\text{II.4}} CH_4 + CO_2$$

$\Delta G^\circ = -37.8$ kcal/reac. $\qquad \Delta G^\circ = -12.6$ kcal/reac.

$$4\ H_2 + 2\ CO_2 \xrightarrow{\text{II.2}} CH_3COOH + 2H_2O \xrightarrow{\text{II.4}} CH_4 + CO_2$$

$\Delta G^\circ = -18.7$ kcal/reac. $\qquad \Delta G^\circ = -12.6$ kcal/reac.

$$CO + H_2O \xrightarrow{\text{II.3}} H_2 + CO_2 \xrightarrow{\text{II.4}} CH_4 + \ldots$$

II.2 + II.4

$\Delta G^\circ = -4.8$ kcal/reac.

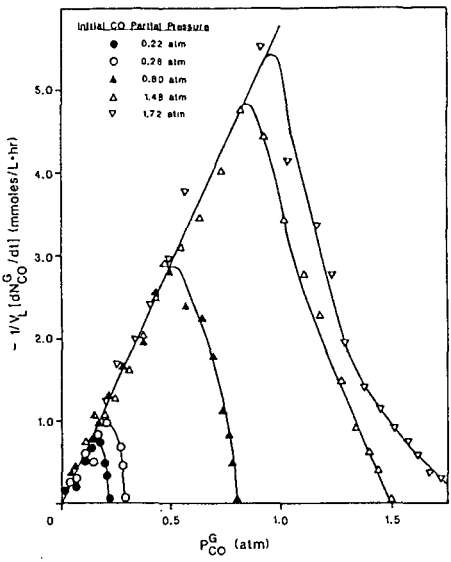

Figure 1. Determination of the volumetric mass transfer coefficient for P. productus in batch culture.

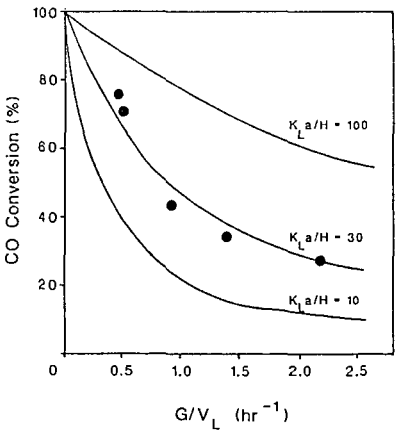

Figure 2. Model results for carbon monoxide conversion as a function of the gas flow rate per unit of culture volume for various volumetric mass transfer coefficients (K_La/H in mmol CO/atm L hr).

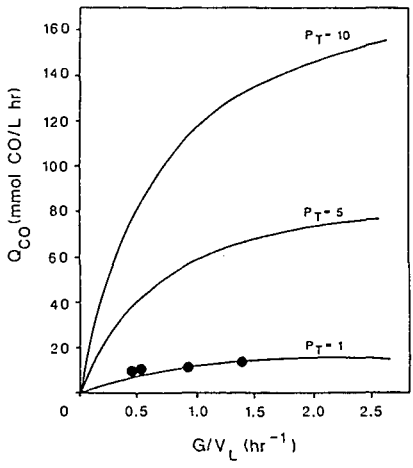

Figure 3. Model of results for carbon monoxide uptake as a function of the gas flow rate for various total operating pressures (P_T in atm).

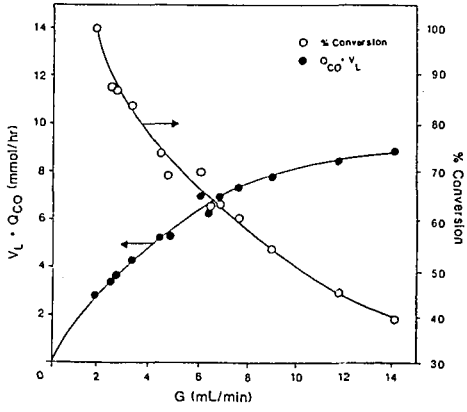

Figure 4. Carbon monoxide uptake rate and conversion level as a function of gas flow rate in the column for *P. productus*.

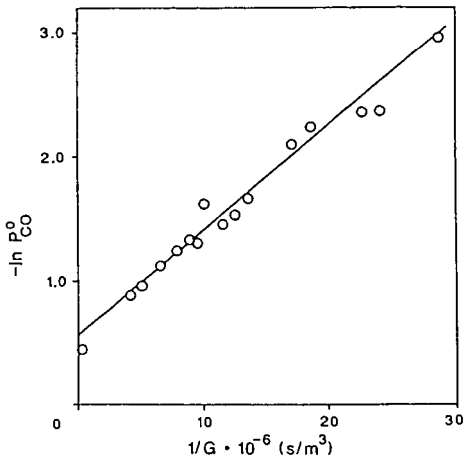

Figure 5. Testing the proposed bubble column model of Equation 1.

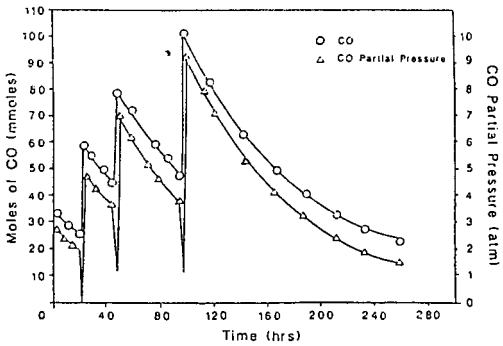

Figure 6. CO consumption and CO partial pressure as a function of time for P. productus start-up with CO alone.

DIFFUSE REFLECTANCE INFRARED SPECTROSCOPY STUDIES OF THE AIR OXIDATION OF COAL SURFACES

E. L. Fuller, Jr. and N. R. Smyrl
Oak Ridge National Laboratory(*)
Oak Ridge, TN 37831-2008

INTRODUCTION

Oxidation of coals is of concern to those interested in the weathering that begins as soon as the mined material is wrested from the humid, reducing, pressurized environment of the underground seam. The loss of energy content comprises an obvious enconomic impact to combustion processes. Floculation and coking processes are both deleteriously effected whereas systematic information regarding the structure and reaction mechanisms can be obtained. This work is directed primarily to defining the surface structures and mechanisms occuring at the air/coal interface.

EXPERIMANTAL

Diffuse Reflectance Infrared Fourier Transform (DRIFT) spectroscopic analyses provide a wealth of information related to the chemical changes wrought in air oxidation of coals, as noted in the spectra of Figure 1. These spectra were obtained by direct observation of an aliquot of powder subjected to the temperature and chemical treatment in the reactor that resides continuously in the analytical beam in the DRIFT attachment within the infrared spectrometer. Detailed descriptions of the equipment and techniques have been reported elsewhere[1,2]. Each spectrum is presented in the Log[R(sample)/R(reference)], "absorbance", format as noted in reference number 1. No numerical values are reported since they are not needed for the qualitative analyses discussed in this report.

RESULTS AND DISCUSSION

Examination of the spectra elucidates several features related to the mechanism of the oxidation of the powder surfaces:

(A) The oxidation progressively consumes the aliphatic hydrogen as witnessed in the loss of characteristic absorbance in the 3000-2800 wavenumber region, generally associated with interaction of the electromagnetic energy with the resonance -C-H, $-CH_2$ and $-CH_3$ stretching vibrations.

(B) Simultaneously there is an insertion of oxygen into the carbonaceous substrate to form carbonyl groups manifesting a marked enhancement of absorbance in the 1900-1600 wavenumber region, long known to be associated with the C=O vibrational

modes.

(C) The band at ca. 1550 wavenumbers due to the O-C-O and/or C-O-C bending mode is enhanced due to the oxygen enrichment of the coal structure in the surface regime penetrated by the reflecting infrared beam (see also Figure 2) In addition, the stretching vibrations of carboxylate salts are known to be manifest in absorption in this energy regime.

(D) The triplet at ca. 800 +/-50 wavenumbers (due to the out-of-plane bending mode of aromatic C-H) becomes less prominent due to the loss of "aromatic" character of the oxidized material. The residual doublet in this region is much akin to the lattice modes of kaolinitic clays, consistent with the hydroxyl bands noted below in (E).

(E) The broad triangular-shaped band 3600-2000 wavenumbers remains relatively unchanged, indicating relatively little or no change in the amount and/or distribution of hydrogen bonded O-H (phenolic, alcoholic, acidic, aquatic, etc.). The narrow bands (3600-3500 wavenumbers) of the clay mineral hydroxyl groups do become more distinct as the 3500 wavenumber feature is broadened.

(F) The "aromatic" C-H band does not seem to be appreciably attacked by the oxygen treatment. Previous workers have generally attributed the band at 3000 to 3200 to an "aromatic" C-H vibrational mode. The peak value appears to shift from ca. 3050 to 3080 wavenumbers as aliphatic (-C-H) and olefinic (=C-H) entities are consumed. This is a tentative interpretation since the effect may involve another distinct type of aromatic C-H entity, not yet defined at this point in time.

Few, if any, techniques are individually able to provide as much information related to the oxidation of coals as does the <u>in situ</u> DRIFT technique. Additional quantitative data will be presented using the analytical techniques developed previously[1].

These qualitative analyses are extremely informative and valuable in elucidating the process of weathering and resultant ramifications related to the processing of coals[3]. In addition a more detailed understanding is obtained by examining the difference spectra, depicting the changes induced with respect to the initial (unoxidized) material. Each of the difference spectra were obtained by direct subtraction without any arithmetic adjustment for sample size, geomtric variations, etc. that pre present in other more classical infrared techniques[1]. By presenting the data in absorbance format (rather than Kubelka-Munk or remission units) we note that we have a distinctly direct ratiometric comparison to the reference material (rather than each mathematically ratioed to a diffusely reflecting reference material, KBr, CsI, NaCl, etc). The spectral changes can then be

observed in their own right on a much expanded scale and with a much more realistic interpretable background base line as noted in Figure 2. Now we can observe not only more accurate measures of the enhanced absorbance and more precise peak locations, but also delineate the progressive increase in the population of four (if not five) discrete carbonyl species based on observed inflection points in the curves formed by connecting the data points comprising the spectra.

These results are consistent with the successive oxygen insertion to form (1) aldo/keto groups, (2) acido groups, (3) acid anhydro groups, and finally (4) carbonato groups all as precursors to the ultimate release of the oxidized products of carbon dioxide and carbon monoxide. Earlier work at 400 C showed similar results albeit with faster rates[1]. In this work we note that the spectral distribution after 400 C oxidation differs from the 200 C result in additional transformation of the low wavenumber intensity to enhance the higher wavenumber bands (see Figure 3). This indicates that there is a greater mobility of the acido groups at 400 C to allow requisite juxtaposition of two precursors subsequent to expulsion of molecular water (dehydration) concomitant to the condensation to form the surface anhydride. This condition is contrasted to the homogeneous reactions in gas phases and/or liquid states where each of the reacting entities is completely mobile and the only activation barrier involves the energy to scission sigma bonds. A schematic representation of the surface reaction is presented below:

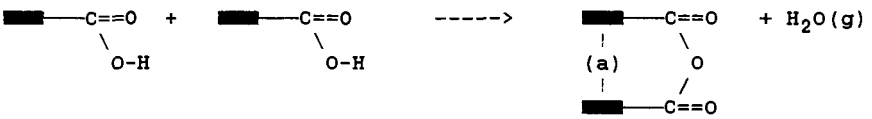

ACID SITE(1) + ACID SITE(2) + THERMAL ENERGY = CONDENSED ACID ANHYDRIDE + WATER VAPOR

The initiation of the reaction requires enough energy to bring the acid entities to within a distance approaching "a" as well as the scission of both a C-O bond and an O-H bond either separately or in concert. Oxidation at 300 C yields intermediate results as shown by the 1810 and 1850 wavenumber feature in Figure 4. The results at 125 C show very little absorbance at 1850 wavenumbers, as revealed in the data of Figure 5. Subsequent elevation to the isothermal oxidation at 400 C is required to form the anydro species. In view of the observations on more mobile configurations, "Phthalic acid melts with decomposition to the anhydride at temperatures ranging from 200 to 230°, depending on the rate of heating and the condition of the glass capillary surfaces."[4] This citation exemplarily refers to the bond

cleavage impediment with little or no migration barrier to the anhydride coalescence. The slight inflection at ca. 1850 wavenumbers is probably due to the small concentration of acid sites formed by oxidation of adjacent susceptible sites on the coal substrate. The migration of more dispersed acid entities is brought about only at the higher temperatures.

Further details and substantiation of the mechanisms are derived from the data of Figure 6. Here we note that the prolonged reaction at 125 C involved only minor amounts of water loss and the DRIFT spectra reveal marked loss of water due to the additional thermal activation to 400 C. These results are still of a qualitative nature but show the benefits of detailed examination to aid in our understanding of the oxidation of coals as related to the important chemical weathering processes, and precursor states to combustion at much higher temperatures.

Our project continues to develop the methodology and technique to acquire more details and more quantitative data. These results are for a single sample of a subbituminous coal from the Wyodak mine of the Roland/Smith seam, Gillette, Wyoming. Even this sample is unique in that it was acquired from a freshly opened mine face, hermetically sealed in a light tight container and maintained at 25 +/-3 C prior to these analyses. Additional studies on "real" materials will aid in there description with respect to our "reference" materials. Not to mention, the need to apply the versatile DRIFT technique to coals of other ranks. This work extends the afirmation, "Clearly, diffuse reflectance has overwhelming advantages in the characterization of high rank coals."[5] to a much broader extent. The major benefits arise from 1. ease of sample preparation, 2. reactions monitored without impediment of matrix (ie. KBr), 3. measurements possible in reaction medium (not inert gas as in photoacoustic), 4. reference spectrum acquired in vacuum, 5. inherently nondestructive (allows other supporting analyses on same alequot), 6. the ability to acquire spectra over a wide range of temperatures (77 to 800 K, at present), and 7. direct measurements in either static (batch) or flowing (continous) modes. The additional information provided by the DRIFT techniques relies on the vast amount of information obtained over the years via the more arduous classical procedures.

SUMMARY

Air oxidation of this sub-bituminous coal proceeds via oxygen insertion into the organic substrate progressively forming aldo/keto groups, acid groups and acid anhydride entities while consuming the hydrogen of the aliphatic hydrocarbon entities. The amount of anhydride is limited (a minority of the total oxidized sites), and serves to measure the number or adjacent susceptible sites on the coal surface. Above ca. 200 C there is sufficient activation to impart the mobility to allow the acid functionalities to come together and dehydrate to form the condensed anhydride species. Above 400 C the anhydro groups

predominate in the steady state production of carbon dioxide and water vapor. These studies show the merits of the in situ, real time DRIFT techniques for the unique definition of the chemistry and structure of coals.

REFERENCES

1. E. L. Fuller, Jr., N. R. Smyrl, and R. L. Howell, Chemistry and Structure of Fuels: Reaction Monitoring with Diffuse Reflectance Infrared Spectroscopy, in "Chemical, Biological and Industrial Applications of Infrared Spectroscopy" edited by James R. Durig, Wiley-Interscience, 1985.

2. E. L. Fuller, Jr. and N. R. Smyrl, Chemistry and Structure of Coals: Diffuse Reflectance Infrared Spectroscopy Equipment and Techniques, FUEL, 64, 1143-1149, (1985).

3. E. L. Fuller, Jr. and N. R. Smyrl, Diffuse Reflectance Infrared Fourier Transform, DRIFT, Studies of Coal Preparation Techiques (Preliminary Results), ORNL/CF-88/27, March 1988.

4. L. F. Fieser and M. Fieser, "Organic Chemistry" D.C. Heath and Co, 1944, p670.

5. P. Painter, B. Bartges, D Plasizynski, T. Plasizynski, A. Lichtus, and M. Coleman, "Novel Methods for FTIR Analyses of Coal" ACS Fuel Chem. Prep. 31 65 (1986).

(*) Operated by Martin Marietta Energy Systems, Inc. for the Department of Energy under contract No. DE-AC05-84OR21400.

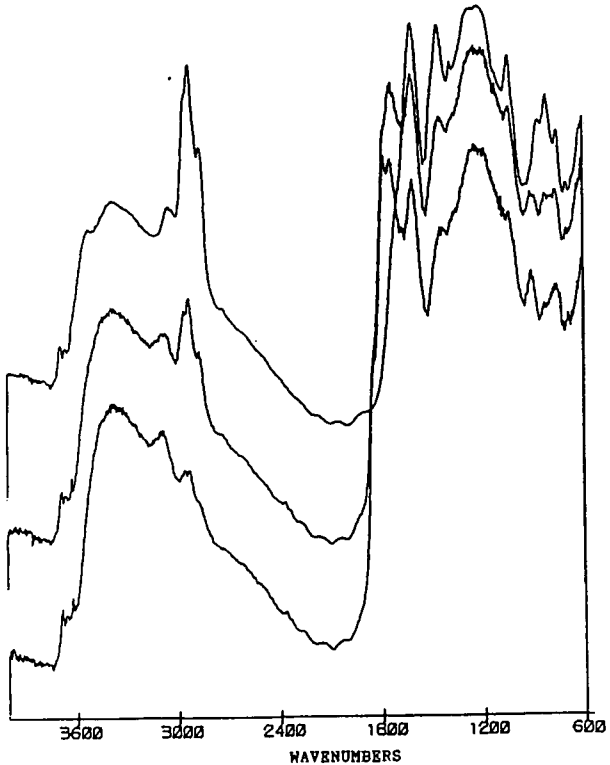

Figure 1. REPRESENTATIVE DRIFT SPECTRA FOR 200 C AIR OXIDATION OF WYODAK COAL POWDER. A. Original (unoxidized)material in vacuo, 200 C; B. 23 hours, 200 C, 100 cc/min; C. 129 hours, 200 C, 100 cc/min.

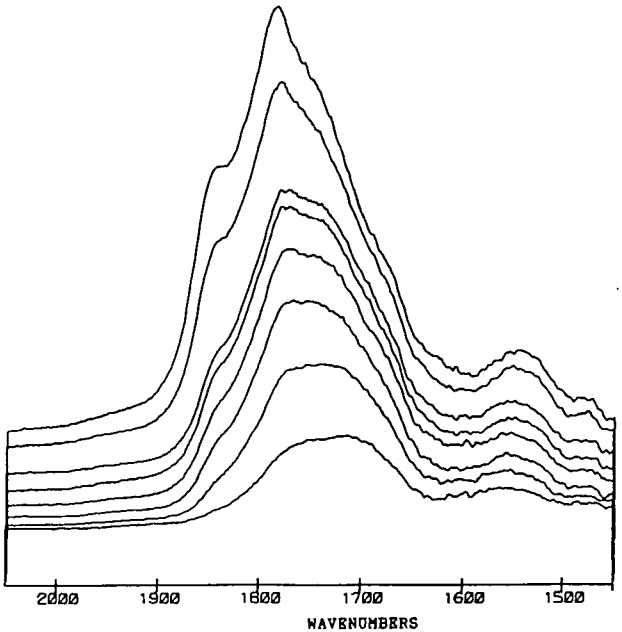

Figure 2. DRIFT DIFFERENCE SPECTRA FOR 200 C OXIDATION OF WYODAK POWDER. Successive spectra for 2, 4, 7, 10, 13, 23, 46, and 129 hours exposure (100 cc/min) isothermally in the beam of the spectrometer.

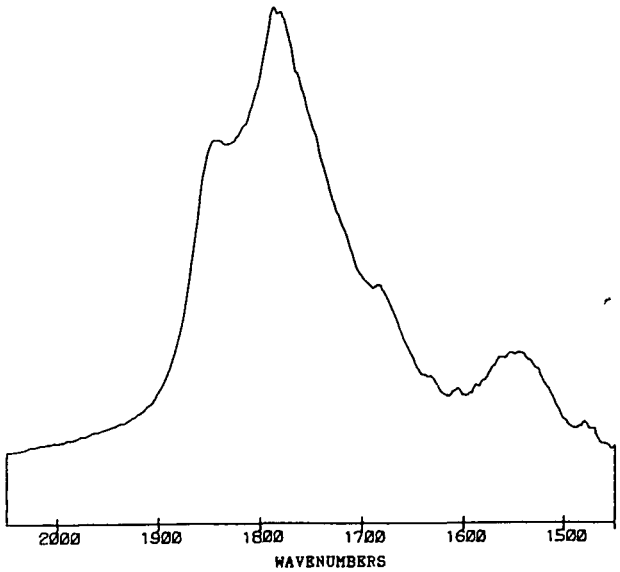

Figure 3. DRIFT DIFFERENCE SPECTRUM FOR 400 C IN SITU OXIDATION OF WYODAK. One hour isothermal exposure at 100 cc/min flow of air through reaction cell.

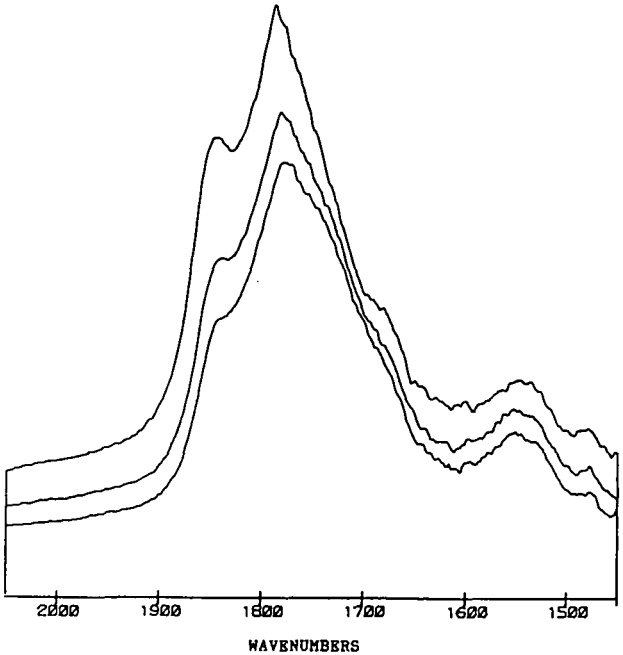

Figure 4. DRIFT DIFFERENCE SPECTRA FOR 300 C AIR OXIDATION OF WYODAK COAL POWDER. Spectra acquired after 1, 2, and 18 hours in situ exposure to 100 cc/min air flow.

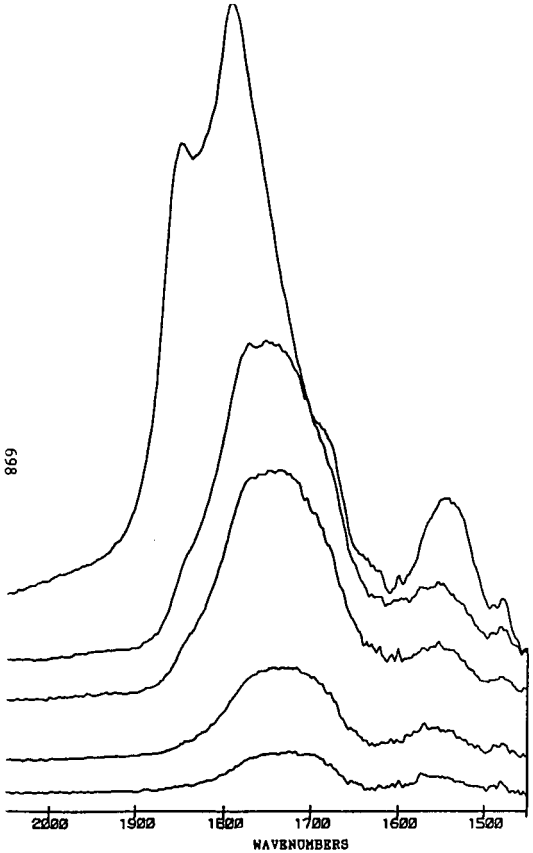

Figure 5. DRIFT DIFFERENCE SPECTRA FOR 125 C ISOTHERMAL OXIDATION OF WYODAK COAL POWDER AND SUBSEQUENT 400 C. Spectra acquired after 24, 48, 124, and 188 hours at 125 C where steady state conditions prevail. The uppermost curve was acquired after an additional 17 hours isothermal reaction at 400 C at the same 100 cc/min delivery of air reactant.

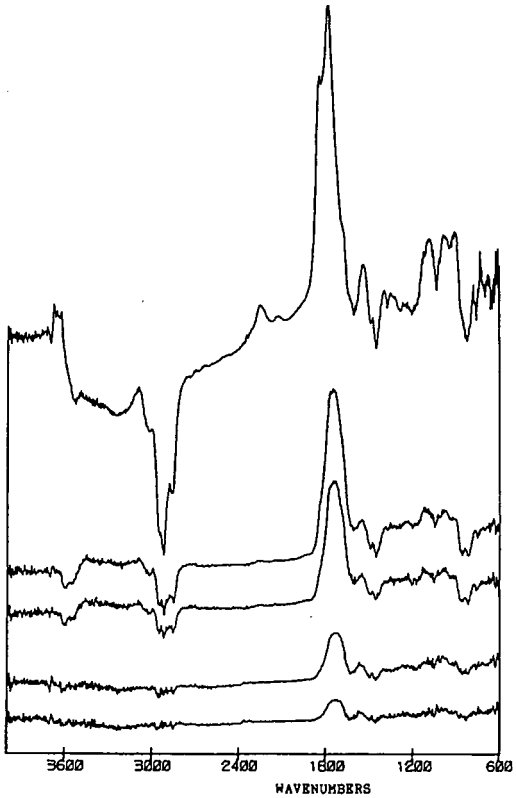

Figure 6. ENTIRE DRIFT DIFFERENCE SPECTRA FOR THE 125/400 C AIR OXIDATION OF WYODAK COAL POWDER. The relevant data are presented in Figure 5. Low temperature oxidation procaeds to the organo acid state and subaequent higher temperaturee are required to dehydrate to the acid anhydride atate as the precursor to carbon dioxide formation.

LOW-TEMPERATURE COAL WEATHERING

M. M. Wu, R. A. Winschel and G. A. Robbins

CONSOLIDATION COAL COMPANY
Research & Development
4000 Brownsville Road
Library, PA 15129

ABSTRACT

Illinois 6 coal (hvBb) was weathered for up to 330 days at 25 and 80°C with humid air. Its behavior was compared with Pittsburgh Seam (hvAb) and Horsepen Seam (mvb) coals weathered under the same conditions. The weathering rate showed a strong dependence on temperature and coal rank. At 25°C, the Illinois 6 coal showed much more substantial changes in chemical and physical properties upon weathering. Spectroscopic data indicate that the concentration of organic oxygen groups in the coal may eventually level off. Two potential causes of this behavior are proposed. Thermal (non-oxidative) treatment at 80°C has little effect on the chemical and physical properties of a fresh hvAb coal.

INTRODUCTION

Weathering can alter organic and mineral constituents of coal, change its chemical and physical properties and affect its utilization (1). Extensive laboratory research has been performed to study this important phenomenon. However, published studies have come to significantly different conclusions concerning the chemical nature of coal weathering (or oxidation). The rate of changes in coal properties induced by coal weathering or oxidation are dependent on temperature. Most reported coal weathering simulation experiments have been conducted at temperatures greater than 100°C to accelerate the oxidation rate. However, the reaction mechanism is reportedly different at temperatures above and below 70 to 80°C (2,3).

Three separate coal weathering reactions (two oxidative and one thermal) were recently proposed by Gethner (4,5) based on a coal oxidation study conducted at temperatures of 25 to 100°C. The rate of each reaction had a different temperature dependency. Gethner concluded, and we concur, that ill-defined or poorly controlled coal weathering or oxidation experiments can result in inaccurate conclusions (5). In addition to temperature, coal weathering is also known to depend on coal rank, humidity and oxygen partial pressure (1,3,6). The work reported here is a systematic study of coal weathering performed at realistic conditions. Different ranks of coal, including Illinois 6 (hvBb), Pittsburgh Seam (hvAb) and Horsepen Seam (mvb) coals, were weathered for up to 500 days at 25 to 80°C with humid air under well-controlled conditions. The work with Pittsburgh Seam and Horsepen Seam coals was reported previously (7). This paper includes the recent results of this study, most of which were obtained using the Illinois 6 coal. For present purposes, we will define oxidative weathering as the progressive changes in coal properties that occur as coal is exposed to humid air at temperatures of 80°C or less.

In addition to oxidative weathering, experiments were also performed with a different Pittsburgh Seam coal and a slightly weathered Illinois 6 coal under

flowing humid N_2 at 80°C. The objective of these tests was to observe any non-oxidative, thermal effects on coal properties and chemical structural changes. This paper also includes recent results of this study.

EXPERIMENTAL

The experimental apparatus and procedures used in the weathering study were described previously (7). The non-oxidative experiment was carried out using N_2 instead of air at otherwise the same conditions. The Illinois 6 coal used in this study is the natural -28 mesh portion of fresh run-of-mine (ROM) coal from a deep mine in Jefferson County, Illinois. The Pittsburgh Seam coal used in the non-oxidative weathering study is the natural -28 mesh portion of fresh ROM coal from a deep mine in Monongalia County, West Virginia. Analyses of these two coals are listed in Table 1. Properties of the Pittsburgh Seam and Horsepen Seam coals used in the oxidative study were reported elsewhere (7).

RESULTS AND DISCUSSION

OXIDATIVE WEATHERING

Changes in elemental composition (H,C,O) observed upon weathering occurred more rapidly for the Illinois 6 coal (hvBb) than for the Pittsburgh Seam (hvAb) and Horsepen Seam (mvb) coals, as shown below.

	Illinois 6		Pittsburgh Seam		Horsepen Seam	
Weathering Time at 80°C, Days	0	46	0	45	0	51
Carbon, wt % MAF	81.8	78.6	82.9	81.1	89.3	87.7
Hydrogen, wt % MAF	5.2	4.7	5.5	5.2	5.0	4.9
Oxygen, wt % MAF (diff.)	9.9	14.0	7.2	9.5	3.1	4.9

These values indicate that rates of change in elemental compositions with weathering time are dependent on coal rank (6).

The FTIR oxidation index is defined as the ratio of the integrated intensity of the carbonyl band (1635-1850 cm^{-1}) to that of the C-H stretching band (2745-3194 cm^{-1}) in the diffuse reflectance FTIR spectrum of coal (7,8). Increases in the oxidation index upon weathering can be attributed to the progressive oxidation of C-H groups to carbonyl groups as the coal weathers (8,9). The oxidation index is plotted in Figure 1 as a function of weathering time at 80°C for the three coals. The oxidation index of Illinois 6 coal not only increases more rapidly with weathering time, but it also has a higher initial value than Pittsburgh Seam and Horsepen Seam coals. This indicates that both the initial value and the rate of change with time of the oxidation index are rank dependent.

The rate of change with time of the oxidation index also depends on weathering temperature. In Figure 2, the oxidation index of Illinois 6 coal is plotted as functions of weathering time and temperature. Changes are rapid at 80°C, and slow, but experimentally significant, at 25°C. Significant changes in the oxidation index of coals weathered at 25°C were observable for the Illinois 6 coal but, as reported previously (7,10), not for the Pittsburgh Seam and Horsepen Seam coals.

Gieseler maximum fluidity was found to be one of the most sensitive indicators of oxidation for the higher rank coals (7,8). However, the lower rank Illinois 6 coal has essentially no fluidity, even when fresh. Though free swelling index (FSI) measurements are less sensitive to weathering than Gieseler fluidity, they do provide an indication of the effect of weathering on the thermoplastic properties (7,8). Figure 3 shows that the rate of change with weathering time of the free swelling index (FSI) of Illinois 6 coal is much greater at 80°C than at 25°C; however, even at 25°C, changes were significant. In contrast, there was very little change in the FSI of Pittsburgh Seam (7) and Horsepen Seam (10) coals weathered at 25°C. This again demonstrates the rank dependency of coal weathering. The FSI and oxidation index of weathered Illinois 6 coal are compared in Figure 4. Figure 4 shows that there is a general linear relationship between the oxidation index and FSI of Illinois 6 coal weathered at both 25 and 80°C, as also noted previously by Huffman et al. (9). The alkali extraction test (11) also shows a general linear relationship with oxidation index for the weathered Illinois 6 coal (Figure 5). Alkali extraction test results are expressed as percent transmittance at 520 nm.

As shown in Figure 1, the oxidation index of Illinois 6 coal weathered at 80°C appears to level off after about 46 days weathering. Results of X-ray photoelectron spectroscopic (XPS) characterizations of the coal weathered at 80°C are consistent with this observation. Table 2 lists the surface elemental compositions of the Illinois 6 coal weathered at 80°C for 0, 46 and 80 days. Organic oxygen was calculated by the method of Perry and Grint (12) in which inorganic oxygen is subtracted from total oxygen assuming inorganic oxygen is associated with Si and Al in oxide forms (12). The organic O/C ratio increased from 0.15 to 0.23 after 46 days weathering at 80°C (Table 2). As shown in Figure 6, an asymmetric C_{1s} peak with a shoulder at high binding energy (287-292 eV) was observed by XPS, indicating that carbon-oxygen functional groups were generated upon weathering for 46 days at 80°C. This is in agreement with FTIR results that show production of carbonyl groups. As weathering time increased from 46 to 80 days, only a slight increase in organic O/C ratio, from 0.23 to 0.24, was observed (Table 2). In addition, there was no significant change in XPS C_{1s} spectrum of the coal between 46 and 80 days (Figure 6).

There are at least two possible explanations for this observation. First, it may be that after 46 days at 80°C, most of the active sites originally available for oxidation had reacted, i.e., few active sites were available for further oxidation at these conditions. Painter et al. (13) reported that coal oxidation is indeed site selective. They concluded that benzylic sites are most easily oxidized to carbonyl groups. Low-temperature weathering work by Larsen et al. (2) supported this concept.

A second possibility is that after 46 days at 80°C, the rate of carbonyl production is matched by the rate of carbonyl destruction, e.g., by decarbonylation and decarboxylation. Gethner (4,5) noted the importance of decarbonylation and decarboxylation reactions during coal oxidation. The rate of carbonyl destruction must depend on the concentration of carbonyl groups. As oxidation proceeds, carbonyl concentrations increase and thus, the rate of carbonyl destruction should increase as well. Eventually, a state may be reached in which the rates of carbonyl production and destruction are equal.

At this point, our data do not confirm or refute either explanation. Additional work is under way to gain a better understanding of this.

NON-OXIDATIVE WEATHERING

A reaction mechanism involving thermal decomposition of carbon-oxygen functional groups (e.g., decarboxylation) was proposed by Gethner (4,5). He noted that this reaction was independent of the oxidative reactions that occur during low-temperature oxidation (4,5). Non-oxidative thermal effects on coal properties and chemical structural changes were examined by treating a Pittsburgh Seam coal under flowing humid nitrogen at 80°C for 48.4 days. No significant changes in elemental compositions were observed over the duration of the test. In addition, Gieseler maximum fluidity, Audibert-Arnu dilitation, FTIR oxidation index and alkali extraction measurements all show little or no change. The Gieseler maximum fluidity and the oxidation index of the Pittsburgh Seam coal treated at 80°C in flowing humid N_2 are plotted as functions of time in Figure 7. These data show that the changes in coal properties that were noted in the oxidative weathering tests with Pittsburgh Seam coal are dependent on the presence of oxygen. Purely thermal effects, except perhaps those involving newly formed oxidized components, were negligible. Since thermal (non-oxidative) effects may be rank dependent, a similar test is now being performed with a slightly weathered Illinois 6 coal.

REFERENCES

1. Cox, J. L. and Nelson, C. R., ACS Div. Fuel Chem. Prepr. 29 (1), 102 (1984).
2. Larsen, J. W., Lee, D., Schmidt, T. and Grint, A., Fuel, 65, 595 (1986).
3. Yohe, G., Illinois State Geological Survey, Report of Investigations, 207, 1958.
4. Gethner, J. S., Fuel, 66, 1091 (1987).
5. Gethner, J. S., Appl. Spectrosc., 4, 50 (1987).
6. Schmidt, L. D., Elder, J. L., David, J. D., Ind. Eng. Chem., 32, 548 (1940).
7. Wu, M. M., Robbins, G. A., Winschel, R. A. and Burke, F. P., Energy & Fuels, 2, 150 (1988).
8. Huffman, G. P., Huggins, F. E., Dunmyre, G. P., Pignoco, A. J., and Lin, M-C, Fuel, 64, 849 (1985).
9. Huggins, F. E., Huffman, G. P., Dunmyre, G. P. and Lin, M-C, Fuel Process. Technol., 15, 233 (1987).
10. Wu, M. M., Winschel, R. A. and Robbins, G. A., "Weathering Effects on the Thermoplastic and Froth Flotation Properties of Bituminous Coal", Presented at the 47th Ironmaking Conference, Toronto, Ontario, Canada, April 18, 1988.
11. Lowenhaupt, D. E. and Gray, R. J, Int. J. Coal Geol., 1, 63 (1983).
12. Perry, D. L. and Grint, A., Fuel, 62, 1024 (1983).
13. Rhoads, C. A., Senfthe, J. T., Coleman, M. M., David, A., and Painter, P. C., Fuel, 62, 1387 (1983).

TABLE 1

ANALYSES OF ILLINOIS 6 AND PITTSBURGH SEAM COALS

	Illinois 6	Pittsburgh Seam (a)
Moisture, wt % as received	2.76	0.64
Proximate Analysis, wt % dry basis		
Volatile Matter	35.74	37.24
Ash	5.30	12.07
Fixed Carbon (Diff)	58.96	50.69
Ultimate Analysis, wt % MAF basis		
Carbon	81.76	84.22
Hydrogen	5.23	5.74
Nitrogen	1.96	1.62
Sulfur, Total	1.19	3.54
Pyritic	0.51	1.97
Sulfate	0.03	0.05
Organic (Diff)	0.65	1.52
Oxygen (Diff)	9.86	4.88
Heating Value, Btu/lb, MAF basis	14,560	15,031
Wet Screen Analysis, wt % Tyler Mesh		
28 x 48 mesh	37.8	26.4
48 x 100 mesh	31.0	32.0
100 x 200 mesh	17.8	19.1
-200 mesh	13.4	22.5

(a) This coal used only in the non-oxidative test.

TABLE 2

FTIR OXIDATION INDEX AND SURFACE COMPOSITION BY XPS OF ILLINOIS 6 COAL WEATHERED AT 80°C

Weathering Time, Days	FTIR Oxidation Index	Atomic Percentage								Organic O/C Ratio
		C	O Total	O Organic	S	N	Na	Si	Al	
0	1.26	75.0	19.3	11.2	0.1	0.8	0.3	2.7	1.8	0.15
46	2.76	68.0	24.6	15.9	0.3	1.1	0.4	3.0	1.8	0.23
80	3.26	68.3	25.3	16.7	0.3	1.1	0.3	3.0	1.7	0.24

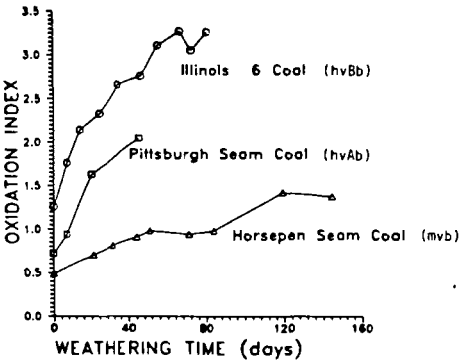

Figure 1. Oxidation Index vs Weathering Time for Coals Weathered at 80°C.

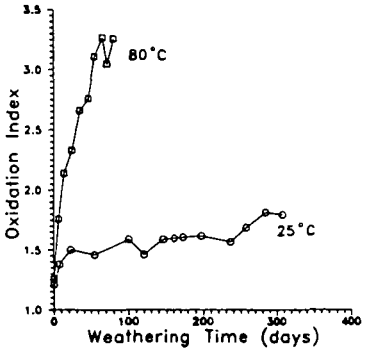

Figure 2. Oxidation Index of Ill. 6 Coal vs Weathering Time and Temperature.

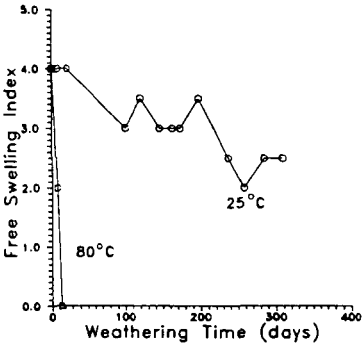

Figure 3. Free Swelling Index of Ill. 6 Coal vs Weathering Time and Temperature.

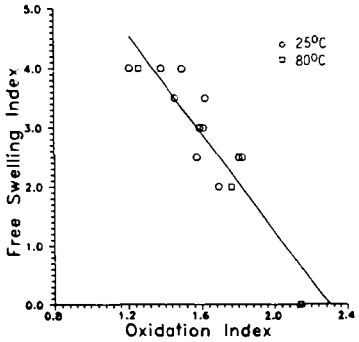

Figure 4. Free Swelling Index of Ill. 6 Coal vs Oxidation Index.

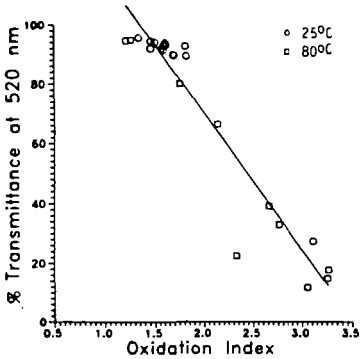

Figure 5. Alkali Extraction Test Results for Weathered Ill. 6 Coal vs Oxidation Index.

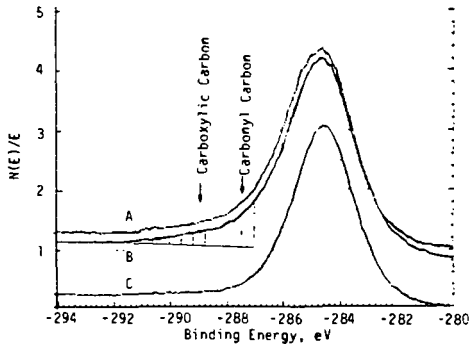

Figure 6. XPS C_{1s} Spectra of Ill. 6

A) Coal weathered at 80°C for 46 days.

B) Coal weathered at 80°C for 80 days.

C) Fresh Coal.

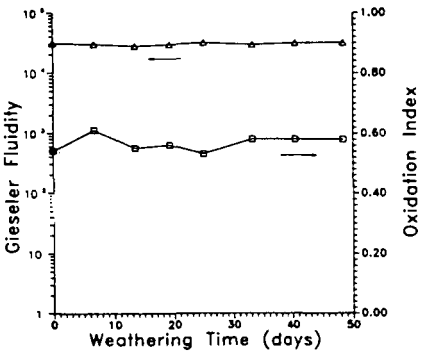

Figure 7. Gieseler Fluidity and Oxidative Index vs Time for Pittsburgh Seam Coal in the 80°C Non-Oxidative Weathering Test.

△ Gieseler Fluidity

□ Oxidation Index

Application of X-Ray Photoelectron Spectroscopy to Coal Oxidation Kinetics

S. R. Kelemen and H. Freund

Exxon Research & Engineering Company, Annandale, NJ 08801

Abstract

Several aspects of the oxidation kinetics of Illinois # 6 bituminous and Wyoming Powder River Basin subbituminous coal were quantified between 295 -398K. XPS was used to determine the changes in the amount of surface organic oxygen and provide an oxygen functional group distribution. GC analysis of the gas phase products and weight changes from TGA experiments were used to place the XPS results in the context of bulk oxidation. The oxidation of Illinois # 6 coal produced mostly solid oxidation products. The rate of increase exhibited Arrhenius behavior with an apparent activation energy of 11.4 kcal/mole. Oxidation of Wyoming Powder River Basin coal at 398K gave mainly gaseous products and a slightly faster total oxidation rate relative to Illinois #6 coal. The amount of oxidized organic sulfur determined by XPS can be used to evaluate the total extent of coal oxidation.

I. Introduction

Oxidation reactions of coal which occur in air near room temperature contribute to the self heating of coal and produce detrimental changes to many coal properties. Both solid and gaseous species are produced as oxidation products.(1) After oxidation many aspects of the solid coal have been investigated and several properties can be used to gauge the extent of oxidation. These include the determination of the changes in the amount of oxygen by difference, by neutron activation analysis(2) and by XPS analysis of the coal surface.(3,4) Relative changes in the properties of coal have also been used to measure oxidation. These include free swelling index,(5) Gieseler fluidity,(6,7) PH,(8) FTIR signatures(9) and changes in pyrolysis response.(10,11)

Despite the many available approaches it is very difficult to quantify the kinetics of low temperature oxidation, T < 350K. The total amount of solid oxidation products after several days near room temperature can be small.(12,13,23-25) There has been a greater number of oxidation studies performed at higher temperatures, T > 350K. The connection between high and low temperature oxidation reactivity is not well established and few have adopted a unified approach to characterize both solid and gaseous oxidation products.

We have quantified several aspects of the oxidation of Illinois # 6 coal and Powder River Basin coal between 295-398K. XPS was used to determine the changes in surface organic oxygen. GC analysis of gas phase products was carried out in conjunction with XPS measurements in order to provide a more complete description of the oxidation process. Thermal Gravimetric Analysis (TGA) results help place the XPS information in the context of bulk oxidation.

II. Experimental

Illinois # 6 coal and Powder River Basin coal were obtained from the Exxon Research and Engineering Company Baytown Texas coal sample library.[26] Upon receipt, the sealed consignment was transferred to a nitrogen drybox. 100-200 mesh cuts were prepared and stored in the drybox for later use.

XPS spectra were obtained with an ion pumped Vacuum Generators ESCALAB instrument using non-monochromatic MgKα radiation. The source was operated at 300W, 20ma, 15KV. A complete XPS analysis took approximately 4 hours. The coal samples were mounted to a metallic sample block by means of double-sided Scotch nonconducting tape. An energy correction was made due to sample charging based on the C(1S) peak at 284.8 (eV) and the unoxidized organic sulfur 2p peak at 164.0 (eV). Samples were introduced using the standard diffusion pumped VG ESCALAB fast entry air lock. As previously observed with other coal samples[3,4,27,28] the elemental composition of the sample remained nearly constant during the measurement period; however, longer-term exposure to the X-ray beam produced damage as evidenced by decreases in the initial amount of carboxyl carbon and by subsequent increased vulnerability to surface oxidation at ambient conditions. New samples were obtained for measurement at every point in the oxidation sequence.

Data acquisition and processing were by means of a VGS 2000 software package using multi-scan averaging. The spectra were obtained at 0.9 eV resolution. Elemental concentrations were obtained relative to carbon calculated from the areas of the XPS peaks corrected for atomic sensitivity. The sensitivity factors relative to C(1s) were determined from VG sensitivity tables and experimentally measured standards.

The organic composition of the starting coal derived from an XPS measurement was compared to a standard bulk determination. The comparison for Illinois #6 coal is shown in table I and for Powder River Basin coal in table II. Both coals have XPS derived organic nitrogen and organic sulfur values in very good agreement with bulk values. The amount of surface organic oxygen also compares favorably with bulk derived values. The amount of organic oxygen was derived from XPS results by taking into account inorganic contributions. The amount of oxygen associated with silicon and aluminum were taken as SiO_2 and $AlO_{1.5}$. With recognition of the surface oxidation of pyrite, the amount of oxygen associated with the inorganic sulfate (2p) signal was taken as SO_4. The difference between the pyrite iron (2p) signal and sulfate sulfur (2p) signal was associated with oxygen as $FeO_{1.5}$.

While there is little inorganic sulfur in Powder River Basin coal it is known from bulk analysis that nearly $^1/_3$ of the total sulfur in this Illinois # 6 coal exists as inorganic forms with the majority as pyrite. Table I also shows that there is a large discrepancy between the surface and bulk values of pyritic and sulfate sulfur for Illinois # 6 coal. The value for surface pyritic sulfur is based on the absence of the pyritic iron (2p) signal. These differences are most likely a result of the surface oxidation of pyrite. The XPS sulfur spectrum from I # 6 coal showed a sulfur 2p peak centered about 171.3 eV. This peak was substantially reduced by a brief water wash at room temperature. The broad peak is interpreted to arise from ferrous and ferric sulfates. The reactivity of coal following the water wash was

identical to the untreated coal. The sulfate peak and the associated iron (2p) signal is shifted by ~-1.5 eV to higher binding energy than the reported literature value.[29,30] This discrepancy is most likely due to a slightly enhanced sample charging of these inorganic components in our samples. We could not observe the iron (2p) signal due to iron pyrite.

We deconvoluted the sulfur (2p) spectrum using a single peak to represent the unresolved 2p spin doublet. We used a mixed Gaussian-Lorentzian line shape and a peak width at half maximum of 2.60 eV for each sulfur species. The organic part of the sulfur 2p spectrum showed two main peaks that occur at 164.0 eV and 168.3 eV. The 164.0 eV peak is characteristic of a variety of unoxidized organic species which includes thiophenes, sulfides and mercaptans. While oxidation to produce sulfoxides (166.0 eV)[31] and sulfonic acid (169.2 eV)[32] will contribute to the development of the main 168.3 eV sulphur (2p) peak, the dominant oxidation products appear as sulfones(168.0).[31-34]

XPS difference curves were made using the C(1s) lines whose areas were normalized to the value of the clean starting spectrum. The following methodology was used to deconvolute the positive peak in each carbon (1s) difference spectrum. We use a mixed Gaussian-Lorentzian line shape and a peak width of 1.80 eV at half maximum for each peak. Four peaks are used in the deconvolution that occur at 286.3 eV, 287.5 eV, 289.0 eV, and 285.2 eV. The 286.3 eV represents carbon bound to a single oxygen bond (i.e. ethers, hydroxyls, hydroperoxides), the 289.5 eV peak to carbon bound to two oxygen bonds (i.e. carbonyl) and the 289.0 eV peak to carbon bound to three oxygen bonds (i.e. carboxyl).[35-40] The intensity of the 285.2 eV peak is fixed to the 289.0 eV peak intensity and represents the carbon adjacent to carboxyl carbon and is referred to as a β peak.

Oxidation experiments for XPS kinetic studies were done in air with <25% relative humidity. Oxidation experiments with gas phase analysis were done in a quartz reactor contained within a furnace. The outlet of the dead-ended reactor was connected to a Bellows pump and a recirculation loop. A gas sample could be taken from the recirculation loop for GC analysis via an evacuated 2 cc gas sample valve. The gas chromatograph used for product analysis was a Hewlett Packard 5840 equipped with a thermal conductivity and a FID detector. The separation column was Porapack Q. Samples were introduced into the quartz reactor vessel and evacuated to $1x10^{-3}$ Torr. The sample size was 100 mg. The reactor volume was then pressurized to 200 kPa with helium. Prior to oxidation the fresh coal samples were heated at the appropriate reaction temperature in He for 18 hours; thereafter the amount of thermal decomposition products were negligible compared to those produced in oxidizing environments. The samples were evacuated to $1x10^{-3}$ Torr before being pressurized to 200 kPa with the reactant gas mixture which consisted of ~6.7% oxygen in Helium. Periodic evacuation and pressurization with new reactant gas was done in order to avoid the build-up of excessive amounts of products and to keep the reactant O_2 partial pressure nearly constant. The closed recirculation reactor arrangement enabled the build-up of products over

long times. The loss of the portion of product gas due to gas sampling was corrected in the product analysis. TGA experiments were done by flowing dry air in a Dupont model 951 thermogravimetric analyzer.

III. Results

We have monitored the increases in the amount of organic oxygen as a function of time and temperature. The results for Illinois # 6 coal are shown in Figures 1 and 2. The curve through the data points at each different temperature is based on a theoretical first order expression with a common asymptote corresponding to 0.085 maximum surface $^{O}/_{C}$ atom ratio increase, or in other words an increase of 8.5 oxygens per 100 carbons. An Arrhenius plot using the XPS derived rate information is shown in Figure 3. The line through the data corresponds to an activation energy of 11.4 kcal/mole and pre-exponential of 4.9×10^{6} $(^{O}/_{C})$ $(day)^{-1}$.

We have measured the corresponding changes in weight as a function of time up to 7 days at 398K. A comparison of these results with the XPS data is shown in figure 4. The same theoretical first order curve is used to fit the TGA data as the XPS data but with an asymptote of 5.0 wt.% $^{O}/C$ increase. The same expression provides an excellent fit to the TGA data.

We have measured the changes in gas composition which occur under similiar experimental conditions following oxidation for 2 days at 398K. Table III shows the changes in the number of gaseous molecules expressed relative to carbon. The Illinois # 6 coal contains 70.87 wt% carbon. With this information we have determined the wt% increase and oxygen atom ratio increase relative to carbon expected on the basis of GC data. We compare the results in Table IV to other experimental information. There is good agreement between the GC and TGA results for the wt% increase. IR analysis of the gas phase shows the presence of a small amount of CO. We did not quantify the weight loss due to CO evolution. The total hydrocarbon production is three orders of magnitude below the levels of CO_2 and H_2O and therefore was not considered. The increase in the surface oxygen concentration is 1.4 times greater than the bulk oxygen increase predicted from an oxygen balance using gas phase data. The fact that the surface enhancement is actually rather small and the similarity of the TGA and XPS kinetics imply that oxidation occurs throughout the bulk and that the surface oxidation process is a reflection of the bulk phenomenon.

The changes that occur in the XPS Carbon (1s) line shape can be related to the changes in the nature of the oxygen functional groups. The use of a difference spectrum facilitates the observation of the changes induced by oxidation. Examples of a C (1s) difference spectrum are found in figure 5 and were obtained after air oxidation of Illinois # 6 coal at 398K. The negative peak in each spectrum occurs near 284.7 eV. A decrease in intensity at this energy is indicative of a decrease in the amount of unoxidized carbon atoms. The presence of positive peaks at higher binding energies is associated with increases in the amount of oxygen functionalities. The fact that the positive going features are different in each spectrum indicates that the functional group distribution changes during the course of oxidation at 398K. Table V

shows the increases in the number of functional groups following oxidation. The information was obtained from the results of the deconvolution of the C (1s) spectrum, the deconvolution of the sulfur (2p) spectrum and the increase of total organic oxygen. Increases in the amount of oxygen associated with carbonyl and carboxyl types are obtained directly from the C (1s) difference spectrum. The amount of oxygen associated with sulfur species comes from the intensity increase in the sulfur (2p) sulfone peak. The amount of oxygen associated with groups bound to carbon by a single bond (i.e. ether, hydroxyl and hydroperoxides etc.) is obtained from the difference between the amount of total organic oxygen and the amount of oxygen associated with carboxyl, carbonyl, and oxidized sulfur.

After approximately 10 days at 398K, the oxygen concentration reaches a plateau. There are, however, changes that happen at longer oxidation times. We find that the carboxyl and oxidized organic sulfur concentration increases while that of the other types decline. Analysis of the gas phase changes, contained in table III, confirm that there is little change in the bulk oxygen to carbon ratio over the same period. The results also show that the Illinois coal continues to participate in oxidation reactions at long times; however, O_2 is consumed at a much slower rate. CO_2 and H_2O are the main gaseous oxidation products. While there are significant changes in the surface oxygen functional group distribution, the total amount of bulk organic oxygen remains nearly constant.

Following oxidation at 294K for 170 days we find that the majority of oxygen increase is associated with the formation of carboxyl structures. Oxidized surfaces produced at slightly higher temperatures and shorter times also show that increases in carboxyl oxygen is responsible for the majority of oxygen increase.

We have used XPS to monitor the changes in the amount of organic oxygen after oxidation of Powder River Basin coal between 294K and 398K, Figure 6. There is very little increase in oxygen concentration even after 170 days at 298K. There is also very little change in the oxygen functional group distribution. Higher temperature oxidation resulted in the build-up of surface products but at much lower levels than that previously observed with Illinois # 6 coal. The changes in surface oxygen concentration were not amenable to a simple kinetic description. The lines in Figure 6 represent a linear connection of data points.

Despite the small or negligible increases in total organic oxygen near room temperature, the relative increase in the amount of oxidized organic sulfur can be substantial. Figure 7 shows the sulfur 2p spectrum of fresh Powder River Basin coal and a spectrum following air oxidation at 295K. The 164 eV peak is due to unoxidized organic sulfur. A peak develops near 168 eV following oxidation and is attributed to the presence of oxidized organic sulfur.

Analysis of the changes in the gas phase composition, Table VI, show that the oxidation of Powder River Basin coal is dominated by gaseous products. These results also support the XPS finding that there are only slight changes in the amount of organic oxygen during the initial oxidation period at 398K.

Discussion

We have found that the oxidation of Illinois # 6 coal produces mainly solid oxidation products. A single kinetic expression was used to model the surface oxidation kinetics between 398K and 295K. TGA and GC gas phase analysis showed that the surface oxidation kinetics reflected bulk oxidation behavior.

Recent FTIR work on thin sections of Illinois # 6 coal indicated the presence of two kinetically distinct oxidative reaction sequences.[23-25] A slow oxidation process was extensively characterized at 393K but was difficult to measure below 343K.[23-25] A fast oxidation process was found to occur over two days at 295K but was complete after 30 minutes at 343K. This reaction is believed to result in a very small net decrease in the amount of organic oxygen. Both the fast and slow oxidation processes can contribute to the observed oxidation response of coal. We were unable to identify the fast oxidation process using XPS. This failure places an upper limit of 0.01 O/C change associated with this process. In another study[12] of Illinois # 6 coal, an increase of 2.4 oxygens per 100 carbons was observed after oxidation for 56 days under external ambient conditions. Nonalkylatable oxygen was the main product, presumably ether oxygen. In the present study near room temperature carboxyl was the main oxygen surface species.

The rate of increase of total oxidation products of Illinois # 6 coal exhibits Arrhenius behavior with an apparent activation energy of 11.4 kcal/mole. Non-isothermal studies[18] of bituminous and subbituminous oxidation, at a heating schedule of 5°C min^{-1}, demonstrate Arrhenius behavior for O_2 consumption above 413K. The apparent activation energy is between 10.0 and 13.2 kcal/mole. Lower temperature oxidation was characterized by much lower activation energies attributed to the influences of diffusion-controlled processes or to physical absorption.[18] A study[22] of subbituminous coal oxidation kinetics demonstrated Arrhenius behavior between 303K-343K with activation energies between 15 to 20 kcal/mole. Apparent global activation activation energies between 12.6 and 24.5 kcal/mole were found based on calorimetric data for a variety of coals of different rank.[46] The energies were determined from data obtained between 373K-423K so as to minimize contributions due to the heat of wetting.

It is generally believed that the oxidation of coal proceeds by way of a free radical oxidation mechanism.[12,14,16-18,21,23-25,41-45] E.S.R. work provides experimental evidence for the changes in free radical population during coal oxidation.[41,42] The variety of oxygen functionalities that we have observed can be accounted for within the framework of a free radical mechanism.[14,16,44,45] It is known that mineral oxidation reactions occur simultaneously with organic oxidation in coal.[6,29,47-53] The catalytic participation of inorganic components toward low temperature organic oxidation has been considered[52,53] but not confirmed. Low temperature inorganic reactions are generally regarded as separate processes. Nevertheless, the presence of inorganic matter complicates the interpretation of the oxidation kinetics based solely on gas phase oxygen uptake or heat release.

Most agree that a radical chain oxidation mechanism, involving decomposition of hydroperoxides, explains coal oxidation behavior at moderate temperatures. The dominant reactions that take place near room temperature are less certain. We find that our XPS results fit a single kinetic expression. The oxygen functional group distribution observed at 295K after long times is similiar to that found after shorter oxidation periods at 398K. We therefore conclude that under our experimental conditions the same basic chemistry occurs over the temperature range. Consideration of the errors associated with the XPS measurement enables us to place an upper limit of 0.01 $^{O}/_{C}$ surface increase that can be associated with faster oxidation processes.

The oxidation behavior of Illinois # 6 coal changes at long times at 398K. The surface and bulk oxygen concentration remains nearly constant but CO_2 and H_2O are still being produced. The total oxidation rate is much slower than the well defined kinetic process found at earlier times. The surface functional group distribution changes. The amount of oxidized organic sulfur continues to rise along with carboxyl oxygen, while other species decline.

We have made a limited study of Powder River Basin Coal. The initial oxidation at 398K gives mainly gaseous products. The total extent of oxidation after 2 days is 1.3 times that found with Illinois # 6 coal. We have monitored the changes in the surface composition at lower temperatures and find only small changes in the amount of organic oxygen. An earlier study indicated a high selectivity toward gaseous products for a low rank coal.[1] Previous work on this coal[13] at room temperature indicated that the change in bulk oxygen content was small. Chemical decarboxylation was offset by increases in the amount of nonalkylatable organic oxygen. Despite the small changes in total organic oxygen, we have found a substantial relative increase in the amount of oxidized organic sulfur.

Conclusions

1) A single kinetic expression can be used to describe the surface oxidation of Illinois # 6 coal from 398K to 295K.

2) The surface oxidation kinetics observed at 398K reflects bulk oxidation behavior. We were unable to identify any faster oxidation process for Illinos # 6 coal. This failure places an upper limit of 0.01 O/C on the amount of surface oxygen change that can be associated with faster oxidation processes.

3) A much slower oxidation process was identified at 398K after reacting Illinois # 6 coal for long times. The total surface oxygen concentration remains nearly constant but the oxygen functional group distribution shifts towards carboxyl and oxidized sulfur. CO_2 is the main gaseous product.

4) The initial oxidation of Powder River Basin coal at 398K produces mainly gas. The total oxidation after 2 days is 1.3 times greater than observed with Illinois # 6 coal.

5) There is a significant relative increase in the amount of oxidized organic sulfur during 295K oxidation of Powder River Basin coal. The total amount of organic oxygen remains almost constant.

References

1) P. D. Swann and D. G. Evans, Fuel 58 (1979) 276.

2) W. D. Ehmann, D. W. Koppenaal, C. E. Hamrin, Jr., W. C. Jones, M. N. Prasad and W. Z. Tian, Fuel 65 (1986) 1563.

3) D. T. Clark and R. Wilson, Fuel 62 (1983) 1034.

4) D. L. Perry and A. Gint, Fuel 62 (1983) 1029.

5) J. W. Larsen, D. Lee, T. Schmidt and A. Grint, Fuel 65 (1986) 595.

6) G. P. Huffman, F. E. Huggins, G. E. Dunmyre, A. J. Pignocco and M. Lin, Fuel 64 (1985) 849.

7) A. Grint and D. L. Perry, Proc. Int. Conf. Coal Sci. (1985) 879.

8) Y. Yun, B. Hoesterey, H. L. C. Meuzelaar and G. R. Hill. ACS Fuel Div. preprints 32 (1987) 302.

9) P. M. Fredericks and N. T. Moxon, Fuel 65 (1986) 1531.

10) B. S. Ignasiak, D. M. Clugston and D. S. Montgomery, Fuel 51 (1972) 76.

11) H. Iyuhara, R. Tanibata and S. Nishida, Proc. Inter. Conf. Coal Sci. (1985) 491.

12) R. Liotta, G. Brons, and J. Isaacs, Fuel 62 (1983) 781.

13) J. J. Isaacs and R. Liotta, J. Energy & Fuels 1 (1987) 349.

14) G. Alberts, L. Lenart and H. Oelert, Fuel 53 (1974) 47.

15) A. Y. Kam, A. N. Hixson and D. D. Perlmutter, Chem. Eng. Sci. 31 (1976) 815.

16) C. A. Rhoads, J. T. Senftle, M. M. Coleman and A. Davis, Fuel 62 (1983) 1387.

17) D. C. Cronauer, R. G. Ruberto, R. G. Jenkins, A. Davis, P. Painter, D. S. Hoover, M. E. Starsinic and D. Schlyer, Fuel 62 (1983) 1124.

18) D. C. Cronauer, R. G. Ruberto, R. S. Silver, R. G. Jenkins, I. M. K. Ismail and P. Schlyer, Fuel 62 (1983) 1116.

19) T. Handa, T. Nishimoto, M. Morita and J. Kodama, Fire Sci. Tech. 5 (1985) 21.

20) T. Nishimoto, M. Hosoya, J. Kodama, and M. Morita, Fire Sci.Tech. 5 (1985) 123.

21) W. S. Kalema and G. R. Gavalas, Fuel 66 (1987) 158.

22) M. Rahman, A. R. Hasan and D. N. Baria, Chem. Eng. Commun 46 (1986) 209.

23) J. S. Gethner, Fuel 64 (1985) 1443.

24) J. S. Gethner, Applied Spectroscopy 41 (1987) 50.

25) J. S. Gethner, Fuel 66 (1987) 1091.

26) R. C. Neavel, S. E. Smith, E. J. Hippo and R. N. Miller, Fuel 65 (1986) 312.

27) D. T. Clark, R. Wilson and J. M. Quirke, Chemical Geology 39 (1983) 215.

28) D. T. Clark, and R. Wilson, Org. Geochem. 6 (1984) 455.

29) A. N. Buckley and R. Woods, Applied Surf. Sci 27 (1987) 437.

30) Handbook of X-ray and Ultraviolet Photoelectron Spectroscopy (Heyden & Sons Ltd., 1978).

31) C. E. Mixan and J. B. Lambert, J. Org. Chem. 38 (1973) 1351.

32) D. T. Clark and H. S. Munro. Polymer Degradation and Stability 8 (1984) 213.

33) J. A. Gardella, Jr., S. A. Ferguson and R. L. Chin, Applied Spectroscopy 40 (1986) 224.

34) H. R. Thomas, Ph.D. Thesis, University of Durham, U.K. (1977) 144.

35) D. T. Clark and H. R. Thomas, J. Polym. Sci. & Polym. Chem. Ed. 14 (1976) 1671.

36) D. T. Clark, B. J. Cromarty and A. Dilks, J. Polym. Sci. Polym. Chem. Ed. 16(1978) 3173.

37) D. T. Clark and A. Harrison, J. Polym. Sci. Polym. Chem. Ed. 19 (1981).

38) D. T. Clark, Adv. Polym. Sci. 24 (1977) 125.

39) D. T. Clark, J. Polym. Sci. Polym. Chem. Ed. 16 (1978) 791.

40) D. T. Clark and A. Dilks, J. Polym. Sci. Polym. Chem. Ed. 17 (1979) 957.

41) S. W. Dack, M. D. Hobday, T. D. Smith and J. R. Pilbrow, Fuel 63 (1984) 39.

42) S. W. Dack, M. D. Hobday, T. D. Smith and J. R. Pilbrow, Fuel 62 (1983) 1510.

43) P. C. Painter, R. W. Snyder, D. E. Pearson and J. Kwong, Fuel 59 (1980) 282.

44) H. A. W. DeVries, C. Bokhoven and H. N. M. Dormans, Brennst. Chem. 50 (1969) 289.

45) E. A. C. Chamberlain, G. Barrass and J. T. Therlaway, Fuel 55 (1976) 217.

46) A. C. Smith and C. P. Lazzara, U.S. Bu. Mines RI 9079 (1987).

47) R. G. Herman, G. W. Simmons, D. A. Cole, V. Kumicz and K. Klier, Fuel 63 (1984) 673.

48) F. E. Huggins, G. P. Huffman and M. C. Lin, Int. J. Coal Geo. 3 (1983) 157.

49) D. C. Frost, W. R. Leeder, R. L. Tapping and B. Wallbank, Fuel 56 (1977) 277.

50) R. G. Wiese Jr., M. A. Powell and W. S. Fyfe, Chemical Geology 63 (1987) 29.

51) D. A. Cole, G. W. Simmons, R. G. Herman, K. Klier and I. Cyako-Nagy Fuel 66 (1987) 1240.

52) D. E. Pearson and J. Kwong, Fuel 58 (1979) 63.

53) F. E. Huggins, G. P. Huffman, D. A. Kosmack and D. E. Lowenhaupt J. Coal Geol. 1 (1980) 75.

Table I

Atom ratio relative to carbon x 100	I #6 coal Fresh XPS	I #6 coal Fresh Bulk Analysis	I #6 coal Water Wash XPS
Organic Sulfur	1.68	1.45	1.65
Sulfate Sulfur	1.19	0.02	0.32
Pyritic Sulfur	0.00	0.62	0.00
Organic Oxygen	10.3	9.9	11.6
Nitrogen	1.4	1.4	1.4

Table II

Atom ratio relative to carbon x 100	Powder River Basin Fresh XPS	Powder River Basin Fresh Bulk Analysis
Organic Sulfur	0.42	0.47
Sulfate Sulfur	0.03	0.027
Pyritic Sulfur	0.00	0.005
Organic Oxygen	19.3	20.1
Nitrogen	1.1	1.0

Table III

Changes in the gas composition after oxidation of Illinois #6 coal at 398K

Time	2 Days	13 Days	48 Days
O_2/carbon (x100)	-1.74	-5.48	-8.73
CO_2/carbon (x100)	0.33	1.68	4.46
H_2O/carbon (x100)	0.16	0.45	1.06
Change in Bulk oxygen/carbon (x100) based on GC data	2.7	7.1	6.9

Table IV

Comparison of the Changes found after oxidation of I #6 coal at 398K for 2 days

	Wt% Increase	Oxygen atom ratio increase relative to carbon x100
From GC Experiment	2.3	2.7
From TGA Experiment	2.7	---
From XPS Experiment	---	3.9

Table V

Amount of oxygen increase per 100 carbons Associated with Various Functional Types Following Air oxidation of Illinois #6 coal

Oxidation Temperature	Oxidation Time	Total Organic Oxygen increase	Carboxyl	Oxidized Sulfur	Carbonyl	Ether hydro-peroxide Alcohol
295K	170 days	3.8	2.1	0.3	0.7	0.7
398K	15 days	8.2	4.2	0.7	2.6	0.7
398K	41 days	8.1	4.9	1.0	1.4	0.8
398K	54 days	8.6	6.4	1.3	0.4	0.5

Table VI

Changes in the gas composition after oxidation of Powder River Basin coal at 398K

Time	2 Days	13 Days
O_2/carbon (x100)	-2.32	-6.33
CO_2/carbon (x100)	2.10	5.37
H_2O/carbon (x100	0.47	1.45
Change in bulk oxygen/carbon (x100) based on GC data	-0.03	0.47

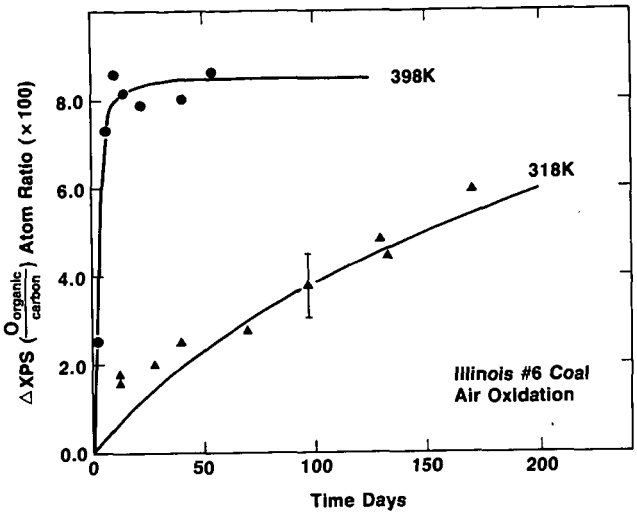

Figure 1. Change in the organic oxygen (1s) to carbon (1s) XPS atom ratio as a function of exposure time at 398K and 318K in air for Illinois # 6 coal

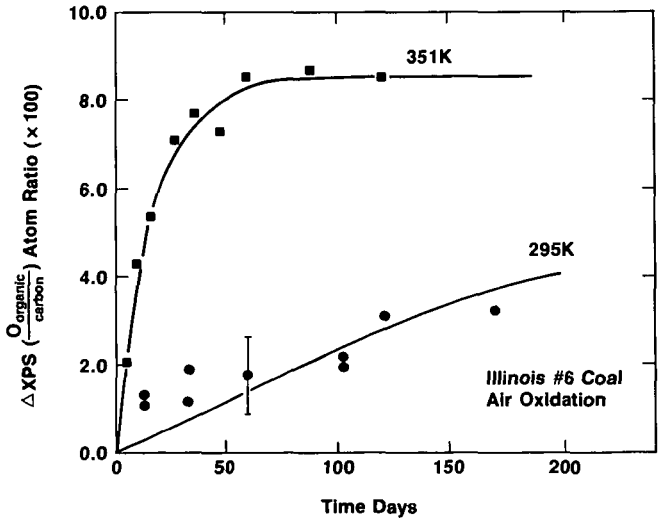

Figure 2. Change in the organic oxygen (1s) to carbon (1s) XPS atom ratio as a function of exposure time at 351K and 295K in air for Illinois # 6 coal

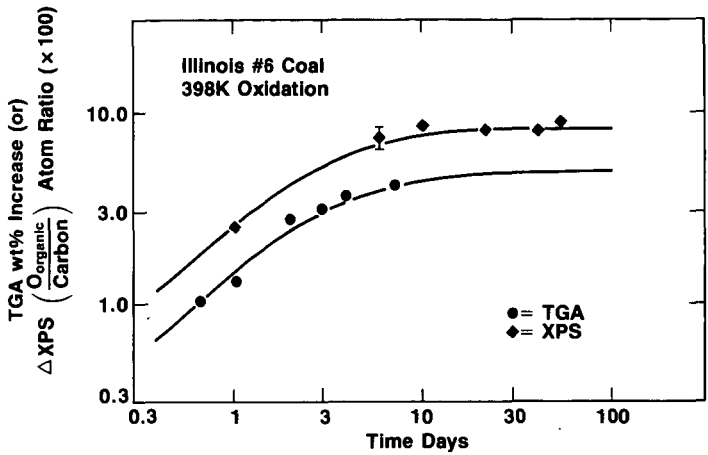

Figure 3. Comparison of the TGA wt% increase and the XPS oxygen (1s) to carbon (1s) atom ratio increase as a function time at 398K for Illinois # 6 coal

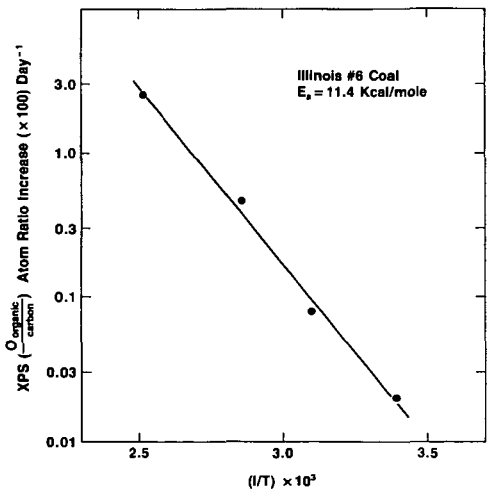

Figure 4. Arrhenius plot of the initial oxidation rate of Illinois # 6 coal based on the XPS data using a first order fit and common maximum $^{O}/_{C}$ increase of 0.085

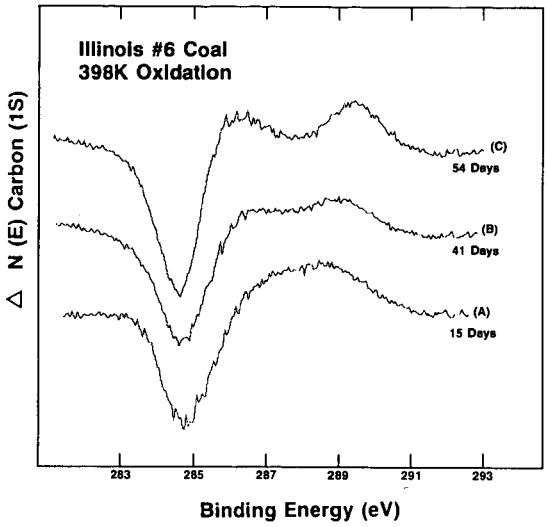

Figure 5. Change in the C (1s) spectrum following oxidation of Illinois # 6 coal for different times at 398K

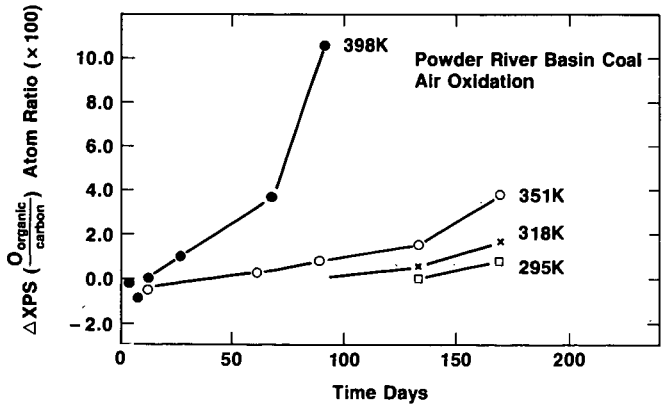

Figure 6. Changes in the Powder River Basin coal organic oxygen (1s) to carbon (1s) atom ratio as a function of exposure time in air at different temperatures.

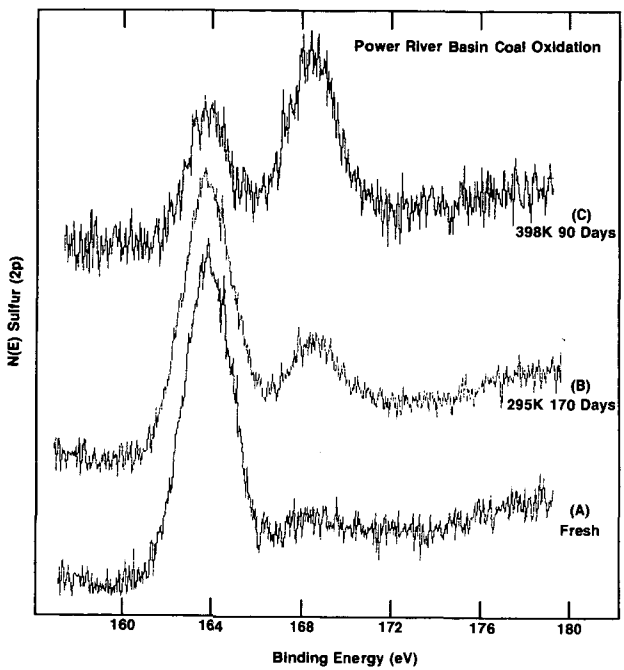

Figure 7. XPS sulfur (2P) spectrum from

A) fresh Powder River Basin coal
B) after oxidation for 170 days at 295K
C) after oxidation for 90 days at 398K

AN ESCA STUDY OF ALKALI-TREATED COAL SURFACES

J.P. Baltrus, J.R. Diehl, and J.R. D'Este
Pittsburgh Energy Technology Center, U.S. Department of Energy
P.O. Box 10940, Pittsburgh, Pennsylvania 15236-0940, U.S.A.

ABSTRACT

The surface interactions of alkali with coal and mineral matter have been studied by ESCA to establish a basis for predicting the relative reactivity of alkali with sulfur during coal beneficiation processes. The speciation of sulfur in several coals doped with various alkali salts was determined and quantified following heating of the samples to 375°C in air or N_2 and after washing them with water. Organic and pyritic sulfur react with the alkali cation when heated, after which the sulfide or oxidized sulfur product can be washed from the coal. The extent of reaction between the alkali salt and sulfur is governed by the size of the cation and the electronic properties of the anion; larger alkali cations are more reactive, as are anions with stronger nucleophilic properties.

INTRODUCTION

Over the years several processes employing alkali have been used for coal beneficiation (1). Presently the process for removing sulfur and ash from coal by treatment with molten caustics (MCL) is continuing to be developed as an alternative method for removing troublesome impurities from coal (1-4). Research has been conducted to determine the effects of process variables on the efficiency of the MCL system and to develop methods for analyzing and regenerating spent caustic (5-7). More fundamental studies have attempted to determine the mechanisms for interaction between the Na and K hydroxides and the components of coal, especially pyrite (8) and organosulfur (9,10).

This study focuses on the surface interactions of alkali with coal and mineral matter as studied by ESCA. Such interactions may be important in several processes in which coal and sulfur in coal are treated with alkali. Changes in the chemical state of the sulfur components of coal were monitored following deposition of various alkali hydroxides and sodium and potassium salts, and after subjecting the coals to various thermal treatments and washes.

EXPERIMENTAL

Preparation of Alkali-Doped Samples. A Pittsburgh No. 8 hvAb coal (2.2% pyrite, 0.4% sulfate, 1.6% organic sulfur) and Rasa lignite (Yugoslavia) (approximately 11% organic sulfur) were ground in air to minus 100 mesh. A 0.75-g sample of coal was mixed with 1 mL of an aqueous solution containing enough NaOH or KOH to produce the desired alkali concentration in the coal. The alkali-doped coals were placed in a ceramic boat and dried overnight at 60°C in a flow of N_2; coals were stored under air in a dessicator.

Four Pittsburgh No. 8 coal samples, the first containing 0.5% Na, the second containing 0.5% K, the third containing 0.25% Na and 0.25% K, and a fourth containing no added Na or K were analyzed after heating them to temperatures up to 375°C for one hour in flowing air or N_2.

A quantitative study of the effects of washing on sulfur removal was carried out on Na-doped and (Na + K)-doped Rasa lignite that had been heated at 375°C for one hour in air or N_2. The lignite samples were doped using the same procedure described above so that the final concentrations of alkali were approximately 5% Na and 5% Na plus 5% K, respectively. After heating, the samples were mixed with approximately 10% to 40% high-surface-area gamma alumina, which was used as an internal standard for monitoring changes in sulfur content during the wash procedure.

The Pittsburgh No. 8 coal was also doped with aqueous solutions of Na, K, Rb, and Cs hydroxides so that 0.75 g of coal contained 1.62×10^{-4} moles of one of the alkali metals. Another series of coal samples was impregnated with aqueous solutions of various Na and K salts (fluorides, chlorides, bromides, nitrates, acetates, and carbonates); the concentration of Na or K was 0.5% in each sample. All of the above samples were heated either in air or in nitrogen at 375°C for one hour.

Instrumentation. The coals were analyzed as powders mounted on double-sided sticky tape using a Leybold-Heraeus LHS-10 spectrometer. The magnesium anode was operated at 12 kV and 20 mA with the analysis chamber at a vacuum of 2×10^{-8} mbar or lower. The S 2p peaks were curve-fitted using the L-H DS-5 data system.

RESULTS AND DISCUSSION

Thermal Treatments. The S 2p region was curve-fitted with two peaks: one at 169.7 eV due to oxidized sulfur, $S_{(o)}$, most likely in the form of SO_4^{2-}; and another at 164.0 eV due to unoxidized sulfur, $S_{(u)}$ (organic sulfur, pyrite, and elemental sulfur) (11). Table 1 shows the results of the curve-fitting analyses of the S 2p spectra for the non-doped, Na-doped, K-doped, and (Na + K)-doped coals after heating to various temperatures in air. It can be seen that heating the coal to higher temperatures in air resulted in the conversion of an increasing percentage of $S_{(u)}$ to $S_{(o)}$ ($\%S_{(u)} = 100-S_{(o)}$); the amount of $S_{(o)}$ was always greater for the alkali-doped coals. Higher $S_{(o)}$ values for Na-doped coals compared to K-doped coals may be due to the somewhat greater Na concentration, on a molar basis.

To investigate the role of oxygen in the oxidation of alkali-doped coals, the coals were heated in a flow of N_2. Table 1 shows that little change in sulfur speciation occurred for the coal containing no alkali, in contrast to the decrease observed in the fraction of sulfur present as $S_{(o)}$ on heating the alkali-doped coals under N_2. Bulk ASTM analyses showed no decrease in sulfur content on heating. The form of sulfur in the latter coals was hypothesized based on the results of subsequent experiments.

The percentages of $S_{(o)}$ are higher for the mixed-alkali-doped coals heated in air when compared to either the Na- or K-doped coals (Table 1). The creation of a eutectic mixture of Na and K hydroxides may enhance their contact with sulfur and promote $S_{(o)}$ formation.

Quantitative Determination of Sulfur Removal. Experiments employing Rasa lignite, which has a high sulfur content (approximately 11% S) that is almost exclusively organic, and Na or (Na + K) hydroxide were carried out to determine whether the alkali hydroxides were reactive toward organic sulfur and how much of the reaction products could be removed from the lignite by washing. The

percentages of $S_{(o)}$ and $S_{(u)}$ in the lignite before and after washing, and the S 2p/Al 2s intensity ratios, are reported in Table 2. There was a small increase in the percentage of $S_{(o)}$ and a 22% decrease in the S 2p/Al 2s intensity ratio following washing for the Na-doped lignite heated in N_2. Therefore, heating of the Na-doped lignite in N_2, followed by washing, led to the removal, or conversion to $S_{(o)}$, of 34% of the total sulfur in the starting lignite. If one were to assume that all of the Na was converted to Na_2S upon heating the lignite in N_2, then 35% of the total sulfur in the lignite would have reacted. This would be in excellent agreement with the results obtained above if washing either oxidized the Na_2S to Na_2SO_4 or removed it from the lignite. Complimentary reductions in sulfur content were obtained for air-heated coal (Table 2) and by increasing the fraction of alkali in the coal.

Rasa lignite must be doped with either NaOH or KOH in order to observe oxidation of sulfur during heating, thereby indicating the importance of the alkali hydroxide for sulfur reactivity. In studies of MCL reactions of alkali with model organosulfur compounds, such as benzothiophene, have shown that nucleophilic attack by OH^- can lead to ring opening and formation of the Na or K salt of the organosulfur fragment (9,10). To systematically evaluate the effect of the alkali cation and its associated anion on the reactivity of sulfur in coal, two sets of experiments were performed. In the first experiment, a Pittsburgh No. 8 coal was doped with various Na and K salts and heated in air or N_2 at 375°C for 1 hour. Coals doped with Na and K salts and heated in N_2 showed no significant difference in the percentages of $S_{(o)}$ and $S_{(u)}$ ($\%S_o = 14.3 \pm 2.4$) because formation of an alkali sulfide renders the reacted sulfur indistinguishable by ESCA from unreacted organosulfur and pyrite.

An easier comparison of the relative reactivity of alkali cations and anions towards sulfur, most importantly organic sulfur, in coal is achieved by heating the coals in air where the product is the alkali sulfate. Table 3 shows that for coals doped with Na salts and heated in air, F^-, NO_3^-, and CO_3^{2-} were least effective for conversion of $S_{(u)}$ to $S_{(o)}$, while the acetate salt was the most reactive. For coals doped with K salts, F^-, Cl^-, and NO_3^- were least effective for $S_{(o)}$ formation compared to acetate, which was most reactive. It is interesting to note that less conversion of $S_{(u)}$ to $S_{(o)}$ occurs in the presence of the small and highly electrophilic (less nucleophilic) anions, F^- and Cl^- (when associated with K) than in the presence of larger and less electrophilic Br^- and acetate anions. Studies of MCL employing model organosulfur compounds have shown that nucleophilic attack of the aromatic sulfur-containing ring is an important step in sulfur elimination (9,10). Therefore, while reactions between Br^- or acetate anions and the sulfur-containing moieties of coal may be sterically hindered, the stronger nucleophilic properties of these anions may play an important role in the overall reaction that leads to sulfur oxidation.

The effects of alkali cation size on the reactivity of the sulfur-containing components of coal can be seen in Table 4, which shows that as the size of the cation increases ($Na^+ \rightarrow Cs^+$), the conversion of $S_{(u)}$ to $S_{(o)}$ for coal heated in air also increases. The extent of reaction of model organosulfur compounds under MCL conditions has been found to increase with cation size (9,10,12). The earlier studies proposed that the increased size of the cation may help to stabilize a reaction intermediate prior to sulfur elimination, thereby promoting the overall reaction.

CONCLUSIONS

These experiments have shown that removal of sulfur from coal may be accomplished by doping with alkali hydroxides followed by heating to moderate temperatures and washing. The types of alkali salts used for treating coal surfaces are important in determining the nature and extent of sulfur reactivity.

ACKNOWLEDGMENTS AND DISCLAIMER

The authors thank Bruce Utz and Yael Miron for helpful discussions. Reference in this report to any specific commercial product, process, or service is to facilitate understanding and does not necessarily imply its endorsement or favoring by the U.S. Department of Energy.

REFERENCES

1. Wheelock, T.D.; Markuszewski, R. In "The Science and Technology of Coal and Coal Utilization"; Cooper, B.R., Ellington, W.A., Eds.; Plenum Press: New York, 1984; pp. 47-123.

2. Masciantonio, P.X., Fuel, 44, 269-275 (1965).

3. TRW Energy Development Group "Gravimelt Process Development," Final Report, DOE/PC/42295-T7 (DE84013743), June 1983.

4. Meyers, R.A.; Jones, J.F.; McClanathan, L.C., TRW Applied Technology Division, "MCL System Integration Project," Presented at Coal Utilization and Environmental Control Contractors' Review Meeting, Pittsburgh, PA, July 1987.

5. Markuszewski, R.; Mroch, D.R.; Norton, G.A.; Straszheim, W.E.; Am. Chem. Soc. Div. Fuel Chem. Prepr. Pap., 30, 41-48 (1985).

6. Criswell, C.D.; Mroch, D.R.; Markuszewski, R., Anal. Chem., 58, 319-21 (1986).

7. Markuszewski, R., "Chemistry of Caustic Regeneration in Chemical Coal Cleaning," Presented at Coal Utilization and Environmental Control Contractors' Review Meeting, Pittsburgh, PA, July 1987.

8. Chiotti, P.; Markuszewski, R., Ind. Eng. Chem., Process Des. Dev., 24, 1137-1140 (1985).

9. Utz, B.R.; Friedman, S.; Sobaczenski, S.K., in: Fossil Fuel Utilization, R. Markuszewski and B.D. Blaustein (Eds.), Am. Chem. Soc., Washington, DC, 1986, pp. 51-61.

10. Friedman, S.; Utz, B.R.; Nowak, M.A.; Fauth, D.J.; Schmidt, C.E., Proc.-Int. Conf. Coal Sci., 1987, 435-438.

11. Wagner, C.D., "Handbook of X-Ray Photoelectron Spectroscopy," Perkin-Elmer Corporation, Eden Prairie, MN, 1979.

12. Wallace, T.J.; Hofmann, J.F.; Schriesheim, A., J. Am. Chem. Soc., 85, 2739 (1963).

Table 1. Percentages of $S_{(o)}$ as Determined by ESCA for a Pittsburgh No. 8 Coal Heated for 1 Hour at Various Temperatures.

Temperature	Non-Doped Coal	Na-Doped Coal	K-Doped Coal	(Na + K)-Doped Coal
Not Heated	30.7	37.5	32.6	45.8
100°C[a]	33.6	36.8	37.5	49.2
150°C[a]	38.0	43.1	43.1	57.2
250°C[a]	46.7	71.4	60.9	81.0
350°C[a]	58.6	82.7	77.0	84.5
375°C[a]	67.4	87.2	80.6	88.2
375°C[b]	31.5	14.6	15.9	23.5

[a]Heated in air.
[b]Heated in N_2.

Table 2. Percentages of $S_{(o)}$ and $S_{(u)}$ and S 2p/Al 2s Intensity Ratios as Determined by ESCA for a Heated-Treated[a] Rasa Lignite Before and After Washing.

	Heated In Air			Heated In N_2		
	$S_{(o)}$	$S_{(u)}$	S 2p/Al 2S	$\%S_{(o)}$	$\%S_{(u)}$	S 2p/Al 2S
Na-Doped (5% Na)						
Before Washing	57.2	42.8	0.796[b]	8.6	91.4	1.40[c]
After Washing	15.5	84.5	0.584[b]	16.0	84.0	1.09[c]

[a]Heated at 375°C for 1 hour.
[b]Mixed with approximately 20% Al_2O_3.
[c]Mixed with approximately 10% Al_2O_3.

Table 3. Percentages of $S_{(o)}$ and $S_{(u)}$ as Determined by ESCA for Air-Heated,[a], Alkali-Doped Pittsburgh No. 8 Coal.

Anion	Na^+ Cation		K^+ Cation	
	%$S_{(o)}$	%$S_{(u)}$	%$S_{(o)}$	%$S_{(u)}$
OH^-	87.2	12.8	80.6	19.4
F^-	76.7	23.3	71.0	29.0
Cl^-	85.3	14.7	74.4	25.6
Br^-	88.2	11.8	82.7	17.3
NO_3^-	80.1	19.9	77.5	22.5
$(C_2H_3O_2)^-$	94.9	5.1	89.9	10.1
CO_3^{2-}	81.1	18.9	78.9	21.1

[a]Heated at 375°C for 1 hour.

Table 4. Percentages of $S_{(o)}$ and $S_{(u)}$ as Determined by ESCA for Heat-Treated,[a], Alkali-Doped Pittsburgh No. 8 Coal.

Cation	Heated In Air		Heated In N_2	
	%$S_{(o)}$	%$S_{(u)}$	%$S_{(o)}$	%$S_{(u)}$
None	67.4	32.6	31.5	68.5
Na^+	87.2	12.8	14.6	85.4
K^+	87.2	12.8	15.9	84.1
Rb^+	91.4	8.6	26.4	73.6
Cs^+	100.0	0.0	22.4	77.6

[a]Heated at 375°C for 1 hour.

FTIR EXTERNAL REFLECTION STUDY OF SURFACE LAYERS ON COAL

J. A. Mielczarski, J. L. Yordan and R. H. Yoon

Department of Mining and Minerals Engineering
Virginia Polytechnic Institute and State University
Blacksburg, Virginia 24061

ABSTRACT

An infrared reflection-absorption spectroscopy (IRAS) technique has been developed to study the structure of adsorbed surfactant layers on coal. Owing to the optical properties of coal, negative as well as positive absorption bands are observed in the recorded spectra which depend on the angle of incidence (θ) and the polarization of the incident radiation. Theoretical calculations make it possible to predict the changes in absorbance with θ and polarization. These changes are a function of the optical properties of the coal and the adsorption layer. The application of the IRAS method to studies of the adsorption layer is presented for several systems, i.e., adsorption of sodium laurate and a nonionic surfactant on coal. In addition, the oxidation layer produced during low-temperature oxidation of coal has been investigated. The results obtained indicate that the IRAS method has an enormous potential for use in determining the structure of an adsorption layer on coal after different treatments.

INTRODUCTION

Systematic studies of coal structure have been carried out in recent years. Since coal is a mixture of various organic and inorganic compounds which are non-crystalline and mostly insoluble, the standard analytical methods of structural determination are of little use. Thus, spectroscopic techniques such as transmission infrared (1,2) and NMR (3,4) are usually applied to characterize the structure of coal and its derivative products.

In most coal cleaning processes, such as froth flotation, the coal surface properties play an important role. Diffuse reflectance (DR) (5,6) and attenuated total reflection (ATR) (7,8) in infrared, and x-ray photoelectron spectroscopy (XPS) (9) are very surface-sensitive techniques and, hence, have been used to study the coal surface. Nevertheless, the study of the surface structure of coal is very difficult because the recorded spectra are the summation of the spectra of heterogeneous bulk coal and those of the surface layers.

In the present paper, the structure of surface layers on coal has been studied using the infrared reflection-absorption spectroscopy (IRAS) technique. To date most of the IRAS studies have been done to study metals surfaces (10-13) which strongly reflect the incident beam. Coal, on the other hand, shows low reflectivity relative to metals, and interpretation of the recorded spectra in terms of an oriented surface structure is more complicated. However, the theoretical analysis presented in this paper makes it possible to predict the changes in the absorbance of polarized light, which makes it easier to interpret the recorded spectra. Moreover, as shown in this work, the IRAS method provides a means of distinguishing the spectrum of the thin surface layer from that of the substrate, and provides a means of examining the flat surface of a large coal slab directly after treatment.

EXPERIMENTAL

Preparation of Thin Layer

Coal slabs 10x30 mm in size were cut by means of a diamond wheel using water as the cooling medium. The coal sample was from a Pittsburgh seam in West Virginia. Each specimen was wet-polished with emery paper (No. 600 and 1200) and washed in water in an ultrasonic bath.

For the study of adsorbed layers, the samples were immersed into 100 ml of $2x10^{-4}$ M solution of nonylphenolpolyethyleneglycol ether with a pH of 7.2 $\pm$ 0.2 for 5 minutes or 12 hours, and for 1 hour in 100 ml of 10^{-3} M sodium laurate with a pH of 6.0 $\pm$ 0.2. After adsorption, the samples were removed from solution, dryed at room temperature and placed into the FTIR spectrometer to record the spectra.

Low-temperature oxidation of the coal specimens was carried out at 125°C in air for a period of 24 hours. The oxidized sample was examined spectrometrically and then treated with barium hydroxide (0.05 M) to change the surface carboxyl groups to ionic form. The spectrum of the sample was recorded again after this treatment.

The reagents used were nonylphenolpolyethyleneglycol ether (Tergitol NP-9), a nonionic surfactant obtained from Union Carbide Corporation, with an average of 9 ethylene glycol groups per molecule. The sodium laurate was obtained from Pfaltz and Bauer, Inc. Both reagents were used as received with no further purification. Double distilled water produced in an all-glass still was used in all the experiments.

Measurement

The infrared spectra were recorded on a Perkin-Elmer Model 1710 FTIR spectrometer with an MCT detector using an external reflection attachment (Spectra Tech, Inc) with a single reflection. A wire grid polarizer (Harrick Scientific Company) was placed before the sample and provided polarization selection. The spectra were taken at 4 cm^{-1} resolution by co-adding 64 scans in the 4000-500 cm^{-1} region. The unit of intensity is given in terms of $-\log(R/R_o)$, where R and R_o are the reflectivities of the samples after different treatment and freshly exposed coal, respectively. The transmission spectra of lauric acid and coal in KBr pellets, and chloroform solution of Tergitol NP-9 were prepared and measured in the standard way.

Calculation of Reflection-Absorbance

Figure 1 shows a model of the three-phase system investigated and the interaction of an electromagnetic wave with the system. The optical properties of each phase are characterized by the complex refractive index $\hat{n}_j = n_j + ik_j$, where n_j is the real refractive index and k_j is the absorption constant. The thin film has a thickness, d_2.

The theoretical calculation of the intensity of an absorption band in the reflection spectra is described in several papers (14-17). In this paper, a recently reported (17) theoretical analysis was used. The calculation was made for the following data: for ambient (air) $n_1 = 1.0$ and $k_1 = 0$; for the adsorption layer of lauric acid, $n_2 = 1.5$ and $k_2' = 0.3$ at 1705 cm^{-1}; and for the adsorption layer of a nonionic surfactant, $n_2 = 1.5$ and $k_2'' = 0.38$ at 1103 cm^{-1}. The thickness of the adsorbed monolayer was assumed to be $5x10^{-9}$ m.

The optical constants of coal were calculated to be $n_3 = 2.05$ and $k_3 = 0.02$ at 1800 cm^{-1}. These latter data were obtained on the basis of transmission spectra of KBr pellets of coal and measurements of the ratio of reflectivities of p- and s-polarization at different angles of incidence. These particular optical data for the three phases are only approximations of the real values and were chosen to simulate the optical properties of adsorption layers on coal.

RESULTS AND DISCUSSION

Adsorption of Nonylphenolpolyethyleneglycol Ether on Coal

The infrared transmission spectra of the coal and nonionic surfactant used in this study are shown in Figures 2 and 3, respectively. Figure 4 shows the reflection spectra of the thin surface film of Tergitol NP-9 on the coal after 12 hours of treatment time in a $2x10^{-4}$ M solution. Since the absorbance was measured in terms of $-\log(R/R_o)$, any spectrum recorded showed the effect of the treatment. It should also be noted that no spectrum is recorded after only 5 minutes of treatment, indicating slow adsorption kinetics. It is shown that the intensity of the absorption bands vary with the polarization and the angle of incidence. The negative absorption bands observed in the recorded spectra are not unique for the system studied in the present work. Others were theoretically predicted (14,18) for low-absorption substrates and observed experimentally for water (16) and cuprous sulfide (17) substrates.

In order to explain the changes in IRAS spectra observed, theoretical calculation of the absorbance for the system has been carried out, and the results are shown in Figure 5. The solid lines represent the changes of absorbance (A) at 1100 cm^{-1}, as a function of the angle of incidence for both s-polarization ($A_\perp$) and p-polarization ($A_\parallel$). This calculation was performed for an isotropic layer of the nonionic surfactant. The experimental points obtained after 12 hours of adsorption from the $2x10^{-4}$M solution are shown as circles and crosses for s- and p-polarization, respectively. In general, a reasonable agreement between the experimental results and the theoretically predicted values is observed. For s-polarization, negative absorption bands are predicted and, in fact, only negative bands are observed. For s-polarization which has electric field components which are only parallel to the interface plane (Figure 1), only those molecular groups that have transition moment components parallel to the substrate surface can interact with the incidence radiation, allowing absorption to be observed. The difference between the relative intensity ratios of the observed bands in IRAS (Figure 4, s-polarization) and transmission spectra (Figure 3) indicates that adsorbed molecules are oriented on the surface of coal.

The same conclusion can be obtained from the spectroscopic results for p-polarization. An intense absorption band is observed at 1103 cm^{-1} for p-polarization and at an 80-degree angle of incidence, while the calculated values of absorbance, A , under these conditions is close to zero (Figure 5). This discrepancy can be explained by consideration of the two components, $E_{\parallel x}$ and $E_{\parallel z}$, of p-polarization of the incident beam (Figure 1). The theoretical calculation of the $A_{\parallel x}$ and $A_{\parallel z}$ components has been done in the same way as reported recently (17), and the results are shown in Figure 5 as dashed lines. According to this calculation, an intense positive absorption band should be obtained at an angle of incidence of 80 degrees for molecular groups which have transition moments parallel to the surface of the substrate. Since the absorption band at 1103 cm^{-1} can be assigned to (C-O-C) stretching, the presence of this intense absorption band in the recorded spectra indicate that the polyethylene glycol part of the adsorbed molecule is positioned parallel

to the surface of the coal. However, the nonylphenol unit of the adsorbed molecule is inclined to the plane of substrate.

Thin Layer of Lauric Acid on Coal

The adsorption was performed from 10^{-3} M solution of sodium laurate at pH 6.0 $\pm$ 0.2. Under these conditions, the reagent exists in solution as lauric acid (pK=4.7). It was found that a significant part of surfactant was deposited on the coal surface from a thin film of solution during drying of the sample.

The reflection spectra of the thin film of lauric acid on coal are shown in Figure 6. Theoretical calculations performed for the coal-lauric acid system (Figure 7) allow an explanation of the results obtained in a similar way as was discussed for the non-ionic surfactant. Generally good agreement is observed between the experimental data and the theoretical analysis. This agreement also suggests that the lauric acid molecules in the thin layer on the surface of coal are randomly oriented. Data presented in Figure 7 was calculated for a thin layer of 50 Å. Since the experimental intensities for the absorption bands are nearly 5 times higher than those calculated, the thickness of the lauric acid could be considered to be as thick as 250 Å. The real thickness of the lauric acid layer is probably much thinner. Various reasons for the discrepancy between real and theoretically calculated values have been discussed recently (17).

Low-Temperature Oxidation of Coal

During the oxidation, the following changes in the reflection spectra (Figure 8) are observed: the bands at 1700, 1555 and 1180 cm^{-1} appear and the intensity of the band at 1440 cm^{-1} decreases. These results indicate that the oxidation products, such as carbonyl and carboxyl groups (band at 1700 cm^{-1}), ionized $-COO^-$ groups (band at 1550 cm^{-1}) and C-O groups in ether, alcohol or phenyl (band at 1180 cm^{-1}), are formed while the aliphatic groups (band at 1440 cm^{-1}) present in the coal are oxidized.

The band at 1700 cm^{-1} is markedly distorted due to the anomalous dispersion of the refractive index of the oxidation products. Notably, band shape distortion when using the reflection method has also been reported (19).

For p-polarization at a 70-degree angle of incidence, positive absorption bands in the spectrum are observed. However, for the other measurement conditions, i.e., different angles and polarization, only negative absorbances are recorded (Figure 8). Hence, for oxidized coal samples, the negative and positive absorption bands appeared at the same angle of incidence and polarization as was found for the adsorption layer from solution (Figures 4 and 6).

The barium hydroxide-treated oxidized coal sample shows intense absorption bands at 1550 and 1400 cm^{-1} (Figure 9). These bands can be assigned to asymmetric and symmetric stretching vibrations of the COO group, respectively. A notably strong increase in the intensities of these bands is due to the change of the -COOH groups to the ionized $-COO^-$ form.

A significant increase in the intensity of the band at 1555 cm^{-1} after oxidation (Figure 8) relative to the band at 1440 cm^{-1} could indicate that the ionic groups $-COO^-$ which are formed during the oxidation process are oriented with both of the oxygen atoms oriented toward the ambient (air).

CONCLUSIONS

The infrared reflection-absorption spectroscopy (IRAS) method has been developed for characterizing the surface layer on coal. The absorbance is shown to be a function of the optical properties of the coal and the surface layer, as well as of the angle of incidence and the polarization of the incident beam.

The results obtained show that the IRAS method makes it possible to determine both the chemical nature and the structure of the adsorbed layers on the coal substrate.

REFERENCES

1. Painter, P. C., Starsinic, M. and Coleman, M. M., 1985. in Fourier Transform Infrared Spectroscopy, Vol. 4 (J. R. Ferraro and L. J. Basile, Eds,), Academic Press, New York, p. 169 and references therein.
2. Gethner, J. S., 1987. Appl. Spectrosc., 41:50.
3. Fredericks, P. M., Warbrooke, P. and Wilson, M. A., 1983. Org. Geochem., 5:89.
4. Painter, P. C., Kuchn, D. W., Starsinic, M., Davis, A., Havens, J. R. and Koenig, J. L., 1983. Fuel, 62:103.
5. Fuller, M. P., Hamadeh, I. M., Griffits, P. R. and Lowenhaupt, D. E., 1982. Fuel, 61:529.
6. Smyrl, N. R. and Fuller, E. L., 1987. Appl. Spectrosc., 41:1023.
7. Mielczarski, J. A., Denca, A. and Strojek, J. W., 1986. Appl. Spectrosc., 40:998.
8. Bubnowskaia, L. M., Popov, W. K. and Rusianova, 1982. Koks i chimia, 5:9.
9. Perry, D. L. and Grint, A., 1983. Fuel, 62:1024.
10. Golden, W. G., 1985. in Fourier Transform Infrared Spectroscopy, Vol. 4 (J. R. Ferraro and L. J. Basile, Eds,), Academic Press, New York, Chapter 8.
11. Swalen, J. D. and Rubolt, J. F., 1985. in Fourier Transform Infrared Spectroscopy, Vol. 4 (J. R. Ferraro and L. J. Basile, Eds,), Academic Press, New York, Chapter 7.
12. Mielczarski, J. A. and Leppinen, J., 1987. Surface Science, 187:526.
13. Liedberg, B., Carlsson, C. and Lundstrom, I. J., 1987. Coll. Inter. Science, 120:64.
14. McIntyre, J. D. E., 1973. in Advances in Electrochemistry and Electrochemical Engineering, Vol. 9 (R. M. Muller, Ed.), Wiley Interscience, New York, Chapter 2.
15. Allara, D. L., Baca, A. and Pryde, C. A., 1978. Macromolecules, 11:1215.
16. Dluhy, R. A., 1986. J. Phys. Chem., 90:1373.
17. Mielczarski, J. A. and Yoon, R. H., 1988. J. Phys. Chem.; submitted.
18. Hansen, W. N., 1970. Symp. Faraday Soc., 4:27.
19. Porter, M. D., Bright, T. B., Allara, D. L. and Kuwana, T., 1986. Anal. Chem., 58:2461.

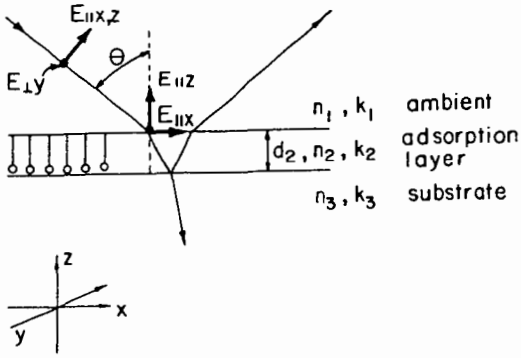

Figure 1. Electric field vectors in a three-phase system. Parallel (p) ($E_{\parallel z}$, $E_{\parallel x}$) and perpendicular (s) ($E_{\perp y}$) components are shown for incident radiation.

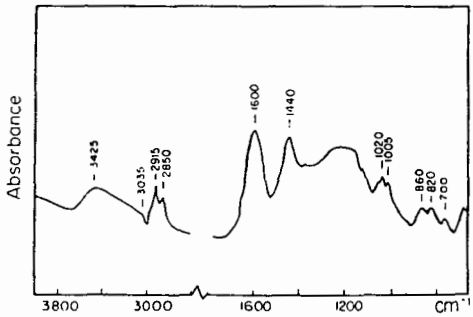

Figure 2. Transmission spectrum of Pittsburgh seam coal.

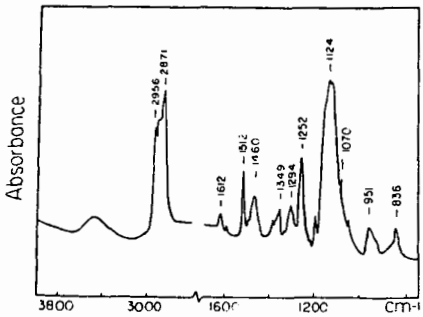

Figure 3. Transmission spectrum of nonylphenolpolyethyleneglycol ether.

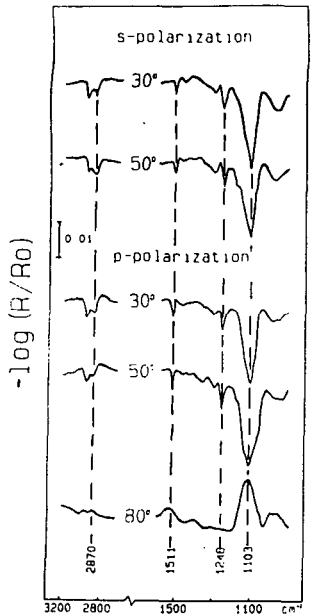

Figure 4. IRAS spectra of the adsorbed layer of nonylphenolpoly-ethyleneglycol ether on coal recorded at various angles of incidence with s- and p- polarization.

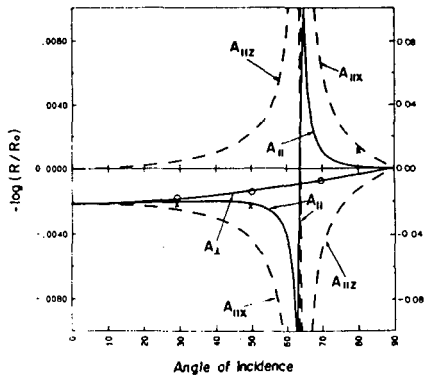

Figure 5. Calculated absorbance for hypothetical layer of nonylphenolpoly-ethyleneglycol ether (n_2 = 1.5, k_2 = 0.38, λ = 9.09, d_2 = 5×10^{-9} m) on coal (n_3 = 2.05, k_3 = 0.02) (solid and dashed lines). Experimental results (note different absorbance scales) shown as circles for s-polarization and as crosses for p-polarization.

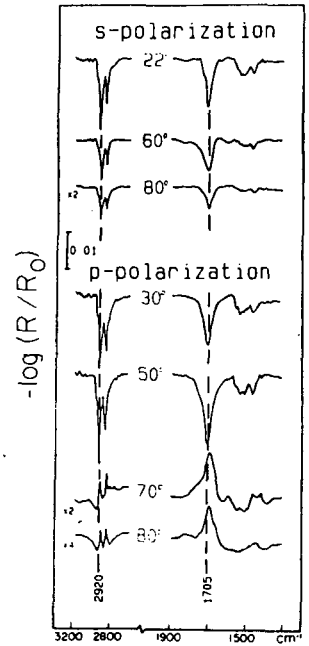

Figure 6. IRAS spectra of lauric acid layer on coal recorded at various angles of incidence with s- and p-polarization.

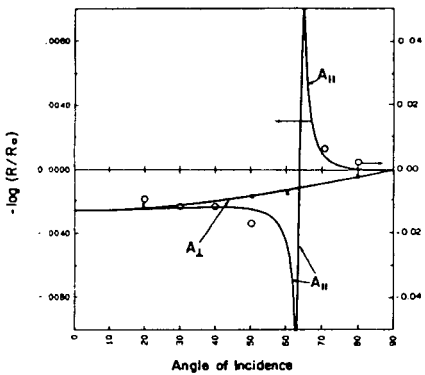

Figure 7. Calculated absorbance for hypothetical layer of lauric acid (n_2 = 1.5, k_2 = 0.3, λ= 5.85, d_2 = 5x10^{-9} m) on coal (n_3 = 2.05, k_3 = 0.02) (solid lines). Experimental results (note different absorbance scales) shown as circles for s-polarization and as crosses for p-polarization.

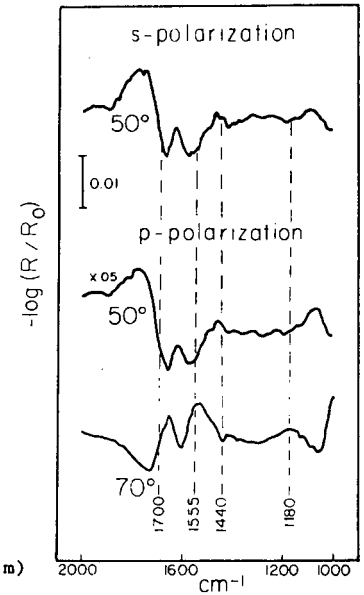

Figure 8. IRAS spectra of low-temperature oxidized coal recorded at different angles of incidence for s- and p-polarization.

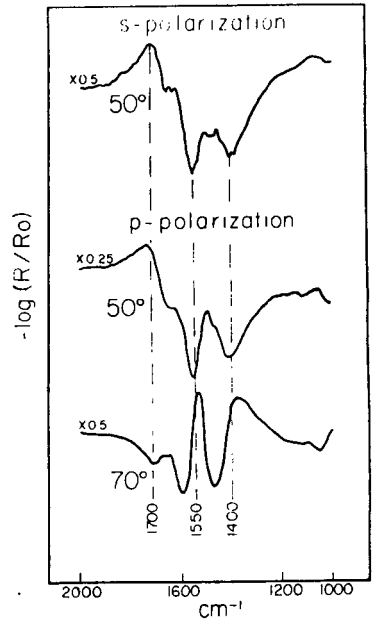

Figure 9. IRAS spectra of barium hydroxide treated oxidized coal recorded at different angles of incidence for s- and p-polarization.

APPLICATION OF THE DUBININ-ASTAKHOV EQUATION TO THE EVALUATION OF THE BENZENE AND CYCLOHEXANE ADSORPTION ISOTHERMS ON STEAM GASIFIED HUMIC ACIDS CHARS FROM BROWN COAL

Teresa Siemieniewska, Kazimierz Tomków, Jan Kaczmarczyk, Andrzej Albiniak
Institute of Chemistry and Technology of Petroleum and Coal, Technical University, Gdańska 7/9, 50-306 Wrocław, Poland

Yves Grillet
Centre de Thermochimie et de Microcalorimétrie du CNRS, 26, rue du 141 RIA, 13003 Marseille, France

Michèle François
Centre de Recherches sur la Valorisation des Minerais, École Nationale Supérieure de Géologie, BP 40, 54501 Vandoeuvre Cedex, France

INTRODUCTION

The Dubinin's theory of volume filling of micropores (1) is applied to the evaluation of adsorption isotherms to characterize the capillary structure of microporous carbonaceous solids (2-15). Recently, this theory is frequently represented by the Dubinin-Astakhov (DA) equation (16):

$$W = W_0 \exp\left[-(A/\beta E_0)^n\right] \qquad (1)$$

where W is the volume of micropores filled with the adsorbate at temperature T and relative pressure p/p_0, W_0 is the total volume of micropores, $A=RT \ln(p/p_0)$ is the differential molar work of adsorption. The product βE_0 is equal E, where E_0 and E are characteristic adsorption energies for a standard and a chosen adsorptive, respectively. The coefficient β is a similarity factor, related to the adsorptives (β is usually calculated as the ratio of molar volumes or parachores of the adsorptives), and it enables the characteristic curves (plots of W/W_0 versus A) of different adsorptives on the same solid to be superimposed. The value of the parameter n is chosen so that the experimental data would fit equation 1.

The proper choice of n may present some difficulties. Also, the question arises, if the rectilinearity of the plot in the coordinates corresponding to the logarithmic form of equation 1: ln W versus $(A/\beta E_0)^n$, even if it should be attained for a given n, can be considered as a sufficient indication for the physicochemical validity of the resulting parameters W_0 and βE_0.

The aim of this work was to establish, for a suite of carbonaceous materials, the values of n for which a satisfactory agreement would be obtained between the experimental adsorption data and the DA equation, trying also to verify the obtained DA parameters referring to related results calculated, or obtained experimentally, independently.

As adsorptives benzene (frequently used as standard) and cyclohexane (to avoid the presence of π - electrones in the molecule) were chosen. To have a suite of samples characterized by a systematically changing porosity, humic acids steam gasified chars were prepared with varying burn-offs. Humic acids from brown coals can be obtained with a low mineral matter content and they are thought to be representative for the organic substance of low rank coals. Additionally, two industrial active carbons, described elsewhere (17) were investigated.

EXPERIMENTAL

Humic acids (HA) were obtained from a Polish humodetrinitic brown coal (containing about 70 wt %, daf, HA), by extraction with diluted NaOH solution, followed by precipitation with hydrochloric

was taken. The lower limit of p/p_o results from our possibility of accurate adsorption measurements; the higher limit is connected with the fact that at relative pressure above 0.1, before the beginning of the histeresis loop, capillary condensation might, in some cases, occur, due to the tertiary process of adsorption in wider micropo - res (20). For each of the assumed value of n, correlation coeffi - cients were calculated, and for each of the adsorbate/adsorbent system the correlation coefficients were closest to unity when n=2 (in a few cases n=1.5 or n=2.5) was chosen (upper part of figure 5). This indicates that the best coincidence of experimental points with the DA equation is achieved, within the considered limits of relative pressures, for n=2 (if integrars are to be consi - dered). However, this does not necessarily mean that the values of W_o and βE_o corresponding to n=2 are of true physicochemical significance.

Applying, for the calculation of the values of n, the method of Dubinin(21), for benzene adsorption on HA 850/10 .... HA 850/85 the following values were obtained: n=6, n=6, n=5, n=3 and n=4, and on the charcoals 208 C and 264: n=6 and n=4. Similar values of n were obtained for cyclohexane adsorption on these samples.

To gain some additional information concerning the validity of the values of W_o obtained for n=2 (and also to check the remaining W_o values), an independently calculated value of the volume of micropores was necessary. We thought this purpose might be served by the volume of micropores, as given in figures 3 and 4 (V_{mic}). We tried also to assess the position of the values of V_m calculated by application of the Brunauer, Emmett and Teller(BET) equation(22) in relation to the respective values of V_{mic}. Because in the BET co - ordinates practically no straight lines were obtained from the isotherms in figures 3 and 4, a modification of the BET procedure, according to Joyner, Weinberger and Montgomery (23) was applied.

It appears that here the values of V_m (according to the theory of BET, V_m is the monolayer capacity of the adsorbent) are in a very good agreement with respective values of V_{mic}, the correlation coefficient being equal 0.998 (figure 6 a). This means that V_m , in case of the investigated samples, might represent the volume of adsorbate contained in the micropores only, not including the ad - sorption in the monolayer of the mesopores (V_{Smes}). If to the values of V_m the values of V_{Smes} are added, an approximate position of point B of the isotherms in figures 1 and 2 is reached. This is seen in Table II, where the amounts adsorbed are expressed directly in mmol/g.

Table II. Benzene adsorption (mmol/g) and corresponding p/p_o

Sample	a_{mic} (p/p_o)	a_m (p/p_o)	$[a_m + a_{Smes}]$ (p/p_o)	a_o (p/p_o)
HA 850 10	1.43 (0.10)	1.43(0.10)	1.53 (0.22)	1.40(0.07)
HA 850 25	2.77 (0.07)	2.73(0.06)	2.92 (0.18)	2.77(0.07)
HA 850 50	4.26 (0.05)	4.27(0.05)	4.76 (0.16)	4.34(0.06)
HA 850 75	4.99 (0.05)	4.93(0,04)	5.71 (0.14)	5.12(0.06)
HA 850 85	4.95 (0.04)	4.94(0.04)	5.81 (0.16)	5.04(0.05)
Charcoals:				
208 C	4.23 (0.08)	4.23(0.08)	4.42 (0.16)	4.27(0.09)
264	3.25 (0.06)	3.40(0.08)	3.90 (0.19)	3.32(0.07)

For all the investigated samples correlation coefficients were calculated for the relationships between W_o obtained for different values of n and the respective values of V_{mic} and V_m. In all cases

acid. The carbonization was carried out at a rate of 5°C/min to the final temperature of 850°C. The obtained char, designed as HA 850, was gasified, in a thermogravimetric apparatus, with steam at 800°C to following burn-offs: 10, 25, 50, 75 and 85 %. The obtained samples were designed as: HA 850/10..... HA 850/85. Active carbons: charcoal 208 C and charcoal 264, based on coconut shell and on coal, correspondingly, were obtained from the firm Sutcliffe Speakman Ltd. Sorption measurements of benzene and cyclohexane were carried out at 25°C in a gravimetric vacuum apparatus (McBain quarz springs). Mercury porosimetry was used for the determination of macropore volumes of the steam gasified HA chars.

RESULTS AND DISCUSSION

The characteristisc of samples is presented in Table I.

Table I. Proximate and ultimate analyses (wt %)

Sample	Proximate analysis			Ultimate analysis		
	Moisture	Ash dry	Volatile matter daf	C daf	H daf	$(O+N+S_o)_{diff}$ daf
Brown coal	52.1[1)]	9.5	57.1	70.8	6.0	23.2
HA	6.3	0.4	53.2	69.1	6.0	24.9
HA 850	1.1	0.6	1.7	97.1	0.5	2.4
HA 850 10	0.5	0.7	1.8	96.3	0.7	3.0
HA 850 25	0.6	0.8	1.7	96.3	0.7	3.0
HA 850 50	0.6	1.2	1.6	96.4	0.7	2.9
HA 850 75	0.7	2.4	1.6	97.6	0.6	1.8
HA 850 85	0.6	3.0	0.8	98.6	0.7	0.7
Charcoals:						
208 C	6.2	5.4	3.2	96.1	1.2	2.7
264	4.7	14.8	3.0	95.4	1.1	3.5

[1)] Total moisture of raw coal.

Isotherms of benzene and cyclohexane adsorption are given in figures 1 and 2. Basing on the desorption branch of the benzene isotherms, the pore size distributions of mesopores were calculated (18,19). The volume of micropores (V_{mic}) was calculated as the difference between the Gurvitch volume (the amount adsorbed at p/p_o = 0.96, corresponding to the effective radius of 50 nm, was taken) and the volume of mesopores. Within the micropores volumes, the volumes of super- and ultramicropores were distinguished, in which primary and secondary (cooperative) adsorption processes occured (20). The results are shown in form of bar graphs in figures 3 and 4. For the HA steam gasified chars, also the volumes of macropores are indicated. With increasing burn-offs systematic changes of each kind of considered porosity are visible.

On the basis of standard adsorption isotherms on a non-porous carbon black - Spheron 6-2700, the benzene and cyclohexane isotherms in figures 1 and 2 were corrected, substracting at successive relative pressures the respective amounts adsorbed on the surface of mesopores (S_{mes}). The values of S_{mes} for the samples HA 850/10 ... ...HA 850/85 are: 25.3, 51.1, 133.2, 206.6 and 228.8 m^2/g, and for the charcoals 208 C and 264: 49.0 and 132.3 m^2/g, respectively.

The corrected isotherms were used to calculate the values of W_o and βE_o according to the DA equation, assuming different values of the exponent n, from 1 to 6. The results are shown in figure 5. For these calculations the relative pressure region between 0.01 and 0.1

the best correlation was obtained, if W_o values corresponding to n=2 were considered. It follows from figure 6 b, that there exists almost an identity between the W_o values calculated from the DA equation for n=2 and the respective V_{mic} and V_m values. For all the investigated samples, if W_o is calculated for n=2, for benzene adsorption: points of the plots $V_m=f(W_o)$ and $V_{mic}=f(W_o)$, and for cyclohexane adsorption: points of the plot $V_m=f(W_o)$, are placed on a straight line which passes almost through the origin of the coordinate system with a slope very close to 1. This is not the case, if for the calculation of W_o in the DA equation other values of n are used.

Examples of DA plots for n=2, for chosen samples, are presented in figure 7. These plots confirm the proper choice of the upper limit of the relative pressure region (p/p_o=0.10) considered for calculations.

An attempt was made to determine the micropore volumes of the samples, employing the α_s-method (20), using Spheron6-2700 as standard. For samples with a low surface area of mesopores (HA 850/10, HA 850/25 and charcoal 208 C) a fairly good agreement was obtained with W_o values for n=2.

To test the validity of the values of βE_o obtained for n=2, the method presented by Stoeckli and Kraehenbuehl (6,8) was applied. The enthalpies of immersion in organic liquids $(-\Delta H_{im})_{mic}$ of microporous solids with negligible external and mesopore surface areas can be related to the characteristic energies of adsorption(βE_o) according to the equation:

$$(-\Delta H_{im})^{*}_{mic} = \beta E_o \, (\sqrt{\pi}/2)(1+\alpha T) \qquad (2)$$

where α is the thermal expansion coefficient of the adsorbate at temperature T; for benzene and cyclohexane the values of α were taken as 8.87×10^{-4} and 9.80×10^{-4} K^{-1}, respectively, calculated on the basis of their densities at the boiling and critical points (21).

$(-\Delta H_{im})^{*}_{mic}$ is expressed in the same units as βE_o, e.g. in kJ/mol. In order to express the enthalpy per mass unit, e.g. in J/g, it is necessary to take account of the amount adsorbed in the micropores corresponding to this unit of mass, i.e. $a_o = W_o/d$ (where d is the density of the adsorbate, taken as the density of the adsorbate as liquid at corresponding temperature):

$$(-\Delta H_{im})_{mic} = (-\Delta H_{im})^{*}_{mic} \times a_o \qquad (3)$$

These calculations were carried out for the steam gasified HA chars. To the obtained values of $(-\Delta H_{im})_{mic}$ corrections for the evolution of heat on the mesopore surface area were added: $(-\Delta H_{im})_{S_{mes}}$. These corrections were calculated on the basis of the respective $a_{S_{mes}}$ values of the HA chars and the βE_o values of Spherone 6-2700. The sum: $(-\Delta H_{im})_{mic} + (-\Delta H_{im})_{S_{mes}} = (-\Delta H_{im})$, considered as the calculated total enthalpy of immersion of the char, was compared with the respective enthalpy value determined experimentally by microcalorimetric measurements (24).The results are shown in figure 8, and (with the exception of samples with highest burn-offs) a satisfactory agreement between the calculated and experimentally determined enthalpy values can be stated.

These considerations point to the fact that the values of W_o and E_o calculated from the DA equation with n=2, represent, in all probability, the real properties of the capillary structure of the investigated samples. Deviations obtained if othe values of n are chosen, are shown in figure 9. Values of W_o and E_o for n=2 are given in Table III (for benzene β =1; for cyclohexane β = 1.22).

Table III. Parameters W_0 (cm^3 g), βE_0 and E_0 (kJ mol) for n=2

Sample	Benzene adsorption		Cyclohexane adsorption		
	W_0	E_0	W_0	βE_0	E_0
HA 850 10	0.125	28.6	0.074	24.9	20.4
HA 850 25	0.248	26.6	0.211	26.7	21.9
HA 850 50	0.388	23.0	0.381	21.1	17.3
HA 850 75	0.458	20.1	0.474	17.0	13.9
HA 850 85	0.451	19.9	0.458	14.2	11.6
Charcoals:					
208 C	0.382	29.1	0.350	23.6	19.3
264	0.297	18.6	0.313	13.9	11.4

A comparison of the W_0 values resulting from adsorption of benzene (molecular sizes: 0.37 and 0.70 nm) and of cyclohexane (molecular sizes: 0.48 and 0.68 nm), indicates the presence of slit-like micropores of widths below 0.48 nm in the microporous system of the HA chars of low burn-offs and the charcoal 208 C. In all cases the values of E_0 for benzene are higher from the respective values for cyclohexane.

CONCLUSIONS

(a) The parameters W_0 and βE_0, calculated for the considered adsorption data, are in a satisfactory agreement with the independently calculated micropore volumes and calorimetrically determined enthalpies of immersion, if in the DA equation the exponent n=2 is assumed.

(b) These results were obtained for micro- and mesoporous carbonaceous materials, which can be considered as being representative for the majority of active carbons.

(c) It is very probable that the values of W_0 and βE_0 for n=2 are closely related to real properties of the capillary structure - the micropore volume and the integral enthalpy of immersion.

ACKNOWLEDGEMENTS

This work was sponsored by the Technical University of Wrocław and the Polish Academy of Sciences (Scientific Program CPBP 01.16).

REFERENCES

1. Dubinin,M.M. in Chemistry and Physics of Carbon(P.L.Walker,Jr., Ed.); Dekker:New York,1966;Vol.2,pp 51-120.
2. Rand,B. J.Colloid Interface Sci. 1976,56,337-343.
3. Huber.U.; Stoeckli,H.F.; Houriet,J.P. J.Colloid Interface Sci. 1978,67,195-203.
4. Dubinin,M.M.;Stoeckli,H.F. J.Colloid Interface Sci.1980, 75, 35-42.
5. Walker,Jr.,P.L. Phil.Trans.R.Soc.London 1981,A300,65-81.
6. Stoeckli,H.F.; Kraehenbuehl,F. Carbon 1981,19,353-356.
7. Masters,K.J.; McEnaney,B. J.Colloid Interface Sci.1983, 95, 340-345.
8. Stoeckli,H.F.; Kraehenbuehl,F. Carbon 1984,22,227-229.
9. McEnaney,B.;Masters,K.J. Thermochimica Acta 1984,82,81-102.
10. Stoeckli,H.F.; Kraehenbuehl,F.; Lavanchy,A.;Huber,U. J.Chim. Phys.1984,81,785-790.
11. Ali,S.;McEnaney,B. J.Colloid Interface Sci.1985,107,355-361.
12. Carrott,P.J.M.; Roberts,R.A.;Sing,K.S.W. Carbon 1987,25,59-68.

13. Marsh,H. Carbon 1987,25,49-58.
14. McEnaney,B. Carbon 1987,25,69-75.
15. Barton,S.S. Carbon 1987,25,77-80.
16. Dubinin,M.M.; Astakhov,V.A. Izv.Akad.Nauk SSSR Ser.Khim.1971 No 1,5,11.
17. Everett,D.H.; Parfitt,G.D.; Sing,K.S.W.; Wilson,R. J.appl.Chem. Biotechnol.1974,24,199-219.
18. Pierce,C. J.Phys.Chem.1953,57, 149-152.
19. Kankare,J.; Jantti,O. Soumem Kemistilehti 1967,B40,51-53.
20. Gregg,S.J.; Sing,K.S.W. Adsorption,Surface Area and Porosity; Academic Press:London, 1982.
21. Komarov,W.S. Adsorbents and their Properties (Russian language); Nauka i Tech.:Minsk, 1977; pp 231-239.
22. Brunauer,S.; Emmett,P.H.; Teller,E. J.Am.Chem.Soc.1938,60, 309-319.
23. Joyner,L.G.; Weinberger,E.B.; Montgomery,C.W. J.Am.Chem.Soc. 1945,67,2182.
24. Grillet,Y.; François,M.; Torralvo,M.J.; Guerrero,A.; Siemieniewska,T.; Tomków,K.; Kaczmarczyk,J.; Albiniak,A. Proc.IUPAC Symposium on Characterization of Porous Solids, Bad Soden,F.R.G. 26-29 April 1987; Elsevier.

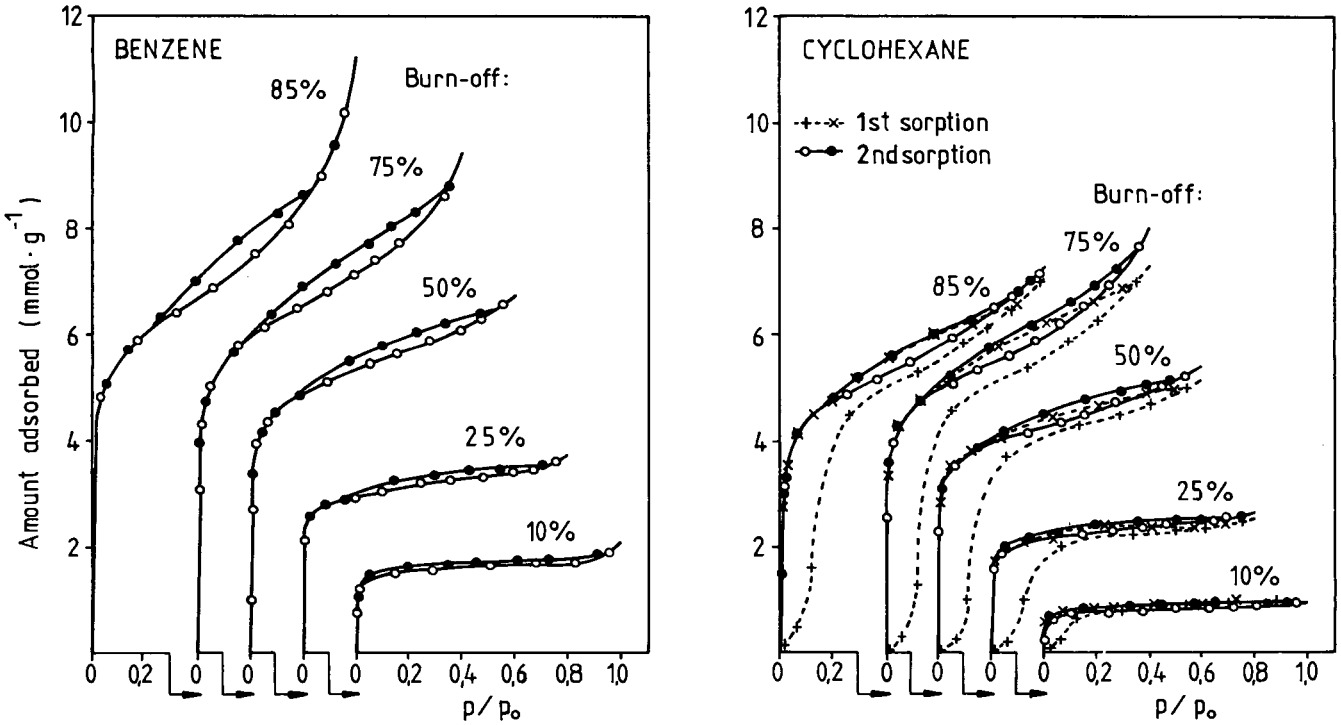

Figure 1. Benzene and cyclohexane sorption isotherms at 25°C on steam gasified (800°C) humic acids char HA 850.

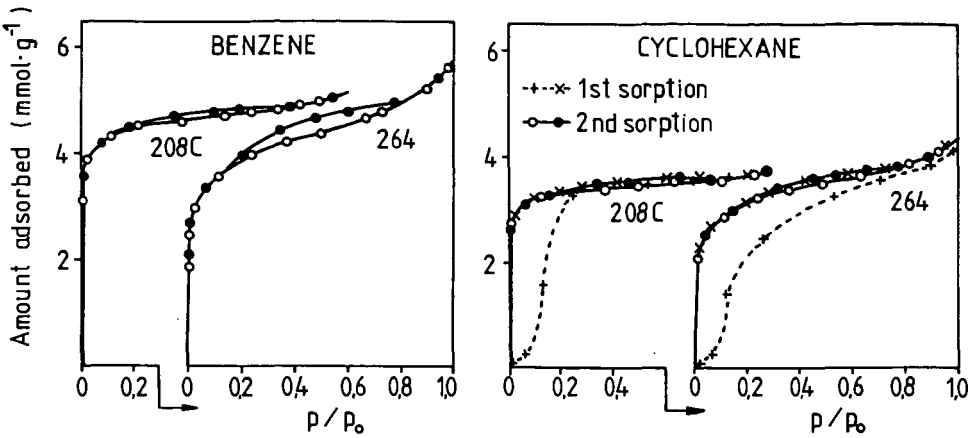

Figure 2. Benzene and cyclohexane sorption isotherms at 25°C on charcoals 208C and 264.

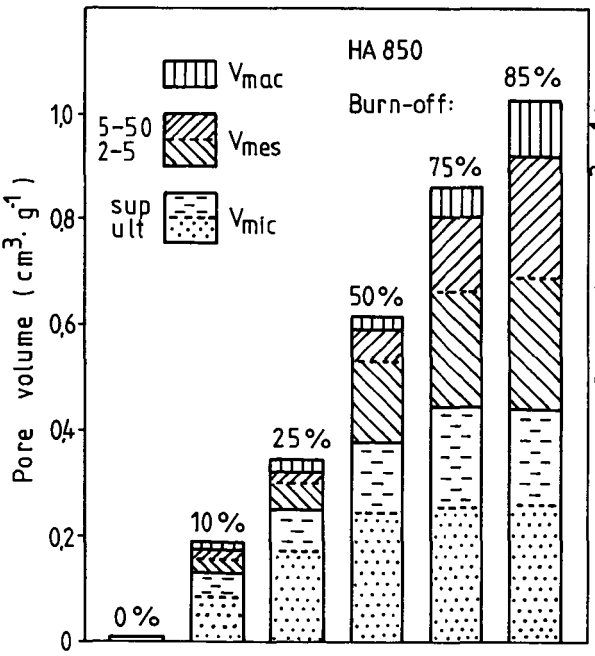

Figure 3. Infuence of burn-off on the pore size distribution of steam gasified (800°C) humic acids char HA850.

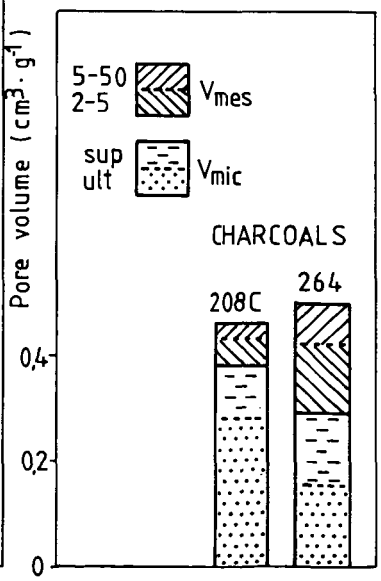

Figure 4. Pore size distribution in charcoals 208C and 264.

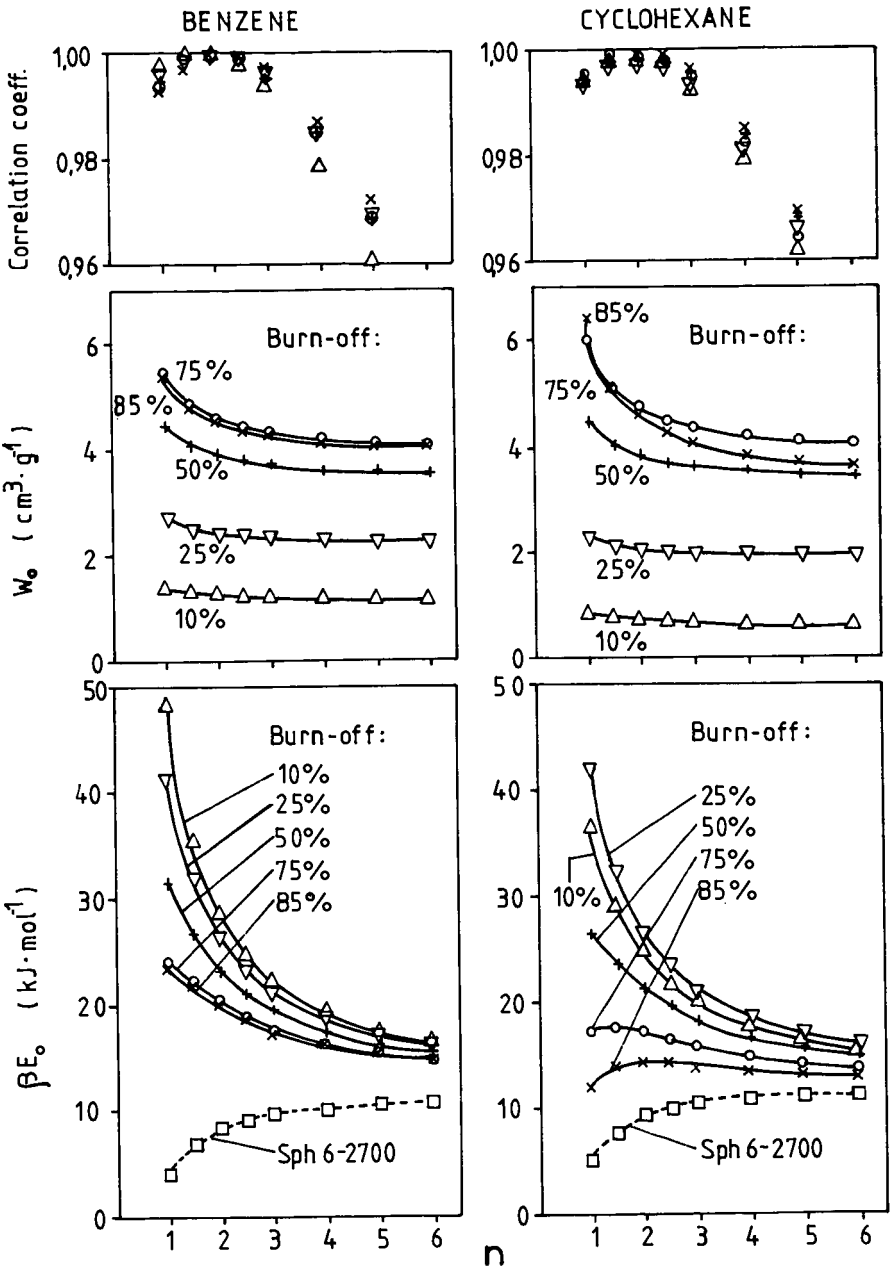

Figure 5. Influence of n used in calculations on the resulting values of W_o and βE_o of the DA equation.

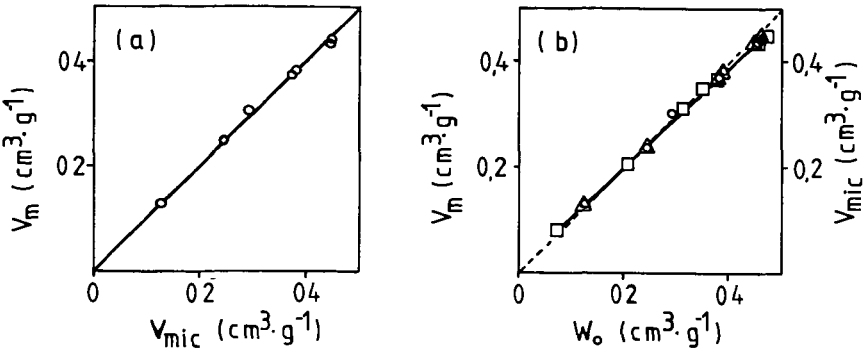

Figure 6. Plots: (a) V_m vs V_{mic} (○, benzene); (b) V_m vs W_o (○, benzene; □, cyclohexane); V_{mic} vs W_o (△, benzene).

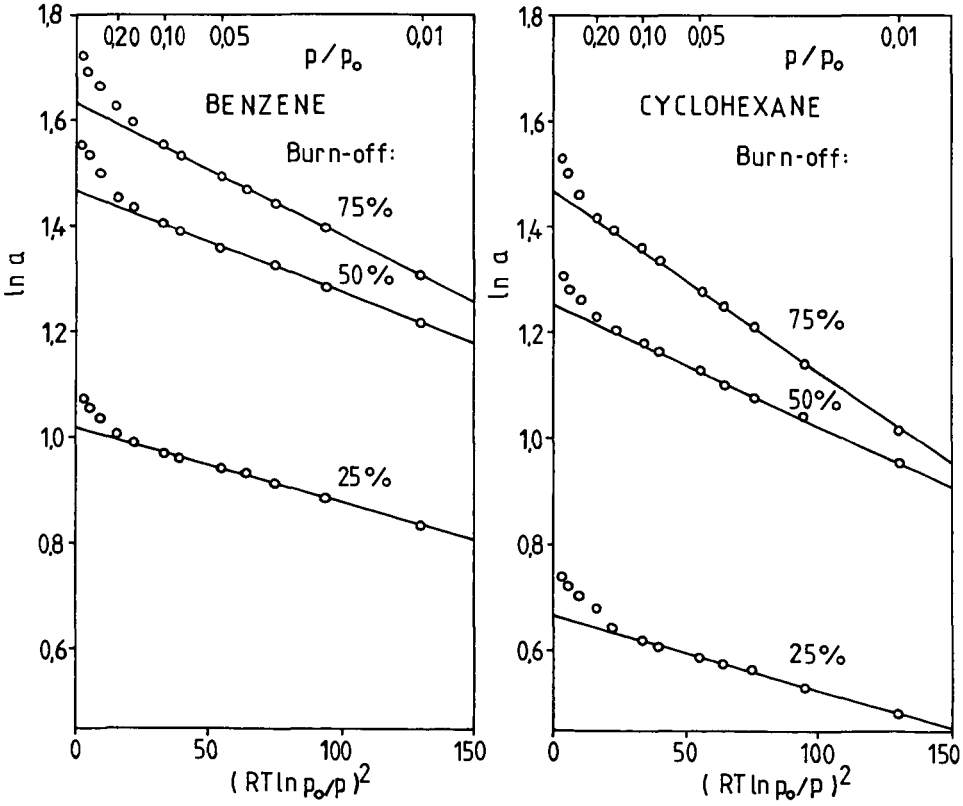

Figure 7. Plots: ln a vs $(RT \ln p_o/p)$ for steam gasified humic acids char HA850; a in $mmol \cdot g^{-1}$, RT in $kJ \cdot mol^{-1}$.

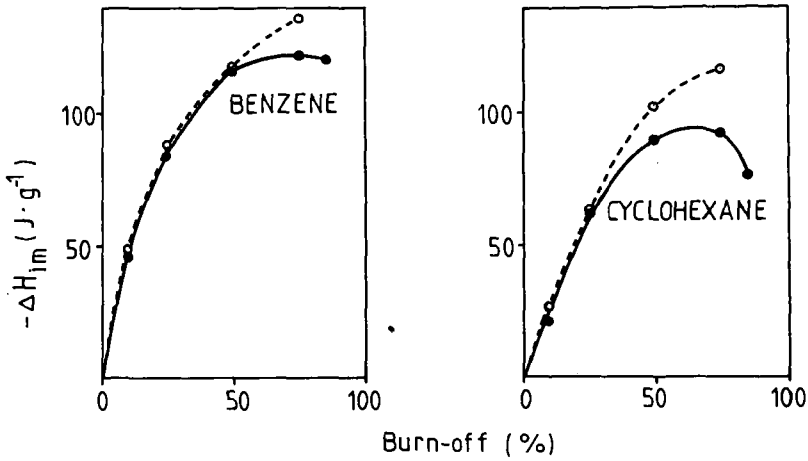

Figure 8. Enthalpies of immersion of steam gasified humic acids char HA850: o - experimental and ● - calculated from parametres βE_o and W_o of the DA equation for n = 2.

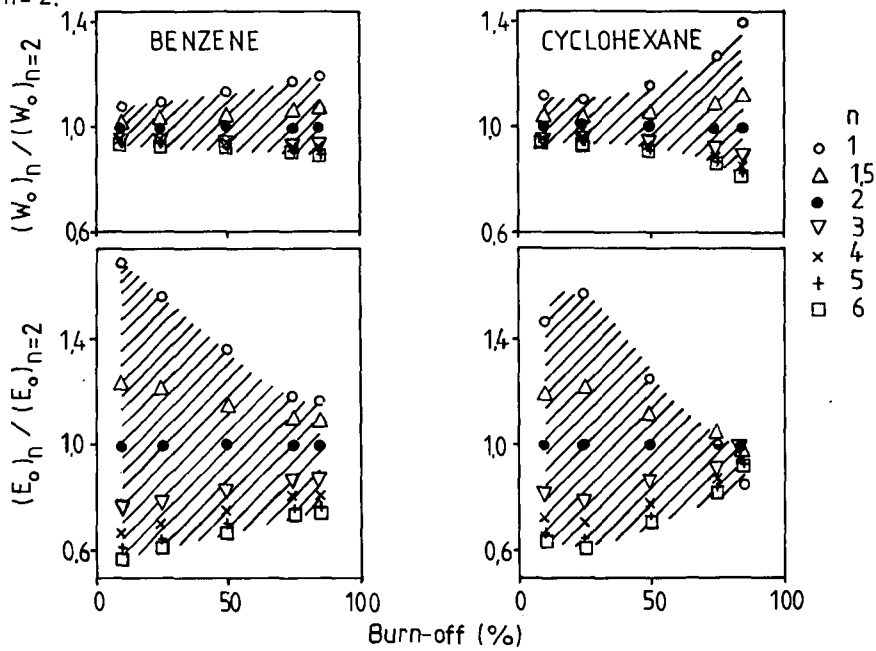

Figure 9. Influence of n in the DA equation on the ratios $(W_o)_n / (W_o)_{n=2}$ and $(E_o)_n / (E_o)_{n=2}$ for steam gasified humic acids char HA850.

CHARACTERIZATION OF COAL PARTICLE SURFACES BY FILM FLOTATION

D. W. Fuerstenau, J. Diao and J. S. Hanson
Dept. of Materials Science and Mineral Engineering
University of California
Berkeley, CA 94720

ABSTRACT

Because of the heterogeneity of coal, particles may vary in composition and, consequently, each particle may have its own unique set of surface properties. The distribution of surface properties of coal particles was determined through film flotation with a series of aqueous methanol solutions. This paper shows how such measurements of the critical wetting surface tension can be used to determine the contact angle (θ) of particles and the distribution of lyophobic sites on the surface of the particles. The mean contact angles calculated from film flotation results for sulfur, graphite and a number of different coals are in reasonable agreement with the values reported in the literature.

INTRODUCTION

Characterization of coal particles in terms of their wetting properties is important for understanding the behavior of coal in such surface-based processes as flotation, agglomeration, filtration and dust abatement. The wetting properties of solids have commonly been studied by measuring contact angles on a flat surface (1) and determining the critical wetting surface tension from the well-known Zisman plot (2). This method has been very successful for assessing the wettability of homogeneous materials, such as polymers. However, because of the heterogeneity of coal, the results obtained using this approach by different researchers are inconsistent (3,4).

Because of the heterogeneity of coal, the properties of coal particles can range from those of a virtually pure inorganic mineral species to that of an organic material. Consequently, each particle may have its own unique set of surface characteristics. Standard measurements of liquid penetration rates, heat of immersion, immersion times, and freezing-front points can assess only average properties of particulate samples. Recently, a film flotation technique was developed wherein the fraction of particles that sink or float on liquids of different surface tensions can be determined (5,6), and from such determination the distribution of wetting surface tensions (surface energies) can be determined.

In this study, the distribution of the surface properties of coals was determined with 100 x 150 μm particles by film flotation on a series of aqueous methanol solutions (of different compositions). By separating the particles into the lyophobic fraction (those remaining on the surface) and the lyophilic fraction (those imbibed into the solution) at each surface tension, the distribution of coal particles in relation to their wetting surface tension was determined. This paper shows how such information can be used to delineate the surface characteristics of the particles.

THEORETICAL CONSIDERATIONS

The critical wetting surface tension of a solid is an important parameter that represents the wettability of the solid. It was defined by Zisman as the surface

tension of a liquid which forms a zero contact angle on the solid (2). In our earlier research (7,8), we have verified theoretically and experimentally that for practical film flotation, the critical wetting surface tension of coal particles can be taken to be the surface tension of the liquid at which the particles sink into the liquid and that the effect of particle size and density are negligible.

Since we are familiar with the concept of contact angle and because we cannot measure the contact angle of a small particle directly, it is useful to calculate it. The calculation is possible only when γ_c of the particles can be determined by film flotation. By using the Young equation

$$\gamma_{SV} - \gamma_{SL} = \gamma_{LV}\cos\theta \qquad (1)$$

and the Neumann/Good equation of state (9):

$$\gamma_{SL} = \frac{(\sqrt{\gamma_{SV}} - \sqrt{\gamma_{LV}})^2}{1 - 0.15\sqrt{\gamma_{SV}\gamma_{LV}}} \qquad (2)$$

we can calculate the contact angle of a particle for a liquid of a given surface tension, γ_{LV}, from the values of γ_c measured in the film flotation experiments. It has been shown that γ_c can be taken as being equivalent to γ_{SV} (9).

Because coal is a mixture of inorganic minerals and organic substances, the surface will appear as a patchwork assembly of carbonaceous material, hydrocarbon, oxygen functional groups and mineral matter. The carbonaceous and hydrocarbon materials contribute to the lyophobic character of coal, whereas the oxygen functional groups and mineral matter contribute to the lyophilic behavior of coal. Therefore, the Cassie-Baxter equation (10) for a composite surface can be used to account for the variation of the contact angle with coal rank (11,12).

To calculate the fraction of lyophobic sites on the surface of coal particles α_{HB} and the fraction of lyophilic sites α_{HL}, we assume that i) the lyophobic sites have a contact angle in water $\theta_{HB} = 105°$ (i.e. paraffin wax) and ii) the lyophilic sites have a contact angle in water $\theta_{HL} = 0°$. Thus,

$$\alpha_{HB} + \alpha_{HL} = 1 \qquad (3)$$

By using Eq. 3 and the Cassie-Baxter equation for a composite surface, we obtain

$$\cos\theta = \alpha_{HB}\cos\theta_{HB} + \alpha_{HL}\cos\theta_{HL} \qquad (4)$$

and can calculate α_{HB} and α_{HL} of coal particles from their contact angles in water.

MATERIALS AND METHODS

Materials used in this study included a number of U.S. coals, Ceylon graphite (99.0% carbon) and sulfur (Nevada). For all materials 100 x 150 μm particles were prepared by grinding the as-received materials in a small ceramic to avoid iron contamination, followed by sizing with sieves. Paraffin wax-coated coal particles were prepared by a simple vapor deposition procedure (11). Oxidation of the coal was carried out thermally in air for 19 hours at 200°C in a mechanical convection oven.

Film flotation experiments (5,6) were conducted by sprinkling the 100 x 150 μm particles onto the surface of the aqueous methanol solutions, with compositions varying from pure water to pure methanol so that the surface tension could be controlled between 22.4 and 72.8 mN/m. For each solution, the fraction of particles remaining at the liquid/vapor interface was determined. All film flotation experiments were carried out at 20°C.

RESULTS AND DISCUSSION

Because of the heterogeneity of coal, the wetting properties of coal particles may change continuously from that of lyophobic organic materials to those of the lyophilic inorganic matter. Figure 1 shows the cumulative distribution of Cambria #78 coal particles as a function of their critical wetting surface tension obtained by film flotation using aqueous methanol solutions. From the results in Fig. 1, the frequency distribution of Cambria #78 coal particles was determined as a function of their critical wetting surface tension and are presented in Fig. 2. These two figures clearly show the heterogeneous nature of coal particles.

From such distributions, four wetting parameters have been defined (5,6). The critical wetting surface tension of the most lyophobic particles in the assembly, γ_c^{min}, is the surface tension of the liquid at which none of the particles remains at the liquid surface. The critical wetting surface tension of the most lyophilic particles in the powder, γ_c^{max}, is the surface tension of the liquid at which all the particles remains at the liquid surface. The mean critical wetting surface tension of all particles, $\bar{\gamma}_c$, can be calculated from the film flotation frequency distribution using the equation:

$$\bar{\gamma}_c = \int \gamma_c \, f(\gamma_c) \, d\gamma_c \qquad (5)$$

where γ_c is the critical surface tension of particles and $f(\gamma_c)$ is the frequency distribution function. $\bar{\gamma}_c$ represents the wettability of the assembly of particles. The standard deviation $\sigma_{\gamma c}$ of the frequency distribution function reflects the heterogeneity of the surface. High $\sigma_{\gamma c}$ values correspond to heterogeneous materials.

Figure 3 shows the frequency distribution of Cambria #78 coal particles as a function of their contact angle in liquids with surface tension of 60.0 and 72.8 mN/m, respectively. The contact angle of the particle for the given liquid surface tension was calculated from their γ_c using Eqs. 1 and 2. The weight percent of particles in different intervals of the contact angle was taken from the distribution presented in Fig. 2. The figure clearly shows that coal particles in an assembly have a wide range of contact angles and that the lower the surface tension of the liquid the smaller the contact angle of the coal particles. This distribution of contact angles serves to illustrate why the coal particles reside at the liquid/vapor surface in film flotation.

The surface composition of coal particles can be related to their wetting properties by calculating the fraction of lyophobic sites on the surface of the particles from their contact angles in water using Eqs. 3 and 4. The frequency distribution of Cambria #78 coal particles as a function of their percentage of lyophobic sites on the surface of the particles is given in Fig. 4. The weight percent of particles in the different intervals shown in Fig. 4 was again taken from Fig. 2. This figure shows that coal particles are covered by varying amounts of lyophobic materials and gives some insight into the extreme heterogeneity of the coal surface.

Table 1. Wetting parameters of as-received, wax-coated and oxidized Cambria #78 coal obtained from film flotation results.

Treatment	$\bar{\gamma}_c$, mN/m	θ, deg.	α_{HB}	$\sigma_{\gamma c}$, mN/m
Wax-coated	25.3	100	0.92	2.60
As-received	43.0	68	0.49	4.53
Oxidized at 200°C for 19 hours	67.0	24	0.07	----

The validity of the film flotation method for characterizing particle surfaces was tested by conducting film flotation tests on wax-coated and oxidized Cambria #78 coal. Figure 5 shows the cumulative distribution of as-received, wax-coated and oxidized Cambria #78 coal particles as a function of their critical wetting surface tension as determined by film flotation. The wetting parameters calculated from the film flotation results are given in Table 1. It can be seen from Fig. 5 and Table 1 that the cumulative distribution of wax-coated coal particles moves to lower wetting surface tensions as compared with that of the as-received coal particles. Also $\bar{\gamma}_c$ of wax-coated coal particles is less than that of as-received coal particles, and the value of θ and α_{HB} for wax-coated coal particles are higher than that of as-received coal particles. This increase in lyophobicity is due to the presence of additional lyophobic sites on the wax-coated coal. On the other hand, the cumulative distribution curve of oxidized coal particles moves to higher wetting surface tensions and its $\bar{\gamma}_c$ value is higher than that of as-received coal particles. The value of θ and α_{HB} oxidized coal particles are smaller than that of as-received coal particles, indicating, as expected, that coal particles are more lyophilic when they are oxidized due to the destruction of lyophobic sites by the oxidation process. These findings serve to confirm our film flotation approach.

To further verify our new approach, the mean contact angle of a particle assemblage was compared with the values reported for direct measurements on the flat surface of a bulk sample. Since a flat surface of a bulk sample can be considered to be a composite of small particles with different contact angles, the contact angles

Table 2. The contact angles, θ, of sulfur, graphite and coals in water calculated from film flotation results, and measured by captive-bubble (CB) and sessile-drop (SD) methods.

Mineral	Film Flotation θ, degrees	Contact Angle Measurement θ, deg.	Method	Ref.
Sulfur	86	87	SD	(13)
Graphite	71	77	CB	(14)
Braztah Coal	87	90	SD	(15)
Somerset Coal	74	56	SD	(15)
Cambria #33 Coal	62	57	CB	(14)
		85	CB	(4)
		91	SD	(4)
Geneva Coal	81	72	SD	(15)
		86	SD	(15)
		64	CB	(14)

obtained from both methods should agree with each other if our approach is correct and if the polishing procedures used in preparing the flat surface do not change its wetting properties significantly. The contact angle of sulfur, graphite and various coals in water calculated from film flotation results are presented in Table 2. This table also shows the contact angle measured by captive-bubble and sessile-drop methods on a flat surface of the same samples in our laboratory. From this table it is seen that the two sets of values are in quite good agreement with each other, especially for the more homogeneous minerals. This further supports the model for the estimation of the contact angle of particles from their critical wetting surface tension.

SUMMARY AND CONCLUSIONS

The distribution of the critical wetting surface tension of an assemblage of particles was determined using the film flotation method. A model has been developed to estimate the contact angle of coal particles from the critical wetting surface tension distribution and to estimate the fraction of lyophobic sites on the surface of these particles from this calculated value. The estimated mean contact angle of particles is in good agreement with measured values on flat surfaces. This model provides insight into the heterogeneous nature of coal particles.

ACKNOWLEDGEMENTS

The authors wish to acknowledge the U. S. Department of Energy, Pittsburgh Energy Technology Center, Grant No. DE-FG22-86PC90507

REFERENCES

1. R. J. Good, Surface and Colloid Science, R. J Good and R. R. Stromberg, Eds., Plenum Press, New York, 11, 1-30, 1979.
2. W. A. Zisman, Contact Angle, Wettability and Adhesion, ACS, Adv. in Chem. Series, R. F. Gould, Ed., 43, 1-51, 1964.
3. B. K. Parekh and F. F. Aplan, Recent Developments in Separation Science, CRC Press, Florida, 4, 107-113, 1978.
4. G. C. C. Yang, Ph.D. Thesis, University of California, Berkeley, 1983.
5. D. W. Fuerstenau, M. C. Williams and J. Diao, AIME Annual Meeting, New Orleans, March 1986.
6. D. W. Fuerstenau and M. C. Williams, Colloids and Surfaces, 22, 87-91, 1987.
7. J. Diao, MS. Thesis, University of California, Berkeley, 1987.
8. D. W. Fuerstenau, J. L. Diao, K. S. Narayanan and R. H. Urbina, Int. Symp. on Interfacial Phenomena in Biotechnology and Materials Processing, Boston, MA, August 1987, accepted for publication.
9. A. W. Neumann, R, J. Good, C. J. Hope and M. Sejpal, J. Col. Interfac. Sci., 49, 291-304, 1974.
10. A. B. D. Cassie and S. Baxter, Trans. Farad. Soc., 40. 546-551, 1944.
11. J. M. Rosenbaum and D. W. Fuerstenau, Int. J. Minl. Proc., 12, 313-316, 1984.
12. D. V. Keller, Jr., Colloids and Surfaces, 22, 21-35, 1987.
13. D. Olsen, R. Moravec and A. Osteraas, J. Phys. Chem., 7, 4464-4466, 1967.
14. A. S. K. Osoka, Ph.D. Thesis, University of California, Berkeley, 1983.
15. J. M. Rosenbaum, Ph.D. Thesis, University of California, Berkeley, 1981.

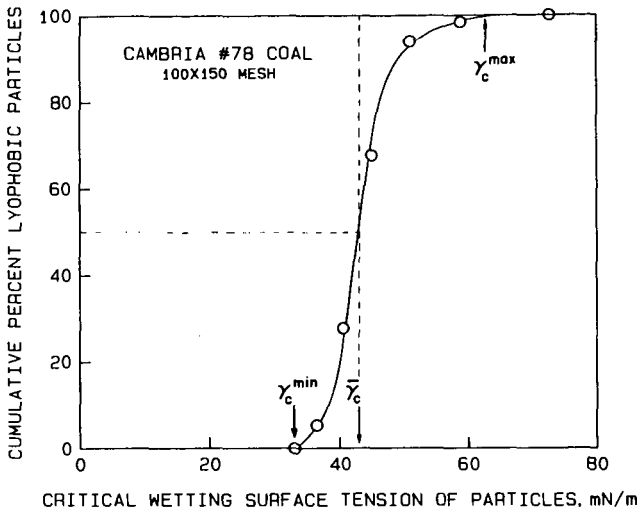

Fig. 1- The cumulative distribution of Cambria #78 coal particles as a function of their critical wetting surface tension obtained from film flotation with aqueous methanol solutions.

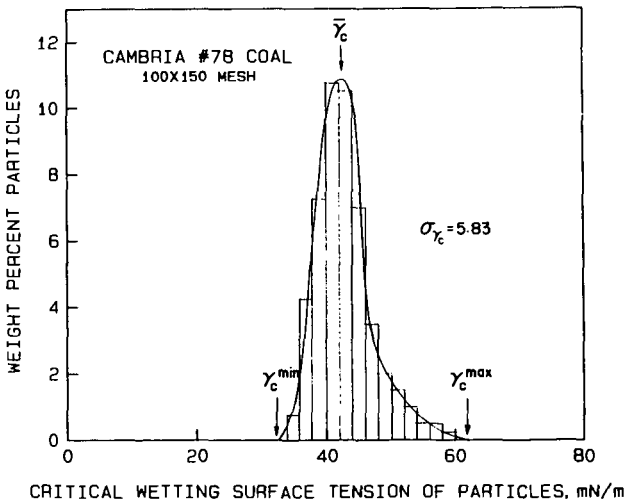

Fig. 2- Frequency distribution of Cambria #78 coal particles as a function of their critical wetting surface tension determined from film flotation with aqueous methanol solutions.

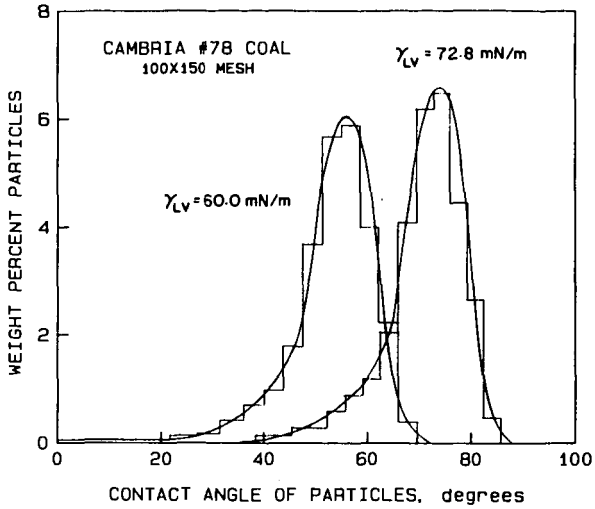

Fig. 3- Frequency distribution of Cambria #78 coal particles as a function of their contact angle in the liquid with surface tension of 60.0 and 72.8 mN/m, respectively.

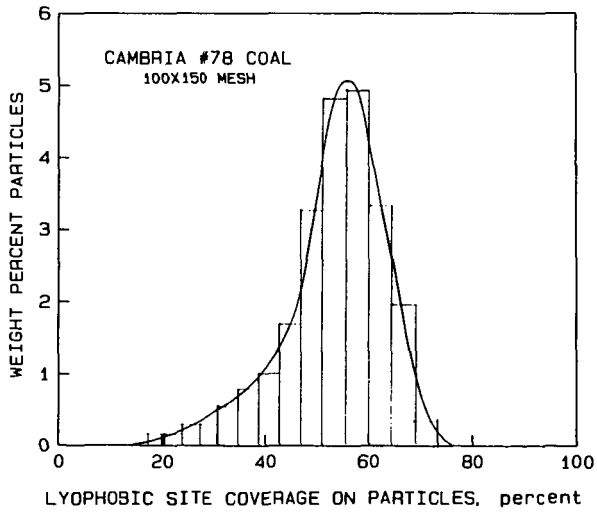

Fig. 4- Frequency distribution of Cambria #78 coal particles as a function of lyophobic sites on the surface of the particles.

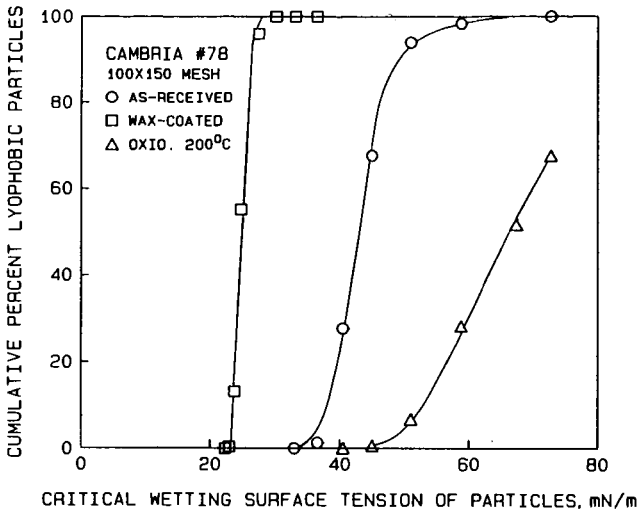

Fig. 5- Cumulative distribution of as-received, wax-coated, and oxidized (200°C, for 19 hours) Cambria #78 coal as a function of their critical wetting surface tension determined from film flotation with aqueous methanol solutions.

Oil Agglomeration of Coal in Salt Solutions: Effects of Hydrophobicity and Other Parameters on Coal Recovery

C.-W. Fan, R. Markuszewski, and T. D. Wheelock

Ames Laboratory and Department of Chemical Engineering
Iowa State University
Ames, Iowa 50011

Abstract

The recovery of fine coal or graphite particles suspended in water by agglomeration with heptane was observed to be highly dependent on the relative hydrophobicity of the solids as indicated by the measured induction time, i.e., the time required for attachment of one or more particles to a small gas bubble when brought into contact. For highly hydrophobic coal or graphite particles, an increase in ionic strength of the suspending medium caused an increase in agglomeration recovery and a decrease in measured induction time. For weakly hydrophobic coal or pyrite particles, an increase in ionic strength caused a decrease in agglomeration recovery and an increase in induction time. Due to the opposing effects of ionic strength on the recovery of a highly hydrophobic coal and pyrite, it was possible to improve the separation of these materials by an increase in ionic strength. On the other hand, because the recovery of pyrite and a weakly hydrophobic coal were affected similarly by ionic strength, it was not possible to improve the separation of these materials by a similar increase.

Introduction

A number of processes have been proposed for cleaning and recovering ultrafine coal particles suspended in water by selective agglomeration of the carbonaceous solids with oil (1-4). Since most of the ever present mineral impurities are unaffected by oil, an agglomerated suspension can be screened to recover the agglomerates and effect a separation from the unagglomerated mineral particles. The method takes advantage of the difference in surface properties of the organic and inorganic components of coal. Generally the organic material is significantly more hydrophobic than the inorganic minerals found in coal. Therefore, the carbonaceous particles are more readily wetted by oil than the mineral particles, and agglomeration occurs when oil-coated particles become connected by oil bridges. Among the common mineral impurities in coal, only iron pyrite appears to be sufficiently hydrophobic to interfere with separation from coal by this technique. However, the hydrophobicity of pyrite is quite variable and depends on treatment conditions.

It has been recognized that strongly hydrophobic coals respond more readily than weakly hydrophobic coals to this method of treatment (1,5,6). Generally, high recoveries of the more hydrophobic coals can be achieved with relatively small amounts of the lighter, paraffinic hydrocarbons such as heptane, whereas high recoveries of the less hydrophobic coals can only be realized by employing heavier, more complex hydrocarbons in larger amounts. Moreover, for highly hydrophobic coals even less oil is required when the material is suspended in a salt solution (7,8).

An improvement in the separation of coal and pyrite as well as a reduction in oil consumption would improve the economic feasibility of the oil agglomeration method. Minimizing oil consumption by adding salt to the system would reduce one of the major costs of the method. However, preliminary indications suggested that this approach would not work with all types of coal. Therefore, this study was undertaken to determine the effect of coal hydrophobicity on oil agglomeration recovery and to determine how the recovery of different types of coal was affected by salt concentration.

While it was known previously that coal hydrophobicity played an important role in oil agglomeration, it was difficult to measure this role quantitatively. The most popular traditional method for determining wettability by measuring the three-phase contact angle for a water drop on a polished coal surface was difficult to apply in practice. Also it was questionable whether the wettability of a polished surface was the same as that of the small granular particles used in oil agglomeration. In addition, the method was not very sensitive.

Another method of investigating wettability which does not suffer the disadvantages listed above is based on measuring the so-called induction time or, more accurately, the time required for attachment of one or more particles to a small gas bubble when brought into sudden contact under water (9). The measured time is believed to be a combination of the time required to thin the water film between a particle surface and an air bubble to the point of rupture (true induction time) and the time required to displace the film (10,11). Since the attachment time or induction time is based on a dynamic measurement, it depends on the kinetics and hydrodynamics as well as the thermodynamic properties of the system (9-12). Therefore, it differs from the equilibrium contact angle which depends only on the thermodynamic properties of the system. Because of this difference, the induction time depends on certain properties which do not affect the equilibrium contact angle such as particle size and density or the ionic strength of the solution in contact with the particles. Thus, Laskowski and Iskra (12) observed that the induction time of a hydrophobic solid was affected by the concentration of potassium chloride in which the solid was suspended whereas the three-phase contact angle was unaffected. Consequently, certain parameters must be controlled carefully when using induction time measurements to study changes in hydrophobicity.

In the present investigation, the surface of coal and graphite particles was characterized by measuring the induction time, and the response of these materials to agglomeration with heptane was determined by measuring the recovery or mass yield. Different types of coal were utilized which appeared to range from weakly hydrophobic to strongly hydrophobic. In addition, the effect of salt concentration on coal recovery and induction time was determined for a strongly hydrophobic coal (Upper Freeport) and a weakly hydrophobic coal (Illinois No. 6). Also the effect of salt concentration on pyrite recovery and induction time was determined.

Materials and Experimental Methods

Samples of coal were obtained from various sources as indicated in Table 1. The Upper Freeport coal is a medium volatile bituminous coal whereas the other coals are high volatile bituminous coals. Relatively pure samples of graphite from Sri Lanka and mineral pyrite from Huanzala, Peru, were obtained through Ward's Natural Science Establishment. These materials were ground in the dry state with a high-speed impact mill and then screened. For the agglomeration experiments the materials were suspended in deionized water having a resistivity of 17.9 megohm-cm and agglomerated with n-heptane from Eastman Kodak Company. The specified normal boiling point of this material was 98°C which indicated a high level of purity.

The agglomeration experiments were carried out with a specially designed closed system so that the operation was conducted without air present (13). The system utilized the motor and agitator from a 14-speed kitchen blender, but the open container furnished with the blender was replaced by a 500-ml glass jar which was nearly square in cross section. A small hole had been drilled in the bottom of the jar which was plugged with a rubber septum. During operation the jar was inverted, and heptane was introduced through the septum with a hypodermic syringe. For each experiment the jar was completely filled with an aqueous suspension containing either 10 g coal or graphite or 3 g pyrite. In some experiments a suspension containing a mixture of coal and pyrite was employed. The suspension at its natural pH was conditioned for 3 min. at high speed (about 18,000 rpm), and then a predetermined amount of heptane was introduced. Agitation was continued at high speed for 3 min.

Table 1. Sources and properties of coal samples

	Upper Freeport	Pittsburgh	Illinois No. 6	Iowa
Source	Indiana County, PA	Belmont County, Ohio	St. Clair County, IL	Monroe County, IA
Mean diameter[a], μm	34	39	43	42
Total sulfur, %	2.10	4.03	2.62	3.06
Proximate analysis, %				
Fixed carbon	62.4	48.2	46.5	45.0
Volatile matter	26.8	40.6	34.5	39.1
Ash	10.4	9.8	9.7	12.4
Moisture	0.4	1.4	9.3	3.5
Total	100.0	100.0	100.0	100.0

[a]Mean diameter of particles used for oil agglomeration.

to produce agglomerates. The agglomerates were recovered on a 100-mesh screen (U.S. Standard), dried in an oven at 100-110°C, and weighed. When a mixture of coal and pyrite was treated, the total sulfur and ash contents of the product were determined and sulfur and ash balances were used to calculate the recovery of the coal and pyrite, respectively.

The so-called induction time of the various materials was measured with the apparatus manufactured by Virginia Coal and Mineral Services, Inc., using the procedure described previously (9-11). For this measurement, -100/+140 mesh coal or graphite particles and -200/+325 mesh pyrite particles were employed. The particles were spread in a thin layer under water and a 2-mm diameter air bubble was formed on the end of a capillary just above the layer of particles. The initial gap between the captive bubble and the surface of the particles was set at approximately 0.1 mm. The bubble was subsequently brought into contact with the particles for successively longer contact times, and the number of particles which adhered to the bubble was noted. The induction time was taken to be the contact time which resulted in particle attachment in five out of ten trials.

Results and Discussion

Graphite and the four coals listed in Table 1 were found to encompass a wide range of hydrophobicity as indicated by the measured induction time. As the results in Table 2 indicate, the induction time ranged from 0.31 ms for graphite (a highly hydrophobic material) to 5.4 ms for Illinois No. 6 coal (a weakly hydrophobic material). For this series of measurements, the particle size was controlled by screening the materials and using only the particles between 100 and 140 mesh. It was necessary to use somewhat larger particles than were used for agglomeration (-200/+400 mesh) to avoid disturbing the bed of particles in the measuring cell when the particles were contacted with a gas bubble. The induction time of the particles used for agglomeration would have been smaller than that of the particles used for determining induction time since the results of Ye et al. (11) indicated that induction time is proportional to particle size raised to a power which depends on particle density. For coal particles of similar density (1.3 to 1.4 g/cm^3) the dependency of induction time on particle size was second order, whereas for molybdenite particles (density = 4.7 g/cm^3) the dependency was third order. In the

Table 2. Induction time and agglomeration recovery of various carbonaceous materials with heptane

Material	Induction time, ms	Agglomeration recovery, %	
		5 v/w % C_7H_{16}	10 v/w % C_7H_{16}
Graphite	0.31	94	100
Upper Freeport coal	1.96	32	76
Pittsburgh coal	2.25	29	70
Iowa Coal	4.85	6	21
Illinois No. 6 coal	5.40	4	17

present study the induction times of the different coals used for agglomeration should have been approximately 10% of the values listed in Table 2 because of the smaller particle size, and the induction time of graphite even less. The effect of particle size should have been more pronounced for graphite due to its greater density (2.2 g/cm^3). Even so, the relative relationship between the induction times of the materials which were agglomerated should have been about as indicated in Table 2.

When the different carbonaceous materials were agglomerated separately with heptane, the recovery decreased monotonically as the induction time of the material increased or, in other words, as the hydrophobicity of the material decreased (see Table 2). This was the case with either 5 or 10 v/w % heptane (i.e., with either 0.5 or 1.0 ml heptane/10 g solids). Thus, there appeared to be a good correlation between recovery and induction time.

The relationship between agglomeration recovery and induction time was explored further by conducting a series of experiments in which different carbonaceous materials were suspended individually in salt solutions and agglomerated with heptane. The results achieved with different salt concentrations are presented in Figures 1 and 2 for Upper Freeport coal and Illinois No. 6 coal, respectively. In the case of the highly hydrophobic Upper Freeport coal, the recovery increased markedly as the salt concentration was raised to 1.5 M, but then it increased only slightly as the salt concentration was raised further to 3.0 M. At this salt concentration, a recovery of 77% was achieved with only 3 v/w % heptane. To obtain a comparable recovery of Illinois No. 6 coal required using 40 v/w % heptane or more. For this weakly hydrophobic coal, the highest recovery was realized when the material was suspended in deionized water, and the recovery decreased when the material was suspended in a salt solution. Moreover the recovery decreased as the salt concentration was increased, and an increase in salt concentration from 0 to 1.5 M produced a greater change in recovery than a further increase from 1.5 to 3.0 M.

The effect of increasing salt concentration on induction time was to reduce the induction time of the highly hydrophobic Upper Freeport coal and increase the induction time of the weakly hydrophobic Illinois No. 6 coal (see Figures 1 and 2). Consequently, the resulting induction time curves were almost mirror images of the recovery curves for the corresponding coals; thus again there seemed to be a close correspondence between recovery and induction time.

The recovery curves and induction time curves for Pittsburgh coal and graphite, while not presented here, were generally similar to those noted above for Upper Freeport coal. Therefore the recovery and induction time of all of these highly hydrophobic materials were affected in the same way by salt concentration. For such materials it appears that the underlying effect of increasing salt concentration or ionic strength of the suspending medium is to compress the electrical double layer surrounding the individual particles (7,8). This in turn destabilizes the water film in contact with the solid according to Laskowski and Iskra (12). Consequently the water film is more easily ruptured between colliding particles and oil droplets or between oil-coated particles. In a similar way the induction time is reduced because the water film between any given particle in contact with a gas bubble also is more easily ruptured.

A different mechanism is required to explain the behavior of Illinois No. 6 coal since an increase in salt concentration produced results which were opposite to those produced in the case of the more hydrophobic coals. One plausible explanation is that the Illinois No. 6 coal adsorbed hydrated sodium ions from the salt solution which made the coal particles more hydrophilic. This would increase the induction time and reduce the agglomeration recovery. Adsorption of sodium ions could likely be due to the presence of oxygen functional groups on the surface of the coal. It is well known that Illinois No. 6 coal has a higher oxygen content than the more hydrophobic coals. Therefore, it would have a greater affinity to adsorb sodium ions.

Pyrite is also known to adsorb sodium ions, with the quantity adsorbed being proportional to the concentration in solution (14). As in the case of Illinois No. 6 coal, this could explain why the pyrite induction time increased and agglomeration recovery decreased when the salt concentration was increased (see Figure 3). Although the curves for pyrite in Figure 3 appeared similar to those for Illinois No. 6 coal in Figure 2, the pyrite was less hydrophobic than the coal. Since pyrite is much denser than coal, smaller particles had to be used for measuring induction time. Because of differences in density and particle size, the induction time of pyrite is therefore not directly comparable with that of the carbonaceous materials. However, the induction time for pyrite was relatively high. Also the agglomeration recovery of pyrite was relatively low, even when 50 v/w % heptane was used.

The opposing influences of salt concentration on the agglomeration recovery of pyrite and Upper Freeport coal suggested a series of experiments in which a mixture of these materials was agglomerated with heptane. The results which were presented in an earlier publication (8) show that coal recovery increased and pyrite recovery decreased as the salt concentration was raised (see Figure 4). Thus the results achieved with the mixture corresponded well with the results of agglomerating the materials separately. Also shown in Figure 4 is the separation efficiency as defined below:

$$\text{Sepn. Eff. } (\%) = \text{Coal Recov. } (\%) - \text{Pyrite Recov. } (\%)$$

It can be seen that the separation efficiency increased with salt concentration until the concentration reached 1.5 M and then remained constant. When a similar set of agglomeration experiments was conducted with a mixture of Illinois No. 6 coal and pyrite, the results were surprising in that the recovery of pyrite was greater than the recovery of coal (see Table 3). On the other hand, when salt was added to the system, the recovery of both materials decreased as expected and the separation suffered.

Conclusions

When aqueous particle suspensions of graphite or various types of coal were agglomerated individually with heptane, the recovery correlated well with the measured induction time which seemed to reflect the natural hydrophobicity of the

Table 3. Results of agglomerating a mixture of Illinois No. 6 coal (5 g) and pyrite (5 g) with heptane

Heptane ml	NaCl M	Final pH	Recovery, % Coal	Recovery, % Pyrite	Separation Eff., %
0.5	0	4.3	15	47	-32
1.0	0	4.3	27	73	-46
2.0	0	4.2	37	87	-50
0.5	1.5	4.1	12	28	-16
1.0	1.5	4.1	19	40	-21
2.0	1.5	4.0	23	43	-20

material. A close correspondence between agglomeration recovery and induction time was also observed in other experiments in which the carbonaceous materials or pyrite were suspended separately in salt solutions of various concentrations. In these experiments, increasing salt concentrations enhanced the recovery and shortened the induction time of highly hydrophobic solids but reduced the recovery and lengthened the induction time of weakly hydrophobic solids. The effect of salt concentration on the highly hydrophobic solids appeared to be due to compression of the electrical double layer surrounding individual particles, whereas the effect on weakly hydrophobic particles seemed to be due to adsorption of hydrated cations. Because of these differing effects, it was possible to improve the separation of highly hydrophobic Upper Freeport coal and pyrite by increasing the salt concentration of the agglomeration system, but it was not possible to improve the separation of weakly hydrophobic Illinois No. 6 coal and pyrite.

Acknowledgement

Ames Laboratory is operated for the U.S. Department of Energy by Iowa State University under contract No. W-7405-Eng-82. This work was supported by the Assistant Secretary for Fossil Energy, through the Pittsburgh Energy Technology Center.

Literature Cited

1. C. E. Capes and J. R. Germain, "Selective Oil Agglomeration in Fine Coal Beneficiation," Chapter 6 in: Physical Cleaning of Coal, Y. A. Liu (ed.), Marcel Dekker, New York, 1982.

2. V. P. Mehrotra, K. V. S. Sastry and B. W. Morey, "Review of Oil Agglomeration Techniques for Processing of Fine Coals," International Journal of Mineral Processing, 11, 175-201 (1983).

3. T. D. Wheelock and R. Markuszewski, "Coal Preparation and Cleaning," Chapter 3 in: The Science and Technology of Coal and Coal Utilization, B. R. Cooper and W. A. Ellingson (eds.), Plenum Press, New York, 1984.

4. W. G. Steedman and S. V. Krishnan, "Oil Agglomeration Process for the Treatment of Fine Coal," Chapter 8 in: Fine Coal Processing, S. K. Mishra and R. R. Klimpel (eds.), Noyes Publications, Park Ridge, New Jersey, 1987.

5. R. Venkatadri, R. Markuszewski, and T. D. Wheelock, "Oil Agglomeration of Weakly Hydrophobic Coals and Coal/Pyrite Mixtures," Energy & Fuels, 2 (2), 145-150 (1988).

6. Z. Sadowski, R. Venkatadri, J. M. Druding, R. Markuszewski, and T. D. Wheelock, "Behavior of Oxidized Coal during Oil Agglomeration," Coal Preparation (in press).

7. G. C. C. Yang, R. Markuszewski and T. D. Wheelock, "Oil Agglomeration of Coal in Inorganic Salt Solutions," Coal Preparation, 5 (3-4), 133-146 (1988).

8. C.-W. Fan, R. Markuszewski, and T. D. Wheelock, "Coal and Pyrite Separation by Oil Agglomeration in Salt Solutions," Fizykochemiczne Problemy Mineralurgii, 19, 17-26 (1987).

9. J. L. Yordan and R. H. Yoon, "Induction Time Measurements for the Quartz-Amine Flotation System," Preprint No. 86-105 for Society of Mining Engineering Annual Meeting, New Orleans, March 2-6, 1986.

10. Y. Ye and J. D. Miller, "Bubble/Particle Contact Time in the Analysis of Coal Flotation," Coal Preparation, 5, 147-166 (1988).

11. Y. Ye, S. M. Khandrika and J. D. Miller, "Induction-Time Measurements at a Particle Bed," presented at 117th AIME Annual Meeting, Phoenix, Arizona, Jan. 25-28, 1988.

12. J. Laskowski and J. Iskra, "Role of Capillary Effects in Bubble-Particle Collision in Flotation," Transactions Institution Mining and Metallurgy, Sec. C Mineral Processing and Extractive Metallurgy, 79, C6-C10 (1970).

13. J. Drzymala, R. Markuszewski and T. D. Wheelock, "Influence of Air on Oil Agglomeration of Carbonaceous Solids in Aqueous Suspension," International Journal of Mineral Processing, 18, 227-286 (1986).

14. A. M. Gaudin and W. D. Charles, "Adsorption of Calcium and Sodium on Pyrite," Transactions of AIME, 196, 195-200 (1953).

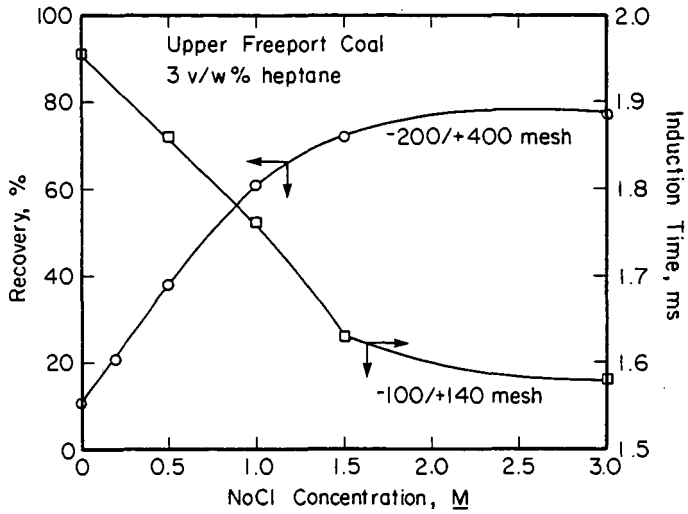

Figure 1. Effect of salt concentration on Upper Freeport coal recovery and induction time.

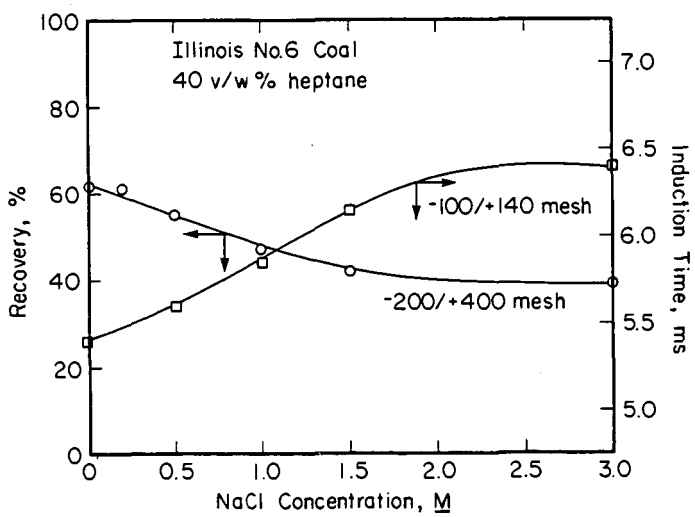

Figure 2. Effect of salt concentration on Illinois No. 6 coal recovery and induction time.

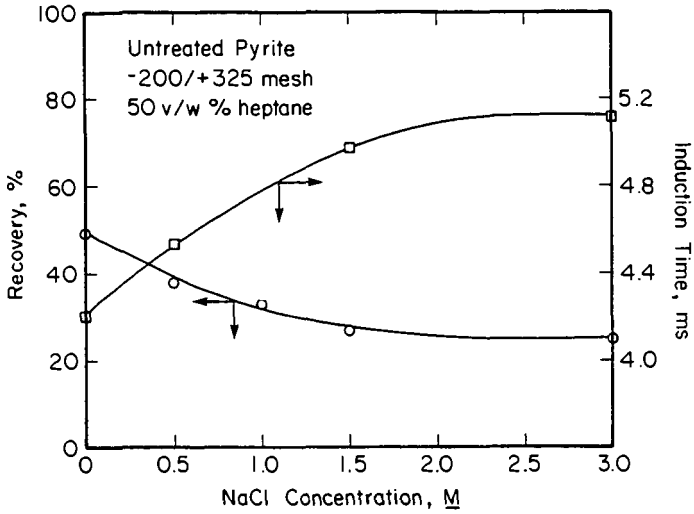

Figure 3. Effect of salt concentration on mineral pyrite recovery and induction time.

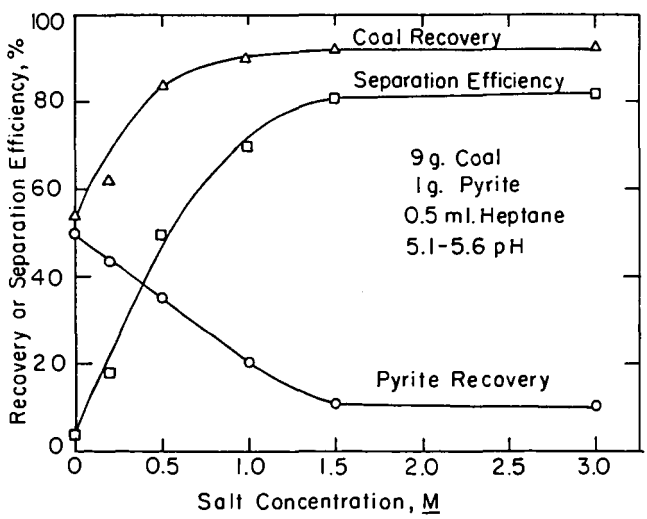

Figure 4. Results of agglomerating a mixture of Upper Freeport coal and pyrite (Ref. 8).

Surface Properties of Coal-Oil Agglomerates in the Floc Regime

K. Darcovich, C.E. Capes* and F.D.F. Talbot

Department of Chemical Engineering, University of Ottawa, Ottawa, Ontario, Canada, K1N 9B4

**National Research Council of Canada, Division of Chemistry, Chemical Engineering Section, Ottawa, Ontario, Canada, K1A OR6*

1 Introduction

Agglomeration processes bring together fine powders into larger masses in order to improve powder properties. In conventional coal mining procedure, much of the fine coal (typically -100 mesh) is rejected with tailings as it is impractical to recover. Due to the heterogeneous nature of coal, smaller particles tend to be individually richer in ash or carbonaceous matter compared to the overall composition of the coal. This discretization facilitates effective separation. The tailings are handled in water slurry form and in an agglomeration/separation treatment, an immiscible oil phase (usually any liquid hydrocarbon of size C_7 or greater) is added under high-shear mixing conditions to enhance surface wetting. The oil selectively adheres to the carbonaceous surfaces and also acts as a bridging liquid to consolidate several oiled coal particles into an enlarged agglomerate. The ash is excluded and is separated via screening or by selective bubble flotation. [1,2,3] Yield-ash results are shown for the agglomeration flotation of a Pennsylvania coal in Figure 1. [4] The results compare well with other recovery methods.

The agglomerate flotation technique has been known since the turn of the century [5], but to date, there is a considerable gap in understanding of the fundamentals involved. Since the coal-oil agglomerates in this context are a product of an upstream formation process, the material properties of the system are more or less fixed, and work has shown that such properties are favourable for flotation. [6] Flotation performance depends on both hydrodynamic and surface chemical interactions. [7,8]

Thus, it is the objective of this study to investigate the surface properties of a coal-oil agglomerate system to provide a database for subsequent work on their flotation properties.

2 Experimental

The coal selected for this work was a high-grade metallurgical coal provided by the Cape Breton Development Corporation. It contains 2.18% ash by weight (proximate analysis), and hence can be used as is to study its agglomeration properties.

2.1 Agglomerate Preparation

Prior to making any surface property measurements, the procedure for agglomerate preparation had to be established.

Agglomerates were prepared at a 10% pulp density. The coal (density = 1.3 g/cm) was mixed with distilled water and stirred under vacuum in a baffled flask for about 90 minutes to remove complications arising from the presence of air in the system. [9] After de-airing, a required volume of hexadecane was added and the mixing continued for a further thirty minutes to form the agglomerates. Agglomerates were prepared at hexadecane levels ranging from (based on weight percent of coal) 0.25% to 10.0%.

2.2 Surface Tension Measurements

The surface properties of the agglomerates were determined by the adhesion technique. [10,11]

Briefly, this technique involves measuring the extent of particle adhesion to various solid substrates as a function of the composition (surface tension) of the suspending liquid. A water-methanol system was used, since hexadecane is immiscible across their entire binary composition range. [12] Thus the agglomerate structure is not interfered with. Surface tensions of binary water-methanol mixtures span possible coal and/or oil surface tensions. For cases where the surface tension of the suspending liquid differs from the particle surface tension, adhesion should be a function of the substrate surface tension, γ_{SV}. For the case where $\gamma_{LV} = \gamma_{PV}$ the change in free energy due to particle adhesion is zero. Thus the γ_{LV} where the adhesion is not a function of γ_{SV} will be equal to γ_{PV}.

The adhesion method surface tension measurements were carried out as described in detail by Absolom *et al.* [10,11]

Four different polymer film substrates were used to span the possible surface tensions of the coal-oil system. These polymers were polstyrene, sulfonated polystyrene, polyethylene and polyethyleneterephthalate. The adhering agglomerates on these films were then recorded on video tape through a stereo microscope. Using image analysis, the area percent adhesion was determined. Each experiment was duplicated.

2.3 Particle-size distribution Measurements

The particle-size distributions for the agglomerates were obtained using a Malvern model 2600 laser diffraction particle-size analyser. This instrument measures the largest dimension of the particles as they are instantaneously positioned in the laser path, and determines an average over at least 500 pulses. Several measurements were made at each oil level.

Additionally, the particle-size distributions of agglomerates were determined suspended in a mixture of 95% CH_3OH and 5%H_2O, at several oil levels to verify that the methanol in the suspending liquid did not influence the particle-size distributions.

3 Results

Results were obtained for the surface tension of the agglomerate particles and the particle-size distributions at several oil levels.

3.1 Surface Tension Results

The adhesion method was employed to determine the surface tension of hexadecane-coal agglomerates at several oil levels. The procedure outlined in [10] was used to determine γ_{PV} at each oil level. Figure 2 shows the agglomerate surface tensions versus oil level. The surface tension of the unoiled coal was 62.0 dyne/cm, in agreement with other published results for bituminous coal. [10,13,14] At 10 weight% oil, the agglomerate surface tension closely approximates that of pure hexadecane.

3.2 Particle-Size Distribution Results

Figure 3 shows the agglomerate particle-size distributions for each measured oil level. The mean particle-size of the unagglomerated coal is 33 μm. As one would expect, the mean size increases as more oil is added to the system.

4 Discussion

In light of the dependence of the surface tension and the mean size of the agglomerates on oil level, the corresponding three-phase contact angles and bond volumes were evaluated.

4.1 Determination of the Three-Phase Contact Angle

Measured and tabulated surface tension values were used along with an equation of state approach to determine the three-phase contact angle. The addition of

adsorbing oil was not considered to have caused a step change in the agglomerate surface properties at low oil levels since problems such as incomplete wetting and surface roughness [15] will contribute some coal character to the surface.

Neumann *et al.* [16,17,18] have developed an equation of state relating an interfacial tension to two known surface tensions. This is coupled with Young's Equation to determine the system.

Neumann's surface tension equation of state is,

$$\gamma_{SL} = \frac{(\sqrt{\gamma_{SV}} - \sqrt{\gamma_{LV}})^2}{1 - 0.15\sqrt{\gamma_{SV}\,\gamma_{LV}}} \tag{1}$$

and Young's equation,

$$\gamma_{SV} - \gamma_{SL} = \gamma_{LV}\cos\theta \tag{2}$$

Equation 1 gives interfacial tensions for the coal, oil and water system at each agglomerate oil level. Now using equation 2, the three-phase contact angle can be calculated. In Figure 4, the three-phase contact angle is plotted against the agglomerate oil level.

4.2 Calculation of Bond Volumes

It has been shown that bonding structure of agglomerates is determined by the volume ratio of binding liquid to solid present in the system. At the binder levels considered in this work, the bonding should be exclusively pendular. [19,20] Pendular bonds are discrete lens-shaped rings at the point of contact of two particles. With different three-phase contact angles at the different oil levels, the oil bond profile will vary. If the effect of gravity is neglected, the binder-liquid interface will assume a profile of constant curvature and thus can be represented by an arc of a circle of radius b. (Figure 4, inset)

The meridian angle, θ_m can have a maximum size of 45° in the pendular regime, or else neighbouring bonds will coalesce. Now assume the particle has a unit radius, defined by the equation $x^2 + (y-1)^2 = 1$. With θ_m equal to 45°, the three-phase junction will occur at the point $x = 1/\sqrt{2}, y = 1 - 1/\sqrt{2}$.

The meniscus surface can be defined by an arc of a circle defined as,

$$(x-a)^2 + y^2 = b^2 \tag{3}$$

Equation 3 along with the particle profile and θ_C determine the parameters a and b. Thus for a given contact angle, the meniscus profile is defined.

The absolute bond volume, V_{BA}, can be then taken as a volume of revolution of the meniscus area. Let the meniscus surface be $\mathcal{F}_2(y)$ and the particle surface be $\mathcal{F}_1(y)$. y_c is the three-phase contact point y-coordinate.

$$V_{BA} = 2\pi\int_0^{y_c} [\mathcal{F}_2(y)]^2\,dy - 2\pi\int_0^{y_c} [\mathcal{F}_1(y)]^2\,dy \tag{4}$$

Equation 4 was integrated numerically with a 15-point Gaussian quadrature routine. The bond volume as a function of contact angle is plotted in Figure 4. Newitt and Conway-Jones [20] define the bond volume as a function of meridian angle θ as,

$$V_{BA} = 2\pi r^3(\sec\theta - 1)^2[1 - (\frac{\pi}{2} - \theta)\tan\theta] \tag{5}$$

The V_{BA} calculated for $\theta_C = 0°$ is exactly the same result as predicted by equation 5. Define V_{OB} as the ratio of V_{BA} to the volume of two particles.

4.3 Interdependence of the Surface Tension, Oil Level and Enlargement Factor

An informative way of expressing agglomeration data is with an enlargement factor, F. F can be defined as,

$$F = \frac{d_p}{d_{p_o}} \tag{6}$$

where d_p is a mean agglomerate diameter at a given oil level and d_{p_o} is the mean diameter of the unagglomerated coal.

Figure 5 shows F plotted against oil level.

Assume that at low oil levels, only single particles and doublets will contribute to the resulting enlargement factor. Now say that there are n particles and one of them is double size (an agglomerate). Thus,

$$F - 1 = \frac{1}{n} \quad \text{or,} \quad n = \frac{1}{F-1} \tag{7}$$

One bond will exist for every $n + 1$ individual particles, so the fraction of the total solid volume that is bonded in doublets, V_{SB}, is,

$$V_{SB} = \frac{2}{n+1} \tag{8}$$

Thus the bonding volume of oil, V_{OB}, relative to the volume of the two bonded particles is,

$$V_{OB} = \frac{V_O(n+1)}{2} \tag{9}$$

where V_O is the total volume of oil expressed as a fraction of the total solids volume. However, for a given volume of solids, the oil will first be consumed in wetting the solid surface, then any excess will be used up in forming bonds. The total oil volume, V_O, will be composed of two parts, a bonding volume, V_B, and a wetting volume V_W. Thus, V_B is substituted for V_O in equation 9 to account for the wetting volume.

It is of interest to determine how the oil distributes itself to bring about the observed agglomeration results.

Recall equation 9. Since $1/n = F - 1$, it may be re-expressed as,

$$V_{OB} = \frac{V_B F}{2(F-1)} \tag{10}$$

Assume that at low oil levels only pendular bonds will exist. Thus the volume of one bond V_{OB}, is known and can be used to calculate V_B and V_W. Assuming V_W is constant for all oil levels, equation 10 may be used to determine the bond volume per particle pair.

Denote V_{OB} from equation 10 as real volume V_R, and V_T as the theoretical volume. The ratio V_R/V_T will give a mean value of bonds per particle. If $V_R/V_T > 1$, then this implies that agglomerates larger than doublets exist. Figure 5 shows this ratio plotted versus oil level. One may note the similarity between Figures 5 and 2. At an oil level of about 1 to 2 weight%, the slopes on these plots significantly change. The underlying reason for this change should be a fundamental change in the agglomerate structure. Based on the size data and the surface approximating that of hexadecane, it appears that beyond 2 weight% oil, larger, more compact agglomerates are formed.

A number of factors constrain the system. The result must conform to a mass balance of solids, an oil balance, and a weighted sum of various agglomerate sizes that accounts for the observed size. A system of three linear equations may be written which determine the distribution of singlets, doublets and triplets at each oil level based on the above criteria. They may be expressed as follows,

$$\begin{aligned} a_{11}q_1 + a_{12}q_2 + a_{13}q_3 &= F \\ a_{21}q_1 + a_{22}q_2 + a_{23}q_3 &= 1 \\ a_{31}q_1 + a_{32}q_2 + a_{33}q_3 &= V_B \end{aligned} \tag{11}$$

where the q_i's are the fraction of singlets, doublets and triplets, the a_{1i}'s are the mean size of each type of agglomerate, the a_{2i}'s are all equal to 1 by mass balance and the a_{3i}'s are the bond volumes per agglomerate based on the oil level.

This system of equations was solved and it gave positive element solution vectors up to 2 weight% oil. At that point, the number of doublets predicted was negative (physically impossible) thereby indicating agglomerates larger than doublets are present which require substantially more oil due to the increased number of bonds per agglomerate.

The system was remodeled to include four-particle agglomerates that were considered to be in tetrahedral form having six bonds. This required an additional linear equation, and one was formulated based on the strength of the agglomerates. Consider each agglomerate in terms of the probability that it will break up, P_b. In general P_b should be proportional to the inverse of the number of bonds present. That is,

$$P_b \propto \frac{1}{nb}$$

where n is the number of bonds in the agglomerate and b is the bond strength. The probability of break-up of the singlet may be expressed as $k_0 b$, where k_0 is some unknown constant. Thus for singlets through quadruples we have,

$$P_b = k_0 q_1 b + \frac{q_2}{b} + \frac{q_3}{3b} + \frac{q_4}{6b} \tag{12}$$

The strongest system, or minimum probability of break-up will occur when,

$$\frac{\partial P_b}{\partial b} = k_0 q_1 - \frac{q_2}{b^2} - \frac{q_3}{3b^2} - \frac{q_4}{6b^2} = 0 \tag{13}$$

Rewriting equation 13 we obtain,

$$k_0 b^2 q_1 - q_2 - \frac{q_3}{3} - \frac{q_4}{6} = 0 \tag{14}$$

In this form, the coefficient a_{41} of the new 4×4 matrix is indeterminate. However, in view of the agglomerate data, it can be assumed that at 1 weight% oil, the solution element q_4 will be zero and a_{41} can be calculated from the 3×3 system results. The 4×4 system was then solved and gave positive solution element vectors from 1 weight% through 10 weight% oil. Interestingly, the 4×4 system predicts essentially the same distribution of sizes at 2 weight% oil as does the 3×3 system, indicating that the omission of quadruples from the model at very low oil levels is justified.

Figure 6 is a plot of the frequency of each agglomerate size versus oil level as calculated by the system of linear equations. It can be seen from Figure 6 that the frequency of singlets as a function of oil level is a smooth curve supporting the above assumptions.

The above development was also calculated with the assumption of a zero contact angle at the three-phase interface, as assumed in previous papers. [21,22] The results predicted overly large particles at low oil levels as the zero contact angle bond is about half the volume of the finite contact angle bond. Correspondingly the wetting volume with a zero contact angle was found to be much larger as well.

5 Conclusions

The adhesion surface tension method and a laser diffraction particle sizer provided means of measuring respectively the surface tension and particle-size distributions of agglomerates formed from metallurgical coal and n-hexadecane in an aqueous suspension of the agglomerates.

From this study it can be said that the amount of oil introduced to a coal-water slurry for forming agglomerates determines several properties on the agglomerate surface. The net agglomerate surface tension was found to approach that of the pure oil at increased oil levels, and as such the three-phase contact

angle between the agglomerate, the oil meniscus and the suspending water decreased. Thus at oil levels below 2 weight%, the bond volumes were great enough to consume the available oil in forming agglomerates no larger than doublets and triplets. With smaller contact angles at higher oil levels, the particle bonding is more economical and larger more compact oil-wetted agglomerates are seen. A constraining system of linear equations was developed to illustrate this.

A more complete analysis would involve a statistical approach encompassing the entire particle-size distribution instead of the mean particle size used here.

References

[1] Capes, C.E., Coleman, R.D., Croteau, S., Jonasson, K., Thayer, W.L., *Agglomerate recovery methods and yield-impurity relationships in oil agglomeration*, *Proc. Coal Liq. and Alternative Fuel Tech. Meeting*, Halifax, NS, Sept. 29-Oct. 3, (1986).

[2] Wojcik, W., Al Taweel, A.M., *Powder Tech.*, 40, (1984), pp. 179-185.

[3] Hirajima, T., Chan, E., Whiteway, S., Stefanski, M., Stewart, I., *Coal Prep.*, 5, (1987), pp. 85-108.

[4] Capes, C.E., Coleman, R.D., Thayer, W.L., in World Congress III of Chemical Engineering, Tokyo (1986), vol. 1, paper 6b-301, pp. 525-528.

[5] Froment, A., *U.K. Patent No. 12,778*, June 4, (1902).

[6] Brown, D.J., in Aerodynamic Capture of Particles, E.G. Richardson (Ed.), Pergamon Press, London, (1960), pp. 35-43.

[7] Sutherland, K.L., *J. Phys. Chem.*, 52, (1948), pp. 394-425.

[8] Deryagin, B.V., Dukhin, S.S., Rulev, N.N., *Surf. and Coll. Sci.*, 13, (1984), pp. 71-113.

[9] Drzymala, J., Markuszewski, R., Wheelock, T.D., *Int. J. Mineral Process.*, 18, (1986), pp. 277-286.

[10] Absolom, D.R., Eom, K., Vargha-Butler, E.I., Hamza, H.A., Neumann, A.W., *Coll. and Surf.*, 17, 2, (1986), pp. 143-157.

[11] Absolom, D.R., Zingg, W., Thomson, C., Policova, Z., Van Oss, C.J., Neumann, A.W., *J. Coll. Intf. Sci.*, 104, 1, (1985), pp. 51-59.

[12] Stephen, H., Stephen, T., Solubilities of Inorganic and Organic Compounds, Volume 2: Ternary and Multicomponent Systems, Part 2, No. 5160, p. 1740.

[13] Vargha-Butler, E.I., Kashi, M., Hamza, H.A., Neumann, A.W., *Coal Prep.*, 3, (1986), pp. 53-75.

[14] Sablik, J., *Pol. J. Chem.*, 59, 4, (1985), pp. 433-438.

[15] Pietsch, W.B., *Nature*, 217, (1968), pp. 736-737.

[16] Neumann, A.W., Good, R.J., Hope, C.J., Sejpal, M., *J. Coll. Intf. Sci.*, 49, 2, (1974), pp. 291-304.

[17] Neumann, A.W., Absolom, D.R., Francis, D.W., van Oss, C.J., *Sep. Purif. Methods*, 9, 1, (1980), pp. 69-163.

[18] Spelt, J.K., Absolom, D.R., Neumann, A.W., *Langmuir*, 2, 5, (1986), pp. 620-625.

[19] Germain, R.J., Masters Thesis, U. of Waterloo, (1977), 93 pp.

[20] Newitt, D.M., Conway-Jones, J.M., *Trans. Instn. Chem. Engrs.*, 36, (1958), pp. 422-442.

[21] Rumpf, H., in Agglomeration, Intl. Symp., W.A. Knepper, (Ed.), Philadelphia, PA, Apr. 12-14, (1961), pp. 379-418.

[22] Capes, C.E., Germain, R.J., in Drying '80, Hemisphere Publ. Corp., New York, (1980), v. 2, pp. 460-466.

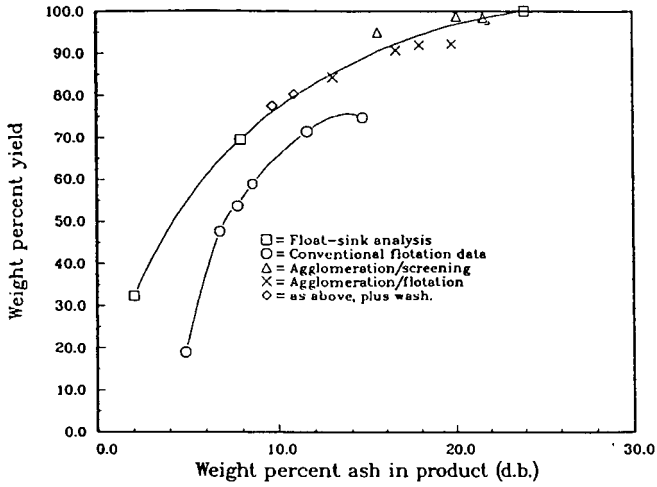

Figure 1: Yield-ash results for a minus 28 run of mine coal from Pennsylvania. (Wt.% reagent levels are based on feed solids).

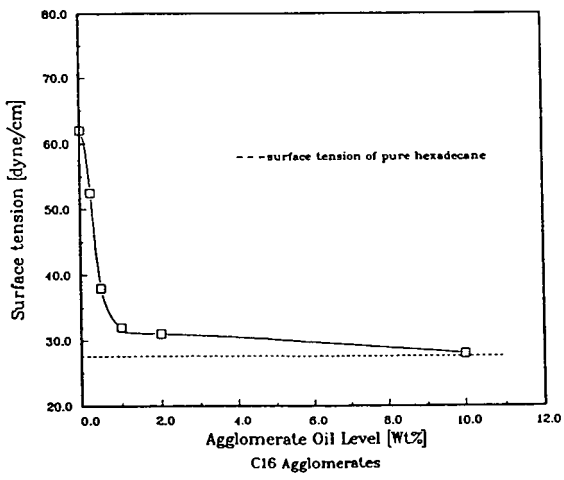

Figure 2: Agglomerate Surface Tension vs. Oil Level

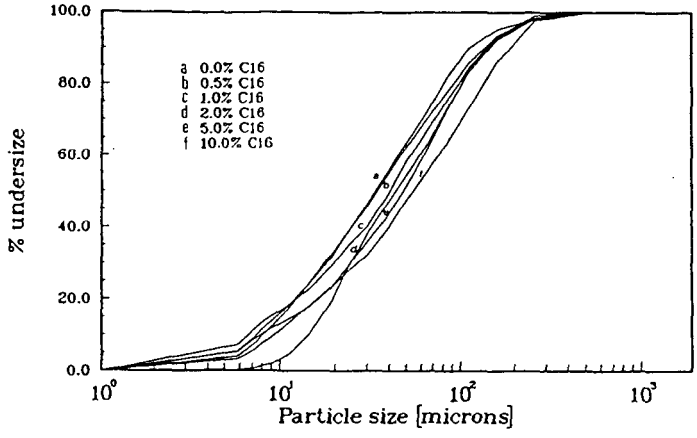

Figure 3: Particle-size distributions of agglomerates for n-$C_{16}H_{34}$ levels from 0 to 10 weight%

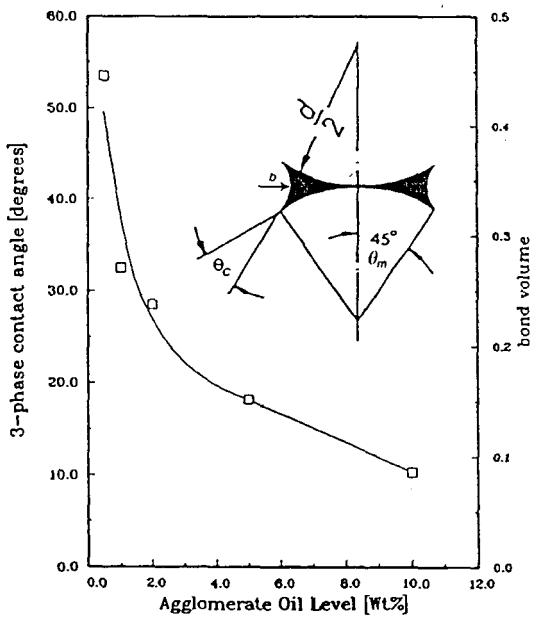

Figure 4: θ_C and V_{BA} vs. Oil Level.
- inset is schematic of 3-phase contact angle in particle-bonding context

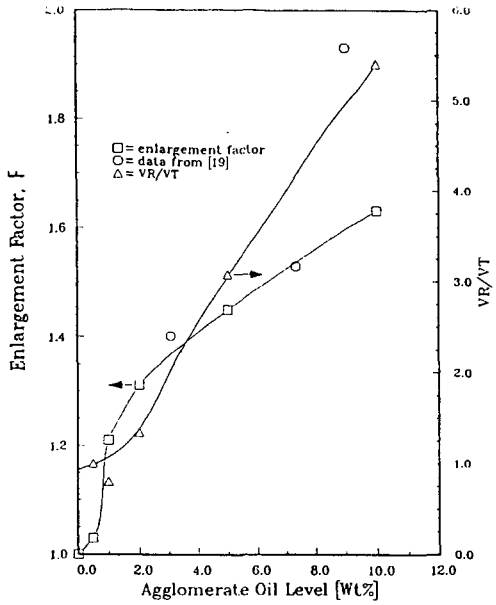

Figure 5: Enlargement Factor and V_R/V_T vs. Oil Level

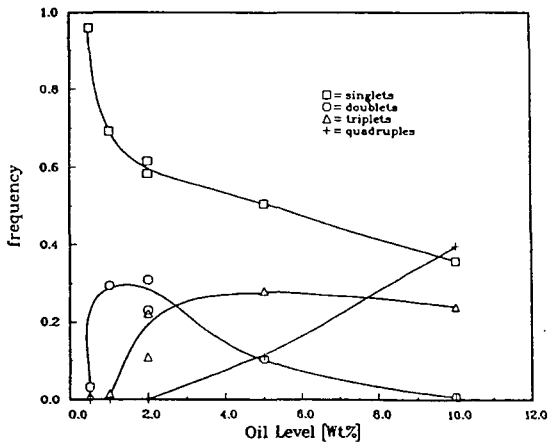

Figure 6: Agglomerate Size Frequency vs. Oil Level

INTERFACIAL PROPERTIES OF LIGNITE, GRAPHITE, KAOLIN, AND PYRITE

S.H. Chiang, Alec Richardson, Anni Wong

Chemical/Petroleum Engrng. Dept., University of Pittsburgh
Pittsburgh, PA 15261

This project consists of four major experiments, in which the surface/interfacial and adsorption properties, particle size, and specific surface area of Lignite (35-, 200-, and 400-mesh), Graphite Powder, Kaolin, and Pyrite, are measured. The first two experiments are minor and yield preliminary results that are combined with later results for specific purposes. These experiments involve measuring the external specific surface area of the six powdered samples using the BET volumetric adsorption apparatus with N_2 as the adsorbate, and measuring five average characteristic particle diameters and the particle size size distribution of these samples with the Omnicon Alpha Particle Field Image Analyzer. From these results, a correlation is determined between particle size and specific surface area. The third experiment involves obtaining the adsorption and desorption isotherms of the samples and determining the effect of pressure, temperature, particle size, and intrinsic nature of the coal mineral on these isotherms. Adsorption isotherms per unit weight and per unit surface area (in conjunction with the surface area results of the BET experiment) of adsorbent are determined with the CO_2 gravimetric spring adsorption apparatus. The relative film pressure, which is proportional to the area under the equilibrium adsorption isotherm on a semilogarithm plot, is also estimated.

Finally, the fourth experiment consists of two parts: 1) The pendant drop method, involving a water pendant drop in the presence of a $CO_2(g)$ or $CO_2(l)$ medium, in which the liquid-vapor and liquid-liquid interfacial tensions are measured as functions of CO_2 pressure (relative to its saturation pressure), temperature, and CO_2 phase used, based on the drop's physical dimensions at equilibrium. 2) The sessile drop method, involving a water sessile drop in equilibrium on a pelletized sample of the coal mineral in a $CO_2(g)$ or $CO_2(l)$ environment. In this three-phase system, the equilibrium advancing contact angle of the drop is measured as a function of CO_2 relative pressure, temperature, and CO_2 phase for each of the six samples. Then, with the preliminary particle size and surface area data, a correlation is drawn between the contact angle and particle size/intrinsic nature of the sample. Using the

contact angle and pendant drop data, the solid-vapor and solid-liquid interfacial tensions are calculated as functions of the above system parameters, using Young's equation and the thermodynamic equation of state:

$$\gamma_{sv} = \gamma_{sl} + \gamma_{lv} \cos\theta \qquad 1)$$

$$\gamma_{sl} = [(\gamma_{sv})^{0.5} - (\gamma_{lv})^{0.5}]^2/[1 - 0.015(\gamma_{sv}*\gamma_{lv})^{0.5}] \qquad 2)$$

Then the works of adhesion and cohesion are calculated from Dupre's relation; and the equation of Boyd and Livingston is used to calculate the equilibrium spreading coefficient, which, like the equilibrium contact angle, is a direct measure of the wetting tendency of the three-phase system under given system conditions:

$$W_{ad} = \gamma_{sv} + \gamma_{lv} - \gamma_{sl} = \gamma_{lv} (1 + \cos\theta) \qquad 3)$$

$$W_{co} = 2\gamma_{lv} \qquad 4)$$

$$S = \gamma_{sv} - (\gamma_{lv} + \gamma_{sl}) = W_{ad} - W_{co} \qquad 5)$$

Then the contact angle and spreading coefficient data are compared for consistency. A system with incomplete wetting is characterized by a high contact angle and negative spreading coefficient at equilibrium; and one with complete wetting is reflected by a zero contact angle and a zero (or positive, indicating the effect of film pressure caused by impurities or an adsorbed vapor film) spreading coefficient. The ultimate objective of this project is to determine the effect of the system parameters (i.e. CO_2 pressure, temperature, CO_2 phase) and nature of the coal minerals (i.e. intrinsic and particle size/surface area) on the relative wettability of the three-phase system of coal mineral-water-CO_2 through an analysis of the interfacial and adsorption properties of the coal minerals.

Results, Discussion, and Conclusions

In the first experiment, involving measurement of the dispersed particle size and size distribution, it is found that all six samples agree in relative magnitude of the five characteristic diameters: Length-, Volume-, Surface-, Surface-Volume-, and Weight-Diameters (Table 1). Pyrite has the largest average diameter of the six samples in all five categories, with the values of 16.9, 30.6, 23.5, 52.7, and 72.5 um, respectively. The sample with the smallest overall particle size is 400-mesh Lignite, with the respective values of 7.5, 12.4, 9.7, 20.6, and 31.1 um. The sizes of the other four samples fall within the ranges of these extreme values. The order of average particle size, from largest to smallest, is determined to be: Pyrite, 35-mesh Lignite, Graphite Powder, Kaolin, 200-mesh Lignite, and 400-mesh Lignite. As expected among the Lignite samples, the 35-mesh sample has the largest particle size; and 400-mesh has the smallest. Prior to this project, the 35-mesh sample is

already provided; and the 200- and 400-mesh samples are prepared by grinding the 35-mesh particles over a controlled time period. Thus, it is concluded that the initial preparation of these samples is successful.

The weight percent and number percent particle size distributions, based on Gaussian and log-normal distribution theory, are also calculated and agree well with the results of the average particle size data. These two curves lie furthest to the right for Pyrite, indicating that the particle size distribution in the Pyrite sample is toward the largest relative sizes. Furthermore, these curves lie farthest to the left for 400-mesh Lignite; and the relative positions of the curves for all the samples agree reasonably well with the order of the average particle sizes of the six samples. The purpose of this experiment is to obtain a relative picture of the particle sizes of the samples, to compare this data with the specific surface area data from the BET experiment to determine a possible correlation, and to later use these results with the interfacial and adsorption results to determine the effect of particle size on the interfacial phenomena of the coal minerals.

From the BET volumetric N_2 adsorption experiment, it is found that Pyrite has the lowest specific surface area of all the samples: 17.4 m^2/g. In contrast, 400-mesh Lignite is found to have the highest value: 21.1. The general order of the samples, from lowest to highest surface area, is: Pyrite (17.4), 35-mesh Lignite (17.8), Graphite Powder (18.1), Kaolin (18.9), 200-mesh Lignite (19.9), and 400-mesh Lignite (21.1). This order is the exact same order as that obtained from the dispersed particle size analysis. Thus, it is concluded that an inverse relationship exists between particle size and specific surface area for the six coal minerals (Table 1). Although this is only a measure of the external (i.e. available) surface area, this relation is still valid because it is safely assumed that, as a sample is ground to smaller particle sizes, the internal surface area (which is found inside micropores) remains constant. Thus, the purpose of this test is coupled with that of the particle size test; and a further purpose is to later use the surface area results to obtain the adsorption/desorption isotherms per unit surface area of adsorbent, from the corresponding isotherm results per unit weight of adsorbent, in order to eliminate the effect of surface area (or particle size) and determine any effect of the solid sample's intrinsic nature on the adsorption properties (i.e. to determine whether adsorption is an extensive or an intensive property.

The goal of the third experiment, using the CO_2 gravimetric spring adsorption apparatus, is to measure the specific amount of CO_2 adsorbate adsorbed on the powdered sample of coal mineral (both per unit weight and unit surface area) as a function of CO_2 relative pressure and temperature for the six samples. Four temperatures (10, 15, 20, and 25°C), and the CO_2 relative pressure in increments of 20% (from 0 to 100%, based on the saturation pressure of CO_2) were tested; and each system parameter was varied independently: CO_2 pressure, temperature, and sample. The specific amount adsorbed ranged from about zero at 0% relative pressure to the order of 0.08 g/g adsorbent (at 10°C) or 0.12 g/g adsorbent (at 25°C) at 100% relative pressure for the six samples. Both the adsorption and desorption isotherms are measured, and it is found in all cases that significant hysteresis occurs, which reflects the energy lost in the adsorption-desorption cycle and hence the "irreversibility" of the process. Figures 1 and 2 show the adsorption/desorption isotherms for 35-mesh Lignite at 10 and 25°C. Similar results are obtained for the other five samples in terms of curve shape and magnitude of hysteresis. The hysteresis is attributed to the pore structure of each of the samples (all of which have mesopores or macropores) and the phenomenon that the vapor pressure of an adsorbate in a pore decreases as the pore size (i.e. radius r) decreases (Kelvin equation):

$$P/Po = \exp(-2V\gamma \cos\theta/rRT) \qquad 6)$$

According to the Ink Bottle Hypothesis, which pictures a pore as having an entrance channel of smaller radius than its bulk volume, adsorption occurs in a pore when the CO_2 relative pressure rises to equal the vapor pressure corresponding to the radius of the "bulk" pore. However, on the desorption curve, as the pressure is reduced, the corresponding desorption does not occur until the pressure reaches a lower value, corresponding to the lower vapor pressure present in the "bottle-neck" of smaller radius, because a meniscus of adsorbate has formed in the bottle-neck. Thus, for a given amount adsorbed, the desorption isotherm lies to the left (i.e. toward lower pressures) of the adsorption isotherm.

This phenomenon also explains the general shape (i.e. concave upward) of the isotherms and the observed change in shape from concave to sigmoidal as the temperature is increased (Figures 1 and 2). Generally, the specific amount adsorbed increases as temperature increases, indicating that some chemisorption (as well as physical adsorption) is present at higher temperatures. The pressure at which the maximum slope of the isotherm occurs decreases as

temperature increases, indicating that the "effective pore radius" decreases: As pore radius decreases, vapor pressure decreases, so that adsorption can occur at lower relative CO_2 pressures; and an increase in temperature increases the vapor pressure in a given pore radius. Since each solid sample is characterized by a pore size distribution, adsorption occurs in different parts of the sample at different pressures, as reflected by the isotherm's shape at equilibrium. The slope is a measure of the increment of adsorption that occurs in response to an increment of CO_2 relative pressure, and thus measures the frequency of pores with a given radius. Thus, for a given sample, it is observed that the adsorption isotherm becomes more sigmoidal (i.e. more like a BET isotherm) as temperature increases: the pressure of maximum adsorption shifts to lower values, indicating that the vapor pressure and "effective" pore size both decrease.

A final observation of this experiment is that the specific amount adsorbed per unit weight of adsorbent increases as particle size decreases (or specific surface area increases) among the six samples and among the three Lignite samples of different particle size. At 20°C and 100% relative pressure, Pyrite showed the lowest specific amount adsorbed (about 0.09 g/g); and 400-mesh Lignite showed the highest amount (about 0.12 g/g). Generally, the order of the amount adsorbed corresponded to the order of specific surface area (or inverse order of particle size) for the six samples at a given temperature and CO_2 pressure (Tables 2 and 3). Finally, these results (per unit weight of adsorbent) are divided by the specific surface area of the corresponding sample (from the BET results) to obtain the adsorption isotherms per unit surface area of adsorbent at each temperature and CO_2 pressure. It is found that this specific amount adsorbed varied very little amoung the six samples, indicating that the intrinsic nature (i.e. hydrophobicity) of the sample has a very little effect on its adsorption properties. Thus, it is concluded that adsorption at equilibrium is an extensive property (i.e. depends on the amount of sample, or the availibility of surface area).

The final experiment involves measuring the equilibrium advancing contact angles and several types of interfacial tension as a function of sample, CO_2 pressure, temperature, and CO_2 phase. As before, each parameter is varied independently to isolate its effect on the interfacial properties. Four temperatures (10, 15, 20, and 25°C) and CO_2 relative pressure in increments of 25% (from zero to 100%) are tested; and $CO_2(g)$ and $CO_2(l)$ are used separately. In

the pendant drop experiment, it is found that the liquid-vapor interfacial tension (Table 4) decreases dramatically as pressure increases (i.e. at 25°C: from 72.03 dyne/cm at 0% to 33.01 dyne/cm at 100% relative CO_2 pressure), decreases slightly with temperature (i.e. at 100% relative pressure: from 35.38 dyne/cm at 10°C to 33.01 dyne/cm at 25°C), and decreases significantly as a switch is made from $CO_2(g)$ to $CO_2(l)$. For example, at 10°C, the tension decreases from 35.38 to 27.09 dyne/cm when the switch is made to $CO_2(l)$. These changes are reflected by the changes in the pendant drop's equilibrium physical dimensions (De, Ds, S = De/Ds, and Hs = f(S)) and by the change in density difference ($p_2 - p_1$) between the water drop and surrounding CO_2 medium. The physical picture is explained mathematically by Laplace's equation of capillarity and the criteria that the surface and gravitational forces are equal at equilibrium:

$$P'' - P' = \gamma \cos\theta (1/r_1 - 1/r_2) = 2\gamma \cos\theta / r \qquad 7)$$

$$Fg = mg = pVg = pg(4/3\,\pi r^3) = 2\pi r \gamma = Fs \qquad 8)$$

Recognizing the nature of curved surfaces, an increase in pressure or temperature decreases the pressure difference across the curved interface and thus decreases the surface force and hence the interfacial tension. As the pendant drop grows in radius, gravitational force increases more rapidly than the surface force. Because of the depressed surface force, the drop has smaller dimensions and a lower interfacial tension at equilibrium, as a result of a pressure or temperature increase. When the switch is made from $CO_2(g)$ to $CO_2(l)$, the density difference between the water drop and CO_2 phase decreases; $CO_2(l)$ has a density comparable to (but still less than) that of water (0.80 vs. 1.00 g/cm^3 at 25°C), as compared to $CO_2(g)$. According to Andreas, Hauser, and Tucker, the interfacial tension in this two-phase system is proportional to this density difference:

$$\gamma = g\,(p_2 - p_1)\,De^2/Hs \qquad 9)$$

Thus, a decrease in interfacial tension is expected when a switch is made from $CO_2(g)$ to $CO_2(l)$ at 100% CO_2 relative pressure.

In the sessile drop experiment, the equilibrium advancing contact angle is measured versus CO_2 pressure, temperature, and CO_2 phase. Generally, it is found that the contact angle increases when: CO_2 pressure increases, temperature decreases, or $CO_2(l)$ is used. These trends can similarly be explained by the above argument, Laplace's equation, and the equilibration of surface and gravity forces at equilibrium. According to Padday, a sessile drop is in equilibrium when the top is flat and at maximum height. For most samples, except the hydrophobic Graphite Powder, the contact angles at all temperatures are

essentially zero at relative pressures less than 50%, indicating a completely wettable system. Thus, the optimal system conditions for enhancing incomplete wetting for a given sample are a high pressure (preferably 100%), low temperature, and the use of $CO_2(l)$ as the surrounding medium. It is also found that, among the Lignite samples, contact angle increases when particle size decreases. At 10°C and 100% relative pressure, the average contact angle values for 35-mesh, 200-mesh, and 400-mesh Lignite are, respectively: 87.50°, 96.25°, and 107.50° with $CO_2(g)$; and 103.75°, 117.50°, and 128.75° with $CO_2(l)$.

Furthermore, among all six samples, no correlation is found between particle size and equilibrium contact angle. Graphite Powder, known to be hydrophobic in nature, is found to have the largest overall contact angle values, ranging (at 10°C) from 90.00° at 25% to 147.50° at 100% with $CO_2(g)$, and 152.50° with $CO_2(l)$. Thus, Graphite Powder is the most incompletely wettable sample. Pyrite shows more intermediate contact angle values, its highest value being 95.00° at 10°C with $CO_2(l)$, and is found to have the second lowest average contact angle at a given temperature, CO_2 pressure, and CO_2 phase. The sample with the lowest average value (i.e. the most hydrophilic sample) is the clay-like Kaolin, which shows a zero contact angle (i.e. complete wetting) even up to 100% relative pressure with $CO_2(g)$. Its largest value is 30.00°, at 10°C with $CO_2(l)$. Thus, the general order of wetting is, from complete to incomplete: Kaolin, Pyrite, Lignite (35-mesh, 200-mesh, 400-mesh), and Graphite Powder, because the magnitude of the equilibrium advancing contact angle is inversely related to the tendency of a three-phase system toward complete wetting. Thus, contact angle is found to be an intensive property, because it depends not only on particle size (or specific surface area) but also on the sample's intrinsic nature (i.e. hydrophobicity).

Using the two-phase equilibrium interfacial tension and contact angle data, the solid-vapor and solid-liquid interfacial tension are calculated using Equations 1 and 2. It is generally found that the solid-vapor tension first decreases and then increases with pressure. This is explained by the fact that complete wetting (i.e. a zero contact angle) is predominant at the lower relative pressures, and film pressure is still negligible; thus, the solid-vapor tension is first constant or decreasesightly. At higher pressures, incomplete wetting sets in; and film pressure (i.e. the presence of an adsorbed vapor film on the solid surface) becomes significant. Thus, based on the interfacial tension of a clean, pure solid in a vacuum, the solid-vapor tension increases with pressure to reflect the

film pressure increase. Generally, as incomplete wetting becomes significant, the solid-vapor tension increases. This argument also explains the observation that this tension increases when the switch is made from $CO_2(g)$ to $CO_2(l)$ at a given temperature.

This tension is also found to be relatively constant with temperature as a result of the cancellation effect of temperature on contact angle and the liquid-vapor tension in Young's equation: As temperature increases, θ decreases, cos θ increases, and the liquid-vapor tension decreases; so the product $\gamma_{lv} \cos\theta$ is essentially constant with temperature. Among the six samples, the solid-vapor tension is lowest for Kaolin (about 88.0 dyne/cm with $CO_2(l)$) and highest for Graphite Powder (about 107.0 dyne/cm with $CO_2(l)$). The order of magnitude for this tension (averaged over the four temperatures) is, in increasing order: Kaolin (88.0 dyne/cm), Pyrite (99.0 dyne/cm), 35-mesh Lignite (101.0 dyne/cm), 200-mesh Lignite (102.5 dyne/cm), 400-mesh Lignite (104.5 dyne/cm), and Graphite Powder (107.0 dyne/cm). This is the same order of increasing contact angle and of decreasing wettability. Thus, among the Lignite samples, this tension decreases as particle size increases. Like the contact angle, the solid-vapor interfacial tension is an intrinsic property, because it depends on contact angle.

Another interfacial tension that is calculated is the solid-liquid tension, which is found to increase with CO_2 pressure continuously (because of the corresponding increase in contact angle and decrease in the system's wetting tensency, and the insignificant effect of film pressure on this tension), remain constant with temperature (because the term $\gamma_{lv} \cos\theta$ is essentially constant with temperature), and increases when $CO_2(l)$ is used (because of the enhancement of incomplete wetting). It is observed among the Lignite samples that the solid-liquid tension decreases as particle size increases. Among the six samples, the order of magnitude for this tension parallels that for solid-vapor tension (reflecting the trend toward incomplete wetting) and is, in increasing order (averaged over the four temperatures): Kaolin (63.0 dyne/cm), Pyrite (98.0 dyne/cm), 35-mesh Lignite (106.0 dyne/cm), 200-mesh Lignite (111.0 dyne/cm), 400-mesh Lignite (120.0 dyne/cm) and Graphite Powder (128.0 dyne/cm). Thus, solid-liquid tension is an intensive property, reflecting hydrophobicities as well as particle size.

The main conclusion obtained from this project is the optimization of reaction conditions to enhance the system's tendency toward incomplete wetting and thus enhance the

potential for separation. Graphite Powder has the highest tendency; and, among the Lignite samples, 400-mesh Lignite has the highest incomplete wetting tendency. For a given sample, incomplete wetting is favored at high relative CO_2 pressures, low temperatures, and the presence of $CO_2(l)$. It is found that, while equilibrium adsorption is an extensive property (i.e. depends only on particle size and thus available specific surface area), the contact angle and interfacial tensions are intensive properties. From the preliminary results, an inverse relation exists between particle size and specific surface area of a powdered sample; and these results make possible and more complete the study of the adsorption and interfacial properties of the six coal minerals.

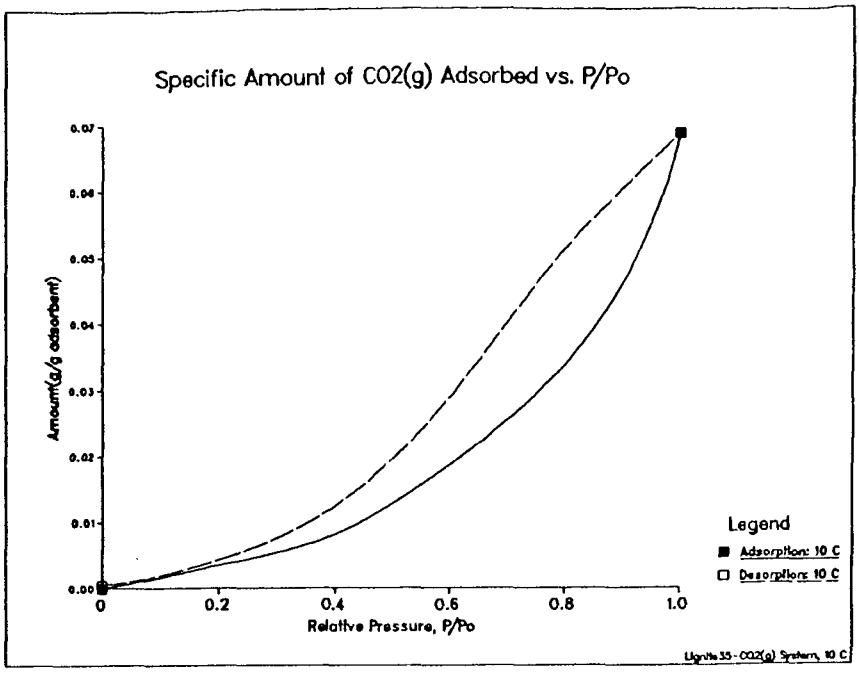

Figure 1 Adsorption and Desorption Isotherms vs. CO_2 Pressure for 35-Mesh Lignite at 10° C

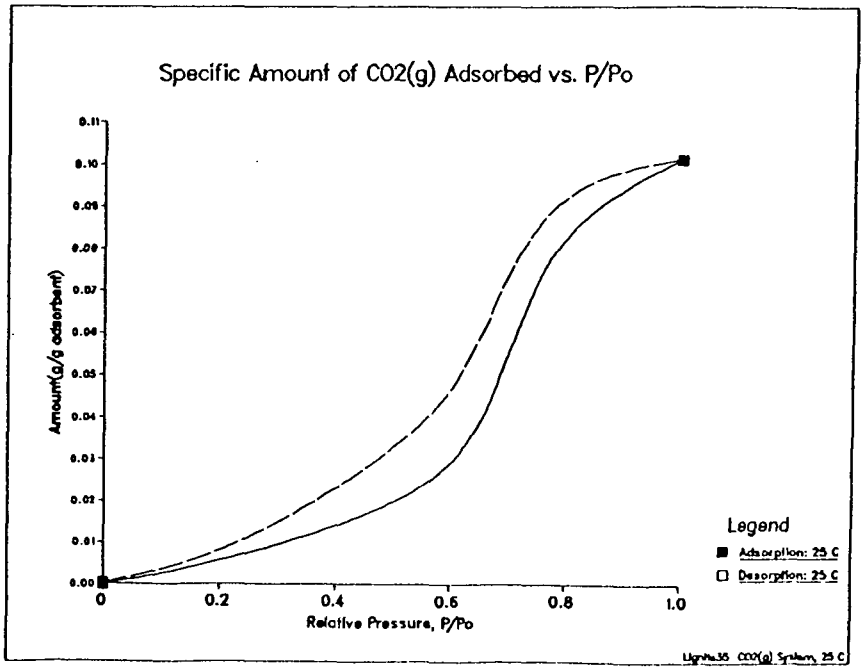

Figure 2 Adsorption and Desorption Isotherms vs. CO_2 Pressure for 35-Mesh Lignite at 25°C

Table 1

Average Characteristic Diameters and Specific Surface Areas of Powdered Particle Samples of Lignite (35-, 200-, and 400-Mesh), Graphite Powder, Kaolin, and Pyrite

Sample	Length Diameter (um)	Volume Diameter (um)	Surface Diameter (um)	Surface-Volume Diameter	Weight Diameter (um)	Specific Surface Area(m^2/g)
35-Mesh Lignite	9.2	17.6	12.8	33.7	54.2	17.8
200-Mesh Lignite	7.6	14.5	10.3	28.9	56.2	19.9
400-Mesh Lignite	7.5	12.4	9.7	20.6	31.1	21.1
Graphite Powder	8.8	16.2	12.0	29.8	46.0	18.1
Kaolin	9.1	15.1	11.6	25.8	44.5	18.9
Pyrite	16.9	30.6	23.5	52.7	72.5	17.4

Table 2

Specific Amount of CO_2 Adsorbed (per unit weight of adsorbent) Along the Adsorption Isotherm for Lignite (35-, 200-, and 400-Mesh) (g/g adsorbent)

35-Mesh Lignite

Temp.(°C)	Relative Pressure (P/Po)					
	0.00	0.20	0.40	0.60	0.80	1.00
10	0.00	0.00350	0.00817	0.01854	0.03367	0.06876
15	0.00	0.00403	0.01094	0.02007	0.05378	0.08830
20	0.00	0.00538	0.01205	0.02723	0.07121	0.09384
25	0.00	0.00568	0.01403	0.02895	0.08239	0.10107

200-Mesh Lignite

Temp.(°C)	Relative Pressure (P/Po)					
	0.00	0.20	0.40	0.60	0.80	1.00
10	0.00	0.00411	0.00928	0.02012	0.03630	0.07286
15	0.00	0.00432	0.01119	0.02187	0.05635	0.09600
20	0.00	0.00574	0.01303	0.03114	0.07820	0.09905
25	0.00	0.00613	0.01635	0.03278	0.08916	0.10980

400-Mesh Lignite

Temp.(°C)	Relative Pressure (P/Po)					
	0.00	0.20	0.40	0.60	0.80	1.00
10	0.00	0.00426	0.00980	0.02140	0.03810	0.07622
15	0.00	0.00471	0.01259	0.02303	0.05957	0.09908
20	0.00	0.00591	0.01376	0.03172	0.10813	0.11794
25	0.00	0.00648	0.01790	0.03359	0.09855	0.12426

Table j

Specific Amount of CO_2 Adsorbed Along the Adsorption Isotherm for Graphite Powder, Kaolin, and Pyrite (g/g adsorbent)

Graphite Powder

Temp.(°C)	Relative Pressure (P/Po)					
	0.00	0.20	0.40	0.60	0.80	1.00
10	0.00	0.00368	0.00878	0.01891	0.03415	0.06957
15	0.00	0.00394	0.01081	0.02013	0.05395	0.09038
20	0.00	0.00532	0.01198	0.02711	0.06940	0.09678
25	0.00	0.00563	0.01411	0.02934	0.08481	0.10537

Kaolin

Temp.(°C)	Relative Pressure (P/Po)					
	0.00	0.20	0.40	0.60	0.80	1.00
10	0.00	0.00382	0.00891	0.01990	0.03467	0.07188
15	0.00	0.00415	0.01121	0.02096	0.05380	0.09160
20	0.00	0.00548	0.01232	0.02751	0.08730	0.10611
25	0.00	0.00571	0.01601	0.03058	0.09110	0.11245

Pyrite

Temp.(°C)	Relative Pressure (P/Po)					
	0.00	0.20	0.40	0.60	0.80	1.00
10	0.00	0.00340	0.00780	0.01816	0.03319	0.06840
15	0.00	0.00376	0.01070	0.01959	0.05361	0.08719
20	0.00	0.00520	0.01170	0.02695	0.06488	0.08843
25	0.00	0.00551	0.01343	0.02789	0.07391	0.09568

Table 4

Equilibrium Liquid-Vapor and Liquid-Liquid Interfacial Tensions from the Pendant Drop Method (dyne/cm)

Liquid-Vapor Interfacial Tension

Temp.(°C)	Relative Pressure (P/Po)					
	0.00	0.25	0.50	0.75	1.00 CO_2(g)	1.00 CO_2(l)*
10	74.27	63.84	53.59	43.42	35.38	27.09
15	73.77	63.51	52.42	43.91	35.07	26.42
20	72.73	61.89	52.87	44.15	34.33	25.37
25	72.03	61.39	51.84	43.40	33.01	23.32

Work of Cohesion (twice the interfacial tension)

Temp.(°C)	Relative Pressure (P/Po)					
	0.00	0.25	0.50	0.75	1.00 CO_2(g)	1.00 CO_2(l)
10	148.54	127.67	107.17	86.85	70.76	54.19
15	147.54	127.02	104.83	87.83	70.13	52.84
20	145.47	123.78	105.74	88.30	68.66	50.74
25	144.07	122.78	103.69	86.81	61.40	47.65

* The first four columns tabulate the liquid-vapor interfacial tensions, whereas the last column lists the liquid-liquid interfacial tensions. They are distinguished by the phase of CO_2 surrounding the pendant drop.

EFFECTIVE SURFACE AREAS OF COALS MEASURED BY DYE ADSORPTION

Donald P. Spitzer
American Cyanamid Company
Stamford, CT 06904

INTRODUCTION

Coals are well known to be more or less porous structures, but just how much porosity and surface area is measured depends very much on the measurement technique. For example, even though N_2 and CO_2 molecules are essentially the same size, surface areas measured by CO_2 adsorption are >100 m^2/g for most coals, but less than 10 m^2/g when measured by N_2 adsorption. This is attributed to the fact that the N_2 measurements are made at 77°K while the CO_2 measurements are made at much higher temperatures, up to 298°K. That is, most of the pores in coals are so small that rate of diffusion of even such small molecules into the pores becomes a limiting factor. This is clearly because most of the surface area in coals is in micropores, <2nm diameter, and even in ultra-micropores, <0.8nm diameter (1).

Similary, use of other small molecules such as methanol vapor (2, 3), water, or butane (3) at temperatures of 273- 298°K also gives high surface areas of 30-400 m^2/g, compared to nitrogen surface areas of only 0.1-1.5 m^2/g for the same coals. This quotation from (2) is relevant: "It is apparent from past work that no absolute method of total surface area measurement exists and that any method will only give the surface area accessible to the adsorbate molecules at the temperature of adsorption." A very similar statement is made by Fuller (4).

Since most coal processing is done in aqueous slurries, adsorption from water is generally of more practical interest than adsorption of vapors. A considerable number of papers dealing with adsorption from aqueous solutions are in print and we can only give some principal conclusions here. The solutes examined include: 1) a variety of surfactants (5-9), which are of interest for dewatering and and for coal/water slurries; 2) alcohols which are used as frothers (10-14); 3) polysaccharides such as dextrin and guar, used for coal depression (15, 16); 4) substituted dioxanes (flotation promoters) (17); 5) phenol (10, 18-20); 6) organic acids (14, 21); 7) dyes (22, 23); etc.

In these various publications, establishment of equilibrium adsorption is stated to require anywhere from one hour to >100 hours. One point of agreement is that adsorption of most reagents on most coals is generally within the range 0.1 - 10 mg of reagent per gram of coal, for a wide variety of types of reagent. Also, it is consistently concluded that nonionic molecules, e.g. alcohols or weak acids, adsorb via their hydrocarbon portion and adsorption therefore decreases as coal is oxidized, although adsorption of stronger acids can occur via the polar end and increase with oxidation. Ionic surfactants apparently adsorb both on fresh and on oxidized surfaces, either via elctrostatic or hydrophobic interactions (5, 6).

An extensive study of dye adsorption on coals is given by Nandi and Walker (23). Using 24 hour equilibration times, adsorption for either an anionic dye, metanil yellow, or a cationic dye, methylene blue was found to be approximately related to nitrogen surface areas for most of the coals examined. Two obvious exceptions, however, were lignites, where dye adsorptions were approximately 20-100 times those expected from nitrogen surface areas.

Most studies of adsorption are concerned with "equilibrium" measurements. Since equilibrium, however, usually requires a day or more, such results may have little relevance to most real coal processing problems, where the time that the coal spends in an aqueous slurry is generally less than one hour (an obvious exception is the case of coal/water slurries, where coals are expected to be stably dispersed in aqueous slurries for weeks or months). Our primary interest has been to examine adsorption behavior expecially at short contact times, ten minutes to an hour, to determine whether such measurements might give useful data on effective surface areas - i.e., the surface that would be accessible to reagents within times comparable to those typical of most coal processing. Accordingly, most of our emphasis is on the effect of time on adsorption, rather than on traditional adsorption isotherms.

Although most literature on cationic dye adsorption Mostly on carbons) uses methylene blue, it happened that we originally used safranin O instead because this dye was reported to be useful in distinguishing oxidized coals from fresh coals (24). Many of our experiments were repeated using methylene blue (in water), with very similar results. It was noted early that swelling of coals in water was common, especially for more oxidized or lower rank coals, and adsorption experiments were also done in another solvent, namely methanol. This produced quite striking differences for some coals.

EXPERIMENTAL

For the aqueous dye solutions, the amount of mixing during adsorption had a considerable effect on the results. Best mixing appeared to be when bottles containing dye solutions plus coal were placed on rollers. A shaker generally gave lower results, since the coals tended to stay at the bottom of the bottle. On the other hand, more vigorous mixing with a magnetic stirring bar gave some results that were far too high, especially in the case of the oxidized coals, indicating breakup from the combination of swelling by the water and the mechanical agitation. For example, stirring of Coals B or C for only an hour in aqueous solution gave some apparent adsorptions greater than 40 mg/g. Adsorptions from methanol solution were little affected by mixing conditions.

Except for the adsorption isotherms (shown here only for Coal A), adsorptions were done from 100ppm safranin O (Kodak Chemical) solutions at room temperature ($23\pm2^{o}C$), with from 0.1 to 10.gm of coal per 100ml of solution, as necessary to give a readily measurable adsorption. Coals were afterwards separated either by centrifuging

or rapidly filtering through a small millipore filter attached to a plastic syringe. Dye concentrations were determined from absorption at 520nm, after appropriate dilution to less than 10ppm.

RESULTS AND DISCUSSION

Adsorption isotherms for Coal A (Fig. 1) are shown from both water and methanol for 16 hour and for one hour adsorptions. From Fig. 2, 16 hours appears adequate to give "equilibrium" adsorption from the aqueous solutions. The one hour curve in Fig. 1 is clearly far from equilibrium, but it is considered significant that a surface area corresponding to just under 0.4 mg/g adsorption is very readily covered by the dye and further adsorption does not take place until high concentrations are reached or longer times are allowed; N_2 area of this coal is 0.4 m^2/g. Isotherms from methanol solutions are nearly independent of time and the maximum adsorption is not too different from that which is quickly attained from water solutions.

The oxidized Coals B and C show the most striking differences between adsorption from water or from methanol. As noted above, such coals are considerably swollen by water; for Coal C, adsorption from water is more than an order of magnitude greater than from methanol. From methanol, there is again nearly a 1:1 correspondence between N_2 suface area and the amount of dye that is quickly adsorbed: for Coal B, S.A. = 1.2 m^2/g, while adsorptions are 1.0 and 2.1 mg/g at ten minutes and one hour, respectively; for Coal C, S.A. = 0.67m^2/g, and adsorptions are o.23 and 0.47 mg/g at ten minutes and one hour, respectively.

To demonstrate that the steep initial increase in adsorption on Coals B and C from aqueous solution was due to swelling by the water rather than just slow diffusion of the dye, the following comparison was made: For Coal B, adsorption from 100ppm aqueous safranin for one hour was 13.5$\pm$1.5 mg/g; similarly, adsorption from 100ppm aqueous safranin for ten minutes was 5.4$\pm$0.5 mg/g; contacting the coal with water for 50 minutes, followed by only ten minutes contact with safranin gave adsorptions of 12.5$\pm$1.5 mg/g (i.e., coal plus water for 50 minutes, then an equal volume of 200ppm safranin was quickly mixed in and kept another ten minutes). Contact with the water is clearly more important in determining adsorption on such coals than is diffusion of the dye. Such swelling must also be responsible for the high adsorption on lignites reported by Nandi and Walker (23), as was suggested by them, but not demonstrated.

For the PSOC coals 217 and 315, adsorptions from aqueous solutions at short times again give numbers that are close to the nitrogen surface areas for these coals, 1.6 and 1.4 m^2/g, respectively. For PSOC 217, adsorption from methanol gives much lower values; it may be that the water helps to open up the pores, but in an experiment similar to that done with Coal B above, we found no obvious swelling.

Note that all of the coals discussed above had quite low surface areas. We did have two other coals with somewhat higher surface areas (3.4 and 7.1 m^2/g) and we also examined two pure clay minerals,

kaolin and illite, and two natural coal/clay mixtures. These latter four samples had surface areas from 15 to 61 m^2/g; unlike high area coal samples, however, the surfaces of the clay would be all external and readily accessible, and the surface areas of the mixtures were undoubtedly determined mainly by the clay minerals. As expected from non-porous particles, adsorption on these samples was essentially constant after only an hour. Quantities of safranin adsorbed from the aqueous solutions again showed a close correspondence with the nitrogen surface areas. Adsorptions from methanol on these clays or clay-rich samples gave distinctly lower capacities, by factors of four to six.

Short term safranin adsorption data for all samples in Table 1, from aqueous or from methanol solutions, are summarized in Figs. 5 and 6, respectively. In Fig. 5 especially, the correspondence between safranin adsorptions from water and nitrogen surface areas is surprisingly good. The only two points that clearly do not fit in are for the Coals B and C, where anomalously high adsorptions were shown to related to swelling by water.

Correlation of N_2 area with adsorption from methanol solutions shows the general trend, but is not as good as from water. Many of the samples show significantly less adsorption from methanol. In the case of highly oxidized coals, however, these lower values from methanol were seen to be much closer to the N_2 areas.

From the correlation in Fig. 5, it happens that 1.0 mg/g of adsorbed safranin is essentially equivalent to 1.0 m^2/g of N_2 surface area. This would require an area of only 0.58 nm^2 per safranin molecule, which is considerably less than the 2.2 nm^2 we estimate for the molecule lying flat. The 0.58 nm^2 would be consistent with an edge adsorption, or alternatively, may indicate multilayer adsorption (3-4 layers stacked flat). Since there is no apparent reason why a 3-4 multilayer configuration would be particularly stable, an edge adsorption is more likely.

Our coal samples were all of rather low surface areas, 0.2-7 m^2/g; the only higher surface areas were for essentially non-porous particles. It is expected that as coal surface areas increase above about ten m^2/g, pores are necessarily smaller and less accessible and the ratio of dye adsorbed to N_2 area must decrease. This is essentially what was found in (23) for coals with surface areas of 10-100 m^2/g. We expect to extend this present work to also include higher surface area coals. In addition, we have some preliminarly results using adsorption of a proprietary reagent that selectively adsorbs only on the coals and not on the ash minerals, permitting a separation of the contributions of the coal and ash to the surface area.

SUMMARY

Coal surfaces that are readily accessible to adsorption by safranin are found to correlate well with N_2 surface areas, with adsorption of 1.0 mg safranin per gram of coal corresponding to essentially a

surface area of 1.0 m^2/g. Highly oxidized coals were found to swell considerably in water, with correspondingly increased adsorption. Areas of such coals can be estimated by adsorption of safranin from methanol solutions.

References

1. Walker, P. L. Jr., Phil. Trans. Royal Soc. London, A300, 65-81 (1981).
2. Carpenter, D. L. and Sergeant, G. D., Fuel, 45, 429-446 (1966).
3. Anderson, R. B., Hall, W. K., Lecky, J. A., and Stein, K. C., J. Phys. Chem., 60, 1548 (1956).
4. Fuller, E. L. Jr., Coal Structure, Gorbaty, M. L. and Ouchi, K., eds., Adv. Chem. Series 192, American Chemical Society, Washington, D. C. (1981).
5. Laskowski, J. and Konieczny, E., Arch. Gorn, 15, 26-36 (1970).
6. Latiff Ayub, A., Al Taweel, A. M., and Kwak, J. C. T., Coal Preparation, 2, 1-17 (1985).
7. Aston, J. R., Deacon, M. J., Furlong, D. N., Healy, T. W., and Lau, A. C. M., Proc. Aust. Coal Prep. Conf. (1981) 358-378.
8. Esumi, K., Meguro, K., and Honda, H., Bull. Chem. Soc. Japan, 55, 3021-2 (1982).
9. Aston, J. R. and Furlong, D. N., Colloids and Surfaces, 4, 121-129 (1982).
10. Przhegorlinskaya, R. V. and Zubkova, Yu. N., Khim. Tver. Topliva, 12, 125-128 (1978).
11. Kelebek, S., Salman, T., and Smith, G. W., Coal: Phoenix of the 80's, Proc. 64th CIC Coal Symp., Al Taweel, A. M., ed., 145-152 (1982).
12. Fuerstenau, D. W. and Pradip, Colloids and Surfaces, 4, 229-243 (1982).
13. Nogly, J. and Laskowski, J., Arch. Gorn. 17, 199-208 (1972).
14. Butuzova, L. F. and Kucher, R. V., Khim. Tverd. Topliva, 11, 119-125 (1977).
15. Huang, H. H., Calara, J. V., Bauer, D. L., and Miller, J. D., Recent Devel. Separation Science, 4, 115-133 (1978).
16. Miller, J. D., Laskowski, J. S., and Chang, S. S., Colloids and Surfaces, 8, 137-151 (1983).
17. Petukhov, V. N., Khim. Tverd. Topliva, 13, 12-20 (1979).
18. Al Taweel, A. M., Farag, H. A., Kwak, J., Hanza, H. A., and Falk, M., Coal: Phoenix of the 80's, Proc. 64th CIC Coal Symp., Al Taweel, A. M., ed., 125-130 (1982).
19. Ayub, A. L., Al Taweel, A. M., and Kwak, J. C. T., Coal Preparation, 1, 1-13 (1984).
20. Eveson, G. F., Ward, S. G., and Worthington, F., J. Inst. Fuel, 29, 540-544 (1956).
21. Zubkova, Yu. N., Basenkova, V. L., and Kucher, R. V., Khim. Tverd. Topliva, 13, 32-37 (1979).
22. Glanville, J. O., Haley, L. H. Jr., and Wightman, J. P., Fuel, 62, 1310-1314 (1983).
23. Nandi, S. P. and Walker, P. L. Jr., Fuel, 50, 345-366 (1971).
24. Gray, R. J., Rhoades, A. H., and King, D. T., Trans. S. M. E., 260, 334-341 (1976).

Table 1. Samples Used

Sample	%C	%H	%O	%N	%S	%Ash	N_2 area m^2/g
Coal A -Virginia	83.0	4.8	10.7	0.9	0.6	7.1	0.4
Coal B -W.V.stockpile	67.4	3.6	27.7	0.9	0.5	16.2	1.2
Coal C -British Columbia surface outcrop	75.4	3.9	19.9	0.6	0.2	18.2	0.67
PSOC 217 -Kentucky	78.9	5.6	8.0	1.8	5.5	17.7	1.6
PSOC 315 -Colorado	76.7	5.8	14.8	2.0	0.8	11.6	1.4
Coal A, oxidized, 200hrs.@150°C	73.7	3.3	21.5	0.9	0.6	6.4	3.4
Coal D -Arizona							7.1
Coal/Ash Mix 1-Kentucky						50.	30.6
Coal/Ash Mix 2-Kentucky						33.	15.1
Kaolin							23.2
Illite							61.2

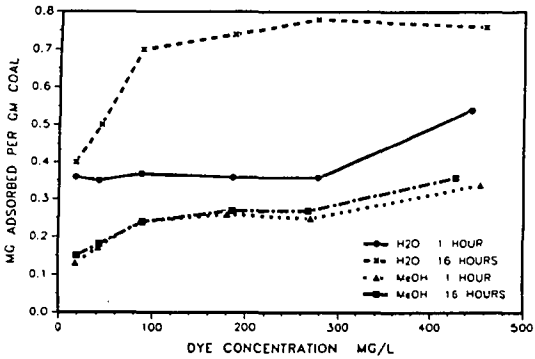

Figure 1. Adsorption isotherms for safranin on Coal A, from water and from methanol solutions and for 16 hour and one hour contact times.

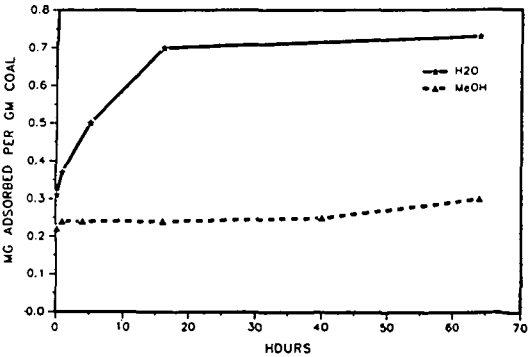

Figure 2. Adsorption on Coal A vs. time, from 100ppm safranin solutions in water and in methanol.

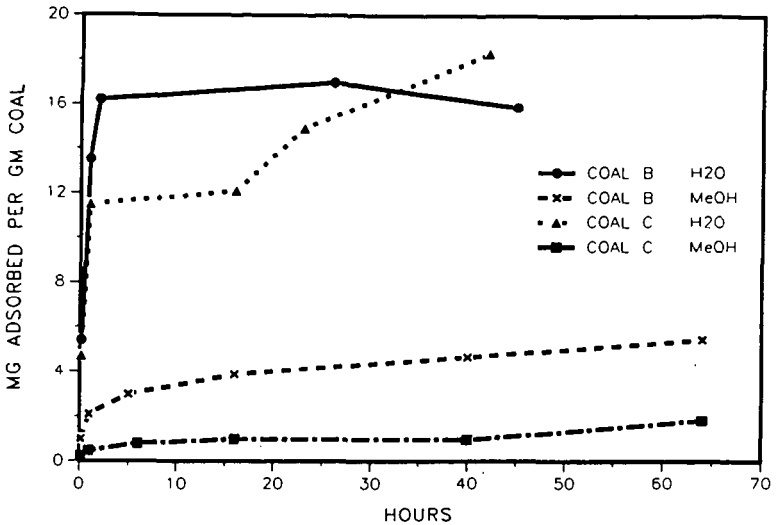

Figure 3. Adsorption on Coal B and Coal C vs. time, from 100ppm safranin solutions in water and in methanol.

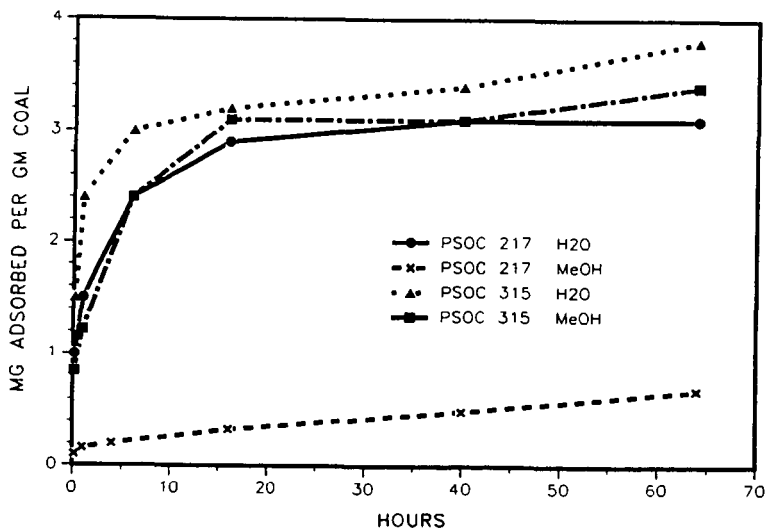

Figure 4. Adsorption on PSOC 217 and PSOC 315 vs. time from 100ppm safranin solutions in water and in methanol.

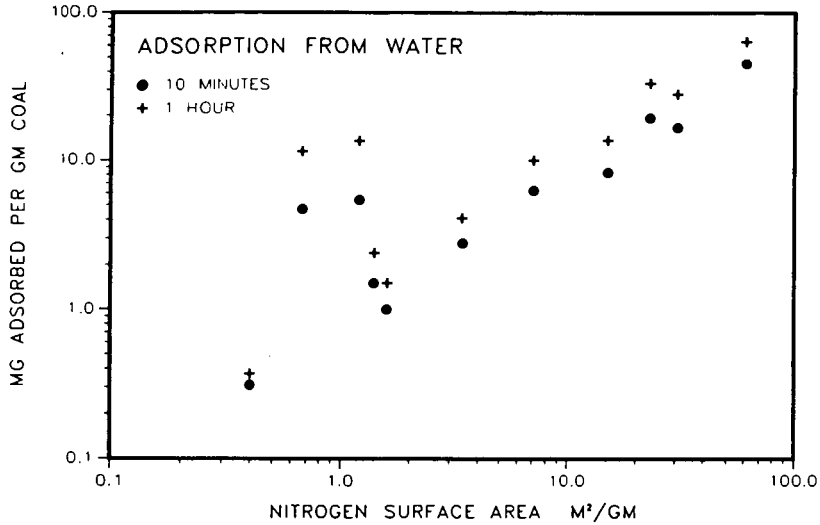

Figure 5. Ten minute and one hour adsorptions of 100ppm safranin from water onto samples of Table 1 vs. nitrogen surface area.

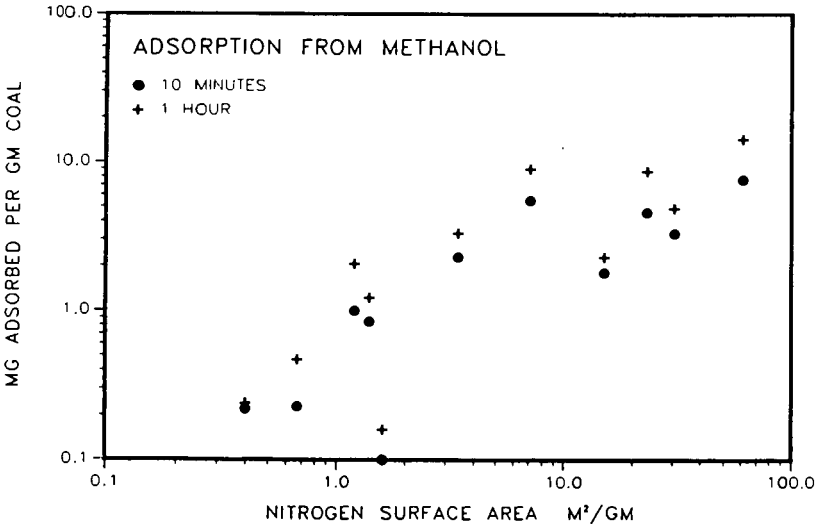

Figure 6. Ten minute and one hour adsorptions of 100ppm safranin from methanol onto samples of Table 1 vs. nitrogen surface area.

CHARACTERIZATION OF MINERAL AND COAL SURFACES BY ADSORPTION OF DYES

Bogdan J. Slomka, M. Robert Dawson and William H. Buttermore,

Ames Laboratory, Iowa State University, Ames, Iowa 50011

ABSTRACT

A dynamic method is described for dye adsorption measurements to characterize mineral and coal surfaces for the evaluation of coal cleaning processes. Samples of increasing mineral content were prepared by density separation of a narrowly sized (300 to 425 μm) wet-sieved coal. The rates and extents of the adsorption of ionic dyes on Illinois No. 6 coal were observed to be highly dependent on mineral content and particle size of ground coal samples. A linear correlation was observed between the adsorbed quantity of dye and the total mineral content of coal samples. Dry-sieved coals were found to be coated by fine material of high mineral ash content which adsorbed greater than 20 times more methylene blue per gram than wet-sieved particles. In preliminary experiments with methylene blue dye, clay was found to adsorb significantly more dye than quartz, pyrite, calcite or low-ash specific gravity fractions of coal.

INTRODUCTION

Adsorption of dyes from solutions has been extensively used for the determination of surface areas and examining the accessibility of porous structures to dye molecules; and has become a standard practice in the qualitative evaluation of active carbons in industry (1, 2, 3). It is well known that surface properties of solid adsorbents govern the adsorption of molecules from liquid solutions. Generally, increasing the surface polarity of active carbons (e.g., by oxidation) causes an increase in adsorption of the more polar component in binary liquid mixtures (4). For instance, adsorption of stearic acid by nonporous carbons, free from surface oxygen complexes, results in a closely-packed monolayer, whereas on surfaces bearing oxygen complexes, the formation of a complete monolayer is not accomplished, even at the highest possible concentrations of the acid solution (5). Similarly, surface acidity of active carbons strongly influences adsorption of aromatic amines and phenol derivatives from organic solutions (6).

For coals, it has been argued that a portion of the mineral matter of coal, predominantly pyrite and alkali metal compounds, interacts with dye molecules, affecting adsorption results. However, adsorption of dyes is not influenced by surface oxygen groups, except in the case of lignites (7).

Literature references dealing specifically with the use of adsorption methods to evaluate either cleanability of coals or the effects of coal-cleaning processes on coal surface properties have not been found. However, adsorption of surfactants has been used for predicting how easily a stable slurry can be made using a given coal (8). With careful selection of an adsorbate (with respect to polarity, acidity, surface activity, molecular area in the adsorbed state, etc.), adsorption from solutions could become a sensitive 'molecular probe' for investigating coal and mineral surfaces. In particular, adsorption from liquid phases appears to

have the potential to become a useful tool for detecting changes in surface properties (e.g., hydrophobicity) which are important for coal preparation processes.

The primary goal of this study was to develop a practical method for quantifying the selective adsorption of dye on coal and mineral surfaces. In these preliminary tests, adsorption profiles were obtained for: coal samples of different total mineral content, specific mineral species, and coal samples of different particle size.

EXPERIMENTAL

Materials

Non-buffered 64.0 mg/l aqueous solutions of methylene blue were prepared by drying the dye under nitrogen at 110°C for 2 hours and dissolving in deionized distilled water.

A bulk sample of coal with a narrow range of particle size was obtained by dry-sieving Illinois No. 6 coal to obtain 330 to 425 µm coal particles. Test samples were then prepared by wet-sieving to remove undersize material from the particle surfaces. Samples of increasing mineral content were prepared by density separation of the wet-sieved particles using aqueous solutions of CsCl at several specific gravities between 1.30 and 1.80 g/cc. Mineral samples for analysis included a single pyrite cube from Ward's Natural Science Establishment; kaolinite flint-clay from A. P. Green quarries of Mexico, Missouri; and single crystals of calcite and quartz obtained from the Department of Earth Sciences at Iowa State University. Mineral samples were ground using a mortar and pestle, and 330 to 425 µm particles were obtained by wet-sieving. Preliminary tests were performed to determine the applicability of the dynamic adsorption technique to fine particle sizes. Illinois No. 6 coal was pulverized and dry-sieved to obtain samples smaller than 150 µm and 44 µm.

Procedures and Analysis

A continuous-flow apparatus was developed for dynamic measurements of adsorption from liquid phases on solids. Figure 1 shows the configuration of the main components. In a typical experiment, a pre-weighed sample of coal is placed in a sample cell and fixed between two 0.5-µm stainless steel frits. The sample cell is then connected to a six-port switch valve and evacuated to remove air. The valve is set initially to direct the solution of dye to by-pass the cell containing the sample, causing it to flow directly through the utraviolet/visible detector (Varian UV-50). As soon as a baseline is established for the dye solution, the flowing solution is directed through the sample of coal to the UV/Vis detector. The absorbance measured for the effluent leaving the sample cell is due only to dye not adsorbed by the coal sample. The apparent absorbance is recorded at a fixed wavelength as a function of time using an A/D converter at a sampling rate of 2 sec^{-1}. This dynamic method of adsorption measurement allows for continuous replacement of the fluid phase in contact with the coal sample, which is not possible in a closed, static system. The rates of adsorption can be continuously measured as a function of time, giving characteristic profiles of adsorption rate, while the total adsorbate uptakes are obtained by integration of the rate profiles over the

time of adsorption. The detector response to dye concentration was linear for the concentrations and wavelenghts used in the experiments. The detector was operated in the visible range at 610 nm. Based on preliminary results, two flow rates of solutions were selected, 1 and 0.5 ml/minute, according to the sample size of the materials tested.

To evaluate the adsorptive components of coal and mineral surfaces, coal samples of uniform particle size and increasing mineral content were analyzed. Total mineral content was determined by standard ash analysis. Samples with very low ash content were used to approximate a non-mineral coal surface. To evaluate specific mineral adsorptive characteristics, mineral samples of uniform particle size and composition were analyzed. Ground coal samples of different mean particle size were analyzed to determine the effect of particle surface area.

RESULTS AND DISCUSSION

Figure 2 shows the correlation between dye uptake and available mineral surface (measured as total ash content) for several coal samples. Quantitative data is presented in Table 1. As shown in Figure 2 and Table 1, increased dye uptakes and adsorption rates are observed for coals with higher mineral content. This implies that methylene blue dye is preferentially adsorbed on mineral surfaces. Figure 3 presents adsorption profiles for samples of different specific gravity (3a), different mineral species (3b), and different particle size (3c). In each graph, the adsorption curve for the head sample of wet-sieved, 300 to 425 µm Illinois No. 6 coal is provided for reference. Data presented in Figure 3a suggest that specific gravity fractions heavier than 1.55 g/cc contain highly adsorbing constituents. Tests are currently underway to identify these constituents from known components of coal mineral matter by testing their behavior during dye adsorption. Figure 3b presents the results of methylene blue adsorption on several common coal mineral species compared to the adsorption pattern for the 300 to 425 µm wet-sieved Illinois No. 6 coal head sample. Based on these data, clay minerals are the most probable single constituent responsible for the high adsorption values reported. Contrary to suggestions by Nandi and Walker (7), pyrite showed the smallest adsorption per gram of sample. In our experiments, pyrite was found to adsorb less methylene blue (Figure 3b) than the coal fraction of 1.30-1.35 specific gravity (Figure 3a).

Early attempts to correlate the extent of adsorption with total coal mineral content using dry-sieved coal samples were unsuccessful. It was later determined that fine-sized material high in mineral content adhered to larger particles and very strongly adsorbed the dye. Figure 3c shows the methylene blue adsorption profiles for dry-sieved and wet-sieved samples of the 300 to 425 µm Illinois No. 6 coal. The integrated uptakes of the dye (Table 1) indicate that the coating of fine material, constituting 20.2% by weight of the dry-sieved sample, adsorbs about 20 times more dye than the wet-sieved coal. Consequently, for later experiments only wet-sieved coals were used.

ACKNOWLEDGMENTS

Ames Laboratory is operated for the U. S. Department of Energy by Iowa State University under Contract No. W-7405-ENG-82. This work was supported by the Assistant Secretary for Fossil Energy through the Pittsburgh Energy Technology Center. We gratefully acknowledge Dr. Robert Cody and the Department of Earth Sciences at Iowa State University for mineral samples and helpful discussions.

REFERENCES

1. Kudo, K., H. Hosada, S. Honma, and M. Komatsu. Journal of the Fuel Society of Japan, 1973, 52:335.

2. Hassler, J. W. "Active Carbon", Brooklyn Chemical Publishing Co., 1951.

3. Rist, L. P. and D. P. Harrison. "Surface Area and Pore Development During Lignite Activation", Fuel, March, 1985, 64:291-7.

4. Jankowska, H., A. Swiatkowski, J. Oscik, and R. Kusak. Carbon, 1983 No. 2, 2:117

5. Kipling, J. J. "Adsorption from Solutions of Non-Electrolytes", Academic Press, New York, 1965, p. 115.

6. Oda, H. and C. Yokokawa. Carbon, 1983 No. 5, 21:485.

7. Nandi, S. P. and P. L. Walker, Jr. "Adsorption of Dyes from Aqueous Solutions by Coals, Chars, and Active Carbons", Fuel, October, 1971, 50:345-66.

8. Liang, W. and L. Jiang. "Effect of Wettability and Adsorptability of Coal on the Slurryability of Coal", Journal of Coal Quality, April, 1987, 44-8.

Table 1. Adsorption of Methylene Blue Dye on Minerals and Illinois No. 6 Coal (adsorption time: 10 minutes)

Sample	Adsorption, mg/g
Minerals	
Pyrite	0.017
Quartz	0.030
Calcite	0.135
Clay	0.577
Coal	
- 45 um, dry grind	4.07
-150 um, dry grind	3.09
-425 + 300 um	
dry-sieved	2.50
wet-sieved	0.51
Specific Gravity Fractions of Coal	
> 1.80	1.15
-1.80 + 1.65	0.671
-1.65 + 1.55	0.585
-1.55 + 1.50	0.535
-1.50 + 1.45	0.462
-1.45 + 1.40	0.357
-1.40 + 1.35	0.291
-1.35 + 1.30	0.185
< 1.30	0.142

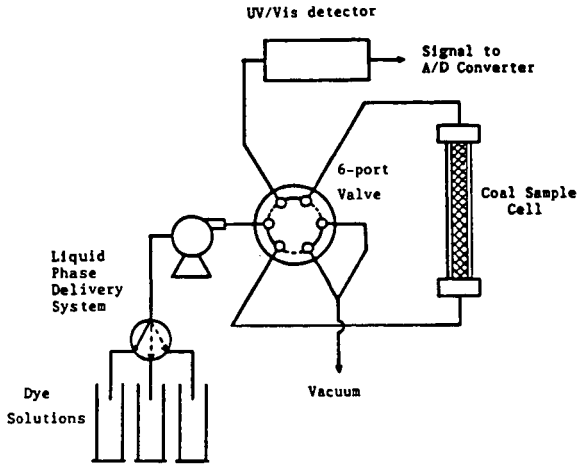

Figure 1. Continuous Flow Dye Adsorption Apparatus

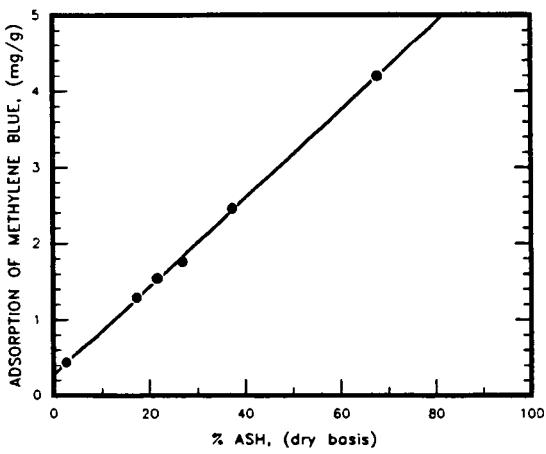

Figure 2. Dye Uptake vs Coal Ash Content (Adsorption time: 6 hours, Flow Rate: 1. ml/min.)

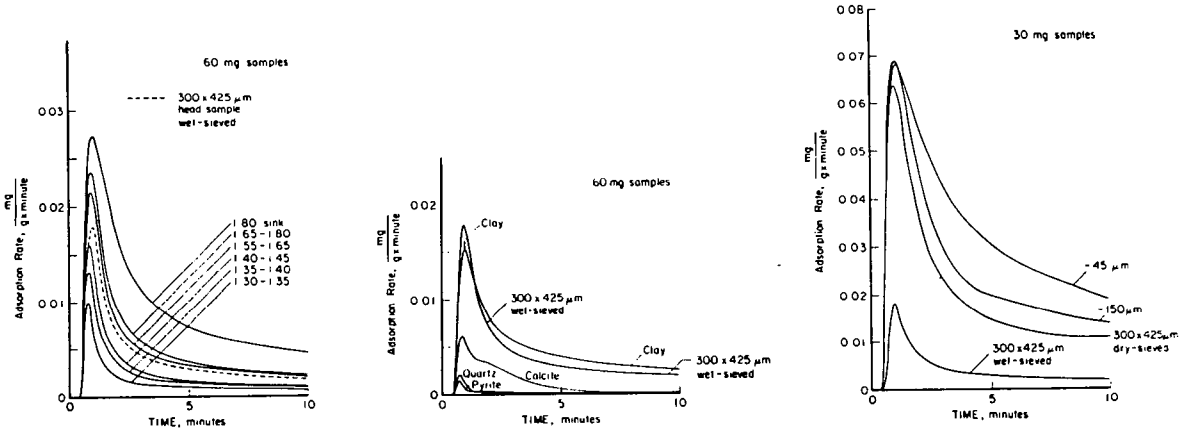

3a. Specific Gravity

3b. Mineral Species

3c. Particle Size

Figure 3. The Effects of Sample Characteristics on Methylene Blue Dye Adsorption.

ASSESSMENT OF THE HYDROPHOBICITY OF FINE COAL PARTICLES IN VARIOUS AQUEOUS MEDIA BY VISCOSITY MEASUREMENTS.

Geatesh K. Tampy, David H. Birlingmair, and Lawrence E. Burkhart
Ames Laboratory, Iowa State University
Ames, Iowa 50011

ABSTRACT

Viscosity measurements have been shown to provide a good indication of the relative hydrophobic and hydrophilic nature of fine coal particles in various aqueous media. Slurries of float and sink fractions of pulverized Upper Freeport run-of-mine coal in various electrolytes showed evidence of structure formation under the influence of shear. This structuring reaches a steady state at very high shear rates; by examining the viscosities at the higher shear rates, the inter-particle interaction effects and hydrodynamic effects may be distinctly determined. When the particles are more hydrophobic, the tendency for structure formation is greater. This is reflected in the response of the slurry to shear. Viscosity measurements of α-alumina particles in slurries of various pH, and corresponding zeta potential measurements, confirmed that the highest viscosity and the maximum structure formation occurred at the PZC, when the particle surfaces are most hydrophobic.

INTRODUCTION

The rheological properties of slurries are influenced both by the surface characteristics of the particles, and by the properties of the suspending liquid(1-4). Measurement of the appropriate rheological parameters offers a simple means of comparing the relative hydrophobicity of particles in different aqueous media and also of comparing the effect of different chemical treatments on the hydrophobicity of the particles. Current work in our laboratories involves surface modification by chemical pretreatment of coal during the size-reduction stage that typically precedes beneficiation in most advanced coal cleaning processes. The rheology measurements can be used to characterize the changes to the particle surfaces that have been brought about by the pretreatment.

THEORY

In the Einstein equation(5) for suspensions of non-interacting spherical particles, the viscosity increase due to the presence of the particles is a function only of the volume fraction of the particles. The equation is valid only for relatively dilute suspensions(6). In a simple shear field, this still represents Newtonian flow, in the sense that shear stress is linearly related to shear rate.

For more concentrated slurries, particle interactions also affect the viscosity of the suspension since various degrees of aggregation or 'structuring' of the particles will occur(7). If the particles are suspended in an aqueous medium and have strongly hydrophobic surfaces, the preference of the water molecules to associate with other water molecules, rather than with the particle surfaces, will promote aggregation. Ionic or polar surfaces on the

other hand, can associate more freely with the polar water molecules and are thus hydrophilic(8). The presence of an electrostatic charge at the surface reduces the tendency for such particles to aggregate. Aggregation causes the viscosity of the suspension to increase for two reasons. The particle assemblages tend to entrap liquid within themselves, increasing the effective volume fraction of the solids, and thus increasing the viscosity in accordance with the Einstein equation(9). Additional energy is also dissipated when the particle assemblages interact with each other during shear flow.

In most slurries containing particles of a few micrometers or smaller in size, the basic flow units are considered to be small clusters of particles and entrapped liquid called flocs(10,11). At rest, the flocs are grouped into larger flow units called aggregates. As shear is imposed on the slurry, the aggregates break down into individual flocs, until at sufficiently high shear, a linear shear stress-shear rate relationship is observed, as shown in Figure 1. This linear portion of the curve represents a steady-state energy relationship between the tendency of the flocs to form doublets, and the tendency of the shear forces to break-up the doublets. The curve is characteristic of pseudoplastic shear-thinning behavior. The Bingham yield stress, τ_B, is defined as the extrapolated intercept of the linear portion of the curve and the apparent viscosity, η, is the ratio of the shear stress to the shear rate at any point on the curve.

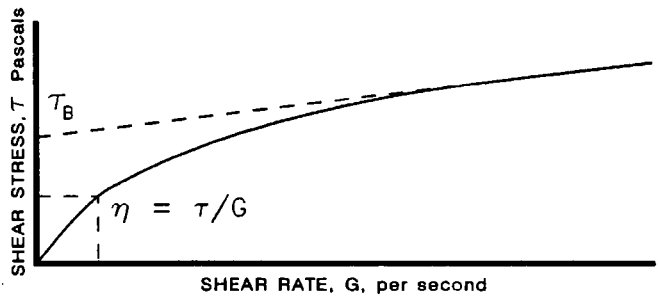

Figure 1. Typical shear stress-shear rate relationship showing pseudoplastic shear-thinning behavior.

Michaels and Bolger(10) found that τ_B increased with the square of the floc volume fraction (Φ_F), and with the strength of the interparticle interactions. The relationship is expressed as:

$$\tau_B = \frac{A}{a \quad d_F^2} \Phi_F^2 \qquad 1)$$

where A is a constant which depends on the net force of attraction between the particles. The parameter, d_F, is the average floc diameter, and 'a' is the distance between flocs and is thus a measure of the attraction between flocs. They also found that the ratio A/d_F^2 was constant and independent of the chemical composition of the liquid used. Thus τ_B depended only on 'a', which is a measure of the degree of interaction between flocs, and on Φ_F, the floc volume. Since the tendency of particles to aggregate is

greater when they are more hydrophobic, this implies that greater hydrophobicity would yield a higher value of τ_B.

Hunter and co-workers(11), who extended the "aggregate-collision" theory of Michaels and Bolger(10), showed that τ_B varied as the square of the zeta potential of the particles in the suspension. τ_B was a maximum when the zeta potential was zero. The tendency for particles to aggregate is also a maximum at this point.

EXPERIMENTAL

To study the effects of the different treatments on the surface properties of the organic and mineral portions of Upper Freeport run-of-mine coal, the coal was first ground to an average particle size of about 10 μm, separated into an organic-rich fraction which had only 4.9% ash, and a mineral-rich fraction which had 55.3% ash. This was done by centrifugal float-sink separation using a liquid of specific gravity 1.4. The organic and mineral-rich fractions were filtered, vacuum dried, and then used to form a variety of different slurries each of which had the same solid concentration (volume fraction). However, the pH of the suspending solutions was different. For each fraction, one additional slurry was made using a 0.1M solution of sodium dithionite. The viscosities of the slurries were measured using a Haake concentric cylinder viscometer. The viscosities of the suspending electrolytes were measured using a Cannon-Fenske capillary viscometer, and very little variation among them was noticed.

As a further test of the method, viscosity and pH measurements were also made on slurries of α-alumina particles, which had more homogenous surfaces. The alumina was obtained from Fisher Scientific Company, and was further ground to an average particle size of about 10μm.

RESULTS

The results of beneficiation tests on separate samples of the same Upper Freeport run-of-mine coal used in this work are given in an accompanying paper(12). Separation was carried out by oil agglomeration, microbubble frit flotation, and microbubble foam flotation. They were made at different pH levels and also in the presence of 0.1M sodium dithionite. In each case the coal which had been pretreated with sodium dithionite ($Na_2S_2O_4$) yielded substantially better results than when only pH control was used. To understand the changes to the surfaces of the particles that might have caused such a response, the viscosity curves obtained in this work were examined.

The shear responses of the mineral-rich fractions of Upper Freeport coal in the various electrolytes are shown in Figure 2. The only difference between the curves is in the liquid used for making each slurry. The curves are all typical of shear thinning behavior. The initial nonlinear portion of the curves represents increasing break-up of aggregates. When these are all destroyed, the curve becomes linear and represents a steady-state relation between the formation and break-up of floc doublets. The slopes of the linear part of the curve is a function only of the

floc volume. These slopes, and hence the floc volumes of the slurries, are essentially equal. This is not unreasonable since each slurry has the same particle concentration, and was subjected to the same shear cycle in the viscometer.

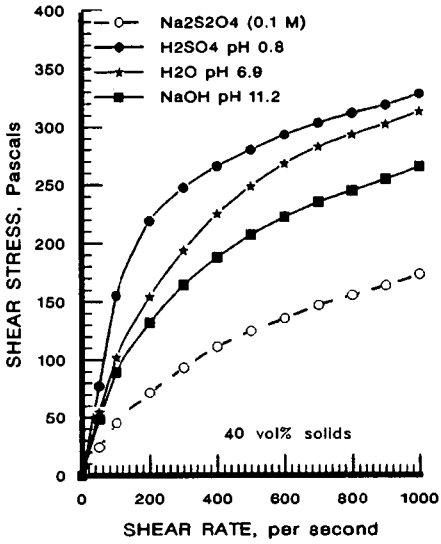

Figure 2. Shear response of slurries of the mineral-rich fraction.

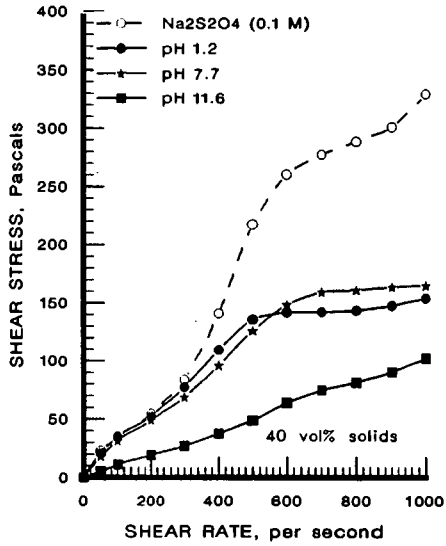

Figure 3. Shear response of slurries of the organic-rich fraction.

Table 1. τ_B values for slurries of the mineral-rich fraction.

pH	τ_B, Pascals
0.8	245
6.9	204
11.2	162
0.1M $Na_2S_2O_4$	85

Table 2. τ_B values for slurries of the organic-rich fraction.

pH	τ_B, Pascals
1.2	130
7.7	150
11.6	11
0.1M $Na_2S_2O_4$	217

The Bingham yield stress, τ_B, found by extrapolating the linear portion of each curve to zero shear rate, is different for each slurry. The values of τ_B are given in Table 1. The Bingham yield stress is a function of both the floc volume and the strength of the net attractive interaction force between flocs. Since the floc volumes are essentially equal for each slurry, τ_B should be directly related to the strength of the particle interactions. Lower values of τ_B indicate a lower net particle-particle interaction (or more correctly, a greater tendency for particle-medium association), a

lesser tendency towards flocculation, and hence a stronger hydrophilic character of the particle surfaces. Clearly, the particles in the slurry treated with sodium dithionite were most hydrophilic; the curve for this slurry is significantly lower than those slurries in which only pH was varied.

Figure 3 shows the shear response of the slurries formed with the organic rich fractions. Although some shear thickening appears at intermediate shear rates, the slurries still showed shear thinning at low and high shear. This type of behavior is not unusual for hydrophobic systems(3,13). For these slurries, the plastic viscosities are not so nearly equal as they were for the mineral-rich slurries. A clear interpretation of the result is difficult and will not be attempted until more data are available. However, the substantial difference in the τ_B values shown in Table 2, for the slurry treated with sodium dithionite, would seem to overshadow any effect of the floc volume difference in reaching a conclusion that the particles in the sodium dithionite slurry were most hydrophobic.

These results suggest that the improved beneficiation results obtained by using sodium dithionite was due to alteration of surfaces of both the organic-rich and mineral-rich coal particles, since the organic-rich particles became more hydrophobic and the mineral-rich particles became more hydrophilic. In other words, the surface characteristics of the two fractions were altered in different ways. Additional evidence, given in the companion paper(12) to this work, is that both sulfur and ash reduction was improved. Reduction of a sulfide surface by an appropriate reductant is known to improve sulfur rejection, but its effect on either carbonaceous surfaces or ash surfaces is less clear and additional work will be required to explain this result.

Figure 4 shows the shear response of α-alumina slurries at various pH values and is included to demonstrate the variation of τ_B with particle interaction effects on slurries made up of particles with more homogenous surfaces. At the point of zero zeta potential, (see Figure 5) the value of τ_B (Table 3) is a maximum, showing maximum particle-particle interaction, minimum particle-liquid interaction, and therefore maximum hydrophobicity. This is only expected, since the particles being least charged can least interact with the polar aqueous medium, and also have the least particle-particle repulsion.

Table 3. Yield Stress (τ_B) at various pH for α-alumina slurries. The corresponding zeta potential values (ζ) are also shown.

pH	ζ, mV	τ_B, Pascals
6.4	+10	76.6
8.3	0	102.4
9.8	-27	33.6
10.0	-29	18.1

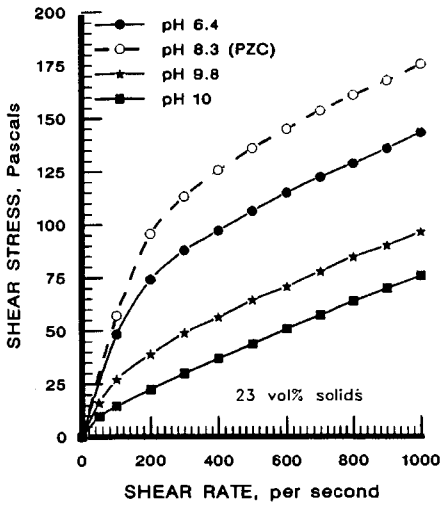

Figure 4. Shear response of slurries of α-alumina.

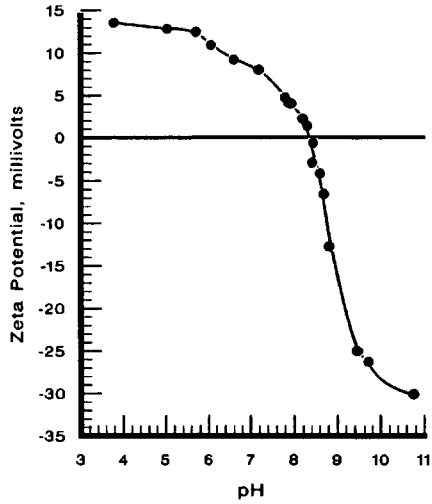

Figure 5. Zeta potential of α-alumina particles at different pH.

CONCLUSIONS

Rheological measurements have been used to study the hydrophobic/hydrophilic behavior of coal and mineral particles in various aqueous media, in an effort to explain why the use of sodium dithionite as an additive during grinding of a coal slurry produced improved beneficiation results. The measurements suggest that this was due to a beneficial effect on the surface properties of both the organic and mineral fractions of the coal. The organic fraction became more hydrophobic and the mineral fraction became more hydrophilic in the slurries containing 0.1M sodium dithionite. These results do not necessarily contradict the contact angle measurements reported earlier(12), if the possibilities of kinetic effects are taken into account. The time taken to prepare the dispersed slurries for viscosity measurements could allow for relatively slow changes to the particle surfaces. These effects would not be expected to show up in the contact angle measurements which did not allow for extended coal-sodium dithionite solution contact. The exact mechanisms that effect these changes are not known at this time. However, additional studies are underway.

ACKNOWLEDGEMENT

Ames Laboratory is operated for the U. S. Department of Energy by Iowa State University under Contract No. W-7405-ENG-82. This work was supported by the Assistant Secretary for Fossil Energy through the Pittsburgh Energy Technology Center.

REFERENCES

1. Adiga,K.C.; Shah,D.O.; Colloids and Surfaces, **1982**, 4, 271-284.

2. Kesavan,S.K., Powder Technology, **1987**, 50, 15-23.

3. Kaji,R.; Muranaka,Y; Miyadera,H.; Hishinuma,Y.; AICHE J., **1987**, 33, 11-18.

4. Tadros,E. in "Polymer Adsorption and Dispersion Stability", Goddard,E.D.; Vincent,B. eds.; ACS, Washington, 1984, pp. 411-428.

5. Jeffrey,D.J.; Acrivos,A.; AICHE J., **1976**, 22, 417-432.

6. Heimenz,P.C.; "Principles of Colloid and Surface Chemistry", Marcell Dekker, New York, 1977, pp. 59-80.

7. Hoffman,R.L.; "Science and Technology of Polymer Colloids", vol 2, Poehlein G.W.; Ottewill,R.H.; Goodwin,J.W.; eds., Martinus Nijhoff, Boston, 1983, pp. 570-588.

8. a) Tampy,G.K; PhD Thesis, Ohio University, March 1988. b) Tampy,G.K., Prudich,M.E.; Savage,R.L; Williams,R.R.; Energy & Fuels, 1988, in press.

9. a) Gillespie,T.; J. Colloid Interface Sci. **1966**, 22, 563-572. b) Gillespie,T.; J. ibid., **1983**, 94, 166-173.

10. Michaels,A.S.; Bolger, J.C.; Ind. Eng. Chem. Fundam. **1962**, 1, 153-162.

11. a) Hunter,R.J.; Nicol,S.K.; J.Colloid Interface Sci. **1968**, 28, 250-259. b) Friend,J.P; Hunter,R.J; ibid. **1971**, 37, 548-556. c) Firth,B.A; ibid., **1976**, 57, 257-265. d) Firth,B.A; Hunter,R.J.; ibid., **1976**, 57, 248-256. e) Firth,B.A; Hunter,R.J.; ibid., **1976**, 57, 266-275. f) van de Ven,T.G.M.; Hunter,R.J.; Rheologica Acta, **1977**, 16, 534-543. g) van de Ven,T.G.M.; Hunter,R.J.; J.Colloid Interface Sci. **1979**, 68, 135-143. h) Hunter,R.J.; Frayne,J.; ibid., **1979**, 71, 30-38. i) Hunter,R.J.; Frayne,W.; ibid. **1980**, 76, 107-115.

12. Tampy,G.K; Birlingmair,D; Burkhart,L.E; Prepr. Conf. Am. Chem. Soc. Div. Fuel Chem. **1988**, 33, in press.see accompanying paper.

13. Umeya,K.; Kanno,T. J. Rheol., **1979**, 23, 123-139.

THE HYDROPHOBIC CHARACTER OF PRETREATED COAL SURFACES

R. Jin, Y. Ye and J.D. Miller
Department of Metallurgy and Metallurgical Engineering
University of Utah, Salt Lake City, UT 84112

INTRODUCTION

In recent years, the production of superclean coal has been of considerable interest in order to partially replace oil and natural gas as fuel sources. Of all the coal-cleaning processes, flotation is one of the most versatile. Carbon dioxide coal flotation is a new technology developed at the University of Utah.(1) Compared with conventional flotation, carbon dioxide flotation enhances the ash rejection and increases flotation recovery for coals of different rank with the exception of lignite. However, significant improvement of the hydrophobicity and flotability of lignite has been found after controlled thermal pretreatment.The potential for the production of superclean coal by carbon dioxide has been demonstrated in bench scale flotation experiments.(2)

EXPERIMENTAL

Coal samples and experimental methods of flotation, contact angle measurement and bubble attachment time measurement have been described in a previous paper.(3)

In addition, a diffuse reflectance FTIR (DRIFT) technique has been used to characterize the coal surface.(3) More recently, an attenuated total reflectance (ATR) accessory, the CIRCLE™ cell with a ZnSe rod from Spectra-Tech Inc., was used in ATR-FTIR spectroscopy. The coal for the ATR-FTIR analysis was ground to minus 1 micron in a ceramic mortar with distilled water at pH 6-6.5 before transferring to the CIRCLE™ cell at a coal/water ratio of 0.5 by weight. A spectrum for each coal was obtained by subtraction of water spectrum from the spectrum of the coal/water suspension. Both spectra were collected under the same conditions with the empty CIRCLE™ cell as a background.

XPS experiments were conducted with the Hewlett-Packard 5950 B instrument using monochromatic Al $K_{\alpha 1,2}$ radiation at 1487 eV. Power at the X-ray source was 400 watts and the chamber vacuum was controlled at 10^{-10} torr. An electron gun at 6 eV supplied a flux of low-energy electrons to the coal surface to minimize heterogeneous charging artifacts in the resulting spectra.

RESULTS AND DISCUSSION

Coal Hydrophobicity

As shown in Figs.1 and 2, it has been found by reagent-less Hallimond tube flotation and by contact angle and bubble attachment time measurements that the hydrophobicity and flotability of coals increase with an increase in coal rank, reaching a maximum for low-volatile bituminous coal and then decreasing with a further increase in coal rank. These traditional methods are excellent indicators of the macroscopic hydrophobicity of the coal surface. However, to better describe the hydrophobic/hydrophilic balance at a coal surface, it is important to establish the corresponding chemical characteristics of these coals.

DRIFT- and ATR-FTIR spectroscopy can provide a more detailed description of the coal surface than elemental bulk composition or chemically determined acid-group content as used by previous investigators.(4) These two FTIR techniques have been used to evaluate the hydrophobicity of fine coals by a spectroscopic criterion--the hydrophilicity index--which contrasts the relative abundance of surface hydrophilic groups OH and COOM with the relative abundance of surface hydrophobic groups ArH and RH.(3) Using the hydrophilicity index determined by both DRIFT- and ATR-FTIR spectroscopy, a rank-dependence of coal hydrophobicity can be plotted as shown in Fig.2. Note that the hydrophobic character of coal estimated by the hydrophilicity index varies with coal rank in much the same fashion as bubble attachment time, contact angle, and flotation recovery. Since the coal rank is essentially classified by the carbon content, the hydrophilicity index determined by FTIR

spectroscopy is obviously a more detailed index for evaluating coal hydrophobicity than coal rank or carbon content.

To ensure the surface sensitivity of the FTIR techniques and confirm the conclusions reached from the FTIR analysis, XPS has also been used to evaluate the hydrophobic character of fine coals.The ratio C/O determined by XPS has also been used to define a hydrophobicity index for the coals. Such a hydrophobicity index for six coals of different rank is presented in Fig.1. Notice that the rank-dependence of coal hydrophobicity estimated by XPS agrees with that evaluated by other methods such as FTIR spectroscopy, flotation response, contact angle and bubble attachment time measurements.

Enhanced Hydrophobicity of Pretreated Coal

Characterization of CO_2-treated coal

As shown in Table 1, it has been found that CO_2 pretreatment increases coal hydrophobicity. Table 2 indicates that enhanced hydrophobicity of CO_2-pretreated coals results in an increased flotation recovery and enhanced ash rejection for coals of different rank with the exception of lignite. It has also been found that coals of middle ranks such as high-, medium-, and low-volatile bituminous coals are most amenable to carbon dioxide coal flotation.(5)

Oxidation can result in a reduced hydrophobicity of CO_2-pretreated coals. Figure 3 illustrates that oxidation of a CO_2-pretreated low-volatile bituminous coal in air reduces the coal hydrophobicity and restores the original lower hydrophobic character after about 20 hours of oxidation. Fortunately, coal oxidation is a slow process. No significant loss in coal hydrophobicity was observed during the first couple hours which was long enough to complete flotation experiments.

The success of CO_2 coal flotation has been attributed to the coal's high adsorption potential for CO_2.(6) It has been found by monitoring the OH absorption band using in-situ FTIR spectroscopy that pore water and hydration water in coal are displaced by CO_2 during pressure treatment, which results in enhanced coal hydrophobicity as shown in Fig.4.

A model for carbon dioxide adsorption by coal is being considered, and a schematic drawing of the microstructure is shown in Fig.5. This drawing represents a final state of the adsorption process, where all the pore water and hydration water have been replaced by CO_2. Before CO_2 pretreatment, the positions of CO_2 molecules in this drawing are predominantly occupied by H_2O molecules. Displacement of the H_2O molecules by CO_2 molecules during pressure treatment and CO_2 nanobubble formation at the coal surface on pressure release are believed to be responsible for the improved flotation performance.

Characterization of thermally-treated coal

It has been found that low-temperature thermal treatment significantly increases the hydrophobicity of lignite as suggested by FTIR hydrophilicity index determinations and confirmed by bubble attachment time measurements/flotation response (see Fig.6). It is believed that the increased hydrophobicity of lignite is attributed to the removal of pore water, hydration water and some organic OH functional groups as well as the diffusion of volatile matter to the surface and the reorientation of surface functional groups. As shown in Table 2, it has been found that controlled thermal treatment can also increase the hydrophobicity of subbituminous coal and anthracite. Finally it should be noted that the thermal treatment improves the flotation separation of lignite from mineral matter.

SUMMARY

Increased hydrophobicity and hence the flotability of coals of different rank has been observed for CO_2 pretreatment and/or controlled thermal pretreatment. DRIFT- and ATR-FTIR and XPS techniques have been used to determine the surface chemical characteristics in order to evaluate coal hydrophobicity. These results agree very well with those determined by traditional methods. The enhanced hydrophobicity of CO_2-treated coal is attributed to the high specific affinity of coal for CO_2 which results in the displacement of pore water and hydration water by CO_2 and on pressure release leads to nanobubble formation at the coal surface in aqueous suspension. Increased hydrophobicity of

lignite by thermal treatment arises from the removal of pore water, hydration water and some organic OH functional groups as well as the diffusion of volatile matter to the surface and the reorientation of surface functional groups.

The financial support provided by the U.S. Department of Energy under Grant No. DE-FG22-85PC80530 is greatly acknowledged.

REFERENCES

1. Miller, J.D. and Misra, M., 1987. U.S. Patent No. 4,676,804.
2. Miller, J.D. and Misra, M., 1985. Coal Preparation, 2:69.
3. Jin, R., Ye, Y. and Miller, J.D., 1987. "Evaluation of coal hydrophobicity by diffuse reflectance FTIR spectroscopy," presented at the 8th National Convention of the Royal Australian Chemical Institute, Aug.24-28, and submitted to Colloids and Surfaces.
4. Miller, J.D., Laskowski, J.S. and Chang, S.S., 1983. Colloids and Surfaces, 8:137.
5. Miller, J.D., Jin, R., Ye, Y. and Sadowski, Z., 1987. "Carbon dioxide for fine coal flotation," Final Report to U.S. Department of Energy, Grant No. DE-FG22-85PC80530.
6. Jin, R., Ye, Y. and Miller, J.D., 1988. "Studies of carbon dioxide adsorption at the surface of coal by in-situ FTIR spectroscopy," presented at the 117th AIME Annual Meeting, Jan.25-28, Preprint No. 88-300, submitted to Fuel.

Table 1 Contact Angle and Bubble Attachment Time for Different Gas Bubbles on a Polished Surface of Low-Volatile Bituminous Coal

Pressure Treatment Using Corresponding Gas Phase at 20 psi	Gas Phase of Bubbles	Contact Angle (degrees)	Bubble Attachment Time (ms)
Yes	Air	49-52	170-190
Yes	N_2	50-51	140-160
Yes	CO_2	54-56	20-25
No	Air	47-49	180-200
No	N_2	50-51	170-190
No	CO_2	51-53	140-150

Table 2 Enhanced Hydrophobicity and Improved Flotation Performance of Pretreated Coals of Different Rank

Coal Rank	Ratio of Attachment Times τ_{CO2}/τ_{air}	Increased Flotation Recovery by CO_2 Pretreatment	Enhanced Ash Rejection by CO_2 Pretreatment	Increased Hydrophobicity by thermal Pretreatment	Enhanced Ash Rejection by thermal Pretreatment
ANT	0.70	Yes	Yes	Yes	
LVB	0.80	Yes	Yes	No	
MVB	0.69	Yes	Yes	No	
HVB	0.66	Yes	Yes	No	
SUB	1.0	Yes	Yes	Yes	
LIG	1.0	No	No	Yes	Yes

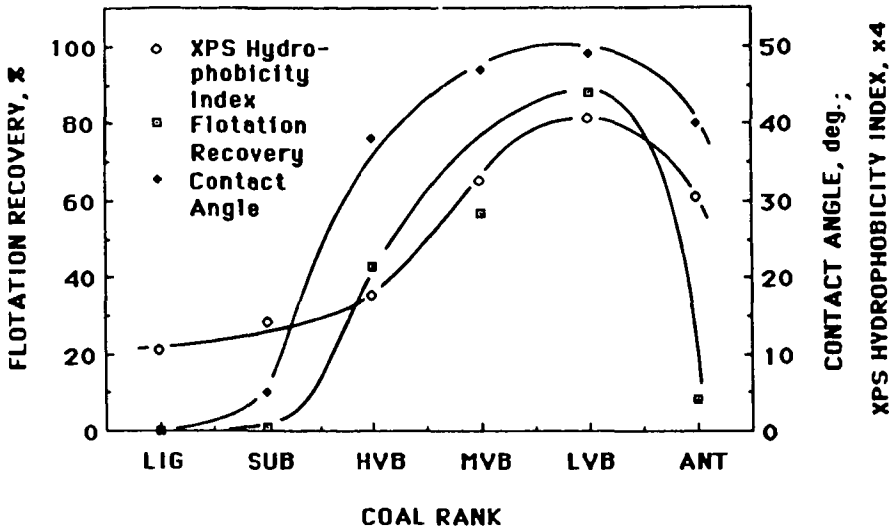

Figure 1 Coal hydrophobicity evaluated by Hallimond tube flotation, contact angle measurement, and XPS analysis as a function of coal rank. ANT = Anthracite, LVB = Low-volatile bituminous coal, MVB = Medium-volatile bituminous coal, HVB = High-volatile bituminous coal, SUB = Subbituminous coal, LIG = Lignite.

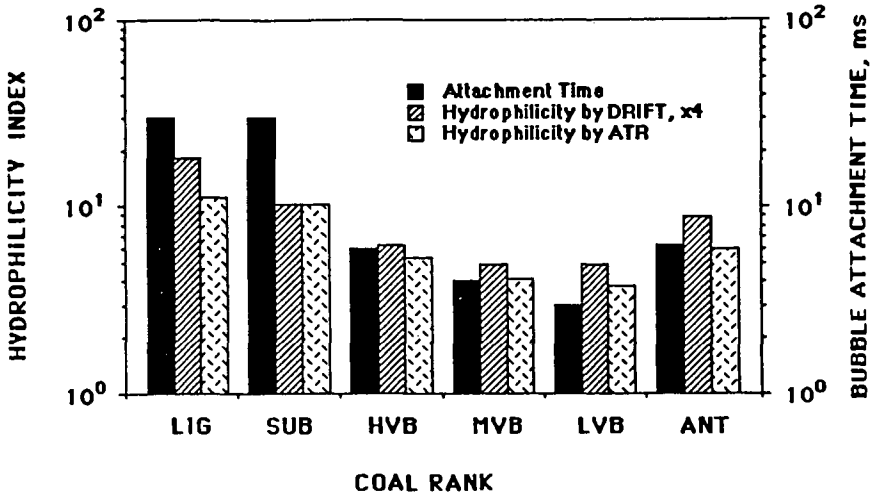

Figure 2 Hydrophobic character of coal as described by bubble attachment time and the hydrophilicity index determined from DRIFT- and ATR-FTIR spectra.

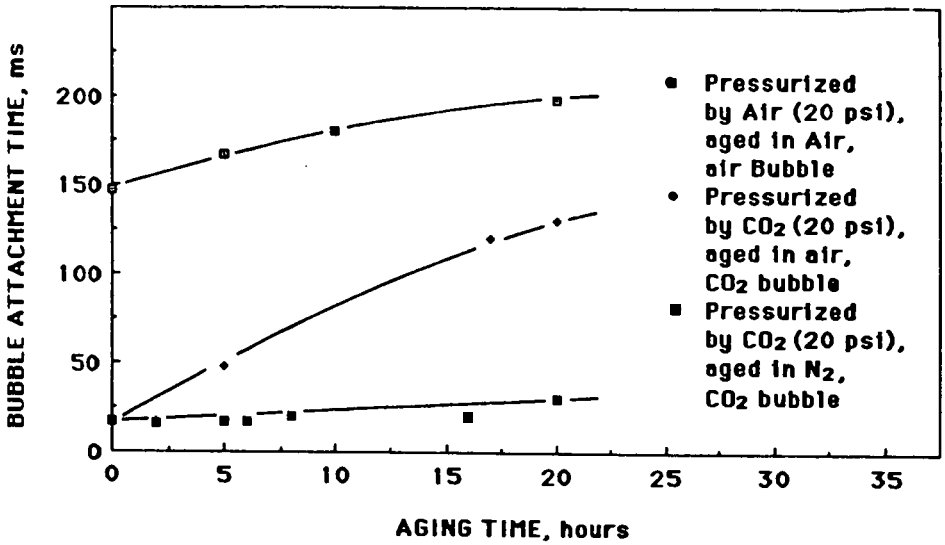

Figure 3 Bubble attachment time measured on the polished surface of a pretreated low-volatile bituminous coal as a function of aging time of the coal.

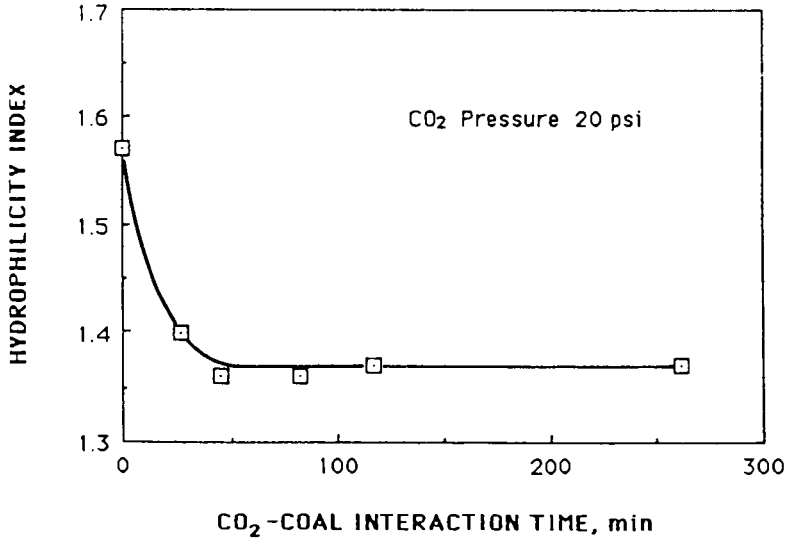

Figure 4 The hydrophilicity index of a CO_2-pretreated high-volatile bituminous coal (-5 micron) at 302 °K determined by DRIFT-FTIR spectroscopy as a function of CO_2-coal interaction time.

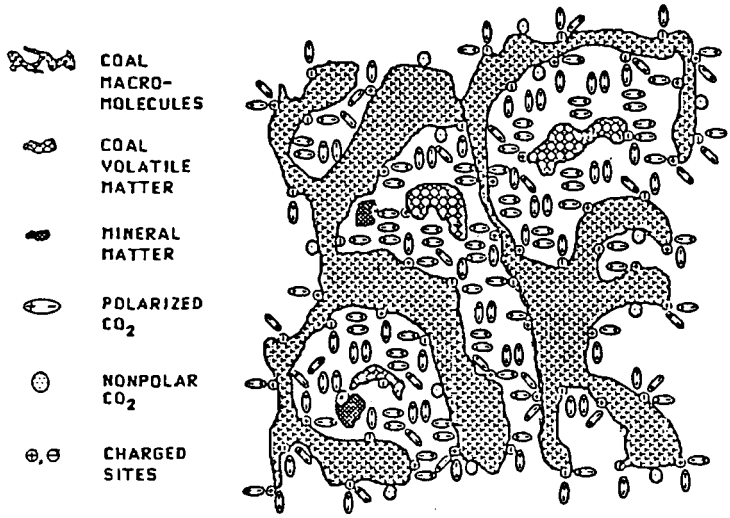

Figure 5 Schematic drawing of carbon dioxide adsorption by coal.

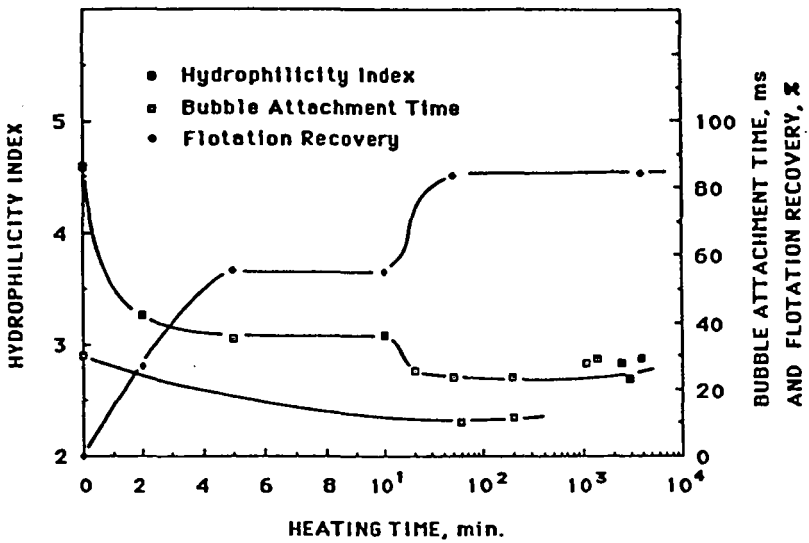

Figure 6 Hydrophobic character of lignite evaluated by the DRIFT-FTIR hydrophilicity index, bubble attachment time and flotation recovery as a function of thermal-treatment time.(3)

IMPROVED SULFUR REMOVAL FROM COALS BY REDOX POTENTIAL CONTROL OF SURFACES DURING GRINDING.

Geatesh K. Tampy, David H. Birlingmair, and Lawrence E. Burkhart
Ames Laboratory, Iowa State University
Ames, Iowa 50011

ABSTRACT

Control of the redox potential of an Upper Freeport run-of-mine coal slurry during wet grinding and subsequent beneficiation gave better sulfur removal, with no decrease in coal recovery, than either potential control during grinding or beneficiation alone. Sodium dithionite, a reducing agent used to depress the sulfur, also gave substantially better results than pH control alone, irrespective of whether the physical beneficiation was by oil agglomeration, foam flotation, or microbubble batch flotation. Three-phase contact angle measurements and pulp potential measurements suggest that slow electrochemical reactions at the particle surfaces may be responsible for the improved results obtained when the reductant is added at the grinding stage.

INTRODUCTION

The purpose of this work was to alter the surface properties of coal and/or associated mineral particles during grinding to enhance the removal of sulfur-bearing minerals during the beneficiation process. This was done by using reducing agents to alter the electrochemical potential during grinding and beneficiation. The fact that sulfide ores can be depressed by electrochemical techniques is well catalogued in the literature(1-5). Studies(6-9) also have shown that electrochemical effects due to "galvanic interaction" of grinding media during size reduction can affect the flotation of sulfide minerals. In this study, however, electrochemical effects were imposed during grinding by the addition of a chemical reagent. It was presumed that the generation of fresh surfaces, improved contact with the freshly generated surfaces, and the presence of an energy-intensive environment, would all contribute towards promoting surface reactions that could result in enhanced beneficiation.

It should be emphasized that adding oxidizing or reducing agents and monitoring the system by measuring the potential of the pulp relative to a reference electrode, yields a potential which has no real thermodynamic significance. However, it may be used as a guideline, and it has been shown to correlate with laboratory flotation results(10).

EXPERIMENTAL

Materials

a) Feed Coal.

A run-of-mine coal sample from the Upper Freeport Seam, Lucerne Mine No. 6, Helvetia Coal Company, Indiana County, Pennsylvania, was used. The sample was dried and reduced to a nominal top size of 9.5 mm (3/8 in) by the Pittsburgh Energy Technology Center. It was further reduced to minus 176 μm in a hammermill, riffled into aliquots, purged with argon, and sealed until use. Its properties are listed in Table 1.

Table 1. Upper Freeport run-of-mine coal, as received.

Moisture %	Ash %	Total Sulfur %	Pyritic Sulfur %	Organic Sulfur %	Sulfate Sulfur %	Heating Value Btu/lb	Hardgrove Grindability (0.7% Moisture)
0.85	32.65	2.41	2.04	0.36	0.01	9970	87

b) Additives.

Reagent grade sodium hydroxide, sulfuric acid, and sodium dithionite ($Na_2S_2O_4$) were used. Kerosene was employed as a conditioner and as an agglomerating oil; Dowfroth 150, Accofroth 76, and methylisobutylcarbinol (MIBC) were used as collectors.

Experimental procedure

Grinding.

Samples of the 176-μm feed coal were wet ground (40% solids by weight coal) for 15 minutes in a stirred ball mill using 1/8-in stainless steel balls as the grinding media. The final average particle size was about 10 μm.

Separations.

After grinding in the stirred ball mill, each slurry was separated from the balls and divided into aliquots for separation by three techniques.

1) Microbubble Frit Flotation

The slurry was diluted to 10% solids, conditioned with kerosene (collector) and MIBC (frother), and placed in a flotation cell. Microbubbles were formed in the flotation cell by admitting a regulated gas flow through a porous glass frit at the bottom of the cell. The coal particles, being hydrophobic, attached themselves to the microbubbles and were thus carried to the top of the cell in a fine froth. The overflowing froth (or concentrate) and the material remaining in the flotation cell (i.e., the tailings) were collected, filtered, dried, and analyzed.

2) Microbubble Foam Flotation

In this process the conditioned pulp was transferred to a flotation tube and a microbubble foam was introduced at the bottom of the tube. The foam was prepared by adding either Accofroth 76 or Dowfroth 150 to water in a modified blending chamber at high speed. The concentrate and the tailings were filtered, dried, and analyzed.

3) Oil Agglomeration

A 10% percent coal/water slurry was agglomerated with 15% (by weight of coal) kerosene in a 500-ml blending chamber for 3 minutes at low shear. The agglomerates were separated from the tailings using 100- and 200-mesh test sieves. They were then filtered, dried, and analyzed.

Variations in pretreatment during comminution in the stirred ball mill included the use of NaOH and H_2SO_4 for pH adjustments and $Na_2S_2O_4$ for control of the pulp potential (ε). Tests were also conducted with no additives and with the same additives introduced after grinding.

Float/Sink

In another series of tests, portions of the feed coal sample were subjected to float/sink separation using Certigrav at a specific gravity of 1.4 to obtain an organic-rich fraction with a

low mineral content and a mineral-rich fraction with a high mineral content. After separation, the samples were dried at 107°C until no odor of Certigrav remained. The float fraction thus obtained contained 4.7% ash and 0.78% sulfur, and the sink fraction contained 55.4% ash and 8.8% sulfur. Since the ideal separation conditions are those in which the organic fractions are more hydrophobic and the mineral fractions are more hydrophilic, by separating the feed coal into organic-rich and mineral-rich fractions, each fraction may be tested separately to determine the surface characteristics under the conditions used. Flotation results, conducted with coal samples soaked in Certigrav and then dried, were compared with flotation results from samples that had not been soaked in Certigrav to assure that exposure to the Certigrav liquid did not affect the particle surfaces.

Contact angle measurements

Three-phase (solid-liquid-water) contact angle measurements at various values of pH and also for an aqueous phase containing sodium dithionite were made using compressed pellets of organic-rich and mineral-rich coal fractions of the Upper Freeport coal which were obtained from the float-sink separation. The pH of the water drops placed on the pellets was adjusted using NaOH and H_2SO_4. A 0.1 M solution of sodium dithionite ($Na_2S_2O_4$) was used. A Rame-Hart contact angle goniometer was used, and the contact angles were measured from enlarged photographs of the drops using a protractor. The contact angles thus obtained were accurate to within 5 degrees, which is the best accuracy that may be expected from a heterogeneous substance like coal.

Potential Measurements

Zeta potential measurements were made with a Komline Sanderson Model 12S zeta meter. Measurements were made for both organic-rich and mineral-rich fractions of coal obtained by float-sink separation in solutions of various concentration of sodium dithionite. The pH and the pulp potential (ε) were monitored with an Orion Microprocessor Ion Analyzer (Model 901) using a combination pH electrode and a combination Pt-Ag/AgCl electrode (0.044 ± 0.001V vs.SCE).

RESULTS

Beneficiation

In the grinding and beneficiation tests, the sample was ground both with and without pH control. The samples ground at pH 3 and pH 7 were each separated at both pH 3 and pH 7. Those ground at the natural pH of 5.5 and at pH 11 were separated at the same pH as during grinding. The results, presented in Table 2, show that under most conditions, the coal recovery was high but with only moderate sulfur reductions and rather poor ash reduction. Since the blender flotation technique yielded poor recoveries, particularly at low pH, some of these tests were repeated using Dowfroth 150 as the frother instead of Accofroth 76. Sulfur removal was poor with Dowfroth, although a slight improvement in coal recovery was obtained.

Table 3 shows the results obtained in replicate runs when sodium dithionite was present during both grinding and separation. This produced significant improvement in the sulfur reduction over those experiments where only pH control was used (Table 2). Average

sulfur reduction values obtained with pH control are compared to those obtained when sodium dithionite was used during both grinding and separation in Figure 1. Figure 2 shows an equally important result; when sodium dithionite was used in only one step, either grinding or separation, lower sulfur reduction was obtained. However, the values still tended to be better than those found during pH control.

Table 2. Results of separations performed under various conditions of pH during grinding and separation.

Grinding pH	Separation Type[e]	Separation pH	% S Conc.	% S[a] Redn.	% Ash[b] Conc.	% Ash[c] Redn.	% Coal[d] Recov.	(additive)
Feed			**3.64**	-	**31.3**	-	-	
Natural	Foam	Natural ~5.5	2.20	39.2	15.9	51.3	84.1	(Accofroth)
	Frit		2.20	39.2	19.9	39.0	97.6	(MIBC)
	Agg		2.32	35.9	13.4	58.9	95.5	(Kero)
7	Foam	7	2.24	38.1	14.3	56.2	90.3	(Accofroth)
	Frit		2.11	41.7	17.6	46.0	97.0	(MIBC)
	Agg		2.39	34.0	13.3	59.3	96.0	(Kero)
	Foam	3	2.19	39.5	15.4	52.8	65.6	(Accofroth)
	Frit		2.22	38.7	19.9	32.1	97.7	(MIBC)
	Agg		2.27	37.3	12.8	60.8	94.1	(Kero)
3	Foam	3	2.59	28.9	19.3	38.4	89.9	(Dow Froth)
	Frit		2.30	36.8	14.3	54.3	88.0	(MIBC)
	Agg		2.25	38.1	14.3	54.3	94.1	(Kero)
	Foam	7	2.22	39.07	16.4	47.8	88.7	(Accofroth)
	Foam		3.20	12.41	24.5	15.5	98.7	(Dow Froth)
	Frit		2.50	33.1	15.4	50.8	95.9	(MIBC)
	Agg		2.34	35.6	14.2	54.8	96.1	(Kero)
11	Foam	11	2.60	28.6	16.5	47.4	95.3	(Accofroth)
	Frit		2.31	36.4	14.8	52.6	91.7	(MIBC)
	Agg		2.43	33.3	13.5	56.8	96.4	(Kero)

a $\% \text{ S Reduction} = \frac{\%\text{Feed S} - \%\text{ Product S}}{\%\text{ Feed S}}$ (all DAF)

b Ash reported on a moisture-free basis; sulfur reported on a moisture- and ash-free basis.

c $\% \text{ Ash Reduction} = \frac{\%\text{Feed Ash} - \%\text{ Product Ash}}{\%\text{ Feed Ash}}$, moisture free.

d $\% \text{ Coal Recovery} = \frac{100 \times (100 - \%\text{ Product Ash})\,(\text{Product wt})}{(100 - \%\text{ Feed Ash})\,(\text{Feed wt})}$

e Foam, Frit, and Agg indicate the type of separation technique used: foam flotation, microbubble frit flotation, or oil agglomeration, respectively.

Table 3. Results of separations performed using 0.1 M sodium dithionite during both grinding and separation[a]. Replicate runs for each technique are shown.

Grinding Condition	Separation Type	Separation Condition pH	Separation Condition ε (V)	% S Conc.	% S Redn.	% Ash Conc.	% Ash Redn.	% Coal Recov.
Feed				**3.64**	-	**31.3**	-	-
0.1 M $Na_2S_2O_4$	Frit	5.0	-0.39	1.56	57.1	9.3	70.3	68.6
	Frit	4.6	-0.43	2.09	42.6	13.0	59.4	92.4
	Frit	4.3	-0.40	1.96	46.3	12.8	59.3	92.6
	Frit	4.8	-0.40	1.93	46.9	16.1	48.6	90.8
	Foam	5.2	-[b]	1.89	48.3	12.8	59.1	71.5
	Foam	5.2	-	2.05	43.8	12.3	60.8	68.5
	Foam	5.2	-	1.89	48.3	12.1	61.4	65.4
	Foam	5.3	-	1.66	54.5	12.5	60.2	58.0
	Agg	5.0	-0.39	2.02	44.5	12.1	61.4	95.4
	Agg	4.9	-0.40	1.98	45.4	12.4	60.7	84.6

[a] Definitions as in Table 1.
[b] The foam flotation technique does not permit sufficient time for pulp potential measurements.

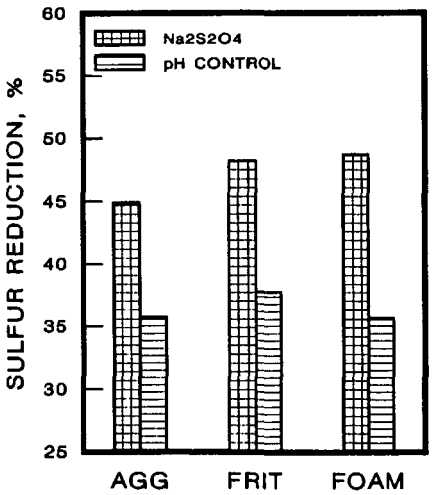

Figure 1. Average sulfur reduction values obtained when $Na_2S_2O_4$ was used during both grinding and separation compared to those obtained with pH control alone.

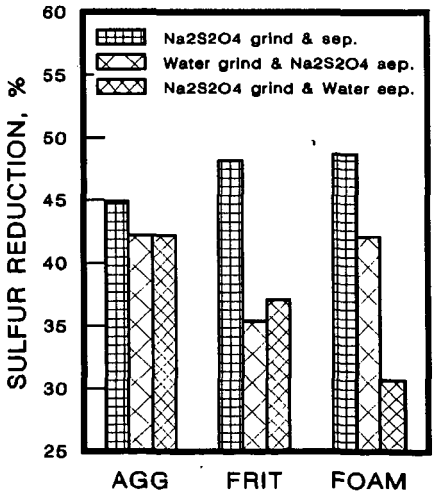

Figure 2. Results obtained when $Na_2S_2O_4$ was used either during grinding or separation only, or during both grinding and separation.

Surface Characterization Tests

Table 4 depicts the results of contact angle measurements made on pellets prepared with material from the float-sink separations. A smaller angle indicates a surface of greater hydrophobicity (see Figure 3). The contact angles measured for the mineral-rich fraction are consistently larger than those measured for the organic-rich fraction, demonstrating that the mineral-rich fraction is more hydrophilic than the organic-rich fraction. Also, the hydrophilicity of the mineral fraction was a maximum at high pH. These are expected results. However, an unexpected result was that the contact angles measured when the aqueous phase contained 0.1 M sodium dithionite were similar to those with the acidic and neutral aqueous solutions.

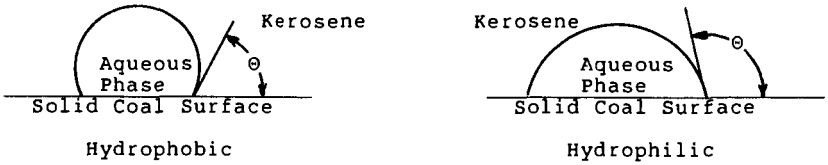

Figure 3. Contact angle measurement.

Table 4. Measured contact angles (θ) of organic-rich and mineral-rich fractions of Upper Freeport coal using the sessile drop technique. Values are averages of 'n' measurements with a standard deviation of σ.

	Mineral-Rich "Sink" Fraction			Organic-Rich "Float" Fraction		
Condition	θ	σ	n	θ	σ	n
pH 11.0	27.5	1.69	8	21.2	5.32	8
pH 7.6	27.3	3.58	8	20.3	4.56	8
pH 3.0	24.4	4.72	8	17.5	3.38	8
0.1M $Na_2S_2O_4$	26.1	3.98	8	20.9	2.10	8
pH 4 Buffer	24.5	0.71	2	16.5	2.12	2
pH 7 Buffer	26.5	2.12	2	15.5	0.71	2
pH 10 Buffer	30.0	0	2	20.0	0	2

An attempt was made to determine the effect of ionic strength on the zeta potential of the organic-rich and mineral-rich fractions in solutions of varying sodium dithionite concentration. During these tests, it was found that both the pulp potential, and the pH of the slurry, changed with time. The change continued over several minutes and the rate of change was a function of sodium dithionite concentration. Thus these experiments provided no information about the effect of the ionic double layer. However, they suggest that the kinetics of reactions at the surface may be important and that slow electrochemical surface reactions may have been taking place.

DISCUSSION

The increased floatability of pyrite and other sulfide minerals is usually attributed to mild oxidation which leads to the formation

of sulfur or sulfur-like entities which enhance the particle hydrophobicity. Hamilton and Woods(11) have explained the effect as the formation of a metal-deficient sulfide; conversely, reduction produces a metal-rich sulfide on the particle surface. These authors state that the attractive interaction between water and the mineral surface is determined by the availability of metal ions in the immediate surface layer (large anions, like sulfide, are generally not hydrated). Thus, removal of metal ions from the surface reduces the opportunity for specific interaction with water molecules. Hydrophobic/hydrophilic effects in solution may also be explained in terms of the free energy of the particle surface(12). When this is done the entropy component of the free energy change of the surface is seen to be significant(12).

Guy and Trahar(13) report that for many sulfides, the oxidation reaction does not proceed rapidly. Firth and Nicol(14) state that a number of factors could affect the rate of reaction on pyrite surfaces. These include: the temperature and humidity, the size distribution and form of occurrence of the sulfides, the time of exposure, and the presence of peculiarities in the crystal lattice, such as sulfur deficiencies and the presence of polymorphs, which may serve as active sites for oxidation reactions. Castro(15) found that, over time the electrode potential of chalcocite decreased when sodium sulfide was added, indicating oxidation of the mineral. More recently, Milley(16) has shown that the electrode potential of a suspension of coal particles in an aqueous solution of a strong oxidizing agent changes over several hours. Thus, observing this change, a general picture of the oxidation process may be obtained, the change being indicative of the "oxidation state" of the coal.

One may envision that the reduction reaction, which has been studied less extensively, may display kinetic effects similar to those observed for oxidation. Chander(17) has reviewed the published literature on the mechanism of reduction of pyrite minerals and states that a unified theory is, as yet, unavailable. According to Chander(17), formation of metastable species in the solution or in the solid phase, nonstoichiometry of the solid phase, and slow reaction kinetics could all lead to nonequilibrium conditions. The variation of the pulp potential and pH with time does suggest slow reaction kinetics.

CONCLUSION

The addition of sodium dithionite to control pulp potential resulted in improved ash and sulfur removal from Upper Freeport coal as compared to pH control. The best results were obtained when the reducing agent was present during both grinding and separation. Contact angle measurements indicated that the improvement was not due to a lesser affinity for the organic portion of the coal toward the dithionite solution. The pulp potential and the pH of the slurries containing the organic-rich and mineral-rich fractions of the coal varied with time, indicating the possibility of slow reaction kinetics. This work is an example in which the grinder has been employed effectively in chemical pretreatment. The concept, often discussed in the literature, has rarely been demonstrated.

ACKNOWLEDGEMENTS

Ames Laboratory is operated for the U. S. Department of Energy by Iowa State University under Contract No. W-7405-ENG-82. This work was supported by the Assistant Secretary for Fossil Energy through the Pittsburgh Energy Technology Center.

REFERENCES

1. Hyde,G.R.; Stojsic,A.; Mining Engineering, **39**(7), 481-484, (1987).

2. Nakazawa,H.; Iwasaki,I.; Minerals and Metallurgical Processing, **2**,206-211,(1985).

3. Ogunsola,O.M.; Osseo-Asare,K.; Fuel, **65**, 811-815, (1986).

4. Biegler,T.; Swift,D.A.; Electrochimica Acta, **24**, 415-420, (1979).

5. Luttrell,G.H., and Yoon,R.H., Int. J. Miner. Proc., **13**, 271 283, (1984).

6. Kocabag,D.; Smith,M.R.; in "Complex Sulfides. Processing of Ores, Concentrates and By-Products", Zunkel,A.D.; Boorman,A.S.; Wesely,R.J.; eds., 55-81, 1985.

7. Learmont,M.E.; Iwasaki,I.; Minerals and Metallurgical Processing, 1, 136-143, (1984).

8. Adam,K.; Natarajan,K.A.; Iwasaki,I.; International Journal of Mineral Processing, **12**, 39-54, (1984).

9. Pozzo,R.L.; Malicsi,A.S.; Iwasaki,I.; SME Annual Meeting, Phoenix, AZ, Jan 25-28 (1988).

10. Hamilton,I.C.; Woods,R.; Proc. Int. Symp on Electrochemistry in Mineral and Metal Processing, Richardson,P.E.; Srinivasan,S.; Woods,R.; eds., The Electroanalytical Society, NJ, 1984.

11. Hamilton,I.C.; Woods,R.; J. Electroanal. Chem., **118**, 327, (1981).

12. a) Tampy,G.K.; PhD Dissertation, Ohio University, March (1988). b) Tampy,G.K.; Prudich,M.E.; Savage,R.L.; Williams,R.R.; Energy & Fuels, in press, 1988.

13. Guy,P.J.; Trahar,W.J.; in "Flotation of Sulfide Minerals", Fossberg,K.S.E.; ed.; Elsevier, 1985, pp. 91-110.

14. Firth,B.A.; Nicol,S.K.; Coal Preparation, 1, 53-70, (1984).

15. Castro,S.; in "Mineral Processing", vol. 2, Laskowski,J.; ed., Elsevier, 1981, pp. 181-202.

16. Milley,J.; Fuel, **67**, 143-144, (1988).

17. Chander,S.; Minerals and Metallurgical Processing, **2**, 26-35, (1985).

EXTRACTION RATES AND POROSITY CHANGES OF COALS IN SUPERCRITICAL THF

E.S. Olson, J.W. Diehl. D.K. Horne and H.D. Bale

University of North Dakota
Energy and Mineral Research Center
and Department of Physics
Grand Forks, ND 58202

Important facets of the thermal processing of coals in a dissolving medium, such as that which occurs in liquefaction or extraction, are the rate of dissolution and the concomitant change in the surface structure of the coal. The interaction between these two related parameters is being studied by extracting coals in a flow-through cell under supercritical conditions and measuring the rates of extraction by on-line ultraviolet spectroscopy and the changes in pore structure of the coal by in situ small-angle X-ray scattering. The advantages of utilizing supercritical fluids in this project are the solvent densities, which are similar to liquids, the high solubility parameters, and yet low viscosities, similar to gases. For these experiments the solvent should be composed of first row elements and not have significant absorption in the uv. In addition, alcohols cannot be used since they destroy the aluminum windows of the extraction cell. Several solvents were tested in these investigations, and supercritical tetrahydrofuran (THF) was the only one found satisfactory for both measurements. The supercritical THF gave good yields of extract from even lignites, and the extracted material remained soluble in liquid THF.

EXPERIMENTAL

The solvent in these studies was uninhibited HPLC grade THF (Fisher), used as received. Coal was dried in an inert atmosphere or in a vacuum prior to the extraction. Ultimate analysis (maf) for the Wyodak subbituminous coal (Clovis Point) was H, 5.2; C, 70.9; N, 0.92; S, 0.60; O (ind.), 22.3. Proximate analysis (mf) was volatile matter, 44.2; ash, 8.4; fixed carbon (ind.), 47.5.

Two different extraction cells have been used for the two types of measurements. The apparatus in which the extraction kinetics were measured by uv absorption consisted of an Isco LC-5000 syringe pump connected to a 5 cm x 4.6 mm (LC precolumn) extraction cell. The cell and steel inlet tubing were heated in a Varian 1400 aerograph GC. The cell capacity was 0.2 g. Effluent from the cell was carried fr. the oven via a 1/16-inch steel tubing to a 1 m x 0.32 mm fused silica capillary (no phase coating), which served as the cell for the uv detector. The polyimide outer coating was removed from a portion of the capillary which was in the beam path of a Kratos 700 LC detector (254 nm). After passing through the uv detector, the capillary was connected to a Whitney SS-21RS2 restrictor valve to maintain the pressure in the system. The eluent was collected, and the weight of extract was determined after evaporation of the solvent.

Analog signals from the uv detector were digitized with an Omega WB-31 12-bit A/D converter and transferred to a Tandy 2000HD computer via RS-232C. Data was collected and stored to disk at 2 points/s. The area under the uv response curve was divided into 100 equal time segments and the proportional area determined for each segment. The

proportional areas were multiplied by the extract weight, giving the weight of extract per unit time. This normalization assumes that the response across the curve remains constant, which was determined to be true for extraction of 3 g of coal in a large cell where individual fractions were collected and weighed.

The extraction cell for the small-angle scattering studies consisted of two electrically heated flanges which hold the aluminum/berylium windows and a stainless steel block which gives a sample depth of 0.07 inches between the two windows. Molybdenum K_α radiation was used in these studies. Details of the collimation system and position sensitive detector are available elsewhere (1). Analysis of the scattering data was based on a model developed by Kalliat, Kwak, and Schmidt (2). Pore structure parameters calculated for thermally treated lignites have been shown to be in close agreement with independent measurements (3).

RESULTS AND DISCUSSION

A series of kinetic experiments were carried out with Wyodak subbituminous coal (Clovis Point) in the flow-through cell with on-line uv detection. In each of these runs, a dewaxing preextraction stage at a temperature of 120°C was utilized to remove an initial surge of material, whose elution was monitored until no detector response was observed. The material extracted at this low temperature (2% mf basis) was mainly aliphatic (fatty acids), similar to the Montan wax, which is normally extracted with noncritical solvents and is not believed to be covalently bonded or "matrix trapped" material.

The X-ray scattering pattern of the Wyodak coal after extraction at 120°C and 4.5 MPa indicated that the dewaxing had an effect on the pore structure, causing a modest increase in the micropore parameters (Table 1). The micropore specific surface increased from 58 m^2/g to about 290 m^2/g. The corresponding increase in micropore volume was 0.019 cm^3/g, which would suggest about a 2% loss of mass if the new pore structure is formed in the wake of the dissolved component.

The supercritical extractions were carried out by rapidly increasing the temperature of the system (30°C/min) in the GC oven to the desired extraction temperature where the temperature was held constant (isothermal stage). UV response data for the Wyodak coal were recorded for four extraction temperatures from 325 to 400°C at 15.2 MPa and flow rates of 1 ml/min. Run times were about one hour. Two extractions were conducted at 380°C at lower pressures (5.5 and 10.3 MPa) for comparison with the 15.2 MPa run. The solvent containing the extracted material was collected after the restrictor valve. The solvent was removed and the extract weighed. The yield data from the four experiments at 15.2 MPa and two experiments conducted at lower pressures are shown in Table 2. The yields at the high temperatures (350° and above) at 15.2 MPa were essentially the same and were approximately three times the yield obtained at either low temperature (325°) or low pressures. We distinguish then, three classes of extracted coal material, the preextraction wax, the low-temperature extract (easily extracted material), and the high-temperature extract (less easily extracted material). The composition of the low- and high-temperature extracts was similar, consisting of high molecular weight aliphatic and aromatic material. The higher yields at the higher pressure may be due to the higher solvating power of the supercritical fluid at higher densities, which are obtained at

higher pressure, or may be due to a physical effect such as solvent being forced into a micropore.

The uv response curve for the 380°C extraction of Wyodak is shown in Figure 1. The curve does not include the preextraction step, instead it begins with the rapid temperature increase. From the uv response curve, the amount of coal material being extracted at each instant and the amount accumulated at each time interval (x) was determined. The natural log of the difference between the total amount of extract (a) and the accumulated amount at each interval (x) was plotted versus time. The first half of the curve was linear, indicating first-order kinetics. The slope of this part of the curve was used to determine an apparent rate constant. Similar curves were obtained for the reactions carried out isothermally at the other temperatures, and the rate constant (k^*) for each of these is shown in Table 2. It is likely that these rate constant values are a composite of reaction rate constants for bond cleavage reactions and other constants for diffusion and dissolution of the coal macromolecules in the supercritical phase. Because of the variety of bonds in the coal matrix which must be broken to solubilize the coal, the range of individual rate constants for bond cleavages which make up the composite might be quite large. Similarly, the polydispersity of molecular sizes in the material released by bond breakage and the solvation parameters of these materials might result in diffusion constants that vary over a large range. Thus one would not expect to be able to derive an activation energy for bond dissociation from the rate constant data at the different temperatures via an Arhenius plot.

Comparison of the rate constants for the 350, 380, and 400°C runs show that they increase generally with the temperature as one would normally expect. The rate constant for the 325° reaction is higher than that for the 350° reaction, but this is for much less extracted material, a 10% yield versus a 28% yield. Thus at 325° we observe the rate constant for the easily extracted material (10% yield) and the rate constant for extraction of this material would be expected to increase with temperature. Then at 350°C the less easily extracted material contributes to the extraction products (an additional 20% yield) but with a lower extraction rate constant, hence lowering the overall rate constant observed. At higher temperatures the rate constant for the less easily extracted material increases. At the lower pressures, lower yields are obtained, presumably because of lower solvent density. This may be the same easily extracted material with the higher extraction rate constant, exhibiting the expected increase with temperature. Thus the less easily extracted material made no contribution to the rate constant at the lower pressures.

For the Wyodak coal extracted at 380° and 4.5 MPa, the micropore surface calculated from the scattering data was 2.7 x $10^3 m^2/g$. This substantial (tenfold) increase was accompanied by a decrease in the transition pore area to 0.39 m^2/g. Progressive isothermal (380°C) extraction as a function of pressure was carried out at 4.5, 7.5, and 10.5 MPa. The curves show an increase in scattering at the intermediate h values, which can be attributed to an increase in the transition pore structure (Table 1). There is also a small increase in the scattering at the larger h values following extraction at 7.5 MPa which suggests additional micropore structure. The progressive changes in the micropore surface area may be due to the increased

solubility of the extract at higher fluid density. The increased transition pore structure is likely a consequence of heterogeneous nature of the coal which results in certain regions dissolving more easily than others.

The change in kinetics as the reaction proceeds may be attributed to an increase in surface area as the micropore volumes develop during the extraction. Thus the greater contact with solvent in the enlarged micropores may result in release of more coal material, even though the activation energies for bond cleavage do not change. Further measurements are needed to confirm this hypothesis.

Experiments were carried out with two additional coals, Beulah (ND) lignite and Pittsburgh #8 bituminous coal (Argonne premium sample), with supercritical THF at 2200 psi and 380°C. The bituminous coal gave a 24% yield of extract in a two-hour run. The uv response had not reached the baseline even after the two hours, indicating that coal-derived material was still being extracted. As expected from this incompleteness of the reaction, the first-order rate constant calculated from the uv response curve for this experiment was considerably lower than that of the Wyodak at the same temperature and pressure, that is 0.014 min^{-1}. Thus the bituminous coal is capable of giving good yields of extract but at a much slower rate than the Wyodak subbituminous coal. Under the same conditions of temperature and pressure, the Beulah lignite gave a yield of 12% over a 80-min period, with the uv response returning to baseline. The uv response curve was unlike that of the Wyodak and Pittsburgh #8 in that the maximum extraction rate was reached more slowly. The first-order rate constant calculated from the curve was 0.022, also lower than that of the Wyodak. These data appear to provide an excellent reactivity index for the coal under nonreductive conditions.

REFERENCES

1. Bale, H.D. Role of Porosity in Supercritical Fluid Extraction of Coal, Technical Progress Report, January 20, 1987.

2. Kalliat, M.; Kwak, C.Y.; Schmidt, P.W. New Approaches in Coal Chemistry, Symposium Series 169; Amer. Chem. Soc.: Washington, DC, 1981; Chapter 1.

3. Bale, H.D.; Carlson, M.L.; Schobert, H.H; Fuel 1986, 65, 1185-1189.

ACKNOWLEDGEMENTS

This research was sponsored by the Department of Energy under DOE contract number DE-FG22-86PC90521.

Table 1
Scattering Results for Wyodak Coal

Conditions	Specific Surface (m^2/g) S_{ma}	S_{tr}	S_{mi}	Specific Volumes x 10^3 (cm^3/g) V_{tr}	V_{mi}
120 C, Ar, 0.2MPa	1.5	3.7	58	2.2	7.1
120 C, THF, 4.5MPa	1.8	3.0	2.9×10^2	2.2	26
380 C, THF, 4.5MPa	1.6	0.39	2.7×10^3	0.15	140
380 C, THF, 7.5MPa	1.2	4.5	4.0×10^3	2.3	250
380 C, THF, 10.5MPa	1.5	10.0	4.3×10^3	4.0	260

Table 2
Yield data and apparent rate constants for Wyodak extractions (THF)

Temperature (^oC)	Pressure (MPa)	Yield (%mf±2%)	$k^*(min^{-1})$
325	15.2	10	0.041
350	15.2	28	0.028
380	15.2	30	0.041
400	15.2	25	0.064
380	10.3	9	0.053
380	5.5	6	0.052

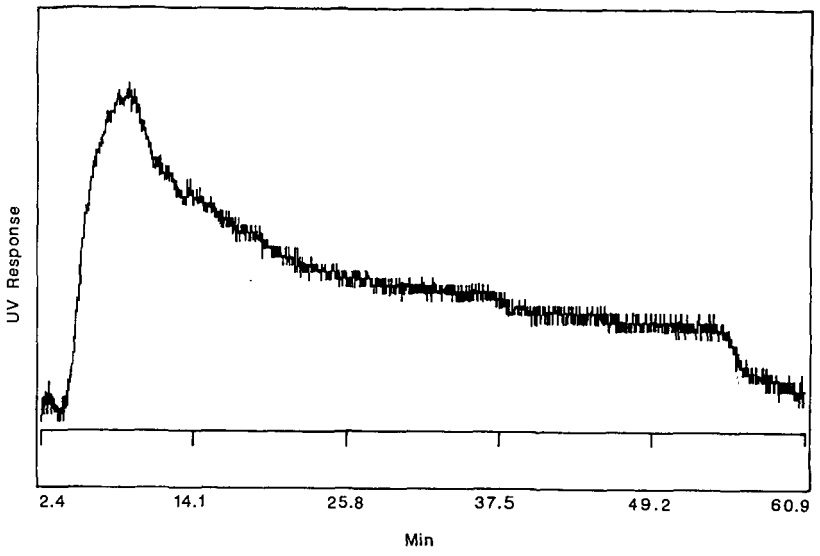

Figure 1: UV response curve for supercritical THF extraction of Wyodak. (THF, 380°, 2200 psi, 1 ml/min).

COAL COMMINUTION BY HIGH PRESSURE WATER JETS
MACHINE DESIGN CONCEPTUAL STUDY

Dr. G. Galecki
Dr. M. Mazurkiewicz
Mr. L. Wijeratne

Rock Mechanics & Explosives Research Center of the University of Missouri-Rolla, 1006 Kingshighway, Rolla, Missouri 65401 U.S.A.

ABSTRACT:

In the offered paper the authors present the results of the work conducted on the coal response for high pressure water jets attack. The paper covers different types of water jets such as: solid jets, cavitating jets, and rotating jets and also the results of coal disintegration effectiveness. The concepts of the models of comminuting machines are presented. The mechanism of the coal disintegration in relationship to these models and the process efficiency are discussed.

INTRODUCTION:

With the advances in the high pressure water jet technology, one of the potential applications of this science is in the area of material disintegration. Coal was chosen as the subject of interest because of the ongoing search for an alternative source of energy. Coal has a structure that is very brittle and filled with micro-cracks. Earlier work by Mazurkiewicz [1] show that material is weaker in tension than in compression. Figure 1 shows the stresses that occur as the water jet penetrates a coal crack. The tip tension stress σ maximum is given by the equation

$$\sigma \max = \sigma_o \left(1 + \frac{2b}{a} \right) \qquad 1)$$

where σ_o is the stagnation pressure developed inside the crack by the jet, 2b the crack length and the 2a the crack width. For even hard coal with a crack dimension ratio, b/a = 10, the pressure necessary to ensure continued crack growth is 15.7 KPa.

For coal, the practical observation yields a ratio between the compression stress versus the tensile stress to be in the range of 20 to 30 times. Also, the theoretical strain energy comparisons show that the compression tension ratio for coal to be 65 in the perpendicular direction to the coal seam and 62 in the parallel direction to the coal seam. These facts combined with the ability of the water jets to penetrate the micro-cracks, creating a zone of tension at the crack tip enhances crack growth and increases the comminution effectiveness.

The theoretical model for comminution of coal by high pressure water jets was based on Griffith's theory [2,3]. Griffith considered an infinite cracked plate of unit thickness with a central traverse crack of length of 2a. The plate is under tensile stress and fixed at its ends. Crack propagation will occur if the energy released upon crack growth is sufficient to provide all the energy that is required for crack growth, which can be expressed by:

$$\frac{dU}{da} = \frac{dW}{da} \qquad 2)$$

where U is the elastic energy and W the energy required for crack growth. Griffith defined the crack driving force as $G = \pi\sigma^2 a/E$. For crack growth to occur G must exceed a certain critical value G_{IC}. Hence the condition for crack growth

$$G_{IC} = \frac{\pi\sigma_c^2 a}{E} \rightarrow \sigma_c = \frac{E\, G_{IC}}{\pi a} \qquad 3)$$

$$\sigma = \frac{Po - Pv}{\rho U_o^2/2} \qquad 4)$$

where Po and Uo are the ambient values of pressure intensity and velocity and Pv and are the vapor pressure and the density of the liquid, respectively. For maximum cavitation in the chamber the outlet pressure should be approximately 1% of the inlet pressure. To control these conditions, a specially designed cavitation chamber was used [5].

Two types of nozzles were used. The first series utilized a nozzle that was not point loaded, but rather contains a cylindrical cavity of air in the center of the jet, which causes very high turbulence (Figure 4). For this series the coal was loaded into the cavitation cell and acted by the high pressure water. In the second series a solid water jet nozzle was used combined with a mixing chamber and slurry nozzle.

Using the cavitation nozzle, tests were conducted for jet action time of 5.0 seconds at an inlet pressure of 5,000 psi for a mass of 200 grams. The results showed that an almost linear relationship existed between the initial coal size and the energy consumption. The lowest energy consumption was for the smallest coal particle size of #30 mesh. As the coal size was increased the energy consumption increased. These results can be explained by the fact that for the same coal mass but smaller grain size, the total surface area of coal which comes into contact with the cavitation bubbles is greater. Cavitation is a micro-phenomenon and the area of contact is very important. For this reason, the erosion process observed during the cavitation phenomenon is proportional to the coal grain size.

For the same initial coal size of #30 mesh, as the time of jet action was increased to 10.0 seconds a drastic increase in the energy consumption occurred (13,502 kWh/ton for the 10 second tests as compared to 839 kWh/ton for the 5.0 second test). These results indicate the importance of the slurry concentration. To further emphasize these results, tests were conducted for constant pressures but for different amounts of initial coal of 200, 400 and 600 grams. The results show that as the initial coal mass was increased the energy consumption decreased.

For the next series of experiments the mechanism of coal feeding was identical to that for solid jets (Figure 2). The coal entering the mixing chamber was attacked by the high pressure water jet and exists through the slurry nozzle into the cavitation chamber. Inside the cavitation chamber erosion of the coal particles takes place due to the cavitation phenomenon and high turbulence in the chamber.

The tests were conducted for a nozzle diameter combination of d=0.041" and D=0.120" for pressures of 3,500 and 5,500 psi. The initial coal particle size was #30 mesh. The tests were conducted for different back pressures, as shown in Figure 5.

The lowest energy level achieved for a final product size of -75 microns was 407 kWh/ton for an inlet pressure of p=3,500 psi. Also, the results show that no significant changes in the energy level was observed at higher pressures. Slight changes in the back pressure caused no significant change in the energy consumption.

As conclusions from this series of experiments it could be concluded that the coal should not be surrounded by water. A higher slurry concentration would produce better results. The importance of the initial particle size was brought out again. As the initial particle size was decreased the energy consumption decreased.

Rotating Water Jets:

A specially designed and machined test rig was used in conducting these experiments. The primary system component was the rotating spindle. Three nozzles were attached to the nozzle head. The rotating spindle was supplied with high pressure water through the rotary coupling. The maximum speed of rotation for this rotary coupling was limited to 600 rpm. The system was driven by an electric motor. A schematic view of the assembly can be seen in Figure 6. The coal was filled into both perforated and imperforated container. The container placed on a mechanical lifter made it possible to give vertical movement to the container.

EXPERIMENTAL EQUIPMENT, PROCEDURE AND DISCUSSION OF RESULTS:

No theoretical value of G_{IC} is given for coal in the literature. The heterogeneous structure of coal would account for this.

To gain a better understanding of material disintegration by water jet action, a model study on material discontinuities has been carried out earlier [4]. The pressure distribution inside a receiving pipe, designed to simulate a representative micro-crack in the material was studied. The results show that the pressure within the receiving pipe depends on the ratio of the injecting nozzle and receiving pipe diameters. As the injecting nozzle diameter increased with respect to the receiving pipe the pressure inside the pipe P 2 increased. Also, the pressure P 2 was strongly dependent on the stand off-distance between the injecting nozzle and receiving pipe. In practice it means that for maximum pressurization of the crack, the jet diameter has to be bigger or equal to the micro-crack. Also, the distance between the jet and the coal is important.

As mentioned, three types of jets were tested, i.e., solid, cavitating and rotating jets. In all tests the comminuted particles below 75 microns (200 mesh) was separated by a wet sieve analysis [4] and the specific energy levels calculated. The calculated specific energy consumption was the energy of the water stream alone and does not include the energy consumed by the system as a whole. In this chapter each series of experimental equipment, experimental procedure and the results achieved will be discussed separately for each kind of jet.

Solid Water Jets:

The first series of tests was concerning the use of solid water jets for coal comminution. The apparatus consists of a solid water jet nozzle connected to a mixing chamber and slurry nozzle assembly. The mixing chamber was connected to a long plexi glass tube by a conical shape adaptor. Figure 2 shows a schematic view of the equipment set up. The coal was fed directly into the mixing chamber to be attacked by the jet emerging from the nozzle. The water jet moving through the mixing chamber creates a vacuum inside the chamber which results in a suction at the coal inlet to the mixing chamber. By taking advantage of this suction, it was possible to get an uniform flow of coal into the mixing chamber. The coal after being attacked in the mixing chamber flows through the slurry nozzle and was collected at the end of the tube.

The initial task was to find the dependence of the initial coal particle size. Tests were carried out for #4 and #30 coal. The energy consumption for the #4 coal was almost 7 times as that for the #30 coal (7147 kWh/ton for the #4 coal as compared to 1032 kWh/ton for the #30 coal).

The next series of tests were for different injecting and slurry nozzle combinations. The initial coal particle size was #30 mesh. The results are presented in Figure 3. These test results show that for a pressure increase that no significant change in the energy consumption occurred. This is an important remark from a practical point of view because lower pressures are easier to generate and does not require expensive equipment. Also, as the slurry nozzle diameter was increased a reduction in the energy consumption occurred. This can be explained by the fact that in a bigger nozzle the possibility of the particles hitting the nozzle wall, deflecting and hitting other particles is greater, thereby, increasing the attrition of particles.

As conclusions from this part of the tests it could be stated that as the initial coal particle size was reduced, the energy consumption was reduced. Also, as the slurry nozzles diameter was increased from 0.086" to 0.120" for the same injecting nozzle of 0.041" a reduction in the energy consumption occurred. Increasing the pressure had an adverse effect on the energy consumption.

Cavitating Water Jets:

The second series of experiments were for cavitating jets. The cavitation number which defines the inception and subsequent growth and collapse of cavitation bubbles is given by the equation

The initial coal particle size was 0.742" <S<0.525". The tests were conducted for a pressure of 5,500 psi using three nozzles each of diameter 0.032".

The initial tests were carried out with the nozzles oriented at 3, 8 and 20 degree angles. The first task was to investigate the importance of increasing the volume of water to the comminution process. Tests were carried out for jet action times of 15, 30 and 75 seconds using an imperforated container. It was seen that as the time of jet action increased the energy consumption increased. To explain this, consider the water jet action on the coal and the time over which it acts. Increasing the jet action time increases the volume of water utilized. The coal particles tend to become suspended in the excess water. They are in effect, surrounded by a coating of water whose protective ability increases with the volume of water utilized. The water jets lose energy in penetrating this protective coating in order to come in contact with the coal particles. This energy is not used to create new surfaces during direct collision with coal particles and hence is wasted.

For the same series of tests a perforated coal container was used and water jet action times of 75 seconds and 150 seconds investigated with vertical up and down axial movement (8 cycles/minute) of the coal container. A test with a jet action time of 75 seconds was conducted without container movement. The results show (Figure 7) that the energy consumption with coal container movement to be almost half those of the case with rotation only. These results clearly indicate the importance of the kinematic movement of the high pressure water jets, which gives a better opportunity for the coal particles to come in direct contact with the water jets.

In the next series the orientation of the nozzles were changed. The nozzles were now oriented perpendicular to the spindle axis. The effect of vertical movement of the coal container was investigated for both 3 and 12 full cycles of motion for 2 minute tests. For the purpose of comparison the coal container was also kept stationary. The energy requirements appear almost 20% less for the case when rotating jets were moved up and down 12 times per minutes as compared to other kinematic conditions of the jets for the tests carried out (Figure 8).

As conclusions from this portion of experiments the importance of the slurry concentration was brought out again. The coal particles should not be surrounded by water. Also the kinematics and dynamics of the interaction between the high pressure water jets and the material to be comminuted plays a very important role in the effectiveness of the comminution process.

GENERAL CONCLUSIONS:

Based on the experimental results presented in this paper the following conclusions can be formulated:

The energy consumption taken into consideration as a criterion of the effectiveness of the comminution process shows a very strong dependence on:

- jet diameter and pressure
- initial coal particle size
- solid concentration in slurry
- kinematics of the interaction between the high pressure water jets and coal

The minimum specific energy input of 400 kWh/ton achieved to date represents a significant improvement in the comminution technology. Typical specific energy consumption levels associated with fluid energy mills are in the range of 700-800 kWh/ton [6]. It is envisaged that application of the knowledge gained from the tests carried out to date will enable further improvement of the comminution technology.

ACKNOWLEDGEMENT:

Support for this project was provided by the Department of Energy, Pittsburgh Energy Technology Center under contract No. DOE-DE-AC22-86PC-91271. The authors are grateful for this support.

REFERENCES:

1. Galecki, G., Mazurkiewicz, M., "Coal Comminution by High Pressure Water Jet" 8th International Symposium of Coal Slurry Fuels Preparation and Utilization., May 27-30, 1986, Orlando, Florida, pp 852-861.

2. Griffith, A.A., "The Phenomena of Rupture and Flow in Solids", Phil. Trans. Roy. Soc. of London, A 221 (1921), pp 163-197.

3. Griffith, A.A., "The Theory of Rupture", Proc. 1st Int. Congress Appl. Mech., (1924), pp 55-63.

4. Mazurkiewicz, M., Galecki, G., Technical Progress Report No. 7 on Contract DOE-DE-AC22-86PC-91271, submitted to Department of Energy, Pittsburgh, Pennsylvania, April 1987.

5. Galecki, G., Mazurkiewicz, M., Summers, D.A., "Cavitation Cell" Invention Disclosure 88-UMR-042.

6. Report of the Committee on Comminution and Energy Consumption "Comminution and Energy Consumption", Publication NMAB-364, National Academy Press, Washington, D.C., 1981, pp. 13-39.

For Illinois Coal:

$\sigma_{\perp} = 26.7$ MPa

$\sigma_{\parallel} = 15.0$ MPa

compression

$\sigma_{\perp} = 3.3$ MPa

$\sigma_{\parallel} = 1.9$ MPa

tension

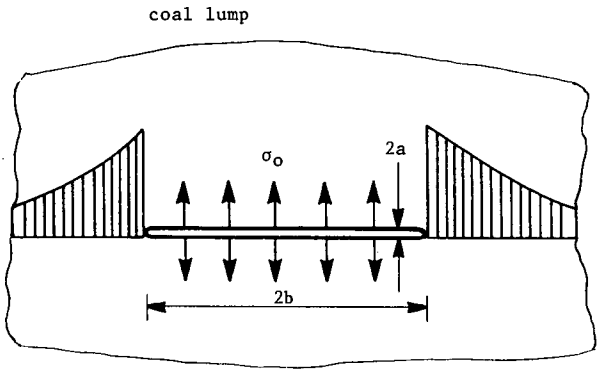

σ_o - stagnation pressure developed inside the crack by jet

σ_{max} - tip tension stress

$$\sigma_{max} = \sigma_o \left(1 + \frac{2b}{a}\right)$$

For b/a = 10, $\sigma_{max} = 21\ \sigma_o = 3.3$ MPa

The stagnation pressure to grow a micro-crack is

$$\sigma_o = 15.7 \text{ kPa}$$

Figure 1. Pressure necessary to propagate coal micro-cracks.

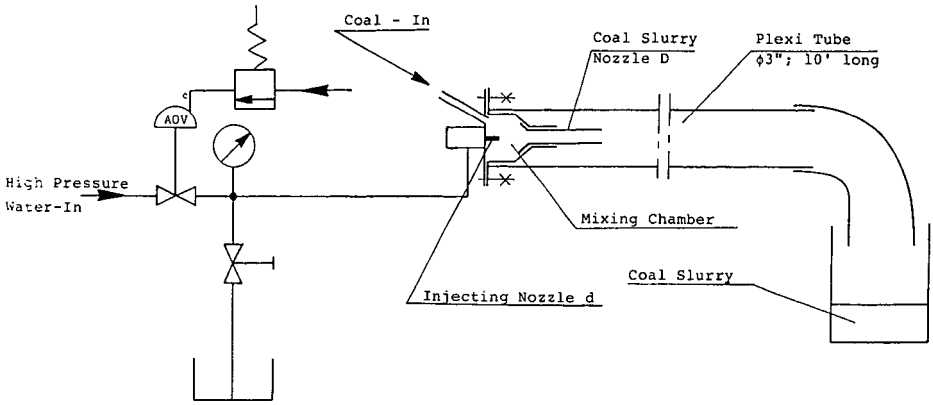

Figure 2. Schematic Drawing of Apparatus for Solid Water Jet Tests with Mixing Chamber.

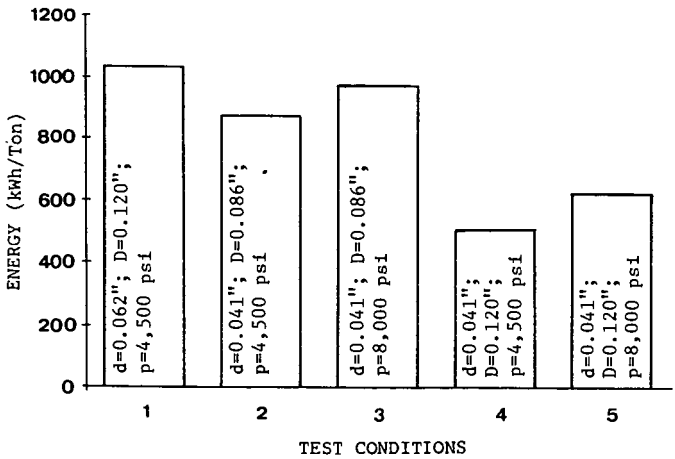

Figure 3. Graph of Energy Versus Different Test Conditions of Pressures and Slurry Nozzle Diameters for Direct Water Jets.

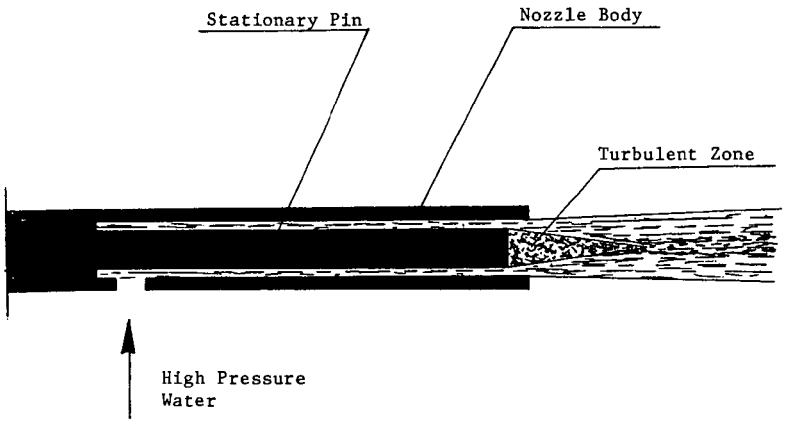

Figure 4. Schematic Drawing of Nozzle with Cylindrical Cavity of Air.

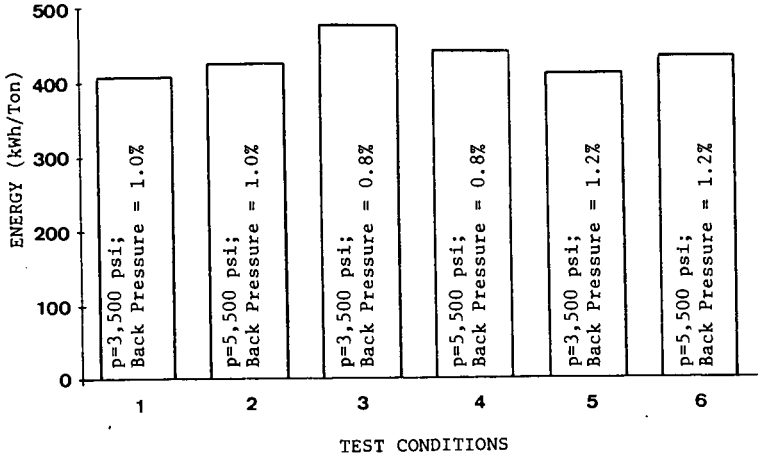

Figure 5. Graph of Energy Versus Different Combinations of Inlet and Back Pressures for Cavitation Tests.

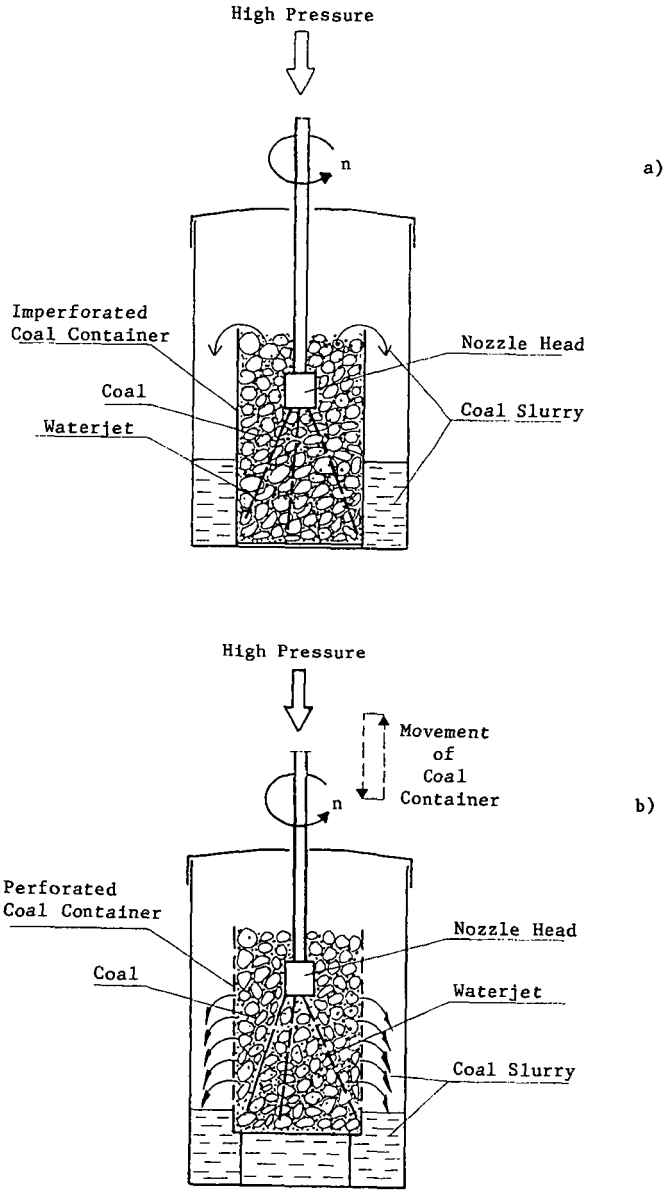

Figure 6. Schematic Drawing of Rotating Water Jet Experimental Equipment.

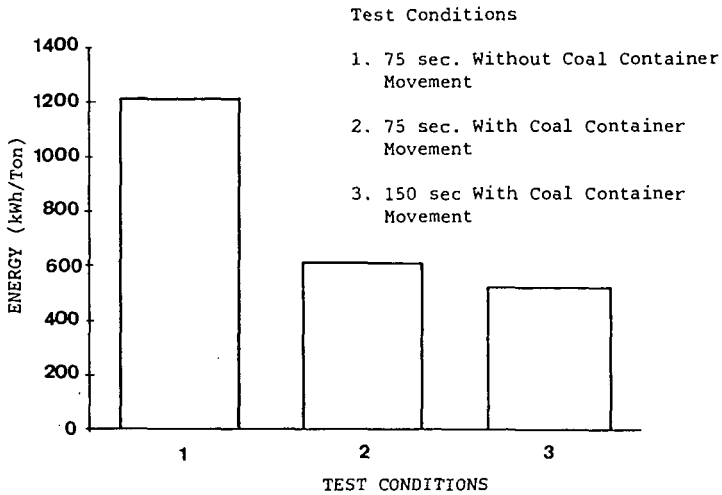

Figure 7. Graph of Energy Versus Different Test Conditions for Nozzles Angled at 3, 8 and 20 Degree Angles.

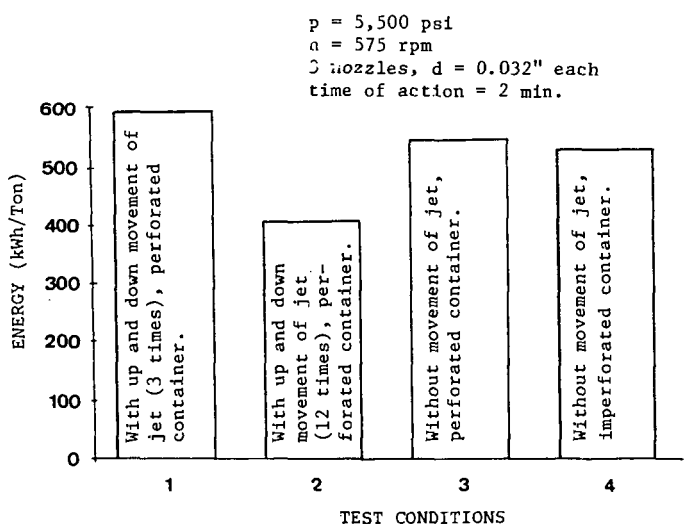

Figure 8. Graph of Energy Versus Different Test Conditions for Nozzles Angled Perpendicular to the Axis of Rotation.

Effect of Maceral Composition and Vitrinite Reflectance on the Combustion Behavior of Six hvA Bituminous Coals

Sung-Tae Kim, Alan W. Scaroni
and
Mohammad Fatemi-Badi

The Pennsylvania State University
Combustion Laboratory
405 Academic Activities Building
University Park, PA 16802

Introduction

A common way of classifying coals is by rank, that is, according to the degree of metamorphism, or progressive alteration of the plant debris as it is transformed into the natural series from lignite to anthracite. In the United States the rank classification system was established by the American Society for Testing and Materials (ASTM), and is based on the percent volatile matter and fixed carbon obtained from the proximate analysis and on a dry, mineral-matter-free basis, and the heating value in British thermal units per pound (Btu/lb) expressed on a moist, mineral-matter-free basis.(1) Each rank of coal from lignite to anthracite has distinctive chemical and physical characteristics which influence the behavior in a given application. This rank classification is commonly used as a guide in the selection of pulverized coal for use in utility and industrial boilers. Although rank can indicate, in some cases, general processing behavior, it is not sufficient to characterize the specific behavior of a coal under specific utilization conditions. This derives, at least in part, from the fact that different maceral compositions for coals of the same rank can give rise to different properties, and hence, different behavior during processing. Therefore, assessment or prediction of processing, particularly combustion, behavior based on rank alone is not reliable. In higher rank coals, however, where the differences between macerals is less significant,(2) the behavioral differences as a consequence of maceral compositon are less significant.

Due to the relatively high vitrinite concentration in American coals, their chemical analyses tend to reflect the composition and properties of the vitrinite. Therefore, the parameters used to classify coals according to rank often reflect the rank of the vitrinite. Further, the characteristics of vitrinite are considered to change in a fairly uniform manner throughout the coalification series. One characteristic of vitrinite which can be measured easily is its reflectance. It is a measure of percent light reflected from a polished surface of coal. Because the degree of petrographic heterogeneity is much greater in lignites than in coals of higher rank, there are some difficulties in determination of vitrinite reflectance in these coals.

It has been observed in practice that a switch from a familiar coal can lead to a change in the amount of unburnt carbon in the fly ash from a utility boiler. There are many possible explanations for this, but in recent years increasing attention is being focussed upon the maceral composition of coals as being a contributor to the problem. From the available published work, relationships between certain petrographic properties and coal combustion behavior can be inferred. In particular, inertinite macerals appear to burn less readily than the so-called "reactive macerals".(3,4) Thus, coals with high inertinite contents may require high temperature and/or long residence time to avoid high unburnt carbon loss. This is supported by results from laboratory experiments and some industrial experience.(3-8) The purpose of the current work was to determine the effect of maceral composition and vitrinite reflectance on the combustion behavior of six maceral-rich hvA bituminous coals.

Experimental

Combustion experiments were conducted in an entrained-flow reactor, a schematic diagram of which is given in Figure 1. The system is composed of a preheater, water-cooled feed probe, cyclone, water-cooled collector probe and char collector. A stream of coal particles was fed by the screw feeder and entrained in a primary gas stream at ambient temperature, then passed through a water-cooled probe and injected at the top of a hot cylindrical reaction chamber, which was maintained electrically at a specified reaction temperature. At the same time, a secondary and larger stream of carrier gas, which was preheated to the reactor temperature, was isokinetically injected around the primary gas stream in laminar flow to ensure that the particles were not dispersed radially to the furnace walls. A ceramic disk was placed above the injector tip to serve as a flow straightener. The secondary gas temperature was adjusted so that upon mixing of the primary and secondary gases the combined gas stream attained the desired reaction temperature. Heating elements around the reactor produced a uniform wall temperature. The estimated heating rate of the particles is 10^3 to 10^4 K/sec. The entrained coal particles travelled in a pencil-like stream down the axis of the reactor. The products of combustion were collected through a water-cooled collector probe that quenched reactions. Solid products (chars) were collected in the cyclone, condensible liquids (tars) were deposited on the filter, and gaseous products were released into an exhaust stack. Detailed design specifications and description of the ancillary equipment are presented elsewhere.[9-11]

In this study, six maceral-rich hvA bituminous coal samples were selected from the D.O.E/Penn State Coal Sample Bank. The selection was based primarily on differences in maceral composition and vitrinite reflectance. The coals were divided into two groups: one group of three having similar maceral composition but different vitrinite reflectance, and the other group having similar vitrinite reflectance but different maceral composition. Full analyses of the six samples are shown in Table 1. By way of example PSOC-1501 is referred to as a low-reflectance, vitrinite-rich coal and PSOC-1374 as a high-reflectance, vitrinite-rich coal of the same rank. A similar relationship holds for PSOC-296 and PSOC-733 (liptinite-rich coals), and PSOC-861 and PSOC-736 (inertinite-rich coals). Three particle size fractions of the six coals, with mean particle diameters of 63, 90, and 127 μm, were prepared and used in this study.

The samples were partially combusted in the reactor at temperatures of 1073 and 1273 K and residence times of typically less than 0.3s. Coal particle residence times in the furnace were determined using a computer flow model. The governing equations and principles of this model have been discussed elsewhere.[7,12] The isokinetic velocity was 128 cm/sec for both the primary and secondary gases. Prior to an experiment the temperature profiles in the reactor were determined using a suction pyrometer. The sample collector probe was then positioned in the reactor, and the coal feeder calibrated to deliver 0.5 g/min.

Proximate analyses of the coals and resulting char samples were obtained using a Leco MAC-400 proximate Analyzer. Weight loss due to the partial combustion was calculated by using ash as a tracer. On a dry, ash-free basis the governing equation is:

$$\Delta W = 100\% \left[1 - \frac{A_0 (100 - A_1)}{A_1 (100 - A_0)} \right]$$

where ΔW is the calculated weight loss on a dry, ash-free basis; A_0 is the proximate ash content of dry coal; and A_1 is the proximate ash content of dry char. An assumption in this calculation is that mineral matter in the coal does not undergo transformations during pyrolysis which would change the quantity of ash produced upon ashing the chars.

Results and Discussion

The terms "reactives" and "inerts" as used in the coke industry will be used throughout this work. The prediction of weight loss, according to the concentration of reactive macerals, would be as follows:

For the low vitrinite reflectance group,	PSOC-1501 > PSOC-296 > PSOC-861
For the high vitrinite reflectance group,	PSOC-1374 > PSOC-733 > PSOC-736

The two vitrinite-rich coals (PSOC-1501 and PSOC-1374) and a liptinite-rich coal (PSOC-296) would be considered as reactive coals, whereas the two inertinite-rich coals (PSOC-861 and PSOC-736) would be considered as less reactive.

The effect of residence time over the range 0.1 to 0.3s on the weight loss during combustion of 100x140 mesh particles of the low and high vitrinite reflectance coals at 1073 K is shown in Figures 2 and 3, respectively. Despite having similar volatile matter contents and ASTM rank, the figures shows that the weight loss by the reactive coals (PSOC-1501 and PSOC-1374) is much higher than those of the inertinite-rich coals (PSOC-861 and PSOC-736). The concentration of reactive macerals for PSOC-1501 and PSOC-1374 were 93.9 and 95.1% compared to 61.7 and 34.9 % for the inertinite-rich PSOC-861 and PSOC-736 coals, respectively. The lower weight loss by the inertinite-rich coals is a consequence of the more aromatic nature of the inertinites. In addition, vitrinite and liptinite contain more oxygen and hydrogen, respectively, than inertinite and are thus likely to be more reactive than inertinite.

As is shown in Table 1, PSOC-296 and PSOC-733 have considerable amounts of inert macerals, 32.4% and 29.1%, respectively. Therefore, it might be expected from the maceral compositions that the weight loss of these two coals would lie between those of the vitrinite-rich and inertinite-rich coals. This can be seen for PSOC-733 in Figure 3. However, despite the relatively high inert content of PSOC-296, both vitrinite-rich PSOC-1501 and liptinite rich PSOC-296 have similar weight losses as seen in Figure 2. Based only on the reactive maceral content, therefore, the difference in weight loss behavior is much smaller than might be expected. This indicates that, during the initial stages of combustion, the concentration of inert macerals seems to have much less influence than the liptinite content. A high liptinite concentration enhances ignition, due in part to the relatively higher hydrogen content. As the H/C atomic ratio of the coal increases, ignition of the volatiles is promoted, thereby increasing the weight loss rate. A comparison of the H/C atomic ratios of the coals shows that liptinite-rich PSOC-296 has a higher H/C atomic ratio (0.83) than vitrinite-rich PSOC-1501 (0.79), Table 1. A general trend is that the low vitrinite reflectance coals (PSOC-1501, PSOC-296, and PSOC-861) tend to have higher H/C ratios than the high vitrinite reflectance coals (PSOC-1374, PSOC-733, and PSOC-736).

The effect of residence time over the range 0.1 to 0.3son the weight loss during combustion of 100x140 mesh particles of the low vitrinite reflectance coals at 1273 K is shown in Figure 4. A comparison with Figures 1 and 3 shows that as temperature is increased the effect of maceral composition on weight loss is decreased.

Figure 5 shows the effect of residence time on the weight loss of 140x200 mesh particles of two vitrinite-rich coals (PSOC-1501 and PSOC 1374) during combustion at 1073 K . The vitrinite reflectance values for PSOC-1501 and PSOC-1374 are 0.73 and 0.89, respectively. As can be seen the low vitrinite reflectance coal showed a higher weight loss. A similar trend was observed in Figure 6 for the inertinite-rich coals PSOC-861 and PSOC-736 with vitrinite reflectances of 0.73 and 0.95, respectively.

The effect of particle size on the weight loss during combustion at 1073 K and 0.1-0.3s residence times is shown in Figures 7 through 10. Figure 7 shows the effect of particle size on the weight loss of PSOC-733. The smaller particles experienced greater weight loss than the larger ones at all residence times. Figure 8 shows a similar trend for the inertinite-rich PSOC-736. Because these coals have a considerable concentration of inert maceral, they are not likely to swell significantly. Therefore, the initial particle size will be the effective size and the weight loss will be related to the initial size. As the data in Figures 7 and 8 indicate, physical factors such as particle size may be important in determining weight loss for the less reactive (inertinite-rich) coals.

The effect of particle size is less well defined for the reactive coals. Figures 9 and 10 show the effect of particle size on the weight loss behavior of vitrinite-rich PSOC-1501 and liptinite-rich PSOC-296 during combustion at 1073 K. The curves in Figures 9 and 10 show similar trends to those observed by Tsai.(7) In both cases, the weight loss behavior was rather insensitive to particle size. Since these coals are considered to be highly reactive, the observed results may be due to their thermoplastic properties. The degree of swelling for these reactive coals is larger than for the inertinite-rich coals and higher concentrations of reactive macerals are thought to change the thermal response of the coal. Thus, the effective particle size for the reactive coals during reaction will be greater than that of the initial particle size. Because particle size changes will affect the time-temperature history of the coal particles, which in turn controls to some extent their behavior in the reactor, the weight loss behavior will vary accordingly.

The ignition delay time is dependent on the gas temperature and particle size. At short residence times (prior to ignition), where the weight loss is due to devolatilization, smaller particles of the reactive coals show higher weight loss, Figures 9 and 10. In larger particles, on the other hand, the escape of volatiles from the coal matrix is retarded, and hence weight loss is reduced. At longer residence times (after ignition), however, the weight loss by the larger particles gradually increases, until the weight loss for all paricle sizes become similar. This may be due to the influence of slip velocity on the mixing of the volatiles and the oxidant at the particle surface, or due to a more reactive char.

Summary and Conclusions

The experimental results indicate that the six hvA bituminous coals studied displayed different behavior during combustion. This was attributed to differences in maceral composition and rank as measured by vitrinite reflectance. Vitrinite-rich and liptinite-rich coals lost more weight than inertinite-rich coals under similar experimental conditions. No significant differences in weight loss were observed between vitrinite-rich and liptinite-rich coals. A lower weight loss rate is believed to be characteristic of high inertinite contents. This is probably due to the existence of high aromaticity and strong cross linkages which exist within the inertinite macerals. For coals with similar maceral compositions, although the weight loss decreased with increasing vitrinite reflectance, there was not a direct and simple correlation between the weight loss and vitrinite reflectance.

Although some smaller particles showed higher weight loss than larger particles of the same coal under similar experimental conditions, there was not a general relationship between the weight loss and the initial particle size. While the weight loss by the less reactive coals (inertinite-rich coals) was sensitive to particle size, the weight loss by the reactive coals (vitrinite-rich coals) was independent of particle size.

In summary, for the high volatile bituminous coals, rank as measured by mean maximum vitrinite reflectance and maceral composition must be considered together with ASTM rank when predicting combustion behavior.

References

1. Annual Book of ASTM Standards, Vol. 5.05, American Society for Testing and Materials, Philadelphia, PA,1986.

2. Van Krevelen, D. W., Coal Science, Elsevier Publishing Co., Amsterdam, 1961.

3. Nandi, B. N., Brown, T. D. and Lee, G. K., Fuel, 56, 125-130, 1977.

4. Sanyal, A., J. Inst. Energy, 56, 92-95, 1983.

5. Shibaoka, M., Fuel, 48, 285-295, 1969.

6. Lee, G. K. and Whaley, H., J. Inst. Energy, 56, 190-197, 1983.

7. Tsai, C. Y., "An Experimental Investigation of the Initial Stages of Pulverized Bituminous Coal Combustion," Ph. D. Thesis, The Pennsylvania State University, 1985.

8. Vleeskens, J. M. and Nandi, B. N., Fuel, 65, 797-802, 1986.

9. Maloney, D. J., "Effects of Preoxidation on Rapid Pyrolysis Behavior and Resultant Char Structure of Caking Coals," Ph. D. Thesis, The Pennsylvania State University, 1983.

10. Morgan, M. E., "Role of Exchangeable Cations in the Pyrolysis of Lignites," Ph. D. Thesis, The Pennsylvania State University, University, 1983.

11. Mallin, J. R., "Pyrolysis of Lignitic and Bituminous Coals in an Entrained-Flow Reactor," M. S. Thesis, The Pennsylvania State University, 1987.

12. Kim, Sung-Tae, "The Effect of Maceral Composition and Vitrinite Reflectance on the Pyrolysis and Combustion of Pulverized Bituminous Coals," M. S. Thesis, The Pennsylvania State University, 1988.

Table 1

Analytical Data for the Coal Samples Used

Sample No	PSOC-1501	PSOC-296	PSOC-861	PSOC-1374	PSOC-733	PSOC-736
Proximate Analysis: (wt%)						
% Moisture	5.80	4.18	3.66	6.76	1.75	3.23
% Ash(dry)	5.55	18.19	10.93	8.82	21.44	8.59
% Volatile Matter(daf)	43.07	44.26	38.10	36.37	34.20	28.12
% Fixed Carbon (daf)	56.93	55.74	61.90	63.63	65.80	71.88
Ultimate Analysis: (wt%, daf)						
% Carbon	80.49	82.09	82.65	84.77	84.81	86.70
% Hydrogen	5.27	5.70	5.42	5.55	5.36	4.88
% Nitrogen	1.55	1.82	1.18	1.58	1.44	1.40
% Total Sulfur	0.68	1.20	0.83	0.80	1.31	0.62
% Oxygen (Diff)	12.01	9.19	9.92	7.30	7.08	6.40
Maceral Composition: (vol%, dmmf)						
Vitrinite	92.4	41.4	60.5	93.3	48.1	24.2
Fusinite	1.9	8.3	5.4	2.2	2.6	8.2
Semifusinite	2.4	7.9	30.9	1.2	19.7	47.0
Macrinite	0.5	2.1	1.0	0.2	1.4	1.9
Micrinite	1.2	14.1	1.0	1.3	5.4	8.1
Sclerotinite	0.1	0.0	0.0	0.0	0.0	0.0
Sporinite	1.4	23.6	1.1	1.8	20.2	10.7
Resinite	0.1	2.5	0.1	0.0	2.5	0.0
Alginite	0.0	0.2	0.0	0.0	0.2	0.0
H/C: (Atomic Ratio)	0.7868	0.8334	0.7880	0.7863	0.7589	0.6760
Mean-Max Vitrinite Reflectance (R_o): (%, in oil)						
	0.73	0.74	0.73	0.89	0.94	0.95
Description	low-reflectance vitrinite-rich	low-reflectance liptinite-rich	low-reflectance inertinite-rich	high-reflectance vitrinite-rich	high-reflectance liptinite-rich	high-reflectance inertinite-rich

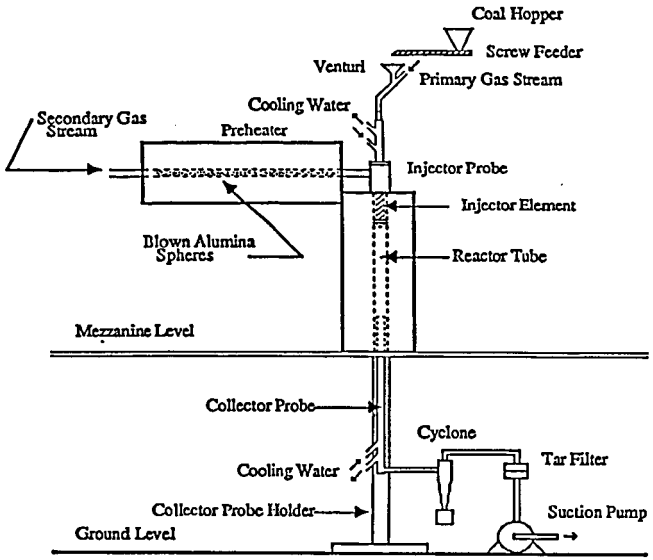

Figure 1. Configuration of Entrained-Flow Reactor and Ancillary Equipment

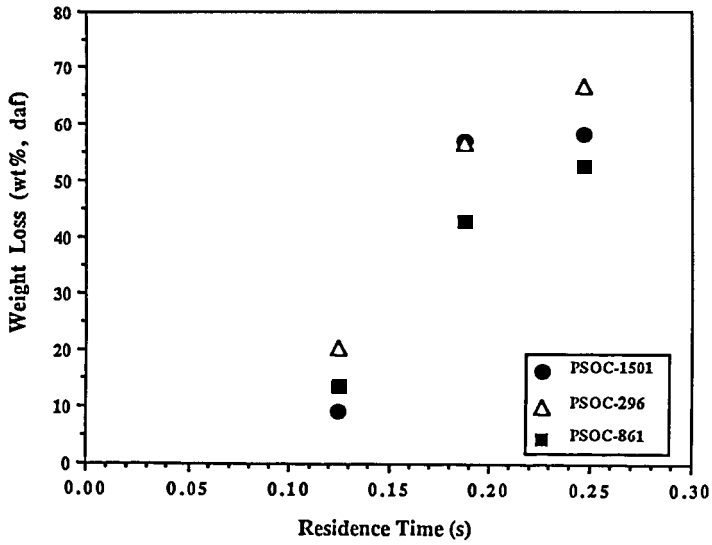

Figure 2. Effect of Maceral Composition on Weight Loss During Combustion of 100x140 Mesh Fraction of Low Vitrinite Reflectance Coals at 1073 K

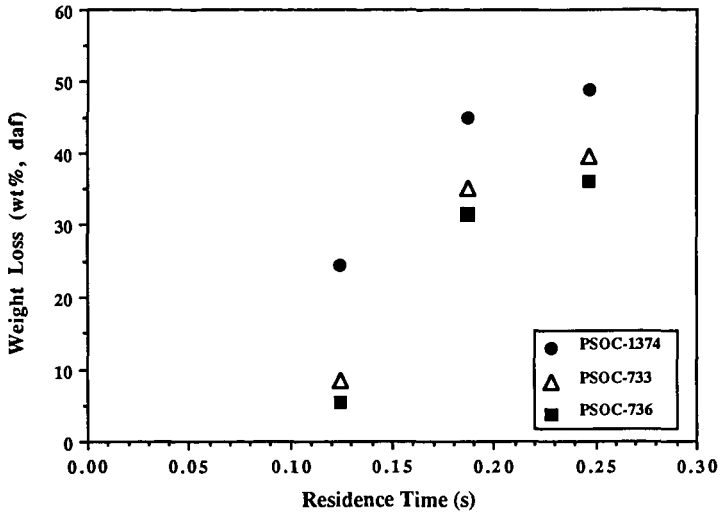

Figure 3. Effect of Maceral Composition on Weight Loss During Combustion of 100x140 Mesh Fraction of High Vitrinite Reflectance Coals at 1073 K

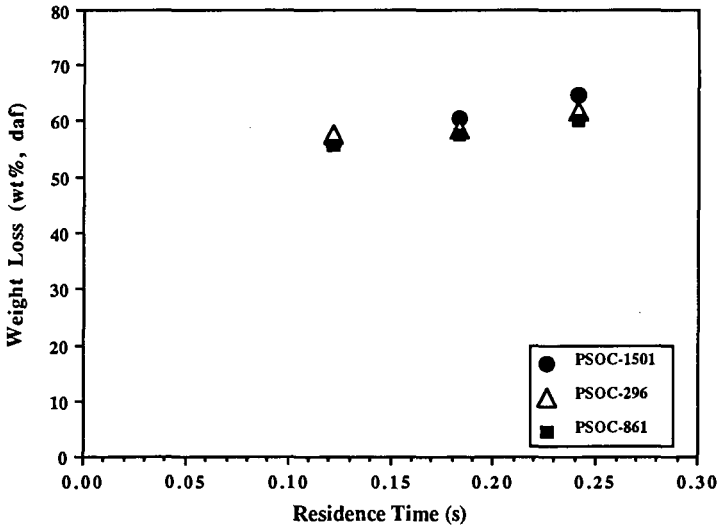

Figure 4. Effect of Maceral Composition on Weight Loss During Combustion of 100x140 Mesh Fraction of Low Vitrinite Reflectance Coals at 1273 K

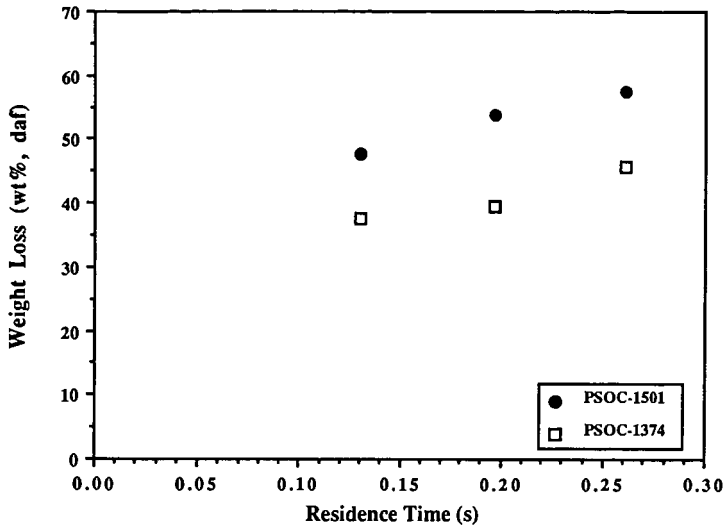

Figure 5. Effect of Vitrinite Reflectance on Weight Loss During Combustion of 140x200 Mesh Fraction of Vitrinite-Rich Coals at 1073 K

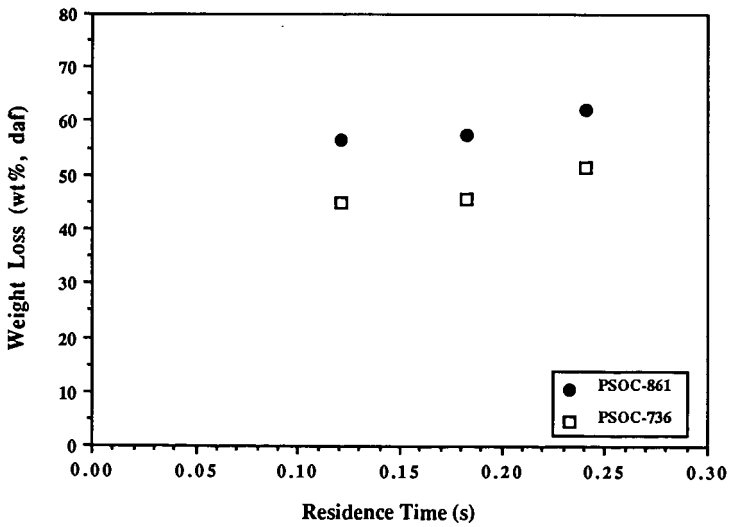

Figure 6. Effect of Vitrinite Reflectance on Weight Loss During Combustion of 100x140 Mesh Fraction of Inertinite-Rich Coals at 1273 K

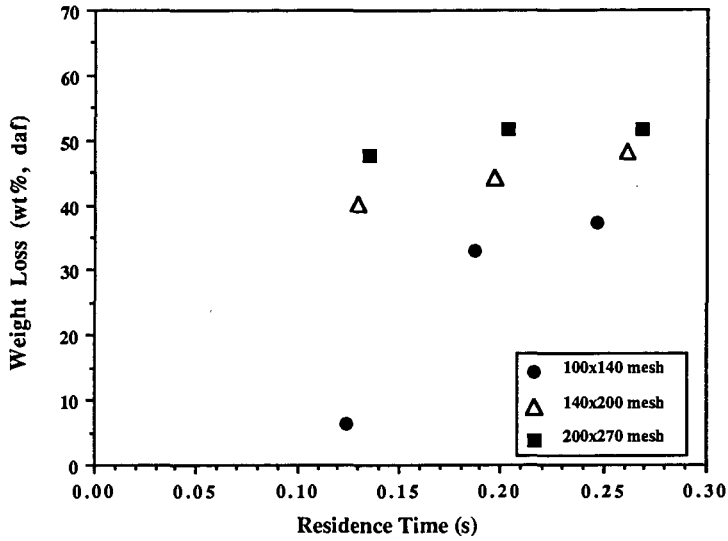

Figure 7. Effect of Particle Size on Weight Loss for Intermediate Coal (PSOC-733) During Combustion at 1073 K

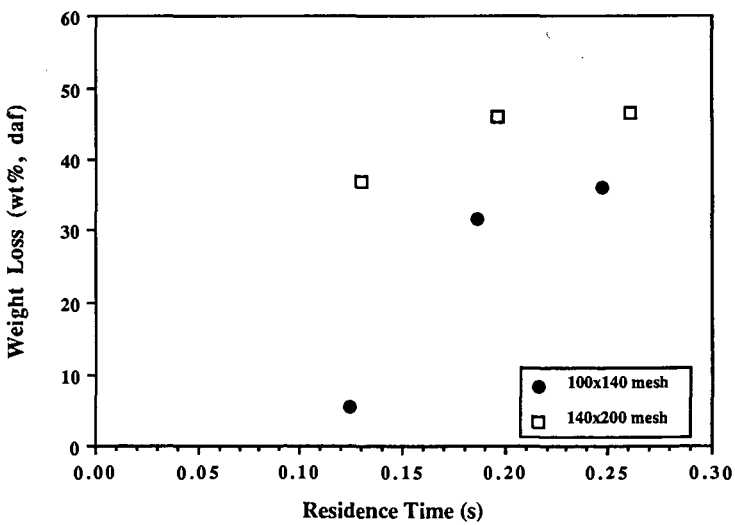

Figure 8. Effect of Particle Size on Weight Loss for Inertinite-Rich Coal (PSOC-736) During Combustion at 1073 K

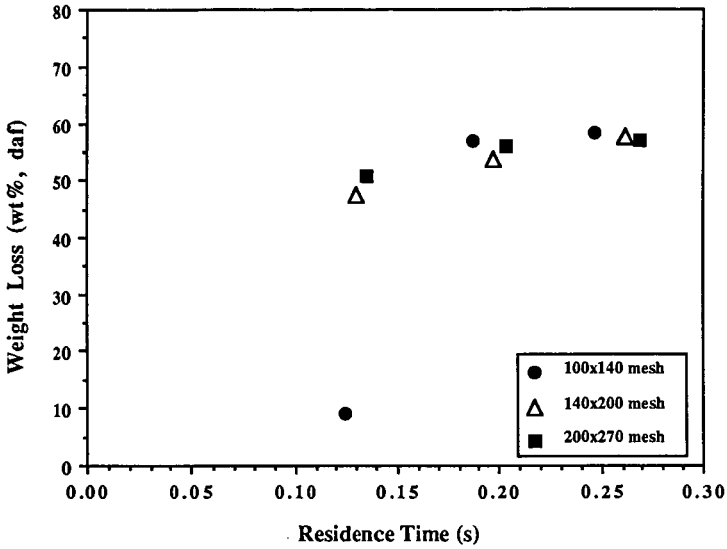

Figure 9. Effect of Particle Size on Weight Loss for Vitrinite-Rich Coal (PSOC-1501) During Combustion at 1073 K

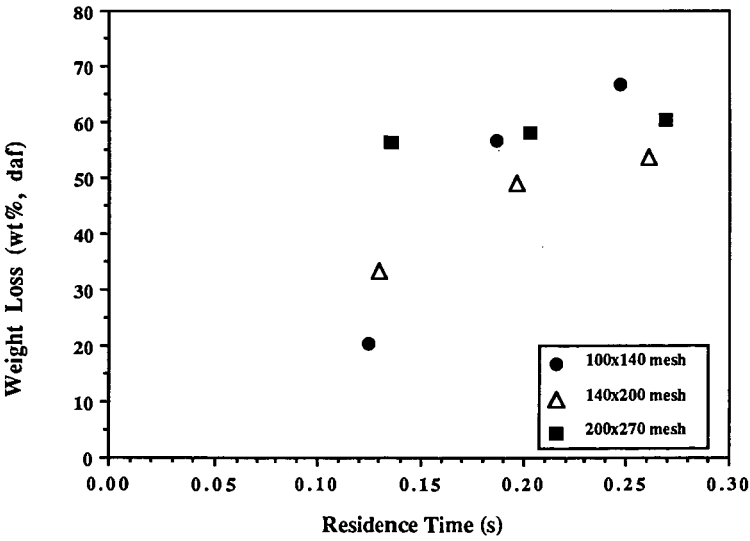

Figure 10. Effect of Particle Size on Weight Loss for Liptinite-Rich Coal (PSOC-296) During Combustion at 1073 K

STUDIES ON IGNITION OF COAL: THE EFFECTS OF RANK, TEMPERATURE, VOLATILE CONTENT, AND LITHOTYPE

Philip G. Sweeny, Dana T. Grow*, and Donald P. McCollor
University of North Dakota Energy and Mineral Research Center

Box 8213, University Station, Grand Forks, North Dakota 58202
*also Department of Chemical Engineering

ABSTRACT

The rates of CO and CO_2 production from single particles of bituminous coal and lignite introduced into a hot, flowing oxidant gas stream were measured as a function of residence time. The time between injection of the particles into the combustion furnace and initial CO_2 production was defined as the ignition delay. These delays, as well as the maximum combustion rates and CO_2:CO product ratios are reported. Two gas temperatures were employed, 923 K and 1273 K. For the bituminous coal studies, temperature was the only parameter varied. For the lignite studies, the effects of volatile content and lithotype were examined in addition to temperature. The effect of volatile matter content was ascertained by comparing a coal to its char. Ignition delays were most affected by the gas temperature, decreasing substantially with increased gas temperature. Activation energies were estimated from the ignition delays. Variations of ignition delay are discussed in terms of the ignition mechanism.

INTRODUCTION

An important consideration in the design of coal combustion systems is ignition delay. In qualitative terms, the ignition delay can be described as the time from the combination of a fuel with an oxidant at high temperature to the beginning of the exotherm. Ignition characteristics of a given coal are important in the prevention of spontaneous ignition, in the production of stable flames, and in the establishment of optimum temperatures in fluidized bed combustion.

Several reviews of pulverized fuel combustion behavior are available (1,2,3). Parameters which affect the ignition behavior of coal and chars include rank and gas temperature. Both ignition delay and gas ignition temperature have been shown to increase with increasing coal rank (4,5). Lignite chars have been shown to be more reactive than other chars (6) and mineral matter has been found to increase the rate of combustion (7). Volatile matter has been shown to affect the mode of ignition of subbituminous and bituminous coals (8,9). Surface area has also been shown to influence ignition behavior (10). The overall objective of this study is to define the effects of moisture content, lithotype, volatile matter concentration, and mineral matter distribution on the ignition delay and combustion rate of single lignite, and subbituminous and bituminous coal particles. To date, data has been obtained from one lignite and one bituminous coal.

The most commonly monitored events used to determine ignition points are visible light production, mass loss, heat effects, and detection of products. Wall, et al. (11) have examined the correlation of light emission with combustion product formation and concluded the latter to be a better

indicator of the onset of stable combustion. Evolution of CO and CO_2 was chosen as the primary means of determining ignition because it is relatively unresponsive to volatile production and provides input for a mass balance.

Apparent Arrhenius activation energies and preexponential factors can be determined from gas ignition temperatures and ignition delays (4,12,13). The analysis assumes heterogeneous ignition and is accomplished through a heat balance on the particle. The unsteady-state balances have been integrated in this work to obtain Arrhenius parameters.

UNSTEADY STATE PARTICLE TEMPERATURES

The ignition process is modeled by assuming that a spherical particle is contacted by hot gas (14,15). The particle is heated by the environment and begins to react with the oxygen present in the atmosphere. The reaction increases the particle temperature which can be substantially higher than the gas temperature. The particle temperature, as a function of time, is determined from unsteady-state energy and mass balances:

$$dm/dt = A_s \rho \qquad 1)$$

$$mC_p(dT_p/dt) = A_s \rho \Delta H - hA_s(T_p - T_g) - \epsilon \sigma A_s(T_p^4 - T_w^4). \qquad 2)$$

Here m is the mass of the particle, while A_s is the surface area. The energy balance equation accounts for the heating of the particle by reaction, where ρ is the overall rate of reaction and ΔH is the enthalpy of reaction, and the loss of heat by conduction to the ambient gas and by radiation to surrounding walls. The temperatures of the particle, wall, and gas are T_p, T_w, and T_g, respectively. The heat transfer coefficient, h, is determined from the Nusselt number, Nu, which is given by

$$Nu = hd/\lambda \qquad 3)$$

The limiting value of the Nu is two and Nu depends on d, the particle diameter and λ, the thermal conductivity of the gas, which is a function of temperature. The emissivity, ϵ, is taken to be unity, and σ is the Stefan-Boltzmann constant.

Mass and area are related to the diameter through

$$m = \pi \rho'_p d^3/6 \text{ and} \qquad 4)$$

$$A_s = \pi d^2 \qquad 5)$$

The overall rate of combustion is determined from the rate of diffusion of oxygen to the surface, ρ_{diff}, and the rate of chemical reaction, ρ_{chem}, where these terms are given by the equations:

$$\rho_{diff} = k_{diff}(P-P_s), \qquad 6)$$

where k_{diff} is given by

$$k_{diff} = 48D_o/dRT_m \qquad 7)$$

and

$$\rho_{chem} = k_{chem}\,(P_s)^n. \qquad 8)$$

Here the chemical rate constant is assumed to have Arrhenius form:

$$k_{chem} = A\exp(-E/RT). \qquad 9)$$

Since the surface pressure (P_s) is unknown, an approximation employed here is to use the maximum rate of both diffusion and reaction and to calculate the overall rate from a resistances in series formula (16)

$$1/\rho = 1/\rho_{diff} + 1/\rho_{chem} \qquad 10)$$

where n has been assumed to be unity. The diffusion coefficient, D_o, depends on temperature and is evaluated at the mean temperature of the particle and the gas.

The enthalpy of reaction and the heat capacity are functions of temperature and in these calculations the char particle is assumed to be composed entirely of carbon. Combustion is assumed to proceed to CO as the product, because, for short times, the temperature versus time curve is insensitive to product mix. The unsteady-state balances, Equations 1 and 2, are solved by numerical techniques to yield particle temperature versus time curves. The initial particle temperature is assumed to be 300 K. This calculation is repeated for several values of the activation energy and preexpponential factor until the calculated and experimental ignition delays agree. Several temperature versus time curves are shown in Figure 1 for gas temperatures of 1273 K and 923 K.

EQUIPMENT AND EXPERIMENTAL PROCEDURE

The ignition apparatus was similar to that employed by Gomez and Vastola (8). A detailed side view of the ignition apparatus combustion zone is shown in Figure 2. The system includes a tube furnace with hot zone, a particle feeder, and a gas mixing system. The combustion products are measured with CO and CO_2 analyzers which are connected to an A/D converter and a minicomputer to collect concentration versus time data. Thermocouples monitor wall and gas temperatures. The particle feeder is a stainless steel tube and is grounded to prevent electrostatic charge accumulation. A quartz window provides optical access for the trigger system.

Coal samples were obtained from the Pennsylvania State University Sample Bank and included a Beulah lignite (PSOC-1507) and Pittsburgh #8 (PSOC-1451) bituminous coal. The lithotypes vitrain, attritus, and fusain were physically separated from the coal samples. Particles were sized under a microscope and were observed to be irregular in shape. Hence, an aspect ratio was calculated from the formula 2a/(b+c), where the axes are ordered a>b>c.

The coal or char particles are first picked up by a suction bulb and

sized under a microscope. The experiment is started by placing the particle in a syringe needle and pushing it into the drop tube with a thin wire. Data collection from the CO/CO_2 analyzers is started when the particle travels past the trigger. The gas flow rate through the apparatus was 200 ml/min and the gas composition was 80% N_2 and 20% O_2. The linear velocity was 26 cm/sec.

The apparatus was calibrated using malonic acid to produce CO_2 at 413 K which acted as a marker to measure the time for flow between the source and the detector. Further details are available (17).

Char of the untreated lignite was produced in an air natural gas flame at approximately 3% excess oxygen. The chars were collected with a nitrogen-quenched extraction probe at 200 mm above the injection point, corresponding to a residence time of 150 ms. Gas temperature varied from approximately 1500 K at the particle injection point to 1050 K at the collection point. After collection, the chars were sieved, and size ranges were selected for combustion tests. The coals and chars were stored over concentrated H_2SO_4 or water at 30°C for two weeks to establish relative moisture contents of 0 and 100%, respectively (18).

RESULTS AND DISCUSSION

The CO_2 concentration versus time curve yields the ignition delay once the system calibration constant is known. The total carbon production is determined from the summation of the CO and CO_2 concentrations. The data is then differentiated to determine the gas production rate as a function of time. Examples of the rate versus time curves are given in Figures 3 and 4. The peaks in these curves give the maximum CO and CO_2 production rates. Arrhenius parameters were estimated by varying the E and A constants in Equation 9 to match the ignition delay time.

Water had no discernable effect on the ignition delay, combustion rate, or CO_2/CO product ratio of Beulah lignite vitrain, as shown in Table 1. Lithotype had an effect on the ignition delay of Beulah lignite with fusain igniting the fastest. Karz et al. (13) have reported that fusains have shorter ignition delays than vitrains obtained from an anthracite and a bituminous coal.

The effect of volatiles on the combustion behavior of Beulah lignite can be seen by comparing the results obtained from char to those obtained from burning the parent lignite (see Table 1). The char reacted as rapidly as the most reactive lithotype and produced a similar, yet somewhat lower, maximum combustion rate. The overall CO and CO_2 production profiles obtained from the char did not differ significantly from those observed for the lignite shown in Figure 4. Heterogeneous ignition of the lignite is indicated since its combustion behavior is similar to that of its char, which can only ignite in a heterogeneous manner.

The effect of material rank on ignition delay and combustion rate can be seen from comparing the Beulah lignite results to those obtained from Pittsburgh #8 bituminous coal. These two materials behaved similarly at 1273 K, however, at 923 K a substantial difference was noted. At 923 K, the bituminous coal was less reactive than the lignite, exhibiting a longer ignition delay and a lower maximum combustion rate. A comparison of the

overall profiles, Figures 3 and 4, shows that the bituminous coal burns in two distinct stages as opposed to the single stage of the lignite. The two stages represent initial volatiles combustion followed by char burnout. The single stage combustion of Beulah lignite indicates that its char is highly reactive, a fact supported by the char data.

Increasing the gas temperature dramatically decreased the ignition delay time for both the Pittsburgh #8 vitrain and the Beulah vitrain. The Arrhenius activation energy is estimated to be about 20 kcal/mole for a preexponential factor of 200 g/(cm^{2}s) when determined from the delay times. The particle temperature versus time curves for two gas temperatures calculated using Equations 1-10 are presented in Figure 1. These compare favorably with the 29.6 and 20 kcal/mole used by Bandyopadhyay and Baduri (4) for bituminous coal and lignite, respectively. In addition, Karcz et al. (13) obtained 17.6 kcal/mole from experiments on bituminous vitrain. Wall and Gururajan (12) cite a value of 17 kcal/mole for a lignite, and Patel et al. (18) used TGA to measure an activation energy of 18 kcal/mole for a char burned for 100 ms at 1030 K in a flame burner.

CONCLUSIONS

The production of CO and CO_2 was measured as a function of time for several low-rank coals and chars. Detection is possible for individual particles of about 200 μm. Activation energies obtained from ignition delay times agree well with measurements from TGA experiments as well as steady-state Semenov analyses. Ignition delay depends strongly on gas temperature and, to a minor extent, on lithotype. The Beulah lignite char was demonstrated to be a highly reactive material and comparison of its ignition behavior to that of the lignite indicated that the lignite ignited heterogeneously.

REFERENCES

1. R.H. Essenhigh in "Chemistry of Coal Utilization", M.A. Elliott, ed., John Wiley & Sons, New York, 1981, p. 1153.

2. M.F.R. Mulcahy and I.W. Smith, Rev. Pure and Appl. Chem., 19, 81, 1969.

3. M.A. Gill, D.W. Gill, B.B. Morgan, and P.G.A. Hawksley, Combustion of Pulverised Coal, The British Coal Utilization Research Association, Leatherhead, 1967.

4. S. Bandyopadhyay and D. Bhaduri, Combustion and Flame, 18, 411, 1972.

5. J.H. Harker and N.S. Mellor, J. Inst. Energy, 59, 154, 1986.

6. B.C. Young and S. Niksa, Fuel, 67, 155, 1988.

7. J.T. Ashu, N.Y. Nsakala, O.P. Majajan, and P.L. Walker, Fuel, 57, 250, 1978.

8. C.O. Gomez and F.J. Vastola, Fuel, 64, 558, 1985.

9. C.Y. Tsai and A.W. Scaroni, Energy and Fuels, 1, 263.

10. J.G. Cogoli, D. Gray, and R.H. Essenhigh, Comb. Sci. Tech., 16, 165, 1977.

11. T.F. Wall, D. Phong-anat, V.S. Guruajan, L.J. Wibberley, A. Tate and J. Lucas, Combustion and Flame, 72, 111, 1988.

12. T.F. Wall and V.S. Guruajan, Comb. and Flame, 66, 151, 1986.

13. H.K. Karz, W. Kordylewski, and W. Rybak, Fuel, 59, 799, 1980.

14. M. Chen, L. Fan, and R.H. Essenhigh, Twentieth Symp. (Int.) on Combustion, The Combustion Institute, Pittsburgh, p. 237, 1984.

15. H.M. Cassel and I. Leibman, Comb. and Flame, 3, 437, 1956.

16. G.R. Thomas, A.J. Stevenson, and D.G. Evans, Comb. and Flame, 21, 133, 1968.

17. D.P. McCollor, P.G. Sweeny, and S.A. Benson "Coal/Char Reactivity Final Technical Progress Report", 1987, Cooperative Agreement #DE-FC21-86MC10637.

18. S.C. Deevi and E.M. Suuberg, Fuel, 66, 454, 1987.

19. M.M. Patel, D.T. Grow, and B.C. Young, Fuel, 67, 165, 1988.

TABLE 1

IGNITION RESULTS FOR SEVERAL COALS AND CHARS

Material	Number of particles	T (K)	Particle Volume x 10^{-6} (cm^3)	Aspect Ratio	Maximum Rate x10^{-6} (g/sec)	CO_2/CO Product Ratios	Delay (ms)
Beulah Vitrain, wet	7	923	8.3 ± 1.5	1.6	3.9 ± 1.1	0.99 ± 0.21	376 ± 62
Beulah Vitrain, dry	11	923	5.4 ± 1.3	1.7	4.5 ± 1.1	0.84 ± 0.16	419 ± 51
Beulah Fusain	7	923	6.7 ± 1.9	1.8	6.3 ± 1.4	0.88 ± 0.33	302 ± 51
Beulah Attritus	9	923	9.8 ± 5.1	2.1	7.2 ± 2.7	0.78 ± 0.25	371 ± 36
Beulah Vitrain	8	1273	6.9 ± 2.0	1.7	5.3 ± 1.2	1.19 ± 0.36	137 ± 38
Pitts #8 Vitrain	7	1273	6.2 ± 1.8	1.4	4.5 ± 1.8	2.01 ± 0.53	120 ± 79
Pitts #8 Vitrain	8	923	6.5 ± 2.9	1.7	0.99 ± 0.25	---[a]	480 ± 34
Beulah Char	7	923	7.4 ± 3.1	2.5	4.2 ± 2.4	1.06 ± 0.30	309 ± 63

a. Not available

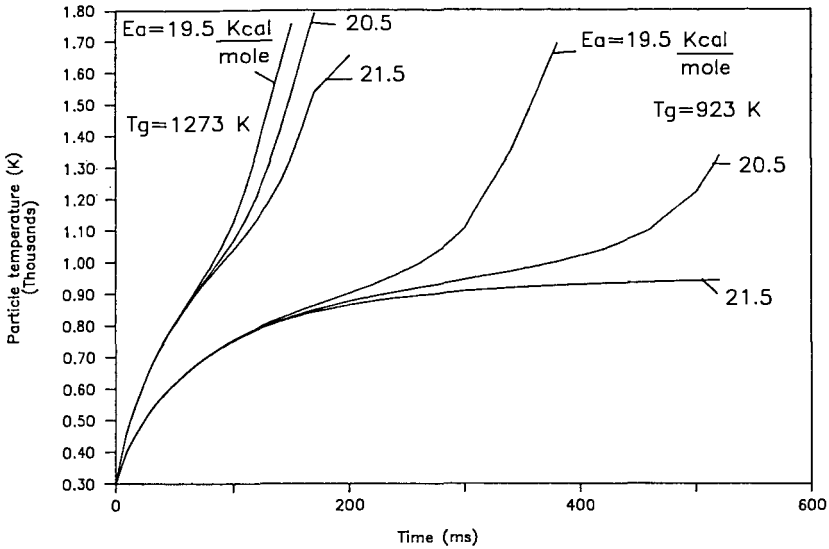

Figure 1. Calculated Temperature Profiles for 200 μm Particles

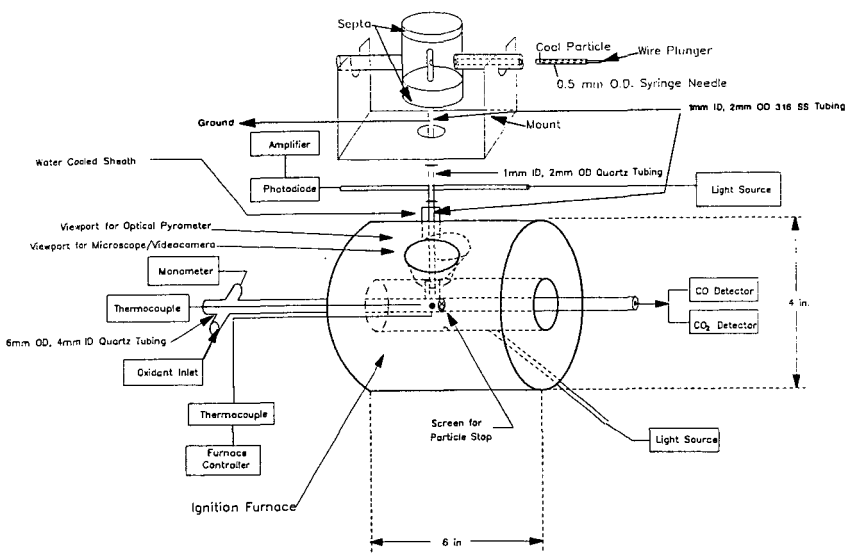

Figure 2. Detailed Side View of the Ignition Apparatus

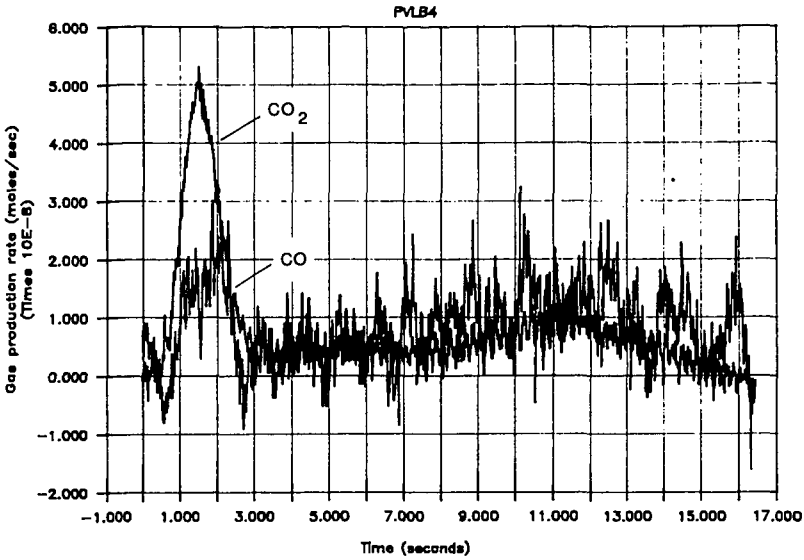

Figure 3. CO and CO_2 Production Rate Profiles of Pittsburgh #8 Coal at 923 K

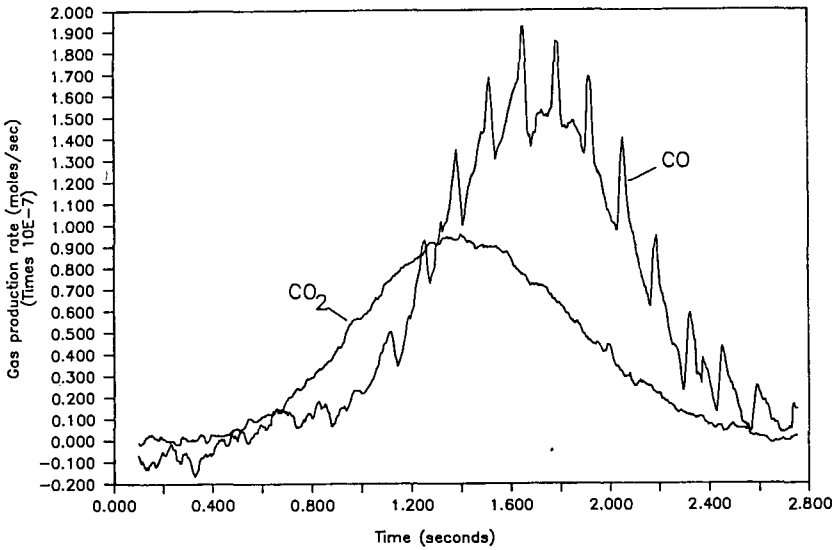

Figure 4. CO and CO_2 Production Rate Profiles of Beulah Lignite at 923 K

CHANGES IN ACTIVATION ENERGY WITH LEVEL OF BURN-OFF FOR BITUMINOUS COAL CHARS

M. Rostam-Abadi, D. L. Moran, J. A. DeBarr

Illinois State Geological Survey, 615 E. Peabody Drive, Champaign, IL 61820

INTRODUCTION

The kinetics of oxidation of coal char has been extensively studied during the last decade (1-4). A common goal of these studies has been to evaluate reactivity of char under diffusion-free conditions and to identify physico-chemical properties of a char which influence its reactivity.

Thermogravimetric analysis has been widely used to obtain rate data for the reaction char oxidation (1-7). Isothermal studies have demonstrated that the oxidation rate changes with conversion and exhibits a maximum at a specific level of burn-off. Data have been analyzed to obtain the intrinsic reactivity and activation energy for char oxidation. In most of the previous studies, however, the activation energy has been calculated at a specific conversion, usually at 50% conversion or at a level corresponding to the maximum rate. Since the value of activation energy has a pronounced effect on the intrinsic reaction rate, it seems appropriate to investigate whether activation energy changes with conversion during oxidation of coal char.

In this paper the results of a study on the oxidation of three bituminous coal chars are presented. The focus is on the variation of activation energy with level of burn-off for the three chars.

EXPERIMENTAL

Char - Chars, also referred to as partially devolatilized (PD) coals, were made from two bituminous coal samples obtained from the Illinois Basin Coal Sample Program, samples IBCSP-3 and IBCSP-4(8). IBCSP-3 is mine-washed coal [a blend of Springfield (No. 5) and Herrin (No. 6)] and the IBCSP-4 is run-of-mine Herrin (No. 6) (see table 1 for analyses).

Two chars (char-1 and char-3) were made from two partially devolatilized (PD-1, PD-3) coals that were produced from IBCSP-3 in the United Coal Company's (UCC) Mild Gasification Pilot Unit (Bristol, Virginia). PD-1 and PD-3 had volatile matter contents of 25.6% and 13.0% (dry-ash-free basis). The details of PD coal production are given elsewhere (9). Chars were made by injecting PD coals into a 5-cm diameter batch fluidized-bed reactor which was preheated to 850°C under a purge of nitrogen. The samples were fluidized at 850°C for 5 minutes and then cooled to ambient conditions. The volatile matter content of char-1 and char-2 were 7.5% and 6.3%.

A third char, hydrodesulfurized (HDS) char, was prepared from IBCSP-4 which was first physically cleaned (14.8% ash and 6.2% S). The char was produced in the batch fluidized-bed reactor from a 74-589 micrometer-size fraction of the clean coal using the following processing steps: 1) preoxidation at 250°C in a 5% O_2 - 95% N_2 gas mixture for 30 minutes, 2) pyrolysis in nitrogen at 850°C for 15 minutes, and 3) desulfurization in hydrogen at 850°C for 90 minutes. The HDS char had 0.4% sulfur and 3% volatile matter.

Reactivity tests - The particle size of char samples was reduced to less than 90 micrometers prior to reactivity tests by crushing, and sieving and recrushing the oversize. Reactivity experiments were performed in an Omnitherm thermogravimetric analyzer (TGA) coupled to an Omnitherm QC25 programmer/controller. The TGA system was interfaced with an IBM XT computer through a Keithley DAS series 500 data acquisition system to provide automated data collection and storage.

In each experiment a sample mass of about 2 mg was placed in the TGA platinum pan and heated in nitrogen (200 cm^3/min) at 50°C/min to the reaction temperature (between 425 and 575°C). The nitrogen was replaced by dry air flowing at a rate of 200 cm^3/min. The percent weight of the unburned char, the rate of weight loss, and the gas temperature in the vicinity of the sample pan as a function of time were monitored by the computer. Data were collected at 5 to 40 second intervals depending on the reaction temperature.

RESULTS AND DISCUSSION

TGA data were used to calculate the apparent reaction rates, R, where

$$R = -\frac{1}{f}\frac{df}{dt} \qquad 1)$$

and

$$f = (M-Ma)/(Mo-Ma) \qquad 2)$$

f = fraction combustible remaining at time t, M = mass of sample at time t, Mo = initial sample mass, Ma = mass of sample at complete conversion, i.e. ash. Figures 1, 2, and 3 show plots of apparent rates versus fraction conversions for the chars at the indicated temperatures. As expected, apparent rates increased with increases in reaction temperature. Also, for each char, the shape of the reactivity curve did not change with temperature. However, there are clear differences among the reactivity curves of the three chars. For char-1, apparent rate increased initially, maximized at about 30% conversion and decreased slightly as the fractional burn-off increased. For char-3, the apparent rate maximized after 5 to 15% conversion, depending on the reaction temperature, and remained relatively constant after about 30% conversion. For HDS, the apparent rates did not show a maximum and increased with conversions up to 90% conversion in the studied temperature range. These results suggest that char formation conditions influence the shape of the reactivity curve.

The differences observed in the reactivity curves could be partially due to the variations that occur in internal pore surface area during char oxidation. In order to gain information with respect to relative available pore surface area, the oxidation rate of char was expressed as:

$$-\frac{df}{dt} = SkP_{O_2}^{n} f \qquad 3)$$

where k = reaction rate constant, g/m^2.atm.min; P_{O_2} = oxygen partial pressure, atm; S = available pore surface area, m^2/g; n = reaction order with respect to oxygen pressure.
The initial rate of the reaction at t=0 (or f=1) is:

$$-\left(\frac{df}{dt}\right)_i = S_o k P_{O_2}^{n} \qquad 4)$$

where S_o is the initial pore surface area. Dividing equation 3) by 4) and solving for S/S_o gives

$$\frac{S}{S_o} = \frac{1}{(-df/dt)_i}\frac{(-df/dt)}{f} \qquad 5)$$

According to equation 5), a plot of $(-df/dt/f)/(-df/dt)_i$ versus conversion should represent changes in available surface area with conversion. Figure 4 shows how the relative available pore surface area of the samples changed with conversion. In these figures, the values of (df/dt/f) were normalized by the corresponding values at the 10% conversion because at the lower conversion levels TGA data could not be obtained accurately. For each char a single curve could adequately represent the data in the studied temperature range. A similar observation has been reported by previous investigators (1,2). This indicates that the rate data were obtained under diffusion-free conditions and surface area development was independent of reaction temperature. Each fuel demonstrates a unique pore area development. HDS which had the lowest initial internal surface area among the fuels tested (because it was subjected to most severe heat treatment condition) exhibited the largest change.

The rate data shown in figures 1, 2, and 3 were used to determine activation energies for the oxidation of the chars. The rate constant was assumed to have Arrehenius form:

$$k = k_o e^{-E/RT} \qquad 6)$$

where k_o is the pre-experimental factor and E is the activation energy (kj/mole). Substituting equation 6) into equation 4), solving for (-df/dt/f), and taking logarithm of both sides yields equation 7)

$$\ln(-df/dt/f) = \ln(k_o P_{O_2}^n) + \ln S - \frac{E}{RT} \qquad 7)$$

According to equation 7) a plot of ln (-df/dt/f) versus 1/T gives activation energy from the slope at a given converion if the values of S are independent of reaction temperature.

The values of ln(-df/dt/f) evaluated at 10%, 20%, 30%, 50%, and 70% burn-off were plotted against 1/T, and are shown in figures 5, 6, and 7. The observed changes in the slopes of the plots demonstrated variations in activation energies with conversion. This is clearly seen in figure 8 where the values of activation energies are plotted against conversion. According to this figure, activation energies may increase, or may show a maximum or minimum as reaction proceeds, depending on the fuel tested. The most often reported value for the activation energy of char combustion at temperatures <600°C is 130 KJ/mole (Radovic, 1983; Khan, 1987). The results obtained in this study indicate values ranging from 107 to 145 KJ/mole, depending on the fuel and the level of burn-off. Results of a recent kinetic study conducted with a sucrose char also indicated that activation energy for the oxidation of the char increased from 136 to 147 kJ/mole as conversion increased from 20 to 90% (10).

The variation in activation energy with the level of burn-off could be partly due to the presence of a distribution or type of active sites in the char with each type having its own characteristic reactivity. Past studies (11) have indicated that two types of surface oxides, stable and fleeting, are formed when oxygen chemisorbs on carbon active sites. Oxidation char is represented by several reactions including formation and desorption of surface oxides as well as direct burn-off of the carbon. These reactions may have different activation energies. Also, the contribution of each reaction to the progress of char oxidation may be significant at different levels of burn-off. This could result in variation of activation energy with conversion as observed in this study.

The results obtained in this study suggest that to more fully describe burning characteristics of a char, reactivity data should be examined at different conversions. This observation was also reported in a recent study in which an average reactivity

the whole char burn-off was used to describe char reactivity rather than one determined at a specific level of burn-off (12).

ACKNOWLEDGEMENTS

This work was funded in part by grants from the Illinois Coal Development Board through the Center for Research on Sulfur in Coal.

REFERENCES

1. Dutta, S. and C. Y. Wen, 1977, Ind. Eng. Chem. Proc. Des. Dev., 16(1), 31-37.
2. Su, J. L. and D. D. Perlmutter, 1985, AICHE J. 3196), 973-981.
3. Tseng, H. P. and T. F. Edgar, 1985, Fuel, 64(3), 373-379.
4. Sahu, R., Y. A. Levendis, R. C. Flagan and G. R. Gavalas, 1988, Fuel, 67(2), 275-283.
5. Radovic, L. A., and P. L. Walker, Jr., 1984, Fuel Processing Technology, 8, 149-154.
6. Khan, M. R., 1987, Fuel, 66(12), 1626-1634.
7. Solomon, P. R., M. A. Serio and S. C. Heninger, 1986, ACD Div. Fuel Chem. preprints, 31(3), 200-205.
8. Kruse, C. W., R. D. Harvey, and D. M. Rapp, 1987, ACS Div. Fuel. Chem. preprints, 32(4), 359-365.
9. Rostam-Abadi, M., 1987, Final Technical Report to the Center for Research on Sulfur in Coal for the period September 1, 1986 - August 31, 1987, 49 pages.
10. Floess, J. K., J. P. Longwell and A. F. Sarofim, 1988, Energy and Fuels, 2(1), 18-26.
11. Laine, N. R., F. J. Vastola and P. L. Walker, Jr., 1963, J. Phys. Chem., 67, 2030-2037.
12. Tsai, C. Y. and A. W. Scaroni, 1987, Fuel, 66(10), 1400-1406.

Table 1. Chemical characterization of coal samples
wt% (moisture-free basis)

Coals	IBCSP-3	IBCSP-4
Seam	No. 5[1]	No. 6
Rank	HVBB	HVCB
Moisture	5.4	10.2
Volatile matter	39.2	30.6
Fixed carbon	52.4	31.3
Ash	8.4	38.1
Carbon	73.8	46.0
Hydrogen	4.9	3.5
Nitrogen	1.7	0.80
Oxygen	8.7	7.4
Sulfur	2.3	4.2
Chlorine	0.2	0.05
Heating value (Btu/lb)	13,437	8,492

[1] Predominantly Springfield (No. 5). Approximately 20% Herrin (No. 6) blended at washing plant.

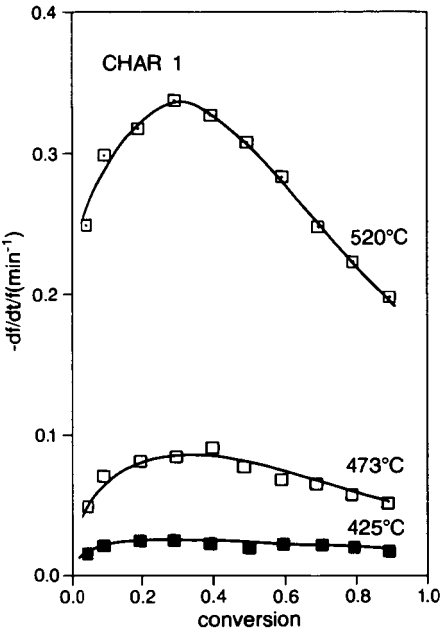

Figure 1. Apparent rate vs. conversion for oxidation of Char 1 in air.

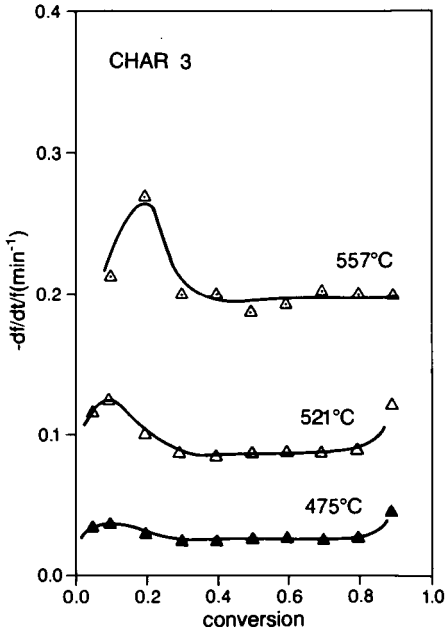

Figure 2. Apparent rate vs. conversion for oxidation of Char 3 in air.

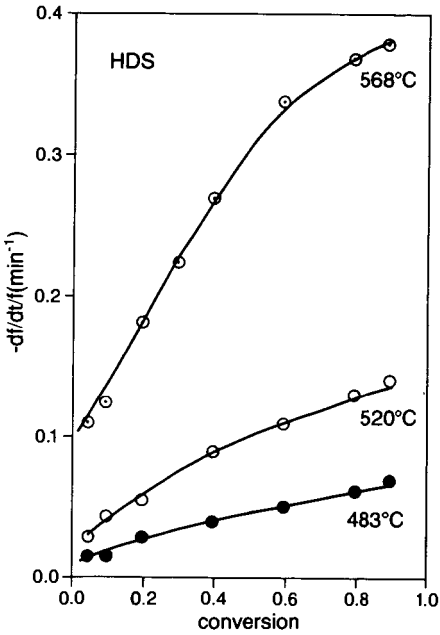

Figure 3. Apparent rate vs. conversion for oxidation of HDS char in air.

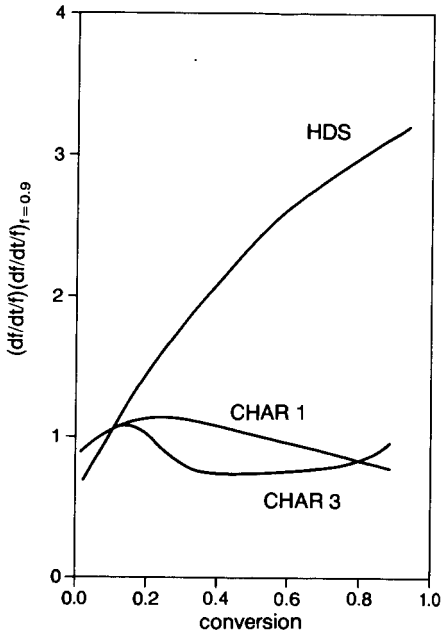

Figure 4. Surface area development vs. conversion for various chars.

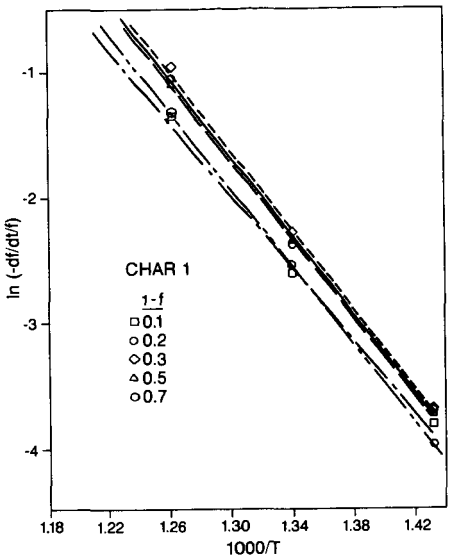

Figure 5. Arrhenius plot with rates observed at various conversions for oxidation of Char 1 in air.

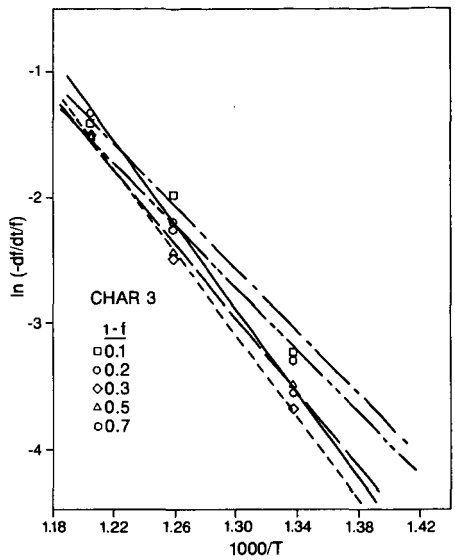

Figure 6. Arrhenius plot with rates observed at various coversions for oxidation of Char 3 in air.

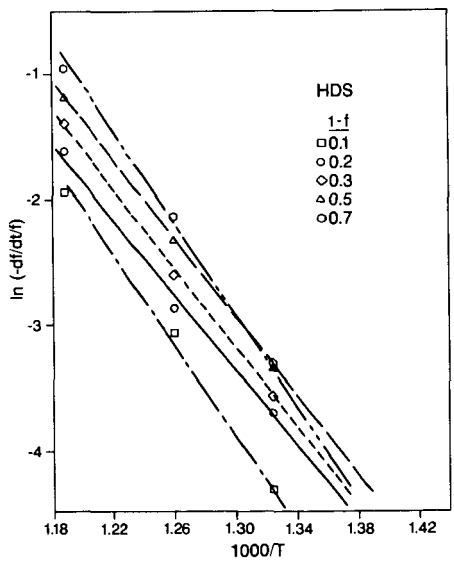

Figure 7. Arrhenius plot with rates observed at various conversions for oxidation of HDS char in air.

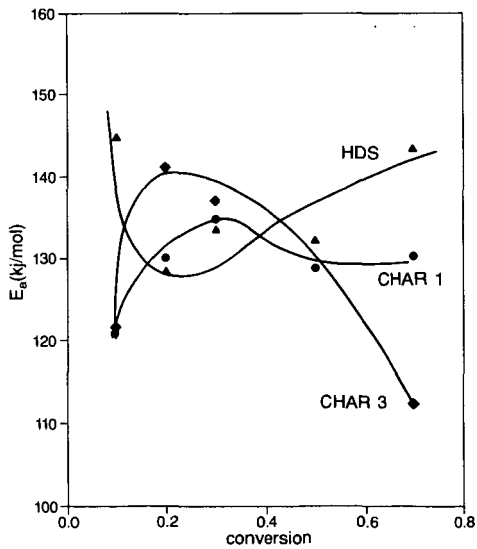

Figure 8. Variation of activation energy with conversions for oxidation of various chars.

BURNING CHARACTERISTICS OF PARTIALLY DEVOLATILIZED COALS

M. Rostam-Abadi, J. A. DeBarr, and D. L. Moran

Illinois State Geological Survey, 615 E. Peabody Drive, Champaign, IL 61820

INTRODUCTION

Thermal and chemical coal-desulfurization processes designed to yield refinable petroleum substitutes and solid fuels for boilers reduce the fuel's volatile matter content. This reduced volatility influences combustion characteristics such as ignition temperature, flame stability, and carbon burn-out.

A variety of studies has been conducted on the oxidation reactivity of coal char (1-5). On the basis of information available from these studies, it can be concluded that the conditons under which a char is prepared influences its reactivity. Some of the production parameters that affect the reactivity are processing gas, heating rate, maximum heat treatment temperature, soak time at peak temperature, and pressure. These factors influence the pore structure and active surface area of the char as well as the accessibility of a reactant gas to the internal surface area of the fuel during combustion or gasification. Recently it has been suggested that char formation conditions that result in a higher H/C ratio or hydrogen content favor reactivity (6-7).

The work presented in this paper is part of a larger study which was undertaken to determine combustion characteristics of partially devolatilized coals.

EXPERIMENTAL

Char - Chars, also referred to as partially devolatilized (PD) coals, were made from a bituminous coal sample obtained from the Illinois Basin Coal Sample Program, sample IBCSP-3 (8). The analysis of the coal is given in table 1.

PD coals were made in two ways: in a pilot-scale fixed-bed reactor at the United Coal Company (UCC) located in Bristal, Virginia, and in a microbalance reactor. The UCC samples were prepared under mild gasification conditions and had volatile matter contents (dry-basis) of 23.3%, (PD-1), 15.4% (PD-2) and 11.4% (PD-3), see table 2. The details of PD production at the UCC are given elsewhere(9). The samples made in the microbalance reactor were produced under the following conditions: heating rates between 5 and 1200°C/min; heat treatment temperatures (HTT) between 400 and 900°C; soak times at maximum treatment temperatures up to 4 hours. These fuels were prepared under nitrogen purge and had volatile matter contents between 2 and 30%.

Reactivity measurement - The particle size of samples was reduced to less than 90 micrometers prior to reactivity tests. An Omnitherm Thermogravimetric Analzyer (TGA) which was interfaced with an IBM-XT computer through a Keithley DAS series 500 data acquisition system was used to obtain burning profiles of the PD coals. In each experiment, a sample mass of about 2 mg was loaded in the TGA platinum pan and was heated at a constant heating rate of 20°C/min in air from ambient to temperatures up to 800°C. The flow rate of air was 200 cc/min (STP).

RESULTS AND DISCUSSION

Burning profile - The term burning profile was first used twenty years ago to refer to a plot of the rate of weight loss versus temperature when a small amount of coal-derived fuel is heated (usually 15-20°C/min) in air(10). Characteristic temperatures from the burning profile corresponding to the onset of burning, peak burning rate and complete burn-out were taken as a measure of a fuel's reactivity, with lower characteristic temperatures indicating more easily burned fuels. The test was used

with past experience and standard reference profiles to predict conditions, such as residence time or excess air, necessary for complete combustion of fuels in large furnaces. The burning profiles were found especially useful for evaluating combustion characteristics of unknown fuels when only small quantities of fuel were available.

In recent years, the concept of burning profiles has been used in coal combustion studies to show the effect of variations in coal rank on reactivity (11), to show the influence of maceral composition on combustion of pulverized coal (11, 12) and to determine the activation energy for oxidation of char (6, 7, 13).

Figure 1 shows typical weight loss and rate of weight loss data obtained in air for coal. The gain in sample weight between 200 and 300°C is due to oxygen chemisorption, i.e., preignition oxidation. A major weight loss began at 375°C (T_I). This temperature was taken at the point where the rate of weight loss was 1%/min. The rate of burning peaked at 490°C (T_P) and the coal was compeletly burned at 630°C (T_B). The burn-out temperature was taken at the point where the rate of weight loss was 1%/min. The weight remaining at 650°C was the ash content of the sample which was approximately 12%.

Combustibility of coal and PD coals - The burning profiles obtained for the coal, PD-1, PD-2, and PD-3 coals are shown in figure 2. The profiles are offset to avoid overlap. The onset of burning was about 375°C for all the samples. However, there are clear differences among the burning profiles. Raw coal exhibited a single-burn profile, while double-burn profiles were observed for PD-1, PD-2 and PD-3. The second burn appeared as a shoulder peak for PD-1 and became more pronounced for PD-2 and PD-3. The double-burn behavior observed for the PD coals suggested the presence of at least two types of combustibles in the fuels. The two portions of combustibles burned in two distinct stages with peak burn rates at approximately 500°C and 550°C. The higher reactivity constituent (low temperature burn) was a coal-like material and was present in larger concentration in PD-1 followed by PD-2 and PD-3 (9). It had burning properties similar to that of the coal. Fuels with higher volatile matter content burned more rapidly. For example at 500°C, the amount of combustible materials burned (not shown) was 70% for the raw coal, 55% for PD-1, 40% for PD-2, and 20% for PD-3. The most pronounced impact of the volatile matter was on burn-out temperatures which were 580, 630, 660 and 690°C for the coal, PD-1, PD-2 and PD-3, respectively. The results indicate that under the conditions used, raw coal was the most readily combusted fuel, followed by PD-1, PD-2 and finally PD-3.

Burning profiles of PD-2 and two 15% volatile PD coals are shown in figure 3. LTC was produced in the microbalance reactor by heating the coal at 5°C/min to 525°C. Coal+HTC was a mixture of coal and a high temperature char (HTC, 3% volatile matter) which was prepared by heating the coal at 5°C/min to 850°C, see table 2. The profiles for the coal and the HTC are also shown in figure 4. LTC exhibited a single burn behavior during burning in contrast with PD-2 and Coal+HTC which exhibited double-burn behavior. The peak burn rate for the HTC occured at 575°C which was 25°C higher than the temperature of the second burn obsorved for PD-2. This was because the HTC was subjected to higher processing temperature than PD-2. The burning profile for the Coal+HTC reveals that the two fraction of this fuel, i.e. coal and the HTC, burned in two stages with peak burn temperatures corresponding to those of the coal and the HTC. LTC was more reactive than PD-2 and the Coal-HTC fuel because it had a lower burn-out temperature. These results indicate that a fuel with inherent volatile matter is more reactive than a fuel with comparable volatile matter prepared by blending raw coal and low volatile char. This suggests that volatile matter alone cannot be used as an index of reactivity.

The influence of volatile matter on characteristic temperatures of PD coals which were made in the microbalance reactor are shown in figure 4. These fuels exhibited a single burn profile during combustion. The results show that there were only slight differences in characteristic temperatures for fuels with volatile matter contents above 10%. However, with further decreases in volatile matter, burn-out temperatures

increased markedly. The burn-out temperatures were particularly sensitive to preparation conditions of a sample. Fuels prepared at the fastest heating rate, i.e. 1200°C/min, and shorter soak times were more reactive and had lower burn-out temperatures than those made at slower heating rates and longer soak times. These observations are in agreement with results reported in a previous study on the reactivity of PD coals derived from an Illinois hvB coal (1). The values of T_B for PD coals prepared at UCC are also shown in figure 4. It is clearly seen that these samples had higher burn-out temperatures than those prepared in the microbalance reactor under controlled pyrolysis conditions. The UCC samples were produced in a pilot-scale reactor and were subjected to different processing conditions than the PD coals made in the microbalance reactor.

CONCLUSIONS

Results obtained in this study suggest that PD coals with comparable volatile matter content produced from the same coal but under different processing conditions had different burning characteristics. Lower preparation temperatures, higher heating rates and shorter soak times at final pyrolysis temperatures favored reactivity. PD coals with inherent volatile matter were more reactive than fuels with comparable volatile matter prepared by blending low volatile char and the coal. It was also concluded that volatile matter alone may not be a valid index of reactivity.

ACKNOWLEDGEMENTS

We gratefully acknowledge the Illinois Coal Development Board and the Center for Research on Sulfur in Coal for their financial support of this project.

REFERENCES

1. Jenkins. R. G., S. P. Nandi, P. L. Walker, 1973, Fuel, 52(10), p. 288-293.
2. Dutta, S., C. Y. Wen, 1977, Ind. Eng. Chem. Process Des. Dev., 16(1), 31-37.
3. Radovic, L. R., P. L. Walker, Jr., 1984, Fuel Processing Technology, 8, 149-154.
4. Wells, W. F., S. K. Kramer, L. D. Smoot, A. U. Blackham, 1984, a paper presented at the 20th International Symposium on Combustion, Ann Arbor, MI, August 12-17.
5. Katta, S., D. L. Keairns, 1984, a paper presented at AICHE meeting, Anaheim, CA, May 20-24.
6. Solomon, P. E., M. A. Serio and S. G. Heninger, 1986, ACS Div Fuel Chem., 32(3), 200-205.
7. Khan, M. R., 1987, ACS Div Fuel Chem. peprints, 32(1), 298-309.
8. Kruse, C. W., R. D. Harvey, and D. M. Rapp, 1987, ACS Div. Fuel. Chem. preprints, 32(4), 359-365.
9. Rostam-Abadi, M., J. A. DeBarr, D. L. Moran and C. W. Kruse, 1987, Final Technical Report to the Center for Research on Sulfur in Coal for the period September 1, 1986 - August 31, 1987, 49 pages.
10. Wagoner, C.L. and A. F. Duzy, 1967, Paper presented at Winter Annual Meeting, ASME, Pittsburgh, PA, Nov. 12-16.
11. Morgan, P. A., S. D. Robertson and J. F. Unsworth, 1986, Fuel, 65(11), 1546-1551.
12. Morgan, P. A., S. D. Robertson and J. F. Unsworth, 1987, Fuel 66(2) 210-215.
13. Cumming, J. W., 1984, Fuel, 63(1), 1436-42.

Table 1. Analysis of coal, wt% (moisture-free basis)

Coals	IBCSP-3
Seam	No. 5[1]
Rank	HVBB
Moisture	5.4
Volatile matter	39.2
Fixed carbon	52.4
Ash	8.4
Carbon	73.8
Hydrogen	4.9
Nitrogen	1.7
Oxygen	8.7
Sulfur	2.3
Chlorine	0.2
Heating value (Btu/lb)	13,437

[1] Predominantly Springfield (No. 5). Approximately 20% Herrin (No. 6) blended at washing plant.

Table 2. Volatile Matter Content of PD Coals and Their Preparation Conditions

Sample	Reactor Type	Temperature (°C)	Residence Time (hr)	Volatile Matter (%)
PD-1	Fixed Bed	760*	1.7	23.3
PD-2	Fixed Bed	760*	2.5	15.4
PD-3	Fixed Bed	760*	3.2	11.4
LTC	Microbalance	525	---	15.0
HTC	Microbalance	850	0.5	3.0
Coal+HTC				17.0

*Reactor tube (8-inch in diameter) was located in a natural gas fired furnace kept at 760°C.

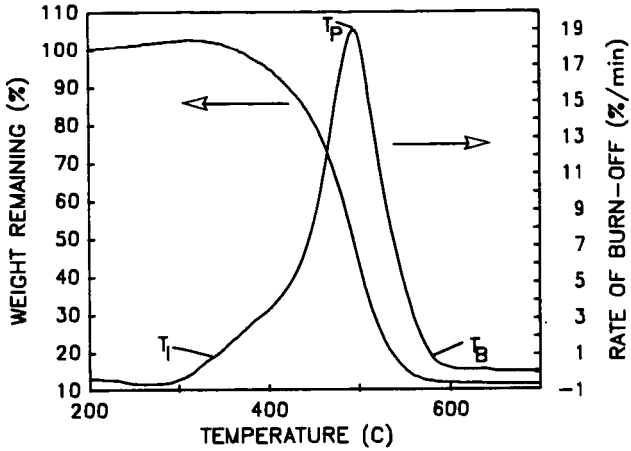

Figure 1. Burning characteristic of coal.

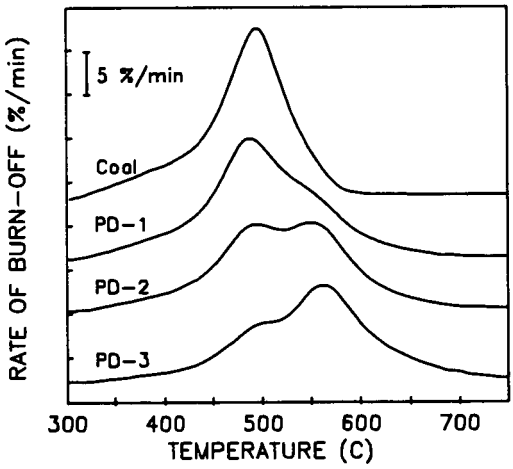

Figure 2. Burning profiles for coal and UCC PD coals

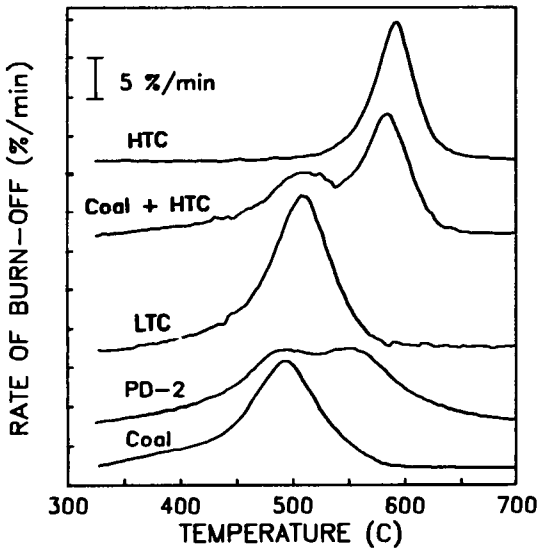

Figure 3. Burning profiles for coal, high and low temperature chars, and a mixture.

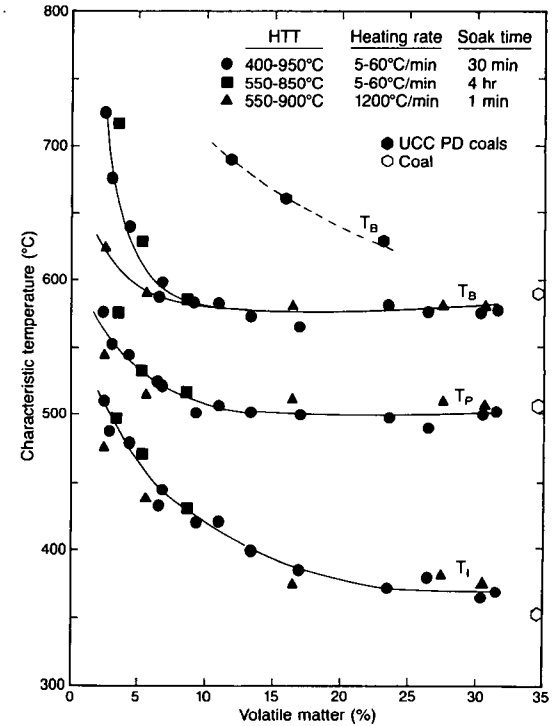

Figure 4. Effect of volatile matter on characteristic burning temperatures of chars produced under varing conditions.

EXPERIMENTAL VERIFICATION OF THE THERMODYNAMIC PROPERTIES OF A JET-A FUEL

Carmen M. Gracia-Salcedo, Bonnie J. McBride, Theodore A. Brabbs

NASA Lewis Research Center, Cleveland, Ohio 44135

INTRODUCTION

Thermodynamic properties for Jet-A fuel are needed for many calculations, including chemical equilibrium calculations. To fulfill this need, various correlations for the estimation of these properties have been published (1,2,3). However, these are difficult to use and may not be practical for all applications. In 1970, Shell Development Company, under a contract for NASA Lewis Research Center, determined the thermodynamic properties for a Jet-A fuel (4). In the present report, we used these thermodynamic data to derive the coefficients necessary to include Jet-A (gaseous and liquid phases) in the thermodynamic data library of the NASA Lewis Chemical Equilibrium Program (5). To verify the thermodynamic data and the polynomial fit, the temperatures of very rich mixtures of Jet-A and nitrogen were measured and compared to those calculated by the chemical equilibrium program.

THERMODYNAMIC DATA AND LEAST SQUARES FIT

To include Jet-A in the thermodynamic data library of the NASA Lewis Chemical Equilibrium Program (5), the thermodynamic functions specific heat C_p°, enthalpy H_T°, and entropy S_T°, need to be expressed as functions of temperature in the form of a fourth order polynomial for C_p°, with integration constants for H_T° and S_T°.

$$\frac{C_p^\circ}{R} = a_1 + a_2T + a_3T^2 + a_4T^3 + a_5T^4 \qquad 1)$$

$$\frac{H_T^\circ}{RT} = a_1 + \frac{a_2T}{2} + \frac{a_3T^2}{3} + \frac{a_4T^3}{4} + \frac{a_5T^4}{5} + \frac{a_6}{T} \qquad 2)$$

$$\frac{S_T^\circ}{R} = a_1\ln T + a_2T + \frac{a_3T^2}{2} + \frac{a_4T^3}{3} + \frac{a_5T^4}{4} + a_7 \qquad 3)$$

The thermodynamic data for a Jet-A fuel used for this report were measured or calculated by Shell Development Company in 1970. Most of these data were in an extensive unpublished table provided to NASA Lewis Research Center by Shell. Part of the data contained in this table and additional fuel information used for this report were published in reference 4. The data used from reference 4 include: heat of combustion value used to calculate the heat of formation of the liquid, and a fuel analysis by hydrocarbon type and carbon number used to estimate the entropy of the gaseous fuel mixture at 298K. The data used

from the unpublished table include: heat capacity and enthalpy values for gaseous Jet-A for temperatures from 273K to 1273K, the entropy and enthalpy of vaporization at 298K, and enthalpies for liquid Jet-A for temperatures from 298K to 650K. The values for enthalpy given in this table were referenced to liquid Jet-A at 273K. The chemical equilibrium program requires an assigned enthalpy value at 298K equal to the heat of formation. For this reason, the enthalphy values from the unpublished table were adjusted to be relative to the enthalpy at 298K.

The entropy values given in Shell's unpublished table were referenced to liquid Jet-A at 273K. The chemical equilibrium program requires the entropy to be zero at 0 K. To estimate the entropy for the gaseous Jet-A, the fuel analysis given in Table XVI of reference 4 was used along with the entropy values of the individual components from reference 6. The entropy of vaporization at 298K was obtained from Shell's unpublished table and substracted from the gas phase entropy to obtain the entropy at 298K for the liquid phase.

An updated version of the PAC4 computer code (7), namely PAC87 was used to extrapolate the thermodynamic functions for the gas to 6000K (8) and fit C_p° and H_T° simultaneously using a least squares method. The data were fitted in two temperature intervals, 298K to 1000K and 1000K to 5000K.

For the liquid Jet-A, the heat capacity values in the unpublished table did not match the enthalpies for temperatures above 600K. Since the enthalpy was the property measured by Shell Development Company (4), it was used in the PAC87 computer code to obtain heat capacity and entropy values for the temperature range 298K to 650K.

The chemical formula $C_{12}H_{23}$ was used to represent Jet-A in the computer program. This results in a molecular weight of 167.3. A value of 166 was reported in reference 4.

The coefficients obtained for the liquid and gaseous phases are the following:

LIQUID: 298K≤T≤650K	GAS: 298K≤T≤1000K	GAS: 1000K≤T≤5000K
a_1 = 0.13993639E 04	a_1 = 0.19935137E 01	a_1 = 0.24875975E 02
a_2 =-0.13440366E 02	a_2 = 0.13383918E 00	a_2 = 0.78259103E-01
a_3 = 0.48492245E-01	a_3 =-0.82891249E-04	a_3 =-0.31556353E-04
a_4 =-0.75524882E-04	a_4 = 0.31180914E-07	a_4 = 0.57891394E-08
a_5 = 0.43166687E-07	a_5 =-0.71528712E-11	a_5 =-0.39838032E-12
a_6 =-0.15588486E 06	a_6 =-0.35903496E 05	a_6 =-0.43110507E 05
a_7 =-0.54852414E 04	a_7 = 0.27744570E 02	a_7 =-0.93633944E 02

VERIFICATION

Experimental Apparatus

Experiments were conducted in the vaporization section of a catalytic flow-tube reactor described in reference 9. Open-end

J-type thermocouples were used to monitor the gas mixture temperature. They were located at 46, 53, 61 and 68 cm from the point of fuel injection.

Two fuel injector designs were used in this work (see Figure 1). Both consisted of seven 10-cm long conical nozzles arranged with six in a circle and one in the center. Fuel was delivered to each cone through tubes of equal length and of 0.04 cm ID. These tubes were located to spray the fuel in the direction of the gas flow. The fuel distribution through the fuel injectors was examined and was found to be uniform within 7% for fuel injector A and 4% for fuel injector B. A nitrogen purge in the fuel line was required to remove any residual fuel in the fuel tubes before shut-down. This eliminated clogging of these small tubes.

Operating Procedure

Nitrogen is heated to about 800K with an electric heater. The standard operating procedure was to warm-up the reactor for about two hours with hot nitrogen to attain a steady state temperature. Then, liquid fuel is added and the mixture temperature 68 cm downstream of the point of fuel injection was monitored. No data was recorded until the temperature was steady for about 5 minutes. This took about 30 minutes for the first point. Then the fuel flow was increased or decreased, and data were taken in the same manner. For the second point on, data could be taken every 10 minutes.

Experimental Approach

The objective of this study is to verify the thermodynamic properties of a Jet-A fuel by measuring the temperatures of very rich vaporized fuel/nitrogen mixtures. In a prior study (9) it was observed that the addition of large quantities of liquid fuel to a high temperature gas stream caused a large reduction in the stream temperature (200 to 300K). This mixture temperature can be calculated using the chemical equilibrium program and the thermodynamic properties of the fuel (liquid and gas) and nitrogen. We found that in such a system, the temperature was very dependent upon the thermodynamic properties of the fuel. For example, a ±5% change in the gas phase heat capacity of the fuel caused a ∓7K change in the calculated mixture temperature.

First, the feasibility of the experimental technique will be demonstrated by studing iso-octane, a fuel for which the thermodynamic properties are well known. Second, the data for iso-octane will be used as a standard for determining any non-adiabatic behavior of the apparatus. Finally, Jet-A will be studied under identical conditions.

Results and Discussion

The initial data were taken with iso-octane and fuel injector A. Temperatures of fuel/nitrogen mixtures were measured for different amounts of fuel injected into the hot nitrogen stream. These measurements were compared to the temperatures

calculated by the chemical equilibrium program for 298K liquid fuel and 800K nitrogen. Since the experimental fuel and nitrogen temperatures could not be maintained at exactly these conditions, small corrections were required to reduce these to the same starting conditions. The data for iso-octane are shown in Figure 2. It was observed that for low fuel mole fractions the experimental temperatures were below the calculated ones. This behavior is expected when the experimental apparatus is not adiabatic. However, at higher fuel mole fractions, the measured temperatures were much higher than the calculated ones and tended to level off. This suggests that complete vaporization had not been obtained at the monitoring station 68 cm downstream of the point of fuel injection. In discussions with Ingebo (10), it was suggested that vaporization could be improved by increasing the gas velocity and providing a constant area section to account for the stream break-up distance (about 2.5 cm). Injector A was modified by attaching a 3.0 cm addition at the inlet of each nozzle, as shown in Figure 1b. The calculated drop size obtained with the modified fuel injector is about 22 μm. With the previous design, calculated fuel drops were about 44 μm at the throat of the nozzles, but droplets 2.5 times larger were calculated at a distance 2.5 cm downstream of the throat. These modifications should significantly improve vaporization.

Fuel injector B proved to be very successful, as shown by the iso-octane data in Figure 3. All the experimentally measured temperatures were below the calculated curve and the data showed a similar shape. This suggests that vaporization was complete. The temperature difference can be attributed to apparatus heat losses. These heat losses increase as the mixture temperature increases, which is the behavior expected for a non-adiabatic system. A curve fit to the experimental data indicated a heat loss varying from 7 degrees at 460K to 23 degrees at 580K. The system was calibrated by plotting the difference between this curve and the calculation as a function of temperature.

The measured temperatures for Jet-A/nitrogen mixtures are shown in Figure 4a. The behavior is exactly that observed for the iso-octane data. Correcting the experimental data points for the heat losses from the calibration curve produced the results shown in Figure 4b. These data are in excellent agreement with the temperatures calculated using the coefficients derived from the thermodynamic data for Jet-A.

The extent of vaporization of a fuel with an end boiling point of 532K (4) was checked by using the Clapeyron equation which relates the boiling temperature (T) of a liquid with its vapor pressure (P),

$$\ln P = A + B/T \qquad 4)$$

Data of vapor pressure reported in reference 4 were used to determine the constants A and B. The line obtained from the equation is shown in Figure 5. The region under the line (region

I) corresponds to only vapor present, and the region above the line (region II) corresponds to liquid and vapor. Data points for the experimentally measured temperatures and partial pressures fall in region I, indicating complete vaporization of the fuel.

CONCLUSIONS

An experimental technique has been described in which the temperatures of very rich fuel/nitrogen mixtures were measured. These temperatures were shown to be dependent on the thermodynamic properties of the fuel. Iso-octane was used to test the feasibility of the technique and to calibrate the apparatus for heat losses. Coefficients were derived from thermodynamic data so that a Jet-A fuel could be included in the NASA Lewis chemical equilibrium program. The experimental data obtained for Jet-A in our calibrated apparatus were in excellent agreement with the calculated temperatures, confirming the correctness of the coefficients for the polynomials used in the program. This experimental technique is an excellent tool for verifying the thermodynamic properties of any multi-component fuel.

REFERENCES

1. "Technical Data Book - Petroleum Refining", Fourth Edition, American Petroleum Institute.
2. Maxwell, J. B.: "Data Book on Hydrocarbons", 1957.
3. "Handbook of Aviation Fuel Properties", CRC Report No. 530, Coordinating Research Council, Inc., 1983.
4. Faith, L. E., Ackerman, G. H. and Henderson, H. T.: "Heat Sink Capability of Jet-A Fuel: Heat Transfer and Coking Studies." NASA CR-72951, July 1971.
5. Gordon, S., and McBride, B. J.: "Computer Program for Calculation of Complex Chemical Equilibrium Compositions, Rocket Performance, Incident and Reflected Shocks, and Chapman-Juguet Detonations." NASA SP-273, 1976.
6. "Selected Values of Properties of Hydrocarbons and Related Compounds", Thermodynamic Research Center, Texas A & M.
7. McBride, B. J., and Gordon, S.: "Fortran IV Program for Calculation of Thermodynamic Data." NASA TN D-4097, 1967.
8. Wilhoit, R. C.: Thermodynamics Research Center Current Data News, Vol. 3, No. 2, 1975.
9. Brabbs, T. A.: "Fuel-Rich Catalytic Preburner for Volume Limited Hydrocarbon Scramjet." NASA TM-87111, 1985.
10. Private communication with Robert Ingebo, NASA Lewis Research Center, Cleveland, Ohio.

Figure 1 – Fuel Injectors

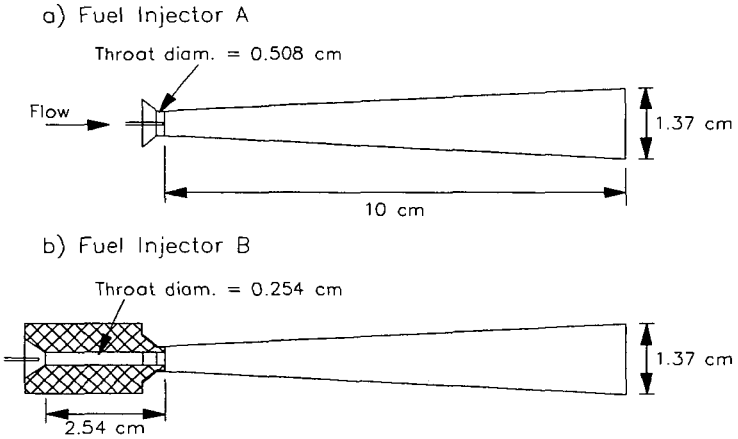

Figure 2 – Experimental Data for Iso–Octane (Fuel Injector A)

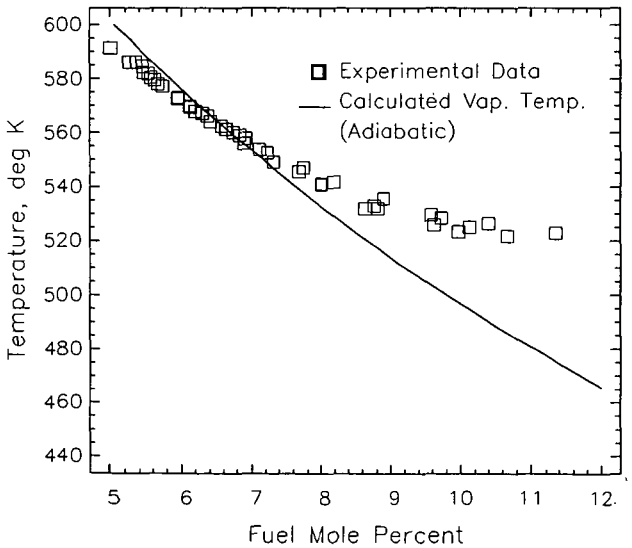

Figure 3 – Experimental Data for Iso–Octane (Fuel Injector B)

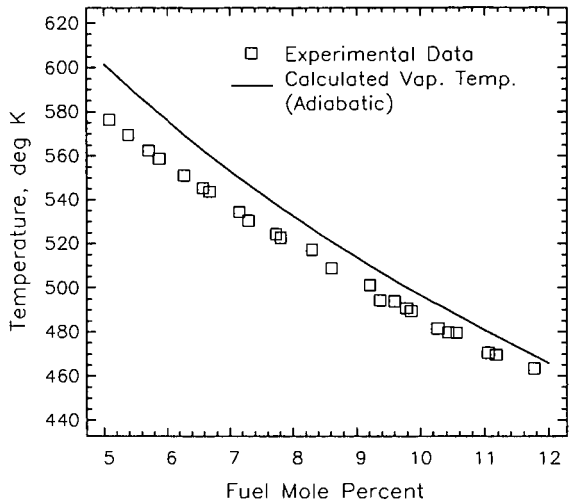

Figure 4 – Experimental Data for Jet–A (Fuel Injector B)

a) Raw Data

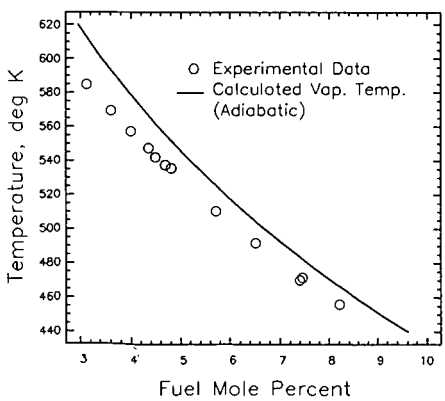

b) Data Corrected for non–adiabatic conditions

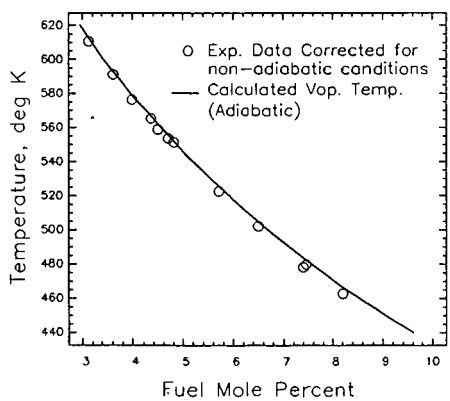

Figure 5 – Vaporization Temperature for Jet–A

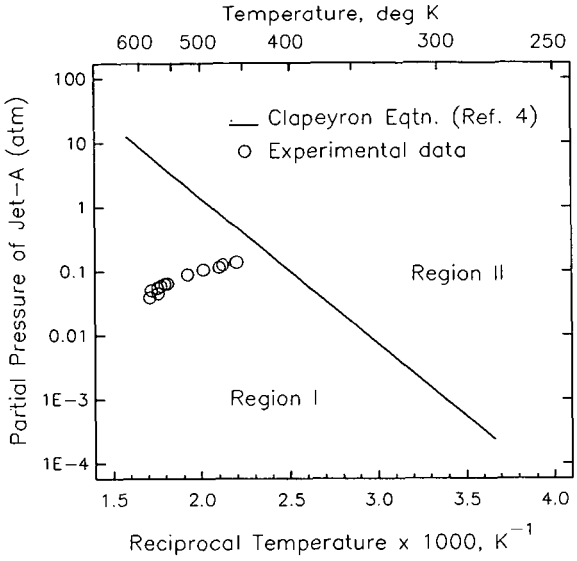

INVESTIGATION OF METHODS FOR AROMATIC STRUCTURAL INFORMATION IN MIDDLE DISTILLATE FUELS

S.W.Lee
Energy Research Laboratories, CANMET
Energy, Mines & Resources Canada
555 Booth St. Ottawa. Canada. K1A 0G1

ABSTRACT

The combustion characteristics of a fuel are related to its chemical and physical properties. The fuel aromatic content is expected to have significant influence on the production of soot in the combustion process. Detailed structural information on the fuel aromatic component is desirable for prediction of soot formation and isolation of certain molecule, responsible for soot formation. Various structural parameters such as the number of aromatic rings and the extent and type of substitution could be provided by ultraviolet spectroscopy, nuclear magnetic resonance, mass spectroscopy, and supercritical fluid chromatography. Information derived from these analytical techniques for a series of middle distillate fuels will be described and relationships among the number of aromatic rings and soot formation will be discussed.

INTRODUCTION

Energy conservation technologies and energy efficiency programs are no longer new in Western world in the eighties. The global increase in demand for petroleum products and the natural decline of existing conventional crude resources reflect the industry's effort to maximize the product yield from the crude barrel and to explore suitable fossil fuel supply sources. While overall demand for distillate oils is expected to increase (1), the transportation fuels are forecast to increase in demand with the fastest rate compared to other middle distillates(2). This scenario could encourage the refiners to maximize the yield of jet fuels and diesel fuels thereby increasing the heavier components in the heating fuel pool.

In Canada, where energy demand per capita is one of the highest in the world, it is expected that, by 1995 more than half of the total domestic production will be derived from the oil sands bitumens, heavy crudes and heavy oil deposits from western Canada(3). Synthetic distillate oils processed from these nonconventional sources have entered the Canadian market over a decade and the supply is increasing. Compositional analysis of synthetic distillates showed larger proportions of aromatics with fewer proportions of paraffins compared to conventional distillates(2). Current energy conservation trends plus the use of synthetic distillate have encouraged the Canadian refiners to produce oils containing higher aromatic components. The problems associated with the use of highly aromatic fuels are widely documented and have prompted performance evaluations on various combustion equipment. At the Canadian Combustion and Carbonization Research Laboratory, a research program is being carried out to study the influence of fuel quality on burner performance in residential heating appliances.

In the course of the study, it has become apparent that reliable analytical techniques for fuel property determinations are critical for accurate interpretation of combustion performance. Especially for aromatics, a method with better accuracy and versatility than commonly used ASTM D1319(fluorescent indicator adsorption;FIA) is desirable since its detection mechanism suffers poor accuracy and its application is restricted low boiling oils only(4). The search for such a method has lead to the development of a new technique utilizing supercritical fluid chromatography (5-7), and the review process of several techniques has provided relevant

information associated with each technique. In addition to total aromatic content, in depth hydrocarbon distribution data of the fuel is desirable in order to establish accurate property-performance correlations. While fuel aromatics are generally considered responsible for excessive particulate emissions, knowledge on how specific aromatic type compounds contribute to the process, could provide the lead to technologies for efficient process quality control in refinery and for reduced combustion emissions.

Initial survey of analytical data from two laboratories indicated considerable variance between a data set provided by the same method and caused concern over the accurate interpretation of results provided by different techniques. Without reliable fuel property data, accurate prediction of combustion performance can not be achieved. This document reports preliminary data from analysis of middle distillate oils, provided by five independent laboratories. Information provided by the techniques of ASTM D1319, nuclear magnetic resonance, mass spectroscopy, supercritical fluid chromatography, ultraviolet spectroscopy and silica-alumina column chromatography are described. More importantly, emphasis is given to the comparison in data supplied by independent laboratories. Correlations between soot production and specific aromatic compound types are also discussed based on the data resulted from two analysis techniques.

EXPERIMENTAL

Ultraviolet spectroscopy (UV)

Ultraviolet spectra of distillate samples were recorded on a UV spectrophotometer within the range of 350 nm to 190 nm after dilution with spectrograde cyclohexane solvent. 1.0., 0.10, and 0.010 cm path sample length cells were utilized with matching reference cells in the analysis depending on the aromatic concentration of the sample. Detailed analytical methodology was described elsewhere (8) and the method is currently under further refinment.

Column chromatography

A modified procedure of the U.S. Bureau of Mines API method (9) as reported by Sawatzky et. al (10) was used to determine saturates, monoaromatics, diaromatics and polyaromatics in distillate samples. In this procedure, the saturates were eluted from the silica/alumina column with n-pentane and the aromatics with different volumetric mixtures of pentane in toluene, followed by careful removal of solvents by air drying. Dried fractions were quantified by a gravimetric method as well as a gas chromatographic method after dilution with suitable solvent.

Supercritical fluid chromatography

The procedure for this new method for the determination of aromatics in diesel fuels and heating fuels was reported in 1987 by Fuhr et. al(5). Saturates and aromatics in distillate fuels are separated on a packed silica column (5 u silica adsorbosphere, 250mm x 2.1 mm) using supercritical carbon dioxide as mobile phase. A Shimadzu model GC-8A equipment with a flame ionization detector was used. A Varian model 8500 syringe pump was utilized to maintain the mobile phase pressure through the chromatographic column.

Nuclear magnetic resonance spectroscopy

The ^1H NMR spectra were obtained on a Varian model EM-390 spectrometer operated at 90 MHz. The samples were prepared by mixing the oil with chloroform-d_1 in a 50/50 volume ratio and a drop of Me_4 Si was added as a reference. Total aromatic content of the fuels were calculated from hydrogen intensities by the

method of Muhl et.al (11). Aromatic breakdown compositions such as mono-,di-, poly- were further derived using other physical properties of the fuels(12).

Mass spectrometry

A Finnigan 4500 quadrupole mass spectrometer was used for the determination of paraffin, olefins, naphthenes, aromatics (PONA) as well as the separation of mono-, di-,and poly- aromatic fractions. The samples were separated using a 1.83m column (3% Dexil 300 on acid washed Chromosorb W) heated from 60°C to 300°C. Chemical ionization(methane) mass spectra were acquired continuously during the gas chromatographic separation on a 3 second cycle. The series of peaks characteristic of paraffins, naphthenes and aromatics were summed continuously throughout the run in characterizing the compound type classes. The olefin content was determined by the ^{1}H NMR method. The detailed PONA method is available in the published literature(13).

Measurement of soot production from combustion process

Soot produced in residential furnaces from the fuels are reported in terms of smoke opacity% per start cycle. It is the maximum peak opacity of the transient soot peak from a cold burner start. It represents the real life soot emission from cold temperature conditions such as in the furnace start-up in the morning after an overnight reduced thermostat setting. Opacity values also indicate general trends of other incomplete combustion products such as carbon monoxide and hydrocarbons. In addition properties of a fuel have the most significant effects on cold start operation of an appliance. The experimental program for measurement of performance characteristics in residential oil combustion has been reported elsewhere(14).

RESULTS AND DISCUSSIONS

Two set of data from two groups of fuels are presented in this paper for discussion. One group of fuels were analyzed by four independent laboratories by NMR, MS, SFC, UV and FIA while the second group was analyzed by two laboratories using MS and column chromatography. Soot production data were available only for the second group.

In Table 1, total aromatic content as determined by four different techniques is presented. Each method determines and describes aromatics in different way. For FIA, volumetric per cent of aromatic compounds are reported whereas in MS-PONA, results are based on the fragmentation pattern and the total number of counts for each compound type. Since the total number of ion counts is proportional to weight of hydrocarbons, it can be considered as pseudo weight per cent or simply a compound type percent. SFC and NMR data are in weight per cent. The table therefore describes the type of information one can obtain from a particular method. Absolute comparison of data were not made for obvious reasons and only the correlation trends between these methods are investigated. Linear regression data are as follows.

Methods	correlation coefficient	slope of the line
SFC(wt.%) vs FIA(vol %)	0.90	0.97
SFC(wt.%) vs NMR(wt.%)	0.96	0.98
SFC(wt.%) vs MS (%)	0.92	0.81

The statistical data indicate generally good agreement between the methods with the strongest correlation between SFC and NMR. The carbon aromaticity data from Laboratory 1, from which the NMR weight per cent data are calculated is

reported in Table 2. These values represent the percentage of aromatic ring carbons present in the total numbers of carbon present in the average fuel molecule. The correlation of NMR aromaticity and SFC weight per cent show a linear relation with a correlation coefficient of 0.89 and a slope of 0.69. The aromatics by SFC are a measure of the amount of molecules having at least one aromatic ring with paraffinic and naphthenic substituents attached. Therefore this SFC-NMR correlation data with a slope of 0.69 indicates that on average, 69% of the carbon atoms in the aromatic molecules of these samples are contained in aromatic rings with the remainder in the substituents.

Table 2 also compares fuel aromaticity dada provided by two independent laboratories. The data indicates that Laboratory 2 has consistently lower values than laboratory 1 for all fuels. Laboratory 2 used Brown-Ledner equation (15) whereas Laboratory 1 derived results from detailed rigorous calculations (11,12). This minor difference alone cannot be accounted for the large difference between the two laboratories. Other variables such as instrument calibration and operator manipulation techniques are more likely the cause of such discrepancy.

Table 3 contains the aromatics ring distribution information provided by NMR, UV, SFC, and MS-PONA techniques. NMR-UV pair describes ring carbon weight per cent while SFC reports aromatic breakdown in total weight per cent. Since MS data is closer to total weight per cent, it was paired with SFC data. It should be pointed out that these SFC data are resulted from preliminary experiments and additional work is being carried out currently. Monoaromatic values from each pair indicate acceptable agreement but none of the pairs show comparable values for diaromatics. Diaromatics from the UV method are significantly lower than NMR method while MS diaromatics show lower values than SFC method to a similar degree.

Table 4 reports aromatic ring distribution in other set of middle distillate fuels. Opacity % reading is the maximum soot opacity measured from a cold start transient cycle from combustion of each fuel. Limited data indicate that both monoaromatics and diaromatics from the column chromatographic method are lower than those from MS method and show no particular relation to the opacity. The column chromatographic is normally suitable for fuels having initial boiling points of at least 200°C, since light fuel components can be lost during solvent removal prior to weighing of the fractions. The method was selected for investigation based on its simplicity requiring only common laboratory equipment. The component loss during solvent removal can be eliminated by analyzing the liquid fractions by gas chromatography instead of gravimetric analysis. This would require a more complicated procedure and trained operator which offsets the simplicity of the method.

Data from column chromatographic method, monoaromatics as well as diaromatics, show no apparent trend of interrelation with soot production. Figure 1 illustrates the correlations between mono- and diaromatic fuel components determined by PONA method and opacity of soot emitted. Diaromatic compounds indicate a general relation with cold start soot emissions with the exception of few outliers. Monoaromatics do not exhibit any particular interrelation.

CONCLUSIONS

1. Based on the information provided by participating laboratories, NMR and SFC show the strongest agreement for total fuel aromatics weight per cent. MS data show the lowest value.
2. Fuel aromaticity determination using NMR technique by two independent laboratories resulted in significantly different values. Regardless of the technique used, the analytical results seem to be more laboratory dependent than method dependent. Due to the highly complex nature of the middle distillate, larger

discrepancies between laboratories are observed.
3. For aromatic ring distribution in fuels, no significant trends between the methods were observed. Further studies are being planned.
4. The survey of analytical techniques suggests that MS and NMR are the most powerful tools for the detailed structural information in fuel analysis. These techniques, however, are not entirely suitable to refinery process quality control.
5. It appears that supercritical fluid chromatography could be the best candidate for a new aromatic standard method for the petroleum industry. The method's agreement with NMR indicates good accuracy and it has potential application for aromatic breakdown analysis. It can handle higher boiling samples using instrumentation of moderate sophistication.
6. Preliminary studies indicates that fuel diaromatics show greater influence on soot production than monoaromatics, in residential combustion.
7. The critical requirement of a reliable analytical methods for fuel aromatic structural information still exists in combustion research.

ACKNOWLEDGEMENTS

The author wishes to thank Dr. B.Fuhr and Dr. C.Reichert of Alberta Research Council for their SFC work, to Dr.B.Glavincevski of National Research Council of Canada for his NMR data and Dr. L.Stavinoha of Southwest Research institute for contribution of UV data. She also wishes to express her appreciation to D.E.Barker for her technical assistance.

REFERENCES

1. Schrepfer, M.W.,Arnold, R.J., Stansky, C.A., Oil & Gas Journal.,Jan 16, 79, 1984.
2. Steere, D.E. and Nunn, T.J.,SAE Technical paper series, Paper No.790922. Society of Automotive Engineers,Inc. Warrendale, PA, 1979.
3. Canadian National Energy Board, "Canadian Energy Supply and Demand 1983-2005" September 1984.
4. "Manual on Hydrocarbon Analysis", 3rd Edition, American Society for Testing and Materials, D1319. Philadelphia, PA, 1977.
5. Fuhr, B.J.,Holloway, L.R., Reichert, C., and Steppler, J., Energy, Mines & Resources Canada, Energy research laboratories Contract Report No. OSQ85-00240. Ottawa. Ont,1987.
6. Fuhr, B.J., Holloway, L.R., Reichert, C., Lee, S.W., and Hayden, A.C., American Chemical Society, Division of Fuel Chemistry preprints,32, No.4, 30,1987.
7. Lee, S.W.,Fuhr, B.J.,and Glavincevski,B., SAE Technical paper series, Paper NO. 872142, Society of Automotive Engineers, Inc. Warrendale, PA, 1987.
8. Newman, F.M. and Greenberg, M.K., U.S. Army Fuels and Lubricants Research Laboratory, Southwest Research Institute. San Antonio, TX. Government Accession No.AD A086654. Tech. Info. Centre, Caneron Station. Alexandria, VA. 1980.
9. Hirsch, D.E.,Hopkins, R.L., Coleman, H.J., Cotton, F.O., and Thompson, C.J. in American Chemical Society, Div. of Petroleum Chemistry preprints. A65, 1972.
10. Sawatzky, H., George, A.E., Smiley, G., and Montgomery, D.S.,Fuel,55, 16, 1976.
11. Muhl, J., Srica, V., Mimica, B. and Tomaskovic, M., Anal. Chem.,54, 1871, 1982.
12. Glavincevski, B., private communications.
13. Ozubko, R.S., Clugston, D.M., Furimsky, E.,Anal.Chem.,53,183,1981.
14. Lee, S.W. and Hayden,A.C., ASHRAE Transections. 92, Part(2), American Society of Heating, Refrigeration and Air-Conditioning Engineers, Inc. Atlanta, GA, 1986.
15. Brown, J.K., and Ladner, R.W., Fuel,39,87,1960.

TABLE 1. Total aromatic content of fuels as determined by different methods.

Fuel	NMR,wt.%	SFC,wt.%	FIA,vol.%	MS,%
1	41.8	40.3	35.0	28.2
2	29.1	30.7	28.9	23.4
3	30.6	34.6	41.8	19.9
4	37.1	37.1	46.7	16.4
5	43.0	42.9	37.0	25.5
6	38.2	39.1	33.3	25.1
7	33.9	30.4	25.0	19.3
8	48.2	46.8	39.1	31.2
9	57.5	55.2	63.9	29.8
10	42.3	46.4	44.7	37.2
11	87.3	80.8	74.2	68.0
12	25.2	23.8	20.6	28.6
13	29.8	28.4	24.1	16.9
14	45.9	50.2	44.9	29.5
15	48.2	49.5	43.7	31.7
16	48.7	51.7	44.2	35.7
17	61.9	69.6	64.0	46.4
18	74.6	79.0	75.0	64.7
19	30.0	37.6	33.3	21.0
20	29.9	37.6	33.0	21.0
21	29.8	37.7	24.9	20.8
22	30.3	25.4	19.6	17.9

TABLE 2. Carbon aromaticity % as determined by two different laboratories.

Fuel	NMR,% (Lab.1)	NMR,% (Lab.2)
1	28.8	20.0
2	19.1	13.0
3	20.9	14.0
4	24.1	21.0
5	29.8	24.0
6	27.2	21.0
7	21.4	14.0
8	33.5	24.0
9	35.1	28.0
10	27.0	18.0
11	59.9	50.0
12	22.4	12.0
13	15.2	12.0
14	34.6	27.0
15	33.1	25.0
16	33.7	29.0
17	47.2	42.0
18	51.9	51.0
19	14.7	16.0
20	14.6	16.0
21	19.3	16.0
22	19.6	11.0

TABLE 3. Aromatics ring distribution in fuels as determined by different methods.

Fuel	Ring carbon wt.% (NMR)			vs (UV)			Aromatics wt.%(SFC)			Aromatics %(MS)		
	mono-	di-	poly-	mono-	di-	poly-	mono-	di-	poly-	mono-	di-	poly-
1	6.7	18.4		7.8	9.2	1.1	16.9	18.4	4.3	19.9	7.0	1.3
2	7.0	9.6		6.8	4.3	0.3	un	28.8	1.1	14.3	7.5	1.3
3	6.3	11.8		6.5	4.4	1.7	un	33.7	0.5	12.8	5.4	1.4
4	6.8	14.2		4.7	4.3	1.9	un	28.8	8.5	10.3	4.8	1.3
5	7.3	18.7		8.5	10.2	0.9	17.3	21.5	2.8	16.5	8.6	0.4
6	6.2	17.4		6.7	9.7	1.0	14.9	19.8	3.4	17.5	7.6	0.1
7	9.9	8.6		9.1	3.3	0.1	un	28.8	1.0	16.7	2.5	0.1
8	7.1	22.3		9.5	11.9	2.2	19.3	20.5	6.0	18.6	12.6	0.1
9	11.6	19.7		8.9	9.1	3.3	un	47.9	6.0	19.0	9.6	1.2
10	14.3	8.8		13.8	3.6	0.2	un	43.8	1.4	30.0	4.3	2.5
11	7.5	46.7		8.3	38.1	3.1	12.7	58.7	7.9	25.1	40.8	2.1
12	na	na		5.1	2.1	<0.1	un	22.7	na	27.2	0.9	0.5
13	na	na		9.3	2.5	<0.1	un	26.8	0.3	15.6	0.8	0.4
14	na	na		10.4	10.3	1.9	22.1	20.7	6.0	25.2	3.6	0.7
15	na	na		10.1	8.2	2.9	21.3	17.7	9.5	21.0	10.1	0.7
16	na	na		10.0	10.1	2.8	20.1	20.5	9.0	24.8	10.6	0.3
17	10.6	6.7		11.4	17.9	6.0	20.3	28.6	1.5	28.9	17.4	0.2
18	13.0	34.6		11.8	22.3	7.5	21.0	36.3	18.3	39.9	24.6	0.2
19	na	na		10.5	3.8	0.4	un	34.8	2.0	19.0	1.8	0.1
20	na	na		10.5	3.8	0.4	un	34.9	1.7	19.0	1.8	0.1
21	10.6	30.8		8.0	3.5	0.3	un	29.2	1.5	9.2	16.4	4.0
22	9.4	7.4		5.3	2.6	<0.1	un	23.9	un	16.0	1.9	<.1

na is for not available

un is for unsatisfactory separation
value reported under di is for both mono & di

TABLE 4. Fuel aromatic ring types and their correlation to soot production.

Fuel	Aromatics Wt.% by CC			Aromatics Wt.% by MS			Smoke opacity % at cold start combustion
	mono-	di-	poly-	mono-	di-	poly	
C	18.2	16.3	1.3	29.8	11,8	0.60	1.3
D	16.2	7.2	0.2	20.7	11.5	0.83	1.2
E	14.9	7.7	0.7	18.1	6.2	0.57	1.8
F	15.9	13.6	1.9	28.9	11.5	0.99	1.5
G	31.1	31.6	1.0	41.4	38.5	0.09	31.7
L	15.9	13.4	0.3	21.3	13.0	1.03	1.9
M	23.8	23.5	0.6	43.0	19.3	2.51	52.3
N	24.5	6.3	0.4	21.5	8.4	0.31	0.7
O	55.9	22.8	0.8	30.6	43.9	1.10	16.8
P	NA			41.9	30.3	1.87	9.1
Q	13.2	6.9	0.8	41.9	30.3	1.87	1.6
S	17.4	6.6	0.9	31.5	4.2	0.12	NA
V	NA			21.6	1.8	0.27	1.6
W	NA			20.4	4.1	0.69	2.03
X	NA			28.3	15.05	0.58	2.12
Y	NA			23.5	21.65	0.71	10.45

TABLE 4. Fuel aromatic ring types and their correlation to soot production. (continued)

	Aromatics Wt.% by CC			Aromatics Wt.% by MS			Smoke opacity % at
	mono-	di-	poly-	mono-	di-	poly	cold start combustion
Z	NA			16.4	6.6	0.20	2.37
AA	NA			15.7	5.7	0.50	14.8
BB	NA			22.9	13.0	0.00	3.3
CC	NA			33.0	18.0	0.30	5.0
DD	NA			25.0	34.1	0.7	15.4
EE	NA			25.5	18.5	0.0	20.9
FF	NA			18.8	9.7	0.0	2.3

NA is for not available.

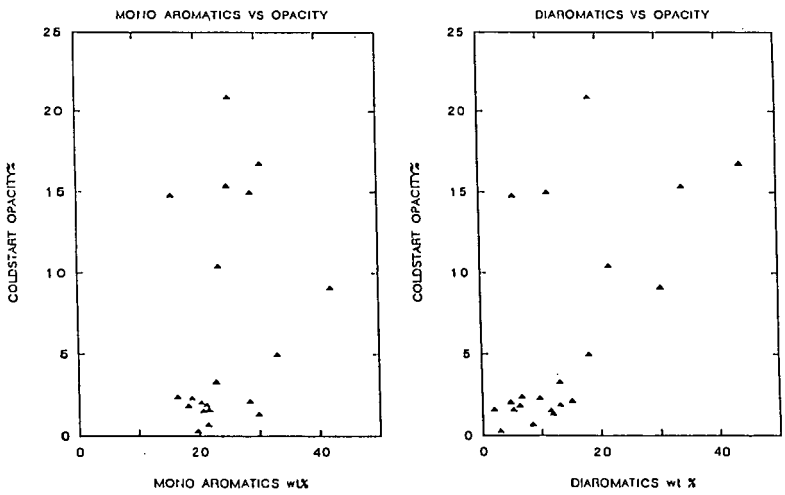

Figure 1. Correlations between fuel monoaromatic and diaromatic components and soot production at cold start combustion.

Radiative Heating of a Conventional and Aromatic Turbine Fuel

George A. Richards

U.S. Department of Energy, Morgantown Energy Technology Center
P.O. Box 880, Morgantown West Virginia, 26507-0880

Introduction

Infrared radiation has long been ignored in the calculation of droplet heating rates for spray flames. Because most hydrocarbon fuels are relatively transparent to infrared radiation, it has been routine to neglect radiative heating as compared to the very effective convective heating present in high-temperature environments. Indeed, in one of the very few detailed investigations of this problem, Berlad and Hibbard (1) found that radiative heating of fuel drops was negligible compared to convection. More recent work has considered the radiative heating of water drops (2). In this case as well, the radiative heating was small when compared to convection.

However, some experimental investigations have suggested that radiation seems to improve combustion efficiency (3) as well as increase flame speeds (4). Because spray combustion is often controlled by evaporation rates, these results suggest that radiation is somehow contributing to the evaporation process. This could be potentially useful for future fuels, which may be more aromatic with lower volatility than conventional hydrocarbon fuels. For example, Myers and Lefebvre (4) found that highly aromatic fuels had flame speeds which roughly cancelled the effects of fuel volatility. They suggest that increased flame radiance via aromatic contributions to soot could heat the fuel spray and diminish the importance of fuel volatility.

While it is certain that earlier conclusions are correct concerning the relative magnitudes of radiative versus convective heating (1,2), previous studies have not considered the situation where an ambient temperature spray approaches a luminous flame. Referring to Figure 1, a room temperature spray flows toward a stationary flame, or conversely, a flame propagates through a room temperature spray. In either case, there is no convective heating of the fuel drops until the drops enter the high-temperature flame front. However, radiation has opportunity to heat the fuel spray well ahead of the flame front. Furthermore, because the drops are bathed in room temperature air, any radiative heating they experience will be rapidly transferred to the surrounding air via convection. One can thus postulate that radiation will heat not just the drops, but the air as well. The magnitude of this effect is unknown. The analysis that follows is a first effort to quantify the radiative effect.

The radiative heating problem can be divided into three subproblems:

- Radiative energy absorbed by individual drops.
- The external radiative field.
- Conservation equations for droplet and air thermal energy.

Each of these subproblems has been treated in detail, but due to space limitations, only the first will be discussed in the current work. Subsequent publications will combine results from all three analyses.

Absorption of Radiation by a Single Drop

The absorption of radiation by small particle is covered in the texts by Van de Hulst (5) and Kerker (6). For the general problem, a laborious calculation from the Mie theory is needed to accurately compute the absorption for a single particle. However, under certain limitations, the spectral absorption cross section is given by an approximate formula:

$$Q_{abs,\lambda} = 1 + 2\exp(-4sn_2)/4sn_2 + 2[\exp(-4sn_2) - 1]/(4sn_2)^2 \qquad (1)$$

where

$s = \pi D/\lambda$; the size parameter of a particle of diameter D subject to radiation at wavelength λ.

n_2 = the imaginary index of refraction at wavelength λ.

The limitations on Equation 1 are that

$$n - 1 \ll 1, \qquad n_2 \ll 1 \qquad (2a,b)$$

where n is the index of refraction. The restriction 2b is easily met for fuels, but the restriction 2a is not precisely met because the index of refraction for most fuels is approximately 1.3. However, for simplicity, Equation 1 will be employed here, as in other investigations. Chan and Grolmes (7) successfully utilized Equation 1 to calculate radiative heating of water drops (n = 1.33) in a nuclear reactor cooling process. Plass (8) has compared the exact Mie solutions to Equation 1 for a range of values of n. From his results, it can be expected that Equation 1 will underestimate the absorption cross section when the restriction 2a is not met precisely. More precise evaluation can be obtained with the program due to Dave (9) or with the elegant ray-tracing procedure of Harpole (10). These complications are excluded in this initial investigation but could be easily adopted in a more comprehensive analysis.

Referring to Figure 2a, it is assumed that the spectral radiant intensity I_λ (W/m^2-str-μm) is uniform in the Θ coordinate but has a specified intensity distribution in ϕ. Note that the radiation direction is defined as positive when leaving the origin, so that the convention to define incident intensity is as shown in Figure 2b. The power absorbed by a drop of diameter D from radiation of wavelength λ is then

$$P_{abs,\lambda} = \frac{\pi}{4} D^2 Q_{abs,\lambda} \int_{4\pi} I_\lambda(\Omega)d\Omega \qquad (3)$$

The integration is over the solid angle Ω. With the assumption that I_λ is independent of Θ and the substitution $\mu = \cos\phi$, Equation 3 reduces to

$$P_{abs,\lambda} = \frac{\pi}{4} D^2 Q_{abs,\lambda} \left[2\pi \int_{-1}^{1} I_\lambda(\mu)d\mu\right] \qquad (4)$$

The term in brackets is the spectral irradiance which will be denoted G_λ:

$$G_\lambda = 2\pi \int_{-1}^{1} I_\lambda(\mu)d\mu \qquad (5)$$

Furthermore, a spectral absorption coefficient is defined for drops of diameter D:

$$C_{abs,\lambda} = \frac{\pi}{4} D^2 Q_{abs,\lambda} \tag{6}$$

Combining Equations 3 through 5,

$$P_{abs,\lambda} = C_{abs,\lambda} G_\lambda \tag{7}$$

Because the drop is heated by the power absorbed across the spectrum, Equation 7 must be integrated over all wavelengths to calculate the total absorbed power:

$$P_{abs} = \int_0^\infty P_{abs,\lambda} d\lambda = \int_0^\infty C_{abs,\lambda} G_\lambda d\lambda \tag{8}$$

The total irradiance G is the integral of G_λ over the spectrum:

$$G = \int_0^\infty G_\lambda d\lambda \tag{9}$$

Then Equation 8 can be written

$$P_{abs} = G \left[\frac{\int_0^\infty C_{abs,\lambda} G_\lambda d\lambda}{\int_0^\infty G_\lambda d\lambda} \right] \tag{10}$$

The expression in brackets will be denoted the total absorption coefficient for drops of diameter D:

$$C_{abs} = \frac{\int_0^\infty C_{abs,\lambda} G_\lambda d\lambda}{\int_0^\infty G_\lambda d\lambda} \tag{11}$$

This reduces the expression for absorbed power to

$$P_{abs} = C_{abs} G \tag{12}$$

If the spectral nature of the incident intensity is given, then the value of C_{abs} can be computed from Equation 11. For a sooting, luminous flame, the spectral output along some direction μ will be approximated as proportional to a blackbody at the flame temperature T_f. That is,

$$I_\lambda(\mu) = k(\mu) I_{\lambda b}(T_f) \tag{13}$$

Here, $k(\mu)$ is an emissivity assumed independent of wavelength but may vary with μ. Because the intensity $I_{\lambda b}$ represents blackbody emission, $k(\mu)$ is obviously restrained to values between zero and one.

Substituting Equation 13 into 11, along with the definition of G_λ from Equation 5, the total absorption coefficient is

$$C_{abs} = \frac{\int_0^\infty C_{abs,\lambda}(2\pi \int_{-1}^{1} k(\mu) I_{\lambda b}(T_f) d\mu) d\lambda}{\int_0^\infty (2\pi \int_{-1}^{1} k(\mu) I_{\lambda b}(T_f) d\mu) d\lambda} \tag{14}$$

Noting that $I_{\lambda b}(T_f)$ does not depend on μ, this reduces to

$$C_{abs} = \frac{\int_0^\infty C_{abs,\lambda} I_{\lambda b}(T_f) d\lambda}{\int_0^\infty I_{\lambda b}(T_f) d\lambda} \tag{15}$$

From Equation 12, the power absorbed by a single drop thus depends upon evaluating the droplet absorption coefficient through Equation 15 and the external irradiance G. Evaluation of Equation 14 can be completed as long as the imaginary index of refraction n_2 is known (versus wavelength) for the drop medium. (Recall that $C_{abs,\lambda}$ depends upon $Q_{abs,\lambda}$, Equation 6, which in turn depends upon $n_2(\lambda)$ through Equation 1.) The value of n_2 may be obtained from transmission measurements of spectral intensity incident on a liquid sample of thickness t:

$$\frac{I_{\lambda t}}{I_{\lambda i}} = \exp(-K_\lambda t) \tag{16}$$

where $I_{\lambda t}$ and $I_{\lambda i}$ denote the transmitted and incident intensity at wavelength λ. The absorption constant K_λ is related to the imaginary index through the following relationship (8):

$$n_2(\lambda) = K_\lambda \frac{\lambda}{4\pi} \tag{17}$$

Transmission measurements as in Equation 16 abound in reference manuals for spectroscopic identification (12). However, such measurements are seldom used for quantitative absorption calculations because of variations in sample thickness, spectrometer response, etc. Despite these limitations, and because no explicit data on n_2 was otherwise found, spectra from several published sources will be used to calculate n_2. Published absorption spectra were corrected for window absorption by evaluating the transmission through the sample at a wavelength where the fuel was transparent. Integration is performed between 2.5 and 5.0 microns because hydrocarbons have no significant absorption bands below 2.5 microns (1) and most of the flame radiation is characterized by wavelengths shorter than 5 microns (13).

Figures 3 through 5 show the resulting calculation of C_{abs} as a function of drop size, at flame temperatures 1,200, 1,600 and 2,000°K. Each plot provides data on the fuels toluene (highly aromatic) and JP-4. The absorption spectra of these fuels were obtained from the reference indicated on the figures, and it is interesting to note that the results for toluene were calculated with spectral data obtained in 1956 (1) and also with more recent data (1985) from reference (9). Despite different test procedures, path lengths, etc., the results are essentially the same, providing confidence that the measured spectra are sufficiently accurate for the present calculations. Further inspection of the plots reveal that the fuel type has only a modest effect on C_{abs}. The modest differences between toluene and JP-4 are of minor importance compared to the order of magnitude variations observed with changes in the drop size. For practical purposes, these results indicate that the difference in radiative adsorption properties for conventional fuels (JP-4) and aromatic fuels (toluene), is surprisingly small. As was stated at the outset, the absorption coefficient can be used to evaluate the importance of radiative heating for the propagating flame where convective heating is absent until the drops enter the flame. Because of space limitations, these calculations will be included in a subsequent publication. However, the current results can be used to verify the established notión that droplet heating is dominated by convection in backmixed flames, i.e., practical burners. If the drops exist in an environment with air temperature $T_\infty = T_f$ and black walls radiating at temperature T_f, then the ratio of convective to radiative heating is

$$\frac{\text{Radiative Heating}}{\text{Convective Heating}} = \frac{C_{abs}\ G}{h\pi D^2(T_f - T_s)}$$

Here, h is the convection coefficient for a sphere in a quiescent environment and may be obtained from the standard Nusselt correlation (13), Nu = 2. Considering conditions which should exaggerate the above ratio (T_f = 2,000°K, D = 100 microns), the above ratio was found to be less than 0.02. The conclusion is that radiation can be ignored when droplet heating occurs by convection and radiation.

Summary

A simple procedure has been described to calculate a droplet absorption coefficient for infrared radiation. The coefficient can be calculated with reasonable accuracy from spectral absorption data on fuel samples. The coefficient was calculated for the fuels JP-4 and toluene. Results were relatively insensitive to fuel type but very dependent on the drop size. As expected, the results demonstrate that convection is more important than radiation in heating the drop. However, the present calculations are necessary to evaluate the radiative heating in situations where no convection operates, i.e., the propagating flame. This situation will be described in a subsequent paper.

References

1. Berlad, A. L., and R. R. Hibbard, "Effect of Radiant Energy and Vaporization and Combustion of Liquid Fuels," NACA Research Memorandum, RM E 52 I 09 (1952).

2. Harpole, G. M., "Radiative Absorption by Evaporating Droplets," Int. J. Heat Mass Transfer, Vol. 23, pp. 17-26 (1980).

3. Nakayama, M., and T. Suzuki, "Studies on Luminous and Nonluminous Flames With Spray Combustion," Bulletin of the Japanese Society of Mechanical Engineers, Vol. 26, No. 216, June 1983.

4. Myers, G. D., and A. H. Lefebvre, "Flame Propagation in Heterogeneous Mixtures of Fuel Drops and Air," Combustion and Flame, Vol. 66, No. 2, pp. 193-210 (1986).

5. Van de Hulst, H. L., "Light Scattering by Small Particles," John Wiley and Sons (1957).

6. Kerker, M., "The Scattering of Light," Academic Press, New York (1969).

7. Chan, S. H., and M. A. Grolmes, "Hydrodynamically Controlled Rewetting," Nuclear Engineering and Design, Vol. 34, pp. 307-316 (1975).

8. Plass, G. N., "Mie Scattering and Absorption Cross Sections for Absorbing Particles," Applied Optics, Vol. 5, No. 2, pp. 279-285 (1966).

9. Dave, J. V., "Scattering of Electromagnetic Radiation by Large, Absorbing Spheres," IBM J. Res., p. 302 (1969).

10. Harpole, G. M., "Radiative Absorption by Evaporating Drops," Int. J. Heat Mass Transfer, Vol. 23, pp. 17-26 (1980).

11. Garbuny, M., "Optical Physics," Academic Press (1965).

12. Coates, J. P., and L. C. Setti, "Oils, Lubricants, and Petroleum Products: Characterization by Infrared Spectra," Marcel Decker, Inc. (1985).

13. Incropera, F., and D. Dewitt, Fundamentals of Heat Transfer, John Wiley (1981).

1A:5-24-88:tk:5a

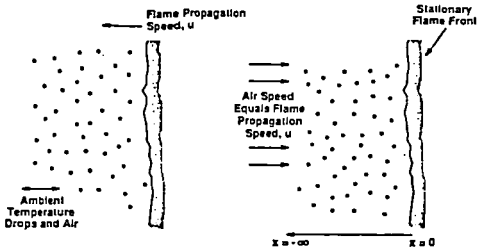

Figure 1

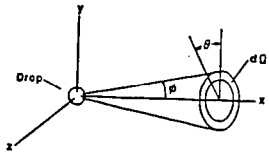

Figure 2a

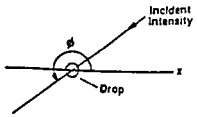

Figure 2b

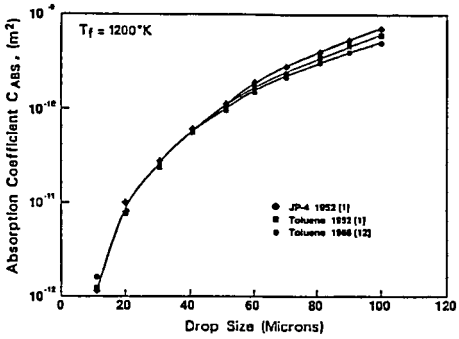

Figure 3

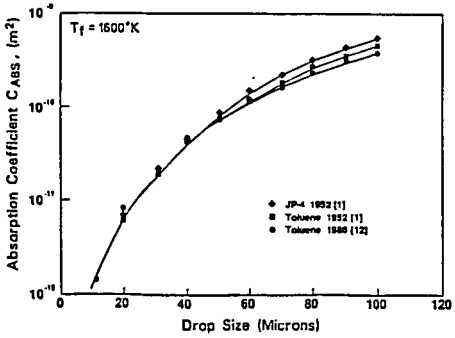

Figure 4

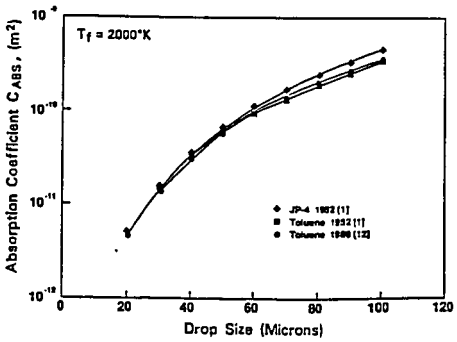

Figure 5

The Effect of Moisture on the Diffusion of Organic Molecules in Coal

Yoshinobu Otake and Eric M. Suuberg
Division of Engineering
Brown University
Providence, R.I. 02912

INTRODUCTION

Diffusional limitations are of importance in a large number of coal utilization processes. Common examples may be seen in many different kinds of processes; in donor solvent liquefaction, the coal must be broken down finely enough so that donor solvent transport into the coal does not become a limiting step (this is generally true at the usual process conditions); in coal devolatilization, during a pyrolysis or combustion process, the rate of escape of tars from coal particles is often limited by diffusional mass transfer in the particles; in natural weathering of coal, diffusional processes limit the rate of oxidation. The potential list of examples is much longer, and it may be quickly concluded that from a technological point of view, knowledge of diffusion rates in coals is generally quite useful. Relatively little such information exists in the literature because the historical method of handling questions of diffusional limitations has involved the empirical approach of grinding particles progressively finer, until no effects of further comminution were seen in the chemistry of interest. As the understanding of the chemical mechanisms involved in coal processing has improved, it now makes sense to improve on the understanding of the transport phenomena as well, and to move away from the empirical approaches to handling questions concerning mass transfer.

The present paper is concerned with diffusional transport occurring in both 1. micropores, and 2.the bulk solid. The distinction between processes in these two nominally distinct places in the coal is unimportant, because the distinction between "micropores" and "gaps between molecules" in a bulk solid is not always clear. The well-known problem of measuring surface areas of coals with N_2 and CO_2 is an example. There are certain portions of the coal porosity that are inaccessible to N_2 that are quite accessible to CO_2, despite the fact that the latter is a larger molecule than the former. This is because diffusion on the micropore level is activated, meaning that thermal motion of the coal structure is required in order for the gas molecules to be able to penetrate the gaps between the molecules. N_2 is apparently less able to penetrate the structure than CO_2 because the experiments with N_2 must normally be performed at very low temperatures (i.e. liquid nitrogen temperatures), and the magnitude of the vibrations in the coal structure are not large enough at this temperature to open up sufficiently large gaps for large amounts of N_2 to penetrate.The magnitude of motions required for penetration by molecules depends upon the size of the penetrant species, and the nature of interactions between the coal and the species. Thus what may appear to be impenetrable bulk solid to one molecule may appear to be porosity to another.

It is the process of activated diffusion in coals that is of principal interest in this paper. There have been a limited number of other earlier studies of activated diffusion processes in coals, particularly concerning the diffusion of small gas molecules (e.g. CH_4,CO_2, light hydrocarbons, noble gases), through bulk coals. This study is, however, mainly concerned with the activated diffusion of larger organic species in coals. In the present case, common "swelling solvents" such as water, pyridine, tetrahydrofuran (THF) are of interest. These are termed swelling solvents because when a dried coal sample is immersed in them, it will physically swell as the solvents are imbibed. The theory of solvent swelling in coals has been well described elsewhere[1], and is based on the classic technique as developed for characterization of crosslinked polymers[2]. The simplest relationship that embodies the essence of the technique is the Flory-Rehner equation, a relationship between the molecular weight between crosslinks in a polymer (M) and the extent to which the polymer is volumetrically swollen by a particular solvent (Q):

$$M = \left[\frac{\rho_c M_s}{\rho_s}\right]\left[\frac{(1/2Q) - (1/Q)^{1/3}}{\ln[1-(1/Q)] + (1/Q) + \chi(1/Q)^2}\right]$$

where ρ_c is the density of the original coal, ρ_s is the density of the solvent, M_s is the molecular weight of the solvent and χ is the solvent-network interaction parameter. The measurement of χ is difficult, as is its estimation for specifically interacting solvents such as pyridine. Values range between 0.3 and 0.6 for typical pairs of solvents and coals. It has been suggested that the Flory-Rehner equation does not hold particularly well for coals, which are highly crosslinked rigid networks[3,4] Its use here is only illustrative, and more sophisticated approaches have been developed[3-6]; unfortunately these new models require more information about the structure of the coal- namely, the molecular weight of repeat units within the coal structure. Since such information is not readily available at present, this will tend to restrict somewhat the use of these more realistic models.

The nature of the combined diffusion and solvent swelling process has also received attention in the literature in recent years[7-9]. This process, observed in "good" solvents-- those that swell the coal structure significantly -- is often non-Fickian in nature. Instead, it is often controlled by what is termed as relaxation of the coal macromolecules, and the process is characterized as exhibiting "Case-II" diffusional behavior. This behavior is well known in polymer systems that are below their glass transition temperatures. It is normally identified by noting that the rate of solvent uptake, or alternatively polymer swelling, is proportional to time, rather than square root of time as in Fickian processes.

What has received relatively little attention thus far in the literature on this topic is the activation energy for the combined diffusion and swelling process. This activation energy will depend upon the nature of the relaxation process that occurs in the glassy coal structure.Below its decomposition temperature, an unswollen coal is below its glass transition temperature[1], but solvent imbibation lowers the glass transition temperature significantly[10]. For the temperatures of interest in this study, the coal will always initially be in the glassy regime.

It is likely that the diffusion rate of a swelling solvent in a glassy material (coal) will be significantly altered by the presence of another swelling solvent. The swelling of coals in mixed solvents has been previously studied in binary mixtures,and co-operative effects noted [11]. But a special case of this effect might involve diffusion in coals that are undried or incompletely dried. In such a case, the water present in the coal may influence the diffusion process, by virtue of being a swelling solvent itself. The swelling and shrinkage behavior of lignites with respect to moisture gain and loss has been reported on in some detail[12,13], and other recent results suggest that even bituminous coals behave similarly, as colloidal materials, with respect to water as a solvent[14]. In the present study, the effect of moisture content on the diffusion behavior of solvents, in various ranks of coal, is considered.

EXPERIMENTAL

The analyses of the coals examined in this study are provided in Table 1. Except where otherwise noted, the coals were ground and sieved to the size range 53-88μm. Special care was given to the lignites to avoid any more drying than necessary while processing. The first four samples in Table 1 were judged to have dried to only a limited extent since mining, and all were crushed in-house from large lumps. To prevent drying, these four samples were stored at 100% relative humidity conditions, at room temperature, by suspending the samples above a large reservoir of clean water, in a sealed container. It is of course difficult in practice to maintain truly 100% relative humidity conditions in such a manner, particularly if the chamber must be occasionally opened for sample removal. There was consequently a small difference in measured moisture contents between bed-moist samples (which are effectively immersed storage samples) and those used in this study. The difficulty in characterizing the initial moisture contents of immersed samples was what prompted us to use this slightly different storage method. Related sample storage and characterization information concerning these lignites can be found elsewhere[13].

The principal experimental technique employed throughout this study was solvent swelling. The technique involves immersion of prepared,sized, coal samples in pure solvents. The measurements were performed in tubes of only a few millimeters inner diameter, and less than 5 cm in length.This technique permitted such measurements to be made with modest quantities of sample. The sample and solvent is frequently stirred during the first phases of the swelling process to prevent plugging in the bottom of the tubes. The tubes are immediately immersed in thermostatted water baths, after mixing coal and solvent. The small diameter of the tubes and the frequent stirring of their contents assure isothermality in the tubes, a necessary prerequisite for obtaining good rate data.

Rate data for swelling are obtained from measurements of the height of the column of coal as a function of time. Since the tubes are of uniform cross-section, the height change of the column of coal is proportional to the volume change in the sample. It is necessary to centrifuge the column of coal in order to obtain reliable measurements. The initial height is obtained by centrifuging the dry sample. Subsequent readings are obtained by first quenching the sample in an ice bath (if necessary because of rapid swelling kinetics) and then centrifuging the partially swollen coal sample for about ten minutes before taking readings. For this purpose, a high speed centrifuge with internal cooling has proven useful.

Thus the raw data of this study are swelling ratios as a function of time, temperature, solvent and coal. Standard Arrhenius plots of log of the swelling rate vs. inverse temperature provide the activation energies for the diffusion/swelling processes.

RESULTS AND DISCUSSION

It has recently been reported that a wide range of coal ranks seem to obey a common relationship between moisture loss and volumetric shrinkage[14]. A correlation was developed for the set of coals shown in Table 1:

$$\% \text{ Volumetric Shrinkage} = 0.94 \text{ (Moisture Loss, wt \%)} - 0.6$$

It was noted that even high volatile bituminous coals, with only a percent or two moisture content, follow this correlation. It is interesting to note that the bituminous coals that show such weakly swelling gel behavior with water as a solvent may typically swell to double their original volume in pyridine. The lignites swell to about 30% extent in water, and also can roughly double their volume in pyridine. The reason for this difference in behaviors is not fully understood. It is obvious that lignites possess much higher amounts of surface oxygen functional groups than do bituminous coals. This would suggest that the value of χ in the Flory-Rehner equation is higher for lignite-water interactions than for bituminous coal-water interactions.But the differences in water swelling behavior may only be partly based on differences in χ values. Another possible explanation is that the apparent molecuar weight (M) between crosslinks in bituminous coals is lower than in lignites, because water is unable to disrupt some kind of non-covalent crosslinking interactions that pyridine is able to disrupt (e.g. interactions between neighboring aromatic clusters). Which of these effects is predominant is, at present, not clear, and indeed both may play some role.

The effect that moisture content in coals may have on diffusion rates of other solvents in the coals is illustrated in Figures 1 and 2, in which the rate of swelling in pyridine is compared for both "wet" and "dry" coal samples. The data in Figure 1 show the 25°C pyridine swelling behavior of the dry and partially moist Texas lignite samples (particle size 212-300μm). The top panel shows the actual raw data, and the lower panel shows the same data, with a correction applied to the data for the moist lignite. The moist lignite has already been partially swollen by water, and in order to compare the data for the moist lignite with those for the dried lignite, it is necessary to express them on a common dry lignite basis. This has been accomplished in the bottom part of Fig. 1 by multiplying the actual swelling ratio (relative to the moist lignite volume) by the swelling ratio observed in going from a dry state to a 9% moisture condition. It is apparent that after such a correction, the final equilibrium swelling ratios in pyridine are identical for the two samples.

The rate of swelling in the case of the wet lignite is, however, considerably higher than the rate of swelling

of the dried lignite. Similar behavior has been noted in the swelling behavior of dried and wet lignites in THF; the swelling of a wet sample is faster than that of a dried sample.

Figure 2 shows that the same conclusion may be drawn in the case of the Powhatan #5 bituminous coal. The particle size range (212-300μm) and temperature (25°C) were identical to those employed in the case of the lignite tests. The presence of moisture accelerates the rate of swelling of the coal by other solvents. Note, however, from the very different timescales in Figs. 1 and 2 that the diffusion and swelling processes in the two coals must be quite different. The swelling rate in the case of the bituminous coal is much higher than that in the lignite. This is consistent with earlier results on the diffusion of pyridine in dried bituminous coals and lignites, in which the activation energy for diffusion/swelling in several bituminous coals was about 13 kcal/mol, and in another lignite it was 18 kcal/mol[14]. Thus it seems in some sense easier for the pyridine to diffuse in and swell the bituminous coal than the lignite. The reasons for this are not yet understood. The effect does not, however, appear related to the presence or absence of moisture in the coals, since the timescale difference exists for both wet and dried samples. In fact, the difference in the rates of the diffusion and swelling processes appears to be a characteristic of the structure of the coals, since, the timescale for THF swelling of the Texas lignite is comparable to that for pyridine swelling of the lignite.Thus, one may conclude that the swelling processes are inherently slower in lignites than in bituminous coals, but that they are affected in the same way by moisture in both cases.

There may be concem that the apparent effect of moisture content on diffusion rates is an artifact, due to some kind of irreversible collapse of the structure upon drying. This was proven to not be the case in an experiment in which samples of the Beulah lignite were dried at vacuum for 3 hours, at 100°C, and then allowed to regain varying amounts of moisture, by exposure to different relative humidity environments. The samples were then subjected to pyridine swelling at 35°C. The effect of moisture content was as noted previously in the case of the Texas lignite. Figure 3 presents a summary of results. The curves show the times required for the samples to reach 30 and 50% of their final extents of swelling (relative to the particular intial volumes of each sample). The conclusion is that the more swollen the coal is to start with, the less time is required to reach any additional extent of swelling.

Indicated for each data point in Figure 3 are the activation energies for pyridine swelling,calculated for each sample at a constant extent of swelling, i.e. either 30% or 50%. These were determined for the range of temperatures 25°C to 58°C. It is interesting to note that while additional moisture appears to accelerate the rate of swelling in pyridine, the presence of moisture also seems to increase the activation energy for additional swelling.

It has been noted in the polymer literature that the higher the glass transition temperature a polymer exhibits, the lower the activation for ordinary diffusion of light gas molecules in that polymer[15]. While the combined swelling and diffusion process in coals is considerably more complex than the diffusion of light gases in polymers, the trends may indeed be related. In Figure 3 it is observed that the activation energy for swelling and diffusion is highest in the highest water content samples. It is well known that the addition of a swelling solvent to a glassy structure will lower its glass transition temperature, and thus the moister the coal, the lower its glass transition temperature. The data are thus in qualitative agreement with trends observed in the polymer literature.

To explore more fully the question of effect of crosslinking and reduced mobility of the coal structure on the rate of diffusion of pyridine in coals, a separate set of experiments was performed at various sets of heat treatment conditions. It has been shown previously that heat treatment of lignites at temperatures in the range 100°C to 300°C results in significant irreversible changes in the structure of the materials, both in terms of collapse of porosity and crosslinking of the structure[13,14]. Based on the trends reported above, one would expect that increasing the severity of heat treatment would lead to increasing crosslinking of the structure, and thus to decreasing activation energy for the swelling and diffusion process. (This is because increased crosslinking in highly crosslinked materials will lead to further increases in the glass transition temperature).The results in Table 2 confirm this hypothesis, and thus lend support to the view that the role of

water in raising the activation energy for the diffusion process is merely in decreasing the glassy character of the coal.

The above observations of decreased activation energy for diffusion and swelling of the coals or polymers, with increased rigidity of the structure (due to crosslinking) might be initially counterintuitive. But it should be noted that the more highly crosslinked and rigid the network structure, the more the activation energy is concentrated in a smaller number of degrees of freedom, in the area in which the activated process is occurring[16]. Thus an increase in activation energy with increased extent of preswelling is likely to be reflecting the fact that there is progressively more mobility in the coal macromolecule, the more it is swollen. Hand-in-hand with increased mobility is the requirement for greater thermal energy to access progressively less probable configurations, which will allow for further swelling. To keep this physical picture in perspective, it should be recalled that the individual "chains" in the coal macromolecule are probably behaving mainly as "entropy springs"- the free energy change associated with swelling, or stretching the chains in the coal macromolecule is positive, due to entropic losses. The negative free energy change that balances this positive free energy change, in the Flory-Rehner analysis, arises from the decrease in chemical potential of the solvent, as it interacts with the structure. The activation energy of the process reflects the need to assume the progressively less probable chain configurations, via thermal motions of the chain segments, as the structure swells.

CONCLUSIONS

The results of the present study confirm the importance of establishing and reporting carefully the moisture content of any coal that is the subject of diffusion rate and/or swelling rate measurements. Likewise, it is important to report carefully how a sample may have been dried, prior to these measurements, since such low temperature procedures also may influence the results.
It may be concluded from the present work that moisture will swell coals of bituminous, subbituminous, and lignite ranks. This swelling will permit faster penetration and swelling of the coal structure by organic liquid diffusants. The activation energies observed for such swelling processes are reduced, as the effective glass transition temperature of the coals are increased, either by drying or pyrolysis.

ACKNOWLEDGEMENT
The support of the USDOE through grants DE-FG22-85PC80527 and DE-AC18-84FC10617, and the Exxon Education Foundation, is gratefully acknowledged.

REFERENCES
1. Green,T., Kovac,J., Brenner,D., and Larsen, J.W., in Coal Structure, R.Meyers, Ed., Chapter 6, Academic Press, 1982.
2. Flory,P.J. and Rehner,J. J.Chem.Phys.,11 ,521 (1943).
3. Larsen,J.W. and Kovac, J., ACS Symp. Ser. No. 71, 36 (1978).
4. Lucht, L.M. and Peppas, N.A. ACS Symp. Ser. No. 169, 43 (1981).
5. Kovac,J., Macromolecules,11,362 (1978).
6. Peppas,N., Lucht, L., Hill-Lievense,M., Hooker,A., DOE Final Tech. Report DE-FG22-80PC3022, US Dept. of Energy, 1983.
7. Ritger,P.L. and Peppas,N.A.,Fuel,66,815 and 1379 (1987) and references therein.
8. Hsieh,S.T. and Duda,J.L., Fuel,66,170 (1987).
9. Brenner,D. and Hagan,P.S., ACS Div.Fuel Chem Prepr.,30(1),71 and 83 (1985).
10. Lucht,L.M., Larson,J.M.,and Peppas,N.A., Energy &Fuels,1,56 (1987).
11. Green,T.K. and Larsen,J.W., Fuel,63,1538 (1984).
12. Evans,D.G., Fuel,52, 186 (1973).
13. Deevi, S. and Suuberg, E.M., Fuel,66,454 (1987).
14. Suuberg,E.M., Otake,Y. and Deevi,S., ACS Div. Fuel Chem. Prepr.,33(1), 387 (1988).
15. Van Krevelen,D.W., Properties of Polymers (2nd Edition), Chapter 18, Elsevier,1976.
16. Rogers,C.E., in Polymer Permeability, J.Comyn,Ed., Chapter 1, Elsevier, 1985.

Table 1-Coals Studied

sSAMPLE	C	H	N	S	ASH	O	Moisture
Beulah lignite[a]	65.6	3.6	1.1	0.8	11.0	17.9	26.0
Freedom lignite[a]	63.5	3.8	0.9	1.4	6.1	24.3	27.9
Glenn Harold lignite[a]	61.1	4.4	0.8	0.4	7.4	25.9	28.9
Gascoyne lignite[a]	60.9	4.2	0.6	1.4	8.2	24.7	30.7
Beulah lignite[b]	65.9	4.4	1.0	0.8	9.7	18.2	32.2
Texas lignite (PSOC1036)[c]	61.5	4.7	1.4	1.3	12.5	18.5	31.8
Belle Ayr Subbit.	69.3	4.4	1.0	0.5	10.3	14.5	30.3
Big Brown Subb.(PSOC785)[c]	62.8	4.6	1.1	1.1	12.6	17.8	27.8
Montana Subbit.(PSOC837)[c]	57.8	4.3	0.8	0.7	11.9	24.6	17.0
Pittsburgh No.8 (HVBit.)[b]	74.2	4.1	1.4	2.3	13.2	4.8	1.7
Bruceton HVBit.[d]	80.4	5.3	1.6	1.0	4.6	6.7	1.7
Powhatan HVBit.	72.3	5.1	1.5	3.6	9.7	7.8	1.1

•All results on a dry weight percent basis, except moisture which is ASTM value on an as-received, bed moist basis.
•Oxygen by difference.
a- Grand Forks Energy Research Center lignite sample bank.
b- Argonne National Laboratory Premium Coal Samples.
c- Pennsylvania State University Coal Sample Bank.
d- U.S. Bureau of Mines Standard Sample.

Table 2- Effect of Drying Temperature on the Activation Energy for Pyridine Diffusion/SwellingProcesses in Beulah Lignite

Drying Temperature (°C)	Q(equilibrium)	Activation Energy (kcal/mol)
100	1.86	17.7
200	1.78	16.5
320	1.70	13.9

•All samples were predried in vacuum for 3 hours,and then subsequently dried at the indicated temperatures for 1 hour additional, under nitrogen.

•All swelling ratios determined in pyridine, at 35°C.

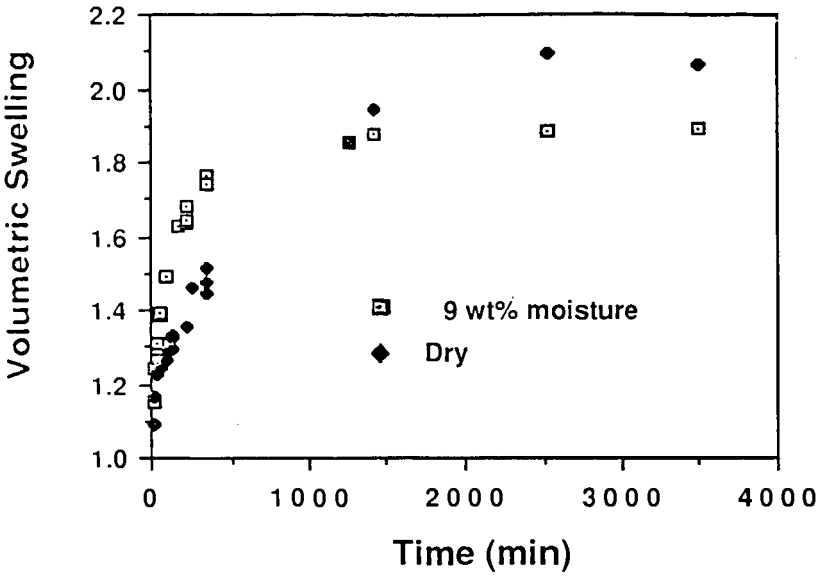

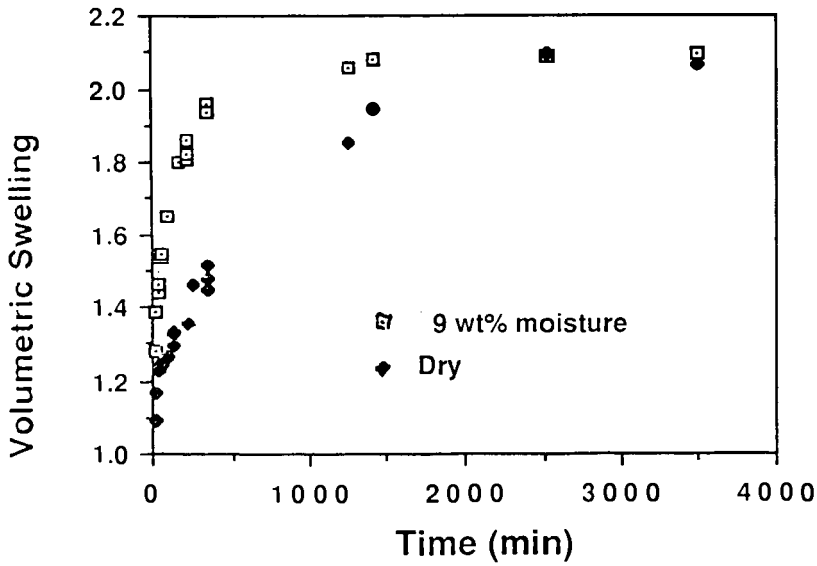

Figure 1. Volumetric swelling ratios (Q) in pyridine, at 25°C, of Texas lignite of 212 - 300 μm particle size. Top panel--raw data; lower panel - raw data for moist lignite corrected for water swelling (see text).

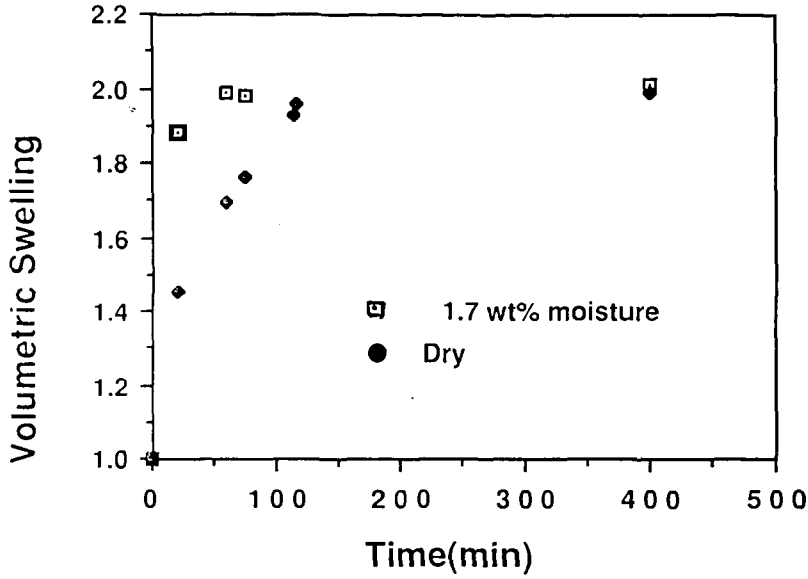

Figure 2. Volumetric swelling ratios (Q) in pyridine, at 25°C, of Powhatan No. 5 high volatile bituminous coal.

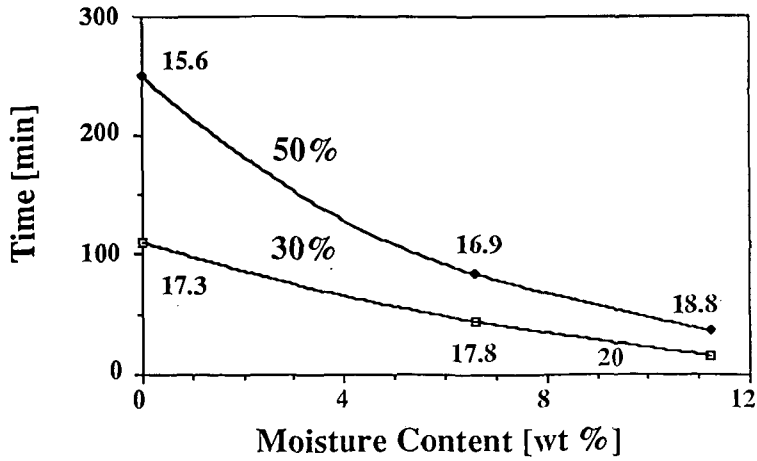

Figure 3. Swelling behavior of Beulah lignite in pyridine at 35°C. The ordinate shows the time required to achieve 30% or 50% of final extent of swelling, as a function of the initial moisture content of the samples. The values next to data points are activation energies for swelling (Kcal/mol).

IDENTIFICATION OF LABILE-HYDROGEN FUNCTIONALITIES
IN COAL-DERIVED LIQUIDS BY ^{31}P NMR SPECTROSCOPY

C. Lensink and J. G. Verkade
Fossil Energy Program, Ames Laboratory
and
Department of Chemistry, Iowa State University
Ames, IA 50011

INTRODUCTION

In recent publications from our laboratories[1-3], the application of ^{31}P Fourier transform nmr spectroscopy to the analysis of -OH, -NH and -SH functionalities in coal extracts and pyrolysis condensates has been described. We initiated these studies with a series of reagents **1**a-e which contain two oxygen atoms in the five-membered phospholane ring system, and varying degrees of ring substitution.

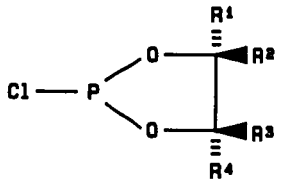

	R^1	R^2	R^3	R^4
1a	H	H	H	H
1b	Me	Me	Me	Me
1c	H	H	H	Me
1d	H	Me	Me	H
1e	Et	Et	Et	Et

These reagents react under mild conditions with the above labile-hydrogen functionalities, R_xEH to give R_xEP linkages in which the phospholane ring remains intact. The HCl liberated is neutralized by triethyl amine in the reaction mixture. In the series **1**a-e, reagents **1**a and **1**b emerged as optimum in terms of minimum overlap of the ranges for each functional group and for maximum resolution within each range of the chemical shifts due to the various R groups attached to the functional group heteroatom E (Figure 1).

To determine the role of the heteroatoms within the ring system of the reagent and the size of the ring system, we are extending our investigations to include reagents such as **2** – **4**. Here we describe our preliminary results with a series of model compounds derivatized with these reagents, and also with a coal low-temperature pyrolysis condensate which was allowed to react with **3**.

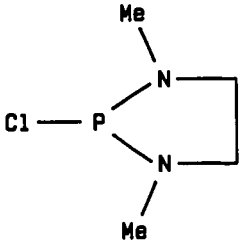

2

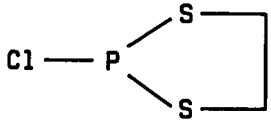

3

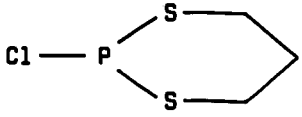

4

EXPERIMENTAL

Reagents **2**,[4] **3**[5] and **4**[6] were prepared according to published syntheses. Chemical shift data for derivatized model compounds were obtained by using a procedure described previously.[2,3] For **2** and **3**, chemical shift data for the individual model compounds were recorded. For reagent **4** only chemical shift ranges for model compounds were recorded by derivatizing mixtures of phenols, alcohols, acids or amines. The compositions of the mixtures are given in Table I.

A low-temperature pyrolysis condensate of a Illinois No. 6 coal sample was obtained as described previously.[2,3]

RESULTS AND DISCUSSION

The chemical shift data for selected model compounds derivatized with **2** – **4** are given in Table II. The regions associated with the ^{31}P nmr resonances for the model phenols, aliphatic alcohols, carboxylic acids, amines and thiols derivatized with **2** – **4** are shown in Figure 1.

Derivatization of phenols with **2** – **4** gives the corresponding phospholanes (**2**, **3**) or phosphoranes (**4**) instantaneously. The observed chemical shift range of 15.2 ppm for phenols derivatized with **3** constitutes a significant improvement over the chemical shift range of approximately 6 ppm reported earlier for dioxaphospholanes **1a** – **3**.[3] Alcohols derivatized with **3** display chemical shifts in the region 143.4 – 151.8 ppm with most of the signals appearing in the 143.4 – 147.2 ppm range. This range is well separated from the chemical shift range observed for derivatized phenols.

An interesting observation can be made from inspection of the data of derivatized pinacol. Derivatization with **3** gives signals at 108.77 and 214.75 ppm. These signals are outside the range of the other derivatized alcohols. The signal at 108.77 ppm is in the range of thiols derivatized with **3** and the peak at 214.75 ppm is in the range of thiols derivatized with **1a** – **e**[3]. These results are consistent with the suggestion that with 1,2-diols, transesterfication occurs to give **5**.

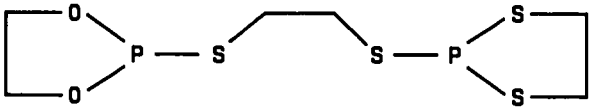

5

Carboxylic acids react rapidly with reagents **2** – **4**. The chemical shift range for carboxylic acids derivatized with **4** could be obtained for a mixture of acids but within a few minutes signals in the range 61.7 – 1.7 ppm started to appear. It is presently not clear what further reactions may be leading to these signals. The chemical shift range observed for carboxylic acids derivatized with **3** overlaps with the region observed for derivatized phenols (Figure 1).

Amines derivatized with dioxaphospholanes of type **1** (e.g., **1a** and **1b** in Figure 1) generally give signals in the ^{31}P nmr spectrum in regions that overlap with signals observed for derivatized -OH functionalities. Amines derivatized with **3**, however, give signals well outside the region for -OH functional groups.

Thiols derivatized with **3** display chemical shifts upfield from derivatized -OH functional groups and downfield from derivatized amines. There also appears to be a separation between aromatic and aliphatic thiols similar to the separation between alcohols and phenols.

Preliminary results with coal-derived liquids derivatized with **3** appear promising. Thus, with an Illinois No. 6 low-temperature pyrolysis condensate (Figure 2) peaks in the 152 - 163 ppm region appear well resolved for identification of specific phenols.

CONCLUSIONS

Of the three new reagents, reagent **2** does not give an improvement over reagents of type **1**. Reagent **2** gives broader ^{31}P peaks, probably owing to the presence of quadrupolar nitrogen nuclei near the nmr-active phosphorus nucleus.

The resolution obtained with reagent **3** is substantially better than any of the reagents investigated so far, paving the way for identification of functional groups and their organic substituents in coal-derived liquids.

Increasing the ring size of the derivatizing reagent from **3** to **4** does not improve the chemical shift ranges observed nor does it lead to less overlap of the functional group chemical shift ranges.

ACKNOWLEDGEMENTS

Ames Laboratory is operated for the U. S. Department of Energy by Iowa State University under Contract No. W-7405-ENG-82. This work was supported in part by the Assistant Secretary for Fossil Energy through the Pittsburgh Energy Technology Center.

REFERENCES

1. Schiff, D. E., Verkade, J. G., Metzler, R. M., Squires, T. G., and Venier, C. G., Applied Spectrosc., 40, 348 (1986).
2. Wroblewski, A. E., Markuszewski, R., and Verkade, J. G., Prep. Pap. Am. Chem. Soc. Div. Fuel Chem., 32, 202 (1987).
3. Wroblewski, A. E., Lensink, C., Markuszewski, R., and Verkade, J. G., Energy and Fuels, submitted for publication.
4. Ramirez, R., Patwardhan, A. V., Kugler, H. J., and Smith, C. P., J. Am. Chem. Soc., 89, 6276 (1967).
5. Denney, D. B., Denney, D. Z., and Liu, L. T., Phosphorus and Sulfur, 22, 71 (1985).
6. Nifantiev, E. E., Sorokina, S. F., Borisenko, A. A., Zavalishina, A. I., and Voiobjeva, L. A., Tetrahedron, 37, 3183 (1981).

Table I. Model Compound Mixtures Used With Reagent 4.

Functional Group Class	Model Compounds in the Mixture
Phenols	m-cresol, p-cresol, 2,3-xylenol, 2,4-xylenol, 2,5-xylenol, 2,3,5-xylenol, p-methoxyphenol, 2,4,6-xylenol, 3,4,5-xylenol, catechol, resorcinol, 2-methylresorcinol, α-naphthol, o-cresol, hydroquinone, m-methoxyphenol, β-naphthol, 3-ethylphenol, 2,6-xylenol, 3,5-xylenol, phenol.
Alcohols	methanol, benzyl alcohol, benzhydrol, isoamyl alcohol, mandelic acid, 2,3-butanediol, menthol, cyclohexanol, t-butanol, t-amyl alcohol, pinacol.
Acids	benzoic acid, p-toluic acid, 2,4,6-trimethoxybenzoic acid, mandelic acid, terephthalic acid, α-methylcinnamic acid, succinic acid.
Amines	aniline, o-toluidine, proline, carbazole, 2,6-methylaniline, diisopropylamine, N-ethylaniline, pyrazole.

Table II. ^{31}P Chemical Shifts of Phenols, Alcohols, Acids, Amines and Thiols Derivatized with **2** and **3**.

Compounds	Reagents	
Phenols	**2**	**3**
2-methoxy-6-methyl phenol	138.4, 136.5	165.24
2,3,6-dimethyl phenol	132.4	160.72
2,6-dimethyl phenol		160.98
guaiacol	135.0	160.45
phenol	131.2	152.51
β-naphthol	132.5	154.32
8-quinolol	135.9	167.38
o-cresol		154.78
p-cresol		152.11
m-cresol		152.87
3,5-dimethyl phenol		153.33
2,4-dimethyl phenol		154.20
Alcohols		
methanol	126.4	145.98
benzyl alcohol	127.3	145.11
isoamyl alcohol	126.5	143.41
menthol	133.1	151.78
t-butanol	124.3	145.66
cyclohexanol	129.1	147.17
pinacol	143.4, 114.1, 113.7	108.77, 214.75
Acids		
terephthalic acid	132.7	insoluble product
benzoic acid	131.2	154.55
d-mandelic acid	132.4	152.18
2,4,6-trimethoxybenzoic acid	130.9	159.83
α-methylcinnamic acid	130.3	153.19
Amines		
2,6-dimethylaniline		103.88
o-toluidine		100.61
di-isopropylamine		92.63
N-ethylaniline		99.97
pyrazole		91.43
Thiols		
2-propanethiol		102.16
thiophenol		113.43
o-thiocresol		112.31
3,4-dimethylthiophenol		112.94

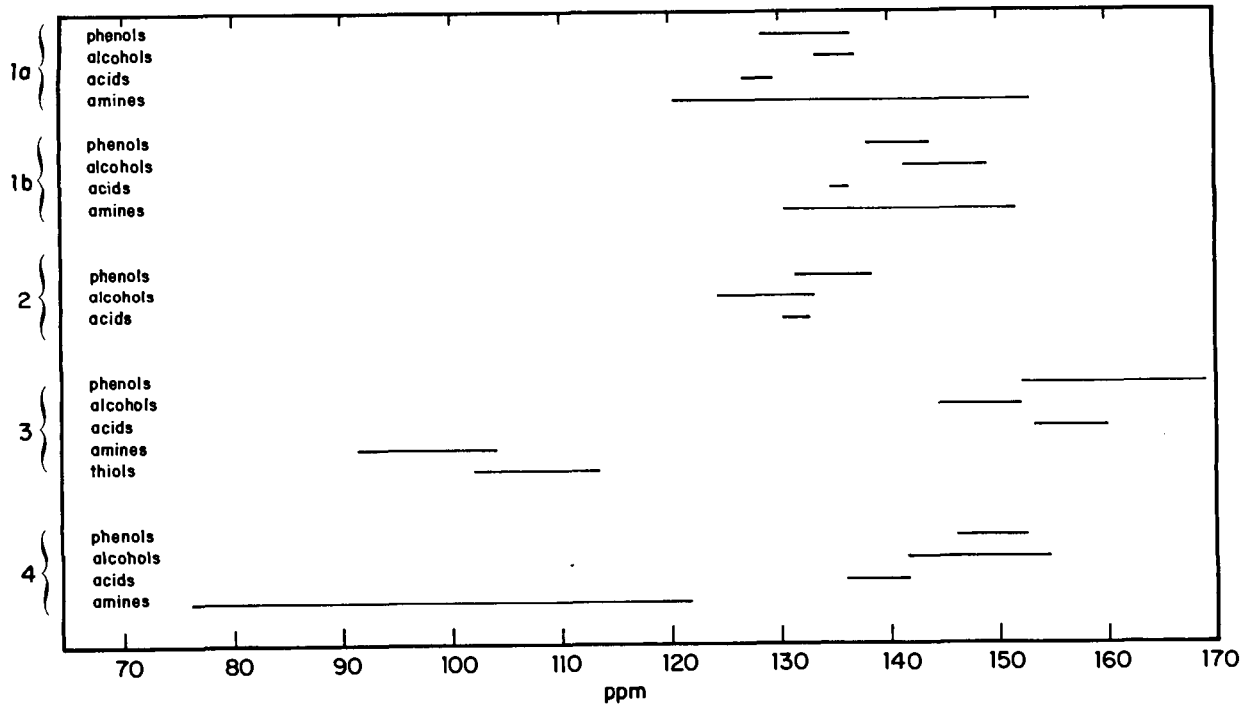

Figure 1. ^{31}P chemical shift ranges for model compound phenols, alcohols, acids, amines and thiols derivatized with reagents **1a**, b and **2** – **4**.

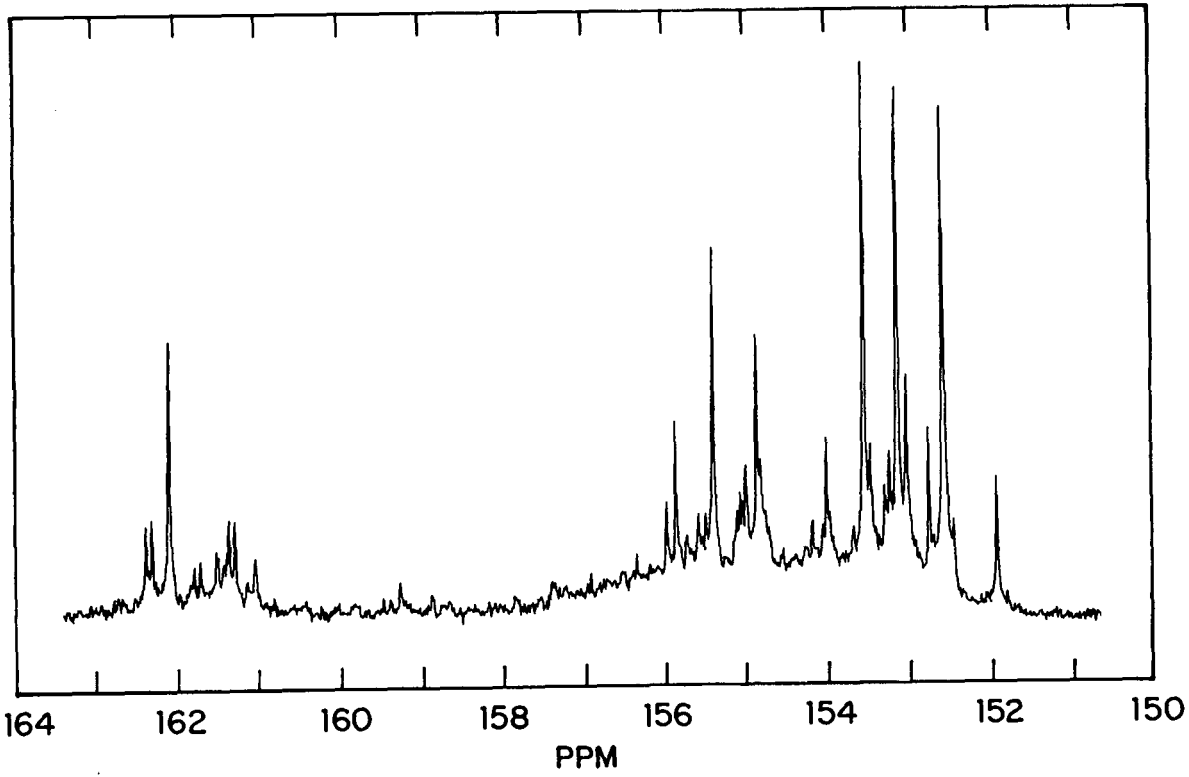

Figure 2. ^{31}P nmr spectrum of the phenol region of an Illinois No. 6 low-temperature pyrolysis condensate.

HYDROPROCESSING OF DESALTED DIRECTLY LIQUEFIED BIOMASS

B. Gevert, P. Andersson, *S. Järås, and S. Sandqvist.
Department of Engineering Chemistry 1, Chalmers University of Technology,
S-412 96 GOTHENBURG, Sweden

* EKA Nobel AB, S-445 01 SURTE, Sweden

ABSTRACT

Desalted directly liquefied biomass from the PERC process was consecutively extracted with iso-octane and xylene. The hydroprocessing was made in a downflow reactor at a constant hydrogen flow and pressure of 85 normal l/h and 10.0 MPa, respectively. The catalyst used was a sulphided cobalt + molybdenum catalyst on gamma alumina. At a liquid flow of 180 ml/h, an hourly liquid space velocity of 1.20 and a temperature of 350°C, the oxygen content of the desalted oil was reduced from 15.3 to 2.3 percent by weight. The effective H/C molar ratio was increased from 1.05 in the starting material to 1.35 and the amount of heavy material with normal atmospheric boiling points above 540°C was reduced from 45.3 to 15.1 percent by weight. Hydroprocessing at 420°C reduced this heavy material further to 4.5 percent by weight. The deoxygenation was only to a small degree dependent on whether the feed oil was desalted or extracted with iso-octane or xylene.

INTRODUCTION

Hydroprocessing is the most important method to reduce the amount of heteroatoms. Oil produced from biomass contains high amounts of oxygen. Downflow trickle bed reactors are the major type used in hydroprocessing of gas oil and heavier types of petroleum fractions. By using similar systems when upgrading oil produced from biomass, known techniques can be used, thereby achieving lower costs. Furthermore, existing refineries can be used without major rebuilding. Elliott and Baker (1-3) have carried out several experiments in an upflow hydroprocessing reactor. When using a downflow reactor they got severe coking and plugging of the flow. They also claim that at low hold up times, which they used, upflow reactors are better than downflow (1).

Petroleum contains small amounts of inorganic salts, mainly sodium chloride. The inorganic salts will be deposited on heat exchange surfaces and on catalysts in destillation towers.By desalting, the inorganic salts are washed out of the oil. The oil used in this study contains approximately 1% of sodium which is considerably more than what is found in petroleum (4).

Earlier work in our laboratory (5) was based upon the assumption that the crudest part has to be separated out before sensitive hydroprocessing catalysts can be used. Since the oil is more thermally instable than petroleum, extraction has been the mehtod employed. By selecting certain solvents it is possible to recieve a predicted yield. However, when separating out the residual part of the oil, large losses occur and the overall yield will be low (4). Therefore, it is of interest to establish a minimum level of amount of residue at which extraction should be performed, without negative effects in the hydroprocessing step.

The purpose of this study was to find a level for suitable yields in the extraction step and still have good conversions without severe deactivation in the hydroprocessing step. Since desalting was included the oil before extraction can also be hydroprocessed. Another important objective was to employ a downflow hydroprocessing reactor. In this paper some preliminary results are presented.

EXPERIMENTAL

Feed oils

The feed oil used was produced from Douglas Fir by the PERC Process in test run 13, in the Albany Liquefaction Plant (6). The oil was mixed with 10 percent by weight of iso-octane, desalted with water at 95°C at a ratio of 1 part oil to 2 parts of water (by volume). It was settled overnight and the desalting was repeated once (referred to as oil D). The sodium content of the feed oil was in this way reduced from 0.92 percent by weight to 0.12 percent. Oil D was consequtively extracted with iso-octane and xylene. The solvents were stripped from the extract in a thin film destillation unit (KDL4 Leybold Heraeus). The two oils will be referred to as oil O and oil X respectively. The residue from the extraction was not treated further. Carbon disulphide was added to the feed oils before hydroprocessing to approximately 100 ppm by weight. The reason for this was to maintain a constant activity and selectivity of the sulphided catalyst (2, 7).

Catalyst

The catalyst used was CoMo on gamma alumina containing 4.2 % CoO and 15.0 % MoO_3 (Akzo Ketjen 742). Prior to use, the catalyst was sulphided with a mixture of 13% hydrogen sulphide in hydrogen at 315°C, 0.3 MPa total pressure and 7 hours of reaction time. In each run 150 ml of catalyst was diluted with 50 ml of carborundum.

Reactor system

The reactor system was a continuous downflow tricle bed designed by Cities Service and modified for heavy feed stocks. The oil was preheated in the feed tank and further heated in the fluidized sandbath before entering the reactor. The liquid product was stripped after reaction (Figure 1).

Analysis

Carbon and hydrogen were determined with a LECO CHN-600 instrument. Oxygen and sulphur were determined with a LECO RO-116 and a LECO SC-132 respectively. Material balance of the liquid products were calculated based on determinations on GC (HP 5880) and GPC according to procedure in reference 4. Coke on catalyst was measured after sohxlet extraction with xylene for 24 hrs. and vacuum drying for 24 hrs. at 110°C. A blank value of 2.04% was reduced from the measurement.

RESULTS AND DISCUSSION

Results of feed stock characterization

Oil O has a higher H/C ratio and a lower oxygen content than the other oils, see Table 1. The fraction of oil O boiling above 540°C is also considerably lower. Thus oil O has good characteristics for being upgraded. Oil D has a higher oxygen content and a poorer H/C ratio than the other two oils. Finally, oil X has the same low H/C ratio as oil D but a considerably lower oxygen content, 9.5 versus 15.5 for oil D.

Results of hydroprocessing

Hydroprocessing of the three oils under similar conditions improved the H/C ratio of all oils but, surprisingly, most in oil D (Tables 1 and 2). Oil O seems to be less active than the other two oils in the HDO reactions since the oxygen content is reduced from 8.2 to 4.8 percent while the reduction of oxygen is higher in the other two oils. The experiments also show that oil O is not cracked to the same degree as the other two oils (Table 3). In biomass the cellulose is built by connecting glucose molecules through C - O - C linkages. Furthermore, lignine is connected with C - O - C bindings although less frequently than in cellulose. A material of the liquefied biomass with large molecules is likely to have large amounts of C - O - C bindings remaining. The C - O - C bindings are easier to break than

C - C bindings in hydroprocessing. This might explain the higher reduction of oxygen and molecular sizes of oil D than that of the other two oils. The residue from the extraction of the feed oil was not further tested since the viscosity was too high. By comparing the cracking and deoxygenation of oil O, X and D and the fact that oil O, X and the residue from extraction together forms oil D. The residue must show a higher activity for cracking and deoxygenation than oil O, X and D. However, on the other hand there might be components in oil O and X which are necessary for deoxygenation and cracking of the residue from extraction.

The largest surface area of the catalyst is found in pores with a diameter between 25 - 80 Å. For a complete pore distribution of the catalyst used, see reference 8. Larger molecules will be limited by diffusion and even not able to enter the smallest pores. The conversion of the largest molecules (C_{44+}) is a strong indication that thermal reactions or homogenous catalysis is important (Table 3). When hydroprocessing in another system, Gevert and Otterstedt (8) showed high conversions without any catalyst present.

Coke on catalyst was measured after the runs and showed high amounts in all cases (Table 4). The high amounts of coke on the catalyst from the experiment with oil O cannot be explained with the limited amounts of experiments in this preliminary study.

In a special run (No. 1) with oil D, a higher temperature, 420°C, was used instead of 350°C (Table 1 and 2). The higher temperature gave considerably more coke on catalyst, 24%, as compared to 11% for the lower temperature (run No. 2). The conversion of heavier material (C_{44+}) was also much higher which has also been found earlier.

CONCLUSIONS

Downflow hydroprocessing of desalted oil from biomass has been successfully done. The preliminary experiments indicate that the the residue after extraction with iso-octane and xylene has a higher activity in hydro-deoxygenation and cracking than the extracted oils. Extraction before hydroprocessing is not necessary.

ACKNOWLEDGEMENT

The authors greatfully acknowledge the Swedish National Board of Energy who sponsored this project.

LITERATURE CITED

1. Elliott, D.K., Baker, E.G. Biotechnology and bioengineering Symposium. 1984, No. 14, 159-174.
2. Elliott, D.C., Baker, E.G. in Proceedings of the 17th Biomass Thermochemical Conversion Contractors Meeting, 1985,CONF-8510167, NTIS 1985.
3. Baker, G.B., Elliott, D.C. Preprint paper - American Chemical Society, Div. Fuel Chemistry. 1987, 32, No. 2, 257-263.
4. Gevert, S.B. Refining of directly liquefied biomass to transportation fuels, IGT Conference on Energy from Biomass and Wastes X, Orlando, March 16-20, 1987.
5. Gevert, S.B., Otterstedt, J-E. Upgrading of liquefied biomass to transportation fuels by extraction. IGT Conference on Energy from Biomass and Wastes X, Washington D.C., April 7-10 1986.
6. Thigpen, P.G., Berry, W.L. In reprints IGT Conference on Energy from Biomass and Wastes VI, Lake Buena Vista, Florida, January 25-29 1982. pp. 1057-1095.

7. Gevert, S.B., Otterstedt, J-E., Massoth, F.E. Applied Catalysis, 1987, 31, 119-131.
8. Gevert, S.B., Otterstedt, J-E. Biomass, 13, 1987, 105-115.

Table 1 Experimental conditions in the different runs

Run No.	1	2	3	4
Oil	D	D	X	O
Temperature (°C)	420	350	350	350
Oil flow (ml/h)	170	180	170	110
LHSV	1.7	1.2	1.13	0.79
Experimental time (h)	6	6	6	6

Table 2 Elemental composition (in weight percent) of the different oils before and after experiments

Oil/Element	C	H	O	H/C*
D	70.6	8.2	15.5**	1.00
X	81.0	8.2	9.5	1.04
O	80.6	9.4	8.2	1.29
1	76.8	10.2	3.1	1.53
2	85.9	10.4	2.3	1.41
3	86.5	9.8	2.5	1.32
4	84.3	9.8	4.8	1.31

*The hydrogen to carbon ratio has been calculated under the assumption that the present oxygen consumes the hydrogen.

**Part of this 15.5 % of oxygen is due to organic oxygen in the oil, some remaining salts and also partly due to oxygen in the water.

Table 3 Boiling point characteristics of the oils in weight percent (values have been normalized)

Oil/Interval	$-C_4$	C_4-C_{12}	C_{13}-C_{20}	C_{21}-C_{44}	C_{44}+
D	0	1.7	25.0	42.1	31.2
X	0	2.9	31.6	44.7	20.8
O	0	5.0	49.3	42.8	2.9
1	0	18.0	43.1	34.6	4.3
2	0.1	20.0	36.5	29.8	13.6
3	0.2	17.9	37.7	29.7	14.5
4	0	13.3	45.9	33.5	7.32

Table 4 Coke on catalyst in weight percent and hydrogen consumption in vol. hydrogen/vol. oil.

No.	Coke	Hydrogen consumption
1	24.0	-
2	11.0	-
3	11.1	152
4	21.4	81

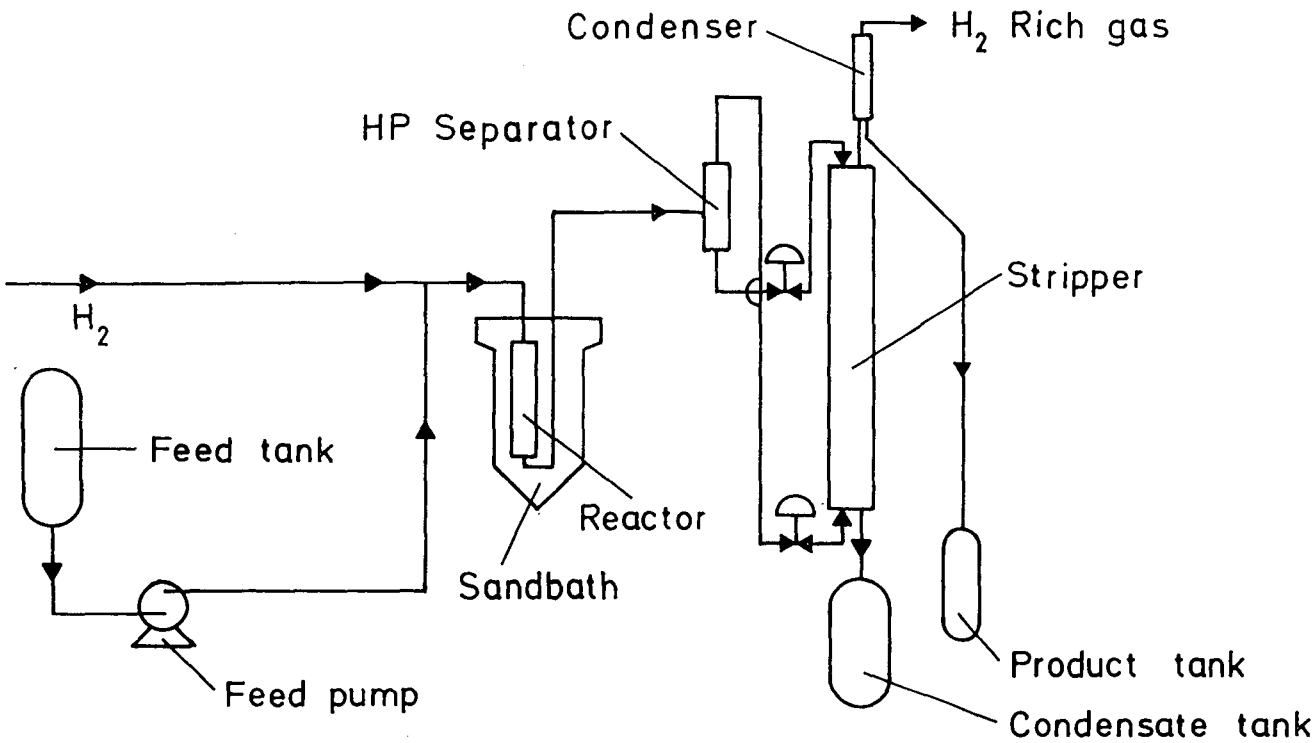

Fig.1 Principle flow diagram of hydroprocessing equipment.

SIMULATED DISTILLATION AND MOLECULAR WEIGHT DETERMINATION BY SUPERCRITICAL FLUID CHROMATOGRAPHY

S. Coulombe and G. Duquette

CANMET, Energy, Mines and Resources Canada
555 Booth St.
Ottawa, Canada K1A 0G1

INTRODUCTION

Supercritical fluid chromatography (SFC) has recently become a popular technique for the analysis of crude oils. It has been demonstrated for simulated distillation (1) and for hydrocarbon type separation (2-3). The advantages of SFC over gas chromatography (GC) in simulated distillation are the wider boiling range and lower temperature thus preventing cracking of heavy molecules during analysis. Previous work with GC (4) has shown that average molecular weight can be determined for aromatic fractions using a technique similar to simulated distillation. The present study on retention time behaviour of standard compounds shows how the same approach can be applied to SFC. Correlations between retention times and boiling point, molecular weight and melting point have been studied.

EXPERIMENTAL

A Lee Scientific Model 600 SFC/GC was used. The separations were performed on a 10 m x 100 µm i.d. DB-5 column (for naphtha range) and two 10 m x 100 µm DB-5 column (for heavier standards) from J&W Scientific, Inc, using carbon dioxide as the mobile phase. The end of the column was connected to a frit restrictor inserted in a 100 µm i.d. fused silica sleeve. The restrictor was directly inserted in the FID detector. The following pressure or density ramps were used: for the naphtha range (IBP- 200°C), initial pressure of 80 atm for 5 min, followed by a 1 atm/min ramp to 200 atm; for the middle distillate range (200- 350°C), initial density of 0.1444 g/mL for 7.5 min, followed by a ramp of 0.0092 g/mL/min to 0.5930 g/mL; for the gas oil range (350-525°C), initial density of 0.3095 g/mL for 5 min, followed by a ramp of 0.006 g/mL/min to 0.7411 g/mL. All runs were isothermal at 100°C. Sample introduction was made via a Rheodyne 7520 valve having a 0.5 µL injection volume.

RESULTS AND DISCUSSION

1- Boiling point

As would be expected from literature on simulated distillation by SFC (1), there is a very good correlation between retention time and boiling point. However, in the light naphtha range, the calibration is not linear. Thus, the pressure (or density) program must be adjusted to provide a linear relation or a proper calibration procedure must be used in order to accurately determine the initial boiling point of a sample. It should be noted that the inflexion point is at about the operating temperature. From this result, it appears that a temperature program would be useful for an adequate calibration of the lighter portion of the sample (low initial temperature) and of the heavier portion (high final temperature).

2- Molecular weight

A previous study (4) has shown that the molecular weight of aromatic fractions from topped (light fractions removed) crude oils can be evaluated by a technique similar to simulated distillation. In that work, after hydrocarbon type separation by column chromatography the aromatics fraction was separated by GC on a non-polar column. Since the compounds are of the same type, boiling points and molecular weights were both well correlated to retention time. This correlation allowed the determination of the boiling range, the average molecular weight as well as the molecular weight distribution of these fractions. A similar approach with SFC would eventually permit monitoring molecular weight of heavier samples.

As shown in Fig. 2, a poor correlation exists between molecular weight and retention time in the naphtha and middle distillate range, except for straight chain paraffins. However, in the gas oil range, the correlation for non-paraffinic standard compounds is improved. As molecular weight increases, it seems that the influence of the functional group becomes less important compared with molecular weight. This could be due to increased steric hindrance or more electron delocalization over the structure of the molecule which reduces the polarity. Thus, it appears that the molecular weight determination would only be effective for heavy fractions.

3- Melting point

Solubility of solids in liquids is determined by intermolecular forces as well as enthalpy of fusion and melting point of the solute (5). Since a supercritical fluid has densities approaching those of a liquid and since the retention time is related to solubility, we investigated how the melting of the solute would be related to the retention time. As shown in Fig. 3, there is no correlation except for the n-paraffins which was expected since their melting point increases regularly with molecular weight.

Melting point was expected to have an influence when the operating temperature was lower than the melting point. All the results shown in Fig. 3 were obtained at 100°C. Although there is some trend in Fig. 3c, there is too much variation to significantly relate melting point and retention time, and the correlation is very poor even within the same family of compounds.

4- Response factors

All simulated distillation techniques assume that the various components of a crude oil sample have nearly identical response factors. Figure 4 shows that response factors can be significantly different. However, within the same class of compounds, it seems that the response factors do not vary to the same extent. Therefore, boiling range determination could lead to erroneous results if the relative quantity of different compound types varies from sample to sample. On the other hand, for hydrocarbon type separation by SFC, results can be reliable if proper response factors are assigned to each compound class. Since the difference between the response factors of saturates and aromatics is small, samples with low heteroatomic content could lead to satisfactory results.

CONCLUSIONS

The study of retention behaviour showed that, for given SFC conditions, retention time is mainly dependent on the boiling point of the solute. Some correlation was found with the molecular weight and no significant link was found with the melting point. Response factors were found to vary between compound classes but to be quite consistent within the same class.

REFERENCES

1. Schwartz, H.E., Brownlee, R.G., Boduszynski, M.W., and Su, F., Anal. Chem., **59** , 1393-1401, 1987.

2. Norris, T.A. and Rawdon, M.G., Anal. Chem., **56** , 1767-1769, 1984.

3. Campbell, R.M., Djordjevic, N.M., Markides, K.E. and Lee,M.L., Anal. Chem., **60** , 356-362, 1988.

4. Coulombe, S. and Sawatzky, H., Fuel, **65** , 552-557, 1986.

5. Reid, R.C., Prausnitz, J.M. and Sherwood,T.K., The Properties of Gases and Liquids, 3rd ed., McGraw-Hill, New York, pp.380-384.

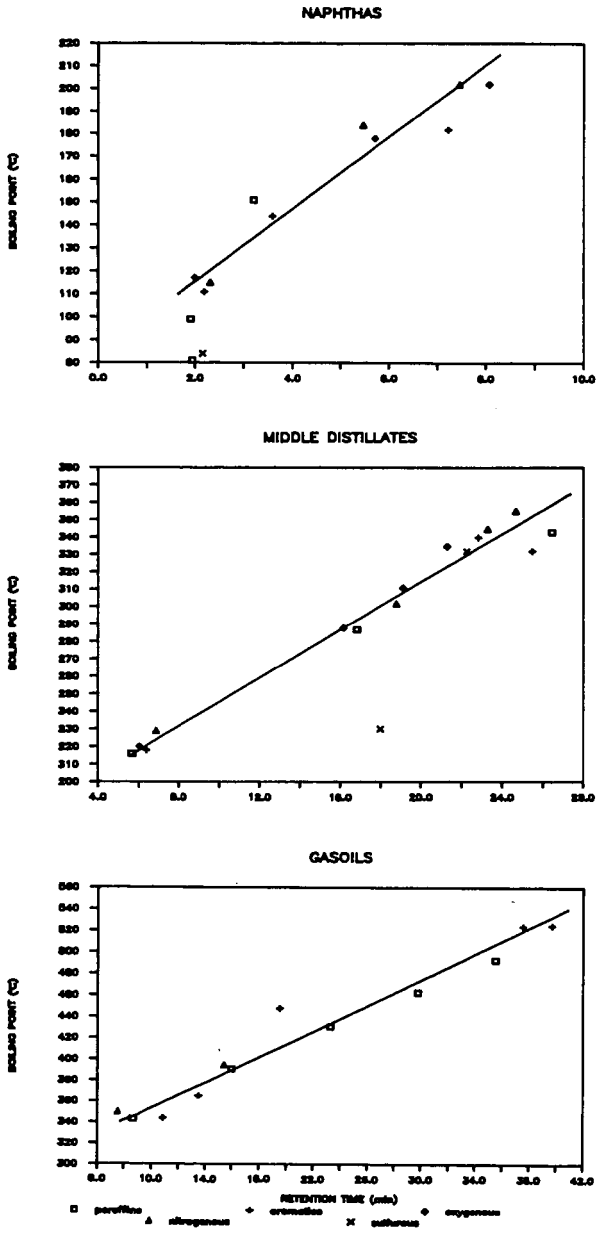

Figure 1 - Correlation between boiling point and retention time

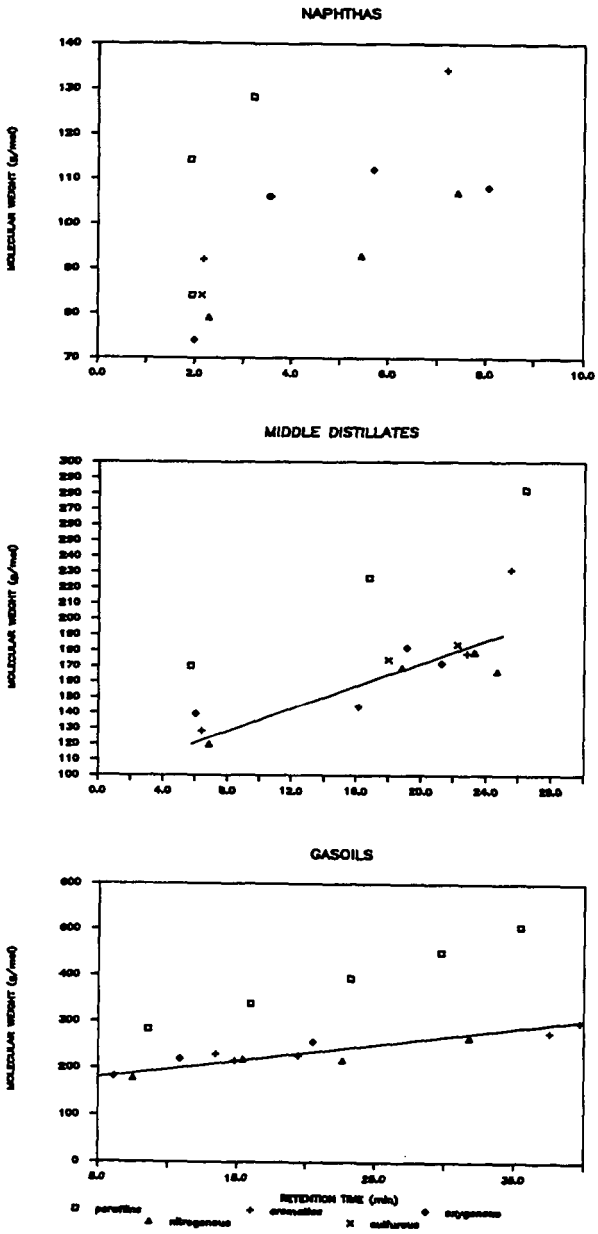

Figure 2 - Correlation between molecular weight and retention time

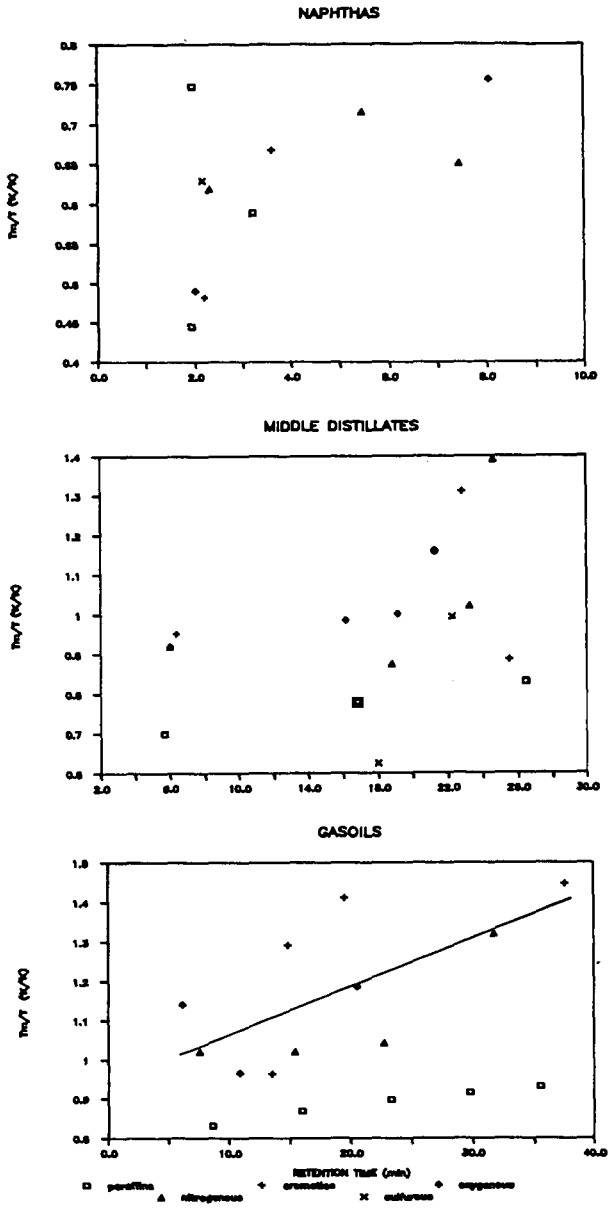

Figure 3 - Correlation between melting point and retention time (Tm: melting point; T: operating temperature)

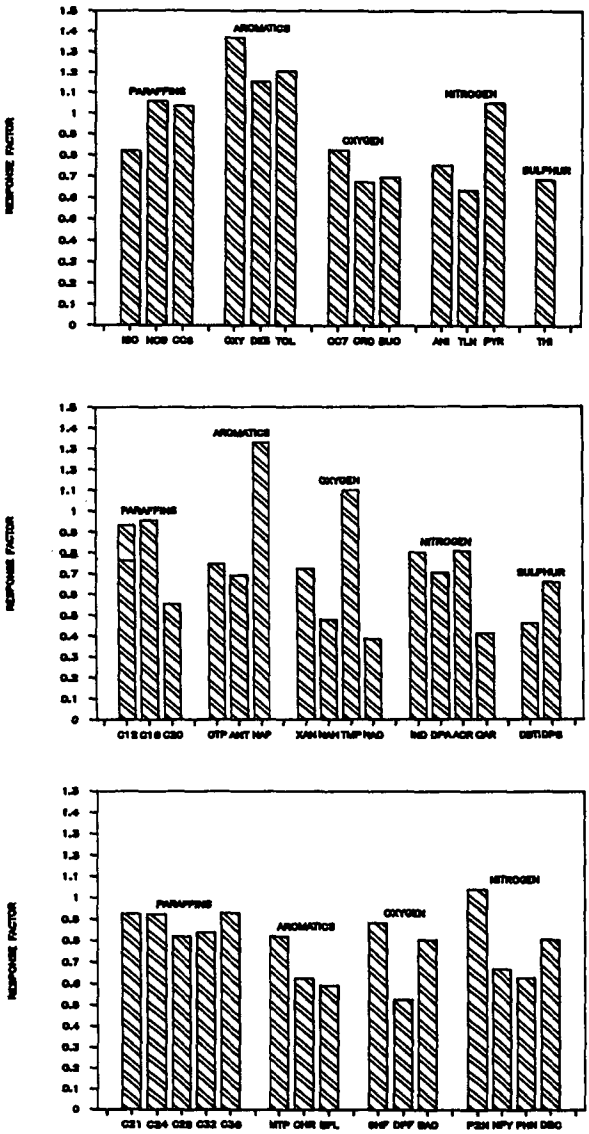

Figure 4 - Response factors (SFC with FID)

ARTIFICIAL SIMULATION OF HYDROCARBON GENERATION IN COAL USING HYDROUS PYROLYSIS TECHNIQUES

S. C. Teerman and R. J. Hwang,
Chevron Oil Field Research
P. O. Box 446
La Habra, California 90633-0446

INTRODUCTION

Coal, which is usually land plant in origin, occurs in many oil-producing basins. Microscopically, coal consists of various macerals (liptinite, vitrinite, and inertinite). The generative potential of coal reflects the hydrocarbon potential of the composing macerals (Kelly et al., 1985). Although most coals consist of predominantly vitrinite, some contain significant amounts (>20% of total maceral content) of oil-prone liptinite macerals. Work by Brooks and Smith, 1967; Connan, 1974; Durand and Paratte, 1982; Thompson et al., 1985; and MacGregor and McKenzie, 1986 suggests that certain coals can be considered as source rocks for liquid hydrocarbons. Their conclusions are based on the close association of coal with liquid hydrocarbon occurrences and promising source potential supported by various geochemical analyses. However, the liquid hydrocarbon potential of coal cannot easily be evaluated because of its variable maceral composition, its unique occurrence compared to most source rocks, and difficulty in quantifying liquid hydrocarbon expulsion.

The overall objective of this study is to complete hydrous pyrolysis experiments to evaluate the liquid hydrocarbon potential of coal. Specific aspects of this study include: (1) a quantitative assessment of the generative potential of coal, and (2) an evaluation of the composition of liquid hydrocarbons generated from coal at various temperatures.

EXPERIMENTAL

Original (Unheated) Samples

Hydrous pyrolysis experiments were completed using Tertiary lignites from North Dakota and the Far East. Both lignites are thermally immature (Ro<0.35%) with respect to hydrocarbon generation. The Far East lignite is liptinite-rich (32% of total maceral content), which is supported by elemental analysis (H/C=1.0) and Rock-Eval pyrolysis (Hydrogen Index= 483 mg HC/g O.C.). Resinite is the most abundant liptinite maceral (13.7%) in the Far East sample. The North Dakota lignite is vitrinite-rich (95% of total maceral content) and

liptinite-poor (3%). Geochemical and microscopic data for the two unheated lignites are listed in Table 1.

Methods and Procedures

Hydrous pyrolysis was used to evaluate product yields, compositions, and the temperature of liquid hydrocarbon generation from the two lignites. This technique has been suggested as a method that best simulates source rock burial and the natural generation and expulsion of petroleum (Lewan et al., 1979; Lewan, 1983; and Winters et al., 1981). These studies suggest that oil-pyrolysate formed under hydrous pyrolysis conditions closely resembles naturally generated products because of the presence of water at high temperatures and pressures in a closed system. However, other pyrolysis methods (closed system anhydrous) can also simulate petroleum generation. Monthioux et al., 1985 suggests that closed-system pyrolysis of coals more closely simulates natural maturation than open-system pyrolysis techniques.

Hydrous pyrolysis procedures used were similar to those described by Lewan et al., 1979. Both lignites were crushed to 0.5 to 1.0mm chips, sieved to remove fines, and thoroughly homogenized. Individual samples were heated to temperatures ranging between 250 and 360°C for 72 hours in 1-liter stainless steel reactors. Both floating and sorbed (solvent rinsed) pyrolysate, as described by Lewan (1983), were included as expelled product. The pyrolyzed lignite residues were geochemically and microscopically characterized to evaluate changes that occur during artificial maturation.

RESULTS AND DISCUSSION

Quantity of Generated Oil-Pyrolysate

A maximum of 48 and 158 mg/g O.C. of oil-pyrolysate is generated from the North Dakota and Far East lignites, respectively (Table 2). Peak generation occurs at 340 and 360°C for the North Dakota and the Far East lignite, respectively (Figure 1). Expelled products consist predominantly of sorbed pyrolysate (Table 2). The differences in oil-pyrolysate yield and temperature of peak generation for the two lignites are probably related to the quantity and type of oil-prone liptinite macerals.

Peak generation temperature for the Far East sample is probably influenced by resinite. Lewan (1987) and Hwang and Teerman (1988) document that large amounts of oil-pyrolysate are generated from resinite, with peak generation occurring at, or above 360°C. Based on a hydrous pyrolysis experiment of a representative sample of solvent (methylene chloride)

extracted Far East lignite (to remove soluble resinite), approximately half of the oil-pyrolysate originates from resinite (Table 2).

Oil-Pyrolysate Composition

Although oil-pyrolysate composition varies with temperature, the pyrolysates generally display a significant amount of n-paraffins and light aromatic and naphthenoaromatic components. Comparison of the Far East and North Dakota oil-pyrolysates at various temperatures are shown in Figures 2 and 3. These oil-pyrolysates are similar to some naturally occurring non-marine oils.

Below 290°C, the Far East oil-pyrolysates are dominated by sesquiterpenoid components, such as cadalene and other alkyl naphthalenes (Figure 2). These (sorbed) oil-pyrolysates consist of soluble resinite rather than a "thermally generated" product. Solvent rinsing the unheated Far East lignite results in a similar quantity of sorbed product. Below 290°C, the North Dakota oil-pyrolysate is dominated by light aromatic and naphthenoaromatic components and contains small amounts of n-paraffins (Figure 3).

Above 290°C, both oil-pyrolysates contain significant amounts of n-paraffins, ranging from $<C_{10}$ to about C_{32}. Although the odd/even predominance in both oil-pyrolysates decreases with temperature, it is still evident at 360°C. Precursors of n-paraffins consist of cutinite, sporinite, and other liptinite macerals, which contain plant waxes (Brooks and Smith, 1967 and Nip et al., 1988). Liptodetrinite and submicroscopic inclusions of bacterial, algal, and plant lipids in desmocollinite (a vitrinite maceral) probably contribute to the n-paraffins. Differences in the distribution and relative abundance of n-paraffins in the two oil-pyrolysates (Figures 2 and 3) are probably related to variation in their precursors.

In the C_6-C_{15} range there is also a significant amount of aromatic and naphthenoaromatic products. These originate mainly from vitrinite and resinite. The Far East oil-pyrolysates display significant amounts of C_2- to C_5-alkyl naphthalenes, which are similar in distribution to a resinite oil-pyrolysate, described by Hwang and Teerman, 1988. This suggests the importance of resinite as a precursor for the Far East naphthenoaromatic components. Generated products from resinite in the Far East lignite are non-paraffinic consisting of cyclic isoprenoids and their aromatic derivatives.

Phenols also occur in significant amounts in both oil-pyrolysates. These compounds are probably derived from

diagenetically altered lignin precursors in vitrinite and inertinite (Chaffee et al., 1984). However, some liptinite macerals (sporinite) may generate phenolic compounds (Meuzelaar et al., 1984). Resinite does not generate phenolic compounds (Hwang and Teerman, 1988). The presence of phenol and alkylphenols in these oil-pyrolysates indicates a contribution from the lignin precursors. However, the contribution to the total oil-pyrolysate is small relative to that of the wax and resin components. The North Dakota lignite yields relatively larger amounts of phenols compared to the Far East sample. This observation is consistent with the vitrinite-rich maceral composition of the North Dakota lignite.

Characterization of Heated Lignites

Atomic H/C and O/C ratios generally decrease with temperature (Table 3). Thermally altered Far East samples plot at the top of the van Krevelen Type III pathway; North Dakota samples plot between the Type III and IV pathways (Figure 4).

Maceral analysis of the Far East samples suggests that hydrocarbon generation from individual liptinite macerals occur at different temperatures. Except for resinite, almost all liptinite macerals have disappeared by 330°C. At 350°C only small amounts of resinite remain. Secondary products consisting of exsudatinite and bitumen smear films still occur at 360°C.

Vitrinite reflectance values increase exponentially with a linear increase in temperature (Figure 5). Differences in the reflectance profiles of the two lignites are probably related to the vitrinite precursor.

Generative Potential of Coal

Based on these hydrous pyrolysis results, coals that contain small to moderate amounts of liptinite (<20% total maceral content) cannot generate significant amounts of liquid hydrocarbons. The contribution of desmocollinite to the liquid hydrocarbon potential of coal in a natural system is uncertain.

The Hydrogen Index of the unheated Far East lignite (483 mg HC/g O.C.) is similar to some Type II kerogens. However, the quantity of generated product is much less than that from hydrous pyrolysis experiments of Type II kerogens, reported by Lewan (1985) and K. E. Peters (personal communication). The large discrepancy in the quantity of generated pyrolysate between Rock-Eval and hydrous pyrolysis (483 versus 158 mg/g O.C.) can be attributed to the different

methods of measuring pyrolysate quantity and pyrolysis techniques (open- versus closed-system). Caution must be used in directly relating Rock-Eval Hydrogen Index to the source potential of coal.

Although the composition of the North Dakota oil-pyrolysate is similar to some naturally occurring waxy oils, the quantity of generated product is insignificant compared to most source rocks. Both the quantity and composition of an artificially generated product must be considered when evaluating the source potential of coal.

REFERENCES

Brooks, J. K. and Smith, J. W. (1967). The diagenesis of plant lipids during the formation of coal, petroleum and natural gas. I. Changes in the n-paraffin hydrocarbons. Geochimica. Cosmochimica Acta, v. 31, p. 2389-97.

Chaffee A. L., Johns R. B., Baerken M. J., de Leeuw J. W., Schenck, P. A. and Boon J. J. (1984). Chemical effects in gelification processes and lithotype formation in Victorian brown coal. In advances in organic geochemistry, 1983 (eds. P. A. Schenck, J. W. de Leeuw and G. W. M. Lijmbach). Org. Geochem. 6, p. 409-416.

Connan, J. (1974). Natural diagenesis and artificial diagenesis of organic matter of predominantly plant constituents. Tissot, B. and Bienner, F., Eds. Advances in organic geochemistry, proceeding of the 6th International meeting on organic geochemistry, 1973, p. 73-95.

Durand, B. and Paratte, M. (1982). Oil potential of coals: A geochemical approach: Symp. Petroleum Geochemistry and Exploration of Europe, J. Brooks, editor, Blackwell Scientific Publications, Oxford, England, p. 285-292.

Hwang, R. J. and Teerman, S. C. (1988). Hydrocarbon characterization of resinite. Journal of Energy and Fuels 2, p. 170-175.

Kelly, P. A., Bissada, K. K., Burda, B. H., Elrod, L. H., and Pheifer, R. H. (1985). Petroleum generation potential of coals and organic rich deposits: significance in Tertiary coal rich basins: Indonesian Petroleum Association Proceedings, 14th Annual Convention, v. 1, p. 1-21.

Lewan, M. D., Winters, J. C. and McDonald, J. H. (1979). Generation of oil-like pyrolyzates from organic-rich shales. Science, v. 203, p. 897-899.

Lewan, M. D. (1983). Effects of thermal maturation on stable organic carbon isotopes as determined by hydrous pyrolysis of Woodford shale. Geochim. Cosmochim, Acta, v. 47, p. 1471-1479.

Lewan, M. D. (1985). Evaluation of petroleum generation by hydrous pyrolysis experiments. Phil. Trans. of the Royal Soc., v. 315, p. 123-134.

Lewan, M. D., and Williams, J. A. (1987). Evaluation of petroleum generation from resinites by hydrous pyrolysis: AAPG Bull., v. 71, p. 207-214.

MacGregor, D. S. and McKenzie, A. G. (1986). Quantification of oil generation and migration in the Malacca Strait region of central Sumatra. Proceedings Indonesian Petroleum Association, 1986, v. 1, p. 305-320.

Meuzelaar, H. L. C., Harper, A. M., Pugmire, R. J., and Karas, J. (1984). Characterization of coal maceral concentrates by Curie-point pyrolysis mass spectrometry. Coal Geol., v. 4, no. 2, p. 143-172.

Monthioux, M., Landais, P., and Durand, B. (1985). Comparison between extracts from natural and artificial maturation series of Mahakam Delta coals. Org. Geochem., v. 10, p. 299-311.

Nip, M., de Leeuw J. W. and Schenck, P. A. (1988). The characterization of eight maceral concentrates by means of Curie Point pyrolysis-gas chromatography and Curie point pyrolysis-gas chromatography-mass spectrometry. Geochim. Cosmochim. Acta 52, p. 637-648.

Peters, K. E. Personal communication of unpublished results.

Thompson, S., Morley, R. J., Barnard, P. C. and Cooper, B. S. (1985). Facies recognition of some Tertiary coals applied to prediction of oil source rock occurrence. Marine and Petroleum Geology, v. 2, p. 288-297.

Winters, J. C., Williams, J. A., and Lewan, M. D. (1981). A laboratory study of petroleum generation by hydrous pyrolysis. In: M. Bjoroy et al. (eds.), Adv. in Org. Geochem. (1981), John Wiley & Sons, Chichester, U.K., p 524-533.

TABLE I

CHARACTERIZATION OF UNHEATED FAR EAST AND NORTH DAKOTA LIGNITES FOR HYDROUS PYROLYSIS EXPERIMENTS

Total Organic Carbon/Rock-Eval Pyrolysis

	Wt.% TOC	Mg HC/g rock	Mg HC/g rock	Mg CO_2/g rock	Tmax °C	S1 / S1+S2	S2/S3	Hydrogen Index Mg HC/g O.C.	Oxygen Index Mg CO_2/g O.C.
Far East	55.01	21.31	265.80	14.06	390	0.07	18.90	483	25
North Dakota	55.29	6.90	67.80	29.02	389	0.09	2.34	123	52

Elemental Analyses and Microscopy

	Far East	North Dakota
Atomic H/C	1.00	0.94
Atomic O/C	0.23	0.35
% Vitrinite Reflectance	0.33	0.29
Maceral Percent		
% Vitrinite (huminite)	65.9	94.9
% Liptinite	31.8	3.0
Exinite	18.1	2.2
Resinite	13.7	0.8
% Inertinite	2.3	2.1

TABLE 2

QUANTITY OF OIL-PYROLYSATE
FAR EAST AND NORTH DAKOTA LIGNITES

Temperature °C	Expelled Pyrolysate Floating (mg/g TOC)[2]	Expelled Pyrolysate Sorbed (mg/g TOC)[2]	Total Expelled Pyrolysate (mg/g TOC)[2]
Far East			
-250	-	68.0	68.0
-270	-	83.5	83.5
-290	-	95.7	95.7
-310	-	97.0	97.0
-330	-	113.5	113.5
-350	68.8	108.1	152.6
-350[1]	-	87.9[1]	87.9[1]
-360	trace	157.6	157.6
North Dakota			
-260	-	11.4	11.4
-270	-	24.0	24.0
-280	-	17.9	17.9
-290	-	7.1	7.1
-310	-	15.8	15.8
-330	-	6.6	6.6
-340	-	46.7	47.7
-350	-	24.1	24.1
-360	-	31.1	31.1

[1] Solvent-extracted lignite

[2] Based on organic carbon value of 64.65 and 63.11 for Far East and North Dakota lignites from elemental analysis

TABLE 3

ELEMENTAL ANALYSES AND VITRINITE REFLECTANCE DATA FOR RESIDUAL (HEATED) FAR EAST AND NORTH DAKOTA LIGNITE SAMPLES

Temp. °C	Atomic H/C	Atomic O/C	% Ro
Far East			
Original	1.00	0.23	0.33
250	1.01	0.15	0.57
270	1.05	0.13	-
290	0.97	0.12	0.72
310	0.92	0.10	-
330	0.91	0.07	1.01
350	0.72	0.06	1.34
North Dakota			
Original	0.94	0.35	0.29
260	0.77	0.25	0.60
270	0.78	0.22	0.70
280	0.71	0.20	0.77
290	0.68	0.20	0.80
310	0.66	0.13	1.08
330	0.68	0.10	1.28
340	0.64	0.10	1.40
350	0.61	0.09	1.45
360	0.60	0.08	1.58

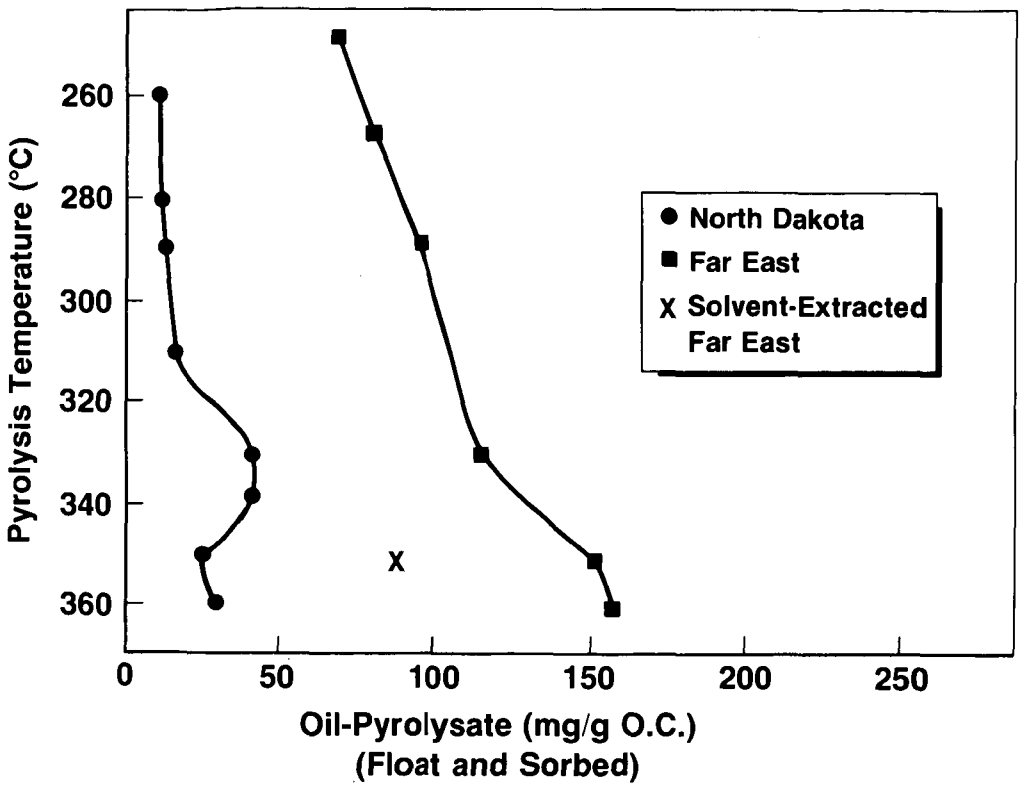

Figure 1

Oil-Pyrolysate from Hydrous Pyrolysis Experiments of Far East and North Dakota Lignites

LE 88—05125

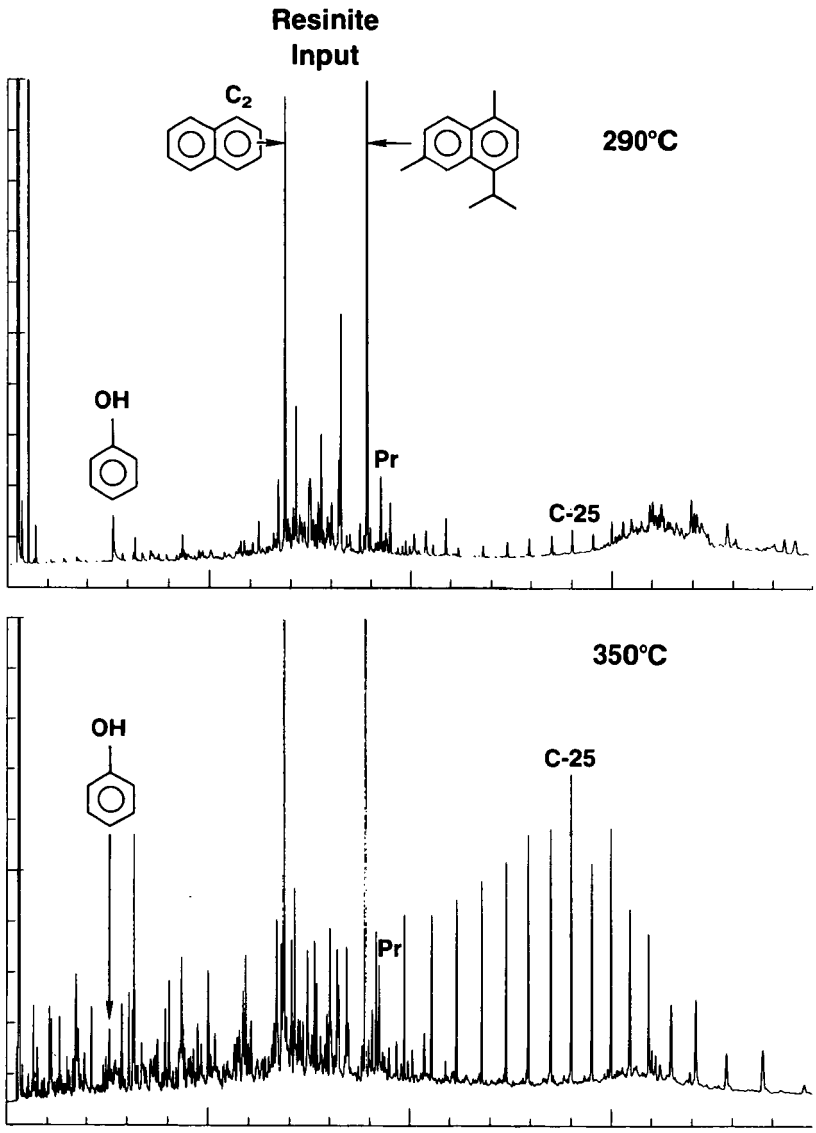

Figure 2

Comparison of Far East Lignite Oil-Pyrolysates, 290° and 350°C

LE 88–05126

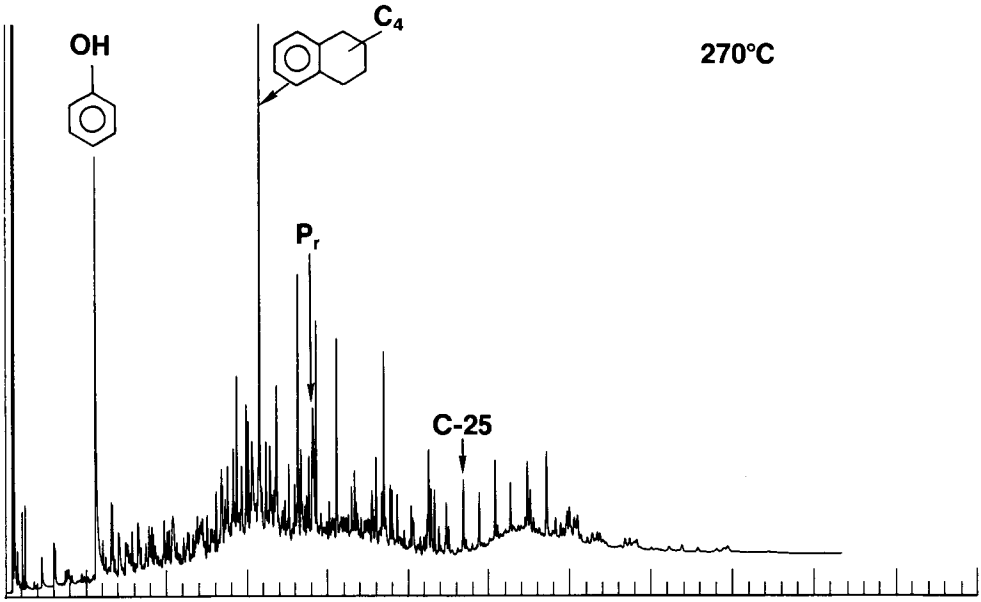

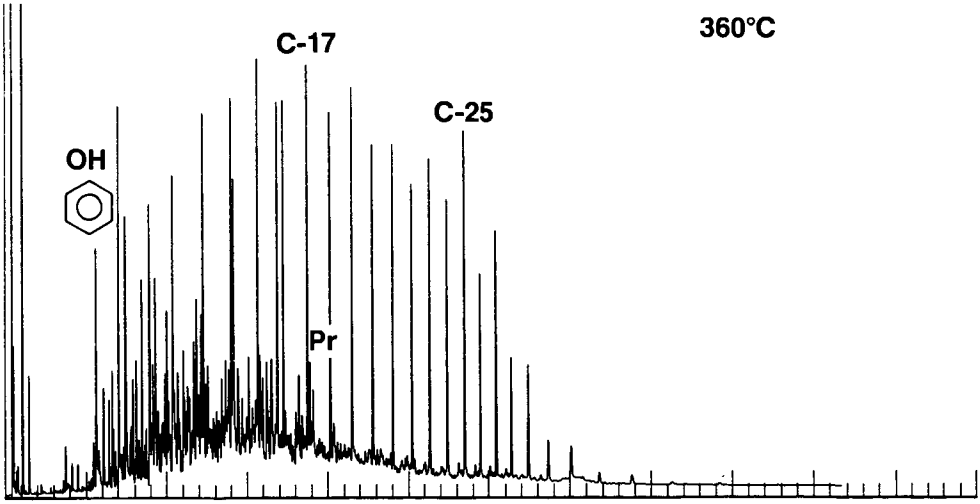

Figure 3

Comparison of North Dakota Oil-Pyrolysates, 270° and 360°C

LE 88–05127

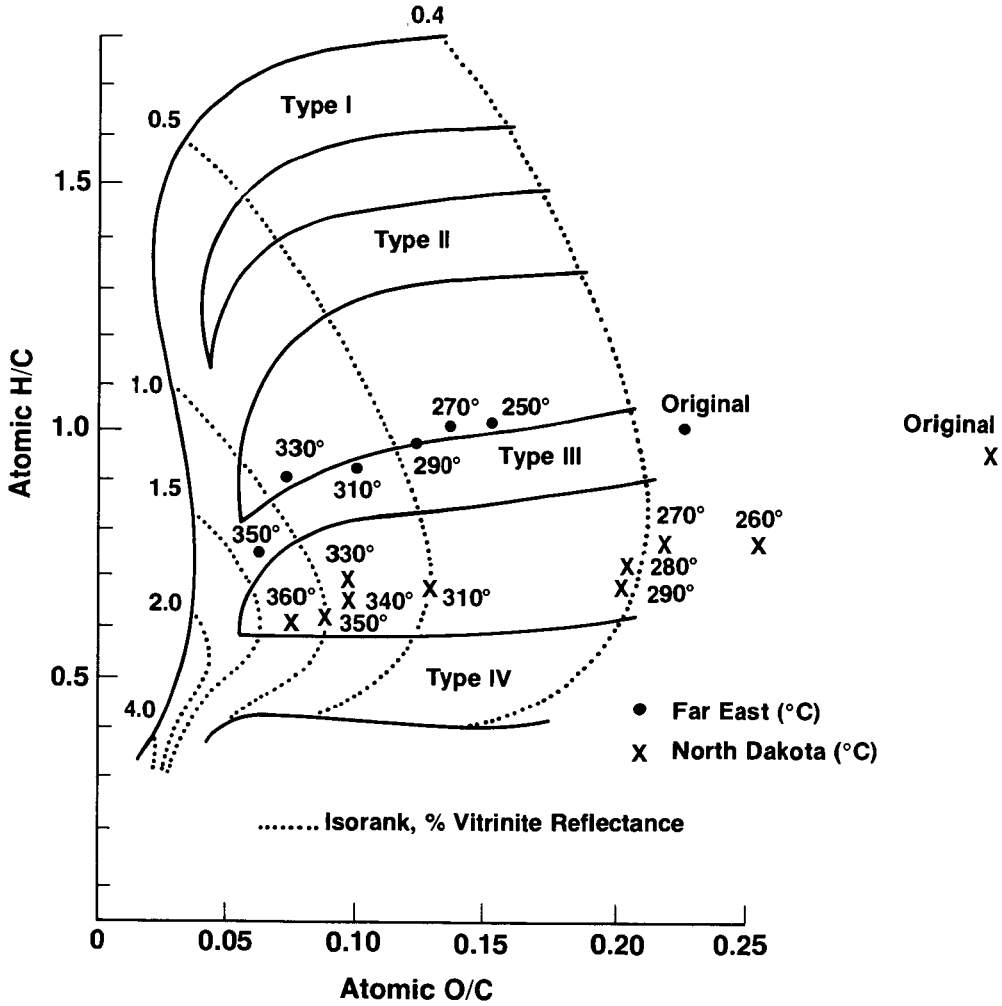

Figure 4

Atomic H/C and O/C Ratios of Far East and North Dakota Lignites from Hydrous Pyrolysis Experiments

LE 88–05128

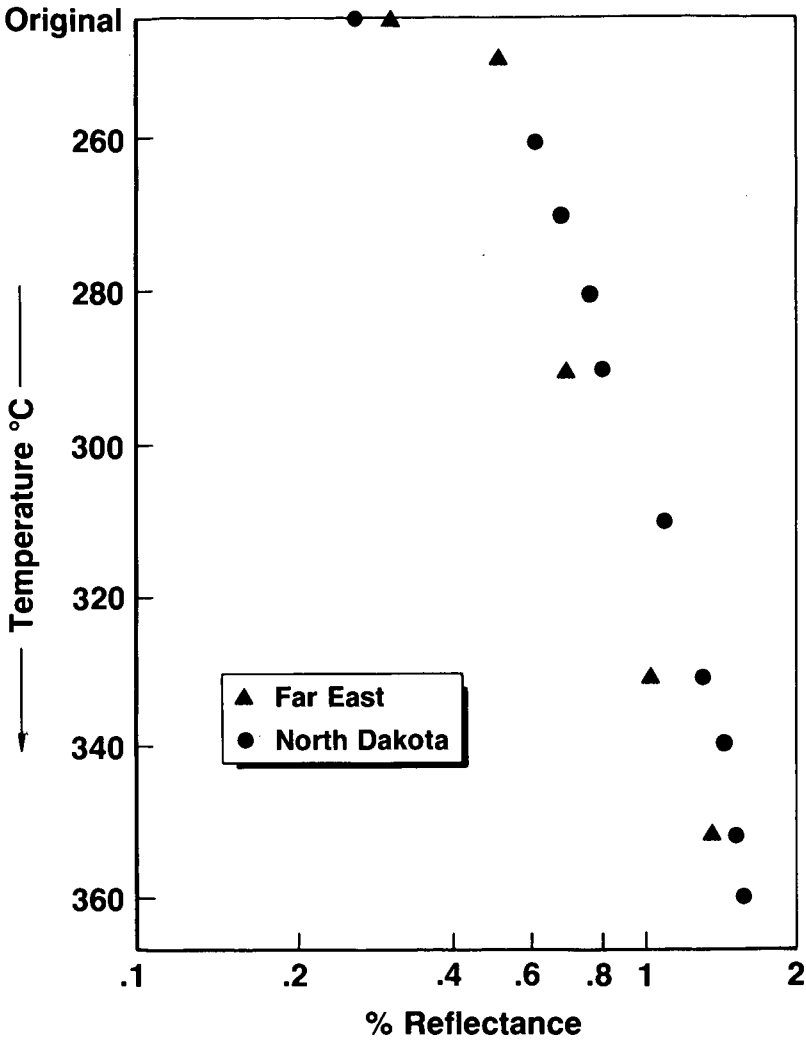

Figure 5

Vitrinite Reflectance for Far East and North Dakota Lignites Versus Hydrous Pyrolysis Temperature

LE 88–05129

CO HYDROGENATION AND OXYGENATE FORMATION OVER RUTHENIUM SUPPORTED ON A BASIC LAYERED DOUBLE HYDROXIDE

M. Rameswaran, Emmanuel Dimotakis and Thomas J. Pinnavaia*

Department of Chemistry and
Center for Fundamental Materials Research
Michigan State University, East Lansing, Michigan 48824

ABSTRACT

Synthetic layered double hydroxides (LDH) such as hydrotalcite (HT), $[Mg_6Al_2(OH)_{16}](CO_3).4\ H_2O)$, provide a highly basic (pK_a<35) environment for supporting transition metals. Ruthenium was grafted onto a HT using $Ru_3(CO)_{12}$ as a precursor and was subsequently reduced under flowing H_2 at 275°C to ruthenium metal. The supported catalyst exhibited substantial selectivity at 275°C for C_1-C_4 alcohols at moderately low pressures (0-190 psig). Methanol was the most dominant oxygenated product. The factors effecting the thermal stability and selectivity properties of this new class of catalyst system are presented.

INTRODUCTION

Layered double hydroxides, such as hydrotalcite $[Mg_6Al_2(OH)_{16}](CO_3).4\ H_2O$ (HT, 3:1 Mg:Al), are anionic clay minerals. These compounds have a brucite-like structure, with positively charged hydroxide layers of aluminum and magnesium. The positive charge is compensated by intercalated carbonate anions along with some water molecules. The thermal decomposition of this material has been investigated by several laboratories [1-3]. These earlier studies indicate that the interstitial water is reversibly lost up to 200°C. Between 250°C-450°C, the loss of water was accompanied by dehydroxylation. Reichle [3] has reported that only above 275°C the formation of MgO phase along with HT phase was observed by X-ray diffraction (XRD). Beyond 550°C the HT phase was irreversibly lost.

Giannelis et al. [4] have grafted metal carbonyl complexes onto the pillars within the galleries of aluminum pillared montmorillonite (APM) clays. They reported that $Ru_3(Co)_{12}$ is more easily transformed into partially oxidized grafted species, even in the absence of air, when compared with other carbonyl complexes. Giannelis and Pinnavaia [5] further extended their studies to include the grafting of Rh and Pt carbonyls to the surfaces of HT. In the present study we show that it is possible to graft these carbonyl complexes onto HT.

*To whom inquires should be addressed.

Bulk Ru is known to be one of the most active syngas conversion catalyst with almost 100% selective to straight chain hydrocarbon [6,7]. However, the acid-base properties of the support are known to effect the selectivity of Group VIII transition metals. Thus, hydrotalcite provided us with an ideal opportunity to investigate the behavior of $Ru_3(CO)_{12}$ and Ru on a very basic oxide surface.

EXPERIMENTAL

HYDROTALCITE PREPARATION

A solution of 51.2g (0.20 mols) $Mg(NO_3)_2.6H_2O$ and 24.8g (0.067 mols) $Al(NO_3)_3.9H_2O$ in 200 ml of water was added drop wise to a solution of 25g (0.20 mols) $Na_2CO_3.H_2O$ and 28g (0.70 mols) NaOH in 200 ml of water. The addition was stopped when the pH of the solution reached 10. This process, which took about 4h, was carried out with vigorous agitation. The resulting heavy slurry was refluxed at 65±5°C for 16h with continuous mixing. Upon cooling, the slurry was washed and centrifuged several times until almost all the salt was recovered. The slurry was then dried in air on a large glass plate [8]. The X-ray pattern indicated a d_{001} spacing of 7.76Å, which is indicative of HT with 3:1 Mg:Al. The thermal stability of the HT thus prepared was analyzed using a CAHN TGA 121 thermo-gravimetric analyzer from 25 to 1000°C at a heating rate of 5°C/min. The weight loss under isothermal conditions at 275°C also was investigated. The isothermal temperature was achieved using the same heating rate indicated earlier.

RUTHENIUM IMPREGNATION

One gram of HT s evacuated at room temperature for 4h. To this HT was added to 45mg of $Ru_3(CO)_{12}$ dissolved in 100 ml of degassed CH_2Cl_2. The slurry was stirred for 20h, filtered in air, and washed with a small amount (~20 ml) of CH_2Cl_2. The percentage of Ru impregnated was determined by atomic adsorption (Galbraith Laboratory) and was found to be 0.34%. A 3.0% mixture of Ru-HT catalyst and KBr was pelletized. The IR spectrum was recorded on an IBM Model IR/44 FTIR spectrometer.

CO-HYDROGENATION

About 0.5g of Ru-HT catalyst was loaded into a 1/4" OD, 316 stainless steel, tubular, single pass reactor. The catalyst sample was reduced in flowing hydrogen (Matheson, UHP) at 275°C for 6h. The reduction temperature was achieved at a heating rate of 5°C/min. The CO hydrogenation reaction was carried out between 225-275°C, and from atmospheric pressure to 190 psig at a conversion of less than 5%, in order to avoid mass and heat transfer limitations. A H_2/CO flow ratio of 2.0 was maintained

using mass flow controllers. The incoming gases were further purified by passing through a manganese/silica [9] oxygen scrubber, Linde 4Å molecular sieve to remove water and through an Al_2O_3 trap maintained at 200 K to remove metal carbonyls. The reactor effluent was transferred through a heated line to a Hewlett-Packard 5890Å GC equiped with automatic gas sampling valve and flame ionization detector. The hydrocarbons were separated using a 60m-long, 0.25 mm dia, 1μm-thick SP2100™ coated, fused silica capillary column.

RESULTS AND DISCUSSIONS

The thermogram presented in Figure 1 for $Mg_6Al_2(OH)_{16}.CO_3.4H_2O$ exhibits four distinct regions, in agreement with the observations of Reichle [3]. The first region (25°-250°C) was attributed to the loss of interstitial water. At the second region (250°-325°C) the loss of water is accompanied by slow dehydroxylation. In the third (325°-500°C), rapid dehydroxylation and loss of carbonate are accompanied by HT phase transformation to mixed metal oxides. In the final region (>500°C), a stable mixed-oxide phase is irreversibly formed. According to Reichle [3], the highest temperature at which the HT phase was stable is 275°C. Therefore, we investigated the thermal stability of HT at 275°C temperature for 4h. As seen in Figure 2, there was no loss in weight after reaching 275°C over 4h period. A similar thermal treatment at 350°C resulted in a significant loss of weight even at the isothermal condition. Therefore, we used 275°C as the reduction temperature for ruthenium and the highest reaction temperature for CO hydrogenation.

The FTIR spectrum for the $Ru_3(CO)_{12}$-HT impregnation product is presented in Figure 3. The two peaks at 2047 and 1965 cm^{-1} were assigned to a mononuclear $[Ru(CO)_x(OM\equiv)_2]_n$, grafted species [4,5,10]. In this case M is either Al or Mg ions. The degradation of the neutral metal cluster carbonyl, due to their reaction with surface hydroxyl groups, results in the formation of partially oxidized grafted species on the surface of HT. Analogous species osmium complex were known to form on bulk silica and alumina supports [11-13].

The selectivity of the hydrogen-reduced Ru-HT catalyst for various hydrocarbon at 275°C at pressures ranging from 0-190 psig is tabulated in Table 1. The production of methane decreased while the total alcohol synthesis increased with increasing pressure. An opposite trend was observed with increasing temperature (Table 2). That is, the methane production increased while the alcohol production decreased when the temperature was raised from 260 to 275°C at a constant pressures of 120 psig. The percentage of various alcohols produced are presented in Table 3 as a function of pressure at 275°C. In Table 4 the selectivity is presented as a function of temperature at a constant pressure of 120 psig. It is interesting to note that

the methanol fraction is independent of pressure, but it increases with increasing temperature at constant pressure.

Metals such as Pt, Pd and Ir are known to non-dissociatively adsorb CO even at high temperature and to produce methanol almost exclusively [14]. Katzer et al [14] observed that the methanol production was related to the concentration of non-dissociatively adsorbed CO. Rhodium, however, is selective to both alcohols and hydrocarbons, depending on the nature of the material that supports it [15-17]. Rh supported on MgO is more selective towards MeOH, but when supported on a non-basic material, it is selective to hydrocarbons.

Ruthenium is known to dissociate CO at reaction temperatures and to produce mainly hydrocarbons. There are a few exceptions, of course. Some workers [18,19] have reported about 20% selectivity to alcohols for alkali promoted Ru and for Ru on MgO catalysts at pressure of 300-1000 psig. It appears that the basic environment of the Ru is responsible for such high selectivity for alcohols. The selectivity toward alcohols for the Ru-HT observed in this study is comparable to that for Ru on MgO or alkali-promoted Ru catalysts [18,19]. It is particularly noteworthy, however, that the reaction pressure employed in this study was far less than the others.

Since HT is an extremely basic material, it appears that it has altered the characteristics of Ru metal by limiting the dissociation of CO. The lower methane production and higher alcohol yield (in particular, the higher MeOH yield) at lower temperature supports this hypothesis. At higher temperatures, the CO disassociation is increased and thus the methanation reaction is promoted; at the same time, the lower concentration of undissociated CO reduces the selectivity of alcohols.

SUMMARY

Our results clearly demonstrate that the support material can alter the CO hydrogenation selectivity of ruthenium. This metal typically is highly selective to straight-chain hydrocarbons, but the selectivity at relatively low reaction pressures has been altered by the presence of a basic support to produce alcohols. In fact, the alcohol selectivities reported here for Ru have not been achieved at such low pressures previously.

ACKNOWLEDGEMENTS

The National Science Foundation Division of Materials Research (DMR-8514154), and the Michigan State University Center for Fundamental Materials Research are gratefully acknowledged for their financial support of this research.

LIST OF REFERENCES

1. Miyata, S., *Clays and clay Miner.*, **23**, 369 (1975).

2. Rouxhet, P. G. and Taylor, H. F. W., *Chima.*, **23**, 480 (1969).

3. Reichle, W. T., Kang, S. Y. and Eherhardt, D. S., *J. Catal.*, **101**, 352 (1986).

4. Giannelis, E. P. and Pinnavaia, T. J., *J. Am. Chem. Soc.*, in press.

5. Giannelis, E. P., Rightor, E. G. and Pinnavaia, T. J., *J. Am. Chem. Soc.*, in press.

6. Vannice., M. A., *Catal. Rev.-Sci., Eng.*, **14(2)**, 153 (1976).

7. King, D. L., *J. Catal.*, **15**, 38 (1976).

8. Reichle, W. T., *J. Catal.*, **94**, 547 (1985).

9. McIlurick, C. R. and Phillips, C. S. G., *J. Phys. E.*, **6**, 1973 (1983).

10. Kuznetsov, V. L., Bell, A. T. and Yermakov, Y. I., *J. Catal.*, **65**, 374 (1980).

11. Deeba, M., Gates, B. C., *J. Catal.*, **67**, 337 (1981).

12. Psaro, R., Ugo, R., Zanderrighi, G. M., Besson, B., Smith, A. K. and Basset, J. M., *J. Organometal. Chem.*, **13**, 215 (1981).

13. Crawford, J. E., Melson, G. A., Makovsky, L. E. and Brown, F. R., *J. Catal.*, **83**, 454 (1983).

14. Katzer, J. R., Sleight, A. W., Gajardo, P., Michael, J. B., Gleason, E. F. and McMillan, S., *Faraday Disc. Chem. Soc.*, **72**, 121 (1981).

15. Sexton, B. A. and Somorjai, G. A., *J. Catal.*, **46**, 167 (1977).

16. van Der Lee, G., Schuller, B., Post, H., Favre, T. L. F. and Ponec, V., *J. Catal.*, **98**, 522 (1986).

17. Ichikawa, M., *Bull, Chem. Soc. Jap.*, **51(8)**, 2268 (1978).

18. Bossi, A., Garbassi, F. and Petrinni, G., *"Preprints of 7th Int. Cong. Catal."*, Tokyo, E4 (1980).

19. Pierantozi, R., Valagene, E. G., Nordquist, A. F. and Dyer, P. N., *J. Molec. Catal.*, **21**, 189 (1983).

Table 1

CO Hydrogenation Selectivity of Ru/HT at Various Pressures (275°C)[a]

Pressure (psig)	Hydrocarbon and Total Alcohol Yields, Wt %							
	C_1	C_2	C_3	C_4	C_5	C_6	C_{7+}	ALC
0	85.5	8.8	5.7	tr				0.0
70	65.2	8.3	7.0	4.5	2.8	1.0	0.9	10.0
120	63.5	7.5	7.4	4.5	2.4	1.1	0.4	13.2
170	54.1	7.6	9.1	6.0	3.3	1.5	1.0	17.6
190	56.7	8.0	9.7	6.1	3.5	2.4	0.7	21.8

[a]$H_2/CO = 2$, Conv<5%, GHSV = 1000 to 3000 h^{-1}, ~ 0.5g of catlyst. Time on stream >24h.

Table 2

CO Hydrogenation Selectivity of Ru/HT at Constant Pressure (120 psig)[a]

Temp. (°C)	Hydrocarbon and Total Alcohol Yields, Wt %							
	C_1	C_2	C_3	C_4	C_5	C_6	C_{7+}	ALC
260	48.0	7.0	9.3	6.7	4.0	3.5	tr	20.8
275	63.5	7.5	7.4	4.5	2.4	1.1	0.4	13.2

[a]$H_2/CO = 2$, Conv<5%, GHSV = 1000 to 3000 h^{-1}, ~ 0.5g of catlyst. Time on stream >24h.

Table 3

C_1-C_4 Alcohol Distribution in the Total Alcohol Product Stream for Ru/HT at 275°C[a]

Pressure (psig)	MeOH	EtOH	PrOH	BuOH
0	0	0	0	0
70	78	22	0	0
120	75	20	5	0
170	78	18	4	0
190	74	17	4	4

[a]H_2/CO = 2, Conv<5%, GHSV = 1000 to 3000 h^{-1}, ~ 0.5g of catlyst. Time on stream >24h.

Table 4

C_1-C_3 Alcohol Distribution in the Total Alcohol Product Stream for Ru/HT at 120 psig[a]

Temperature (°C)	MeOH	EtOH	PrOH
260	81	13	6
275	75	18	4

[a]H_2/CO = 2, Conv<5%, GHSV = 1000 to 3000 h^{-1}, ~ 0.5g of catlyst. Time on stream >24h.

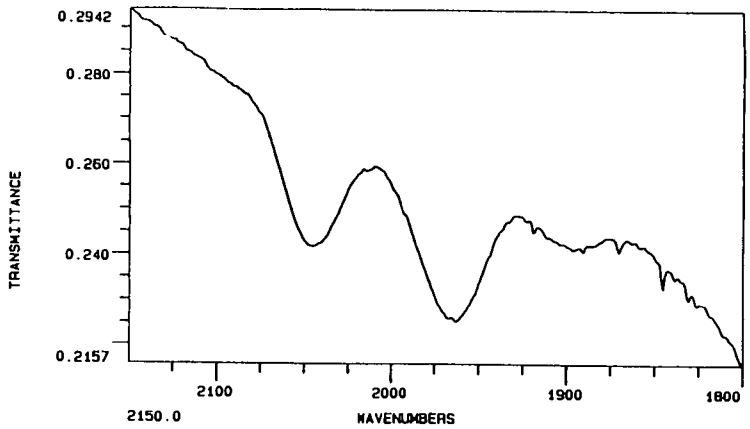

Figure 1 FTIR spectrum of the reaction product obtained from the "impregnation" of $Ru_3(CO)_{12}$ on HT. The two major peaks at 2047 and 1965 cm^{-1} indicate the presence of grafted $Ru(CO)_x(OM\equiv)_n$.

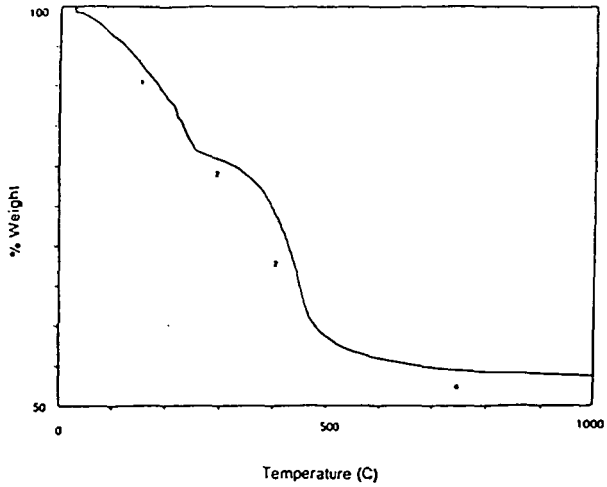

Figure 2 Themogravimetric analysis of HT. The heating rate was 5°C/min. The four (1-4) regions are discussed in the text

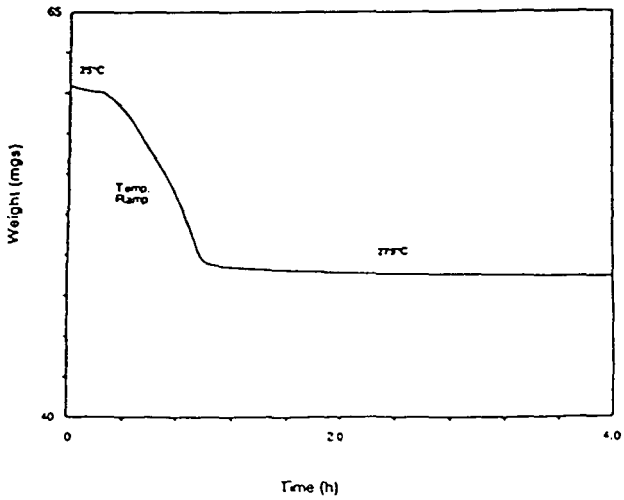

Figure 3. Thermogram of HT. Heating from 25° to 275°C was achieved using a temperature ramp of 5°C/min.

THE EFFECTS OF PYROLYSIS CONDITIONS ON THE MACROPORE STRUCTURE OF COAL CHARS

Kyriacos Zygourakis
Department of Chemical Engineering
Rice University
Houston, TX 77251-1892

INTRODUCTION

Pyrolysis is the first stage of direct coal utilization processes. As coal particles are heated in a reactor, they release most of their volatile constituents in the form of gases and tars. The chemical transformations characterizing the pyrolysis stage are accompanied by complex morphological transformations that determine the pore structure and, consequently, the reactivity of the produced chars during the subsequent combustion or gasification stage. Gasification processes are usually diffusion-limited since the various heterogeneous reactions take place at elevated temperatures. Low utilization of the surface area associated with the micropores present in chars is expected under such conditions. Reactions occur mostly in the larger macropores that are close to the particle exterior and pore accessibility to reactants becomes a major factor in determining gasification rates. Initially, internal pores may be inaccessible to reactants. As the reaction proceeds, however, walls of closed pores will burn away exposing surface area previously unavailable for reaction and leading to substantial particle fragmentation. The opening of closed porosity, the formation of a progressively more tortuous particle exterior and the fragmentation of the original particles can lead to large enhancements of the observed gasification rates.

The major factors affecting the macropore structure of chars are the rank of the parent coals and the pyrolysis conditions. Coals can be broadly categorized as **plastic** or **non-plastic** according to their behavior during pyrolysis. Plastic coals soften as they are heated up and behave as highly viscous non-newtonian fluids over a broad temperature range. Three phases are found to coexist during this plasticity stage: a viscous (but optically isotropic) coal melt, an anisotropic liquid crystalline phase and a gaseous phase. The volatile gases form bubbles that grow and coalesce swelling the coal particles and leading to the formation of highly cellular internal pore structures that are characteristic of chars derived from plastic coals. Non-plastic coals, on the other hand, do not soften and do not undergo drastic macropore structure transformations during the pyrolysis stage. Bituminous and subbituminous coals are generally considered to be plastic, while lignites and other low rank coals belong to the non-plastic category.

The operating conditions influencing most strongly the pyrolysis process are the heating rate, the particle size and the pressure. Existing literature data offer little quantitative information on the effect of operating conditions on macropore structures, since the majority of past studies have concentrated on studying the kinetics of pyrolysis reactions and the distributions of the obtained products. Previous studies (Howard, 1981; Oh et al., 1984), however, indicate that the kinetic and transport processes occurring during pyrolysis (such as the rate of volatile release, the diffusion of volatiles into the bubbles, the transport of volatiles to the particle exterior etc.) will be governed by the time-temperature history of the coal particles. Hence, the pyrolysis heating rate is expected to have the strongest effect on the macropore structure of the chars (Hamilton, 1981).

EFFECTS OF PYROLYSIS HEATING RATE ON MACROPORE STRUCTURE OF CHARS

A plastic coal (Illinois #6) was studied first. Coal particles in the 50-60 mesh (250-300 μm) range were pyrolyzed in a captive sample microreactor at five different heating rates: 0.1, 1.0, 10, 100 and 1000 °C/s. Char particles

collected from ten runs at each set of conditions were embedded in an epoxy-resin block, and one side of the block was polished to reveal random cross-sections. Digitized images for 50 particle sections were acquired from each block and they were analyzed with the digital image processor to obtain the size distribution of the two-dimensional macropore profiles. Fig. 1 presents binary images of representative cross-sections of char particles produced at the various heating rates. The black areas of these images correspond to the char matrix, while the internal white areas are the cross-sectional profiles of macropores.

The lowest heating rate (0.1 °C/s) produced char particles exhibiting a few scattered large cavities with thick walls and several smaller cavities. This is consistent with the accepted pyrolysis mechanism involving formation and growth of volatile gas bubbles. Note that most of the particles shown in Fig. 1A have retained their angular shape and only a few cenospheres were observed. Calculations indicated a moderate pressure buildup in the particle interior, since the volatile production rates are slow enough to let the gas escape before the bubbles can grow to a large size. At faster heating rates, however, the volatile production rates increase substantially leading to considerably higher pressures in the particle interior and, thus, to larger bubble sizes and more particle swelling. At a heating rate of 1 °C/s, the formation of several thin-walled cavities was observed (Fig. 1B) and several pyrolyzed char particles started exhibiting a distinct cellular internal structure. At still higher heating rates, the cellular internal structure was dominant. Chars pyrolyzed at 100 and 1000 °C/s showed exclusively thin-walled cellular structures with a few large cavities and a group of smaller secondary vesicles formed in the thin walls of the larger ones. One should note also that large particle swelling occurs at the higher heating rates leading to particles with very high porosity.

Table I summarizes the basic stereological properties for the five Illinois #6 chars. Estimates of the macroporosity ε can be obtained (Weibel, 1980) from the two-dimensional particle cross-sections using the formula $\varepsilon = A_a/A_c$, where A_a is the total area of pore profiles and A_c is the total area of the char particle sections. An estimator of the macropore surface density S_v (in (cm^2 pore surface)/(cm^3 particle)) is given (Weibel, 1980) by $S_a = B_a/A_c$, where B_a is the total pore profile boundary length and A_c is the total area of particle cross-sections. Both ε and S_v can be estimated from two-dimensional sections without any restricting assumptions concerning the geometrical shape of the pores (DeHoff, 1983). We have also obtained the macropore volume distributions, but these measurements were based on the assumption that the macropores can be modeled as non-overlapping spheres with randomly distributed radius.

Increasing heating rates produced chars with consistently higher porosity and maximum pore radius. The increase in porosity, however, tends to level off at the higher heating rates. An increase in the macropore surface area density S_v was observed as the pyrolysis heating rate increased from 0.1 to 10 °C/s. However, S_v decreased at higher heating rates due to the appearance of very large pore cavities in the highly-swollen char particles (see Figs. 1D and 1E). The property of interest for reaction engineering calculations, however, is the specific macropore surface area S_g expressed in (cm^2 pore surface)/(cm^3 solid char). Table I shows that S_g increased dramatically with increasing heating rates. This is an indication that Illinois #6 chars produced at high pyrolysis heating rates will be more reactive at elevated temperatures where low utilization of the micropores is expected.

Pyrolysis heating rates had a much smaller effect on the macropore structure of chars produced from a non-plastic lignite coal (Wilcox, Texas). Earlier indirect measurements have indicated that the initial macropore network of non-plastic (low rank) coals remains essentially intact during pyrolysis (Gavalas and Wilks, 1980). In order to study the effect of pyrolysis heating rate on the lignite char structure, coal particles in the the 50-60 mesh size range were pyrolyzed in our microreactor at three heating rates (0.1, 10 and 1000 °C/s). Fig. 2 shows

representative images of the polished char sections taken for each sample. In contrast to the Illinois#6 chars, the cross-sections of lignite char particles show almost no visible change as the heating rate is increased. A comparison of particle sections obtained from the pyrolyzed chars and the parent coal revealed that several large fractures and cracks were formed during the pyrolysis stage. Table II presents the basic structural properties for the lignite chars. These stereological measurements show small effects of the pyrolysis heating rate both on the particle porosity and on the specific macropore surface area S_g of the char samples.

EFFECTS OF COAL PARTICLE SIZE ON MACROPORE STRUCTURE OF CHARS

Heat transfer in pyrolyzing coal particles can be significantly affected by the particle size. If external heat transfer controls the pyrolysis process, particle temperature will remain constant during heatup and the heating rate will decrease with increasing particle size. On the other hand, if the rate of external heat transfer is high enough, high heating rates and large particle sizes can lead to significant temperature gradients within the particle. Under such conditions, the pyrolysis reaction rates will vary significantly inside the particles.

In order to quantify the effects of particle size on the macropore structure of chars produced from the Illinois #6 coal, two additional size fractions of coal particles were pyrolyzed at 10 °C/s: 25-28 mesh (589-710 μm particle diameter) and 100-120 mesh (125-149 μm particle diameter). Thus, the mass of individual particles varied by about two orders of magnitude for the pyrolysis runs at 10 °C/s. This heating rate was selected in order to facilitate the detection of differences in the pore structure possibly caused by changes in the internal heating rate of the particles.

Fig. 3 presents representative cross-sections of char particles produced from the additional runs at 10 °C/s. A comparison of the cross-sections shown in Fig. 3 and Fig. 1C reveals very different pore structures for the three chars. For the smallest size fraction (Fig. 3A), we observe fewer pores per particle and the pore shape is rather rounded. The largest size fraction, on the other hand, exhibits numerous macropores per particle. The boundaries of the pore profiles are very tortuous and we see again the characteristic cellular pore structure with small pores embedded in the walls separating the larger cavities.

Table III summarizes the measurements for the macropore properties. The interesting result here is that the macroporosity of the particles was not affected by their size. This indicates that particle size did not affect the internal heating rate, pointing out that external heat transfer is not limiting for our pyrolysis reactor. The maximum pore radius observed fell from 284 μm for the 25-28 mesh sample to 51 μm for the 100-120 mesh sample. This decrease in macropore size was accompanied by an increase in the specific surface area of macropores per unit volume of char particle.

It must be noted here that maceral segregation may complicate the determination of particle size effects on the macropore structure of chars produced from plastic coals. Due to differences in the mechanical properties of the various coal macerals, grinding and sifting procedures may lead to enrichment of certain macerals in certain size fractions (i.e. small size fractions may contain more exinite). Thus, the well-known differences in the plastic behavior and volatile content of coal macerals can affect the macropore structure of different size fractions.

MODELING OF CHAR GASIFICATION

Discrete models were developed to treat the problem of char gasification at high temperatures. Low utilization of the surface area associated with the micropores is expected under such conditions, and the accessibility and surface area of the

macropores become the dominant factors in determining the temporal evolution of reaction rates.

Our earlier discrete models (Sandmann and Zygourakis, 1986) defined the pores of a solid reactant (char) by overlapping regular geometrical entities (circles, spheres or cylinders) of a given size distribution. For example, two-dimensional simulations modeled the pore cross-sections as an assemblage of overlapping circles, grew the pores by increasing the circle diameters by a fixed amount at each time step and then determined which cells had to be changed (from char to pore) to reflect the new pore dimension. As shown in Figs. 1 through 5, however, highly irregular pore structures are observed when char particle cross-sections are viewed under the microscope.

The new discrete models are based on an **erosion algorithm** and they avoid the computational complexities introduced when pores of arbitrary geometry are approximated by overlapping regular geometric entities. These models again employ a computational grid to represent the reacting porous solid and the macropores. However, the initial computational grids are obtained directly from digitized images of actual particle cross-sections viewed under the microscope. These images are accurate discrete approximations of a slice of the actual reacting solid. The incorporation of sophisticated digital image processing techniques in the gasification models is perhaps the most attractive feature of the new approach. For the runs presented below, the following assumptions were made.

- Only the surface area directly accessible to reactants from the irregular particle exterior participates in the reaction. Macropores in the particle interior are not initially available for reaction. When the reaction front reaches these interior pores, however, their surface area becomes available for reaction.
- Diffusional limitations in the macropores that are open to the exterior are neglected. This assumption is not expected to lead to significant errors in model predictions for the Illinois #6 chars given the large size of their internal cavities.
- Internal pores for any cross-section do not become available for reaction due to burn-through occurring at planes above or below the studied one.

The last two assumptions have been relaxed in more recent versions of the erosion algorithm. At each simulation step, the computational grid is scanned and the surface area available for reaction is identified. A statistical method is then used to erode away a single layer of pixels corresponding to the char matrix from the exterior of the char particle (and from the exterior of all particle fragments). A 3x3 neighborhood around each char pixel is examined to determine whether or not it is on an edge boundary and should be reacted. The number of pixels reacting at each step is counted and the solid reactant conversion is calculated. This process can be repeated until a specified conversion has been achieved. Particle fragmentation can also be investigated with this model by identifying all the isolated char fragments.

Fig. 4 presents the temporal evolution of reaction rates for the four particle cross sections presented in Fig. 1A. The dimensionless rate R_e and time θ are defined as

$$R_e = \frac{1}{m_o}\frac{dm}{dt}\Delta\tau \qquad \theta = \frac{t}{\Delta\tau} = \frac{t\ R_s(c,T)}{\Delta x\ \rho_s}$$

where m_o is the mass of unreacted char, (dm/dt) is the rate of change of the reacting char mass, $R_s(c,T)$ is the intrinsic reaction rate per unit of surface area, ρ_s is the density of the solid, Δx is the pixel size of the image and $\Delta\tau$ is the time required to react a layer of solid with uniform thickness equal to 1 μm.

The erosion rate for the particle exhibiting the large cenosphere (ILL106 in Fig. 1A) decreases initially and then jumps to very high levels when the large internal cavity opens up for reaction. At this point, the cross-section fragments considerably and disappears soon thereafter. The ILL102 particle in Fig. 1A has several large cavities with thin walls separating them from the particle exterior. Thus, the erosion rates calculated for this cross-section jump to very high values as these cavities open up at fairly low conversions (less than 20%) The ILL105 cross-section of Fig. 1A, on the other hand, exhibits numerous smaller cavities that open up for reaction at different time levels giving rise to the characteristic jumps in the reaction rate observed in the experiments by Sundback et. al. (1984). In this case the reaction rates remain at relatively high levels for a large time interval. Finally, the more "solid" cross-section of Fig. 1A (ILL101) exhibits a steady decrease in erosion rate for a long period of time until the single large cavity opens up. A large jump in the erosion rate is observed at this point and the rate decreases slowly after achieving its maximum value. Another interesting observation from Fig. 4 concerns the wide range of particle burnout times predicted by the discrete simulations. These variations are clearly attributed to the large internal cavities and the different macroporosities of the individual particles.

Simulation results from runs on all particle sections can provide an indication of the expected average gasification behavior for a char sample. Fig. 5 presents the average reaction rate vs. time patterns for the three Illinois #6 chars produced by pyrolyzing coal particles of different sizes at 10 °C/s. Due to its small particle size and large external surface area, the 100-120 mesh sample exhibits a high initial rate, a sharp rate maximum and very short reaction times. As the particle size is increased, the reaction rates decrease and their burnout times increase significantly.

ACKNOWLEDGMENT

This work was partially supported by the Department of Energy under the contract DE-FG22-87PC79930.

REFERENCES

Gavalas, G.R. and Wilks, K.A., AIChE J., 26, 201 (1980).

Hamilton, L.H., Fuel, 60, 955 (1981).

DeHoff, R.T., J. Microscopy, 131, 259 (1983).

Howard, J.B., "Fundamentals of Coal Pyrolysis and Hydropyrolysis", in Chemistry of Coal Utilization, p. 665, Elliott, M.A., Ed., John Wiley (1981).

Oh, M., Peters, W.A. and Howard, J.B., Procs. 1983 International Conference on Coal Science, p. 483, International Energy Agency (1983).

Sandmann, C.W. and Zygourakis, K., Chem. Eng. Sci., 41, 733 (1986).

Sundback, C.A., Beer, J.M. and Sarofim, A.F., Procs. 20th International Symposium on Combustion, p. 1495, Ann Arbor, Michigan, August 12-17 (1984).

Weibel, E.R., "Stereological Methods", vol. 2, Academic Press (1980).

TABLE I

Macropore Structural Properties of Illinois #6 Chars Produced at Various Heating Rates

Heating Rate	Porosity	Surface Area Density (cm^2/cm^3 particle)	Specific Surface Area (cm^2/cm^3 solid)	Maximum Pore Radius (μm)
0.1	0.356	527	822	135
1.	0.526	759	1,599	173
10.	0.709	908	3,116	153
100.	0.795	700	3,409	194
1000.	0.873	695	5,470	224

TABLE II

Macropore Structural Properties of Lignite Chars Produced at Various Heating Rates

Heating Rate	Porosity	Surface Area Density (cm^2/cm^3 particle)	Specific Surface Area (cm^2/cm^3 solid)	Maximum Pore Radius (μm)
0.1	0.140	1,011	1,176	31.0
10.	0.153	1,107	1,307	25.5
1000.	0.195	1,369	1,700	25.6

TABLE III

Effects of Coal Particle Size on the Macropore Structural Properties of Illinois #6 Chars

Particle Size (mesh)	Porosity	Surface Area Density (cm^2/cm^3 particle)	Specific Surface Area (cm^2/cm^3 solid)	Maximum Pore Radius (μm)
100-120	0.689	1,898	6,106	50.5
50- 60	0.708	908	3,116	153
25- 28	0.688	729	2,339	351

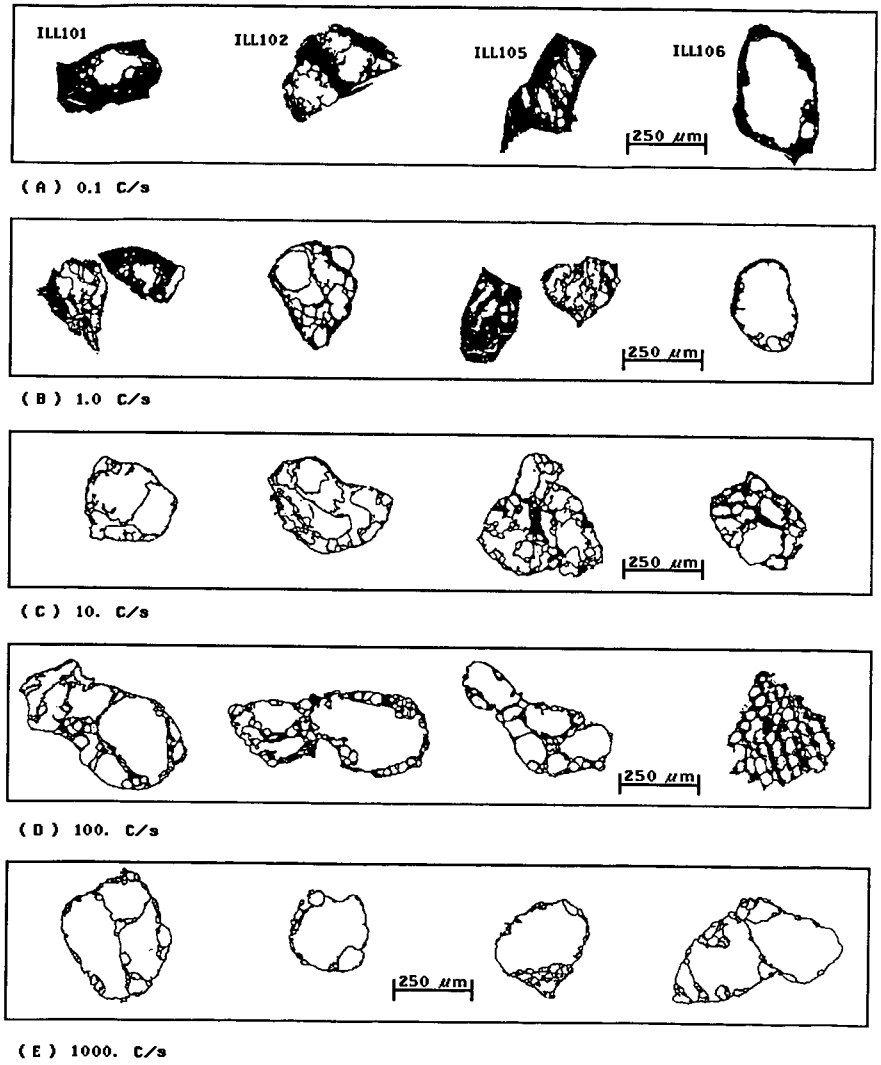

Figure 1: Binary images of particle cross-sections for Illinois #6 chars produced at various pyrolysis heating rates (Coal particle size: 50-60 mesh).

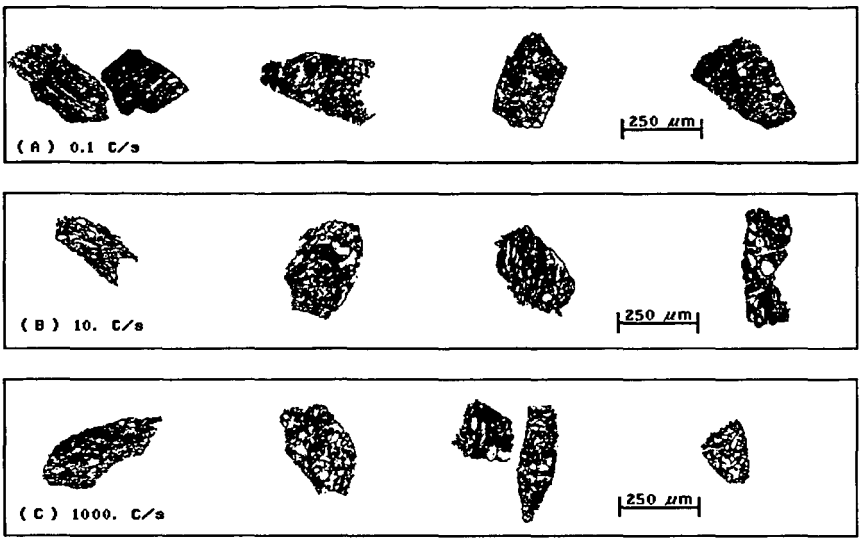

Figure 2: Binary images of particle cross-sections for lignite chars produced at various pyrolysis heating rates (Coal particle size: 50-60 mesh).

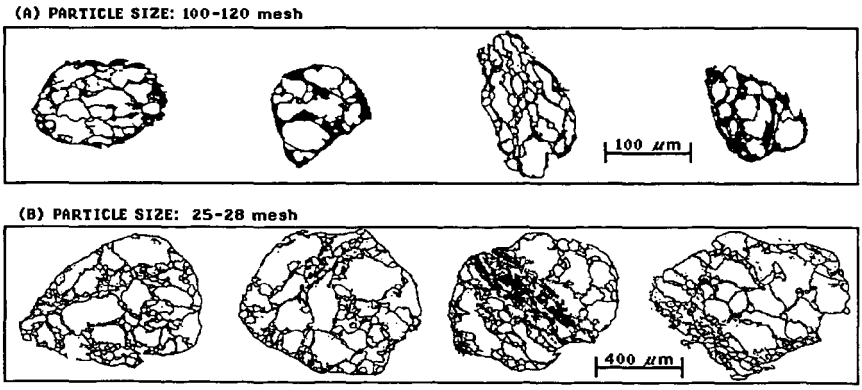

Figure 3: Binary images of particle cross-sections for Illinois #6 chars produced from different sizes of coal particles (Heating Rate: 10 °C/s).

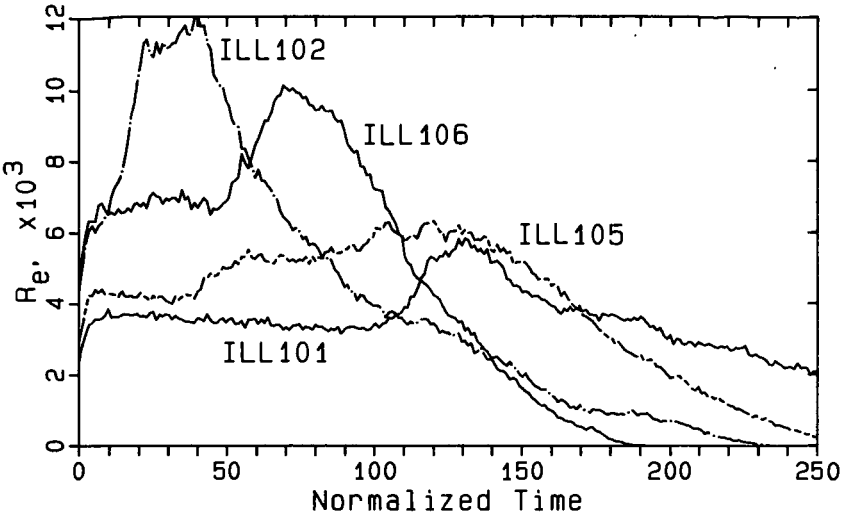

Figure 4: Temporal evolution of predicted reaction rates from four simulation runs with Illinois #6 char particles.

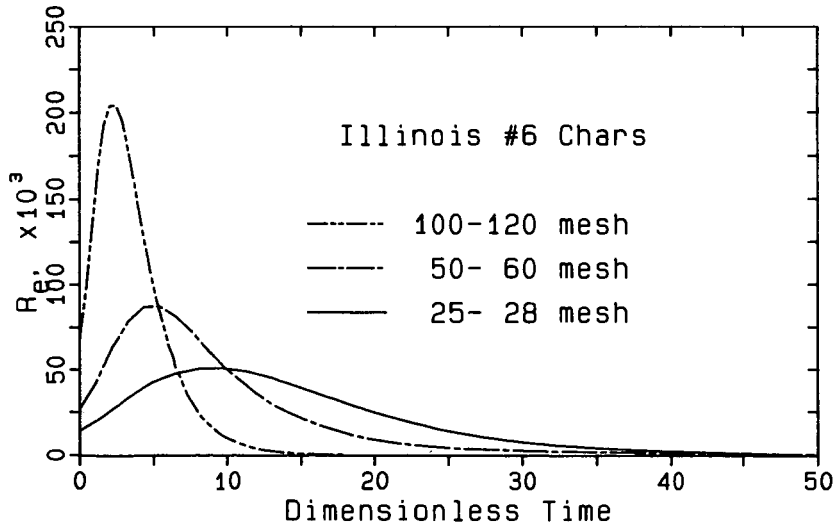

Figure 5: Effect of coal particle size on the reaction rates predicted for three Illinois #6 chars. Model predictions are averages for 48 particle cross-sections.

THE EFFECT OF MILD OXIDATION ON THE THERMAL DESULFURIZATION AND HYDRODESULFURIZATION OF TWO ILLINOIS BITUMINOUS COALS IN A FLUIDIZED BED REACTOR

M. D. Stephenson, A. D. Williams, M. Rostam-Abadi and C. W. Kruse
Illinois State Geological Survey
615 East Peabody Drive
Champaign, IL 61820

ABSTRACT

Two high sulfur Illinois No. 6 coals were desulfurized in a fluidized bed reactor (FBR) to less than one percent sulfur by a thermal and chemical approach which included pyrolysis followed by char hydrodesulfurization. Chars were prepared for hydrodesulfurization by three different procedures; pyrolysis only, oxidation prior to pyrolysis and oxidation after pyrolysis. Pre-oxidizing conditions reduced agglomeration during pyrolysis and for one coal, which was physically cleaned, it led to significantly increased overall sulfur removal compared to the non-oxidized char. Oxidation after pyrolysis had no obvious beneficial effects. Under the best conditions tested, chars were produced having sulfur contents less than one percent for both coals.

INTRODUCTION

Efforts to abate the deleterious impact of burning high sulfur coals are easily classified into three approaches. Post-combustion desulfurization, which includes wet limestone scrubbing, is being utilized by electric utilities but is beset by high capital and operating costs. The second category, desulfurization during combustion, includes fluidized bed combustion. This method of sulfur dioxide control is quite promising, but has not yet gained widespread usage by electric utilities. The third classification is precombustion desulfurization which includes physical and chemical coal cleaning. As yet, only physical cleaning is used commercially but it is limited to inorganic sulfur removal.

One approach to removing sulfur, including organic sulfur, is to first pyrolyze the coal and follow this step with high temperature hydrodesulfurization. This combination of steps is quite effective in removing a significant amount of the total sulfur from high sulfur coals. The products of these two steps include up to one barrel of pyrolysis oil per ton of coal, a low to medium Btu gas, coal char and elemental sulfur [1]. The relative amounts of each product depend on the coal feed and on the conditions used for the pyrolysis and hydrodesulfurization steps.

In the work described here, two Illinois basin coals were pyrolyzed in a fluidized bed reactor under a variety of conditions and then subjected to hydrodesulfurization. Three pyrolysis treatments were employed. The first treatment, denoted as pre-oxidized, consisted of a mild oxidation prior to pyrolysis, followed by pyrolysis under nitrogen. The second treatment, denoted as non-oxidized, was pyrolysis under a nitrogen atmosphere. The third treatment, denoted as post-oxidized was identical to the second or non-oxidized treatment, except that a mild oxidation occurred after the pyrolysis step. Thus, three chars were produced, pre-oxidized, non-oxidized, and post-oxidized, and these were used as hydrodesulfurization feeds.

While preoxidation is effective in decaking highly agglomerating coals [2], it does lower the yield of pyrolysis oil and is undesirable for this reason alone. However, preoxidation apparently leads to larger pores in an otherwise microporous char [3]. This tends to increase both the rate and the extent of hydrodesulfurization [4]. Since pre-oxidation has been effective in producing chars which are more reactive towards hydrogen, it was hypothesized that an oxidation of the char after removal of the volatile matter might also be effective. This processing sequence would permit maximum conversion of coal to pyrolysis oil. Agglomeration would be averted in some other way such as multistaged heating.

EXPERIMENTAL

Coal samples - Two Illinois No. 6 coals were used in this study. The samples were obtained form the Illinois Basin Coal Sample Program (IBCSP) and are referred to as the IBCSP-1 and IBCSP-4 samples [5]. The IBCSP-1 coal is a mine-washed sample containing 4.62% total sulfur of which 3.35% is organic sulfur. The IBCSP-4 sample is a Run-of-Mine sample containing 34% ash and 4.2% total sulfur (equivalent to 9.87 lbs SO_2/MMBtu). In order to reduce the mineral matter and pyritic sulfur content, two types of physically cleaned coal were prepared from the IBCSP-4. A "deslimed" coal was prepared by slurrying and agitating the sample and then sieving it over a 235 mesh screen. The step effectively reduced the clay content of the sample, but retained much of the coarser pyrite and other mineral matter. The sample after treatment had 14.8% ash, 3.05% pyrite and 6.28% total sulfur on a dry ash free (daf) basis. A 28x200 mesh fraction was prepared from the deslimed coal utilizing a staged crushing and screening technique to ensure that the size fraction was representative of the starting material.

A second sample of physically cleaned IBCSP-4 was prepared using a gravity concentrating table in order to reject liberated coarse pyrite grains and other mineral matter. The sample was also deslimed using the above procedure to reject any clays that reported to the coal fraction. Following this treatment, the "tabled" coal had 4.18% total sulfur of which 1.22% sulfur was pyritic. Analyses of the 28x200 mesh fractions of both tabled and deslimed coal appear in Table 1.

Char production - Chars for hydrodesulfurization experiments were prepared in bulk using a 2-inch, batch, fluidized bed reactor. The description of this apparatus appears elsewhere [6]. Basically, 200-gm batches of coal were pyrolyzed in this system and when appropriate, reacted with gaseous streams of dilute oxygen. The reactor was constructed of type 304 stainless steel and was heated externally by a 3-inch, tube furnace. A microprocessor was used to control the bed temperature via a type K thermocouple immersed in the center of the bed.

The three different types of chars prepared here are designated as pre-oxidized, non-oxidized, and post-oxidized. Several batch runs at each treatment regime were necessary to provide kilogram-quantities of each type of char for hydrodesulfurization tests. After combining the appropriate batches, the chars were then riffled into 25-gm portions, and stored under inert conditions in sample bottles which were sealed with paraffin.

Pre-oxidized chars were prepared by heating a 200-gm charge of coal to 250°C in the 2-inch FBR using nitrogen as a fluidizing gas. Once at 250°C, the fluidizing gas was switched to five percent oxygen in nitrogen. The coal was fluidized under these conditions for 30 min. at which time the fluidizing gas was switched back to nitrogen. The temperature was raised to 850°C and held there for 15 min. The reactor was cooled to ambient conditions under a purge of nitrogen.

Non-oxidized chars were prepared using heating schedules similar to those used by the FMC Char Oil Energy Development (COED) process [7]. Multistaged or slow heating of our coals was necessary to avoid agglomeration. For IBCSP-4 coal, four soak temperatures were used, 350, 375, 400, and 425°C. For IBCSP-1 coal, a heating rate of 1.7°C/min was employed without any isothermal soak periods. Agglomeration did not occur. Once the temperature reached 850°C, the char was held for 15 min. before cooling to ambient conditions under a purge of nitrogen.

The post-oxidized samples were prepared in the same way as the non-oxidized samples with one exception. During the cool down period, the bed temperature was allowed to reach 450°C for IBCSP-1 coal or 250°C for IBCSP-4 coal and then held at that temperature while five percent oxygen was admitted as a fluidizing gas. The temperature was lowered to 250°C for the second coal because this temperature was preferable for a comparison of pre-oxidization with post-oxidation. The post-oxidative treatment was continued for 15 min. (IBCSP-1) or 30 min. (IBCSP-4) after which the fluidizing gas was switched back to nitrogen. The reactor was then cooled to ambient conditions.

Hydrodesulfurization - A 1-inch batch fluidized bed hydrodesulfurizer was used for char hydrodesulfurization tests. The reactor was constructed from a 24-inch length of type 446 stainless steel, schedule 40 pipe. A distributor plate of porous Hastelloy-X stainless steel (average pore size of 10 microns) was located nine inches from the bottom of the pipe. The space below the plate was filled with 1/4-inch ceramic Raschig rings which served as a gas preheater. Type 446 stainless steel caps were used at both ends of the reactor and were fitted to accept 1/4-inch tube fittings.

For each hydrodesulfurization (HDS) experiment, approximately 10 grams of char was accurately weighed and charged to the reactor. The sample was heated rapidly to the reaction temperature under a nitrogen flow which generally took about 45 min. Once the system reached the designated reaction temperature (±1°C), nitrogen was shut off and hydrogen was introduced to the reactor for a period of 90 minutes except where noted. When the desired treatment time had elapsed, hydrogen was turned off and nitrogen was once again introduced to the reactor. The reactor system was allowed to cool to near room temperature and the desulfurized char was removed, weighed and analyzed.

RESULTS AND DISCUSSION

Hydrodesulfurization of IBCSP-1 coal - Three chars were prepared from IBCSP-1 coal (pre-oxidation, non-oxidation, and post-oxidation). As shown in Figure 1, it can be seen that after pyrolysis, the post-oxidized char had the lowest sulfur content, approximately 2.4%. The non-oxidized char contained roughly 2.7% sulfur while the pre-oxidized char was marginally higher at 2.8% sulfur. Table 2 shows that hydrodesulfurized chars were produced having sulfur contents of 0.9% sulfur (an average of four combinations of temperature and hydrogen flow rate) from pre-oxidized coal compared to 1.2% average sulfur for the same array of conditions for the post-oxidized sample. By taking an average over the four sets of conditions, the effect of oxidation is measured over a wide range of conditions.

Examination of the percent initial char sulfur remaining after hydrodesulfurization reveals that hydrodesulfurization removed the most sulfur from the pre-oxidized sample. On average, only 27.4% of the sulfur initially present in the HDS sample remained after treatment. For the non-oxidized sample, 34.7%, on average, of the char's sulfur remained after hydrodesulfurization while 42.6%

remained for the post-oxidized char. Apparently, pre-oxidized chars are the most reactive towards hydrogen.

The final sulfur contents of the chars do not show appreciable differences between the treatments. Thus, there is no apparent advantage to post-oxidation as a part of a multi-step process which includes pyrolysis and hydrodesulfurization. As can be seen in Figure 1, sulfur is removed during the post-oxidation. The amount is relatively small but it is presumably converted to sulfur dioxide. Also, the amount of sulfur removed during hydrodesulfurization, the sulfur being removed as hydrogen sulfide, is the least of all three treatments. When considering product differences with regard to ease of gas cleanup, the post-oxidation treatment would be the most troublesome if it produced dilute sulfur dioxide that had to be removed from the gas stream. Mild pre-oxidation is not expected to yield appreciable sulfur dioxide. As there was no overall improvement in desulfurization when post-oxidized chars were used, this treatment was not investigated further with this particular coal.

Hydrodesulfurization of deslimed IBCSP-4 coal - As shown in Figure 2, the sulfur content of post-oxidized chars, non-oxidized chars and pre-oxidized chars produced from this coal with higher pyrite content were all similar. As shown in Table 3, all three types of hydrodesulfurized chars, on average, were similar in sulfur content. Although there is some scatter among the data, there is no treatment that is clearly superior. As with IBCSP-1, the post-oxidation treatment is of dubious merit and was not investigated further.

Pre-oxidation is quite effective in controlling agglomeration although pyrolysis oil yields are usually reduced. For the case of IBCSP-1 and IBCSP-4 (deslimed) coals, the sulfur content of the hydrodesulfurization products were not appreciably affected by pre-oxidation. However, due to its extreme effectiveness in handling caking coals, it was investigated further.

Effect of physical cleaning of IBCSP-4 coal - If a coal contains an appreciable quantity of pyritic sulfur, it is desirable to physically remove as much as possible before any processing. This is due to the thermodynamic limitations imposed by the unfavorable reaction between ferrous sulfide and hydrogen. Pyrite is converted to ferrous sulfide during pyrolysis and in order to remove this remaining inorganic sulfur, high hydrogen space velocities are required [8]. In the case of IBCSP-4, where the pyritic sulfur content was 3.05%, as compared to 1.34% pyritic sulfur in the IBCSP-1 coal, it seemed logical to remove additional pyrite by tabling. This step alone lowered the pyritic sulfur content to 1.22% or roughly that of the IBCSP-1 coal.

Removing pyritic sulfur from the tabled coal resulted in a vastly more effective hydrodesulfurization step. This is clearly demonstrated in the data shown in Table 4. Data in this table are organized in eight sets of two experiments. For each set, the only difference between the experiments is the level of physical cleaning. For the first set, lines one and two, the sulfur content in the product is 2.99% for the deslimed and 2.01% for the tabled coal. This same trend can be seen in each succeeding set of runs. On average the tabled coal resulted in a hydrodesulfurized product which was 1.25 percent lower in sulfur content.

A close inspection of the data in Table 4 reveals a synergistic effect between physical cleaning and oxidation. In lines 1 and 3, all factors remain constant except for oxidation. This is also true for lines 2 and 4, 5 and 7, 6 and 8, etc. For deslimed coal, the effect of oxidation on desulfurization is generally

quite small or nonexistent. However for tabled coal, desulfurization is significantly increased for all cases in which pre-oxidized chars were used. Thus, with this particular cleaned coal, pre-oxidation is quite effective in aiding hydrodesulfurization. The relative merit of a pre-oxidation step compared to no oxidation depends on technical and economic considerations. Pre-oxidation would permit coals to be pyrolyzed faster than by staged heating resulting in a cost savings. However, the decreased oil yields would impact negatively on the economics.

Concluding remarks - A combination of pyrolysis and char hydrodesulfurization is an effective method to reduce the total sulfur content of high sulfur coals to less than one percent. Oxidation, both before and after pyrolysis, generally had little effect on the overall level of desulfurization for two Illinois basin coals, although pre-oxidation markedly increased the extent of desulfurization for physically cleaned IBCSP-4. In fact, the only appreciably desulfurized IBCSP-4 chars had been pre-oxidized and physically cleaned.

REFERENCES

1. Stephenson, M. D. and C. W. Kruse, 1985, in Y. A. Attia, ed., Processing and Utilization of High sulfur coals, Coal Science and Technology 9, Elsevier, pp 373-392.

2. Boodman, M. S., T. F. Johnson and K. C. Krupinski, 1977, in T. D. Wheelock, ed., Coal desulfurization, ACS Symposium Series 64, 248-266, Washington, D.C.

3. Block, S. S., J. P. Sharp and L. J. Darlage, 1985, Fuel, 54(4), 113-119.

4. Fleming, D. K., R. Smith, and M. R. Y. Aquinio, 1977, in T. D. Wheelock, ed., Coal desulfurization, ACS Symposium Series 64, 267-279, Washington, D. C.

5. Kruse, C. W., R. D. Harvey, and D. M. Rapp, 1987, ACS Div. Fuel Chem. Preprints, 32(4),359-365.

6. Stephenson, M. D. and C. Liu, Quarterly Technical Report to the Center for Research on Sulfur in Coal for the period September 1, 1986-August 31, 1987, 40 pp., 1987.

7. Paige, W. A., 1977, Energy Communications, 3(2), 127-150.

8. Stephenson, M. D., M. Rostam-Abadi, L. A. Johnson and C. W. Kruse, 1985. in Y. A. Attia, ed., Processing and Utilization of High sulfur coals, Coal Science and Technology 9, Elsevier, pp 353-372.

ACKNOWLEDGEMENTS

This work was funded in part by grants from the Illinois Coal Development Board through the Center for Research on Sulfur in Coal. The authors gratefully acknowledge Mr. Scott Ellis, Mr. Jeffrey Sprague, and Dr. Gary Clauson for their laboratory expertise and Mr. Dave Rapp for his assistance in preparing physically cleaned coal samples.

Table 1. Analysis of feed coals.

Analysis	IBCSP-1	IBCSP-4	IBCSP-4 Deslimed	IBCSP-4 Tabled
Proximate, wt% as received				
Moisture	14.1	10.2	3.5	1.5
Volatile matter	37.9	27.4	36.6	38.3
Fixed carbon	39.2	28.2	45.1	50.4
Ash	8.8	34.2	14.8	9.8
Ultimate, wt% daf				
Hydrogen	5.42	5.25	5.26	4.64
Carbon	75.41	69.86	77.91	81.66
Nitrogen	1.32	1.22	1.57	1.90
Oxygen	12.96	11.29	8.97	7.61
Sulfur	4.75	6.37	6.28	4.18
pyritic	1.34	3.54	3.05	1.22
organic	3.34	2.67	3.23	2.86
sulfatic	0.07	0.15	tr	0.10
Calorific value, Btu/lb	12,606	8,492	11,554	12,556
Specific sulfur content, lbs SO_2/MMBtu	5.81	9.87	8.88	5.91

Table 2. Hydrodesulfurization of char from IBCSP-1 coal[a].

Experimental Conditions				Sulfur in HDS char %	Initial char S left in HDS char %
Oxidation	Temp °C	Flow cc/min			
Pre	800	500		0.91	27.6
Pre	850	500		1.00	30.5
Pre	800	1000		0.92	28.0
Pre	850	1000		0.83	23.3
			Average	0.92	27.4
Non	800	500		1.33	42.9
Non	850	500		1.13	35.2
Non	800	1000		0.88	27.8
Non	850	1000		1.06	32.8
			Average	1.10	34.7
Post	800	500		1.27	47.2
Post	850	500		1.24	43.8
Post	800	1000		1.03	35.5
Post	850	1000		1.24	44.0
			Average	1.20	42.6

[a]Time, 90 minutes

Table 3. Hydrodesulfurization of char from deslimed IBCSP-4[a].

Oxidation		Sulfur in HDS char wt %	SO_2 from burning HDS char lbs/MMBtu	Initial char S left in HDS char %
Pre		1.84	3.23	45.2
Pre		1.95	3.36	45.5
	Avg	1.89	3.30	45.3
Non		1.95	3.44	40.0
Non		1.67	2.80	38.4
Non		2.04	3.50	46.2
	Avg	1.89	3.25	41.5
Post		1.90	3.34	43.7
Post		2.27	3.97	52.1
	Avg	2.09	3.66	47.9

[a]Temperature, 850°C; time, 90 minutes; H2 flow rate, 1000 cc/min.

Table 4. Hydrodesulfurization of char from tabled and deslimed IBCSP-4[a].

Experimental Conditions					Sulfur in HDS char wt %	SO_2 from burning HDS char lbs/MMBtu	Initial char S left in HDS char %
No.	Coal Type	Pre-Oxi-dized	Temp °C	Time min.			
1	Deslimed	No	750	45	2.99	5.25	70.05
2	Tabled	No	750	45	2.01	3.30	66.40
3	Deslimed	Yes	750	45	3.40	5.88	86.00
4	Tabled	Yes	750	45	1.50	2.42	54.30
5	Deslimed	No	850	45	2.57	4.53	59.40
6	Tabled	No	850	45	1.62	2.65	52.30
7	Deslimed	Yes	850	45	2.51	4.30	58.85
8	Tabled	Yes	850	45	1.22	1.97	43.70
9	Deslimed	No	750	90	2.77	4.88	64.55
10	Tabled	No	750	90	1.76	2.85	57.25
11	Deslimed	Yes	750	90	2.64	4.49	63.10
12	Tabled	Yes	750	90	1.14	1.82	40.95
13	Deslimed	No	850	90	2.24	3.99	51.20
14	Tabled	No	850	90	1.41	2.31	45.60
15	Deslimed	Yes	850	90	2.28	3.86	53.05
16	Tabled	Yes	850	90	0.77	1.24	27.15

[a]Hydrogen flow rate, 750 cc/min.

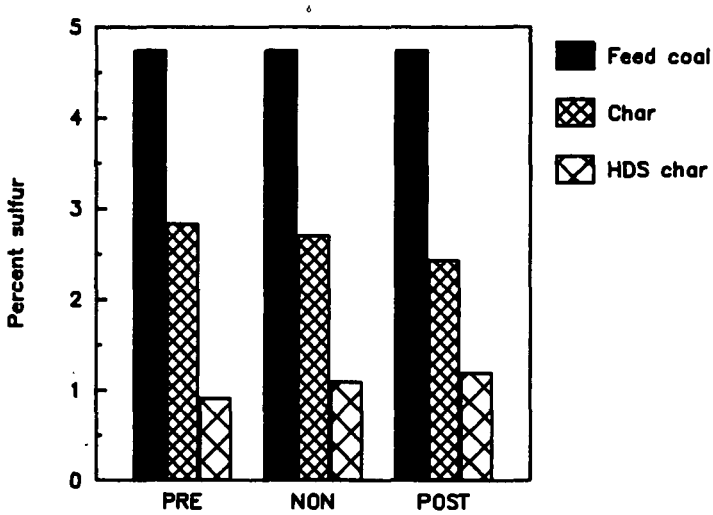

Figure 1. Desulfurization of IBCSP-1.

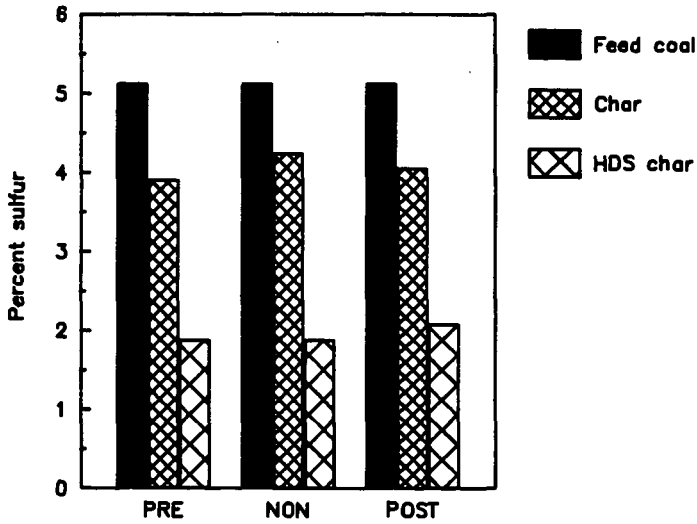

Figure 2. Desulfurization of IBCSP-4.

Coal Gel Chemistry 1. An Aspect of Synergistic Effects on the solvent Swelling of Coal

Tetsuo Aida*[1], Yasuhumi Shimoura[1], Nobuyuki Yamawaki[1], Masayuki Fujii[1]
Thomas G. Squires[2], Masakuni Yoshihara[3], Toshihisa Maeshima[3]

[1]Department of Industrial Chemistry, Faculty of Engineering
Kinki Universirty in Kyushu, 11-6 Kayanomori, Iizuka, Fukuoka 820, JAPAN
[2]Ames Laboratory, Iowa State University, Ames Iowa 50010, U.S.A.
[3]Department of Applied Chemistry, Faculty of Science & Engineering
Kinki University, 3-4-1 Kowakae, Higashiosaka, Osaka 577, JAPAN

INTRODUCTION

For a long time, the mixed solvents, such as alcohol-benzene, are conveniently used for coal extractions(1), in which solubilities of coal products used to be enhanced to those in the individual solvents. Most recently, Iino et al. (2) reported powerful binary solvent systems for coal extractions which were composed of carbondisulfide and aprotic dipolar solvents like a DNF or N-methylpyrrolidinone. Although it has long been pointed out that there was a correlation between the increase of extractability and the increase of swelling(2, 3), the mechanism of the synergistic effect on the solvent swelling of coal has been controversial in the coal chemistry. For examples, the effects observed in the binary solvent systems composed of the amine as a counter component had been discussed by Hombach(4) and Larsen(5), based on the solubility parameters and hydrogen bondidngs in the coal matrix, respectively.

Meanwhile, recently ,we revealed the significant steric requirement on the solvent swelling of coal(6). In the course of the further study on the solvent swelling by using various solvents we have learned that there was a curious similarity on the solvent systems adopted by previous researchers(4,5), which were commonly composed of a sterically hindered and a less sterically hindered solvents, and also have found that the relaxation of the steric requirement of coal by the initial formation of the "Coal Gel" of a less hindered solvent would be responsible to the synergistic effect on the solvent swelling of coal.

This paper presents the results of the studies on the synergistic effects of binary solvents on the solvent swelling of coal, based on the steric requirement.

EXPERIMENTAL

The swelling measurements were carried out as described into previous paper (7). Coal, Illinois #6 coal, used in these studies were from the Ames Laboratory Coal Laibrary. Prior to use, the coal was ground, sized, dried at 110 ℃ overnight under vacuum, and stored under a nitrogen atmosphere. The solvents were distilled by ordinary procedures before use. The quantitative determination of the ratio of the concentrations of solvents in the system were carried out by a gaschromatography using a packed colummn(Φ=1/8',glass colummn, 2m, PDEGS). A typical run was as follows: To Illinois #6 coal(500mg; 60-100mesh), a mixture of triethylamine and methanol(1.5ml; 1:2 vol.) was added, and immersed in the ultrasonic cleaning bath. An aliquot of the supernatant of the mixture was injected into a gaschromatography with appropriate time intervals.

RESULTS AND DISCUSSION

Swelling of Illinois #6 Coal in Binary Solvent System

Figure 1. shows the swelling behavior of Illinois #6 coal in the systems of triethlamine and methanol, and dimethylaniline and methanol.

As Hombach already reported(4), in these case also significant synergistic effects were observed. However, curiouly enouph such effects did not appeared in the systems such as pyridine/methanol or n-propylamine/methanol, in spite of their reasonable ranges of the solubility parameters ,as shown in Figure 2.

Furthermore, in the case of the use of steric isomers of butylamine, n-butylamine and t-butylamine, the synergistic effect was observed only to the sterically hindered isomer system(Figure 3).

Figure 4. shows the solvent swelling behaviors of Illinois #6 coal in the binary solvent systems of which components' solbility parameters are considerded to be quite similar, i.e., hexamethylphosphoramide(HMPA) / dimethylformainde (DMF) or t-butylmethylketone(pinacolone) / acetone, in which also sinergistic effects appeared.

These observations clearly suggest that the sinergistic effects of binary solvents on the swelling of coal were not resulted by such simple parameter as a solbility parameter.

Recently, we have revealed the steric requirement on the solvent swelling of coal(6). Based on our observations, such solvents as triethylamine, dimethyl aniline, t-butylamine, pinacolone or HMPA showed significant retardations on

their penetration rates into coal matrix(8). On this point of view, it is quite likely that because of theire steric bulkiness, the apparent equiliblium swelling ratios(Q-values) of these solvents are forced to keep far below their potential values expected under more relaxed steric requirement of coal. .

Measuring the Relative Concentrations of Binary Solvents During Swelling of Illinois #6 Coal

In order to examine the possibility of the selective penetration of the solvent molecule of the binary system into the coal matrix, the relative concentrations of the solvents in the supernatant of the mixture were determined during swelling the coal.

Figure 5. illustrated the change of the relative concentration of methanol vs. time, together with the swelling behavior of coal.

It is obvious that the penetration of methanol into the coal matrix occured predominantly, that is, the relative concentration of methanol in the supernatant was sharply decreased at the initial stage of swelling of coal, and then kept almost constant value which was still a little below the original concentration.

Table 1. shows the relative swelling rate (retardation factors; V_{Rel}) of the various solvents to Illinois #6 coal at 21℃, which were calcurated as described into previous report(7). In these data, we can see that the penetration rate of methanol is approximately 10^4 times faster than that of triethylamine.

Plausible Mechanism of Synergistic Effect of Binary Solvent on Swelling of Coal.

All of these observations described above may be rationalized as folows: The swelling of coal in the binary solvent systems composed of a sterically hindered and a less sterically hindered solvents(or in general, the solvents posessing different penetration rates) is initiated by the predominant penetration of the less hindered solvent, and then forms , so-called, "Coal Gel", of which steric requirement will be released significantly because of the expansion of the coal matrix by the penetrant, and thus it enable to penetrate more sterically hindered solvent molecule into coal with a "Edge Effect".

Namely, the synergistic effect of binary solvent on the swelling of coal is considered to be resulted by the relaxation of the steric requirement of coal, based on the "Coal Gel" formation.

AKNOWLEDGEMENTS

This research was suported by the special grant from The Environmental Science Institute, Kinki University of JAPAN. We are also grateful for suport from The State of Iowa, and from the U.S. Department of Energy through the Ames Laboratory under Contract No. W-7405-ENG-82.

REFERENCES

1. A. Wielopolski, I. Witt, Koks, Smola, Gaz, 22, 47(1975)
2. M. Iino, J. Kumagai, O Ito, J. Fuel Soc. Japan(Nenryo Kyokaishi), 64, 210 (1985); Proceedings of 2nd Japan-China Symposium on Coal & C_1 Chem., Tokyo, Japan, 309(1988)
3. I.G.C. Dryden, Fuel, 30, 39, 145, 217(1951); D. W. van Krevelen, "Coal", Elsevier Publishing Co., Amsterdam(1961)
4. H-H. Hombach, Fuel, 59, 465(1980)
5. J.W. Larsen, T. K. Green, Fuel, 63, 1538(1984)
6. T. Aida, T. G. Squires, Prepr. Pap.-Am. Chem. Soc., Div. Fuel Chem., 30, 102 (1985)
7. T. Aida, T. G. Squires, Prepr. Pap.-Am. Chem. Soc., Div. Fuel Chem., 30, 95 (1985)
8. T. Aida, K. Fuku, N. Yamawaki, M. Fujii, unpublised results.

Table 1. Comparison of Swelling Rate
(Illinois #6, 60-100 mesh, 21 ℃)

SOLVENTS	$V_{Ret.}$ *
Methanol	1.00
Acetone	0.86
Dimethylformamide	0.24
n-Butylamine	0.10
t-Butylamine	39.75
Dimethylaniline	105.43
Triethylamine	> 10^4
Pinacolone	> 10^3
Hexamethylphosphoramine	> 10^4

* Retardation Factor = V_{MeOH} / $V_{Solvent}$

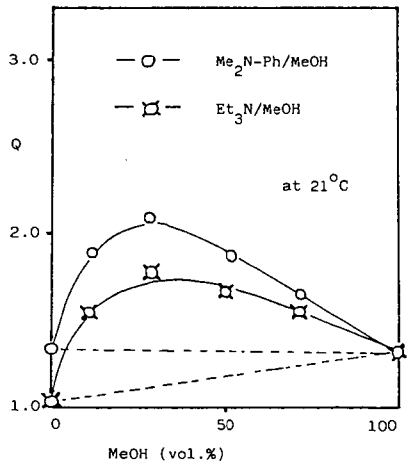

FIGURE 1.

Solvent Swelling of Coal in Binary System
(Illinois #6 Coal,60/100 mesh)

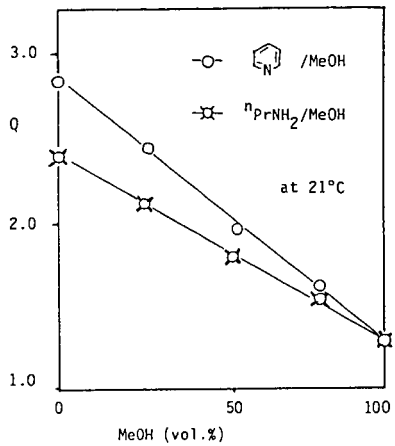

FIGURE 2.

Solvent Swelling of Coal in Binary System
(Illinois #6 Coal,60/100 mesh)

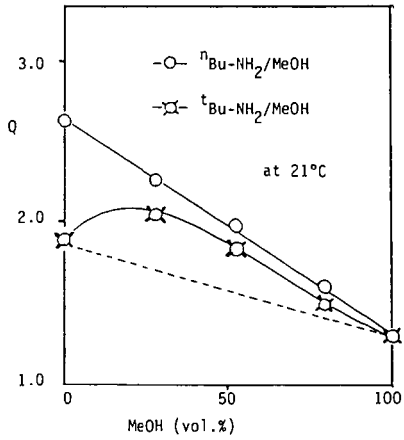

FIGURE 3.

Solvent Swelling of Coal in Binary System

(Illinois #6 Coal,60/100 mesh)

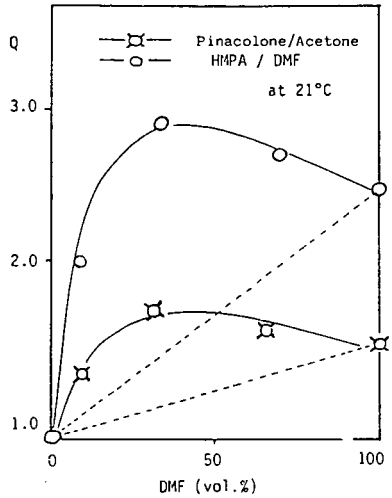

FIGURE 4.

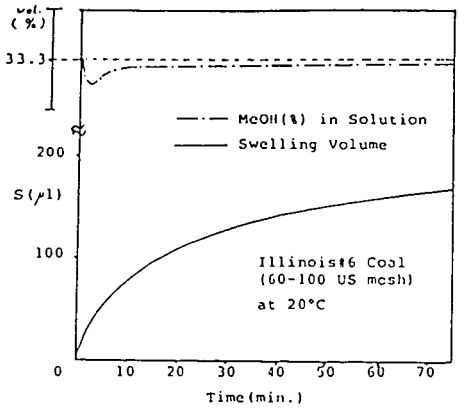

FIGURE 5. Solvent Swelling in Binary Solvent System (Et_3N/MeOH) and Change of Composition in Solution

Utility of Low Value Liquefaction Products as a High Value Additive

Hyon H. Yoon and Arthur R. Tarrer

Chemical Engineering Department
Auburn University, AL 36849

Characteristic to many coal liquefaction processes is that certain streams have objectionable properties in terms of ease of upgrading, and as a result, these streams not only complicate downstream processing but have a very low value. A specific objective of this research was to identify a high value application for these streams. This can impact the entire coal liquefaction processing train and its economics. By finding a high value application for these streams, it becomes economical to remove them early in the processing train for separate processing. This simplifies downstream processing of other streams, reducing overall processing costs, with there being an actual higher value for the entire product slate.

Typical objectionable properties of certain coal liquefaction streams are: 1) high molecular weight distribution, 2) high heteroatomic content, and 3) high metals content.(1) It was thought that these objectionable properties could actually prove to be advantageous for utilizing these fractions as a high value antistripping additive for asphaltic pavement cement.

Stripping of asphaltic cement from pavement aggregates has long been recognized as a major cause of failure in asphaltic concrete pavements. The cause of stripping is attributed to water or moisture penetrating the asphalt-aggregate matrix. Stripping, which is the loss of adhesive bond between the asphalt and aggregate surface, results in a loss in integrity of the asphaltic concrete and subsequent failure, requiring early and costly maintenance.

A number of methods have been developed for reducing stripping damage in asphaltic concrete pavements. Of these methods, the addition of a chemical antistripping (AS) additive has become the most widely practiced method for maintaining pavement durability, because of its relatively low cost and ease of implementation. A large number of AS additives, which are normally surfactants, are commercially available today. According to the 1984 survey of state highway agencies by Tunnicliff and Root (2), more than 100 chemical AS additives are used in the United States.

AS additives are substances added to asphalt cement to promote adhesion of the asphalt cement to the aggregate surface and thus to improve the resistance of the asphalt pavement to stripping damage. Most AS additives are mixtures of proprietary chemical compounds, and detailed characterizations of these compound mixtures are usually not available; however, most of the active compounds are probably amines or chemical compounds derived from ammonia. Usually these compounds act as cationic surfactants to reduce surface tension at the aggregate surface (3). However, it has been shown that many AS additives are susceptible to heat and thus, with storage in hot asphalt cement, the effectiveness of these additives could be severely reduced. Figure 1 shows the loss in effectiveness for different typical commercial AS additives with storage of the additives at 325°F in an asphalt cement. Four

different commercial AS additives from different manufacturers were used in this study. The additives were labeled Additive Nos. 1, 2, 3, and 4. The stripping propensity of an asphalt-aggregate mixture was measured in terms of the percentage coverage of aggregate after the boiling water test. If the asphalt separated from the aggregate surface after boiling the asphalt-aggregate mixture in water for 10 minutes, it was said to have stripped, and the asphalt - aggregate bond was concluded to have been weak and to have a high stripping propensity.

In addition to evaluating the heat sensitivity characteristics of AS additives, it was shown that only a small fraction of the AS additive migrates to the aggregate surface and acts to improve the asphalt cement/aggregate bonding: most of the additive remains in the bulk of the asphalt and never comes in contact with the aggregate surface. For this reason, such chemical AS additives not only change the asphalt cement/aggregate bonding, but can also change the properties of the bulk asphaltic cement significantly.

In order to minimize AS additive dosage requirements, direct application of AS additive to the aggregate surface was investigated. Table 1 shows the result of direct application of an AS additive (Additive No. 1) to the aggregate surface. The additive, which is water soluble, was dissolved in water to form treatment solutions having concentrations ranging from 0.05 to 0.5 wt%. Then the aggregate (granite 3/8 in. - No. 4 mesh size) was immersed in the respective solution for 10 minutes. After towel drying and preheating the aggregate at 275°F, the boiling water test was performed. Based on the results given in Table 1, it was calculated that direct application of AS additive to the aggregate surface requires only about 5% of the amount of additive which would be required to provide an equivalent effective amount of additive at the aggregate surface when the additive is added in the asphalt.

With direct application, the commercial AS additive, a polyamine-type additive, appeared to degrade at relatively high temperatures (250°C) and become ineffective, as shown in Figure 2. The preheating temperature was varied from 135°C to 350°C to simulate the temperature range in which aggregates may be heated in a commercial aggregate dryer. The temperature of combustion gases and air used to dry aggregate in a commercial dryer ranges from about 250 to 315°C.

In an earlier work (4), it was found that stripping of asphalt cement from pavement aggregates was very much an aggregate problem. That is, physico-chemical properties of the aggregate surface have a very significant effect on the stripping propensity of an asphalt-aggregate mixture. Figure 3 shows how the surface charge density (Zeta Potential) varied among some different types of common aggregates. Interestingly, the aggregates which had a relatively high surface charge were found to be more susceptible to stripping as measured by the boiling water test.

It was thought that by impregnating the aggregate surface with an easily polymerized compound prior to its being dried, it would become coated with molecular layers of polymerized (coked) material. This could serve to reduce the surface charge of the aggregate surface and make it easier for the asphalt to adsorb (or bond) to the aggregate.

Aggregate surfaces were assumed to interact strongly with high molecular weight, aromatic compounds in a manner similar to how coke forms on catalyst surfaces. High molecular weight aromatic compounds have high coking propensities. For this reason, a granite aggregate was precoated with a phenanthrene solution (10 wt% in toluene) and then preheated at 135, 250, and 350°C. Figure 4 shows that the effectiveness of the phenanthrene pretreatment increased as the preheating temperature was increased. A similar result was obtained for an actual coal liquid (10 wt% toluene), as is shown in Figure 4. The coal liquid was obtained from the Wilsonville coal liquefaction plant. It was therefore thought that the formation of coke-like compounds on the aggregate surface during the aggregate preheating (drying) period could be the primary cause of the observed pretreatment effect of phenanthrene and/or heavy coal liquid on the asphalt-aggregate bond, as was measured here using the boiling water test.

While performing the above aggregate surface conditioning studies, it was observed that reheating an asphalt-aggregate mixture usually resulted in an increase in its stripping resistance. Asphalt-aggregate mixtures were cured (reheated) by holding the mixtures at a fixed temperature for a set period of time. It was observed that the performance of an asphalt-aggregate mixture was improved with curing at about 300°F for several hours. This apparent improvement in adhesion between the asphalt and the aggregate surface with curing was again thought to be, in part, due to coke-like compounds being formed on the aggregate surface. For this reason, pretreatment of a granite aggregate with phenanthrene, which has high coking propensity, was evaluated for accelerating the curing effect on stripping propensity. Indeed, this was found to accelerate curing, as shown in Figure 5.

It appears then that compounds having a high coking propensity, like phenanthrene and heavy coal liquid, have potential usage as an AS additive.

References

1. Nalitham, R.V., "Parametric and Kinetic Studies on Deactivation and Regeneration of Hydrotreating Catalysts in Solvent Refined Coal Upgrading Process and an Evaluation of the Liquid Vaporization Effects on Hydrotreater Performance." Dissertation, Auburn University, 1983.

2. Tunnicliff, D.G and R.E. Root, "Use of Antistripping Additives in Asphaltic Concrete Mixture." NCHRP Report 274, 1984.

3. Mathews, D.H., "Surface-Active Agents in Bituminuous Road Materials." J. Appl. Chem. 12, February, 1962.

4. Yoon, H.H. and A.R. Tarrer, "Effect of Aggregate Properties on Stripping." Transportation Research Record (In Press).

Table 1. Effect of Aggregate Pretreatment with a Commercial AS Additive (Additive No. 1) on the Boiling Water Test Results.

Additive Content in Water	Water Content of Aggregate after Soaking	Amount of Additive on Aggregate	Percent Coating Retained after Boiling
%	g water/g agg.	g add./g agg.	%
0.5	0.0232	1.60×10^{-4}	100
0.1	0.0281	0.28×10^{-4}	100
0.05	0.0430	0.21×10^{-4}	95
0.05	0.0221	0.11×10^{-4}	65
0.05	0.0201	0.10×10^{-4}	60

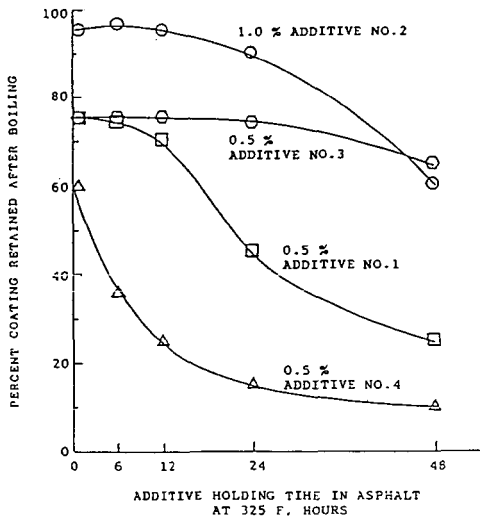

Figure 1. Heat Stability of Antistripping Additives in Asphalt as Determined by the Boiling Water Test.

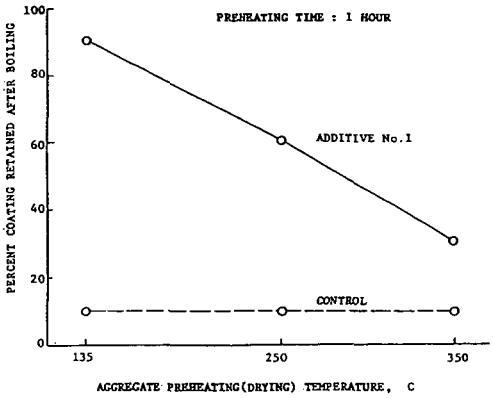

Figure 2. Response in Effectiveness of a Typical Commercial AS Additive to Changes in Aggregate Preheating(Drying) Temperature with Direct Application of the Additive to Granite Aggregate.

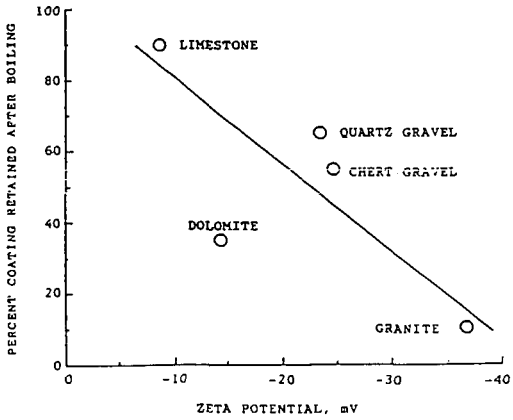

Figure 3. Comparison of Aggregate Surface Potential and Stripping Propensity as Determined by the Boiling Water Test.

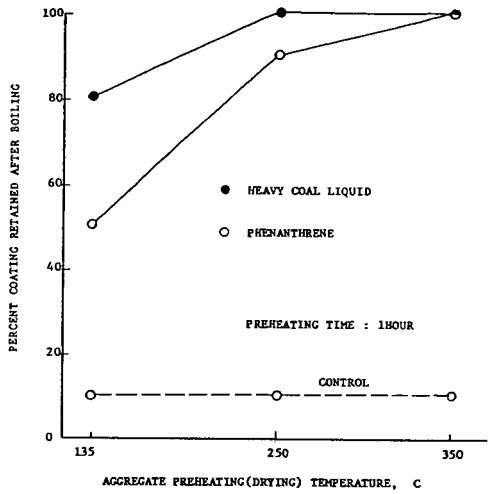

Figure 4. Response in Effectiveness of Phennthrene and of Coal Liquid as AS Additives to Changes in Aggregate Preheating(Drying) Temperature with Their Direct Application to Granite Aggregate.

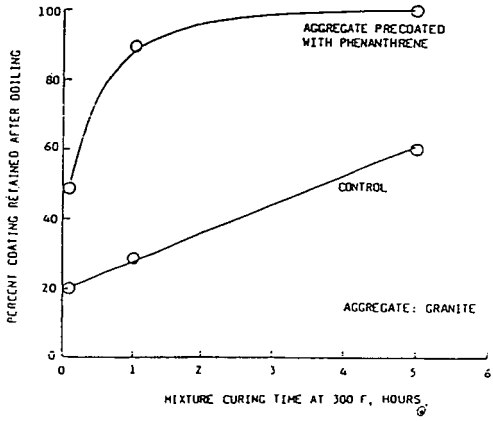

Figure 5. Acceleration of Curing Effect on Stripping Resistance by a High Coking Propensity Additive, Phenanthrene.